REGOLITH MINERALOGY AND GEOCHEMISTRY AT GOONUMBLA PARKES, NSW

Eric K. Tonui

A thesis submitted for the degree of Doctor of Philosophy
(PhD) at the Australian National University

January, 1998

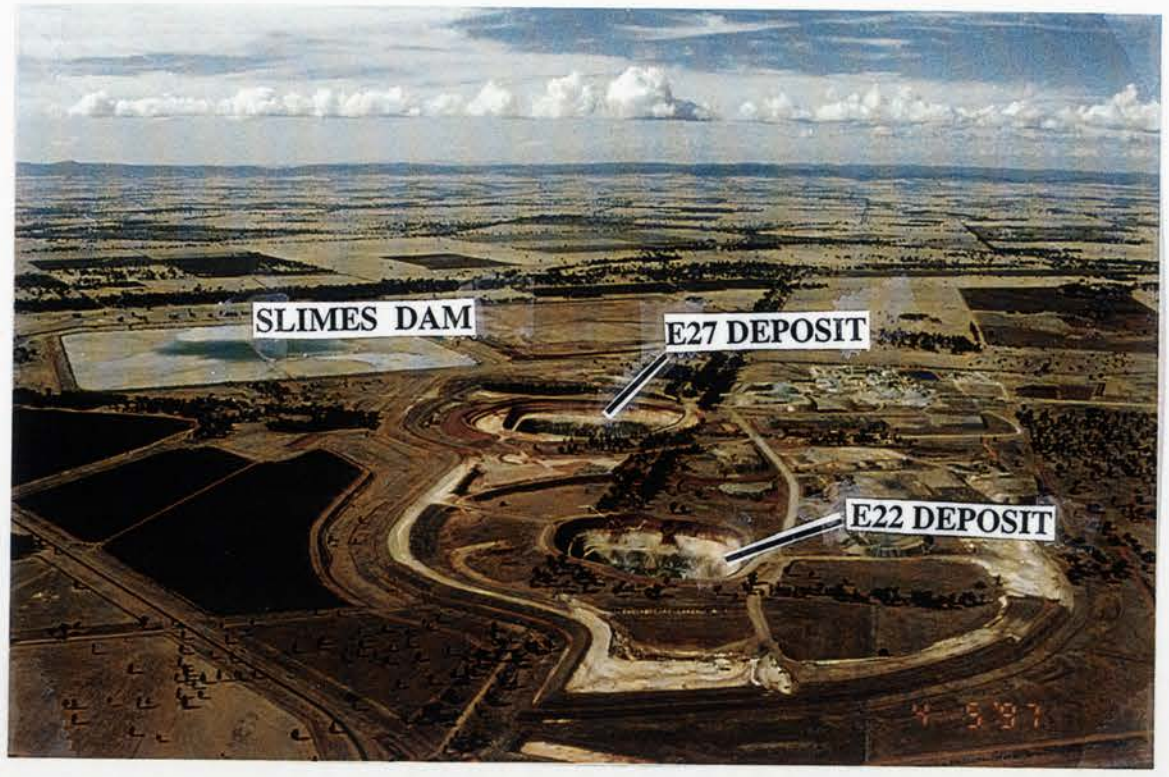

Aerial view of the Northparkes E22 and E27 deposits with the slimes dam in the background. Notice the general flatness of the landscape around the mine area.

Aerial view of the Northparkes E22 and E27 deposits with the company premises in the background.

Aerial view of the Northparkes E22 deposit

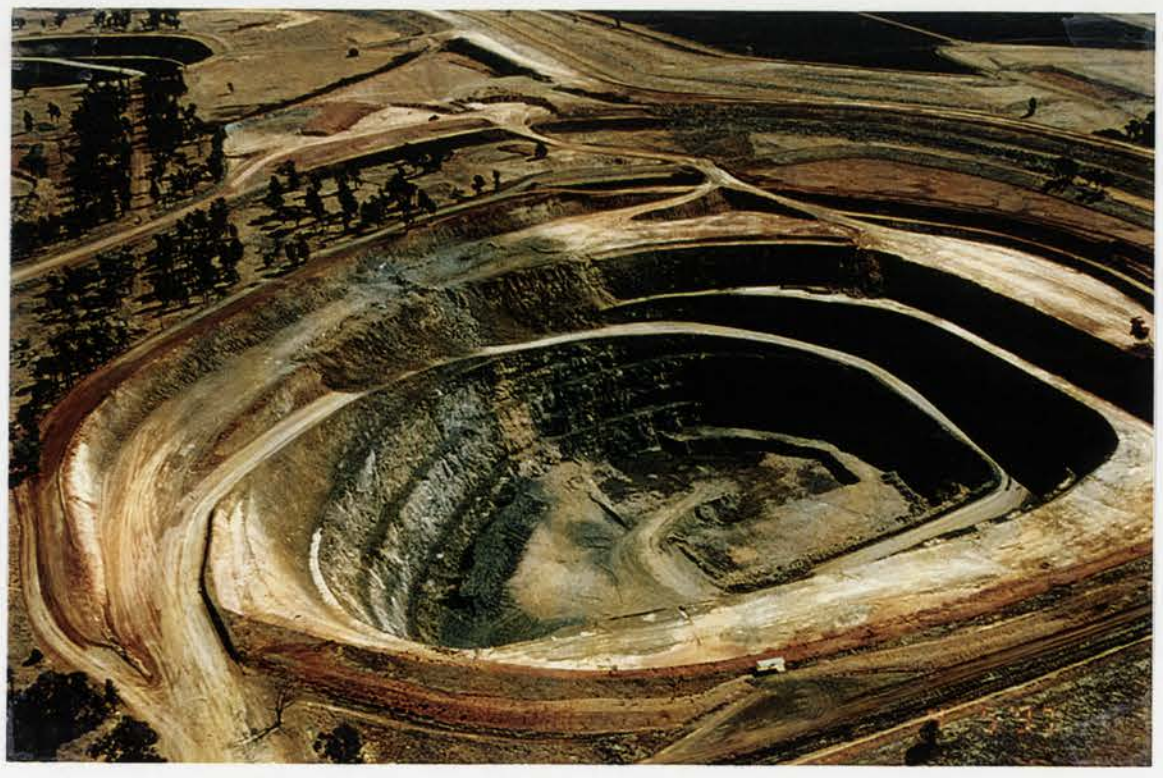

Aerial view of the Northparkes E27 deposit

TABLE OF CONTENTS

CHAPTER 3

CLASSIFICATION OF THE REGOLITH

CHAPTER 4

SAMPLE COLLECTION AND ANALYSIS

PART 2

CHAPTER 5

REGOLITH FEATURES OF THE DEPOSIT

CHAPTER 6

REGOLITH MINERALOGY: DESCRIPTION AND PARAGENETIC SEQUENCES

CHAPTER 7

PART 3

CHAPTER 8

CHAPTER 9

CHAPTER 10

CHAPTER 11

LIST OF FIGURES

LIST OF TABLES

LIST OF PLATES

[After page 88]

ABSTRACT

In the Parkes region of New South Wales, Northparkes Mining Ltd is developing a major porphyry copper-gold deposit occurring in late Ordovician to early Silurian trachyandesites as disseminated or veined sulfides. Detailed mapping of the open cut as mining progressed provided information on the landscape evolution of the area, revealing an older weathered landscape covered by younger, weathered, transported alluvial and colluvial material in palaeotopographic lows. A close study of macro-and-micro regolith fabrics, mineral paragenetic sequences and mineral element associations have been made to determine the nature and extent of weathering processes. Palaeomagnetic dating of the regolith has been carried out to determine the age of weathering.

The determination of the nature of the parent material has been central to the description and classification of the regolith materials. Two major regolith types have been recognized: residual regolith that developed from the weathering of the trachyandesite, and transported regolith that resulted from the weathering of alluvial and colluvial sediments overlying the residual regolith.

The weathering of the trachyandesite transpired within joints, cracks and fissures which presented sites of rapid solution and matter movement and zones of accelerated kinetics and alteration within the rock system. Rock-solution microsystem reactions predominated where primary mineral and solution activity and chemistry exerted roughly equal influence on the production of secondary assemblages. This was exemplified by dissolution of feldspars which was marked by differential shattering and formation of etch pits; commonly regarded as evidence of transport-solution mechanisms operating to induce the dissolution of mineral surfaces. This involved introduction of iron from the weathering of pyroxenes and sulfides into active sites with fissure microsystems prevailing and solution chemistry dictating the type of secondary product. The role of microenvironments in governing the type of secondary product was of major importance with the intensity and amount of solution access regulating nucleation and crystal growth and hence the outward appearance of the secondary products.

The characteristics that define the transported regolith materials include the presence of sub-rounded to sub-angular detrital quartz fragments, the presence of numerous illuviated clay filled channels and voids, laminar or cellular goethite cutans on nodules and formation of rounded to sub-rounded ferruginous nodules. The transported regolith is markedly mottled, with mini-mottles (< 5 mm) occurring in transition with the soil at depths of 4 to 6 m, medium-mottles (5 to 30 mm) in the middle levels at depths of 6 to 18 m and mega-mottles (50 to 300 mm) at the base at depths of 18 to 26 m. Scanning electron microscopy showed the occurrence of thin platy kaolin particles that occurred parallel to one another and in most cases adhering to the detrital quartz grains representing concurrent deposition of quartz and clays in alluvial environments.

The transported materials occur in U-shaped pockets in localized basins in the landscape that have been interpreted as defining palaeotopographic lows. These features are now seen to be widespread in the landscape although their occurrence has not been well documented before. The mineralogy of detrital rock fragments within them was similar to that of the host volcanics indicating a local sediment source rather than derivation from surrounding Palaeozoic sediments. The boundary between the residual and transported regolith is quite conspicuous within the regolith stratigraphy and can easily be delineated throughout.

The study of element mobility was accomplished from extensive geochemical data using a combination of line plots, correlation matrices and scatterplots with additional input

from mass balance techniques. The isocon method was found to be most appropriate for the latter because unlike other weathering indices it has an internal check on the degree to which the so called immobile elements have actually remained immobile during weathering. In studying the element mobility, a close check was carried out between the petrographic work and X-ray diffraction analysis to optimize the interpretation of data. The immobile elements in the profiles studied were found to be Ti, Al and Nb.

These studies showed rapid removal of alkalis and alkaline earth cations (in particular Ca, Mg, Na and Sr) from the weathering profiles and enrichment in the soils corresponding to the presence of carbonates; rapid depletion of sulfur corresponding to the weathering of sulphides; progressive depletion of silica from the profiles; oxidation of iron and fixation largely as hematite and goethite and the close association between Cu, Pb, Zn and Rb defining the mineral alteration zone. For major cations and closely related elements, the slope of the elemental loss curve gave a general order in which elements were lost as: Na>Sr>Ca>Mg>Rb>K>Si.

Selective leaching techniques have also provided an insight into mineral and element host associations during weathering. The Fe and Mn oxides were analyzed for this study because of their ubiquitous occurrence and strong ability to scavenge metals. Extraction by pH 5 acetate dissolved all of the Ca and Mg phases from the carbonate-rich units and only part of that in the residual regolith units because of occurrence of these phases in the more pH 5 acid resistant plagioclase feldspars. The general trend from hydroxylamine extractions showed partitioning of Ag, Ni and Pb into the Mn oxides and Cu into the iron oxides. The low dissolution capacities in the lower residual units was attributed to elements being more tightly bound to resistant mineral phases like muscovite and ferromagnesium silicates. A strong association between Au and goethite in the soil horizons was also determined during this study.

Palaeomagnetic dating of the regolith yielded a late Palaeozoic age for the weathering of the trachyandesite and a mid-tertiary age for the weathering of the overlying transported regolith. Recognition that the weathering has been an on-going process in the Parkes region since the late Palaeozoic provides a challenge to the dimensions of thinking regarding the regolith evolution and landscape evolution processes in the region.

ACKNOWLEDGEMENTS

Many thanks to the following people for their invaluable support and assistance in the production of this thesis:

- Dr. Tony Eggleton (supervisor), Reader in the Department of Geology of the ANU, for introducing me to this project and for his guidance in all aspects of this work. His humble support, accessibility, valuable advice and critical examination of the thesis manuscript ensured optimum delivery of all the outcomes.

- Dr. Graham Taylor (supervisor), Associate Professor of the University of Canberra, for offering similar support and advice and for promptly proof reading each chapter.

- Mr. Roger Jones (advisor), Senior Exploration Geochemist of North Exploration Ltd. For getting me started on the impressive task of statistically analysing and interpreting the geochemical data. Roger was also actively involved in the generation of the 2D geochemical plots utilising North's facilities at Parkes.

- North Exploration Ltd. for provision of field support and accommodation, funding of the ICP MS geochemical data and allowing me the use of their computers, photocopiers etc. when required.

- North Mining Ltd. for providing access to the mines and additional information on the deposit geology.

- Richard Arculus, Head of Department, for allowing me the use of the Geology Departments facilities.

- Technical staff at the Department of Geology and the Electron Microscopy unit at the ANU. Special thanks in particular go to Robyn Westcott and Berlinda Crowther for guiding me in all aspects of analytical work notably X-ray diffraction and optical microscopy and for keeping me disciplined around the laboratory.

- Bruce Chappel, Ulrike Seinff and Tony Phimpisane of the ANU, for their support in the geochemical analysis of the samples.

- Brian Harrold of the Department of Geology, ANU, for his guidance on software utilities

- My colleagues at CRC LEME ANU especially Mehrooz Aspandair and David Tilley for their invaluable support. Profound thanks also go to Nazre Sobhan for being a wonderful officemate and friend.

- My parents Stephen and Mary Sang, brothers Willy and Patrick and sisters Chepkemoi, Cheronoh, Chepngenoh, Cherotich, Chelangatt, Chepkoech and Chebett for their never ending source of inspiration.

My utmost appreciation goes to my wife Joyce and our two boys Kiprutoh and Kiptoo for their unconditional love and for being so understanding throughout the course of this research.

Finally I thank God (Chepongolo) for sustaining me through the ages.

Dedicated to my loving wife Joyce
and sons
Kipruto (5) and Kiptoo (2)

DECLARATION

This thesis is based on work carried out at the Department of Geology, Australian National University.

All results, interpretations and arguments presented in this thesis are the authors, except where acknowledged.

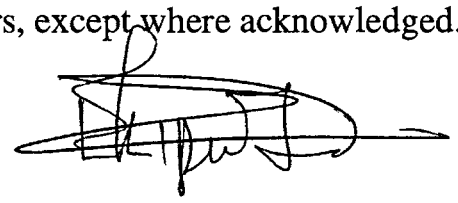

Eric Kipkirui Tonui

AIMS OF THE STUDY

The major objectives of the project include:

1. To establish a systematic classification system of the regolith in the region, based on evidence from the mine open cuts and drill cores.

The major problem confronting regolith research and studies in Australia and elsewhere at present is the lack of a uniform classification system that can be used to accurately describe and characterize regolith materials. The most commonly used terminologies at present include Butt and Zeegers (1992), Nahon and Tardy (1992) and the CSIRO classification of Anand and Butt (1988); Anand et al., (1989); Butt et al., (1991) and Smith et al., (1992). The scheme described in this text has been formulated after taking into account the distribution of the regolith materials in the project area and in conformity with established national and international usage.

2. To elucidate regolith paragenesis and processes of rock alteration in the area.

The description of weathering sequences of the host rocks, the macro and micro regolith fabrics and textures and hence regolith mineralogy is of particular importance to this study. Weathering causes rocks composed of anhydrous or weakly hydrated minerals to alter to friable material composed mainly of hydrated secondary minerals. The description and characterisation of these secondary minerals is important in that they are the ultimate sink for most elements released and dispersed from primary mineralisation during weathering.

3. To determine the distribution of ores and ore-forming metals, their mobility and potential enrichment in the weathering environment and trace element distribution in secondary phases during mineral alteration.

The distribution of these elements in deeply weathered environments is determined by the stability of their primary host minerals, the presence or absence of secondary host minerals and the chemical mobility of these elements in the changing weathering environments to which they have been subjected.

4. To date the regolith and develop a regolith stratigraphy for the study area and to use this to formulate models to explain landscape evolution processes in the region.

The determination of the weathering history and the recognition of the effects of past and present climates on these processes are fundamental to interpretation of geochemical data and hence in formulation of improved exploration procedures.

PART 1

.Geology & Mineralization

.Review of the Literature

.Classification & Terminology

CHAPTER 1

GEOLOGICAL SETTING AND MINERALIZATION

1.1 Introduction

Over the past twenty years, considerable effort and expense has been put into the search for porphyry copper deposits in Australia, particularly in the Palaeozoic rocks of the Tasman Fold Belt. Recent detailed exploration by [1]North Ltd (formerly Geopeko) over a large area of lower Palaeozoic andesitic volcanics in central New South Wales has led to the discovery of a major new porphyry copper-gold province. The deposits are located in Goonumbla, 25 km northwest of Parkes.

Copper mineralization has been known in Parkes district since the late nineteenth century. North selected the region for detailed exploration in 1971. Initial field mapping led to the discovery of a lead-zinc skarn deposit in 1974, now known as Endeavour 27. Further drilling work in 1976 intersected disseminated copper mineralization associated with weak potassic alteration in andesite. Individual centers of mineralization at Goonumbla are referred to as Endeavour prospects or deposits and have accompanying numbers, which run in sequence of discovery date (Figure 1.1). Subsequent work defined the Endeavour 22 and 27 bedrock copper-gold geochemical anomaly. This project has entirely been based on the study of the regolith over the Endeavour 22 and 27 prospects herein also referred to as E22 and E27 deposits.

A recent detailed description of the Goonumbla porphyry copper deposits has been given by Heithersay et al. (1990) who expanded on work previously done by Jones (1985) and Bowman et al. (1977). All these works provide a description of regional geology and deposit geology. Additional work has been presented of petrology (Clarke, 1987), stratigraphy (Krynen, 1984; Sherwin et al. 1987) and tectonism (Tenison, 1983).

1.2 REGIONAL SETTING

Gold and copper mineralization in the Parkes district is hosted by a sequence of Late Ordovician to early Silurian volcanics, intrusives and sediments that occur within the NE portion of the Lachlan Fold Belt system known as the Bogan Gate Synclinorial Zone (Scheibner, 1975).

[1]North Ltd., a major Australian resources company, holds an 80% interest in Northparkes Mines, operators of E22 and E27 deposits. The exploration unit of North Ltd. supported this study.

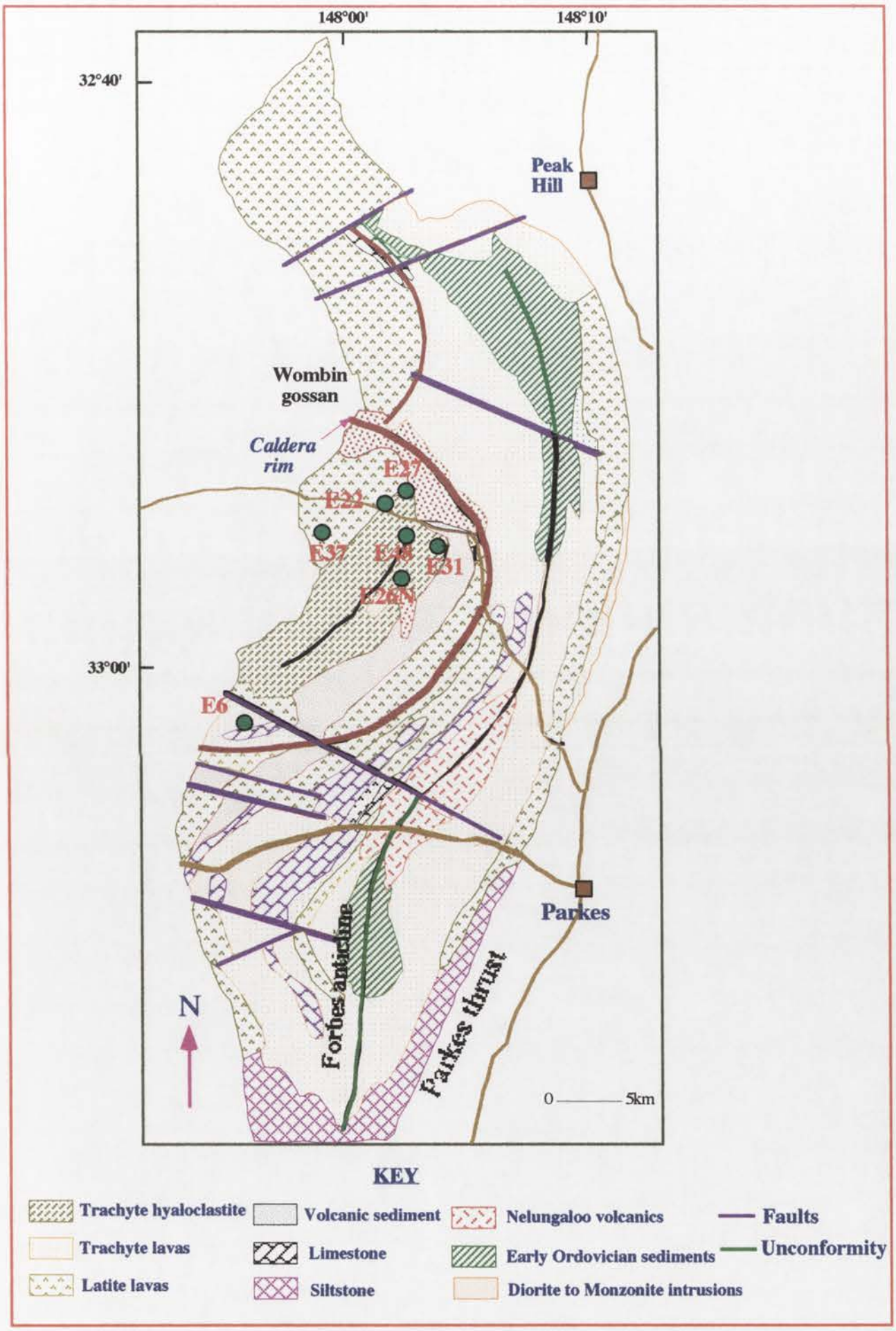

Figure 1.1: Geological setting and location of the Goonumbla Cu-Au deposits (Modified from Heithersay et al., 1990).

This belt can be subdivided into the western Girilambone Anticlinorial Zone dominated by volcanics, and the eastern Tumut Synclinorial Zone dominated by sediments. The deposits are located in the western zone (Heithersay et al. 1990). The volcanics, comagmatic intrusives, volcanic sediments and limestones of the western zone are gently folded with shallow dips and poor cleavage. Metamorphism is weak to absent with occasional zeolite to lower greenschist minerals identified. The sediments, intermediate volcanics and pyroclastics of the eastern zone are tightly folded, with major faulting and widespread quartz veins. The eastern zone is host to the Parkes-Forbes-Peak Hill gold belt (Clarke, 1985).

Several models for the geological setting of the Parkes district during the Ordovician to Early Silurian have been postulated including a subduction-related island arc/arch model (Scheibner, 1975, 1976), a lithospheric tensional model associated with partial melting of the upper mantle and subsequent crustal melting (Wyborn, 1977) and an extensional continental rift model (Jones, 1985).

1.2.1 REGIONAL STRATIGRAPHY

The stratigraphic units of the Parkes district as shown in Figure 1.2 are briefly described below:

ORDOVICIAN-SILURIAN

Nelungaloo Volcanics

These are the oldest rocks in the area. Fossil evidence provides an Early Ordovician or possible Late Cambrian age (Sherwin, 1979). They are exposed in the core of the Forbes anticline and comprise andesitic flows, volcanically derived sediments, conglomerate, chert and limestone.

Goonumbla Volcanics

This dominantly volcanic sequence overlies the Nelungaloo Volcanics though the precise relationship between the two is unknown. The basal sequence of the Goonumbla Volcanics includes the Billabong Creek Limestone Member and the Gunningbland Shale Member. Fossil evidence provides a Late Ordovician age (Sherwin, 1973). The volcanics are potassium rich trachyandesites and consist of interlayered flows, pyroclastics and volcanic sediments.

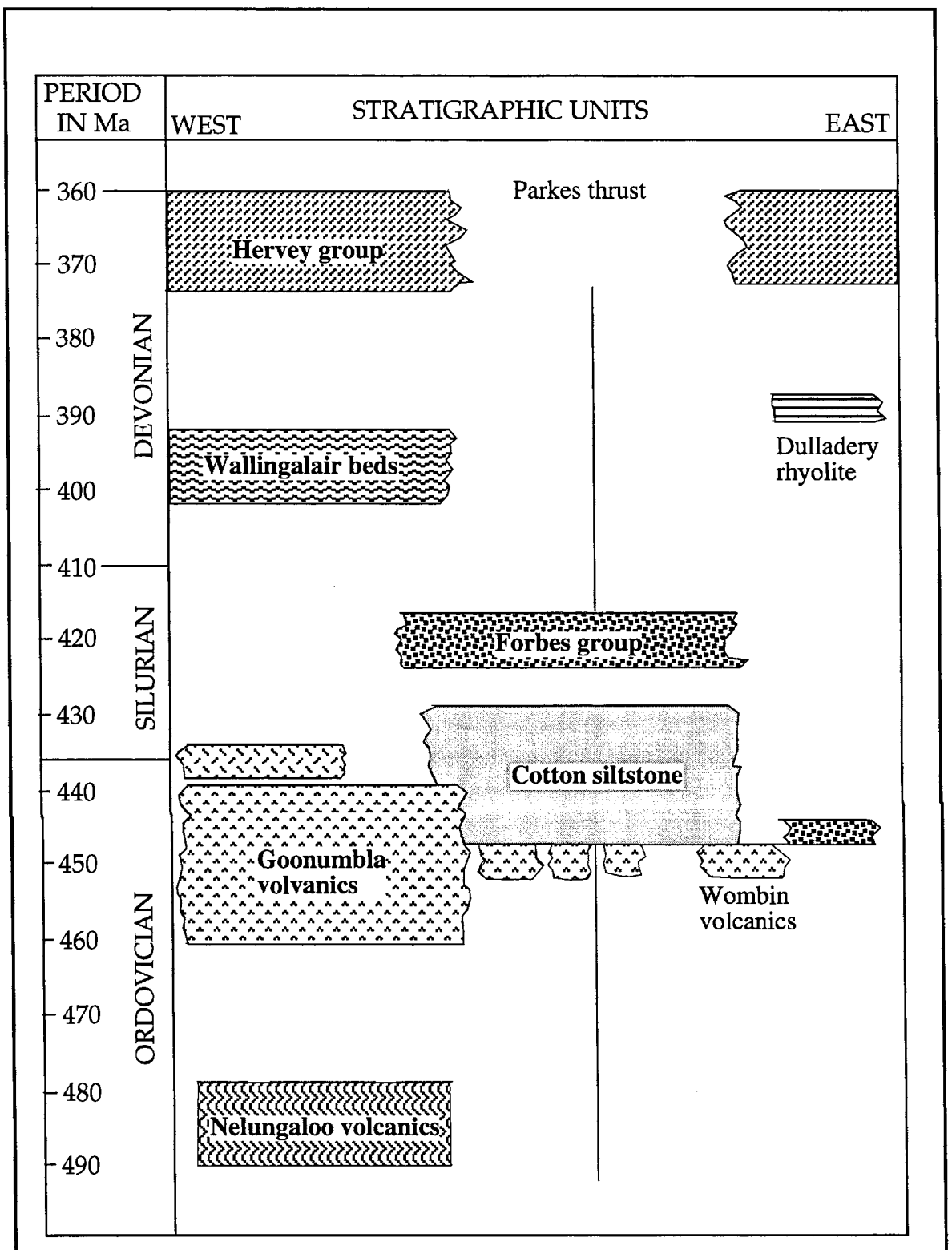

Fig. 1.2: Rock relationships diagram of the region (After Sherwin et al., 1987).

Similar intermediate volcanics occur within the sediments to the east of the Goonumbla Volcanic Complex and include the Parkes Volcanics, Nash Hill Volcanics, Daroobalgie Volcanics and Mingelo Volcanics, all regarded as time equivalents of the Goonumbla Volcanics.

Wombin Volcanics

The relatively loose definition of the Wombin Volcanics (Bowman et al. 1977) has made it impossible to delineate this formation confidently (Heithersay et al. 1990). Jones (1985) included within his 'Wombin Group' a sequence of trachyandesites, now considered to be part of the Goonumbla Volcanics. It is preferable that the term Wombin Volcanics be restricted to a sequence of brown-red potassium rich trachytic flows, pyroclastics and associated epiclastics that immediately overlie the Goonumbla Volcanics (Heithersay et al. 1990). Recent ^{40}Ar- ^{39}Ar dating of alteration assemblages cutting the trachytic volcanics returned a date of 441 ± 2Myr (Perkins unpublished data cited in Heithersay et al. 1990), thereby fixing the minimum age as Late Ordovician. Petrochemical evidence strongly supports the interpretation that the trachytic volcanics are late stage, more differentiated volcanics related to the waning stages of the Goonumbla volcanic event.

Cotton Formation

This formation is dominated by siltstone but includes several conglomerate and chert horizons. Fossil evidence (Sherwin, 1973) provides an age of Late Ordovician to Early Silurian.

SILURIAN

The **Forbes Group** consists of the Bocobidgle Conglomerate, which contains chert, quartzite and monzonite clasts up to 10 cm in diameter in a limy to lithic matrix, and the Mumbigle Formation of silty mudstone and sandstone (Heithersay et al. 1990). Fossil evidence indicates a Middle to Late Silurian age (Sherwin, 1975). It is often difficult to distinguish between the Forbes Group and the Cotton Formation and it is possible that the Forbes Group is more extensive than currently mapped (Heithersay et al. 1990).

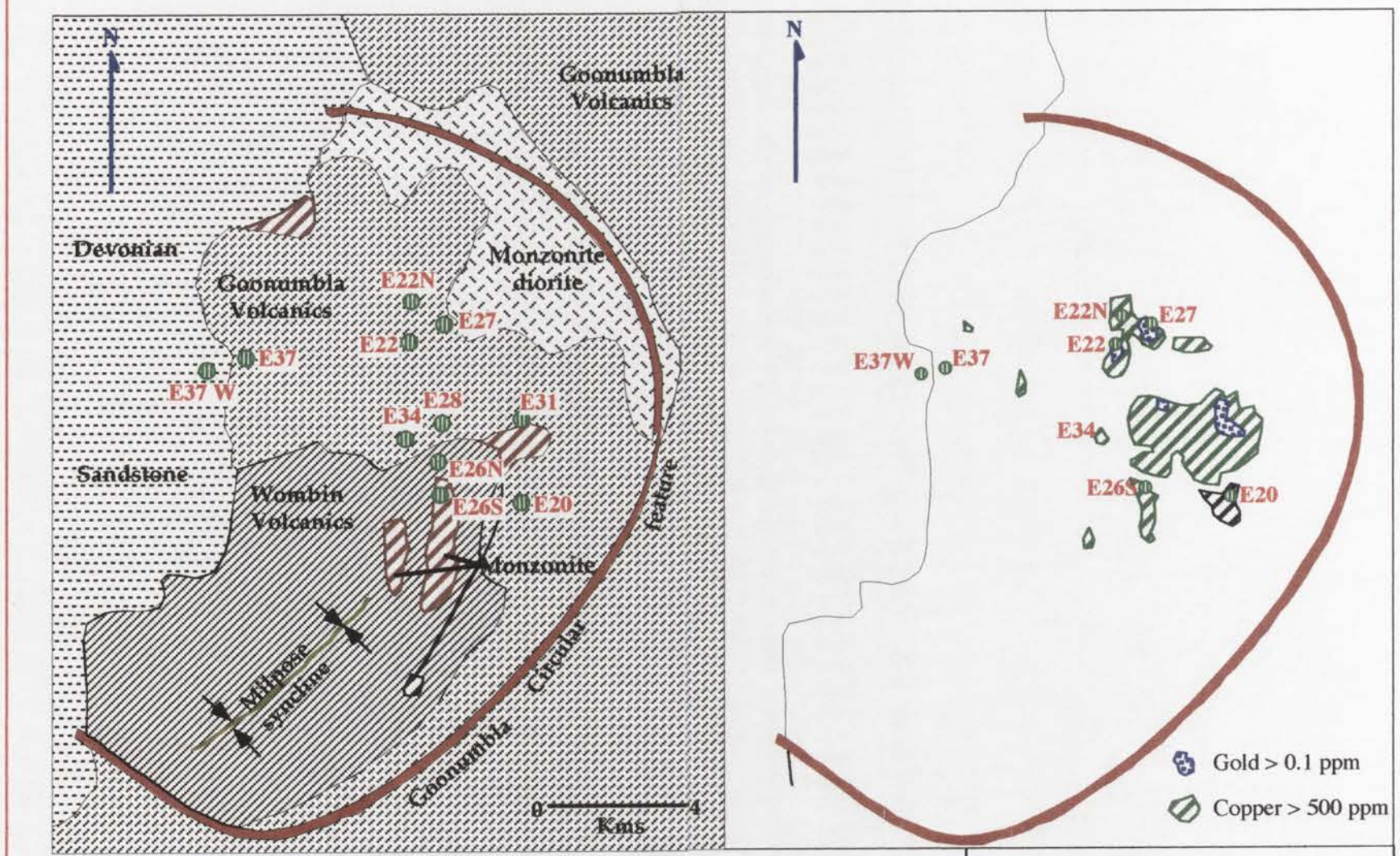

(Modified from Heithersay et al.1990)

Drawn by E.K Tonui

Fig 1.3: The geology and geochemistry of the Goonumbla porphyry Cu - Au deposits

EARLY DEVONIAN

The **Wallingalair Beds** consist of quartz sandstone, conglomerate lenses, shale and impure limestone. On fossil evidence they are assigned an Early Devonian age (Sherwin, 1975). Included are the Calarie Sandstone and the Milpose Volcanics; a sequence of flows and possible intrusions of rhyolitic to granitic composition (Heithersay et al. 1990).

LATE DEVONIAN

The **Hervey Group** is dominantly quartz sandstone and conglomerate, and unconformably overlies the Wallingalair Beds.

MESOZOIC

Towards the West, remnants of a drainage system are apparent in the form of deposits of coarse-grained poorly cemented sandstones and conglomerates. Plant fossil evidence according to Picket (1985), cited in Krynen et al. (1987) suggests a Jurassic age.

INTRUSIVES

Ordovician intrusive activity, as currently known, is restricted to the western zone. Mafic intrusives of dioritic to monzodioritic composition intrude the Nelungaloo Volcanics and a suite of intrusives ranging in composition from diorite to quartz syenite intrudes the Goonumbla and Wombin Volcanics. Quartz monzonite porphyries are intimately associated with porphyry copper-gold mineralization.

1.3 GOONUMBLA PORPHYRY COPPER-GOLD DISTRICT

Jones (1985) interpreted interpreted the circular feature (Figure 1.3) within the volcanics of the western zone to be a collapsed caldera. He postulated that the discrete circular Bouger gravity low resulted from the presence of a large and less dense intrusive body at relatively shallow depths within the caldera. A complex intrusive of monzonitic to dioritic composition, which forms an arcuate dyke along the northern and northeastern perimeter of the circular feature, is regarded as a ring dyke. All porphyry copper-gold mineralization discovered to date is located within the circular feature.

1.3.1 STRATIGRAPHY

Outcrop within the circular feature is poor, however on the basis of limited and relatively sparse drill hole data; a broad open syncline (the Milpose Syncline) plunging to the SW has been discerned (Figure 1.3). Extensive soil cover, structural complexity, sudden facies variations and monotonous rock types characterize the district.

In the northern part of the caldera, the oldest unit exposed is a sequence of high potassium trachyandesitic volcanics (shoshonites) of the Goonumbla Volcanics. They are flows of varying thickness, and pyroclastics ranging from coarse agglomerate to fine ash tuff. Minor interbedded volcanically derived fine-grained sediments indicate shallow water (possibly lacustrine) deposition (Heithersay et al. 1990). Limestones occur outside the caldera rim, however they have not been identified within the caldera.

The Wombin Volcanics overlie and are probably conformable with the Goonumbla Volcanics. They are preserved toward the center of the synclinal feature in the southern half of the caldera and appear to be truncated in the south by a major east-trending structure.

INTRUSIVES

The intrusive history within the caldera is complex. Including the northern ring dyke, approximately 20% of the rocks exposed within the caldera are of intrusive origin. Detailed work by Heithersay et al. (1990) has identified multistage intrusive activity and complex overprinting hydrothermal alteration patterns. They have envisaged a subvolcanic environment for these intrusives.

The porphyry copper-gold mineralization is invariably associated with relatively small, subvertical, pipe-like intrusive bodies of quartz monzonite porphyry (Figures 1.4 and 1.5). Their diameters rarely exceed 100 m but they may have vertical continuity of over 900 m. A typical mineralized quartz monzonite porphyry has a strong pink to pinkish orange colour, and is commonly coarsely porphyritic containing 20-40% plagioclase phenocrysts. Quartz phenocrysts, mostly less than 1mm, may comprise 10 to 20% of the rock and the matrix is fine grained potassium feldspar and quartz.

Multistage intrusive activity of quartz monzonite porphyry is quite common (Heithersay et al. 1990), but contacts between phases are often poorly defined, suggesting that timing

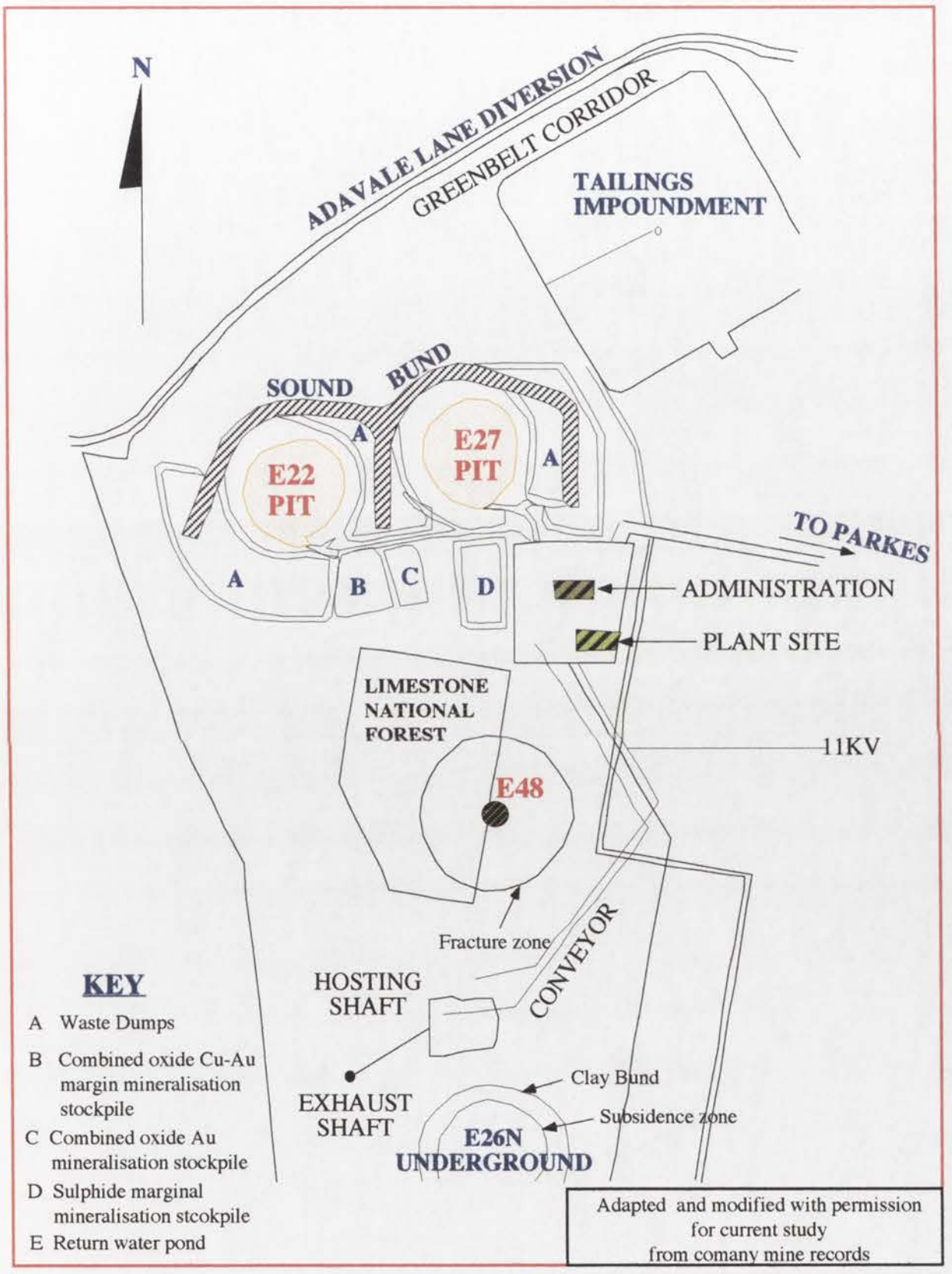

Fig 1.4. The Northparkes mines general arrangement

of the intrusive events may be very close and possibly overlapping. Individual phases are identifiable by slight textural and compositional variations.

Post-mineralization intrusives are common in both E22 and E27 deposits and include porphyritic dykes of monzonitic to syenitic composition. Thin basic dykes, 1 to 2 m wide, and andesitic to basaltic dykes occur but are not common.

1.4 DEPOSITS

1.4.1 ENDEAVOUR 22 (E22) DEPOSIT

The Northparkes mines plan showing the major deposits is shown in Figure 1.6. Selected photomicrographs of some of the lithological units are presented in Figures 1.7. The E22 deposit is 28 km northwest of Parkes and is located near the centre of the caldera. The base of oxidation (referred to as the weathering front in regolith studies) occurs at various depths between 20 and 45 m with the overlying material extensively weathered.

Volcanic lithologies comprise a layered sequence of andesitic flows and associated pyroclastics, notably lithic tuffs, ashfall tuffs and agglomerates. All the volcanics show strong evidence of hydrothermal alteration which has resulted in partial to complete destruction of most primary textures (Jones, 1985).

The andesite is a dark, basic and tuffaceous unit characterized by abundant plagioclase phenocrysts (Figures 1.7.1 and 1.7.6). Compositionally the andesites range from shoshonite to potassium-rich trachyte using the nomenclature of Cox et al. (1979). Latites (potassium rich trachyandesites) dominate the Goonumbla Volcanics. Chemically they range from 50 to 65% SiO_2 with corresponding K_2O range of 2 to 7%; K_2O + Na_2O content ranges from 5 to 10%. The suite is characterized by high Al_2O_3:FeO ratios and low Ti, Zr and Ba contents (Heithersay et al. 1990). These features are consistent with characteristics of shoshonite rock association outlined by Joplin (1968) and Morrison (1980).

Three varieties of intrusives have been identified in E22. The most important is a quartz monzonite porphyry, also considered as the active mineralization intrusion. It is a pink to pinkish-orange finely porphyritic rock containing abundant K-feldspar and euhedral phenocrysts of oligoclase 2-3 mm in size and set in an equigranular groundmass of quartz and feldspar (Figure 1.7.7). Biotite and hornblende are minor phases and

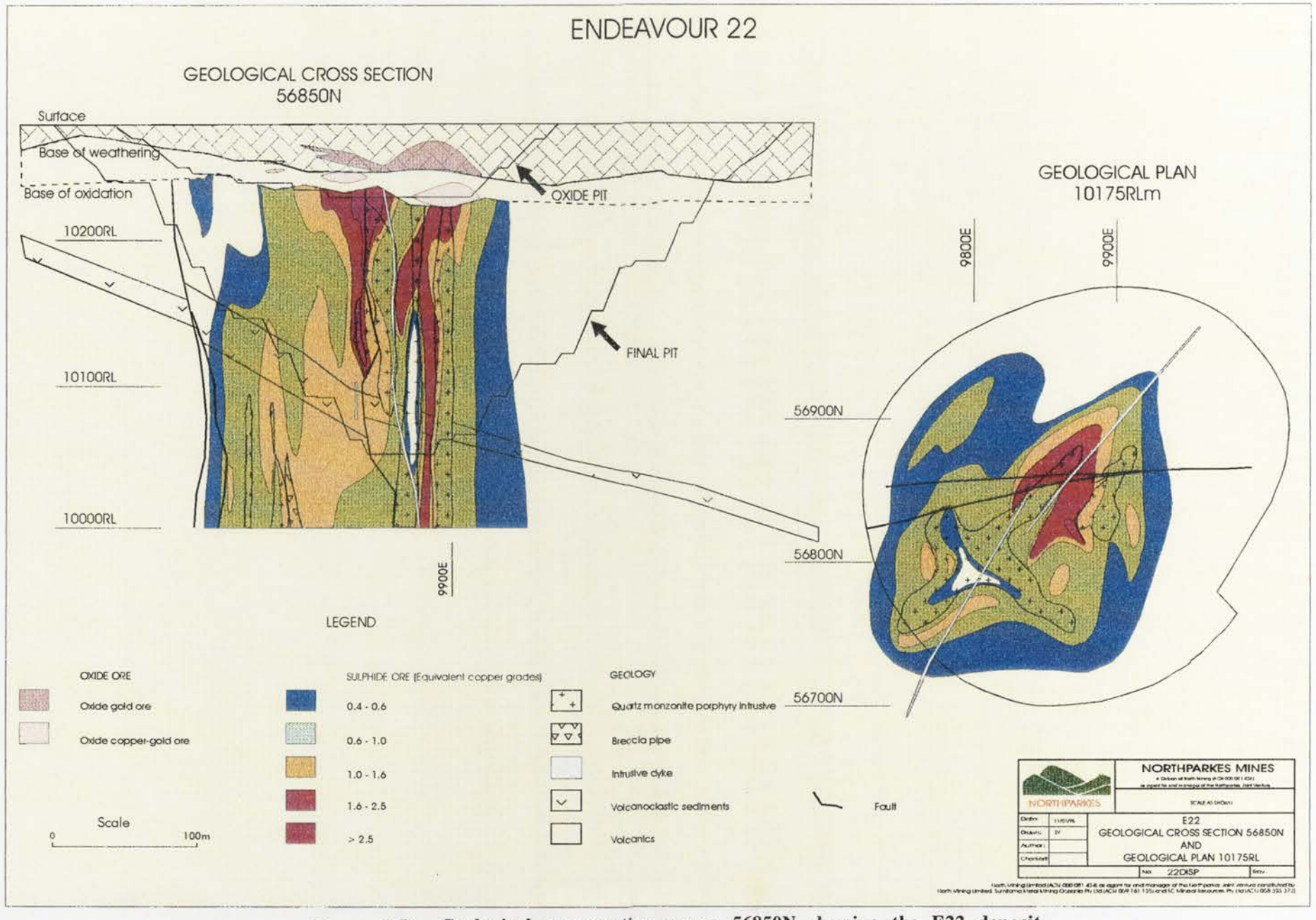

Figure 1.5: Geological cross-section across 56850N showing the E22 deposit.

magnetite, sphene and apatite are accessories. The other intrusives are felsic monzonite and picrite basalt dykes.

ALTERATION

The most abundant alteration product is pink K-feldspar, which is present principally in the andesitic wall rocks surrounding the quartz-monzonite porphyry intrusive. It occurs in veins and as vein envelopes, irregular blebs and as pervasive matrix flooding (Heithersay et al. 1990). The potassic alteration occurs in a cylindrical zone centered around the quartz monzonite porphyry and extending for distances between 80 to 200 m outward into the wall rocks (Jones, 1985).

Lesser but important alteration products include carbonate which occurs as narrow veinlets in the groundmass. Away from the deposit, calcite has been observed to replace quartz as the dominant gangue mineral. This is associated with the marked decrease in the number and thickness of the veins (Jones, 1985; Bowman, 1987). Secondary biotite also occurs as pervasive alteration of the groundmass and as pseudomorphs of primary mafic phenocrysts. Sericite alteration occurs as incomplete replacement of plagioclase phenocrysts and as subordinate to biotite in altered groundmass (Figures 1.7.2 and 1.7.5). A broad (200 m) propylitic halo surrounds the K-feldspar zone. Here pyrite occurs as disseminations and veinlets with minor sphalerite and galena in association with epidote and chlorite (Jones, 1985).

MINERALIZATION

Copper-gold mineralization in E22 is dominantly fracture controlled. The deposit is a sulfur poor system with Bornite (Figure 1.7.10) being the dominant copper sulfide, followed by chalcocite and chalcopyrite (Figure 1.7.11) which is dominant in the marginal and lower grade peripheral zones (Heithersay et al. 1990). Pyrite occurs in outer zones rarely exceeding 1% of the rock. Gold occurs within and rimming bornite usually as fine blebs less than 5 μm in diameter. Mean grades of copper range from 0.55 to 0.78% and gold content varies between 0.40 and 0.83 g per metric ton.

1.4.2 ENDEAVOUR 27 (E27) DEPOSIT

The Endeavour 27 deposit, situated 1 km east of Endeavour 22 is the smallest of the three larger deposits. It is completely masked by weathered cover with the interface between the weathered zone and rock occurring at vertical depths between 25 to 50 m.

The volcanics here show a higher proportion of massive porphyritic andesitic flow rocks than in the sequence at E22. Definition of individual flows is difficult but in many cases the tops of these flows are marked by minor pyroclastic material, commonly tuffaceous sediment. The porphyritic andesite is dark grey to green in colour. The dominant feldspar is plagioclase commonly occurring as euhedral phenocrysts 6 mm in length. Subordinate hornblende and augite are other rock forming minerals with apatite and magnetite as accessories (Jones, 1985). The dominant pyroclastics include crystal lithic tuffs, dark tuffaceous sediments and hornblende porphyries.

The E27 quartz monzonite porphyry stock is a large coherent pipe-like body (Figure 1.5). An uncommon feature is the presence of large (10-15 mm) isolated megacrysts of orthoclase scattered throughout the groundmass. This scattering has been accompanied by localized contact brecciation, dyking and disruption (Heithersay et al. 1990) clearly linked to the emplacement of mineralization. The matrix has a typical granular crystalline texture comprising a mixture of quartz and feldspar with quartz up to 15% by volume. Minor biotite is present. Other intrusives include the mafic monzonite and basalt dykes.

ALTERATION

By comparison, the potassic alteration at E27 is far more restricted than the equivalent zone at E22, attributed mainly to the presence of high proportion of andesitic flow rocks in contrast to the largely pyroclastic wall rock sequence at E22. The K-feldspar generally forms envelopes to mineral-bearing quartz and carbonate veinlets and also occurs as blebs and irregular shaped masses (Bowman, 1987). Carbonate occurs in association with K-feldspar and quartz in veins (Figures 1.7.3 and 1.7.8) and as small patches that are randomly distributed throughout the andesites. Partial carbonate replacement of plagioclase phenocrysts have also been noted. Sericite typically occurs as dusting and replacement mineral of plagioclase with lesser effects on orthoclase. Minor hydrothermal alteration minerals include secondary biotite, chlorite, zeolite, prehnite, apatite, fluorite, epidote and green amphibole.

MINERALIZATION

Porphyry copper mineralization at E27 comprises both disseminated and vein bornite, chalcopyrite and chalcocite. Vein mineralization typically occurs in the central core of narrow (3-5 mm) quartz and quartz-calcite veins, which form irregular stockworks. Most of the higher-grade copper-gold mineralization (greater than 0.8% Cu) occurs

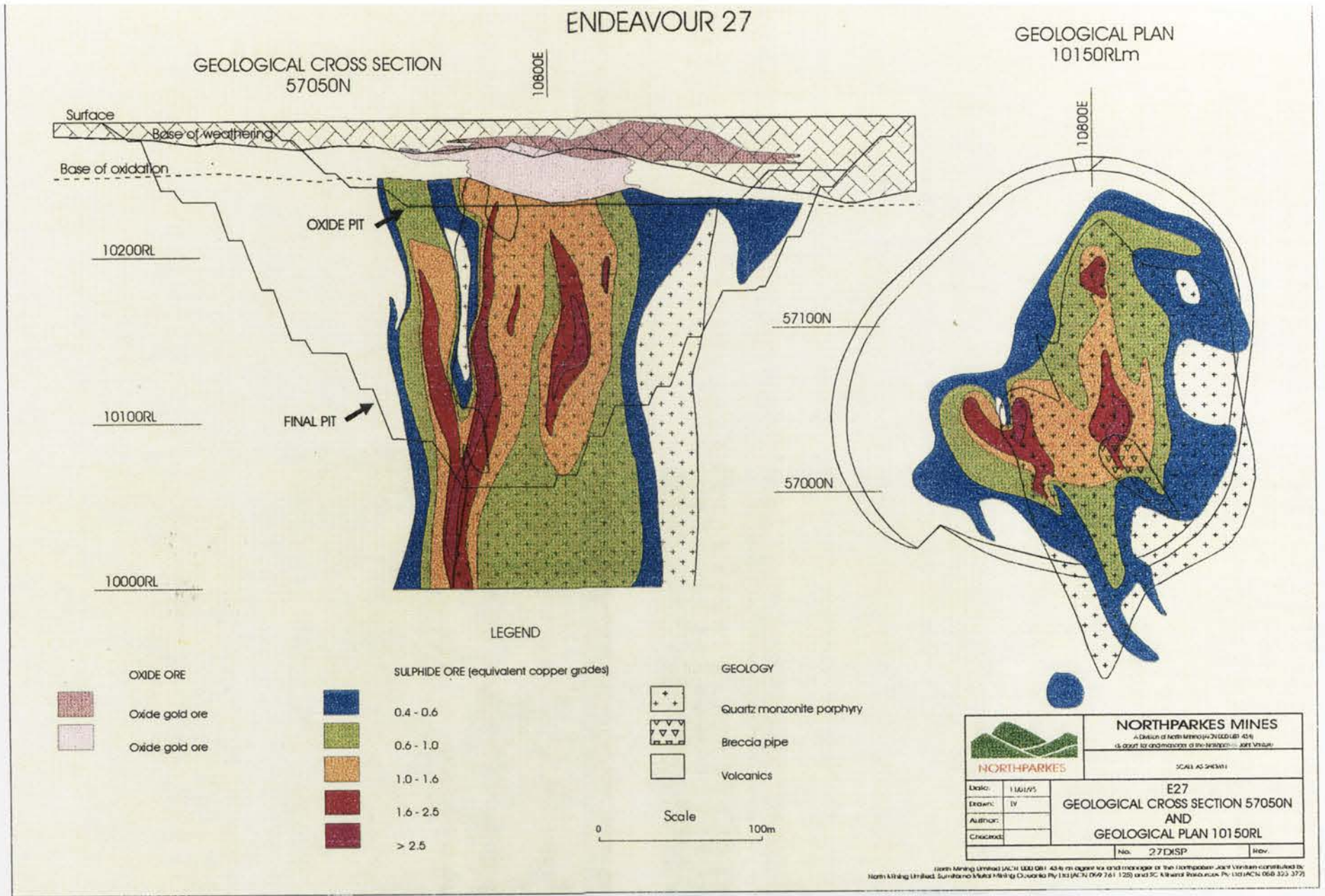

Figure 1.6: Geological cross-section across 57050N showing the E27 deposit.

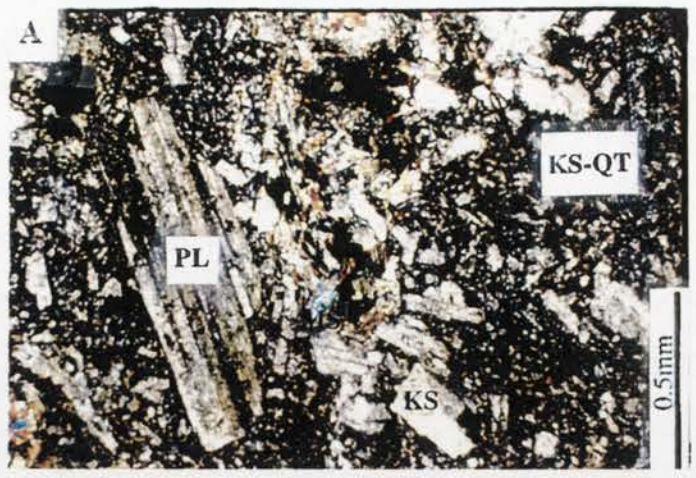

Fig. 1.7.1: Trachyandesite rock showing a partially altered plagioclase lath (PL) with K-feldspar (KS) and muscovite (MS) in a groundmass of K-feldspar and quartz (KS-QT). Hydrothermal alteration resulted in partial destruction of the rock fabric. Specimen E27 TR4. Depth (46m). Photomicrograph with crossed polars.

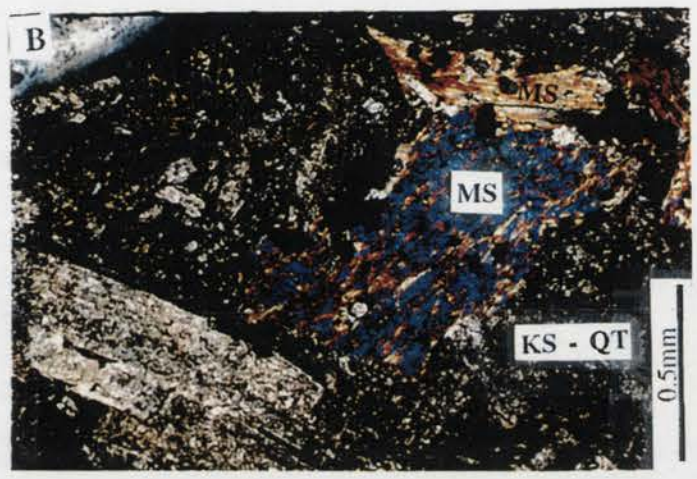

Figure 1.7.2: Muscovite (MS) pseudomorphically replacing plagioclase within the K-feldspar and quartz (KS-QT) groundmass. Specimen E27 TR1. Depth (46m). Photomicrograph with crossed polars.

Figure 1.7.3: A quartz-calcite vein within the quartz monzonite showing tabular prehnite (PR) within the quartz (QT) and calcite (CL) groundmass. Specimen E22 MZ 3. Depth (44m). Photomicrograph with crossed polars.

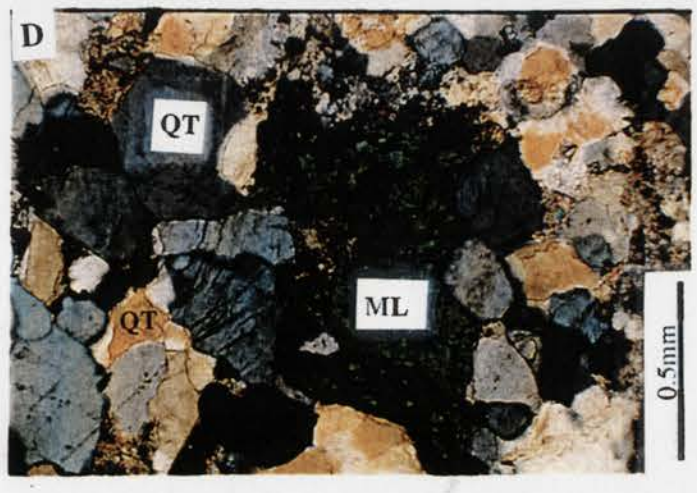

Fig. 1.7.4: Malachite (ML) engulfed within a quartz vein associated with the quartz monzonite. Specimen E22 MZ 1. Depth (46m). Photomicrograph in normal light.

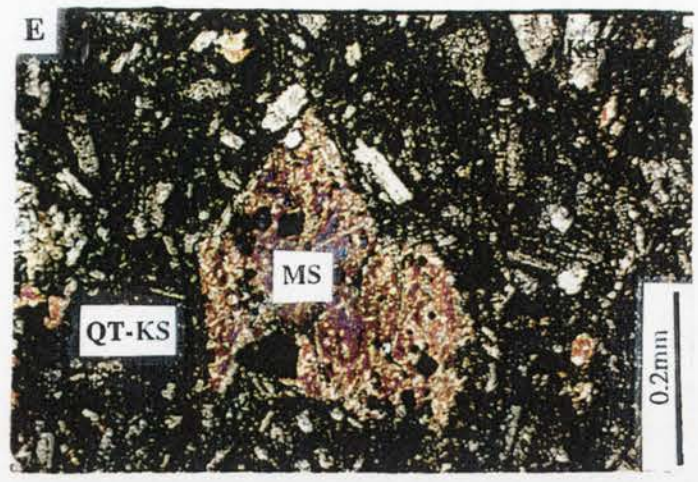

Fig.1.7.5: Muscovite (MS) with plagioclase (PL) laths in a quartz-feldspar groundmass (QT-KS). Specimen E22 TR1 (trachyandesite).
Depth (42m). Photomicrograph with crossed polars

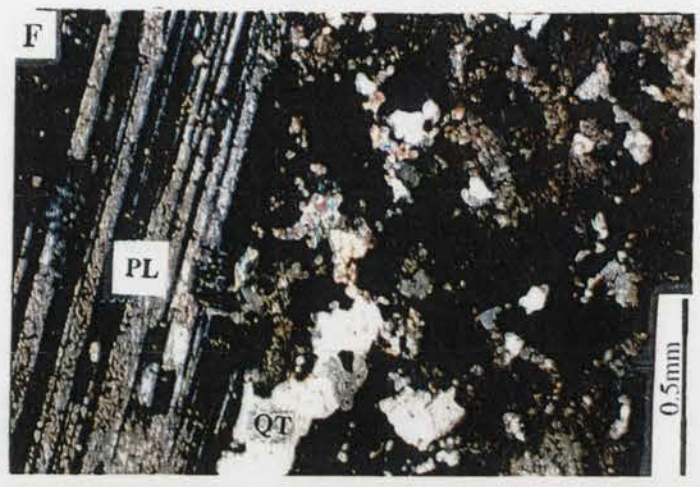

Fig.1.7.6: Twinning in plagioclase (PL) set in a quartz- rich (QT) matrix and opaques (sulphides and oxides). Dominant oxides include magnetite, sphene and hematite. Specimen E27 TR 4. Depth (46m). Photomicrograph with crossed polars.

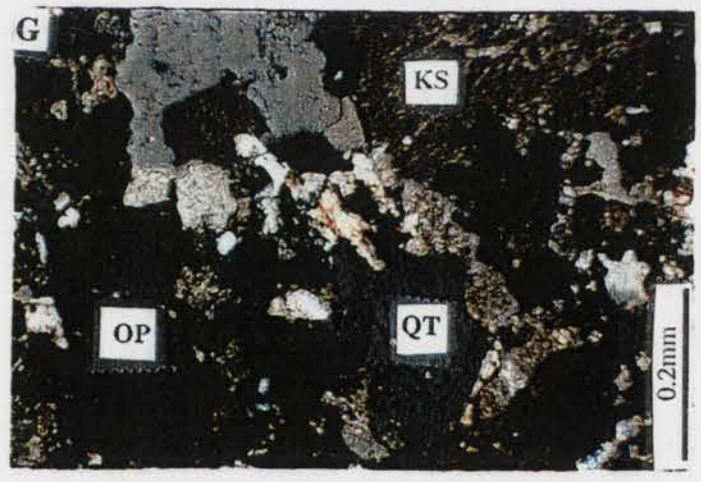

Fig. 1.7.7: K-feldspar (KS), quartz (QT), and opaques (OP) within a quartz monzonite rock. Specimen E22 MZ 2. Depth (46m).
Photomicrograph with crossed polars

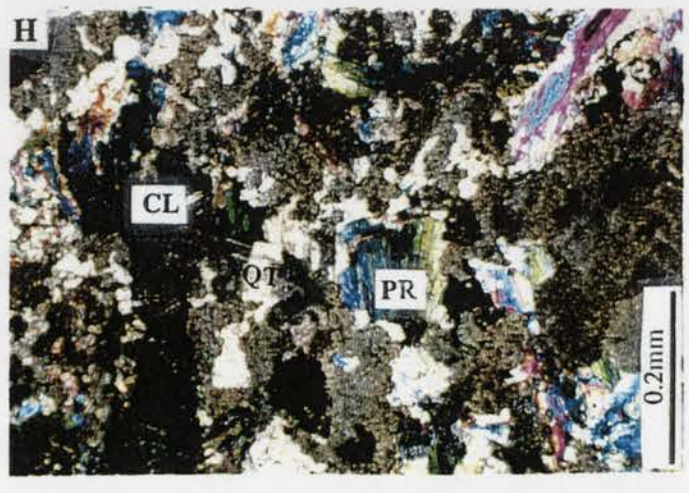

Fig. 1.7.8: Quartz-calcite vein within the quartz monzonite showing intergrowths of prehnite (PR) crystals within the calcite (CL) and quartz. Specimen E22 MZ 3.
Depth (44m). Photomicrograph with crossed polars.

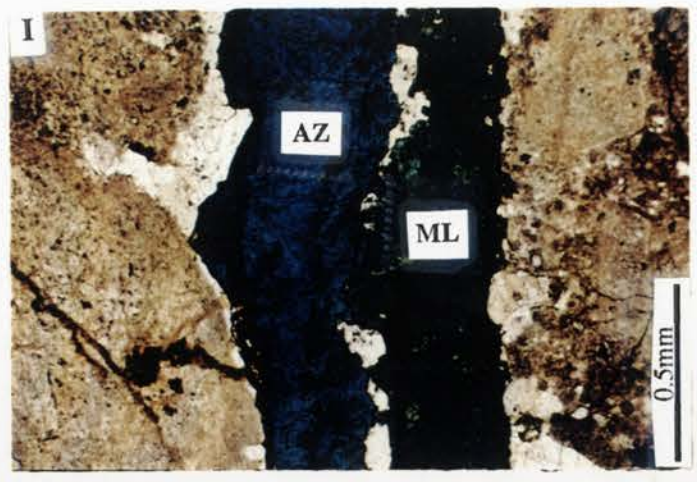

Fig.1.7.9: Malachite (ML) nad azurite (AZ) vein within a quartz monzonite rock. Specimen E27 MZ 4. Depth (46m). Photomicrograph in normal light.

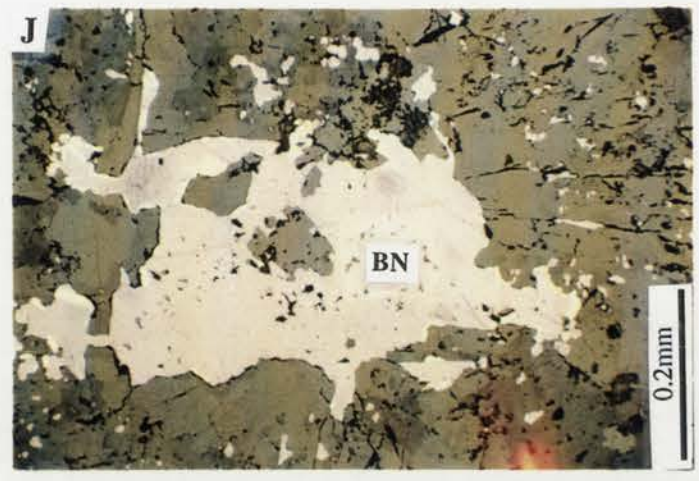

Fig. 1.7.10: Bornite (BN) aggregates within a relatively fresh trachyandesite. Specimen E27 TR4. Depth (46m). Phtomicrograph in normal light.

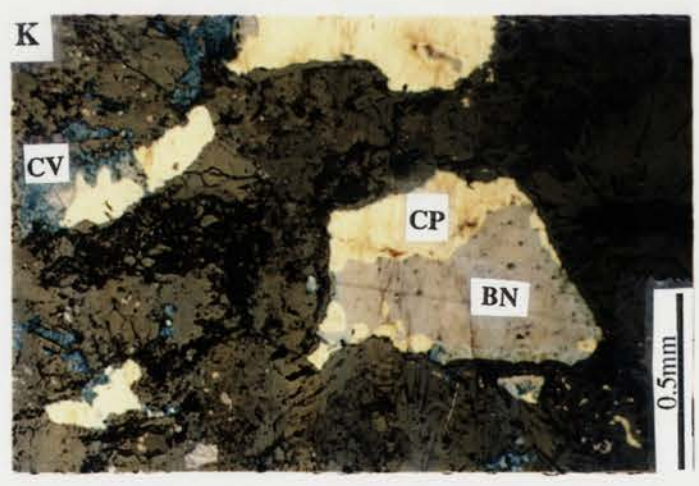

Fig.1.7.11: Covellite (CV) repalcing chalcopyrite (CP) which in turn is replacing bornite (BN) in the alteration zone. Specimen TR 1. Depth (46m). Photomicrograph in normal light.

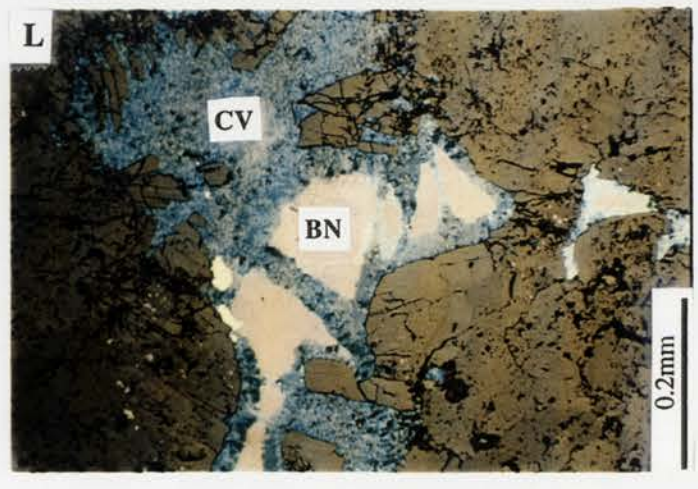

Fig.1.7.12: Chalcopyrite (CP) and covellite (CV) pseudomorphs after bornite (BN). Specimen E27 TR 1. Depth (46m). Phtomicrograph in normal light.

within the stock. Gold accompanies the copper mineralization with average grade for the deposit being 0.65 g per metric ton. Minor pyrite, galena and sphalerite occur in areas of chloritization associated with minor faulting and shearing. Secondary copper minerals comprise malachite (Figures 1.7.4 and 1.7.9) and covellite (Figure 1.7.11 and 1.7.12). Secondary manganese oxide infilling of fractures is also common.

1.4.3 ENDEAVOUR 26N DEPOSIT

The deposit is 4 km south of E22 and E27 deposits. It has been worked as an underground deposit and the study of regolith was limited to the decline access to the deposit. Samples over the decline were collected for comparison with those from E22 and E27 deposits.

The E26N is a stockwork quartz-bornite pipe centered on small, multiphase, subvolcanic quartz monzonite porphyry intrusions. It is hosted by trachyandesitic rocks and pyroclastics similar to those described for E27. At the base of the sequence are porphyritic trachyte lavas with interbedded ash and lapilli tuffs. They are commonly flow-banded and consist of euhedral plagiocalse phenocrysts and minor pyroxene. The upper part of the sequence is dominated by volcanic breccia (Krynen, 1984).

Mineralization is predominantly bornite with minor chalcopyrite, chalcocite and digenite. Gold is associated with bornite with important gold bearing phases being free gold, cuprian gold and telluride (Heithersay et al., 1990). The most important supergene effect here is the occurrence of a gypsum line at 200m. The gypsum has been removed by leaching leaving holes and open fractures above a deep horizontal line. Jones (1985) suggested that the line points to the presence of a chemical interface between groundwater systems. A possible explanation, he said, lies in fresh groundwater sourced from a caldera margin interacting with the hot sulfate rich hydrothermal brines.

1.5 STRUCTURAL GEOLOGY

Volcanic rocks surrounding the intrusives are generally strongly fractured and veined by quartz, potassium feldspar and calcite. Gypsum veining, which is common at the E26 deposit (Heithersay, 1986), is very rare at E22 and E27.

Several post-mineralization faults occur at each deposit. Many faults are partially healed by quartz-carbonate veins which carry up to 5% combined galena, sphalerite, chalcopyrite and pyrite, and are accompanied by zones of strong sericite alteration. At E22 a major

070° trending subvertical fault or fault system bisects the deposit. An apparent 20 m vertical movement, south block down, is indicated by the displacement of the volcanic marker horizon. Displacements on other faults appear to be small (Heithersay et al. 1990).

The faulting at E27 is less well understood. Information to date suggests that there are two subvertical faults similar in trend to the major fault at E22, one at the southern end of the deposit and another at the northern end. Displacements along these and other minor faults are interpreted to be relatively small.

1.6 Dating

K-Ar dating (AMDEL geological reports, 1978) of biotite from a fresh intrusive mafic rock, and of a total rock sample of trachyandesitic volcanics from the Goonumbla porphyry copper district, reyurned dates of 427± 6 Myr and 423 ± 6 Myr respectively. By using more recent decay constants the dates become 435 and 431 Myr respectively. Recent ^{40}Ar -^{39}Ar dating (C. Perkins, unpublished data, cited in Heithersay et al. 1990) on sericite separates from the E26 potassic alteration zone returned an age of 441 ± 2 Myr.

Given the above information, the preferred age for the Goonumbla porphyry copper-gold mineralization is Late Ordovician, using the time scale of Cooper and Grindley (1982).

CHAPTER 2

LANDSCAPE EVOLUTION, CONCEPTS OF ANDESITE WEATHERING AND GEOCHEMICAL DISPERSION IN THE REGOLITH

2.1 MORPHOTECTONICS

This section briefly discusses the physiographic and tectonic evolution of the South Eastern Highlands and the models that propose mechanisms to explain the regional uplift of the South Eastern Highlands. The effect of the formation of Canobolas Divide on drainage evolution in the study area is also examined.

The South Eastern Highlands of Australia form a broad, low, asymmetrical arch that rises in some places to 2000 m above the sea level. The crest of the highlands is not uniform in height and consists of three distinct high regions: the Northern, Central and Southern Tablelands. Low saddles near Cassilis, at the head of the Hunter River and the city of Goulburn, NSW (Bishop et al. 1985), separate these regions.

The South Eastern Highlands are located within the Tasman Fold Belt. The tectonic evolution of the Tasman Orogenic Belt can be summarized into four events. The first event, from the late Proterozoic to early Paleozoic was a period of variable tectonic settings with deep marine turbidite sedimentation and submarine volcanism, with local deformation, metamorphism and plutonism (Cooney et al. 1990). The second epoch from the mid Palaeozoic, was a period of deformation, volcanism and plutonism that consolidated the belt of lower Palaeozoic interior terrains into Australia (Cooney et al. 1990). The third period was the accretion of the New England belt of terrains from the late Palaeozoic to the Mesozoic (Cooney et al. 1990). The final phase was extensional, resulting from the break up of Gondwanaland in the Late Mesozoic. It continues to the present (Cooney et al. 1990).

2.1.1 THE EVOLUTION OF THE SOUTH EASTERN HIGHLANDS

A number of models have been proposed to explain the evolution of the South Eastern Highlands. These include a passive Mesozoic and Cainozoic erosion of the older highlands (Lambeck et al. 1986), dynamic Late Mesozoic and or Cainozoic uplift (Wellman, 1979B; 1987) and passive Cainozoic subsidence of Mesozoic highlands punctuated by dynamic intermittent uplift (Jones & Veevers, 1982; 1983). While much

controversy surrounds these models, all agree on long-term landscape stability. However, apatite fission track data of O'Sullivan (1995) and Kohn & Gleadow (1994) propose kilometre scale denudation, which is at odds with the accepted view held by geomorphologists.

2.1.2 PHYSIOGRAPHIC EVOLUTION OF THE SOUTH EASTERN HIGHLANDS

Prior to the extensional phase in the Late Mesozoic, Australia was attached to parts of Gondwana and Pacifica located to the east. The Palaeo-Tasman Divide was located 300 kilometers to the east of the present day coastline. The rivers formed in the water shed on the western side of the Palaeo-Tasman Divide carried sediment to the Eromanga-Surat basin (Ollier & Pain, 1994).

During the Cretaceous, an east west trending ridge line known as the Victorian Divide extended from the Tasman Divide through the Victorian Highlands and separated the Eromanga-Surat Basin from the Otway, Torquay and Gippsland Basins (Ollier & Pain, 1994). Drainage carried sediments to the north from the Victorian Divide to the Eromanga Basin and south to the Otway and Gippsland Basins.

The Tasman Sea opened by rifting, followed by seafloor spreading, forming the modern day coastline approximately 80 Ma ago. The formation of the Great Divide cut off sediment supply from the Old Tasman catchment, restricting deposition in the Eromanga-Surat and Gippsland Basins (Ollier & Pain, 1994).

At the commencement of the Tertiary, the Murray Basin began to subside. Northward flowing rivers from the Victorian divide no longer reached the Eromanga-Surat Basin and began to flow in a westerly direction following a course similar to the present day Murray River (Ollier & Pain, 1994).

A new divide, the Canobolas Divide, formed between the Murray and Surat Basins during the Tertiary. Traces of the ancient northward trending drainage channels can be found crossing the Canobolas Divide near Parkes (Rosylyn Chan Pers. Comm. 1997). The eastern margin of Australia was downwarped to form the present coastline, leading to reversal of the major rivers.

2.1.3 CANABOLAS DIVIDE

The Great Divide is parallel to the New South Wales coastline and separates the Murray and the Eromanga-Surat Basins from the Tasman Sea. A majority of the Great Divide is located on the eastern margin of a palaeo-plain that slopes gently to the west and is cut off on the eastern side by the Great Escarpment (Ollier, 1982).

Unlike the great divide, the Canobolas divide is not a topographically significant feature. This divide is named after the Canobolas volcanic complex situated near Orange. The Canobolas Divide leaves the Great Divide at a height of approximately 1300 metres, descends to 400 m in the Parkes region, and runs in a westerly direction across geological structures (Ollier & Pain, 1994). Lava flows from the Canobolas volcano, dated by Wellman & McDougal (1974), to the north and south show that the Canobolas Divide was established by the Middle Eocene.

West of the Canobolas Volcano, the divide crosses granite and Silurian and Devonian sedimentary rocks. A large portion of the divide is relatively flat although in some places the divide runs along the tops of strike ridges of Devonian quartzite locally known as ranges. North-South flowing rivers crossed the divide during the late Mesozoic, evident from the large volumes of quartzose sediments deposited in the Coonamble Embayment and fluvial sediments of Cretaceous age preserved at low points in watersheds (Ollier & Pain, 1994).

2.1.4 SUMMARY

The Canobolas Divide has formed in response to the subsidence of the Murray Basin. The effect of the divide on the drainage channels in the South Eastern Highlands has been reviewed by Chan (1996) and in the Parkes region by Adamson (1996). According to Chan (1996), the development of the Canobolas Divide has caused previously northward flowing channels to divert towards the south. Regional aerial photo interpretation has showed that the formation of the divide has disrupted drainage systems north of the divide less than those located south of the divide. According to Chan (1996), this is evidenced by the fact that the channels developed along the southern parts of the divide run parallel to the divide drainage in a westerly direction.

Close to the study area, the channels in the northern watersheds appear to be structurally controlled by the Hervey Range and flow west prior to establishing a dominantly

northwards direction, whereas on the western side the channel morphology is dendritic with well established northwards flowing channels (Adamson, 1996). The depth of regolith formation in the region would appear to be beyond the fluvial energy of the present headwaters of the Bogan River to transport such large volumes of material. This suggests a river capable of greater bed load once flowed in the area (Adamson, 1996).

2.2 INTRODUCTION TO WEATHERING PROCESSES

Definitions

2.2.1 Regolith

The term *regolith* was first coined by Merill in 1897 and is derived from the Greek *rhegos* meaning blanket and *lithos meaning* stone (Joyce, 1996). Chan et al. (1986) defines regolith as a general term for the layer of mantle of fragmented and unconsolidated rock material, whether residual or transported, that nearly everywhere forms the surface of the land and overlies or covers the bedrock. Taylor (1996 pers.comm.) has offered a simplified definition thus: "regolith is everything from fresh rock to fresh air".

The regolith comprises the entire altered, unconsolidated or secondarily recemented cover that overlies more coherent bedrock and that has been formed by the weathering, erosion, transport and/or deposition of older material. The regolith thus includes fractured and weathered basement rocks, saprolite, soils, organic accumulations, glacial deposits, colluvium, alluvium, evaporitic sediments, loess and other aeolian deposits (Butt & Zeegers, 1992). The regolith in deeply weathered terrains is particularly complex and may exhibit great variations in mineralogical and chemical composition, fabric and origin even within a single profile or toposequence.

2.2.2 REGOLITH EVOLUTION PROCESSES

Regolith evolution is the result of interactions between primary minerals and chemical agents particularly H_2O, O_2 and CO_2 that circulate below the earths surface. The weathering zone is hence the transitional boundary between the lithosphere and atmosphere in which the physical, mineralogical and chemical properties of fresh bedrock are progressively modified, ultimately forming soil at the surface (Trescasses, 1992). In the presence of water, the chemical constituents tend to seek a new equilibrium in the

form of secondary minerals. Primary minerals only react with a chemical agent when they are in contact; however this occurs at specific sites that are closely controlled by access to solutions. For this reason, weathering usually starts at contacts between adjoining primary minerals, or along their microfractures (Trescasses, 1992). The primary minerals are progressively altered into secondary minerals, which are important constituents of the regolith and may also be of direct economic interest themselves.
There are three mechanisms in which primary rock forming minerals weather to become stable secondary minerals i.e. dissolution, oxidation and hydrolysis (Trescasses, 1992).

2.2.3 Dissolution

Dissolution affects only a restricted number of minerals, essentially those minerals with a high solubility product. Such minerals include salts (e.g. halite), sulfates (e.g. gypsum) and carbonates (e.g. calcite and dolomite). The solubility of calcite, for example, increases with the partial pressure of CO_2, which is $10^{-3.5}$ bar in the atmosphere, but can be 10-100 times higher in soils, as the result of organic matter and root respiration (Trescasses, 1986). Even quartz can be dissolved, by a hydration mechanism thus:

$$SiO_2 + 2H_2O \text{ <<>> } H_4SiO_4 \text{ (aq)}$$

The solubility of the molecule H_4SiO_4 is approximately 20 times that of quartz at 25°C and pH<9 (6 mg/l SiO_2 for quartz in these conditions).

2.2.4 Oxidation

Some elements such as iron, manganese and sulfur can be present in several oxidation states in rock-forming minerals. In the primary environment, the fugacity of oxygen ($f O_2$) is generally very low so that these elements are generally present in a reduced state. In the weathering zone, however, atmospheric oxygen is introduced by percolating solutions and oxidation may occur (Trescasses, 1992). Pyrite, which is a common accessory mineral in many rocks, is also weathered under oxidizing conditions:

$$4FeS_2 + 8H_2O + 15O_2 \text{ <<>> } 2Fe_2O_3 + 16H^+ + 8SO_4^{2-}$$

This reaction contributes to strong acidification of the environment surrounding the weathered pyrite grains. Oxidation is usually accompanied by hydrolysis, i.e. reaction with water.

2.2.5 Hydrolysis

Hydrolysis causes dissociation of water molecules, consumption of H^+ ions and production of OH^- ions, causing the pH to rise and the solution to become more alkaline. The hydrolysis of silicates produces hydroxyl anions, cations, dissolved silica and secondary minerals (Trescasses, 1992).

$$Mg_2SiO_4 + 4H_2O <\!\!> 2Mg^{2+} + 4OH^- + H_4SiO_4\,(aq)$$

During the weathering of sulfide deposits, a major control on the nature and mineral assemblage of the resulting gossan is the separation of the cathodic oxygen-consuming and alkali-producing reactions from the anodic, dissolution and oxidizing reactions (Thornber & Taylor, 1992). For example, in massive Ni sulfide ores, the anodic supergene weathering can be 100 m or more beneath the cathodic oxygen reduction at the water table.

On the other hand, in disseminated sulfide ores, sulfide minerals are sufficiently dispersed so as to be insulated from each other. Access of oxygen-containing solutions will determine where leaching will occur and the chemical composition of the grains will influence the reaction rate, pH conditions and the secondary minerals that form (Thornber & Taylor, 1992). Anodic leaching can take place within the cracks, fissures and open grain boundaries where the solutions have penetrated without the necessity for dissolved oxygen to be present to complete the reaction. In most metal sulfide ores, pyrite, covellite and chalcocite are less reactive than pentlandite, violarite, chalcopyrite, sphalerite and galena and consequently can remain higher in oxidized profiles (Thornber & Taylor, 1992). Metal cations released into solution-filled cracks within the sulfide assemblage can form precipitates by metal hydrolysis reactions. The precipitates develop a fabric that accentuates the solution channels and replicates the morphologies of the minerals being leached. This results in the development of the box work fabrics sometimes used as diagnostic features in gossan evaluation (Thornber & Taylor, 1992).

The solubilities of Cu, Ni, Zn, Co and Pb are all controlled to some degree by the oxidizing Fe (II) present. The amount of Fe relative to base metal is important in determining the composition of the precipitate, while the oxidizing Fe-oxide also controls the pH of the environment where the precipitate is forming (Thornber, 1979). Oxidation and dissolution of primary sulfides occurs *in situ*, consuming oxygen and producing both sulfate and acid. At the same time, pseudomorphic replacement of sulfides by Fe-oxide

at the initial stages also occurs and could create a localized low pH value of about 3. When ground water passes through and away from a sulfide orebody, the pH increases while sulfate content decreases. Subsequently, base metals will be fixed on existing goethite surface or coprecipitate with oxidizing Fe (Thornber, 1979; Thornber & Wildman, 1979).

As weathering proceeds under conditions of a progressively falling water table, the environment close to sulfide mineralization becomes increasingly leached and acid. Recently-formed gossan that is found just above actively leaching sulfides commonly differs from the gossan that is exposed at the surface, because considerable reworking of the gossan minerals takes place above the water table. Repeated wetting and drying as well as periodic flushing by water and the penetration of silica-rich solutions changes the water chemistry. Hence, the resulting gossan has a complete loss of mobile elements bound in the original precipitates as well as previously stable primary and secondary minerals, but an increase in Fe hydroxides and quartz (Thornber & Taylor, 1992).

2.3 REGOLITH MINERALOGY

2.3.1 Chemical weathering of andesites

Experimental studies on a large number of rock types and minerals under varying conditions, have greatly increased understanding of the reactions and mechanisms of weathering (e.g. Pedro, 1964; Wollast, 1967; Dolmas, 1979; Berner & Holdren, 1979 and Berner et al. 1980). Much of the literature dealing with clay mineral genesis from basic volcanic rocks has concentrated on basalt weathering (e.g. Eswaran, 1979; Eswaran & Coninck, 1971; Siefferman & Millot, 1969; Singer, 1970; Velde, 1985). Critical to this study is examination of literature dealing with the Goonumbla host rocks i.e. trachyandesites. A limited number of workers have described the weathering products of andesites and they include Hendricks and Whittig (1968), Augustithus & Vnegopoulous (1981), Colman (1982) and Glassman (1982). The only study of the regolith development around the study area has been done by Aspandiar (1990) who described the regolith features of a number of outcrops in the area.

The resistance of rocks to chemical weathering depends on the susceptibility of the component minerals (Goldich, 1938). Andesite mineralogy is composed of plagioclase, augite, pyroxenes, volcanic glass, biotite, hornblende and accessories such as apatite, magnetite and sphene. Andesite alteration progresses from the rock's surface inward along transmineral porosity (Glassman, 1982). Transmineral pores traverse the rock

without following grain boundaries and may develop upon cooling of the parent lavas or reflect tectonic shattering (Stoops et al. 1979). Several processes are associated with the initial phase of alteration. The interstitial glass becomes discoloured and shows the development of weakly anisotropic granular forms associated with pale, yellowish brown staining and reduced birefringence of feldspar microlites (Colman, 1982). Such groundmass alteration is most pronounced bordering transmineral pores and decreases rapidly away from the pore.

Initial phenocryst alteration consists of congruent dissolution of augite and surface etching of plagioclase (Glassman, 1982). Pyroxene weathering begins at grain boundaries and cleavages with the entire mineral replaced uniformly (Colman, 1982). Products of pyroxene weathering in volcanics are either smectites (Glassman, 1982) or iron oxides (Hendricks & Whittig, 1968). Olivine generally alters to goethite via an iddingsite phase (Eggleton et al. 1987). The general susceptibility of minerals to weathering in Goonumbla volcanics according to Aspandiar (1990) is established as:

Glass < Olivine < Pyroxene < Plagioclase < Opaques.

2.4 Weathering of major silicates in andesites

2.4.1. Feldspars

Feldspars are framework silicates in which the tetrahedra are linked through all four oxygen atoms in a three-dimensional configuration. Al substitution for Si within the tetrahedra creates a negative charge on the framework, which is balanced by addition of a Na^+, K^+ or Ca^{2+} ions. Dissolution of feldspars proceeds via loss of these mono- or divalent cations, but the tetrahedral framework must rupture in order to release the cations. Alkali feldspars and sodic plagioclase have an Al to Si ratio of 1:3, and calcic plagioclase 1:1. Despite the similarities in structure of the feldspars, there is a considerable difference in their weathering stability (Goldich, 1938), and alkali feldspars are considerably more resistant to weathering than plagioclase feldspars. However, once the metallic ions are lost, the framework structure breaks down (Loughnan, 1969, Anand et al. 1985).

Feldspar alteration begins with surface etching that eventually leads to the formation of intramineral porosity as the crystals are penetrated by a network of cracks (Glassman, 1982). Propagation of the pores probably occurs along crystal dislocations or compositional zonations (Berner & Holdren, 1977; Wilson, 1975). Once the

intramineral porosity penetrates the andesine-rich surface zone, complex alteration of labradorite core zones occurs rapidly, resulting from the alteration of discrete zones of host material (Stoops et al. 1979).

The non-stoichiometric dissolution of feldspars has been attributed to the presence of a depleted surface layer (Sjoberg 1989, Shotyk & Nesbitt, 1990, Hellman et al. 1989). Eswaran & Bin (1978) and Eggleton (1986) noted the transformation of feldspars to smectite via an amorphous aluminosilicate material called a 'protocrystalline' stage by Banfield & Eggleton (1990), and also observed feldspar alteration directly to kaolinite. This 'protocrystalline' surface layer was depleted in Ca, Na, K and Si and significantly enriched in Fe. On plagioclase the protocrystalline material may be replaced by Ca-Fe-K smectite, another unidentified protocrystalline material and spherical halloysite. Feldspars can also alter to halloysite and kaolinite (Hughes & Brown, 1977; Wilke et al. 1978), gibbsite (Parham, 1969; Lodding, 1972) and muscovite mica or illite (Exley, 1976; Eggleton & Buseck, 1980).

Several authors have suggested that the chemical weathering of feldspars takes place by diffusion of ions through a residual coating of hydrous aluminium silicate (Correns & Von Engelhardt, 1938; Correns, 1961; Wollast, 1967; Parham, 1969; Hengelson, 1971; Busenberg & Clemency, 1976). However, weathering of feldspars can occur without the development of a cation depleted surface layer (Holdren & Berner, 1979). Scanning electron microscopy (SEM) images show that weathered feldspars from soils and those from laboratory simulations have similar morphologies. Holdren & Speyer (1986), showed experimentally that the release rates of Al and Si were markedly different at different pH values, and the reaction rates were not proportional to the exposed surface area.

Electron microscope studies (Tchoubar 1965, Wilson, 1975, Berner & Holdren 1977) confirm that dissolution during the weathering of silicates occurs mainly at the sites of excess energy on the crystal surface such as dislocations, microfractures and other crystal defects, and not by uniform attack over the entire mineral surface. Distinctive etch pits develop on the feldspar surface, and with continued weathering may produce a very porous honeycomb microstructure with irregularly scattered clay mineral flakes (Dearman & Baynes, 1979; Moore, 1989).

Feldspars can also weather differently in differing environments. In alkaline environment for example, plagioclase alters to montmorillonite with small amounts of amorphous aluminosilicates present (Eswaran,1979). In acid environments, plagioclase feldspar

weathers to metahalloysite and some amorphous aluminosilicates. In a freely draining environment, the weathering of plagioclase leads to kaolinite formation, and locally to gibbsite. DeJou et al. (1982) observed that, at the top of a weathering anorthosite profile, where the drainage was good, the clay separate was dominated by kaolinite. Near the base of the profile where the drainage was poor, feldspars altered to smectite and vermiculite in addition to kaolinite. The rate of silicate weathering may also be affected by the presence of organic substances (Schenk et al. 1989).

Parham (1969) experimentally leached microcline (alkali-feldspar) and plagioclase in conditions simulating a hot, high rainfall climate and a site with good drainage. Electron microscope examination of the weathered surfaces identified bumps of amorphous material at various sites on cleavage surfaces and at grain edges. These grew into tapered projections and flame shaped sheets, which rolled to form tubes of halloysite on the microcline. Sheets formed on the plagioclase feldspars developed into a platy material, probably boehmite. Hence, the observed weathering sequence for the feldspars tested was feldspar to allophane to halloysite and boehmite.

Wilson (1975) observed that in a confined environment, mica may form during the weathering of feldspar, but in more open systems the K^+ ions are removed and halloysite, vermiculite or montmorillonite form. In intensely weathered profiles, feldspars may be converted to gibbsite either directly or through an intermediate halloysite stage. Kitigawa & Katitani (1977) studied the alteration of plagioclase in granite and proposed a sequence of feldspar weathering from plagioclase through allophane, halloysite and metahalloysite to kaolinite. However, they found it is possible for plagioclase to alter directly to halloysite or kaolinite.

Aspandiar (1990) noted the following alteration paths for plagioclase weathering in the Goonumbla trachyandesites:

PLAGIOCLASE >> Smectite >> Fe-Kaolinite >> Al-Iron oxides

Chemistry

Plagioclase is the most abundant mineral in many basic lavas in both the phenocryst and groundmass assemblages. Plagioclase feldspars form a solid solution series from Na-rich to Ca-rich anorthite. All plagioclase feldspars contain some K, and may also contain Ti, Fe^{3+}, Fe^{2+}, Mn, Mg, Ba and Sr. Fe^{2+} substitutes for Ca^{2+} while Fe^{3+} substitutes for

Al^{3+}. Sodic plagioclase feldspars are more resistant to weathering. Minor or trace elements in feldspars are Sr, Rb, Cs, Cu, Pb, REE and possibly Fe^{2+}, Mg and hydronium (H_3O^+) (Huang, 1989).

2.4.2. Pyroxene

The weathering of pyroxenes produces etching, disaggregation and eventual depletion of these minerals in weathering profiles. Pyroxenes are chain silicates and have a structure of tetrahedra arranged in chains bonded together by metallic ions. The most common metallic ions incorporated are those which enter into octahedral coordination with oxygen, such as Mg^{2+}, Fe^{2+}, Fe^{3+} and Al^{3+}. Some Al may replace Si in tetrahedra. Access of water by way of the cleavages promotes solution of the weakly bonded cations.

Craig and Loughnan (1964) during a study of the weathering of basic volcanic rocks in New South Wales, found that pyroxenes weathered directly to saponite. Loughnan (1969) suggested that chains of silica tetrahedra are released from the weathering of pyroxenes and polymerise into sheets incorporating free Al and Mg, thereby forming chlorite or smectite or both. Free ferrous ion is stabilized by oxidation to the ferric state, while Ti combines with oxygen to crystallize anatase. A general weathering sequence proposed by Loughnan (1969) for pyroxene weathering is:

		Chlorite		
	Partial loss of	Montmorillonite		Complete loss of
PYROXENE >>	Mg^{2+}, Ca^{2+}, Fe^{2+}	>> Calcite	>>	Ca^{2+} and Mg^{2+}
	Oxidation of Fe^{2+}	Ferric oxides		Partial loss of SiO_2
		Anatase		

If excess Ca results from the breakdown of the pyroxene, calcite may form. With increase in weathering intensity, Ca, Mg and Si are lost and remaining soil-forming material becomes enriched in kaolinite, anatase and oxides, and hydroxides of ferric iron. This corresponds with earlier findings by Craig & Loughnan (1964) that montmorillonites are rendered unstable by the more intense weathering conditions (better drainage) near surface, leading to the formation of halloysite, kaolinite and poorly crystallized montmorillonite. In addition, iron as goethite, hematite, or an amorphous precursor of these minerals is concentrated in the oxidized parts of the weathering zone. Subsequent intense weathering may cause the desilicification of clay minerals and the formation of bauxite minerals.

However, in north east Scotland, Barsham (1974) recorded the gradual alteration of pyroxene to vermiculite pseudomorphs, the c-axis of the vermiculite being normal to that of the pyroxene, indicating topoaxial growth of the secondary vermiculite. Velde (1985), discusses the presence of vermiculite as a secondary mineral and observes that it forms as a result of continued weathering and oxidation. The formation of vermiculite reflects the loss of Ca and Mg from earlier formed trioctahedral phases, incorporation of Al into the clay, and oxidation of iron within clay from Fe^{2+} to Fe^{3+}.

Nahon & Colin (1982) described a three-stage dissolution of orthopyroxene due to weathering. The first stage is the appearance of amorphous products with a similar chemical composition to the parent material. The second stage is the formation of smectites and ferruginous talc-like minerals and the third stage features the appearance of iron oxyhydroxides in which well-crystallized goethite is observed. Eggleton & Boland (1982) acknowledged the formation of a talc-like mineral as an intermediate stage in the weathering of enstatite (Mg, Fe orthopyroxene) to smectite.

Augite dissolution and subsequent smectite precipitation in the resulting voids leads to the formation of pseudomorphs. The pseudomorphs after augite may have similar compositions to plagioclase pseudomorphs (Eswaran, 1979; Glassman, 1982; Glassman & Simonson, 1985).

Aspandiar (1990) noted the following alteration paths for pyroxene in the Goonumbla trachyandesites:

PYROXENE	>>	TALC	>>	SMECTITE	>>	IRON OXIDES
		Solid-solid transformation - Mg		Crystallization from amorphous phase - Mg - Ca -		Crystallization from amorphous phase - Si - Ca-

Chemistry

The clinopyroxenes augite and titanaugite are the typical pyroxenes of basic volcanic rocks but the orthopyroxene enstatite may be present in olivine tholeites. Al, Fe^{3+} and Na are present to a limited extent in most augites. Si and Al fill the tetrahedral sites, but Fe^{3+} is may also be taken in. Cr is an important minor constituent in Mg-rich augites and the highest Mn concentrations are in Fe-rich augites. K is not present and Na has very low concentrations (Deer et al. 1992).

2.4.3 Olivine

Olivine is an orthosilicate composed of silica tetrahedra bonded together by ferrous and magnesium ions in octahedral coordination. The divalent cations may be mobilized from the outer surface of the mineral and along its inner fractures during weathering as they are largely unprotected by silica tetrahedra at these sites (Delvigne et al. 1979). Individual silica tetrahedral units are released exposing the fresh surface of the olivine to attack.

A number of different intermediate products are encountered. Brown & Stephen (1959) described rims of iddingsite on olivines from poorly drained profiles. "Iddingsite" is described as an oriented intergrowth of iron oxide and trioctahedral layer silicates (Eggleton et al. 1987, Smith et al. 1987). Subsequently, Banfield et al. (1990) described hematite-rich smectite rims on weathering olivines, and suggested that a metastable hexagonal phase in iddingsite rims described by Eggleton (1984) but not identified, may be proto-hematite. Hence iddingsite is a reddish brown substance which consists of a combination of smectite, (chlorite), goethite and/or hematite. It is formed as a result of diffusion of H^+ ions into the olivine structure where they temporarily attach to O^- ions releasing Mg^{2+} and Fe^{2+} and Si^{4+} ions from their sites, permitting replacement by Fe^{3+}, Al^{3+} and Ca^{2+} (Siefer & Woodford, 1979; Eggleton, 1984; Deer et al. 1992).

The presence of an X-ray amorphous intermediate product in the weathering of olivine to smectite clays was acknowledged by Grandstaff (1986) who suggested that, in oxic conditions, olivines weather rapidly and congruently to X-ray amorphous material. This material then slowly recrystallizes to layer silicates (Eggleton, 1986). Hisingerite, a partially X-ray amorphous product of the weathering of olivine, was thought to be an intermediate phase between nontronite and saponite (Kohyama & Sudo, 1975). Clark et al. (1978) did not support a layer-structure for Hisingerite, and considered it part of the solid solution series between neotocite and hisingerite, and concluded that it was gel-like or very poorly crystalline. Brigatti (1982) described a more crystalline phase, and found it was similar to trioctahedral Fe saponite clay rather than dioctahedral nontronite clay. This was refuted by Eggleton et al. (1983) who confirmed an amorphous or gel structure for minerals of the neotocite-hisingerite series.

Sherman et al. (1962) found nontronite (dioctahedral Fe-smectite) the initial product of the weathering of olivine at Lualualei, Hawaii. Craig (1963) has shown that olivine may alter directly to Mg-rich montmorillonite. Loughnan (1969) suggests that the released silica tetrahedra can polymerise into sheets, fix some of the magnesia and yield serpentine as the first alteration product. Most of the ferrous iron if released above the water table, is

oxidized, and crystallizes as either hematite or goethite. Wilson (1975) also found that ferromagnesian minerals weather relatively easily and alter mainly to Mg-rich mixed layer trioctahedral expandable minerals as well as chlorites.

Delvigne et al. (1979) suggested that the intermediate weathering product of olivine is a mixture of iron oxide and hydrated magnesium silicate which produces smectites if silica and magnesium are partly retained in the profile, or forms a mixture of iron oxide or hydroxide with opal if magnesium is removed. Nontronite and Fe^{3+}- bearing beidellites are frequently found as alteration products of olivine, especially in areas of poor drainage. In areas of better drainage, when magnesium and silica are totally released, nontronite is lost and a mixture of goethite and hematite may develop (Trescasses, 1975). Similarly Smith et al. (1987) observed that with increased weathering, smectite is lost from the olivine rim leaving a porous aggregate of goethite. In this situation, it is very difficult to distinguish optically between original iddingsite and the residual goethite, because the micromorphological features of both phases are the same (Delvigne et al. 1979).

Chemistry

Ni and Cr are commonly present in Mg rich olivines. The chromium usually occurs in minute exsolved plates of chromite, while the nickel is enclosed within the silicate. Fe^{3+} is usually present and may be related to small exsolved grains of magnetite but more frequently to an oxidation rim formed during the dissolution of olivine. Relatively small amounts of Ca are present in olivine and P^{5+} is present in trace amounts replacing Si^{4+}. In order to maintain charge balance there is an empty site elsewhere in the structure when P^{5+} substitutes. There is some replacement of Mg and Fe in olivine by Mn and Ca but this is more common for Fe-rich olivines (Deer et al. 1992).

2.4.4 Micas

The micas yield diverse weathering products depending on various environmental factors as well as the composition and structure of the parent material (Wilson, 1975). The influence of structure is well illustrated by the greater susceptibility to weathering of trioctahedral micas compared with their dioctahedral counterparts. In particular, the former are much more readily converted to vermiculite- a process that is apparently connected with the orientation of the hydroxyl dipole in the octahedral sheet (Basset, 1960). This is normal to the silicate structure sheet in trioctahedral micas, so that the protonic charge is adjacent to the potassium ion, which is in a stable environment.

Many studies in the field and laboratory by workers such as Walker (1949), Norrish (1972) and Newman (1972) have shown that the mica-vermiculite transformation is a complex process. Walker (1949), suggested that loss of potassium was accompanied by oxidation, substitution of hydroxyl for oxygen and loss of octahedral iron and magnesium. Norrish (1972), showed by chemical analysis of natural vermiculites that charge reduction can be accounted for by oxidation of octahedral ion. Newman & Brown (1966) showed that other mechanisms are operative especially where low iron micas like muscovite and phlogopite are involved. Churchman (1980), showed from X-ray and chemical evidence that muscovite weathered by loss of K from alternate interlayers, leading first to mica/dioctahedral vermiculite, then to mica/beidellite interstratifications before altering entirely to beidellite.

The weathering of biotite on the other hand can bring about the stronger retention of interlayer potassium by oxidation (Barshad & Kishk, 1968). This occurs with little or no vermiculization (Farmer et al. 1971), even though a substantial proportion of total potassium may have been lost (Seddoh & Pedro, 1974). According to Gilkes & Suddhiprakarn (1979), packets of a hydrobiotite-like phase develop within biotite and the hydrobiotite then alters to kaolinite, goethite, gibbsite and hematite. Eggleton (1976) noted though that biotite appears to weather initially in a manner similar to muscovite, but a process complicated by the oxidation of iron.

Under extreme weathering conditions, both muscovite and biotite can be converted to kaolinite, which tends to occur as distinct intergrowths within exfoliated flakes (De Kimpe & Tardy, 1968). Banfield (1985) also finds somewhat irregular biotite-vermiculite interstratification in the early stages of alteration, a process she associates with a relatively slow weathering rate. Vermiculite, she postulated, forms by loss of interlayer potassium and expansion of this region by 2Å followed by introduction of brucite-like interlayer using Mg released by dissolution elsewhere in biotite. Some 2:1 layers are stripped of their tetrahedral sheets, leaving a single octahedral sheet as an interlayer, in a manner analogous to the alteration of biotite to chlorite (Eggleton & Banfield, 1985).

2.4.5. Ferromagnesium minerals

Amphiboles are generally considered to be more resistant to weathering than olivine or pyroxenes, but they nevertheless appear to yield similar weathering products (Wilson, 1975). Stephen (1952), demonstrated that hornblende weathered to chlorite and subsequently to interstratified vermiculite-chlorite. Wilson & Farmer (1970) showed that fresh hornblende contained discrete lamella intergrowths of an iron-rich amphibole phase,

which broke down preferentially to yield, interstratified chlorite-saponite. No orientation relationship between the clay mineral and the parent hornblende lattice was observed except for a tendency towards parallelism with cleavage planes.

2.4.6. Opaque oxides

Magnetite, titanomagnetite and ilmenite are the more common opaque accessory minerals of basaltic rocks. These minerals oxidize during weathering to yield hematite, maghemite, or goethite and ultimately oxidized to anatase (Loughnan, 1969). However, in a more arid environment, magnetite and ilmenite are very stable and show only slight decomposition, as a result of physical and chemical weathering. Magnetite and ilmenite therefore, persist into the weathering crust (Singer, 1984).

Chemistry

The ideal formula for ilmenite is $FeTiO_3$ but generally some Mg and Mn substitute for Fe resulting in the composition $(Fe,Mg,Mn)TiO_3$. If magnetite and ilmenite co-exist, the Mn is always partitioned into the ilmenite. Ilmenite weathers to rutile, ± pseudorutile, hematite, anatase and secondary Fe-oxyhydroxides. Exsolution lamellae of hematite may form during the dissolution. Ilmenite is a common accessory mineral in many igneous rocks and is often associated with orthopyroxene in tholeiitic basalts. Ilmenite has a hardness of 5-6, is relatively resistant to weathering and is a common detrital mineral (Deer et al. 1992).

In magnetite, small amounts of Al may substitute for Fe^{3+} and Ca, Mn and Mg substitute for Fe^{2+}. A considerable amount of Ti can enter the magnetite structure forming titanomagnetite. Other substitutions are Cr and V for Fe^{3+} and Ni, Co and Zn for Fe^{2+}. Magnetite has a hardness between 7.5 and 8, hence it resists weathering and is a common detrital mineral (Deer et al. 1992).

2.4.7 Glass

Devitrification of glass occurs early in weathering as glass is particularly susceptible to dissolution. Glass reactions consist of an initial rapid surface ion exchange followed by a slower solid state diffusion (White & Claussen, 1980). At low pH (abundant H^+ ions) surface exchange between aqueous hydrogen ions and surface cations produces aqueous compositions which reflect the mole fractions of the species in the glass (congruent dissolution). At neutral pH (fewer H^+ ions) hydrogen ions selectively exchange for

surface ions. Eggleton & Keller (1982) discuss the breakdown of glass to form palagonite, a smectitic mineral that shows compositions variable between amorphous phases (Wada, 1982) and dioctahedral Mg-bearing smectite. Ti and Fe remain relatively stable during the dissolution of glass, but loss of other constituents follows the order Na~ Ca~K> Al > Si > Mg (Eggleton & Keller, 1982).

A summary of the alteration pathways of the common rock-forming minerals is presented in Figure 2.1.

2.5 Chemistry of andesite weathering

Hendricks & Whittig (1968) have described the chemistry of weathering of andesites to saprolite. Using isovolumetric method of analysis, they observed that all the major chemical constituents except ferric iron and lattice water suffered loss during weathering of hypersthene-and olivine-andesite in acid leaching environments.

They observed that during the weathering of hypersthene andesite, Si rapidly decreased in forming the saprolite, but less rapidly as weathering progressed. Ca, Na and K along with Si were also rapidly removed while Mg tended to remain. By the end of the weathering sequence, the alkali and alkali earth metals were also entirely removed. Fe^{2+} decreased and Fe^{3+} increased throughout the course of weathering. The total Fe also decreased in the early weathering stages, and become stable as weathering continued. Of the major constituents, Al remains unchanged. It underwent a moderate decrease initially, but became quite stable with further weathering.

Hendricks & Whittig (1968) noted similar trends for olivine andesite. Decreases occurred in the total Fe, Al and Ti though they were considerably less especially in the hypersthene andesite. They concluded that in acid leaching weathering environments, Si is being removed in the early stages of weathering. Pickering (1962), found that the rate of dissolution and removal of Si during leaching of quartz-free rocks increased as the acidity of acid leaching solutions increased in the pH range of 7 to 3. Nakamura & Sherman (1965), have also demonstrated the rapid release and removal of Si during weathering of Mugearite in Hawaii.

The tendency of Mg to resist weathering is explained by the fact that the pyroxene phenocrysts and to a lesser extent the olivine phenocrysts are fairly resistant to weathering as compared to the matrix minerals. Mg is combined in these ferromagnesium mineral grains until the grains are decomposed. The moderate amount of Al loss could also be

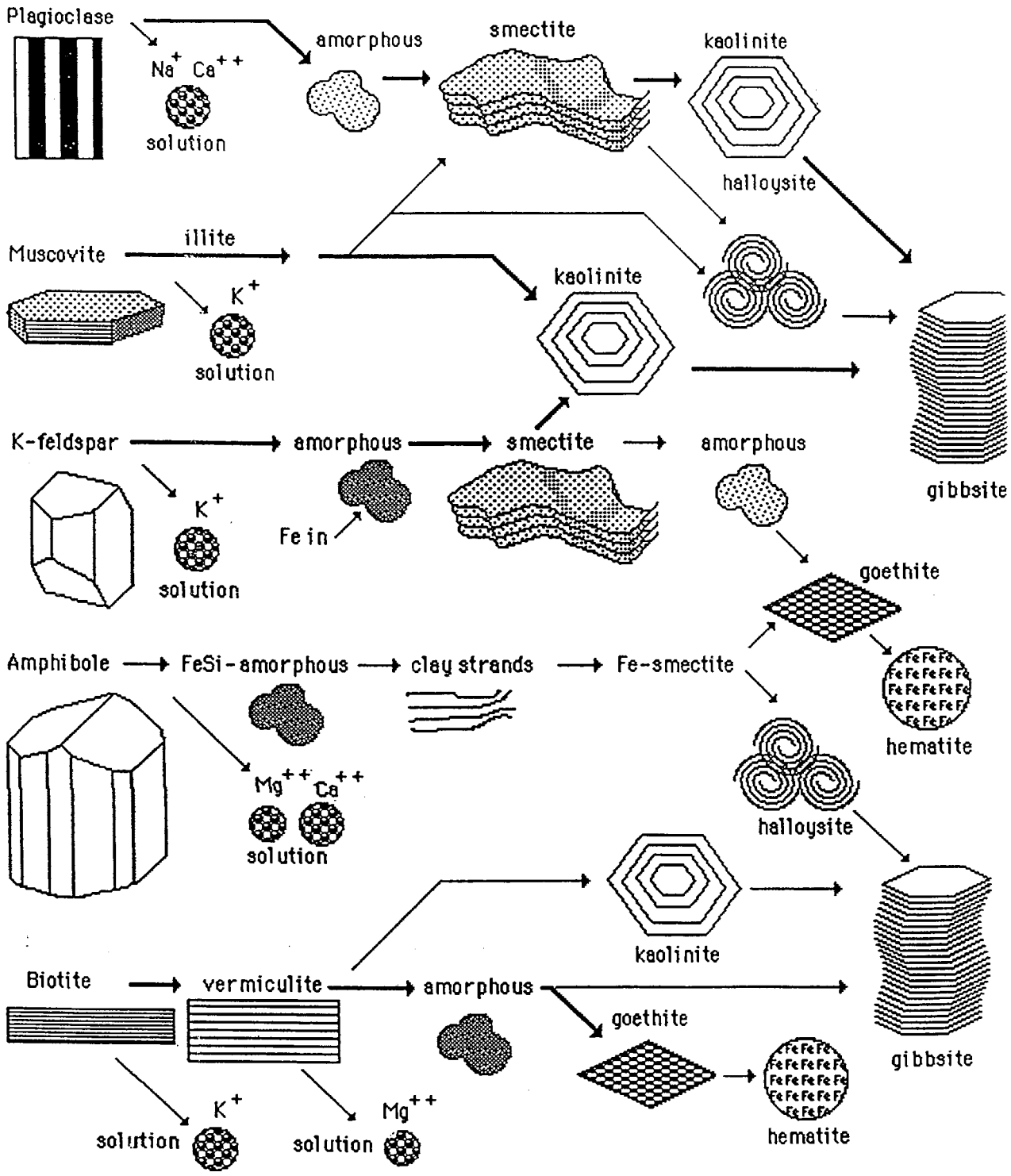

Figure 2.1: Alteration pathways of the common rock forming minerals (Eggleton, 1996)

attributed to acid leaching conditions (pH < 5) or its common behaviour of forming complexes with chelating agents (Pickering, 1962).

Colman (1982), noted the following sequence of mobility based on abundance of each element in weathering rinds compared to the unaltered rock:

$$Ca > Na > Mg > Si > Al > K > Fe > Ti$$

These weathering rinds were studied from different localities in the USA. This conforms with the general sequence:

$$Ca > Na > Mg > K > Si > Fe > Al$$

which has been determined by several workers studying stream waters draining igneous rocks or the weathering of igneous rocks themselves (Goldich, 1938; Tiller, 1958).

As for the trace elements, Augustithus & Vgenopoulous (1981) observed that Na, Ca, Rb, Sr were relatively leached out in comparison to Al for trachyandesites from Ethiopia. They further observed that Ca was relatively leached out in comparison to K, Na, Fe and Rb and Sr in comparison to Rb. In addition, Cu was leached out in comparison to Pb, Zn, Co and Y in comparison to Nb.

2.6 GEOCHEMICAL DISPERSION IN THE REGOLITH

2.6.1 Introduction

Geochemical dispersion is the outward spread of elements from a source with higher than background concentrations of these elements. It is the process that underpins the whole subject of geochemical exploration. Geochemical dispersion can result in dispersion haloes with element concentrations intermediate between those of the source and background. These anomalies represent targets much larger than the source concentration or orebody. Primary dispersion generally refers to geochemical dispersion in unweathered rocks (or in the primary environment) as distinct from secondary dispersion, which occurs near surface, around and above the watertable, as the result of weathering, erosion and hydromorphic processes (secondary environment, Figure 2.2).

However, primary dispersion has taken on a broader meaning and can be considered to include dispersion that occurs around an ore deposit or source at the time of its formation

(syn-depositional dispersion). Clearly many types of ore deposits form in the secondary environment and this allows a distinction between dispersion that accompanied the formation of the deposit and subsequent dispersion (post-depositional) that occurred after the deposit was formed and then exposed to later weathering and erosion.

2.6.2. Chemical mobility and transport of elements in the weathering environment

The study of element mobility and geochemical dispersion in the regolith has attracted a number of workers over the last decade. Published accounts include those of Thornber (1982), Mann (1984), Smith (1982), Butt (1981), Baker (1978), Webster (1986), Fletcher (1985) and Lecomte & Colin (1987).

The aqueous solution, transport and precipitation of elements is of central importance to weathering and geochemical dispersion. The hydrolysis and redox reactions hitherto mentioned are responsible for the destruction of the primary rock forming secondary minerals of the regolith (Trescasses, 1982). Of particular importance to geochemical exploration, however, are those reactions that affect the less abundant elements associated with mineralization (Thornber, 1982). This is because these reactions are ultimately responsible for the nature and surface expression of mineralisation in the regolith, particularly its size, intensity and location. Geochemical anomalies formed as a result of the chemical reactions and transport involving water are referred to as hydromorphic and the process as hydromorphic dispersion (Trescasses, 1982).

Mobility is a geochemical term used to describe the ability or the potential ability of an ion to migrate via the solution phase (Mann, 1984). The extent to which particular elements are mobilized by groundwater during weathering depends upon:

1) Controls of solubility in aqueous solutions having various amounts of other dissolved species (cations, anions and organic materials), and
2) The interaction between these solutions and the complex surfaces of primary and secondary minerals.

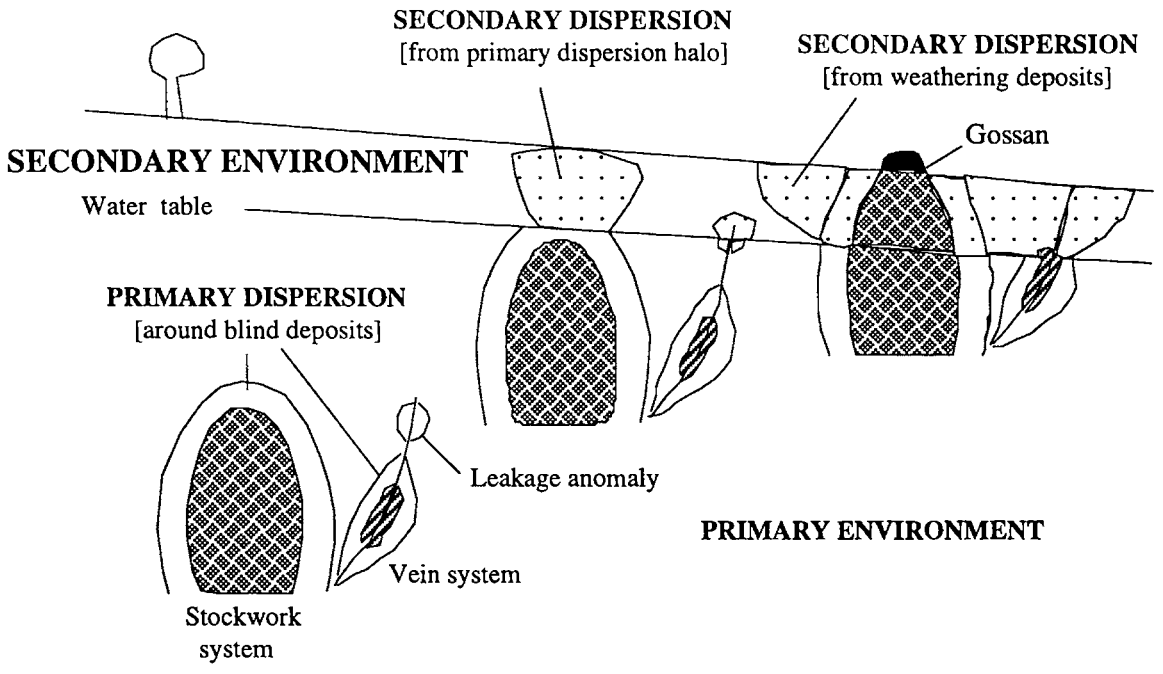

Figure 2.2: Generalized patterns of primary and secondary dispersion patterns around ore deposits

2.6.3 Element mobility and behaviour during weathering

The various elements within the primary and secondary minerals may be held within the mineral crystal lattice or loosely bound within a layer of the changing potential field at the interface. In addition they may be mobile in solution, either solvated by the water molecules or 'complexed' with one or more soluble ions (Thornber, 1982). Mobility is also possible as colloidal particles.

Quantum mechanics dictate that no two elements behave the same. Elements have different numbers of electrons in their atoms (atomic number) and these fill energy fields (orbitals) around the nucleus. The way in which electrons fill the orbitals is referred to as an element electronic configuration and characterizes the element and its chemical behaviour (Lawrence, 1994). An element's electronic configuration will determine whether it is likely to form a positively or negatively charged ion in solution. The charge an element adopts is referred to as the oxidation state. The oxidation state of an element varies with solution chemistry, but is predictable. The state in which elements may occur can be divided into five groups (Table 2.1) thus:

State	Form	Fe	As	Cu	
(1) Anions	Negatively charged free ions	-	As^{3-}	-	Most reduced form
(2) Metals	Uncharged solids	-	-	Cu^0	
(3) Cations	Positively charged free ions	Fe^{2+}	-	Cu^+/Cu^{2+}	
(4) Oxides	Various charged insoluble solids	Fe_2O_3	As_2O_3	-	
(5) Oxyanions	-vely charged soluble oxide ions	-	AsO_3^-	-	Most oxidized form

Table 2.1: Element states (Lawrence, 1992)

The oxidation state of the weathered profile controls the oxidation state of an element. The major factors controlling the mobility of the chemical elements in aqueous solutions and normal temperatures are discussed below.

2.6.4 Solubility

The solubility of an element in aqueous conditions is controlled by its oxidation state (Langmuir, 1979). As elements become more oxidized by losing the electrons, they become smaller in size and more positively charged. The solution chemistry of an element is affected by changes in oxidation state, e.g. Fe^{2+} is far more soluble than the smaller sized, higher oxidized state Fe^{3+}. A comparison of the six coordinated radii of all elements with their particular oxidation states that can occur within the range of Eh and pH expected during weathering is shown in Figure 2.3.

The most important and abundant of the elements grouped as having variable oxidation states is iron. The change in oxidation state from from Fe^{2+} which is soluble as a cation to Fe^{3+}, which is insoluble as the oxide Fe_2O_3, falls directly in the range of Eh and pH expected in the weathering environment (Thornber, 1982).

Low oxidation potentials (Eh) and low pH values (i.e. reducing acid conditions) produce greater iron mobility than higher oxidation potentials and higher pH values, hence iron precipitates when a solution comes into contact with air. Manganese behaves somewhat similarly. Elements such as Mo, V, Cr and W that readily oxidize to +5 and +6 oxidation states show an increased solubility with higher pH due to formation of oxyanions. For U, the change in oxidation state is more complex, with oxycations such as $U_2O_4^{2+}$ forming mobile species (Langmuir, 1978).

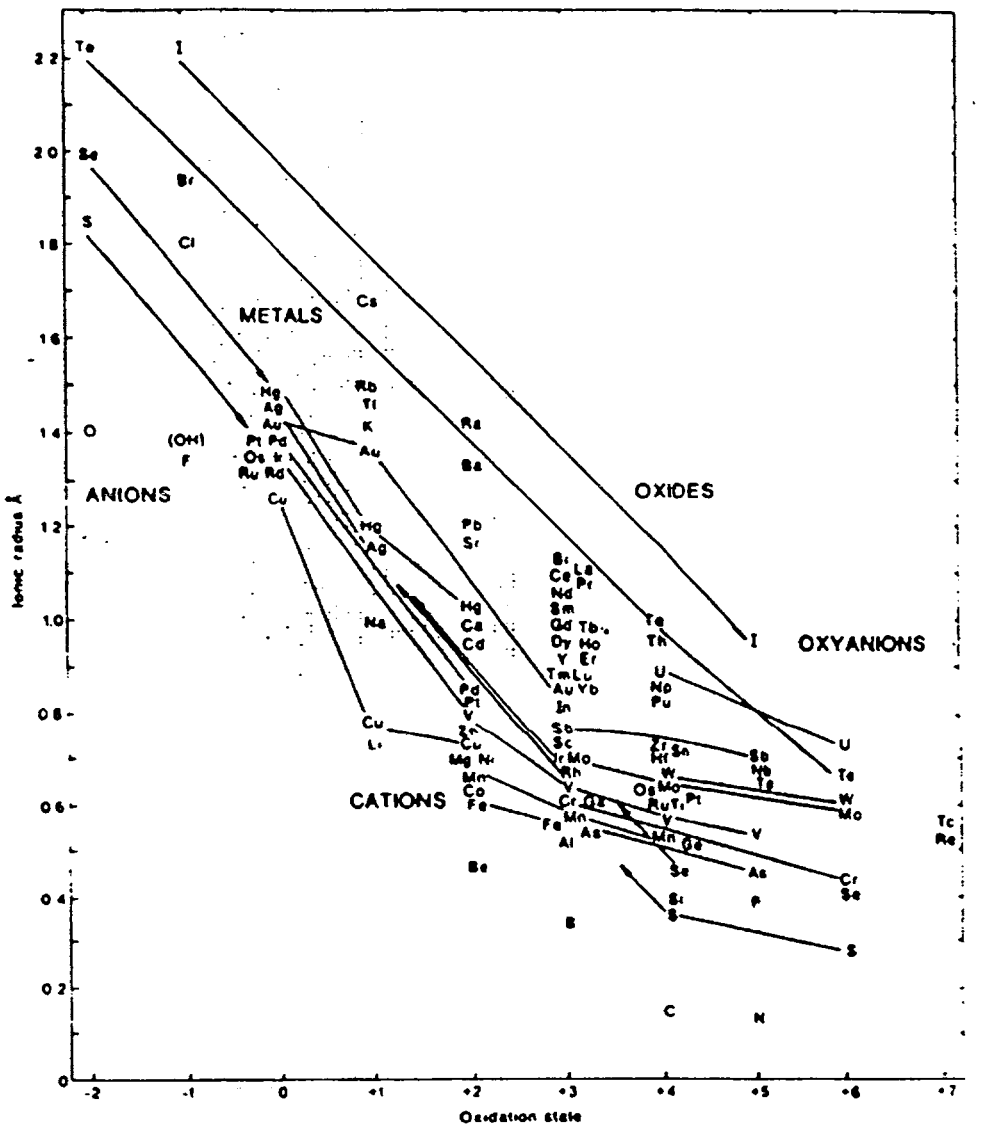

Figure 2.3. A plot of ionic radius, for six coordination, of the chemical elements as a function of the oxidation state possible in natural weathering conditions. Derived from Shannon (1976), and Hume-Rothery & Raynor (1958). Diagram adapted from Thornber (1982).

Cu, Ag and Hg have the oxidation state of either metal or cation. They are assisted in their mobility by highly oxidative environments associated with solutions of high ionic strength in which soluble complexes with anions can form. However, in the presence of sulfides, a lower oxidation potential could help mobility by the incomplete oxidation of the sulfide allowing metastable thiosulphate and other metastable oxysulphur anions to be present and form soluble complexes (Webster & Mann, 1974; Webster, 1984).

2.6.5. Formation of inorganic and organic complexes

The solubility of most cations can be increased by bonding with anions, both organic and inorganic, to give complexes having lower overall charge. Organic complexes become important in waters in which organic materials are decaying. Because the dissociation of these organic ions is affected by pH, complex formation can be pH dependent. Complexation plays an important role in the processes of adsorption, coprecipitation, humic interaction and microorganism activity discussed below.

2.6.6 Adsorption

Adsorption refers to the binding of elements at the solution/mineral surface. Like solubility, it is pH dependent. Many oxide surfaces including goethite, hematite and Al oxides change from being positively charged at low pH to negatively charged at high pH (Thornber, 1982). With increasing OH^- concentration, such surfaces become increasingly negatively charged and thus more cations become adsorbed from solution. On decreasing the pH, the reverse occurs; surfaces become more positively charged, decreasing the adsorption of cations, but increasing the adsorption of anions. The pH at which the change-over occurs i.e. the point at which there is a net zero charge (pzc) can be used to give a measure of whether the surface is likely to be negatively or positively charged at a particular pH. The pzc for various common minerals are given in Table 2.2.

In natural systems, however, the properties of individual minerals are subject to interference by other components e.g. humic substances cause the surfaces of goethite to become more negatively charged (Tipping & Cooke, 1982).

2.6.7. Co-precipitation

Co-precipitation is the term describing the precipitation of elements from solutions in which they would normally be soluble, as the result of the precipitation of some other

abundant elements (Thornber, 1992). It is influenced by the same factors as solubility and adsorption being greatest at high cation exchange concentrations and high pH values, whether the cation can be co-precipitating with Fe oxides (Thornber & Wildham, 1984) or with carbonates (Thornber & Nickel, 1976). Co-precipitation of anions is similarly influenced by the same factors with anions of low solubility and low pH favouring greater co-precipitation (Thornber & Wildham, 1984).

Common minerals	pzc	Reference
Amorphous SiO_2/quartz	1.8 - 3.5	1
Feldspars $(NaK)AlSi_3O_8$	2.0 - 2.4	1
Olivine $(MgFe)SiO_3$	4.1	1
Kaolinite/Illite $Al_4Si_4O_{10}(OH)_8$	3.3 - 6.0	1 and 2
Montmorillonite $Na_2Mg_2Al_{10}Si_{24}O_{60}(OH)_{24}$	2.5 - 6.0	1 and 2
Allophanes	6.0 - 7.0	3
Augite $(CaFeMg(AlSi)_2O_6$	4.5	1
Calcite $CaCO_3$	8.0 - 9.0	1
Gibbsite $Al(OH)_3$	9.5	3
Hematite Fe_2O_3	6.5 - 8.6	4
Goethite FeOOH	7.6 - 8.1	3
Ferrihydrite Fe_4O_5 $(OH)_2$	6.9	3

Table 2.2. Some point of zero charge (pzc) pH values for various common minerals and soils. [References: 1: Parks (1967); Farrah & Pickering (1979); 3: Parfitt (1980); 4: Parks & De Bruyn (1962)].

2.6.8 Chelation by humic materials

The strong interactions between decaying organic material and inorganic ions may cause either enhanced solubility or complete immobility, depending on the molecular size of the humic material. Organic matter has the greatest exchange capacity (150 to 400 mev per 100 g) of any of the soil fractions due to the presence of humic materials. The humic acids have adjacent carboxylic acids or phenolic -OH groups that allow the formation of chelation bonds with metal ions (Cline et al., 1983). The reaction is represented by the equation:

$$HA + M^{2+} = MA + H^{+}$$

Humic acid — Humic complex — M = divalent metal; A = humic ion

Humic substances are generally subdivided into humic acids, fulvic acids and humin (Thornber, 1982). Humic acids are those fractions that can be extracted into strongly alkaline solutions but are insoluble in strong acids; fulvic acids are soluble in both acids and bases whereas humin is soluble in neither. This separation is related to molecular size, with fulvic acid<humic acid< humin, the latter possibly bound firmly to soil grains. Chelation of a cation with humic material may render it more soluble with a fulvate molecule, chelate with two soluble humates to form a large molecule, which precipitates or could be chelated into an immobile humin.

Fulvate molecules are important in increasing the mobility of many cations by attacking otherwise stable minerals. An example is hydroxamate siderophors (complex compounds produced by microorganisms within rhizophere) which form strong chelates with Fe^{2+} that it becomes mobile even in an oxidising environment and hence may be responsible for leaching iron oxide minerals (Cline et al. 1983). They can also form solutions that can keep other metals such as Al^{3+}, Mn^{2+}, Zn^{2+}, Cu^{2+}, Ca^{2+} and Mg^{2+} dissolved under conditions in which they would normally precipitate.

2.6.9. Microorganisms

The involvement of microorganisms with weathering is generally accepted. They play two major roles:

(1) They accelerate the rate at which reactions occur by making use of the energy so released. This is exemplified by many species of microorganisms, mainly anaerobic bacteria, which are capable of reducing iron oxides (Schwertmann et al. 1985). This reduction occurs wherever O_2 needed for metabolic oxidation of biomass by aerobic soil organisms (mainly microbes) becomes deficient such as in poorly drained soils. The details of the biological reduction process are not yet fully understood. A possible mechanism has been provided by Scwertmann & Taylor (1989).

Electrons produced during metabolic oxidation of organic compounds have to be transferred to an electron acceptor. When O_2 is lacking, and the redox potential, Eh, has been lowered Fe^{3+} can take up these electrons. They probably are bound to an enzymatic system, which is excreted from the bacterial cell to its outer surface where electron

transfer to Fe^{3+} ions at the oxide surface occurs. This process is facilitated if the organism is in contact with the Fe^{3+} oxide particle (Munch & Ottow, 1983). The resultant Fe^{2+} will then go into solution as a divalent cation where it is reoxidized when O_2 is again introduced, or moved to zones of higher pH. Thiobacillus ferrooxidans are microorganisms that can oxidize Fe^{2+} in aqueous solutions and they are well adapted to very acid conditions (pH<3).

(2) They change the conditions of the system, for example one organism may change the pH so that another organism can then operate in a preferred environment to complete an oxidation reaction; the two organisms thus act together as a symbiotic system (Nissenbaum & Serbam, 1987).

Microorganisms can also derive energy by breaking down large, immobile molecules into smaller, more mobile ones (Thornber, 1982).

Table 2.3 provides a summary of the mobilities of selected elements under the different conditions that have been discussed in this section (section 2.6).

Element	Mobile in:			Precipitated when:		
	Eh	pH	Organic matter	Eh	pH	Copreci-pitated with
Fe	Low	Low	No	Low	Low	-
Mn	Low	Low	No	Low	Low	-
Cu	High	Low	No	High	Low	-
Zn	High	Low	No	High	Low	Fe-oxides Mn-oxides
Ag	High	Low	No	High	Low	Mn-oxides
As	High	Low	No	High	Low	Fe-oxides Mn-oxides
Au	High	Low	No	High	Low	Fe-oxides
Mo	High	High	No	High	High	-
V	High	High	No	High	High	-
Cr	High	High	No	High	High	-
W	High	High	No	High	High	-

Of these elements, Fe and Mn are more mobile in low pH and Eh conditions and are precipitated under the same conditions. Cu, Pb, Ag, Zn, As and Cu are more mobile in high Eh and low pH conditions and apart from Cu are all co-precipitated with Fe and Mn oxides. Mo, V, Cr and W are mobile in high Eh and pH conditions and are precipitated under similar conditions. All the elements show limited mobility when organic matter is present in the substrate.

2.7 Geochemistry of regolith profiles

During weathering distinct Eh-pH zones develop in the profile. Typically, Eh and pH increases towards the surface. Limited oxygen fugacities below the watertable generally result in at least mildly reducing conditions in the lower part of the weathered profile. With the exception of those profiles that have become locally water saturated (e.g. salt lakes), the upper profile is generally oxidizing. The access of oxygen and water from the surface cause the upper part of the profile to be most oxidizing; elements will be at their most oxidized state in the near surface (Lawrence, 1994).

Those oxides that form the insoluble oxides in their most oxidized state are the most strongly affected by a change in redox conditions. Under reducing conditions, for example, iron weathered from iron-bearing minerals is mobile as the ferrous ion (Fe^{2+}). Where the profile becomes sufficiently oxidizing, the Fe^{2+} is destabilized and converted to the ferric ion (Fe^{3+}). The Fe^{3+} is insoluble, except at very low pH, and is hydrolyzed and precipitated to red, brown and yellow iron oxides. This iron oxidation front is referred to as the redox front (Lawrence, 1994).

Reducing environment		Oxidizing environment
$2Fe^{2+} + 0.5\ O_2 + 3H_2O$	=	$2FeOOH + 4H^+$
Mobile ferrous ion		Goethite

This reaction is irreversible in the supergene environment, except by specialized organic processes. Hence the iron oxide is insoluble, and therefore represents a permanent, highly visible record of the position of the redox front within the regolith (Lawrence, 1994).

This production of acid at the redox front enhances the mobility of cations (e.g. Ag^+, Li^+, Cu^{2+}, Zn^{2+} and Cd^{2+}) within the oxidizing environment of the upper profile. However under strongly oxidizing conditions some elements are capable of losing up to five or six

electrons. These strongly positively charged ions are unstable and readily react with oxygen to form oxyanions, which have a negative charge. Elements which do this are As, Se, Nb, Mo, Sb, Te, Ta, W and Bi. Thus, under strongly oxidizing conditions these elements behave as anions.

2.8 Mobility of gold in weathering environments

The mobility of gold, gold nuggets and particulate gold in the weathered zone has long been a subject of conjecture and intense discussion. Various laboratory studies have shown that gold is soluble in chemical solutions, which may occur naturally in weathering profiles. McCuaghey (1909) showed that solutions of ferric salts could dissolve gold and that the addition of ferrous ions to the solutions inhibited their ability to dissolve gold. Smith (1943), found that gold could be dissolved in, and subsequently precipitated from sodium sulfide solutions at low temperature. He also noted that these sulfide solutions, if left to oxidize in air, formed sulfates and thiosulphates.

The importance of the chloride ion, low pH and oxygen content (or redox potential) on the solubility of gold was deduced by Krauskopf (1951) on theoretical grounds. A series of experiments at low pH with NaCl by Cloke & Kelly (1964) demonstrated that gold was dissolved at an appreciable and observable rate when pyrolusite (MnO_2) was present in acid chloride solutions. Lakin et al. (1974), showed that a wide range of ions and agents, including Cl^-, I^-, Br-, $S_2O_3^{2-}$, SCN^-, CN^- and organic substances, could dissolve gold.

The Goonumbla deposit is a Cu-Au-Ag system. Because of the importance of gold to the mine economy and future exploration work in the region, it is important to review its behaviour in the weathering environment in more detail.

2.8.1 Dispersion of gold and its main aqueous species during regolith formation

Gold, silver and copper are traditionally assigned to a subdivision of the alkali metals (Cuff & Doherty, 1982). Many of the qualities of gold can be traced to its electronic properties. Gold has 79 electrons in six shells with a lone electron in the outermost orbit, which is free to bond with other atoms. Therefore, Au^+ is the predominant oxidation state of gold in aqueous systems although it has another oxidation state of Au^{3+}. The activity of Au^{3+}, however, is negligible in comparison to that of Au^+ in aqueous fluids (Seward, 1984).

The most active and abundant ligands necessary for complexing and dissolving gold in the weathering environment are thiosulphate ion, humic acid, chloride ion and cyanide ion (Butt, 1981). During periods of lateritization, conducive environments for the mobility of gold and related silver are developed. It has been observed that Au-Ag alloys dissolve more readily than pure Au (Mann, 1984).

Low pH and a high concentration of chloride appear to be requisite for gold and silver mobilization in laterite profiles (Mann & Webster, 1984). In acid chloride solution, gold forms chloride complexes, the most important being $AuCl_4$- (Sillen & Martell, 1964). Oxygen was found by Krauskopf (1951) to be most likely oxidant for gold. The oxidation of gold by oxygen in the presence of the chloride ion, is shown by this reaction:

$$4Au^{\circ} + 16Cl^- + 3O_2 + 12H^+ = 4AuCl_4^- + 6H_2O.$$

2.8.2 Role of Fe and Mn

Iron and manganese are the most important redox state buffers influencing gold transport and precipitation since they are the major elements, which have different valencies. Oxidation of Fe^{2+} in sulfides to Fe^{3+} is one of the main reasons for decomposition of sulfides during weathering processes and forming sulphate- or thiosulphate-gold complexes (Gray et al. 1992).

Lateral dispersion of gold is evident towards to the top of the lateritic profile, particularly in the ferruginous and mottled horizons (Freyssinet et al. 1987; Michel, 1987). Precipitation of gold in a solution in which it has been dissolved and exists as the $AuCl_4^-$ complex could take place as a result of lowering of the Cl^- ion concentration by dilution, raising the pH or reduction of the $AuCl^-$ ion. The reaction for the precipitation of gold by reduction of $AuCl_4^-$ with Fe^{2+} can be written as:

$$AuCl_4^- + 3Fe^{2+} + 6H_2O = Au^{\circ} + 3FeOOH + 4Cl^- + 9H^+$$

Goethite

implying a simultaneous deposition of both iron oxide and gold.

According to experimental work, gold concentration may be up to 0.2 ppm as gold-chloride complexes in a solution which is highly saline (3.5% Cl), very acidic (pH=3)

and highly oxidized (Eh > 800 mmV). Such high oxidizing condition can be approached by the MnO_2 buffer (Gray et al., 1992):

$$Mn^{2+} + 1/2O_2 + H_2O = MnO_2 + 2H^+$$

On the other hand, Mn^{2+} may also play the same role as Fe^{2+} to reduce gold from a gold- chloride complex (Figure 2.4).

The chemical characteristics of an active weathering profile are such that there is an increase in Eh and decrease in pH from the weathering bed-rock interface up to the watertable (Lawrence, 1994). Implicit in the chemical model for such a profile where ferrolysis is active is that there is diffusion of ferrous ion, Fe^{2+} upward in the profile (Mann, 1983). A chemical model for the dissolution of primary gold (for example) a quartz vein or a lode system and the reprecipitation of gold in the mottled zone of such a profile is illustrated in Figure 2.4.

Dissolution of gold (and silver) from the vein of the lode system occurs at or close to the watertable where Cl^-, H^+ and O_2 are abundant and there is little or no Fe^{2+} present. Chloride complexes of both Au and Ag migrate away from the vein system, but the mobility of Au is restricted because of the presence of Fe^{2+} in the profile. Reprecipitation of high purity gold occurs in conjunction with the precipitation of FeOOH in the mottled zone (Mann, 1983).

2.8.3 Role of humic acids

Lateral dispersion of gold in this zone can also be possible if there is residual concentration and surface wash during landsurface reduction, and in part to mobility, either in solution or as colloids, complexed by humic acids produced by the rapid degradation of organic matter (Butt, 1981) as shown by the equation:

$$\underset{\text{(electrum)}}{Au^0} + H^+ + \text{organic acid} + O_2 = Au\,(\text{humate})^{3+} + H_2O$$

Gold precipitation occurs by reduction thus:

$$Au[\text{ humate }] + Fe^{2+} = \underset{\text{(fine gold)}}{Au^0} + \text{organic acid} + Fe^{3+}$$

It is also possible that gold may react with organic matter to form soluble gold-organic complexes or form colloids which may be stabilized by organic matters (Gray et al., 1992). These colloids are negatively charged, and may be mobile in negatively charged host environments, then precipitate when it reacts with positively charged particles e.g.. iron and manganese oxides. However, no quantitative data is available to support this suggestion.

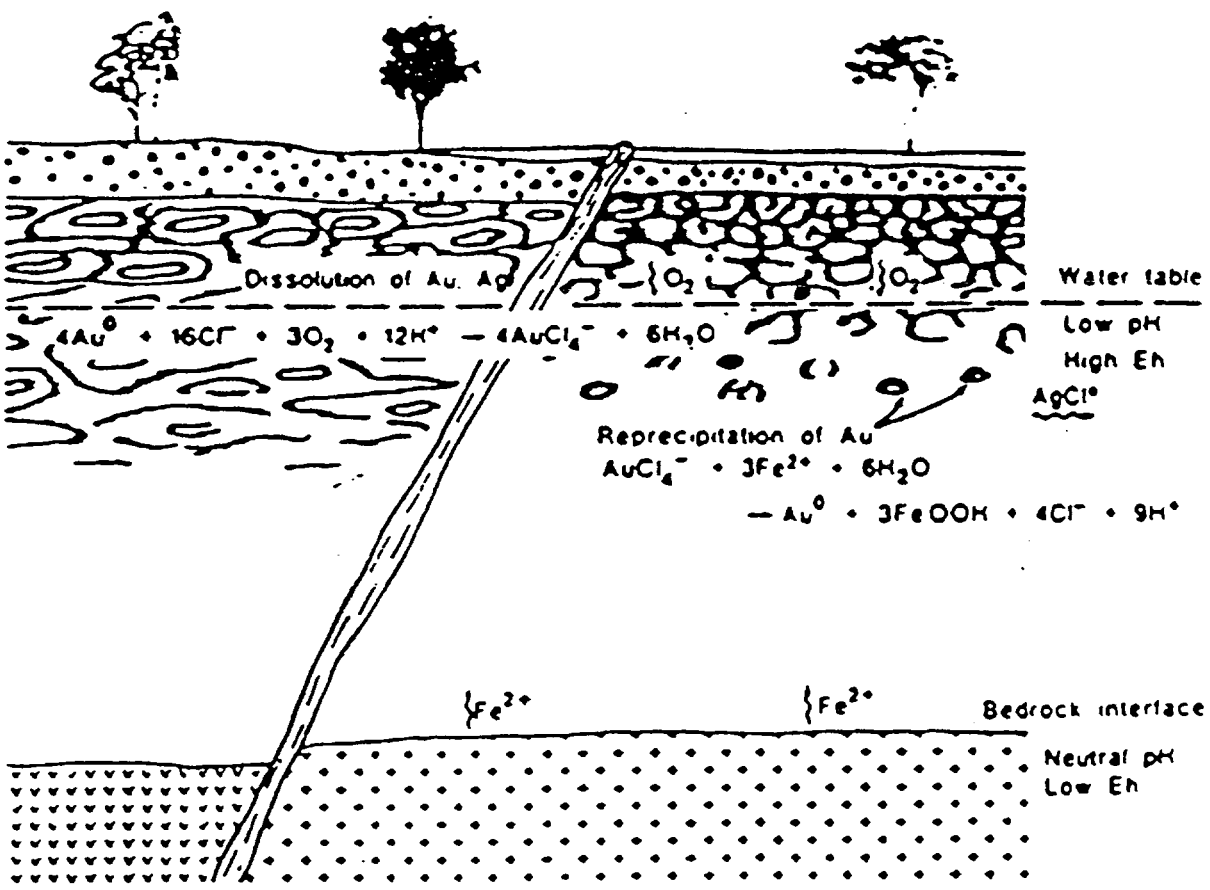

Figure 2.4. Chemical model for the redistribution of gold and silver from a quartz vein or lode system into the weathering zone of a lateritic profile + = granite, v = greenstone (Mann, 1984)

2.8.4 Role of Carbonates

Free gold (and silver) may also be mobilized if high concentrations of carbonate are present in primary mineralization, because the oxidation of pyrite proceeds under an alkaline environment to produce thiosulphate as in the equation:

Pyrite oxidation:- high carbonate, alkaline, mildly oxidizing:

$$2FeS_2 + 4CaCO_3 + 3H_2O + 3.5O_2 = 2FeOOH + 4Ca^{2+} + 4HCO_3^- + 2S_2O_3^{2-}$$

This mechanism has been invoked to explain the solution and reprecipitation of electrum in humid, tropical Papua New Guinea (Webster & Mann, 1984). Stoffregan (1986) suggested the possibility of solution and immediate reprecipitation of gold and silver by thiosulphate under near-neutral conditions, the principal effect being a reduction of grain size. The mechanism is as follows:

Pyrite oxidation:- low moderate carbonate, mildly acid-mildly alkaline, oxidizing

$$FeS_2 + 3O_2 = 2Fe^{2+} + 2S_2O_3^{2-}$$

Gold dissolution

$$\underset{\text{(electrum)}}{Au^0} + 2S_2O_3^{2-} = Au(S_2O_3)_2^{3-}$$

Gold precipitation:- reduction, acidification

$$2Au\,(S_2O_3)_2^{3-} + 2H^+ = 2Au^{2+} + 4S^0 + SO_4^{2-} + H_2O$$

$$Au^+ + Fe^{2+} + 2H_2O = \underset{\text{(electrum)}}{Au^0} + FeOOH + 3H^+$$

It is also notable that carbonate solubility is correlated with temperatures in that the release of pressure and increase of pH are probably critical for carbonate formation (e.g.. calcrete) during weathering processes or in soils.

When gold is carried as complexes in an acidic fluid, and the fluid reacts with carbonates, decomposition of carbonates and removal of oxygen from the environment will increase

the pH values and lead to gold precipitation. This may explain some of the gold anomalous in calcrete:

$$AuCl_2^- + CaCO_3 + 3H^+ + 1/4O_2 = Au + Ca^{2+} + CO_2 + 2Cl^- + 3/2H_2O$$

Laboratory experiments have shown that the Au associated with the carbonate is very soluble even in deionised water (Gray & Lintern, 1994).

2.9 Summary of environmental effects on element mobility

The two most important effects are physico-chemical conditions and climate.

2.9.1 Climate

The chemical and physical processes of weathering, soil formation and landscape development are essentially the same as those of secondary geochemical dispersion. Thus, the determination of the weathering history and the recognition of the effects of past and present climates on these processes are fundamental to the interpretation of geochemical data (Butt, 1982). Two climatic regimes are of significance in regolith evolution i.e. warm and wet conditions and the present arid to semi-arid conditions.

2.9.2 Warm and wet climates

High watertables and large volumes of water during profile formation, under warm and wet conditions leaches mobile components with the resultant residual accumulation of stable primary and secondary minerals, and the precipitation and accumulation of iron oxides above a high watertable in the near surface. This iron oxide accumulation results in the formation of laterite at the surface (Thornber, 1982). Acid conditions produced by ferrolysis enhances weathering in laterite and mottled clay horizons.

2.9.3 Arid conditions

Under increasing arid conditions, an excess of evaporation over precipitation lowers the watertable and decreases ground water flow resulting in decreased weathering and accumulation of weathering products. Ground water salinity also increases. The net effect is that iron oxides are precipitated down the profile (Thornber, 1991).

Arid conditions above the descending redox front, causes further intensive leaching of the upper saprolite and the formation of the upper leached saprolite. With progressive lowering and further still-stands in the water table, under periods of constant climate, a series of palaeo-redox fronts generally indicate that there was not just a continuous downward progression of the redox front, but that in some situations, it also rose in the profile, with perhaps a reversal of climate or change in topography, such as tectonic uplift.

During the decline of the watertable, oxygen is readily available and the deposition of iron oxides and intensive weathering are uninhibited. However, when the watertable becomes static, redox processes are slowed, because eventually the reaction front will descend to level of anoxic conditions. With a rising watertable, redox processes are limited by a decline in oxygen access and weathering is greatly reduced.

The intensity of iron oxide accumulation at the redox front depends on the length of time of the stand-still and the availability of iron in the profile. Iron oxides may also move as colloids and, hence, precipitate on fracture surfaces, indicating fluid movement within the profile. It is the deposition of these iron oxides at the redox front and on fracture surfaces that indirectly controls most element mobility and deposition and, hence, supergene mineralization (Lawrence, 1994).

2.9.4 Physico-chemical environment

The two most important factors controlling the solubility of an element are oxidation potential (Eh) and hydrogen ion activity (pH). The oxidation state has the overriding control on the mobility of an element in solution. The effect on element mobility of each factor has already been discussed.

CHAPTER 3.

CLASSIFICATION OF THE REGOLITH.

3.1 Introduction.

Regolith evolution as hitherto mentioned is the result of interactions between primary minerals and chemical agents particularly H_2O, O_2 and CO_2 that circulate below the earth's surface. The regolith profile is considered to be an assemblage of 'differentiated and superficial mantle displaying several units of organization or structural order (Nahon, 1991). Thus observing and analyzing the attributes of the differentiated weathered units in the field has consequences for understanding of the regolith and the processes that shape it, and subsequently provides the framework for laboratory characterization of the mineralogy and chemistry of the regolith.

Weathering reactions differ from site to site in response to climatic factors, nature of parent rock, topography, time and microfauna. Weathering environments are thus strongly heterogenous both spatially and chemically (Ildefonse et al. 1979). The structural units or horizons which are essentially products of weathering, succeed each other genetically and historically in the upward direction (Bocquier, 1973), and consequently their study is undertaken commencing from the fresh rock upwards to the more weathered zones (Millot, 1970; Hough, 1982; Velde, 1985). The intensity is maximum at the surface and decreases progressively with depth resulting in the development of horizontal or near horizontal zones or 'facies' of weathered rock which together constitute the regolith profile. The bottom to top of the profile approach was adopted in this study of the regolith allowing structural units in the profile to be distinguished, unless later events e.g. erosion and sedimentation have occurred.

Well-defined systems of terminology and classification are essential to provide an accurate description of regolith materials and units and to permit valid comparisons between sites (Anand et al. 1989). The regolith is polygenetic, hence descriptive attributes must recognize characteristics due to different events. The classification must be able to discriminate these characteristics accordingly.

In much of Australia, the regolith consists of a deep, mostly, lateritic weathering profiles which have been modified by physical and chemical alterations induced by later tectonic and climatic changes (generally, uplift and a change to an arid climate). Accordingly, the

terminology and classification are based on the fundamental characteristics of this profile, with modifications due to later events or features added as descriptors. The present-day formation of calcrete for example may, because of erosion, be superimposed on different horizons of the pre-existing profile. The classification of the product, therefore may be either according to the later event (i.e. the presence of calcrete) or to the earlier event (i.e., the horizon in which the calcrete has precipitated). As long as the descriptions of the material are adequate, classification according to either event should be appropriate (Anand et al. 1989).

One of the major problems confronting regolith scientists today is the lack of a universally accepted system for the terminology of deeply weathered regolith, whether for whole profiles, individual horizons or for many distinctive secondary structures. This is because there is a wide range of materials within the regolith, with great variations in mineralogical and chemical composition, fabric and origin, even within a single profile or toposequence. Many of the terms are used in different senses by different authors. Accordingly, comparisons of like situations in widely separated regions are greatly hindered by the inadequacy of existing terminology and lack of consensus in its use.

This chapter aims to present a classification system for the description of the regolith in the study area by using terms that conform as much as possible, with established and currently available national and international usage. Most of the commonly used schemes include those of Butt & Zeegers (1992), Nahon & Tardy (1992) and the CSIRO scheme of Anand and Butt (1988), Anand et al. (1989), Butt et al. (1991) and Smith et al. (1992).

3.2 CLASSIFICATION AND TERMINOLOGIES OF REGOLITH PROFILES

The classification and terminology according to CSIRO (Anand et al., 1989), Nahon and Tardy (1992) and Trescasses (1992) are summarized in Figure 3.1. The two most dominant profiles in the study area are presented in Figure 3.2. As will be discussed later in the chapter, they have been subdivided on the basis of the nature of the parent material into residual and transported regolith. The classifications presented in this section are broadly hierarchical, with subdivisions of each unit defined in terms of a given set of attributes. The profiles encountered in the study area do not exhibit the ferruginous cappings typical of 'lateritic' environments with the classification system of Trescasses (1992) depicted in Figure 3.1(c) closely typifying the profiles encountered in the study

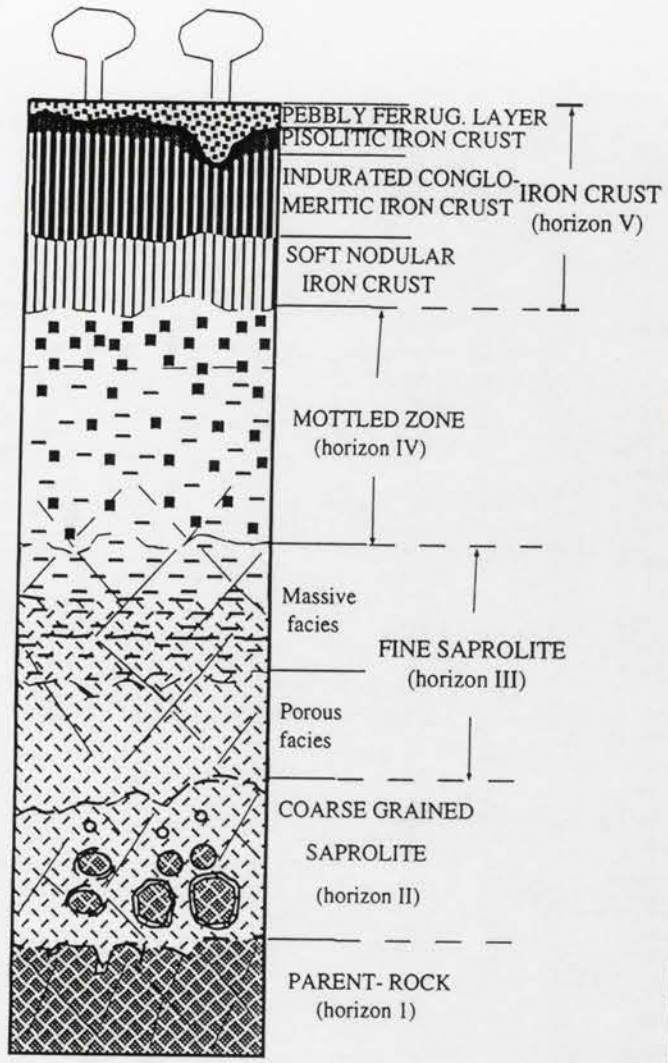

Figure 3.1(a): Nahon and Tardy (1992)

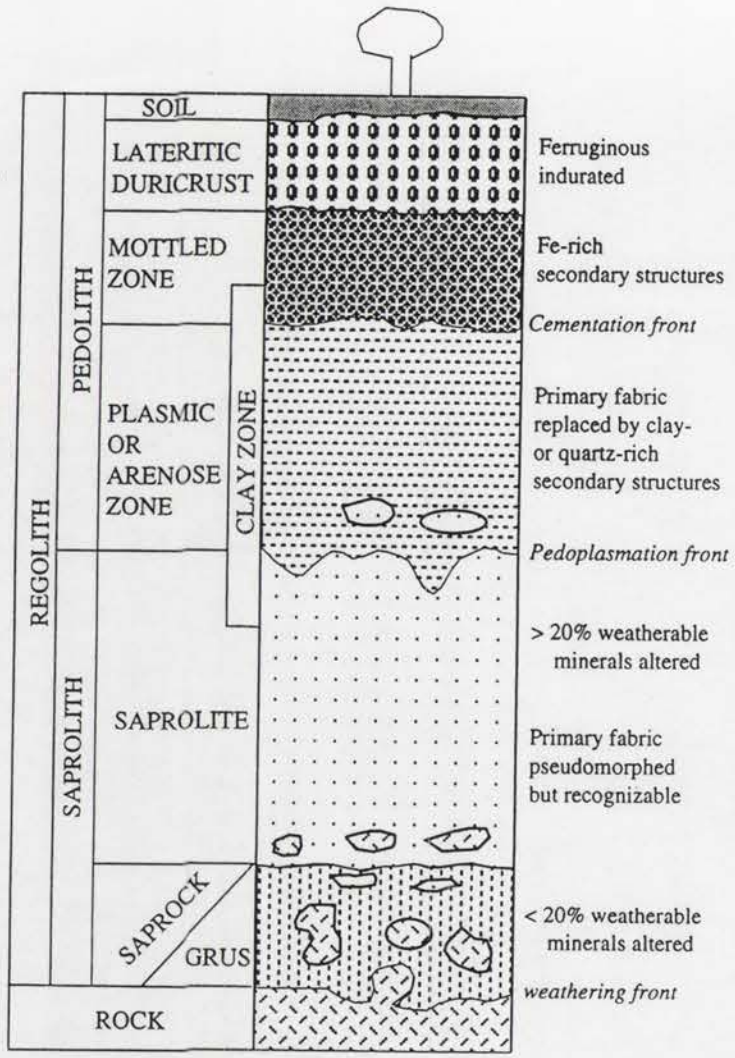

Figure 3.1 (b): Anand et al., (1989)

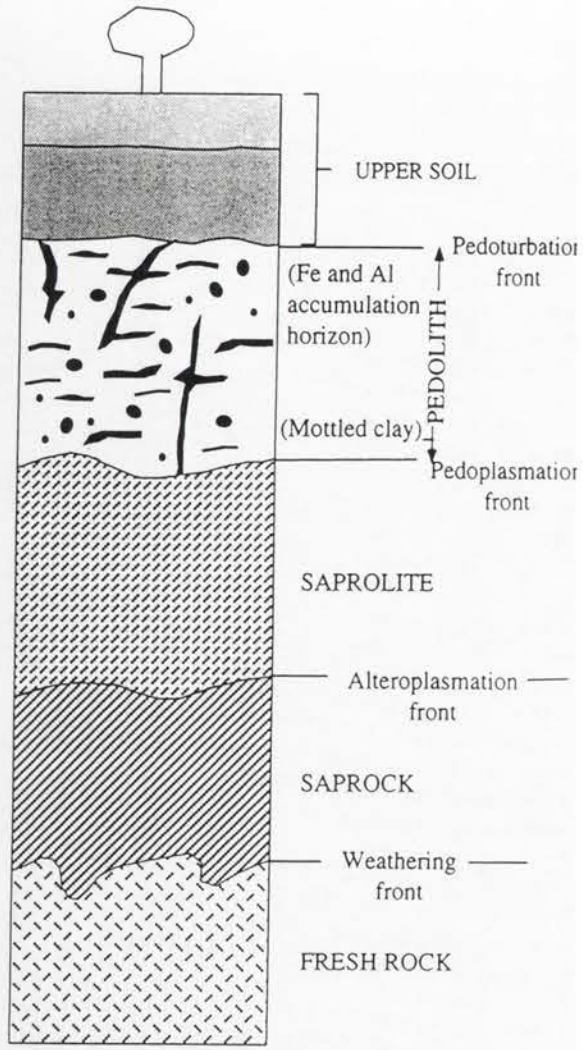

Figure 3.1 (c): Trescasses (1992)
(modified)

Figures 3.1 (a), 3.1 (b) and 3.1 (c): The distribution of the regolith in systems formulated by Nahon and Tardy (1992), Anand et al., (1989) and Trescasses (1992)

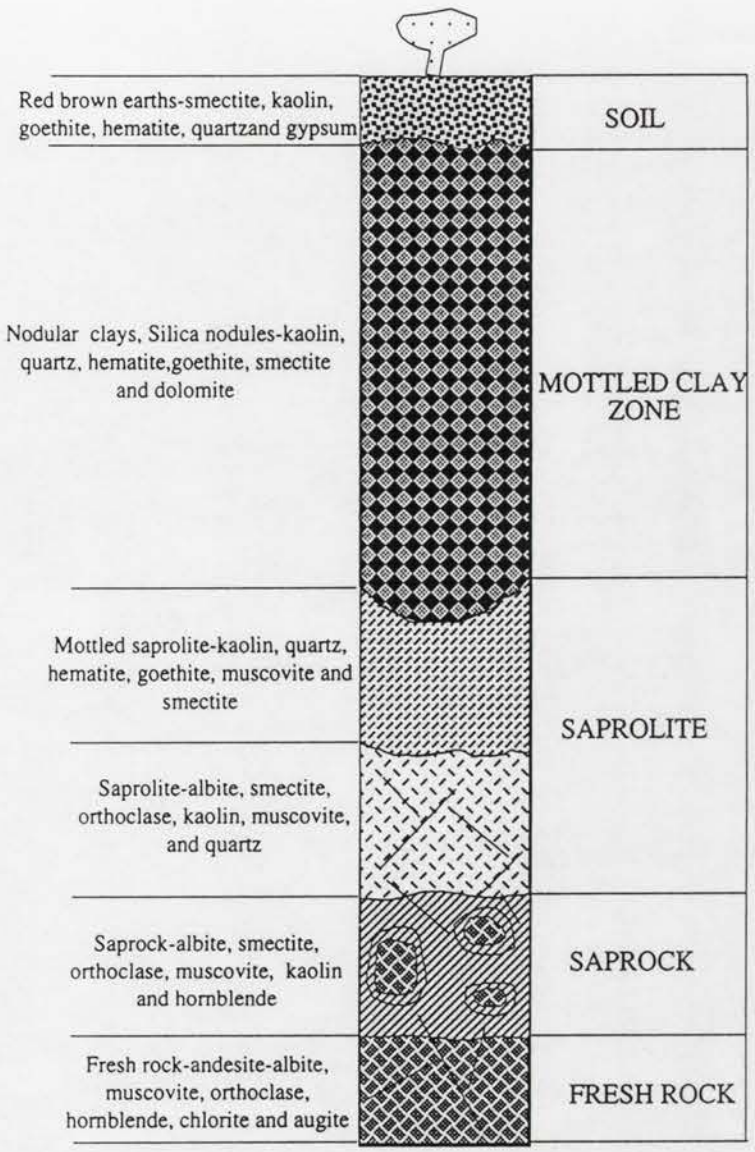

Figure 3.2 (a)

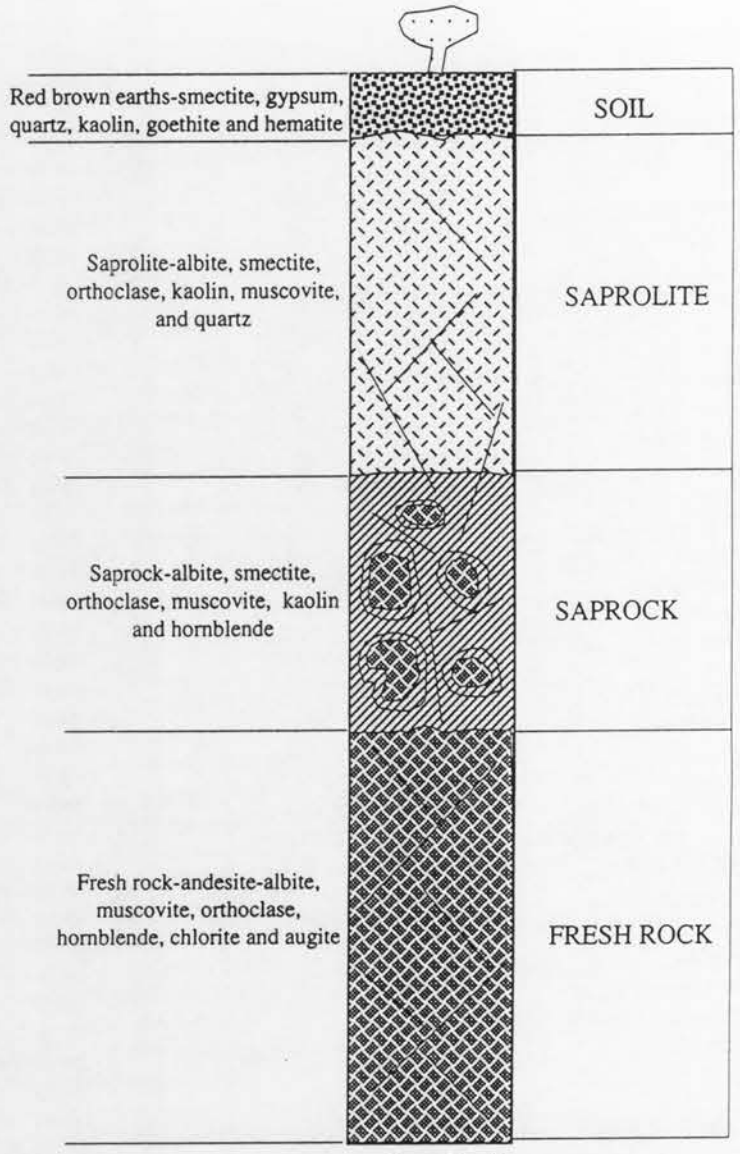

Figure 3.2 (b)

Figures 3.2: Typical weathering profiles at the Goonumbla Cu-Au deposits developed; (a) on inferred initially transported alluvial/colluvial sediments and (b) on the host rock (trachyandesite).

area. Consequently the description of terms in this chapter shall only be limited to the characteristics features in the Parkes profiles that are also described in these terminologies. The vertical succession of horizons from the base is as follows.

3.2.1. Fresh or parent rock.

This is the horizon where the minerals remain unaltered. The weathering front marks the commencement of weathering in the regolith. It is important to note that some secondary minerals such as carbonates, phyllosilicates and iron oxides may occur in fissures and cracks down to considerable depths in this horizon although much of it is imported (Anand et al. 1989; Nahon & Tardy, 1992). The first signs of weathering are usually the oxidation of primary sulfides and the dissolution of carbonates (Nahon & Tardy, 1992)..

3.2.2. Saprock

According to Anand et al. (1988), the saprock is a compact slightly weathered rock of low porosity with less than 20% of the weatherable minerals altered. The weathering effects are present along mineral boundaries and intra-mineral fissures, along cleavages, shears, joints and fractures. Nahon & Tardy (1992) refers to this zone as forming the lower part of the coarse grained saprolite (sometimes referred to as "grus" or "arene" in French literature) which they define as forming the porous, basal horizon in which some parent rock fragments, feldspars, micas and other primary minerals remain unweathered. On granitic rocks, the coarse saprolite or saprock is referred to as "arene" (from latin *arena*, sand; Leneuf, 1959; Millot, 1964; Tardy, 1969).

Weathering products in the saprock may be either a single mineral phase such as vermiculite, smectite, kaolinite, gibbsite, imogolite and hydrated aluminosilicates, or assemblages such as vermiculite-kaolinite, smectite-kaolinite, kaolinite-gibbsite (Leneuf, 1959; Tardy, 1969; Novikoff, 1974 and Novikoff et al. 1972). In a normal succession of minerals, the most soluble phases (calcite, smectites) appear in closed systems, while the less soluble ones (kaolinite, gibbsite) appear in open systems, at the contact with circulating solutions (Nahon & Tardy, 1992).

The term "grus" is applied to mean fragmental disintegration product of largely unweathered granitic rock. It is commonly applied to surface products, although it is also present as a porous horizon ranging from a few centimetres to 10 m or more thick at the

base of the saprolite. Grus differs from saprock in that it is friable rather than compact (Anand et al. 1989).

3.2.3. Saprolite

The term saprolite was first used by Becker (1894) and was defined as 'structurally coherent, thoroughly decomposed crystalline rock formed in place by chemical weathering'. This is the zone in which the weathered bedrock retains much of the fabric and structure of the parent rock (Leneuf, 1959; Millot, 1964; Tardy, 1969; Anand et al. 1989 and Nahon & Tardy, 1992). The progress of weathering is petrographically expressed by an increase in porosity, a complete or partial transformation of most of the parent rock minerals and a decrease in induration of the rock (Tardy, 1969; Nahon, 1986). Compared to saprock, more than 20% of the weatherable minerals are present (Anand et al. 1989).

Nahon and Tardy (1992) refer to this horizon as the fine grained saprolite which they define as the horizon in which most primary minerals have been altered to secondary minerals such as kaolinite, goethite or amorphous iron oxyhydroxides with the exception of quartz and resistant minerals which remain unweathered or partly weathered.

The definition may be extended to include weathered rocks in which only larger structures such as bedding, schistosity, veining or lithological contacts are preserved (Anand et al. 1989). Nahon & Tardy (1992), have also used the term lithomarge , "argiles bariolees" and pallid zone to refer to the fine saprolite. However, term pallid zone should not be used to refer to saprolite because it may exhibit a variety of colours (Anand et al. 1989; Nahon & Tardy, 1992).

3.2.4. Mottled Zone

The mottled zone is the horizon, which is characterized by localized spots or segregations of iron oxides in a clay rich matrix. Trescasses (1986) refers to this zone as the pedolith which he defines as the zone where the structure of the 'primary' plasma is progressively modified into 'secondary plasma' which includes formation of ferruginous patches (mottled clay zone) and nodules (nodular horizons). Nodule growth progressively destroys pre-existing fabrics, although pseudomorphic lithic plasma or arenose fabrics and micro-fabrics may be preserved in the core.

Nahon & Tardy (1985), mentioned that the mottled zone lies above the watertable in the unsaturated (vadose) zone. The reorganization they say, is a result of two factors. Firstly, vertical and lateral percolation of water in the unsaturated zone leading to the formation of a network of channels and tubular voids of large diameter (approximately 10 mm). Secondly, ferruginous spots (5-150 mm) and nodules (10-30 mm) develop, becoming more abundant and indurated towards the top of the mottled zone. The implication is that iron is mobilized from areas around large (> 1 mm) pores and reprecipitated and concentrated in clay-rich areas. The formation of mottles and nodules is discussed in Chapter 6.

Generally, loss of fabric and the accumulation of Fe-and Al-oxides appear to coincide fairly closely, defining the mottled zone. Where such accumulations occur without substantial loss of fabric, the material remains classed as saprolite (Anand et al. 1989). The pedoplasmation front marks the boundary between the saprolite and the pedolith in deeply weathered terrains and is the zone at which the lithic fabric is destroyed although commonly with little chemical reworking.

3.2.5. Soil

Soil is the primary zone of interaction between the regolith and vegetation and fauna. Strong reworking of the regolith reorganizes components into what is the soil profile. The *solum* is the upper-most part of a soil profile and consists of a sandy textured layer over a more clay-rich brighter coloured layer. The *sub-solum* is that part of the profile where the effects of the biota and consequently the reorganization are not as strong as in the solum.

Most soils are developed from, rather than with, the material they overlie, whether these are the ferruginous zones of complete profiles or the exposed horizons (e.g., the mottled zone, saprolite, fresh rock) of truncated profiles, and have characteristics inherited from these parent materials.

3.4 Classification of the regolith in the study area

A detailed description of the distribution of regolith materials in the study area is presented in the next chapter. The scheme formulated for the study area (Table 3.1) conforms very closely with the CSIRO scheme although most of the terms with the exception of mottled and clay saprolite are common to all the other schemes.

Two types of soils have been recognized in both E22 and E27 deposits and they differ in their depths, colour, pH, mineralogy and geochemistry as a result of their source or parent materials. Those that have developed over the inferred transported material of the mottled clay zone are more deeper (up to 4.5m) and have higher pH values (7-9) and higher contents of carbonates and gypsum while those that have developed over the trachyandesite have slightly lower pH values (5-7) and lower contents of carbonates and gypsum and higher contents of the primary rock forming minerals. The detailed characteristics of these soils are discussed in Chapter 5.

The term ferruginous saprolite has been used by Anand et al., (1989) to define the clay-rich saprolite that has been formed by infusion with goethite. This zone is described as being hard, massive to mottled, and dominated by kaolinite and goethite with yellowish brown, non-magnetic fragments. It may also have an incipient nodular structure and often form a continuous blanket generally overlain by collapsed ferruginous saprolite because soluble, less ferruginized material has been removed by leaching, causing the whole structure to collapse.

This part of the saprolite in the study area is yellowish brown to red in colour, friable to firm, mottled and dominated by kaolin (50-60%), goethite (10-20%), quartz (10-15%), muscovite (5-10%) and hematite (< 5%) in order of their abundance. This zone is stratigraphically situated directly below or on the fringes of the mottled clay zones. Ferruginous nodules of between 5-20 mm when present are dominated by goethite relative to hematite. The collapsed portions and the hard and massive character mentioned above are almost absent in this saprolite. The content of iron oxide infusion often used to describe this portion of the saprolite is between 40-50% (Anand pers. comm.). This unit is distinguished from the other saprolite units in the field by its highly mottled nature as defined by yellowish brown (10 YR 5/8) to yellowish gray (2.5 Y 5/4) and hence the term mottled saprolite has been adopted to describe this unit in this study. The common terms, subdivisions and major characteristics of the regolith in the study area are presented in Table 3.3.

Some pertinent field attributes have been employed to differentiate some regolith materials that have similar characteristics under their broad definitions. Colour, for example, has proved to be a good attribute in differentiating between the different types of saprolite in the study area. The greenish-grey (8/5 GY) saprolite has acquired its colour from its high content of the olive-green iron rich smectite known as nontronite and

COMMON TERMS	PREFERED TERMS	SUBDIVISIONS	MAJOR CHARACTERISTICS
Soil	Soil	-Soil over transported parent material	-High pH (7-9); High carbonate and gypsum content; High depths (3-4.5m)
		-Soil over residual parent material	-Moderate pH (5-7); Shallow depths (1.5-2.5m; Lower contents of gypsum and carbonates; Higher contents of primary minerals.
Mottled zone	Mottled clay zone	-Mini-mottled clay zone	- Zone of incipient development of mottling in clay; Nodules present; Mottle size-<5mm
		-Medium-mottled clay zone	- Nodular horizon; Size of mottles- 5 to 30mm
		-Mega-mottled clay zone	- Nodules absent; Size of mottles- 30 to 300m
Saprolite	Saprolite	- Mottled saprolite	- Infused with iron from the mottled zone. Iron oxide contents of between 15 to 30%
		- Greenish-Grey saprolite	- High amounts of green smectite (nontronite), plagioclase and kaolin
		- Orange-Pink saprolite	-High amounts of K-feldspar, muscovite, kaolin and iron oxides
		-White clay unit	-High amounts of white to whitish- grey kaolin and smectites; High dolomite content.
Saprock	Saprock	- Nil	-High amounts of nontronite and primary rock forming minerals and opaques (sulphides, iron oxides and ferromagnesians.
Bedrock Unweathered rock	Fresh rock	- Nil	-High amounts of primary rock forming minerals, opaques (iron oxides and sulphides) and ferromagnesians

Table 3.4: The common terms, subdivisions and major characteristics of the regolith of the study area

the orange-pink (2.5 YR 8/4) saprolite by its high content of K-feldspar which occurs as a matrix flooding in this unit. The two types of saprolite occupy different positions in the regolith stratigraphy and display differences in both their mineralogy and geochemistry. The subdivision on the basis of colour then has proved to be an additional tool in further subdivision of the profiles . The use of other additional terms such as lower, middle or upper saprolite in this study relates to the positions of these units in the regolith profiles. These terms are purely descriptive and are not formally defined.

A third colour distinction is the use of the term white clay unit. This zone occurs between the orange-pink saprolite and the soil in the flanks of the mottled clay portions of the pit . It consists of massive white, whitish-grey to light gray (7.5YR 8/1; 7.5 YR 7/1; N 8/0) clays commonly with mesoscopically homogenous fabrics. The loss of lithic fabric in this unit has probably resulted from solution and authigenesis of saprolitic clays (kaolin and smectite) and mechanical processes such as shrinkage and swelling. Mineralogically, it is composed of smectite (10-15%), kaolin (50-70%), muscovite (10-15%) and minor amounts of orthoclase, dolomite and goethite. Because of these distinctive characteristics, this zone is herein referred to as the white clay unit.

The different horizons of the mottled zone have also been distinctively subdivided on the size of their iron accumulations (mottles) into mini, medium and mega-mottled clay. Mini-mottled clay has iron oxide segregations of 2-5 mm, medium-mottles, 5-30 mm and mega-mottles, 50-300 mm or above. These subdivisions were necessary when carrying out detailed descriptions because these mottles have subtle differences in their fabrics, texture, mineralogy and geochemistry as outlined in the next chapter.

3.3 Modification of the regolith after formation.

A number of events can occur to modify the regolith after its formation. Some of these events have been observed in the study area and they include the following features.

3.3.1 Partial truncation

Erosion can occur after the establishment of a weathering profile either due to instability resulting from climatic change or drainage rejuvenation. Removal of the upper horizons of the profile may result in the lower horizons, including weathered rock, being exposed at the surface. The exposed lower horizon may crop out, become the parent material of newly formed soils or be overlain by transported overburden. The erosion products will

then occur as extensive transported overburden including alluvium, colluvium, sheet-wash, evaporitic sediments and aeolian material.

The regolith developed over the trachyandesite shows evidence of partial stripping down to the middle saprolite. This is evidenced by the lack of a well defined contact between the soil and the saprolite and the development of a thin soil cover with mixed components of the andesite parent and alluvial/colluvial sediments. The significance of this event is discussed in Chapters 6 and 7.

3.3.2 Cementation by secondary components

Cementation is one of the most recognizable modifications to regolith profiles after formation. The most common cements are iron oxides (ferricrete), silica (silcrete, hardpan), Ca and Mg carbonates (calcrete), aluminosilicates and gypsum. Of these cements, the most significant in the study area are gypsum, calcite and dolomite.

One of the most commonly encountered cementing agents in semi-arid parts of Australia is calcrete. Calcrete is a term commonly used to refer to indurated material formed by the *in situ* cementation or replacement, or both, of pre-existing regolith by secondary carbonates. They vary widely in carbonate content and properties, from friable, fine-grained soils to coarse nodular horizons to limestone rock. There are two principal genetic types, namely (1) pedogenic or vadose calcretes and (2) groundwater or phreatic calcretes. Most consist of calcite and/or dolomite; magnesite occurs over ultramafic rocks. Groundwater calcretes may have minor aragonite and magnesian clays such as sepiolite. In Western Australia, pedogenic calcretes are most abundant south of 30^0S (the Menzies Line) and groundwater calcretes to the north (Lintern, 1996).

In the study area, cementation occurred in the form of dolomite coating of silica aggregates and as fracture and void infills within the saprolite and also manganese coating of fractures within the saprolite and the mottled clay. Iron oxide cutanic accumulations were also common within the saprock and the saprolite. Translocation of fine quartz, gypsum and clay particles was also evident in the mottled clay units. This process of illuviation was quite intense in the voids and fractures in these units and occurs in response to a number of processes. Firstly, it may have involved the downward movement in solution by percolating waters of clay constituents derived by weathering in solution often resulting in precipitating of clay minerals in the lower solution. Secondly, the clays could have moved as particles in suspension in the downward percolating water

to accumulate in the lower horizons because of flocculations, constrictions in the pores through which the water moves, or because the bases of the lower units marked the lower limit of water movement (Birkeland, 1974).

3.5 FACTORS AFFECTING REGOLITH PROFILE DEVELOPMENT

3.5.1 Role of meteoric agents

The chemistry and rate of weathering is controlled by the availability of water and temperature. These are governed by the two fundamental factors that define the climate, namely annual average precipitation and temperature (Strakhov, 1967; Loughnan, 1969; Barshad, 1974; Ollier, 1984). Rain is the principal source for recharge of groundwater. Water is essential for dissolution of soluble constituents of the rock and mobilization of these species around and out of profile. Reaction rate is governed by the availability of water, and is influenced by temperature. Experimental investigations have confirmed that water is an important agent of chemical weathering, acting through the process of dissolution and hydrolysis (Pedro, 1961; Pickering, 1962; Parham, 1969 and White & Sarcia, 1978).

Temperature plays a dual role in chemical weathering. On one hand, increasing temperatures promote weathering by greatly accelerating the rates of chemical reactions while on the other hand temperatures create greater evaporation and hence tend to retard chemical weathering by reducing the quantity of water percolating through the weathering zone. The effective temperature of an area is also modified by surface relief. For every 50 m in elevation, the temperature decreases by approximately 1°C while aspect and steep slopes may considerably reduce the amount of sunlight reaching certain areas (Loughnan, 1979).

Many soil properties show distinct trends with the regional climate in going from the equator to the poles, as shown in Figure 3.4. These variation in the soils originate in such processes as organic-matter influx and decomposition, presence or absence of chelating agents, soil-water chemistry, and the depth and rate of leaching of water through the soil. These processes are in turn controlled by climate. The tropical forest regions are characterized by intense, deep weathering, with iron and aluminium oxides and hydroxides predominant close to the surface. With depth clay minerals of the 1:1 and finally 2:1 varieties are found. Organic matter in these soils varies, because even though the amount annually added to the soil is high, the decomposition rate of organic matter

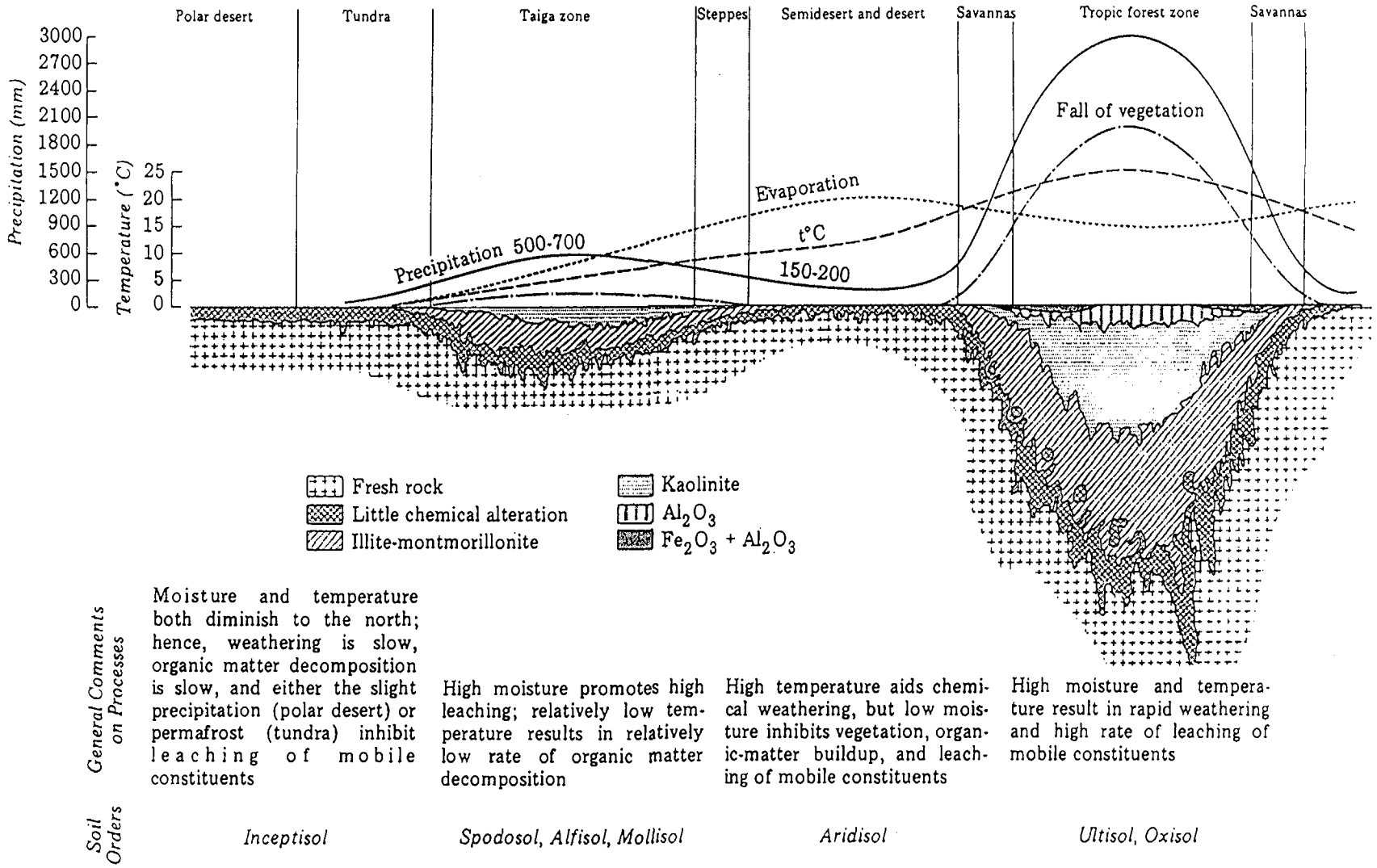

Figure 3.3: Diagram of relative depth of weathering and weathering products as they relate to some environmental factors in a transect from the equator into the north polar region (Strakhov, 1967)

varies. The above trends diminish to the north in the savannah region. the deserts on the other hand are characterized by low organic-matter input relative to the rate of decomposition and low organic matter content (Strakhov, 1967).

The influence of climate on the formation of regolith in question, can be studied by reviewing the past climate of Australia. The evolution of Tertiary climate in Australia commenced with the separation of Australia from Antartica in the late Cretaceous (~ 90 Ma). Since then Australia has drifted 30° north and has consequently experienced different climates. The onset of aridity in Australia is suggested to have developed in response to the clearing of Antartica in the south and initiation of circumpolar circulation in the ocean (Quilty, 1982; 1994). Figure 3.3 shows the relative depth of weathering and weathering products as they relate to some environmental factors in a transect from the equator into the north polar region while Figure 3.4 shows the intensity of chemical weathering in relation to temperature and rainfall.

This period of aridity altered landscapes, reduced the drainage extent and dried up the flourishing flora and also advanced the birth of the deep regolith profiles (Veevers, 1984). In arid regions where evaporation exceeds rainfall, water may penetrate the rocks but, during the ensuing long dry spell, it is returned to the surface and ultimately becomes lost through evaporation. As a result, soluble constituents of the rocks are not removed and the reactions slow down accordingly. Oxidizing conditions ensure retention of iron in the ferric state and this imparts red, brown and yellow hues to the surfaces of the rocks. Loughnan (1969) stated that the characteristic secondary minerals in arid settings are montmorillonite, illite and chlorite or, more probably, mixed layers of these minerals, and suggested that kaolin is rare unless present in the parent rock, in which case it persists unaltered in composition.

In contrast, the rocks of humid areas are generally intensely weathered as a result of the continual downward movement of percolating waters. Most of the soluble products of the hydrolyzing reactions taking place at mineral surfaces are carried down to the water table and are lost through the subsurface drainage. Because of high ground water recharge in wet areas, the water table is often at shallow depth and much of the altered zone may be permanently saturated, and hence in a reduced state. The concept that weathering processes, lead to the ultimate development of lateritic profiles with good fluid thoroughflow has gained increasing support in recent years (Bird & Chivas, 1988, Bird et al. 1990b, Taylor et al. 1990).

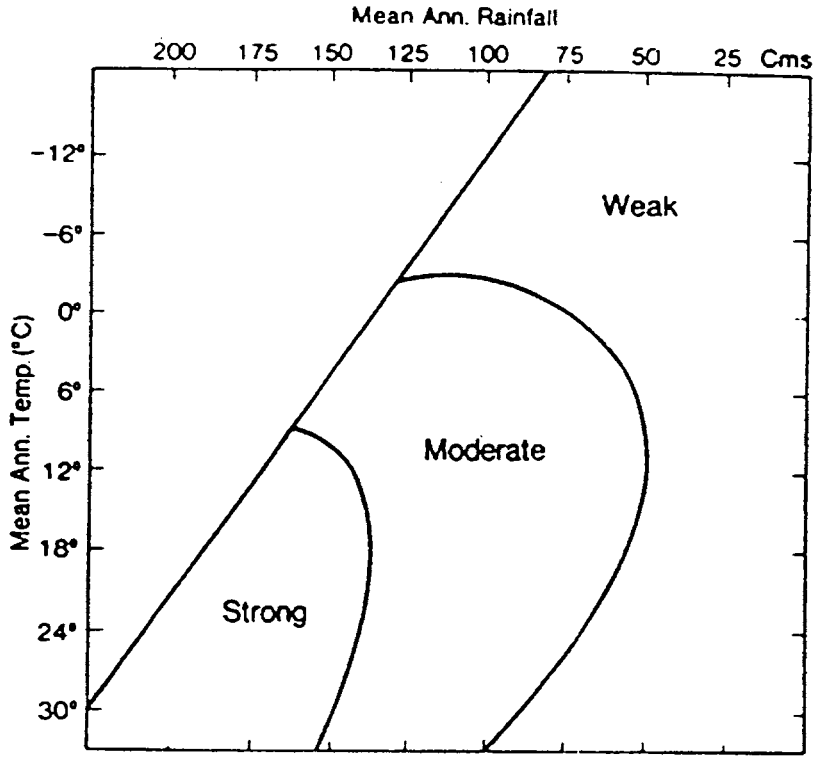

Figure 3.4: Intensity of chemical weathering in relation to rainfall and temperature (From Ollier, 1984)

The main period of production of laterites and weathering profiles in Australia is indistinctly defined. Smith & Embleton (1978) defined the main period as having been during the late Oligocene to early Miocene but evidence based on stable $^{18}O/^{16}O$ isotope studies of kaolinite and gibbsite suggests that weathering did initiate before Oligocene (Bird & Chivas, 1988). The Goonumbla volcanics have been exposed to weathering processes since the Carboniferous though the main weathering phase might have been sustained in the Tertiary (Chapter 8).

3.5.2 Topography

Topography in combination with climate, has a marked effect on the rate of chemical weathering and the nature of the resulting products (Barshad, 1957; Loughnan, 1969 and Tardy et al. 1973). It exerts this influence by controlling the rate of surface runoff and hence the rate of fluid infiltration, the rate of subsurface drainage and therefore the rate of removal of the soluble constituents, and the rate of erosion of the weathered products and thereby the rate of exposure of fresh mineral surfaces (Loughnan, 1969). On very steep

slopes, most of the rainwater is lost through surface runoff and little penetrates the parent rock. Steep slopes with good drainage facilitate erosion and efficient removal of alkalis and silica resulting in the development of a thin profile. Undulating gentle slopes lead to the formation of both 1:1 and 2:1 phyllosilicate layer types and are characterized by thicker weathered horizons because clay is considered to be transported downslope (Tardy et al. 1973; Birkeland, 1974).

Flat, low-lying areas (typical of the study area at present), experience little runoff, and infiltration of water is at a maximum especially if the soil has a high infiltration capacity. However, in this type of environment, subsurface drainage tends to be sluggish and soluble products released by the hydrolyzing reactions persist in the waters. Where the parent rocks are relatively rich in the alkalis or alkaline earth's, or where the drainage waters from nearby hills are charged with such ions, the environment may become distinctly alkaline. Generally, in low-lying areas the water table is at shallow depths and may, in places, rise above ground level forming swamps and promoting the accumulation of organic matter. In these circumstances, a reducing environment may develop.

Such observations of the physical configuration of weathering environments with associated change in redox regimes in different topographic positions reflects the catena model where crestal to upper slope free draining profiles are more likely to be oxidising while lower slope to valley profiles may be more saturated and hence more reducing. There is some gradation between these end members. Perched groundwaters also provide some variation to this basic model. In a study of weathering on basalts in northern New Zealand, Carr et al. (1980) noted that deeply weathered deposits form where thin basalt flows cover an irregular topography yielding a series of relatively flat surfaces which have excellent drainage. However, even in rolling country, local variations in topography can create distinctly different environments, which may find expression in contrasting weathering products.

The broad flat basin topographic setting of the study area facilitate the preservation of the regolith and hence the characteristic deep weathering. The regolith is interpreted as having been sourced from the surrounding regions although some developed residually on the host rock. Weathered material may not only be transported via surface processes, but can also escape through the lower weathered horizons to the topographically lower areas by the process of elutriation (Velde, 1985). The tectonic evolution of the south eastern highlands has already been discussed in section 2.1 of Chapter 2.

3.5.3 Nature of parent rock.

Primary minerals only react with a chemical agent at specific sites closely controlled by access to solutions (Trescasses, 1987). Weathering starts at contacts between adjoining primary minerals, or along microfractures within the minerals. The physical characteristics of the parent rock then are considered vital in promoting leaching processes (Loughnan, 1969). These structures i.e. fractures, joints, cleavages and bedding planes increase the intensity of weathering by providing channels for easy access of water to internal sections of the rock. Dissolution along cracks allows enhanced percolation in weathered materials. In addition, a more open microstructure and corresponding increase in porosity and permeability of most weathered materials enhances fluid percolation. Exceptions are weathered materials where the microstructure has collapsed forming dense, less permeable material, and laterally continuous layers of water saturated clays through which water can no longer permeate.

Texture of the parent rock then is important in that it influences permeability and therefore the degree of infiltration of rainwater into the rock. Laterally continuous clay layers may inhibit penetration of water when saturated. If layers of water-saturated clays are concentrated near surface, this may reduce the amount of fluid percolating through a profile and enhance surface runoff. Where there are subsurface water-saturated clay concentrations, permeability contrasts may cause ponding of fluids, and sometimes lateral transport of fluids above the impermeable layer (Moore, 1997).

Many weathering experiments have been concerned with simulating the chemical effects of weathering (Pedro, 1961; Pickering, 1962; Parham, 1969 and White & Sarcia, 1978) rather than physical weathering processes. Physical disintegration caused by weathering, however, can be of considerable importance in affecting the weathering of rock, for example the effects of wetting and drying of rocks containing expanding minerals (Cawsey & Mellon, 1983).

The chemical composition of the parent rock also controls weathering reactions in a given environment. The reaction rates for the chemical reactions that occur during the dissolution of the minerals forming the trachyandesites are governed by the chemistry of this rock as mentioned in Chapter 2. The greater the reaction rate, the more rapid the conversion of parent rock into secondary clay minerals and metal ion bearing hydroxides.

As a consequence of increased reaction rate, the weathered rock zone would be thinner and saprolite-soil zone would be thicker.

The Goonumbla Volcanics of the wall rock sequences were well jointed and revealed abundant veins and fractures. On a regional context, the volcanics exhibited some jointing although the rocks were generally devoid of any abundant structures which might have ensured strong leaching.

3.5.4 Time and organisms

Rock and mineral weathering and the development of prominent soil features are time dependent. The time necessary to produce various weathering and soil features varies, however; those soil properties associated with organic-matter buildup develop rapidly, but those associated with the weathering of the primary minerals develop rather slowly (Birkeland, 1974). A number of studies are available in literature on the rates of development of various weathering features, soil orders and clay-mineral alteration products some of which are mentioned in this section.

Rocks and minerals weather at different rates. The majority of the data on durations of weathering for which the time factor is reasonably well known come from the study of Quaternary unconsolidated deposits. Tombstones or other man-made structures for example are good indicators of the rates at which weathering can proceed above the ground surface. At any rate, rocks that weather quite rapidly, such as some limestones, can lose their tombstone inscriptions in as little as 100 years in a warm and wet climate. With more resistant rock, such as some sandstones and igneous rocks, it may take several centuries before the tombstone shows distinct signs of weathering (Rahn, 1971). This suggests therefore that several centuries are sufficient for weathering to be visible on almost any rock type in warm and wet climate. Arid-climate weathering proceeds at much slower rates (Barton, 1916).

Studies of glacial tills and outwash deposits are ideally suited to the determination of weathering of different lithologies as a function of time because all factors, except paleoclimate, can be kept constant. In weathering studies of glacial tills, one can compare the amounts of subaerial versus subsurface weathering with time (Figure 3.6) as has been shown for example in granitic rock types from the Cordilleran region of America (Birkeland, 1964). The initial weathering of the granitic clasts is characterized by rates of subaerial weathering that exceed those of subsurface weathering. With time, however,

subsurface rates are greater than subaerial rates. Thus, in old tills, most granitic stones at the surface have been at the surface for a long time i.e they are not lag gravel from depth. This difference in weathering with position relative to the surface is basic to an understanding of the origin of topographic features in granitic terrain (Wahrhaftig, 1965). It should also be noted that in the time necessary to alter a sound granitic boulder to grus in a soil, dense volcanic rocks may show only thin weathering rinds (Birkeland, 1964). Figure 3.5 shows the variation in subaerial weathering and subsurface weathering as a function of time in Sierra Nevada, California.

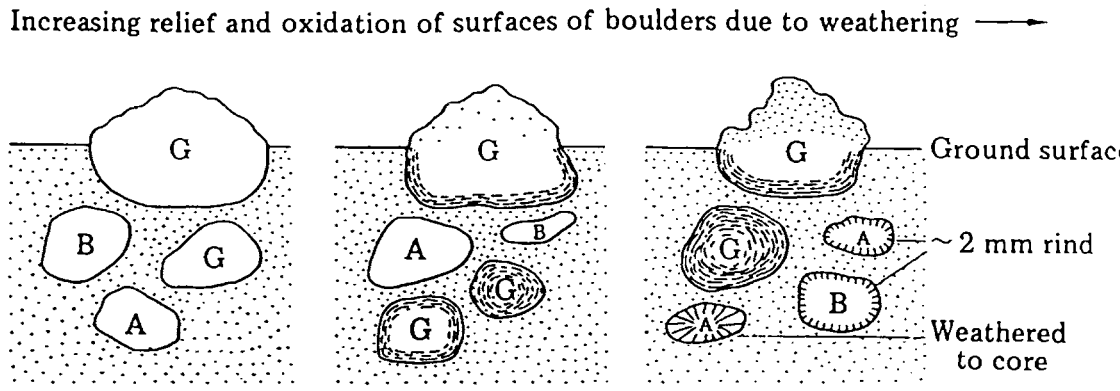

Glaciation:	Late-Wisconsin	Early-Wisconsin	Pre-Wisconsin
Approximate duration of weathering (years)	10,000	40,000	200,000

Key
Boulder lithology: G, granitic rock; A, andesitic rock; B, basaltic rock
Surface oxidation: slight; moderate
Subsurface weathering: grus; weathering rind

Figure 3.5. Variation in subaerial weathering and subsurface weathering as a function of time, northern Sierra Nevada, California (Birkeland, 1964).

The rate of mineral weathering can be determined in two ways. In one, the uniformity of the parent material can be established, and then the ratio of resistant to non resistant minerals for dated surfaces gives the rates at which the more weatherable minerals are

depleted. Ruhe (1965, 67 a), has done this for an area in Iowa, USA, where erosion surfaces of varying age are cut on Kansan till. Ruhe (1965) estimated that the soil related to the Wisconsin surface may have weathered 6800 years, the soil related to the late-Sangamon surface no less than 13,000 years or much longer and that related to the Yarmouth-Sangamon surface 10^5 years or more. The ratios also showed that the surface horizons were the most strongly weathered and that the weathering extended into the C-horizons of the older soils.

There is also a fairly good correlation between soil orders and the age of underlying deposits or landscapes in some regions. The Oxisols of the world seem to have required long periods of time to form. Maignien (1966), has reviewed most of the data on them and shows that many Oxisols date from the tertiary or early Quaternary. Although climate in Australia, may have been different during the time of Oxisol formation, these soils are so highly weathered that formation times of tens to hundreds of thousands of years or more do not seem unreasonable.

Microorganisms such as bacteria, algae and fungi on the other hand play a vital role in provoking initial disruption of fresh rock. These microfauna accelerate mineral alteration by enzymic oxidations and reductions (Berthelin, 1987; Weaver, 1989). Bioturbation by soil microfauna (e.g., worms, insects and other small animals) plays a significant role in alteration of soils and mixing of soil components in near-surface horizons.

Of these, the role of termites has received the most attention from exploration geochemists. In the drier savannahs and semi-arid regions of Africa, India and Australia, termite mounds 0.5 to 3.0 m or more high are features of the landscape. Termite burrows to great depths in search of water-for example, they have been observed at 70 m at Jwaneng, Botswana (Lock, 1985) and at 45 to 55 m in the Sahel (Cloud et al. 1980). Termites use soil and weathered material to build their mounds and in so doing transport minerals from deep horizons to the surface. Bioturbation has been credited with transporting metal enriched clays to give surface expression to otherwise concealed targets for example in Zimbabwe and Southern India (d'Orey, 1975). At Goonumbla, bioturbation has been observed to depths of up to 15 metres and hence, the microrganisms might have played a significant role in the evolution of the regolith especially in the higher horizons.

CHAPTER 4

SAMPLE COLLECTION AND ANALYSIS

4.1 Introduction

The objective of the sampling program was to obtain a suite of samples in order to investigate regolith mineral paragenesis and to illustrate the vertical and lateral distribution of a range of elements in the regolith developed over gold and copper mineralization and its wallrocks. The study area was entirely restricted to the locality in and around open cut mines.

Mining commenced on the E27 deposit in August 1993 and on E22 in January 1994 about the same time as this project was conceived. The stripping of the overburden offered an opportunity for a detailed regolith study as mining on the two deposits continued. Additional samples were collected from profiles previously exposed in the current position of the crusher pit and the decline bench to E26N deposit for control purposes.

4.2 Sampling

In total about 600 samples of soil, mottled clay, saprolite and fresh rock were collected for analysis. The samples were collected at horizontal intervals of 100 m to define individual profiles and in some instances 50 m where transition in regolith characteristics necessitated close interval mapping. The vertical interval depth of sampling was 2 m. When collecting these samples, at least one sample was taken from each weathering unit that could be defined in the field. For each profile a field description was done detailing the depth of sampling, location, textural and fabric characteristics, colour and field pH.

All the samples were analyzed for mineralogy and 300 selected samples for geochemistry using a combination of techniques. Another 40 samples were collected for optical microscopy and Scanning Electron Microscopy (SEM). 30 representative samples were selected from the 300 geochemical samples for selective leaching to determine the host minerals for ore-forming elements. Sixteen samples were additionally selected for a subproject on appropriate sample collection techniques for use in this study area and Broken Hill, the results of which are reported in this Chapter.

4.3 Mineralogy

4.3.1 Mineral identification

Mineral identification was performed using a combination of the techniques: X-ray Diffraction (XRD), optical microscopy and Scanning Electron Microscopy (SEM). The X-ray Diffraction and optical microscopy was carried out at the ANU Geology Department and Scanning Electron Microscopy at the ANU Research School of Biological Sciences.

Optical microscopy was carried out using oriented polished and unpolished samples mounted in polyester resins for the friable un-consolidated materials from the weathered sections. Determination of the clay mineralogy (< 2μm fraction) was accomplished by dispersion in distilled water (containing 0.5% sodium tripolyphosphate) with ultrasonic treatment and then by gravity settling and centrifugation in order to separate the clays from the bulk fractions. Different size fractions were obtained by sedimentation in accordance with Stoke's Law. Particle sizes are expressed as equivalent spherical diameters (e.s.d) which are related primarily to the a-b dimensions of clay particles rather than their thicknesses (Brindley & Brown, 1984).

Besides air dried samples of XRD analysis, glycolation treatment was carried out by incubating slides of clay samples for 24 hours at 65° C in a vessel containing ethylene glycol vapour in order to expand the smectite layers. The sample was then analyzed immediately by XRD. An example is shown in Figure 4.1.

Specimen dehydration was also carried out where necessary for 24 hours at 330° C. At this temperature, swelling clay minerals should lose their interlayer water yet retain basic structural integrity (Brindley & Brown, 1984). Only air-dried specimens were used in heating experiments. To reduce the possibility of smectite re-hydration, samples were analyzed with minimal exposure to atmospheric water.

Cambridge S360 and Jeol 6400 scanning electron microscopes were used in combination with energy dispersive X-ray analysis (EDXA) to determine the morphology and composition of the mineral grains.

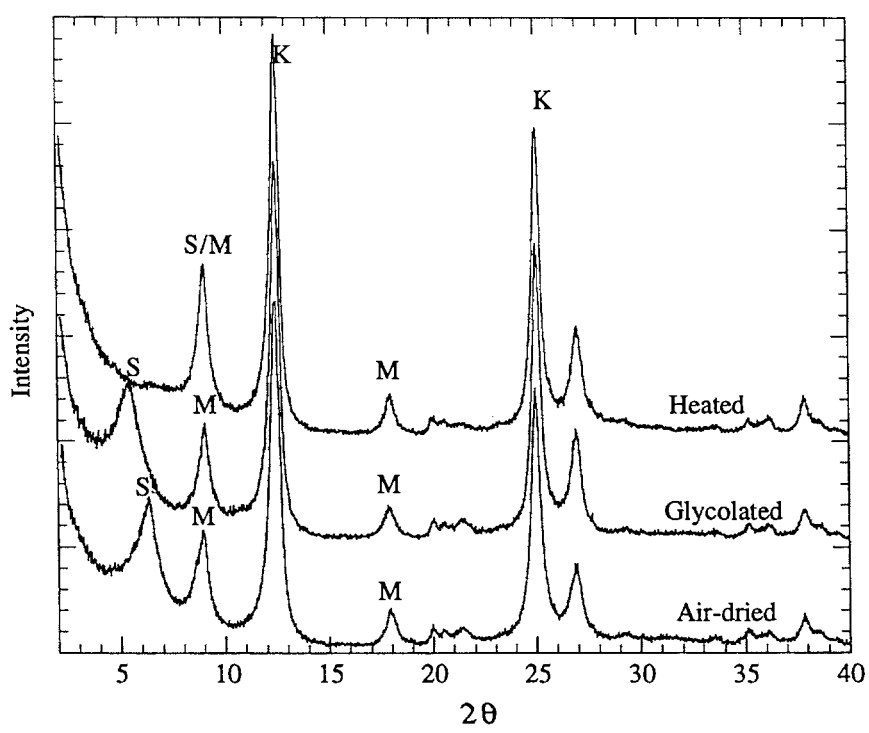

Figure 4.1. XRD traces of oriented samples from the saprolite of the 0.5-1μm size fraction after various treatments: K-Kaolinite; S-Smectite; M-Mica; S/M- Smectite and mica.

The grains were mounted on aluminium stubs and a thin coating of gold (200 Å) was applied to their surfaces. The scanning electron microscope was normally operated at 15kV unless charging was a problem, in which case the voltage was reduced. To obtain high resolution images, a working distance of less than 12mm and a lower than normal filament current was used.

The X-ray diffraction (XRD) studies for this work was done on a Siemens D501, θ-2θ powder diffractometer at the Department of Geology, Australian National University using CuKα radiation and a graphite post-sample monochramator, collimated by 1° divergence slits. For quantitative analysis, samples were usually run from 2-70° at steps of 0.02° 2θ and a counting time of 1.2 seconds/step. Bulk samples, clay separates and individual mineral grains were analyzed by this method. Two samples were employed in sample preparation. The traditional method involved milling of the bulk sample in an agate mortar and pestle with acetone until a grain size <10 μm was achieved, then the

sample was coated on a glass slide and allowed to dry before analysis. Clay mineralogy was carried out by analyzing oriented samples of material that had been taken from suspension after about 8 hours of settling time (<2 μm). The fraction was oriented simply by mounting the suspension directly onto a glass slide and letting it dry.

The other modern method of sample preparation was developed by the Centre for Australian Regolith Studies (CARS) group at the Department of Geology, Australian National University halfway through this project. This method involves loading the finely crushed and milled sample (< 2 μm fraction) onto a U-shaped aluminium holder, the sample being held in place during preparation by frosted glass. This ensures optimum random orientation of the sample during analysis and avoids minor displacement of peaks which often occurs when the previous method is used. Because some of the samples had been analyzed using the glass slide coating method, a quality check on the data was carried out to determine any major differences, if any, when either method is used on a similar sample. The results of this quality check are reported later in the Chapter.

Figure 4.2 shows a typical XRD scan of mega-mottled clay, with major peaks indexed for the minerals present. One of the essential elements of this study was the determination of the quantitative mineralogy of the samples in order to facilitate proper correlations with geochemical data and to discern differences in mineral contents between profiles. Quantitative X-ray diffraction techniques traditionally involved the measurement of the intensity of chosen peaks and subsequent comparison with those in standard calibration mixtures. However, these methods were tedious and relatively inaccurate, as standards needed to be made up for a variety of situations and intensity anomalies caused by angular dependent aberrations such as preferred orientation often made the method unreliable.

The foundations for multiphase profile analysis of the complete powder diffraction pattern were first laid down by Rietveld (1969). He showed that it was possible to replicate a measured diffraction profile with a calculated pattern. The advantage of full profiling is that residual errors caused by intensity aberrations inherited from the sample preparation stage or from using imperfect structural models tend to be positive and negative over the full diffraction profile leaving the Rietveld phase scaling factors largely unaltered (Taylor, 1991). Other workers including Hewt (1973), Wiles & Young (1981), Will et al. (1983), Hill & Howard (1986) and Taylor (1991) have since refined the technique, culminating in the writing of *Siroquant* 2.

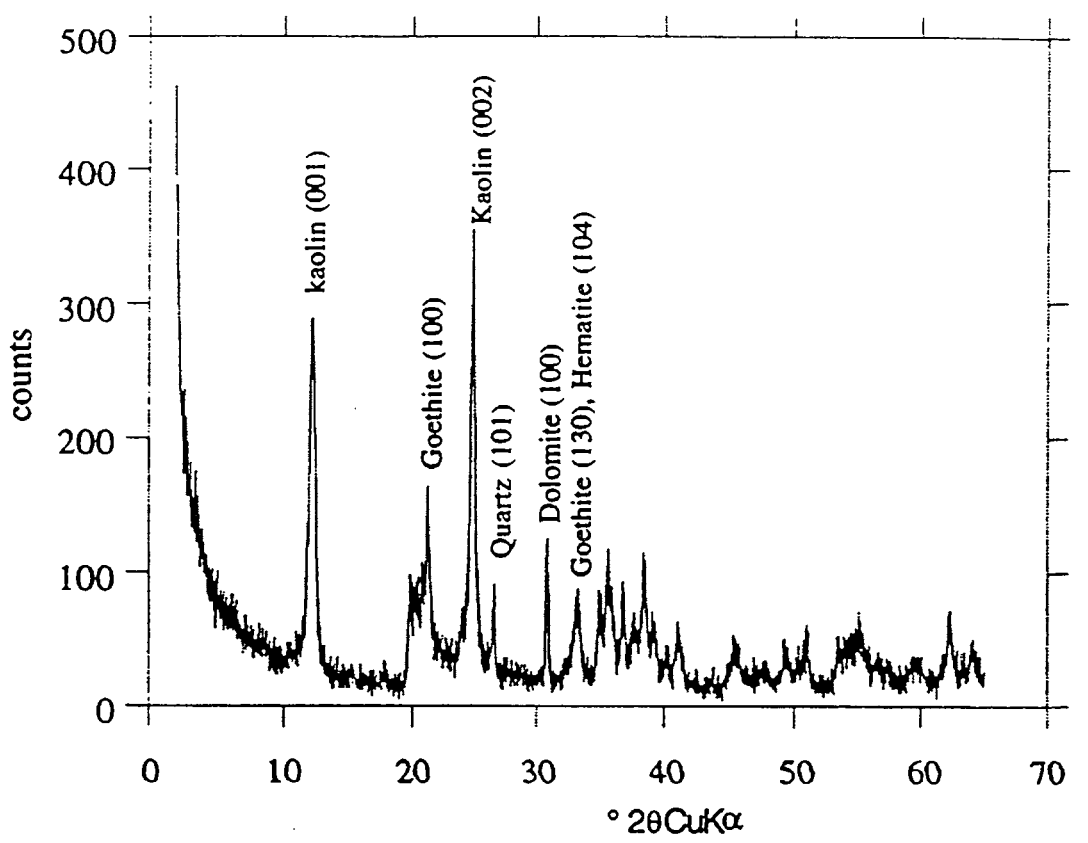

Figure 4.2 Typical XRD scan of mega-mottled clay with major peaks indexed for the minerals present.

Siroquant is a Rietveld-type multiphase analysis program which replicates a measured diffraction pattern by employing a least-squares fitting routine which adjusts the scaling factors until the calculated profile best approximates the measured one (Figure 4.3). In the process, a differential pattern is produced which indicates the degree to which the calculated pattern replicates the measured one. As an additional means of determining the degree of fit, the statistical parameter, χ^2 (chi-squared), is displayed after each least

[2]*Siroquant* is marketed and distributed by Sietronics Pty. Ltd, P.O Box 3066, Belconnen, ACT 2617, Canberra, Australia.

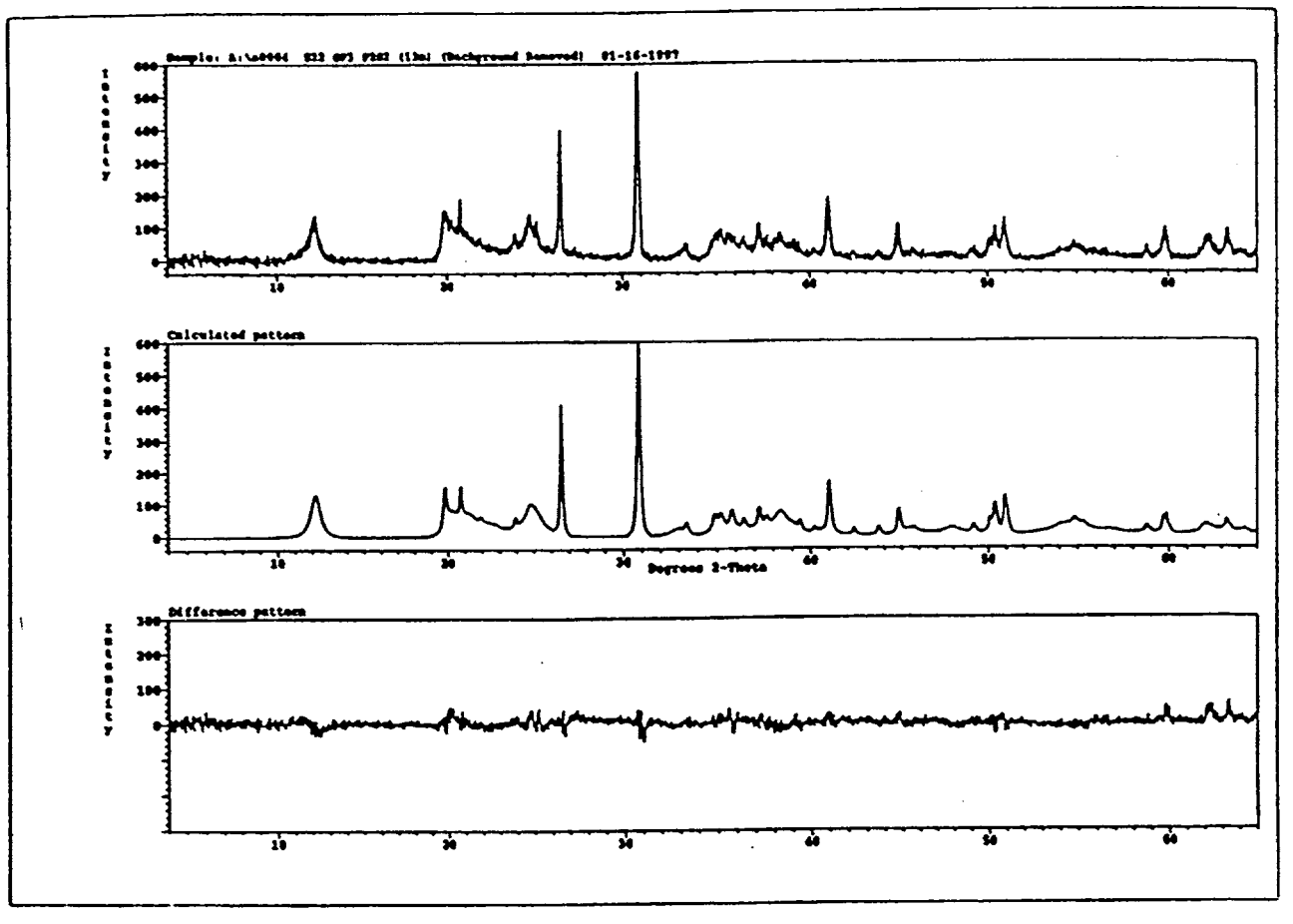

Phase	Weight %	error %
Quartz	7.5	0.13
Kaolinite	49.6	0.50
Hematite	4.0	0.34
Goethite	7.1	0.45
Dolomite	25.6	0.30
Anatase	6.1	0.26

Figure 4.3

A typical *Siroquant* output showing the measured (background removed), calculated and difference patterns.

squares fitting routine. Ideally, a perfect match is attained when $\chi^2=1$, however this seldom occurs. Generally, a good fit is indicated when the χ^2 value is less than 3. The quantity of individual minerals present within a sample is calculated from their respective scaling factors and absorption coefficients. A typical measured and calculated pattern from *siroquant* is shown in Figure 4.3.

Siroquant also has the provision for quantifying the amorphous mineral content of a sample. The presence of such poorly diffracting material (PDM) in a sample causes a reduction in the diffracted intensity of the crystalline phases. The amorphicity of a sample may be due to a number of reasons. Minerals that are composed of particles smaller than several hundred Å, have broad diffraction patterns. The diffraction lines may be so broadened that they are lost in the background. Glassy materials have no three-dimensional periodicity and therefore give no diffraction lines. Disordered structures may have streaking in the reciprocal lattice, thereby contributing as well, to the poorly diffracting material content of a sample (Tilley, 1996).

Rietveld analysis alone cannot quantify amorphicity. However, the addition of an internal standard (ZnO or quartz are recommended by Taylor & Clapp, 1992) of known concentration, facilitates the quantification of the poorly-diffracting weight fraction.

Siroquant uses the following equations in the quantification of poorly-diffracting material (Tilley, 1996):

$$X_D = 1 - Y_S/X_S$$
$$X_I = X_D/(1-Y_S)$$

X_D=weight fraction of PDM in the sample containing an internal standard,
Y_S=weighed weight fraction of the internal standard
X_S=Siroquant weight fraction of the internal standard
X_I=weight fraction of PDM in the original sample containing no internal standard.

As the addition of the internal standard causes dilution of the sample and a subsequent loss in accuracy, it is preferable to run a sample without an internal standard, as well (Tilley, 1996). This sample is used specifically for the purpose of quantifying well-crystallized phases while the sample containing the internal standard is used only for the

amorphicity determination. To obtain the final quantification, the results from both samples are combined and normalized.

Chemical analysis using either X-ray fluorescence (XRF) or energy dispersive X-ray analysis (EDXA) shows good agreement with *Siroquant* analyses when poorly diffracting material is absent (Figure 4.4). When it is present, the chemical composition of the material is determineable by subtracting the *Siroquant* results from the chemical analyses (Tilley, 1996).

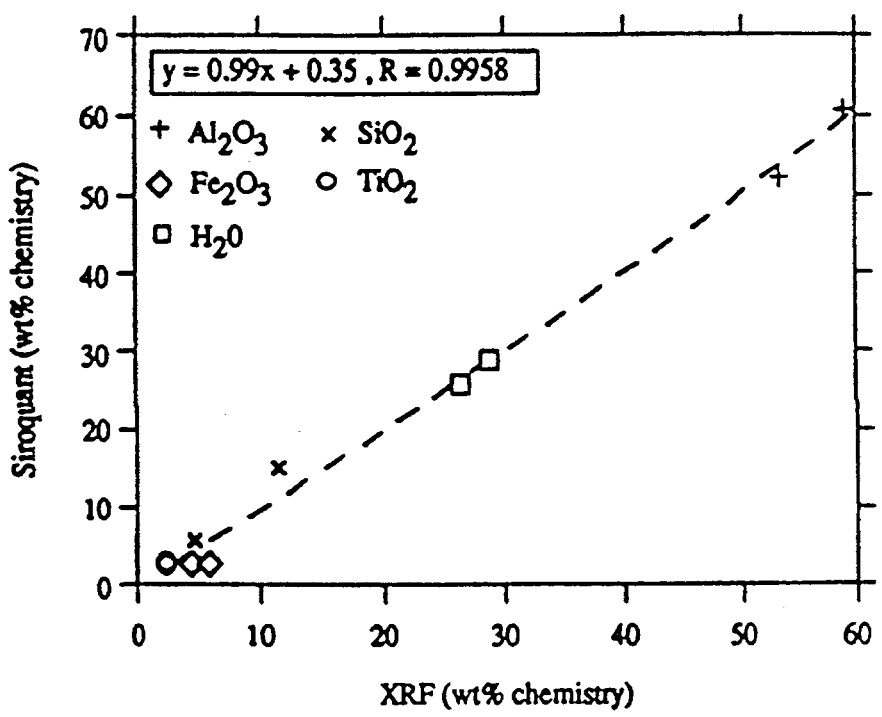

Figure 4.4 Correlation between the chemistry of bauxite analyzed by XRF and that determined by Siroquant, when poorly diffracting material is present (Tilley, 1996).

4.3.2 Creation and loading of a task file

An integral part of the *Siroquant* system is the concept of a hkl-file. Contained within a hkl-file, is data which enables the sub-program TRCSCAL, to calculate an XRD pattern for a particular mineral. Data contained within a hkl-file includes values for the intensity

(F_C(hkl)), multiplicity (M), d-spacing and orientation a-angle for each hkl powder diffraction line. A task file is created which consists of a collection of hkl-files of minerals to be quantified in the observed XRD pattern.

4.3.3 Background subtraction

After loading an observed XRD pattern into *Siroquant*, removal of the background is required before applying the quantification process. The background of an XRD pattern is composed of the low-angle scattering curve, ambient radiation and scattering bands associated with amorphous and poorly diffracting material (Figure 4.5). Low angle scattering is represented by an intensity curve which asymptotically approaches, the ambient radiation level, as the 2θ angle becomes larger. When quantification of such material is required, it is advisable to subtract the scattering bands during the background removal procedure, otherwise the quantity of well-crystallized material may be over-calculated. An apparent increase in the background level may be caused by peak overlap. In such cases, care must be exercised to ensure that not too much background is removed, otherwise phases associated with the peak overlap may be under-calculated.

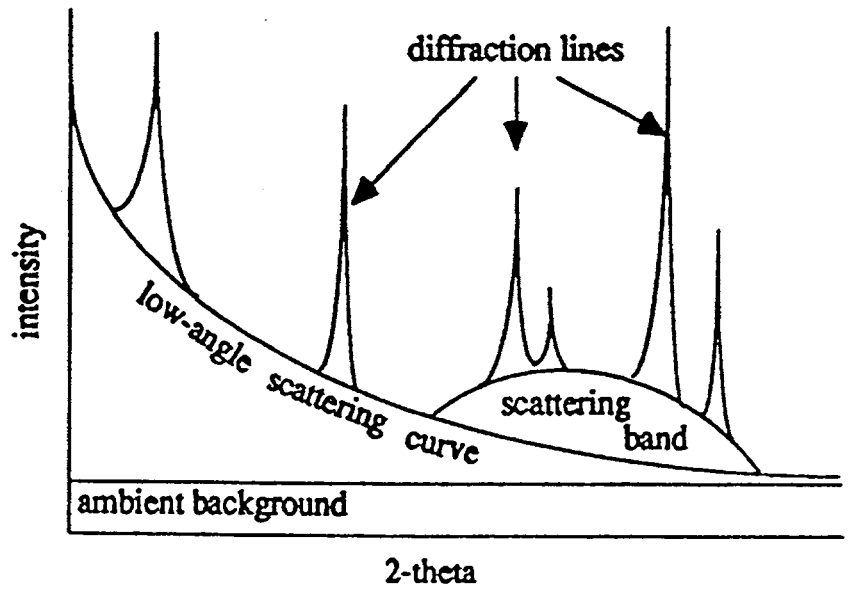

Figure 4.5. The background of an XRD pattern associated with amorphous and poorly diffracting material

Tilley (1996), analyzed mixtures of synthetically prepared gibbsite and boehmite to gauge the accuracy of the *Siroquant* program that has also been used in this study. The gibbsite he used was commercially made and sold under the name *Higilite* (grade H-43, mean particle size of 0.6μm and purity of 99.5%) and the boehmite by dehydrating gibbsite hydrothermally. The results showed a good correlation as in Figure 4.6.

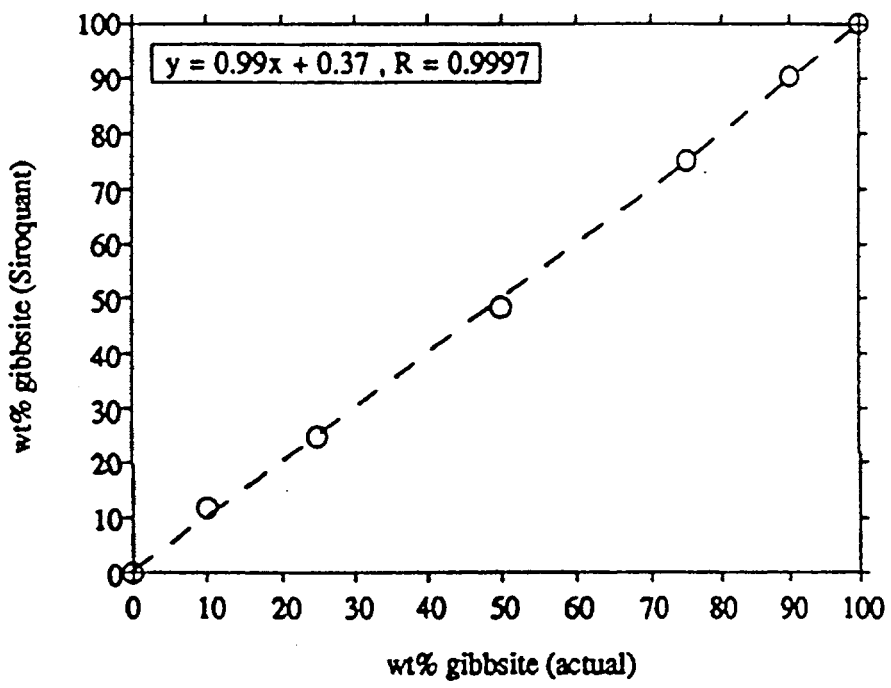

Figure 4.6 Correlation between the weight percent of gibbsite-boehmite mixture and that determined by Siroquant (Tilley, 1996).

4.4 Geochemistry

Instrumentation and methods

The samples to be analyzed geochemically were dried and powdered in a mechanical, tungsten-cobalt mortar and pestle. All the powdered samples were analyzed at the

Department of Geology, Australian National University (ANU) and the Australian Laboratory Services (ALS) in Orange. The major elements expressed as oxides, were analyzed at the ANU using X-ray Fluorescence (XRF). The description of the method has been provided by Potts (1987). The trace elements were analyzed using a combination of XRF at the ANU, and Inductively Coupled and Atomic Absorption Spectroscopy (AAS).

4.4.1 X-ray Fluorescence

Samples were analyzed on a PW1400 XRF spectrometer in the Geology Department, Australian National University. Major elements were determined using the method of Norrish and Hutton (1964) whilst trace elements were determined by procedures developed by Chappel (1991) and Norrish & Chappel (1977). All software algorithms used in converting X-ray intensities to concentrations were written by B. ChappelL.

4.4.2 Inductively Coupled Mass Spectrophotometer (ICP-MS)

Analysis was carried out under the propriety of Australian Laboratory Services (ALS) using two methods i.e. IC580 and PM204. The former was for Cu, Pb, Zn, Ag and As determination and the latter for Au analysis.

4.4.2.1 IC580.

The procedure used by ALS involved the weighing of 0.25g of sample into a disposable test tube and addition of 1ml of perchloric immediately afterwards. The solution was then placed on a sand bath at 220° C for 90 minutes, with shaking after 45 minutes. It was then allowed to cool after which 9 ml of distilled water was added. The tubes were then covered with cling wrap and foam-covered board. It was then shaken to mix and run on ICP.

4.4.2.2 PM204

This method involved the weighing of 30g of sample into a beaker and addition of 12.5ml of nitric acid. The solution was then allowed to stand to let any reaction subside. 40 ml of hydrochloric acid was then added, and the solution stirred and covered with watchglass. It was then digested on hotplate at 220° C for 2 hours with constant stirring. It was then allowed to cool and flocculant and water added to 100mls. 25mls of

supernatant liquid was then taken into a test tube and extracted into 10mls of MIBK (4-methyl 2-pentanone). The aqueous phase was then removed and the organic layer backwashed twice with acid solution. The organic phase was then analyzed by carbon rod (graphite furnace).

Table 4.1 shows the detection limits of the various analytical techniques employed in this study.

Element	Detection Limit	Analytical Technique	Analytical Labotatory
Rubidium (Rb)	0.5 ppm	XRF	ANU
Strontium (Sr)	0.5 ppm	XRF	ANU
Barium (Ba)	1.0 ppm	XRF	ANU
Zircon (Zr)	1.0 ppm	XRF	ANU
Niobium (Nb)	0.5 ppm	XRF	ANU
Yttrium (Y)	1.0 ppm	XRF	ANU
Lanthanum (La)	1.0 ppm?	XRF	ANU
Cerium (Ce)	1.0 ppm	XRF	ANU
Chromium	1.0 ppm	XRF	ANU
Nickel (Ni)	1.0 ppm	XRF	ANU
Copper (Cu)	1.0 ppm	XRF	ANU
Copper (Cu)	2.0 ppm	IC580	ALS
Zinc (Zn)	1.0 ppm	XRF	ANU
Zinc (Zn)	2.0 ppm	XRF	ANU
Arsenic (As)	1.0 ppm	XRF	ANU
Arsenic (As)	1.0 ppm	IC580	ALS
Silver (Ag)	1.0 ppm	XRF	ALS
Gold (Au)	0.001 ppm	PM204	ALS
Lead (Pb)	1.0 ppm	XRF	ANU
Lead (Pb)	5.0 ppm	IC580	ALS
Thorium (Th)	0.5 ppm	XRF	ANU
Uranium (U)	0.5 ppm	XRF	ANU
Gallium (Ga)	1.0 ppm	XRF	ANU
Scandium (Sc)	2.0 ppm	XRF	ANU
Vanadium (V)	1.0 ppm	XRF	ANU

Table 4.1. The analyzed trace elements, their respective lower limit of detection (LLD) and the analytical techniques used. XRF, X-ray Fluorescence, IC580: ANU: Australian National University; ALS: Australian Laboratory Services.

4.5 Quality of the geochemical data

4.5.1 Duplicate analysis

Duplicate analysis was performed to check the precision of the geochemical data. The major element XRF analysis was very precise, all analyses duplicated and 96% of these had duplication results within 1% of each other. Samples yielding duplicate results differing by more than 1% were re-analyzed.

There were notable differences between concentrations of elements from the XRF and ICP MS analysis as a result of the Lower Limits of Detection (LLD) using these methods (Table 4.1). Because of this, the ICP MS results for Au, Cu, Pb, As and Zn have been utilized and XRF for the rest of the elements.

4.6 Regolith sample selection

To determine the appropriate sample size for use when geochemically sampling regolith, the Centre for Australian Regolith Studies (CARS) group formulated a sub-project in regolith sample selection for initial sampling at Goonumbla (this study area) and Broken Hill

The scale of element concentration in the regolith (the nugget effect) and precise determination of the sites and surfaces where elements concentrate, is hard to determine in most field sampling situations. The strategy of this sub-project was to determine the scale of variation by taking a typical sample bagfull and analyzing subsamples. The samples were selected from different mottled horizons at the E27 deposit. The mottled zones were specifically selected because of the diverse nature of the composing materials i.e, white to grey clays, iron segregations, nodular aggregates etc.

4.6.1 Procedure

Each sample (approximately 2 kg) was split into two visually similar halves. One half was randomly sampled by taking the samples as collected and breaking it into several roughly equal sized portions. The sample was crushed to the sub-milimetre size and then split into quarters. Each quarter was determined for mineralogy using XRD, quantitative mineralogy by *Siroquant* and geochemistry by XRF. All the fourth quarters of each sub-sample were then blended from each of the individual sub-samples into the a fifth sub-sample. XRD and XRF was then performed again on the blended sample and the results compared. The procedure is shown in Figure 4.7.

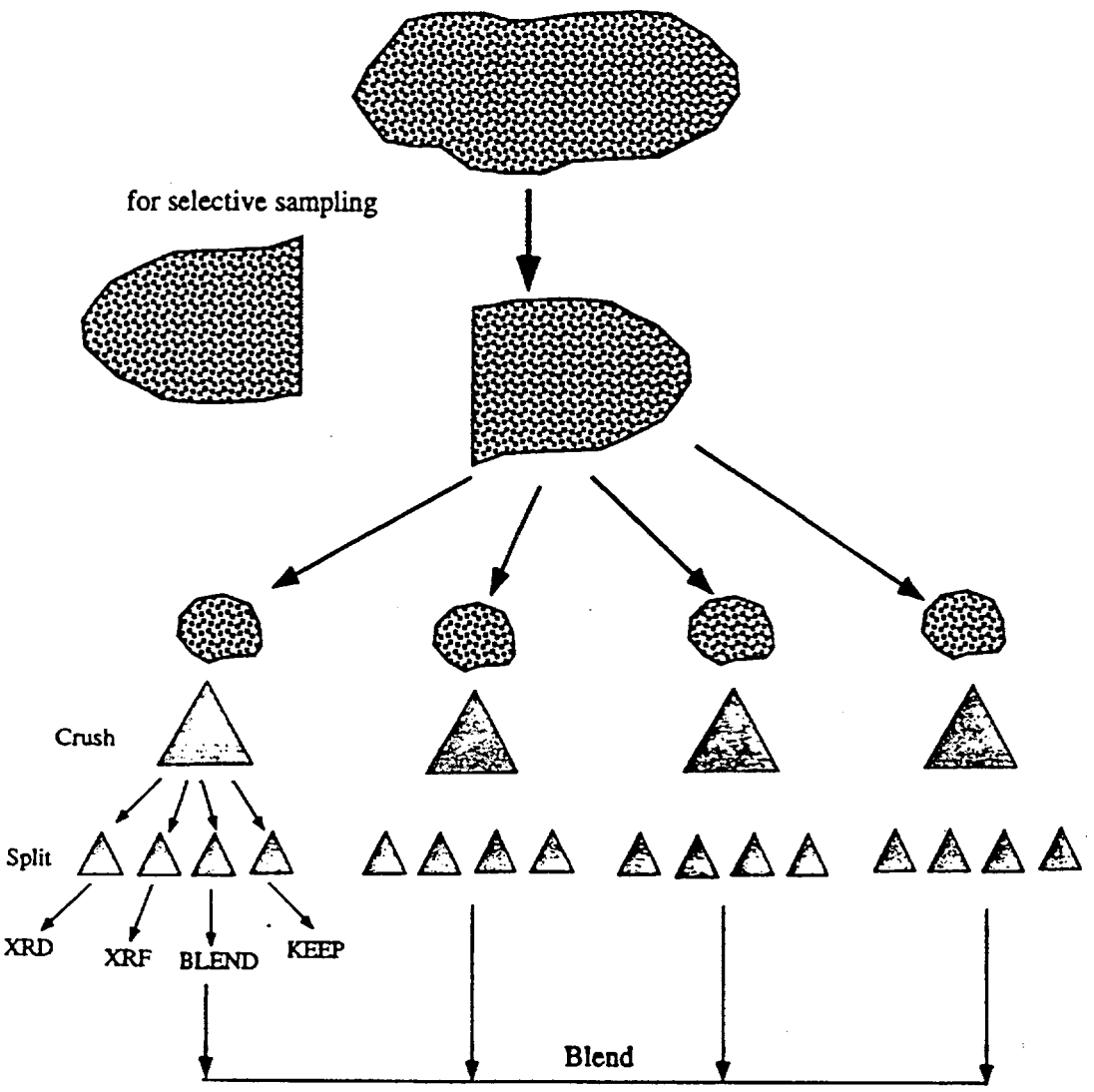

Figure 4.7: Procedure for regolith sample selection

4.6.2 RESULTS:

MINERALOGY

The mineralogical contents of the samples are presented in Table 4.2

Table 4.2a: Sample source: Mottled clay unit - E27 P6S5 (10m)

[All values in weight %]

SAMPLE	Quartz (%)	Kaolin (%)	Goethite (%)	Hematite (%)	Smectite (%)
Sample 1	16.9	65.5	9.1	6.4	2.1
Sample 2	14.0	68.9	8.4	5.3	1.8
Sample 3	15.2	70.1	8.4	6.1	0.2
Sample 4	14.2	66.4	8.6	8.1	2.8
Average	**15.1**	**67.7**	**8.6**	**6.5**	**1.7**
Blend	**17.0**	**66.4**	**7.8**	**6.0**	**2.7**

Table 4.2b: Sample source - Mottled clay unit-E27 P5S5 (8m)

[All values in weight%]

SAMPLE	Quartz	Kaolin	Goethite	Hematite	Smectite
Sample 1	20.5	61.9	1.5	5.6	10.5
Sample 2	19.2	53.3	3.9	9.4	14.3
Sample 3	12.6	67.4	4.1	7	8.9
Sample 4	18.5	58.7	2.3	8.1	12.4
Average	**17.7**	**60.3**	**2.9**	**7.5**	**11.5**
Blend	**16.6**	**64.2**	**2.7**	**7.4**	**9.1**

Table 4.2c: Sample source - Zone of incipient development of mottling in clay- E27 P4S3 (5m) [all values in weight %]

SAMPLE	Quartz	Kaolin	Goethite	Hematite	Smectite	Albite
Sample 1	25.6	49.7	8.1	4.6	4.1	7.9
Sample 2	26.8	48.1	7.1	5.4	4.1	8.5
Sample 3	28.9	52.2	5.5	3.6	3.3	6.5
Sample 4	23.8	49.6	6.2	6.9	4.5	8.1
Average	**26.3**	**49.9**	**6.7**	**5.1**	**4.0**	**7.8**
Blend	**24.8**	**49.5**	**5.6**	**6.9**	**4.5**	**8.7**

Tables 4.2a, b and c: The mineralogical contents of mottled clay samples [P-Profile; S1-Sample 1; 8 m-depth]

GEOCHEMISTRY

Major elements

Table 4.3a: Sample source: Mottled clay unit - E27 P6S5 (10m)

OXIDE	SiO_2	TiO_2	Al_2O_3	Fe_2O_3	MnO	MgO	CaO	Na_2O	K_2O	P_2O_5	S
Sample 1	53.45	1.41	19.3	12.12	0.02	0.66	0.12	0.61	0.17	0.04	0.1
Sample 2	53.71	1.38	18.87	12.49	0.02	0.68	0.13	0.62	0.19	0.04	0.1
Sample 3	56.59	1.45	20.43	8.15	0.01	0.70	0.13	0.61	0.19	0.03	0.1
Sample 4	55.12	1.41	18.81	11.59	0.02	0.64	0.12	0.63	0.20	0.04	0.1
Average	**54.72**	**1.41**	**19.35**	**11.09**	**0.018**	**0.67**	**0.13**	**0.62**	**0.19**	**0.038**	**0.1**
Blend	**54.43**	**1.41**	**19.19**	**11.25**	**0.02**	**0.63**	**0.12**	**0.64**	**0.19**	**0.04**	**0.1**

[All values in weight %]

Table 4.3b: Sample source - Mottled clay unit-E27 P5S5 (8m)

OXIDE	SiO_2	TiO_2	Al_2O_3	Fe_2O_3	MnO	MgO	CaO	Na_2O	K_2O	P_2O_5	S
Sample 1	49.22	1.33	24.76	8.43	0.01	0.58	0.16	0.32	0.15	0.03	0.1
Sample 2	48.19	1.27	24.21	10.77	0.01	0.55	0.13	0.32	0.12	0.03	0.1
Sample 3	46.44	1.23	23.68	12.59	0.01	0.54	0.13	0.29	0.13	0.04	0.1
Sample 4	44.11	1.23	22.62	16.07	0.01	0.50	0.12	0.31	0.12	0.04	0.1
Average	**45**	**1.26**	**23.82**	**11.97**	**0.01**	**0.54**	**0.135**	**0.31**	**0.13**	**0.035**	**0.1**
Blend	**46.8**	**1.26**	**23.82**	**12.05**	**0.01**	**0.53**	**0.13**	**0.30**	**0.13**	**0.04**	**0.1**

[All values in weight %]

Table 4.3c: Sample source - Zone of incipient development of mottling in clay- E27 P4S3 (5m)

OXIDE	SiO_2	TiO_2	Al_2O_3	Fe_2O_3	MnO	MgO	CaO	Na_2O	K_2O	P_2O_5	S
Sample 1	51.4	1.13	19.35	12.19	0.02	0.78	0.35	0.33	0.25	0.03	0.0
Sample 2	49.2	1.38	24.88	8.15	0.01	0.59	0.31	0.22	0.15	0.03	0.0
Sample 3	50.44	1.16	20.58	12.24	0.02	0.74	0.35	0.31	0.21	0.03	0.0
Sample 4	46.91	1.43	26.24	8.9	0.01	0.57	0.28	0.28	0.09	0.03	0.0
Average	**49.50**	**1.28**	**22.80**	**10.4**	**0.015**	**0.67**	**0.33**	**0.29**	**0.18**	**0.03**	**0.05**
Blend	**49.06**	**1.30**	**23.34**	**9.91**	**0.01**	**0.70**	**0.32**	**0.27**	**0.17**	**0.03**	**0.0**

[All values in weight %]

Tables 4.3 a, b and c: The major element chemistry of the mottled clay samples [P-Profile; S1-Sample 1; 8 m-depth]

Trace elements

Table 4.4a: Sample source: Mottled clay unit - E27 P6S5 (10m)

Sample	Cr	Mn	Ni	Cu	Zn	Ga	As	Rb	Sr	Zr	Nb
Sample 1	32	155	8	134	96	21	14	10	111	10	12
Sample 2	32	145	8	116	86	21	16	12	107	10	10
Sample 3	36	115	8	102	82	22	9	12	111	10	12
Sample 4	32	140	8	116	86	21	13	13	116	10	12
Average	**33**	**138.8**	**8**	**117**	**87.5**	**21.3**	**13**	**11.8**	**111.3**	**10**	**11.5**
Blend	**32**	**140**	**10**	**122**	**88**	**21**	**14**	**14**	**112**	**10**	**12**

[All values in ppm]

Table 4.4b: Sample source - Mottled clay unit-E27 P5S5 (8m)

Sample	Cr	Mn	Ni	Cu	Zn	Ga	As	Rb	Sr	Zr	Nb
Sample 1	40	60	10	216	28	29	8	11	73	198	10
Sample 2	42	65	8	256	30	28	11	8	69	188	10
Sample 3	34	80	10	256	34	28	12	10	66	184	10
Sample 4	32	70	10	250	30	28	14	8	71	180	8
Average	**37**	**68.8**	**9.5**	**244.5**	**30.5**	**28.3**	**11.3**	**9.3**	**69.8**	**187.5**	**9.5**
Blend	**34**	**70**	**8**	**248**	**30**	**29**	**12**	**10**	**67**	**182**	**10**

[All values in ppm]

Table 4.4c: Sample source - Zone of incipient development of mottling in clay- E27 P4S3 (5m)

Sample	Cr	Mn	Ni	Cu	Zn	Ga	As	Rb	Sr	Zr	Nb
Sample 1	46	165	12	282	40	23	13	17	124	226	10
Sample 2	30	90	8	260	24	29	6	11	96	202	12
Sample 3	38	25	12	276	36	25	11	15	122	216	10
Sample 4	48	65	10	336	20	32	8	8	78	194	12
Average	**40.5**	**86.3**	**10.5**	**288.5**	**30**	**27.3**	**9.5**	**12.8**	**105**	**209.5**	**11**
Blend	**40**	**100**	**10**	**292**	**28**	**28**	**8**	**12**	**105**	**206**	**10**

[All values in ppm]

Tables 4.4 a, b and c: Trace element chemistry of the mottled clay samples [P-Profile; S1-Sample 1; 8 m-depth]

4.7 DISCUSSION

4.7.1 Mineralogy

The samples from the mottled clay zones exhibit similar mineralogical distributions, the only differences occurring in the abundance of these minerals. The zone of incipient of mottling is the zone below the soil 'B' horizon where the mottles are starting to form in the clay groundmass. Albite is a constituent mineral of the host trachyandesite and its present in this sample as a detrital constituent.

The mottled clay sample E27 P6S5 (10 m) shows minor differences in the distribution of smectite and quartz than the rest of the minerals as depicted by the average values compared with those of the blended samples. Notable differences did not exist in the other mottled clay sample E27 P5S5 (8 m). Minor differences exist in the amounts of smectite and kaolin in this sample. The samples from the zone of incipient mottling on the other hand shows minor differences in the distribution of quartz and hematite as compared to the other minerals.

In general, these variations were less than the *Siroquant* error. The results also demonstrate that the variation between horizons was significantly greater than the sum of variations within horizons and analytical errors. These disparities can be regarded as minimal especially in this project where the emphasis was on the study of the trends in profile mineralogy rather than in absolute mineral percentage values.

4.7.2. Geochemistry

4.7.3 Major elements

The major oxides, Fe_2O_3, SiO_2 and Al_2O_3 exhibit minor differences in distribution compared to the other elements for most of the samples. Fe_2O_3 is the most affected as exemplified by sample E27 P5S5 (8 m) with the highest and lowest values being 16.07% and 8.43% Fe_2O_3 respectively. The average value of the split samples (11.97%) almost equals that of the blend (12.05%). The same case is true of SiO_2 distribution as in sample E27 P5S5 (8 m) where the highest value is 49.22% and the lowest 44.11%. The average value is 45% while that of the blend is 46.8%. Al_2O_3 from the zone of incipient development of mottling shows the highest and lowest values of 26.24% and 19.35%

respectively. The average and blend values are 19.35% and 19.19% respectively. The values of the other samples did not show any major variation. TiO_2 on the other hand showed similar average and blend values samples E27 P6S5 (10 m) and E27 P5S5 (8 m) while sample E27 P4S3 (5 m) showed the highest and lowest values of 1.43% and 1.13% respectively. The average value of 1.28% almost approximates that of the blend (1.30%).

The other major oxides do not show marked differences in either the values of the split samples, the average and the blend. The differences in the distribution of Fe_2O_3, SiO_2 and Al_2O_3 is dictated by the site and nature of iron segregation within the sample. The nodular portion is expected to contain more Fe_2O_3 relative to the other elements than the non-nodular clay rich portion depending on which part of the sample the split is taken from. The clay rich portion is expected to contain more Al_2O_3 and SiO_2 and less Fe_2O_3 since these elements make up the kaolin structure. In selecting the ultimate sample for analysis, care should be taken to ensure that an homogeneously blended sample from all these portions is presented.

4.7.4 Trace elements

The trace elements, Cu, Mn and Ba show appreciable differences in the values of the split samples although the values of the average and the blend do not differ markedly. The highest value of Cu in sample E27 P4S3 (5 m) for example is 336 ppm compared to the lowest value of 260 ppm. The average and blend values for the same sample is 288.5 ppm and 292 ppm respectively. Mn in the same sample has the highest and lowest values of 165 ppm and 65 ppm respectively. The values of these elements in the other samples do not differ markedly although the disparities are much higher compared to those of the other samples. The most affected element is Ba where the disparity between the average and blend is as much as 61.2 ppm as in sample E27 P6S5 (10 m).

To explain these differences, one has to determine the host minerals which tend to concentrate these elements by selectively leaching the various constituents. It is not considered necessary to cover this aspect at this stage since this topic is comprehensively discussed in the latter part of this text where similar samples as the ones used in this sub-project were utilized.

4.7.5 Conclusions

Effective interpretation of geochemical data relies heavily on proper sampling and sample preparation procedures. As this study shows, one has to selectively ensure that an homogeneously prepared sample is ultimately presented for geochemical analysis because the process of presenting sub-samples, which could partly solve the problem, is both expensive and tedious.

The results of this study proved to be invaluable in the follow up systematic sampling program. To ensure this homogeneity, each representative portion of the sample was crushed and blended and the ultimate sample presented for analysis. As the study showed, the average and blend values do not differ markedly in most of the analyzed samples whereas the sub samples showed some 'nugget effect'. Because of these differences, it is recommended that a 500 g of the bulk sample should at least be utilized for geochemical determinations in the regolith of this type.

4.8 Mineralogical sample preparation techniques

4.8.1 Quality control experiment

During the initial stage of the project, the main sample preparation technique involved the milling of a bulk sample with an agate mortar and pestle with acetone until a grain size <10 μm was achieved. The sample was then coated on a glass slide and allowed to dry before analysis. Almost halfway through this project, a new technique involving the side packing of pre-crushed powdered sample into a U-shaped aluminium holder (the sample being held in place during preparation by a frosted glass) was adopted by the Centre for Australian Regolith Studies.

To ensure that this change in sample preparation technique did not significantly affect the quantitative mineralogy results, samples of soil 'B2' horizon, mottled clay, iron nodules, saprolite and the fresh rock by XRD were prepared using the two methods and the results quantitatively analyzed by "*Siroquant*". The results are shown in Table 4.5.
The observed XRD peaks of some of these samples are shown in the Figure 4.8.

4.8.2 Conclusions

The results show that the differences between the two techniques are less than the *Siroquant* error though minor differences exist mainly in the amounts of feldspars, muscovite and kaolin as compared to the other minerals. Kaolin and quartz contents for example are higher in the smear than in the side packed sample though in general the results of analyses are method independent.

The side packing powder preparation technique is preferred to the smear technique because it results in random orientation of crystals in the ray beams. Though *Siroquant*t can correct for preferred orientation, it is always better to eliminate such systematic variation before analyses, rather than correct for it after. Refinement of feldspars and clays often presents problems because of the complex nature of the structures of these minerals and the numerous solid solution phases present in each of these mineral species.

Sample	Method	Kaol	Qtz	Hem	Goe	Smc	Alb	Orth	Mus	Calc	Chl.	Dps	Hrn
Soil	Smear	28.9	40.6	3.2	0.3	14.9	9.8			2.4			
[E27 P6S3]	Powder	30.1	39.1	2.9	0.5	15.4	8.9			3.1			
Mottled clay	Smear	47.1	9.9	14.9	28.1								
[E27 P6S4]	Powder	49.1	9.3	12.5	29.1								
Iron nodules	Smear	66.3	11.6	0.3	21.8								
[E22 MGN 1]	Powder	68.5	11.1	0.5	19.9								
Saprolite	Smear	39.0	1.3	0.8	0.3	8.0	7.5	20.6	22.2				
[E27 P4S20]	Powder	40.2	1.4	0.7	0.2	8.2	6.3	23.6	19.0				
Fresh rock	Smear				3.6		52.9	11.1	15.0		8.4	7.2	1.9
[E27 P5S25]	Powder				1.5		55.3	10.1	14.4		6.3	8.4	4.0

Table 4.5. Quantitative mineralogy results of smeared and powder prepared samples of soil, mottled clay, iron nodules, saprolite and fresh rock. [Kaol=kaolin; Qtz=Quartz; Hem=Hematite; Goe=Goethite; Alb=Albite; Orth=Orthoclase; Musc=Muscovite; Calc=Calcite; Chl=Chlorite; Dps=Diopside and Hrn=Hornblende].

The use of the smear method can result in minor loss of random orientation of the crystals. However, as the results show this did not in any way significantly affect the weight percentages of the respective mineral species. As the major purpose of quantifying these minerals was to decipher trends in mineral distribution along the

regolith profiles, the results of this experiment more than qualified the use of either method to achieve this aim.

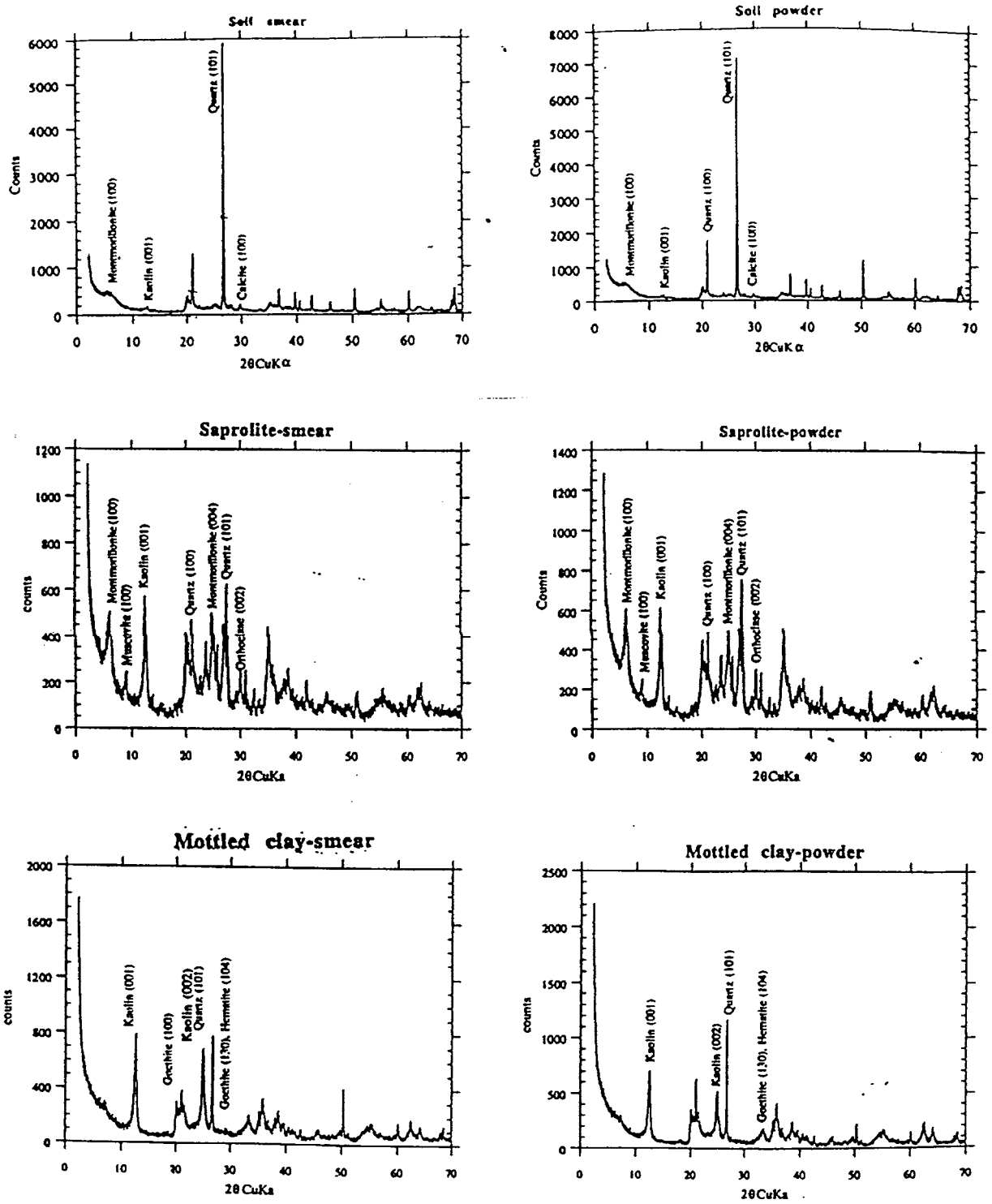

Figure 4.8: XRD peaks of smeared and powder samples from the soil, mottled clay and saprolite zones

PART 2

.Regolith features of the deposits

.Regolith mineralogy: Description and paragenetic sequences

.Regolith mineralogy: Origin and distribution of products

CHAPTER 5

REGOLITH FEATURES OF E22 AND E27 DEPOSITS

5.1 Introduction

Primary mineralisation at the E22 and E27 deposits is overlain by deeply weathered regolith. The depths of weathering in the two deposits are variable. In E22 the weathering front occurs at a depth of 20-25 m to the west and 45-50 m in the more weathered sections to the east (Figure 5.1). In E27 it occurs at depths of 10-20 m in the least weathered sections to the west and 50-60 m in the more weathered sections to the east (Figure 5.2).

The two deposits exhibit similar regolith features as shown in Figures 5.1 and 5.2. Notable differences occur in the depths and positions in which these features occur in the regolith stratigraphy. The principal profiles are shown in Figures 5.3 and 5.4.

5.2 REGOLITH DISTRIBUTION

The principal regolith units are described below. The regolith units have been given informal codes for identification in figures, tables and the data listings.

5.2.1 Soil horizons

The depth of the soil horizon varies from 0-200 cm in the shallow weathered sections to the west of the open pit to 0-350 cm in the more deeply weathered parts to the east. The soils from the two locations exhibit minor characteristic differences that arise because they have originated from different parent materials. The soils from the shallow weathered section have been derived from the weathering of the host trachyandesite whereas the ones from the more deeply weathered section have been derived from weathering of initially transported alluvial and colluvial sediments. These regolith materials will be described later in the text.

The main horizons for the soil situated on the shallow weathered section to the west of the open pits are:

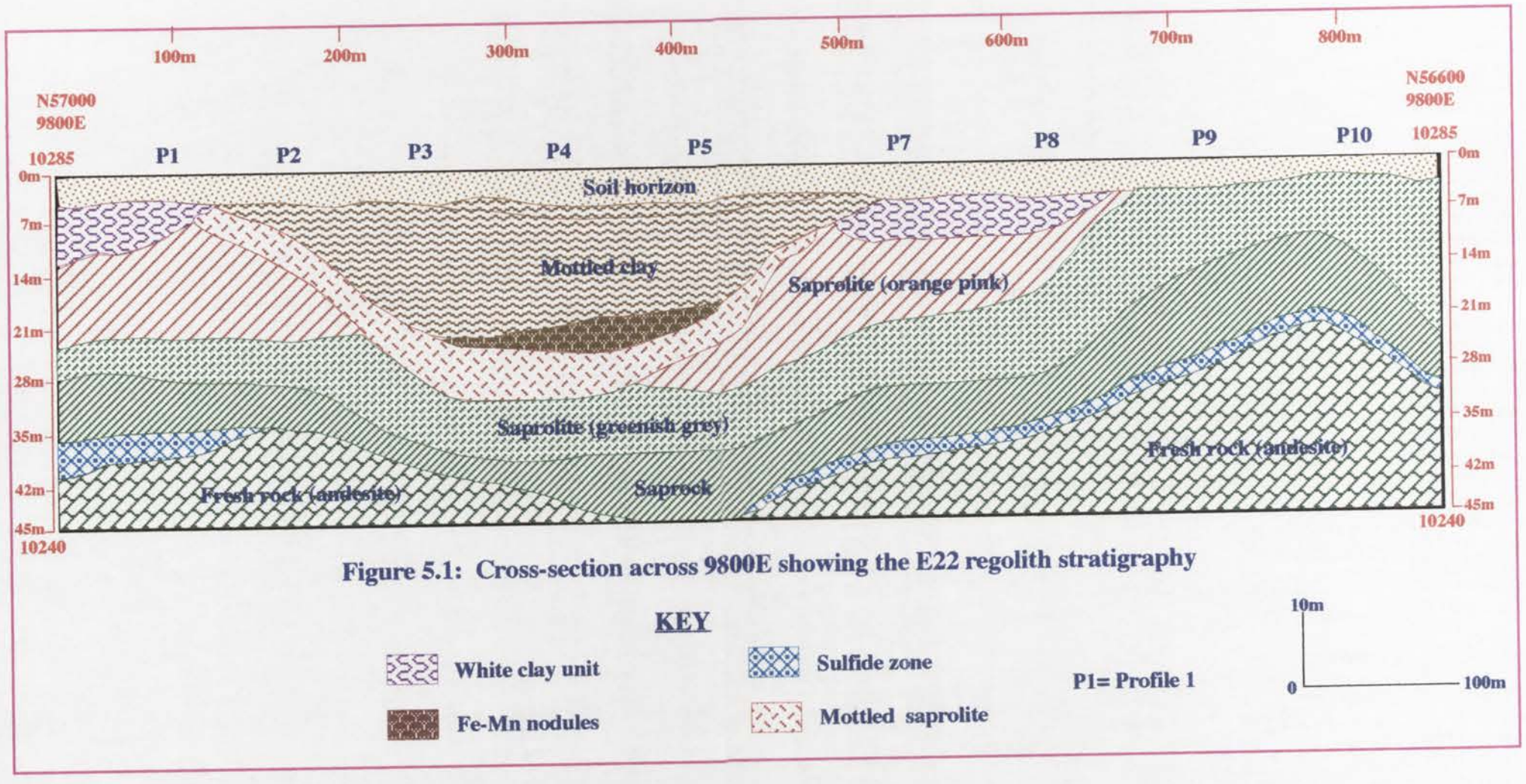

Figure 5.1: Cross-section across 9800E showing the E22 regolith stratigraphy

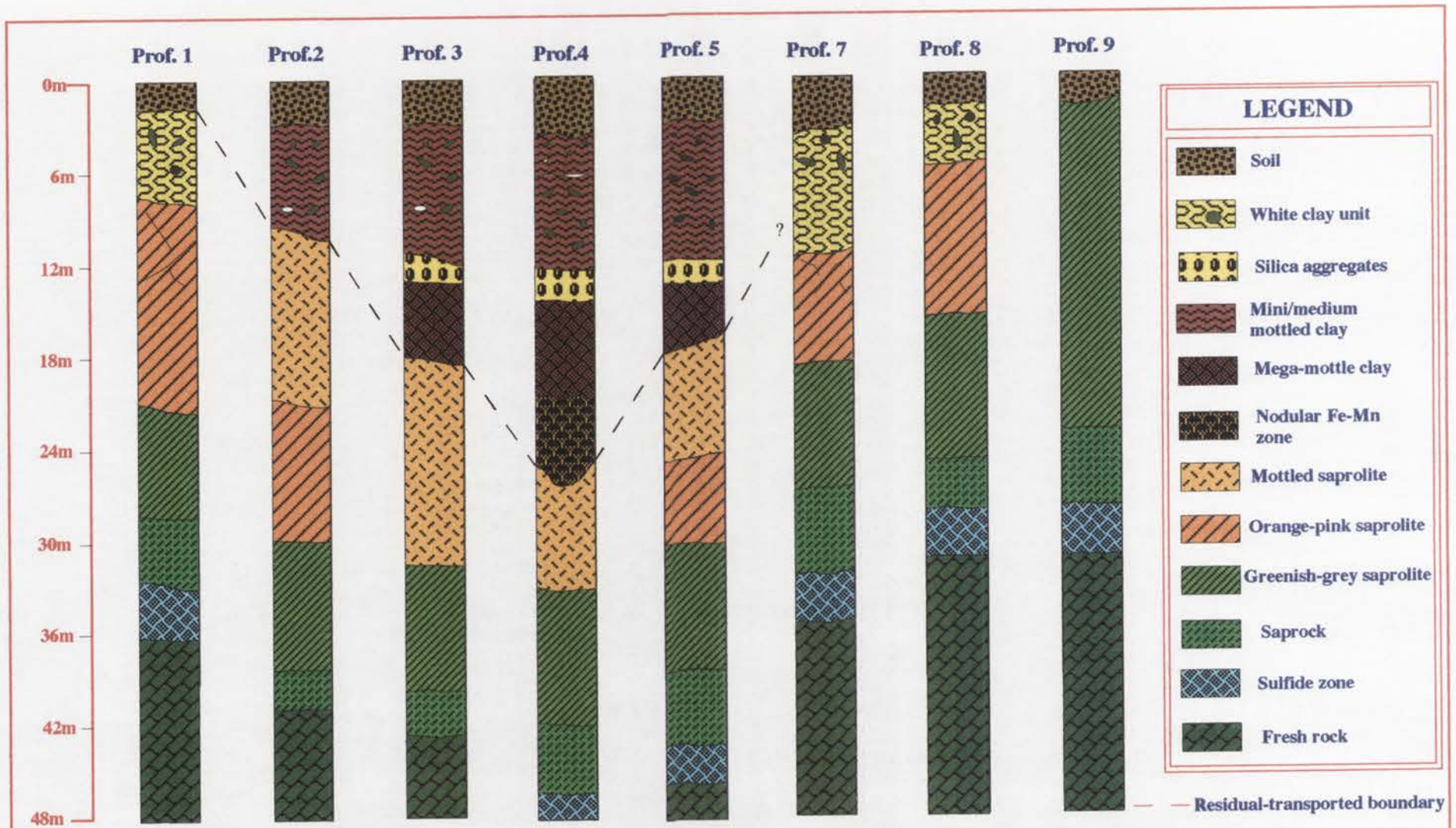

Figure 5.3: W-E Cross section along line 9980E showing the major profiles of the E22 deposit

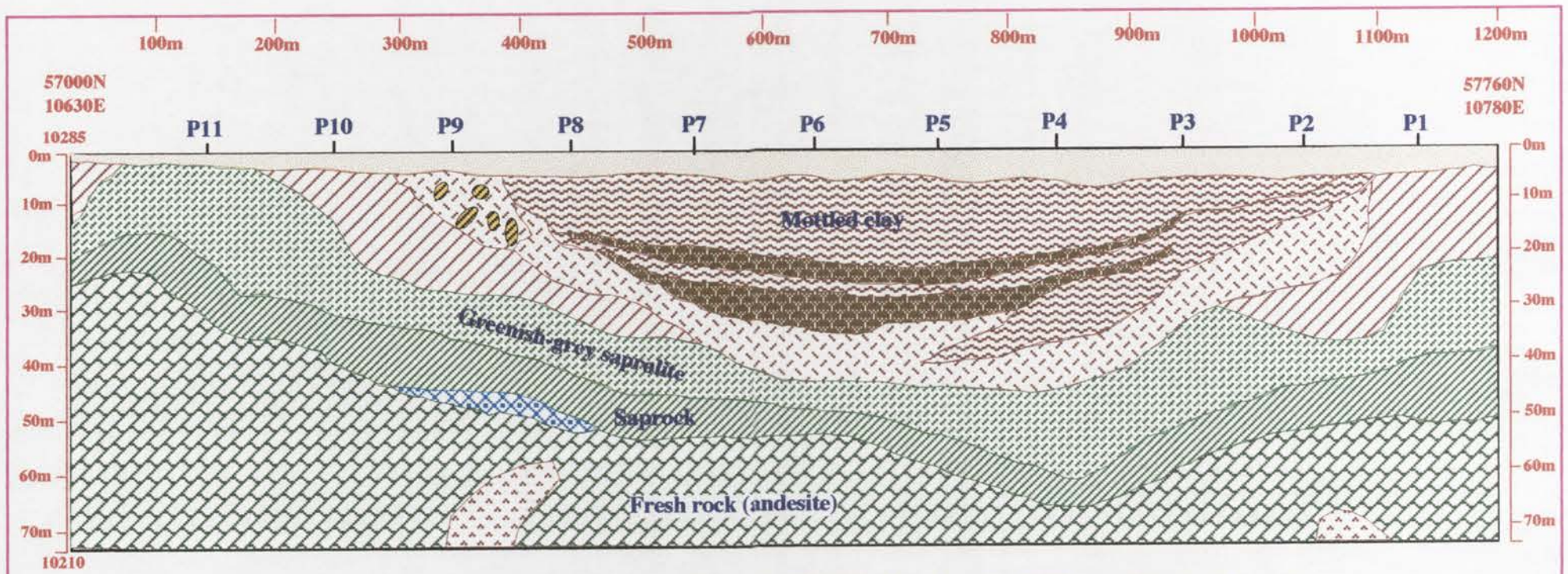

Figure 5.2: Cross section across 10630 and 10780E showing the E27 regolith stratigraphy

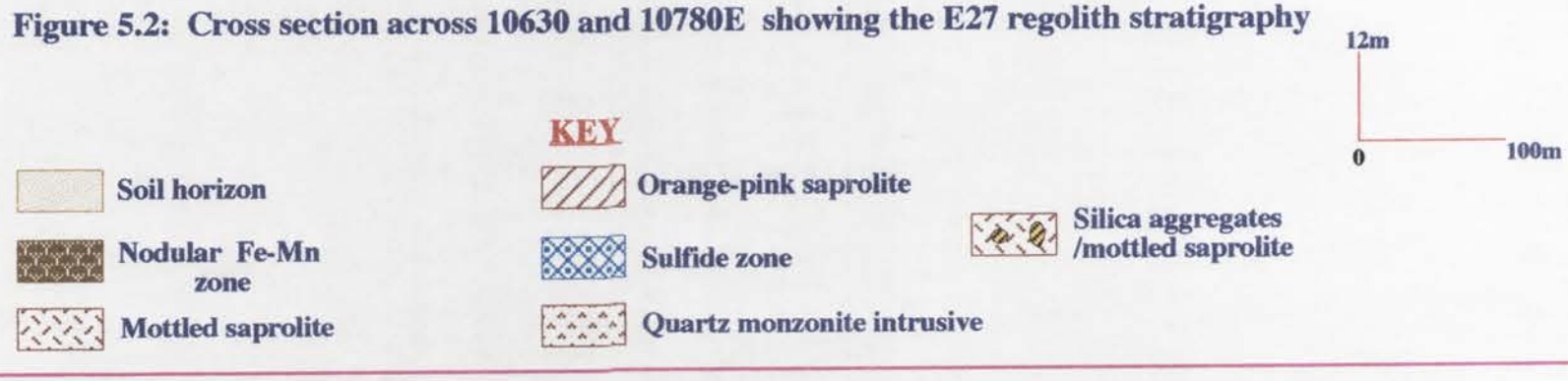

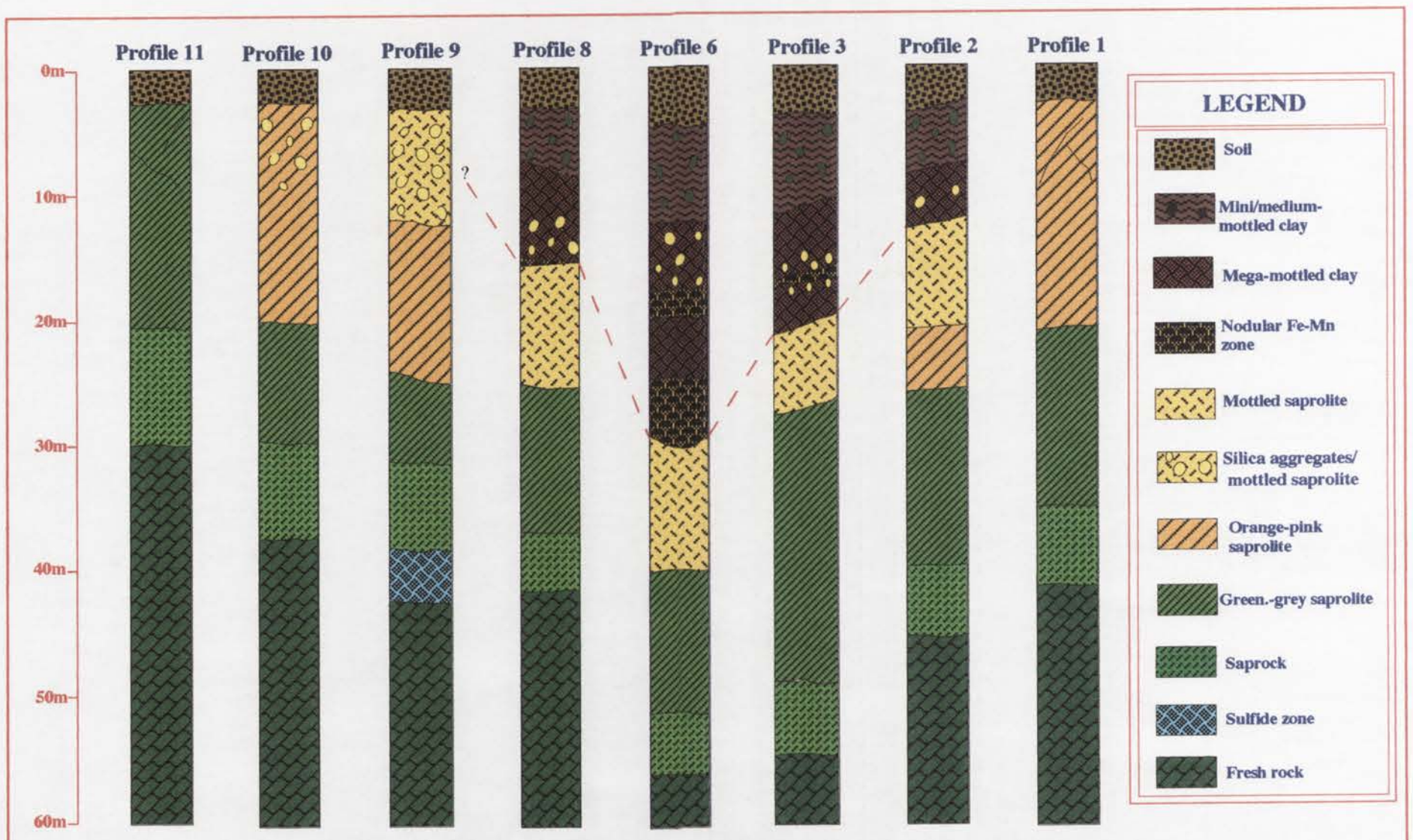

Figure 5.4: West-East cross section across the E27 deposit (along 10850E grid line) showing the major regolith profiles.

0-100 cm. Soil 'A'horizon: Dark reddish brown (2.5 YR 3/3) soil with high contents of clay and organic matter. Quartz occurs as small rounded to subrounded detrital fragments 5-10 mm in size. Carbonates when present occur as thin veneers or as friable creamy yellow to white aggregates in fine earth matrix. Gypsum occurs in moderate amounts as transparent to near transparent crystals 5 to 10 mm in size. The pH of the soil varies from 6 to 7.5.

100-200 cm. Soil 'B' horizon. Red (2.5 YR 4/6) to dark reddish grey (5 YR 4/2) clay loams. The zone is marked by an increase in the amounts of carbonate, which still occur as friable, creamy to yellow to white aggregates. Gypsum is present in very low amounts. The pH varies from 5 to 6.5.

This soil type is mainly composed of quartz, kaolin, smectite, muscovite, orthoclase, albite, gypsum goethite and rarely hematite.

The main horizons for the soil situated on the more deeply weathered section to the east are:

0-100cm. Soil 'A' horizon: Reddish brown (2.5 YR 5/4), clay and organic rich soil. Carbonate is present in the lower levels of this horizon (80-100 cm) where the pH is between 8 and 9. It occurs in moderate amounts as soft, creamy white to yellow masses in fine earth matrix. It imparts a yellow-white (dusty) appearance to dry soil. Gypsum is present in very low amounts as transparent or near-white crystals ranging in size from 2-6 mm while quartz occurs as small rounded to subrounded detrital fragments 5-10 mm in size. Manganese segregations may also be present as diffuse, hard small nodules within matrix. The pH varies from 6 in the upper levels of this subhorizon to 9 in the lower levels. Overall depth varies from 50-150 cm.

100-250 cm. Soil 'B1' horizon: Reddish brown (5YR 5/4) to yellowish red (5 YR 5/6) clay rich loams. This horizon is marked by an increase in clay and gypsum content. The carbonate content is less than in the horizon above. Kaolin imparts a characteristic whitish grey to brown colour to the soil matrix. The pH varies from 7 to 8.5.

250-350 cm. Soil 'B2' horizon: Red (2.5YR 4/6) to dark reddish grey (5 YR 4/2) clay and iron oxide rich loams. The iron oxide occurs as diffuse impregnations within the soil matrix. Gypsum is still present in very low amounts within this soil while the carbonates are absent. The transition zone with the mottled zone below is both irregular and

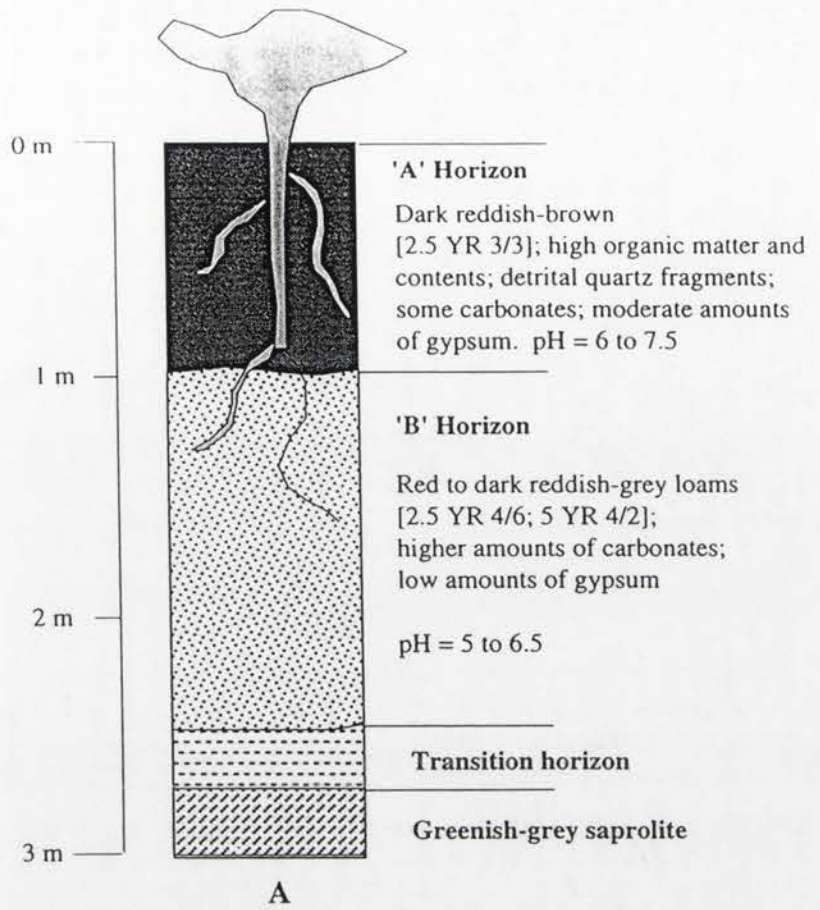

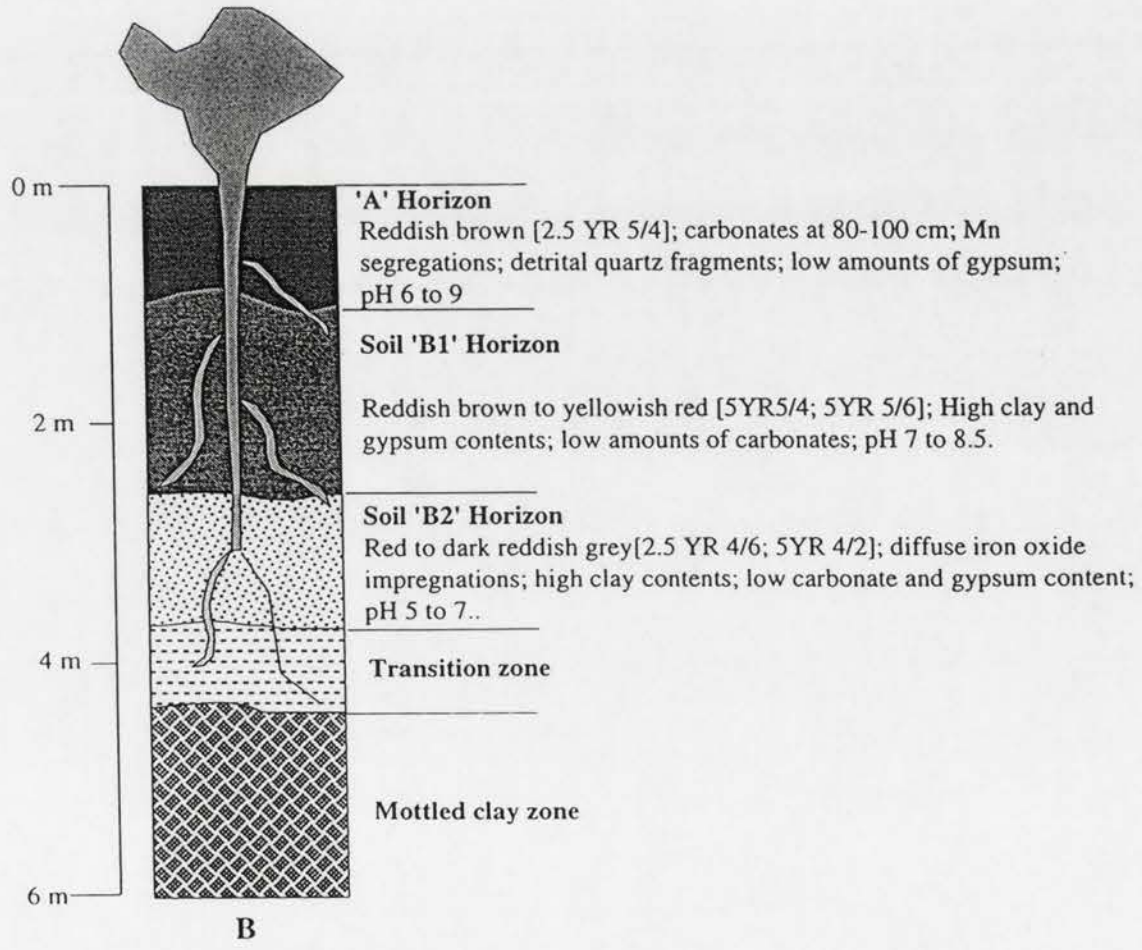

Figures 5.5: The two different types of soils at the Goonumbla deposits; [a] developed at the least weathered section over the trachyandesite and [b] developed at the more deeply weathered section over initially transported weathered sediments.

undulating and can reach 400 cm in some parts (Figures 5.1 and 5.3). The pH varies from 5 to 7.

The mineralogy of this soil is dominated by kaolin, quartz, gypsum, smectite, calcite, dolomite, goethite and hematite. The high contents of detrital quartz fragments in the soil 'A' horizon suggests that this part of the soil has formed from recently transported materials while the B1 and B2 horizons have developed from the underlying residium. Figures 5.5 shows the major characteristics of the two soil types.

5.2.2 Mottled clay units

This zone occurs between the soil and the saprolite. It consists of whitish grey to pale green-grey to pink clays strongly coloured by iron oxides. The iron oxides can occur as diffuse impregnations within the clay matrix or as secondary structures such as rounded to subrounded nodules and aggregates.

Three different types of mottles are encountered in both E22 and E27 and they have been subdivided on the basis of size of iron accumulations into mini, medium and mega-mottles (Table 5.1). The mini-mottled clay zone is the zone marking the incipient development of mottling in the clay. It is generally 1 to 2 m in depth, reddish grey to reddish brown (5YR 4/2; N 8/0) in colour and is composed of small (< 5 mm) rounded to sub-rounded iron oxide nodules. The nodules are dark silvery red (7.5 R 4/4) to reddish grey (7.5 R 4/1) or yellowish gray (2.5 Y 5/4) in colour and exhibit a sub-metallic lustre. The matrix is mainly composed of a light grey (7.5 Y 8/1) to whitish grey (N 8/0) kaolin rich clay. Mineralogically, it contains kaolin, quartz, hematite, goethite and smectite.

The medium sized mottles are reddish brown (5 YR 3/4) to reddish gray (2.5 YR 6/1) in colour. The depth is variable and locally it can extend from 4 to 6 m. The zone is characterized by the presence of metallic red to yellowish gray (2.5 Y 5/4) to brown (2.5 Y 7/6) rounded to sub-rounded nodules 5 to 30 mm in size. The matrix is mainly composed of light gray (7.5 Y 8/1) to whitish grey (N 8/0) kaolin-rich clay. One characteristic that differentiates this sub-zone from the others is its columnar crack parting structures between the clay rich and iron rich portions (Plates 5.2a and 5.2b). These partings have been locally infilled by massive (>50 mm) kaolin rich clays along what appears to be old root channels. These partings must have facilitated rapid access of

solutions, which resulted in local-scale migration, and accumulation of iron oxides that form the mottles.

Subdivision	Size of mottles	Mineralogical composition	Colour
Mini-mottled clay	2 - 5 mm	Kaolin, hematite, quartz and goethite	Reddish to reddish brown [5YR 4/2; N 8/0]
Medium-mottled clay	5 - 30 mm	Kaolin, hematite quartz and goethite	Reddish brown to grey [5YR 3/4; N 8/0]
Mega-mottled clay	50 - 300 mm	Kaolin, quartz, hematite, goethite and dolomite	Brown to reddish grey [5YR 4/4; N 8/0]
MEDIUM-MOTTLES (Fabric)		MEGA-MOTTLES (Fabric)	

Table 5.1. Types, size, mineralogy and the dominant colours of the subdivisions of the mottled clay zone.

The mega-mottles are brown (10 YR 4/6) to reddish gray (2.5 YR 6/1) to brown (5YR 4/4) irregular iron accumulations 50-300 mm in size. The mottles have a dull earthy lustre and an irregular to an abrupt boundary with the surrounding clay (Plates 5.4a and b). Root systems although not as columnar as in the medium sized mottles are also present. Large shrinkage cracks are still evident within the dense and massive clays. The clays are highly bleached (iron deficient) and can be light gray (2.5 Y 8/1) to pink in colour. Magnetic, black ferruginous granules are also present. The depth of this sub-zone is generally 5 to 10m. The mineralogy is dominated by kaolin, quartz, hematite, goethite, smectite and dolomite.

5.2.3 Silica aggregates (Sa)

The upper contact of the mega-mottled zone in contact with medium-mottles at the E22 deposit is marked by the presence of a narrow band (2-4 m) of opaline silica-rich-carbonate-coated aggregates. These aggregates are present in E27 at the margins of the mottled clay zones in transition with the mottled saprolite (Figure 5.2). They are sub-angular to angular and elongate in shape with lengths varying from 20 to 50 mm (plates

5.3a and 5.3b). The matrix is composed of whitish grey (7.5 YR 7/2) kaolin-rich clays. The carbonate coating is predominantly dolomite. The dolomite can also occur as sugary white masses in the transitional zone between the medium and mega-mottles (Plate 5.3b). In E27, the opaline silica aggregates are present within the kaolin rich portions of the mega-mottles, as independent angular aggregates or as white friable masses (< 5 mm) within the clay matrix.

Mineralogically, the silica aggregates contain quartz, dolomite, kaolin and smectite.

5.2.4 Nodular iron-manganese aggregates

This zone is transitional between the mottled zone and the saprolite in the more deeply weathered portion to the east of the open pits (Figures 5.1 and 5.2). It is 5 to 7 m in depth and is characterized by rounded to sub-rounded nodules which range in size from 5 to 300 mm. They are stained dark (Plates 5.5 a &b) because of their high content of poorly crystalline manganese oxides. The matrix is composed of greenish-grey to pale-pink kaolin rich clays. Rounded to sub-rounded detrital quartz fragments or pebbles are also common within the matrix.

Micromorphological studies show that the nodules are goethite rich and the manganese occurs as a coating which is gradually replacing goethite within the matrix. These manganese aggregates are poorly diffracting on X-ray diffraction because of their amorphous nature but XRD step scanning and SEM EDXA probe analysis shows it to be a mixture of hollandite and lithiophorite. The results of these studies are reported in Chapter 6.

These nodules consist of quartz (5-15%), goethite (30-50%), hematite (10-30%), kaolin (25-50%) and poorly diffracting material (PDM) contents of between 10 to 15%.

5.2.5 White clay unit (Wcu)

This restricted regolith unit occurs on the flanks of the mottled zones directly above the orange pink saprolite (Plates 5.7 a & b). It consists of white, light gray (N 8/0) to yellowish white (7.5 YR 8/1; 7.5 YR 7/1), massively bleached clays, commonly with mesoscopically homogenous clay fabric. Incipient nodular structures composed of goethite, kaolin and quartz sporadically occur within the clay groundmass. The unit is 5

to 10 m thick and is composed of smectites (10-15%), kaolin (60-70%), dolomite (5-10%), goethite and muscovite. Its boundary with the soil horizon above is quite sharp.

5.2.6 Saprolite (Sgg, Sm)

The saprolite occurs below or on the flanks of the mottled zone. It is about 10 m thick on the flanks of the pit and 20 to 30 on the more deeply weathered portions of the pits. The transition from the unweathered to weathered rock occurs between 15 to 20 m on the flanks and 45 to 50 m on the deeply weathered portions.

Three types of saprolite units have been identified in both E22 and E27 deposits and they have been differentiated on the basis of their distinct colour differences into:

i) The yellowish-pink (10 YR 5/4) saprolite, located below or on the flanks of the mottled zone. It is mainly yellowish-brown (10 YR 5/8) to yellowish gray (2.5 Y 5/4)) in most parts. It is also friable to firm, moderately massive and mottled (Plates 5.6a & b) and thus its name. Incipient nodular structures (5 to 20 mm in size) composed of goethite, kaolin and quartz are present in some parts. This saprolite unit is mainly composed of kaolin (50-60%), goethite (5-10%), quartz (10-15%), muscovite (5-10%) and hematite (5-10%) in order of abundance.

The depth of the mottled saprolite is between 5 to 10 m. It has been interpreted as having formed by infusion of clay rich saprolite with iron oxides and hence the use of the term mottled saprolite to describe it.

ii) The orange-pink (2.5 YR 8/4) saprolite that occurs between the white clay unit and the greenish-grey saprolite in the regolith stratigraphy (Figures 5.1 and 5.2). It is a soft, highly friable and leached saprolite that emphasizes the distinct orange-pink colour used to describe it (Plates 5.8a & b). The orange-pink colour is attributed to the predominance of K-feldspar within the groundmass. Scattered phenocrysts of orthoclase are also recognizable within the matrix in some parts. Dolomite when present occurs as vein or fracture infills and as coatings on the remnants of quartz veins that often occur as massive perpendicular cross-cutting structures, rarely exceeding 3m in length.

The depth of this saprolite is between 10 to 20 m. The mineralogy is dominated by kaolin (50-70%), muscovite (15-20%), orthoclase (15-25%), quartz (5-10%) and

dolomite (5-10%) although two samples E27 P1S6 (10 m) and E22 P1S7 (12m) contained 34.1% and 22.9% dolomite respectively.

iii) The greenish-grey saprolite (8/5 GY) is soft, friable and clay-rich (Plates 5.9a and b) occurs below the ferruginous saprolite or the orange-pink saprolite. It has been weathered directly from the trachyandesite rock below. Its fractures and veins have been infilled by an olive-green nontronite. Remnants of quartz veins can be traced through sections of this saprolite. The depth varies from 15 to 25 m.

Compositionally, it contains kaolin (30-45%), quartz (5-15%), muscovite (10-25%), orthoclase (10-20%), albite (10-20%) and smectite (5-15%).

5.2.7 Saprock (Sck)

The saprock is greenish-grey, hard and jointed. The joints have been infilled by the olive-green smectite (nontronite) as the greenish-grey saprolite. It is commonly 5 to 10 m thick and is composed of kaolin (<5%), albite (15-40%), muscovite (20-30%), smectite (10-20%), orthoclase (10-20%), and hornblende, chlorite and epidote (each rarely exceeding 5%). Its boundary with either the sulfide zone or the fresh rock is sharp (Plate 5.10).

Table 5.2 provides a summary of the physical properties of these regolith units.

SAMPLE NUMBER	DEPTH (m)	REGOLITH UNIT	COLOUR (Munsell) [Mottle/background]	pH
E27 P6	0.5m	Soil 'A' over transported regolith	2.5 YR 4/4	8.5-9
E27 P6	3.0m	Soil 'B' over transported regolith	5YR 4/2	4.5-6
E27 P11	0.5m	Soil 'A' over the host rock	2.5YR 4/6	5-6.5
E27 P11	1.5m	Soil 'B' over the host rock	5YR 4/2	5-6
E22 P4	5.0m	Mini-mottled clay	5YR 4/2 N 8/0	4.5-6
E22 P5	9.0m	Medium-mottled clay	5YR 3/4 2.5 YR 6/1 N 8/0	4.5-5
E22 P4	16m	Mega-mottled clay	5YR 4/4 10 YR 4/6 N 8/0	7-8.5
E22 P4	31m	Mottled saprolite	10YR 5/4 N 8/0	6.5-8.5
E22 P7	10m	White clay unit	7.5 YR 8/1 7.5 YR 7/1 N 8/0	6-7.5
E22 P7	16m	Orange-Pink saprolite	2.5YR 8/4	6-7
E22 P9	18m	Greenish-Grey saprolite	8/5 GY	5-6
E27 P5	44m	Saprock	8.5 GY	-
E27 P6	52m	Fresh rock	8.5 GY	-

Table 5.2: A summary of the physical properties of the regolith units

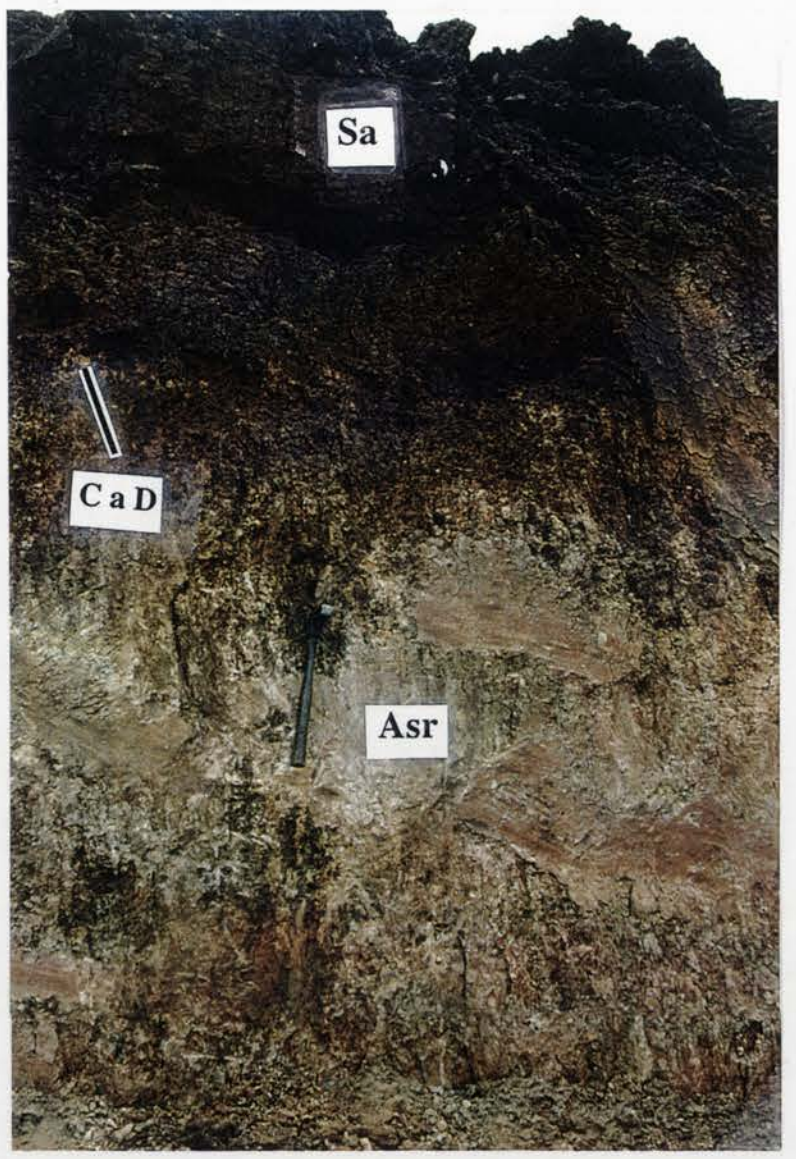

Plate 5.1a: Dark reddish brown [2.5 YR 3/3] loamy earths (Sa) developed over weathered andesitic saprolite (ASr). Notice the yellow creamy carbonate dusting (CaD) within the soil

The unit is approximately 1.5 to 2.5m thick. It is a dark reddish brown, clay and organic rich earthy soil often with yellow to white carbonate aggregates and minor amounts of gypsum. It grades straight into the saprolite below. It is composed of:

Mineralogy

Kaolin	Quartz	Smectite	Gypsum	Calcite	Hematite	Goethite	Muscovite	Orthoclase
42.3%	28.2%	2.6%	1.7%	7.8%	0.4%	3.8%	9.9%	1.3%

Geochemistry:

SiO_2	Al_2O_3	Fe_2O_3	MgO	CaO	Na_2O	K_2O	TiO_2	Au	Cu	Pb	Zn	As
52.3%	22.1%	8.57%	0.77%	1.65%	0.27%	1.67%	0.86%	37ppb	710ppm	11ppm	57ppm	7ppm

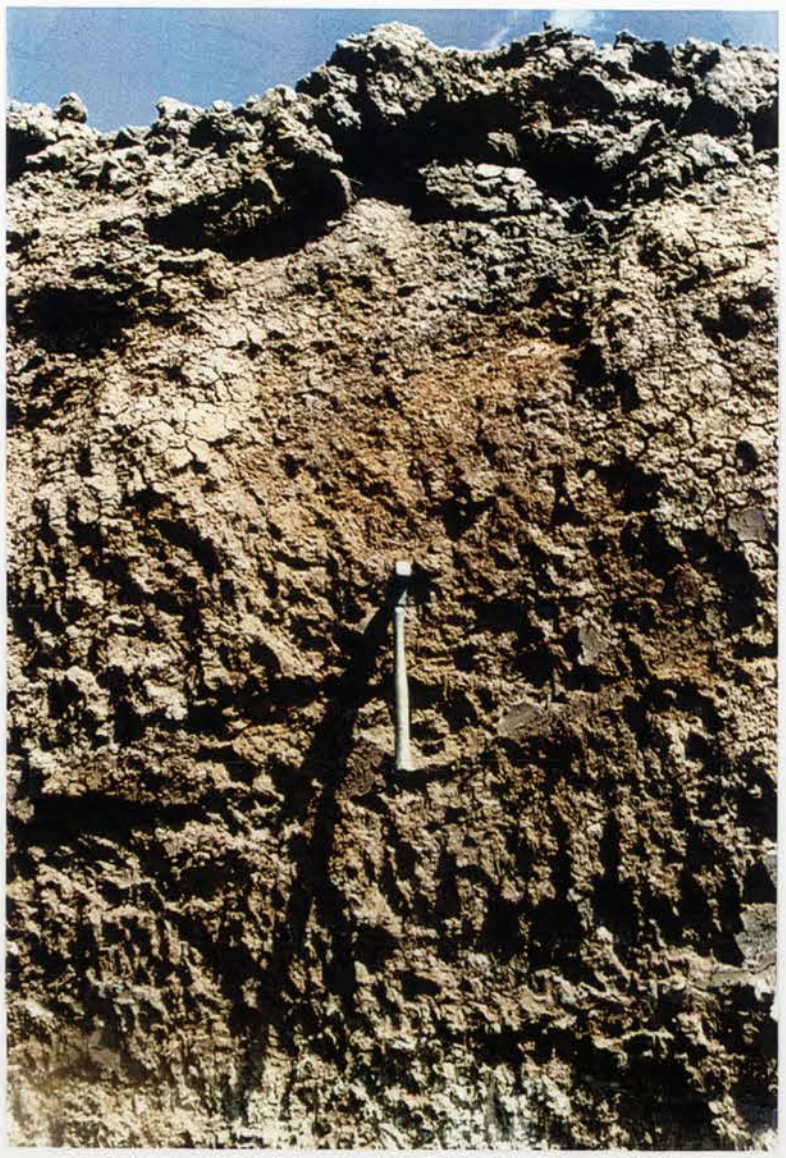

Plate 5.1b: Reddish brown [2.5 yr 5/4] earthy loams developed over weathered transported material [E22 Profile 4].

This unit is approximately 3 to 3.5 m in depth. It is a reddish brown clay and organic rich earthy soil with abundant carbonates and gypsum (not conspicuous in the plate). It grades into the mottled clay below. It is composed of:

Mineralogy:

Kaolin	Quartz	Smectite	Calcite	Gypsum	Dolomite	Hematite	Goethite
11.3%	38.5%	22.6%	13.5%	7.3%	0.8%	3.3%	2.7%

Geochemistry:

SiO_2	Al_2O_3	Fe_2O_3	MgO	CaO	Na_2O	K_2O	TiO_2	Au	Cu	Pb	Zn	As
48.1%	9.21%	3.96%	1.04%	9.45%	0.39%	0.55%	0.65%	24ppb	78ppm	13ppm	48ppm	6ppm

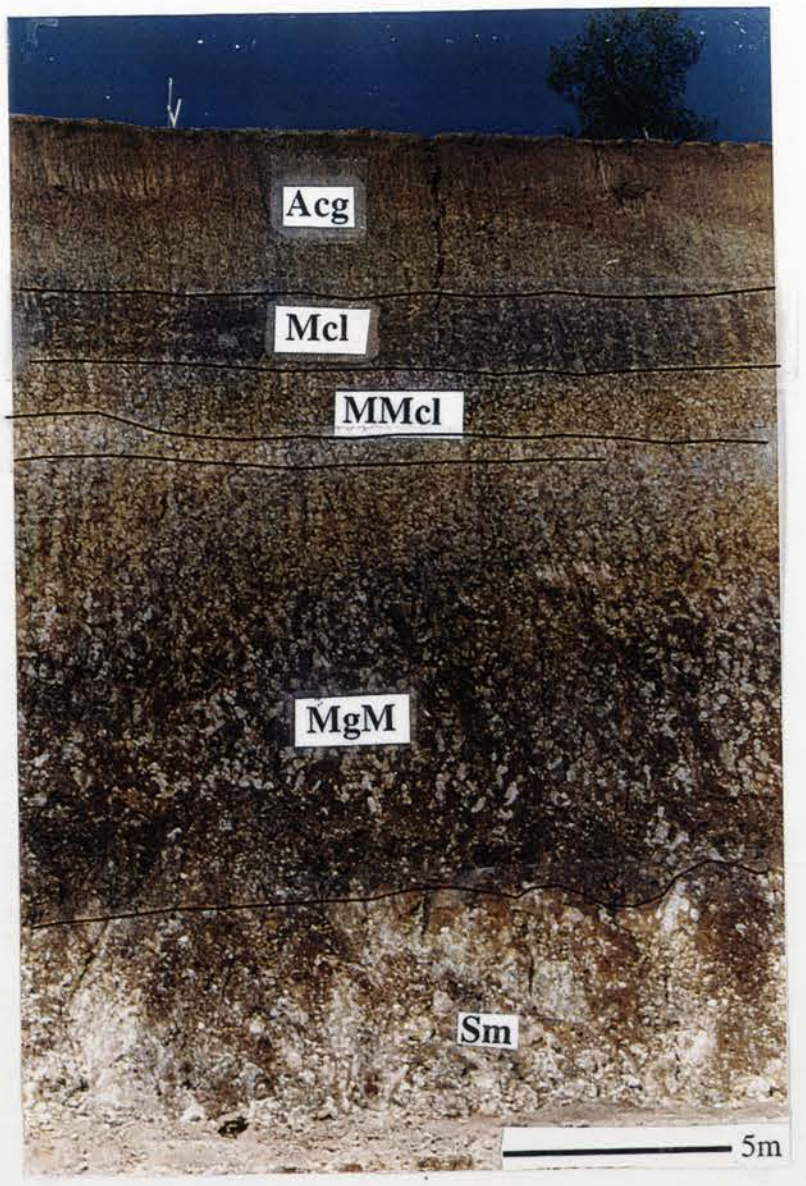

Plate 5.2a: The mottled clay profile is defined by the soil horizon (Acg), mini-mottles (Mcl), medium-mottles (MMcl) and mega-mottles (MgM). The mottled saprolite (MS) occurs below the mottled clay in the profile.

The mini-mottled clay zone is the unit below the soil where the mottles start to form within the clay. This unit is generally 1 to 2m in depth and is marked by increase in clay content and the development of small rounded to subrounded nodules (<5mm in size). Gypsum crystals may also be present within the groundmass. It is composed of:

Mineralogy:

Kaolin	Quartz	Hematite	Goethite	Smectite	Gypsum
53.9%	32.0%	6.2%	4.1%	3.4%	0.5%

Geochemistry:

SiO_2	Al_2O_3	Fe_2O_3	MgO	CaO	Na_2O	K_2O	TiO_2	Au	Cu	Pb	Zn	As
54.6%	16.7%	12.6%	1.04%	0.22%	0.59%	0.32%	1.08%	2ppb	101ppm	87ppm	120ppm	17ppm

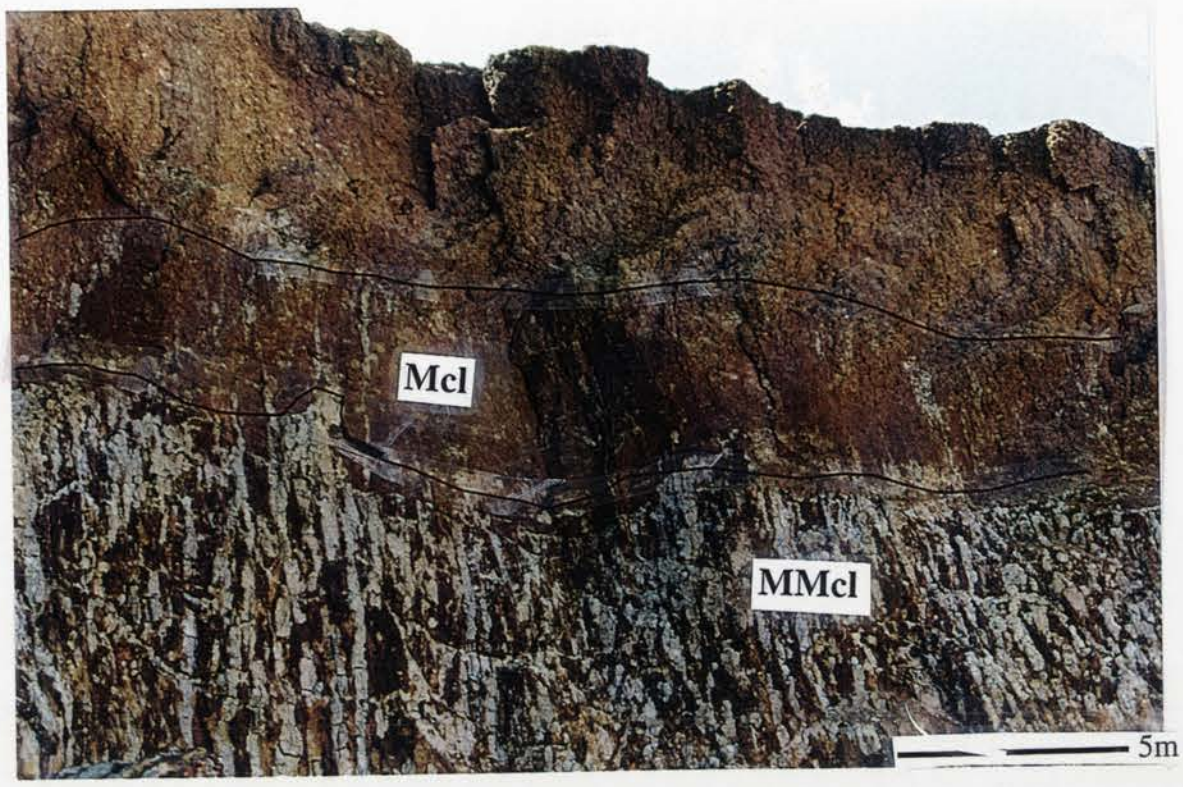

Plate 5.2b: A close-up view of the mini (Mcl)-and-medium (MMcl) mottles showing the collumnar parting structures separating the clay and iron-rich portions.

The medium mottled clay occurs to depths of about 4 to 6m. This unit is characterized by metallic red to yellowish red rounded to sub-rounded nodules 5 to 30mm in size. It also exhibits a characteristic columnar cracking structure between the clay and the iron accumulations as shown in Plate 5.2b. The matrix is kaolin rich.

Mineralogy:

Kaolin	Quartz	Hematite	Goethite	Anatase
66%	7.1%	12.9%	10.5%	3.5%

Geochemistry:

SiO_2	Al_2O_3	Fe_2O_3	MgO	CaO	Na_2O	K_2O	TiO_2	Au	Cu	Pb	Zn	As
40.4%	26.0%	16.5%	0.38%	0.09%	0.19%	0.07%	1.12%	10ppb	113ppm	80ppm	16ppm	12ppm

Plates 5.3. Silica aggregates (Sa)

These aggregates occur as a narrow band (2 to 4 m) of angular and opaline silica-rich-carbonate-coated aggregates in E22 deposit. Elsewhere they occur as sugary white masses or as distinct nodular units within the clay rich portions of the mega-mottles. The nodular fractions are angular and elongate in shape with lengths which vary from 20 to 50 mm. The carbonate cement or coating is mainly dolomite.

Plate 5.3a: Nodular silica aggregates (NSa) occurring within the kaolin-rich clays in the mottled saprolite.

Plate 5.3b: Dolomite (DL) occurring as sugary white horizontal fracture infills within the mega-mottles.

Plates 5.4. Mega-mottled clay unit-E22 Profile 4

The mega-mottles are reddish brown irregular iron accumulations 50-300 mm in size. They exhibit a dull earthy lustre and an irregular to an abrupt boundary with the surrounding clay. The clays are kaolin and smectite rich and are highly bleached. Manganese aggregates and dolomite is quite common within the groundmass. The dolomite occurs as discrete sugary white masses. The mega-mottled zone grades into the nodular and pisolitic iron-manganese aggregates or the mottled saprolite below.

Mineralogy:

Kaolin	Quartz	Hematite	Goethite	Smectite	Dolomite
59.9%	10.7%	2.7%	21%	0.5%	5.1%

Geochemistry:

SiO_2	Al_2O_3	Fe_2O_3	MgO	CaO	Na_2O	K_2O	MnO	Au	Cu	Pb	Zn	As
40.9	24.3	9.8	3.41	5.03	0.33	0.19	0.71	40	214	24	52	4

[Major oxides=weight %, Au-ppb; other trace elements-ppm]

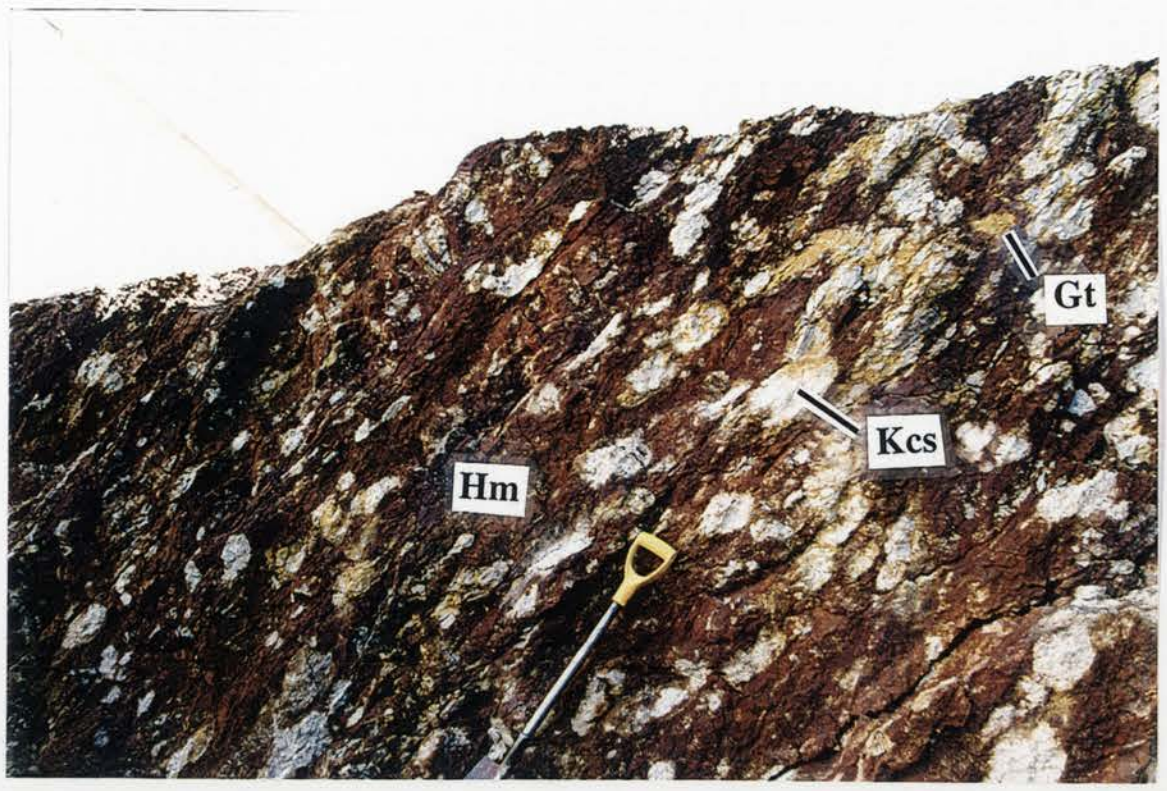

Plate 5.4a: Mega-mottles showing massive kaolinitic clays (Kcs) in contact with dull earthy hematite (Hm) and goethite (Gt) rich portions.

Plate 5.4b: A close up view of the massive white kaolin-rich clays (Kcs) in close contact with pink kaolin-rich clays (PKcs), managanese aggregates (Mna) and hematite-rich portions (Hm).

Plates 5.5. E27 P6-Nodular iron and manganese aggregates (FMn)

This zone is transitional between the mottled zone and the mottled saprolite and marks the deepest portions of the transported regolith at between 27 and 32 m. It is characterised by grey to dark rounded to sub-rounded nodules and pisoliths which range in size from 5 to 300 mm.. The matrix is composed of greenish-grey to pale-pink kaolin rich clays. Rounded to sub-rounded detrital quartz fragments and pebbles (5-20 mm in size) are also common within the matrix.

Mineralogy:

Kaolin	Quartz	Hematite	Goethite	PDM
21%	13.7%	11.7%	42.1%	11.5%

(PDM= Poorly diffracting material)

Geochemistry:

SiO_2	Al_2O_3	Fe_2O_3	MnO	CaO	Na_2O	K_2O	TiO_2	Au	Cu	Pb	Zn	As
27.1	10.6	33.5	8.85	0.45	0.18	0.18	1.27	31	783	16	354	12

[Major oxides=weight %, Au-ppb; other trace elements-ppm]

Plates 5.5 a and 5.5b

Nodular iron-manganese rich zone (FMn) occurring in betwen the mega-mottled clay (MgM) and above the mottled saprolite.

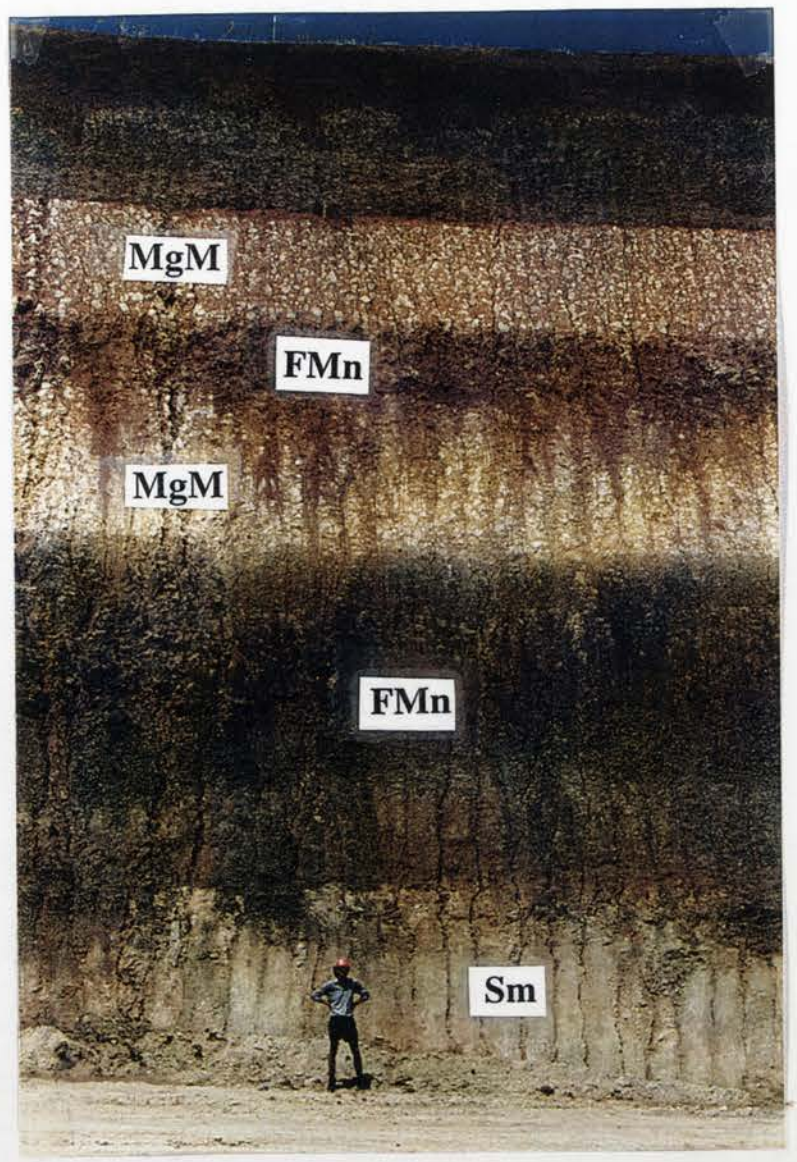

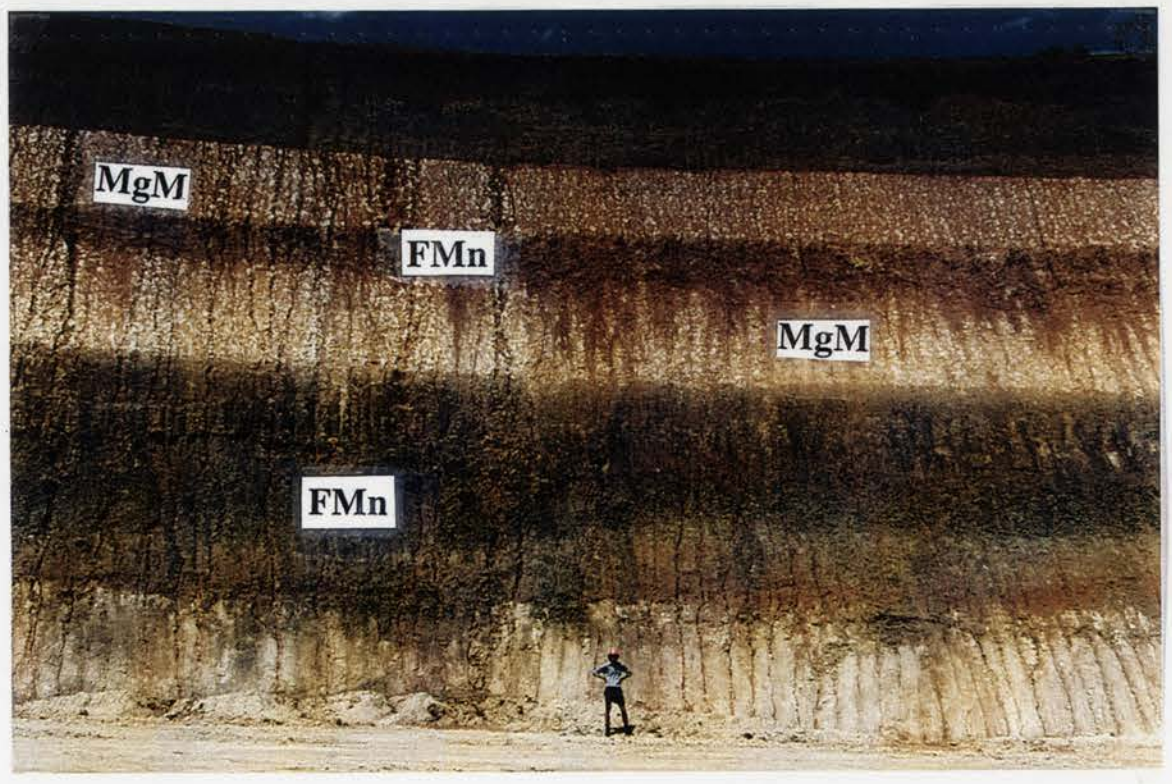

Plates 5.6. E22 P6-Mottled saprolite (Sm)

This zone is located below or on the margins of the mottled clay. It is yellowish-pink to yellowish red, friable to firm, moderately massive and mottled saprolite. Incipient nodular structures (5 to 20 mm in size) are common. Overall depth is 5 to 10 m.

Mineralogy:

Kaolin	Quartz	Hematite	Goethite	Muscovite	Smectite
50.4%	3.3%	5.6%	9.9%	29.6%	1.2%

Geochemistry:

SiO_2	Al_2O_3	Fe_2O_3	CaO	MgO	Na_2O	K_2O	TiO_2	Au	Cu	Pb	Zn	As
48	24.8	12.7	0.14	0.27	0.52	4.55	1.39	74	482	56	11	12

[Major oxides=weight %, Au-ppb; other trace elements-ppm]

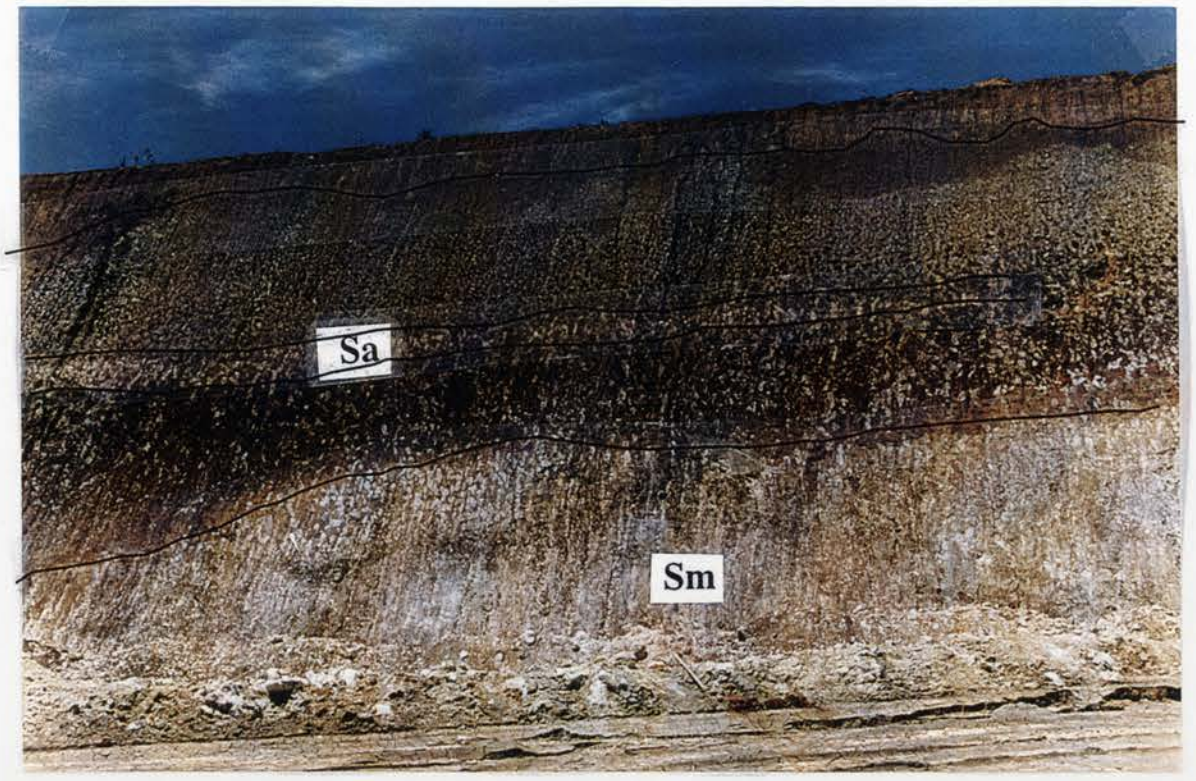

Plate 5.6a: Mottled saprolite (Sm) underlying the mottled clay in the regolith stratigraphy. Notice the narrow band of silica aggregates (Sa) within the mottled clay.

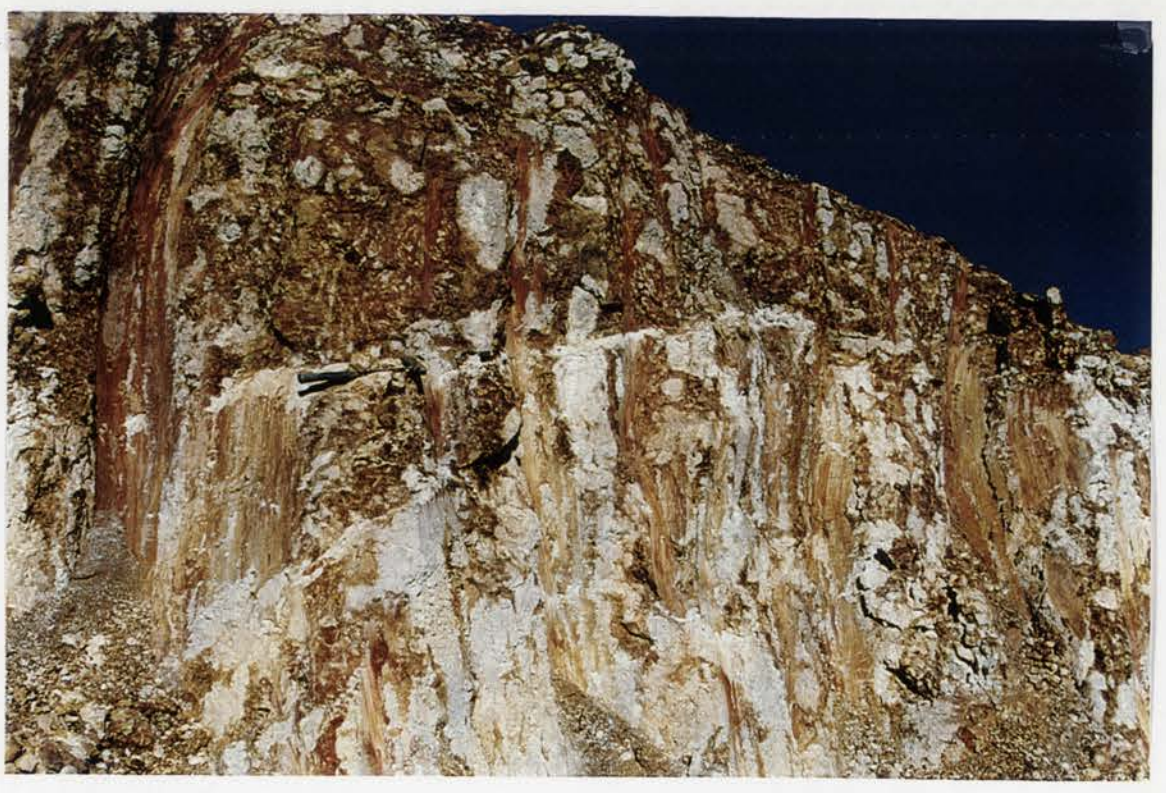

Plate 5.6b: A close up view of the mottled saprolite showing the clay and iron-rich portions.

Plates 5.7. E22 P7-White clay unit (Wcu)

This unit occurs on the margins of the mottled zone directly above the orange-pink saprolite. It consists of white to yellowish white, massively bleached clays with mesoscopically homogenous fabric. Incipient nodular structures are common within the matrix. Depth varies from 5 to 10 m.

Mineralogy:

Kaolin	Quartz	Hematite	Goethite	Muscovite	Smectite	Dolomite
48.2%	3.5%	6.3%	6.1%	26.5%	1.5%	7.9%

Geochemistry:

SiO_2	Al_2O_3	Fe_2O_3	CaO	MgO	Na_2O	K_2O	TiO_2	Au	Cu	Pb	Zn	As
33.6	24.4	10.5	5.5	4.4	0.14	1.96	0.70	132	267	5	9	2

[Major oxides=weight %, Au-ppb; other trace elements-ppm]

Plates 5.7a and 5.7b

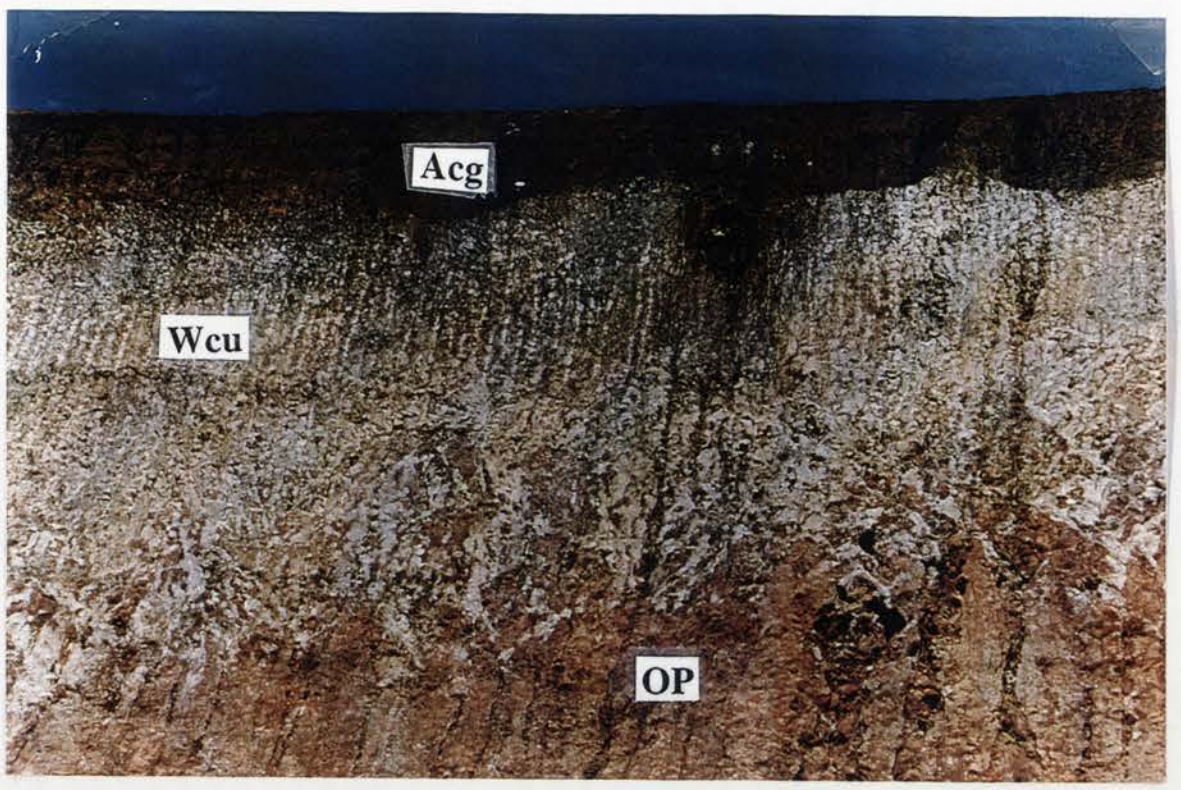

White clay unit (WCU) overlying the Orange-Pink saprolite (OP) in the regolith stratigraphy.
Noticethe highly bleached nature of the clays and the sharp contact with
the soil horizon ab(ACg) above.

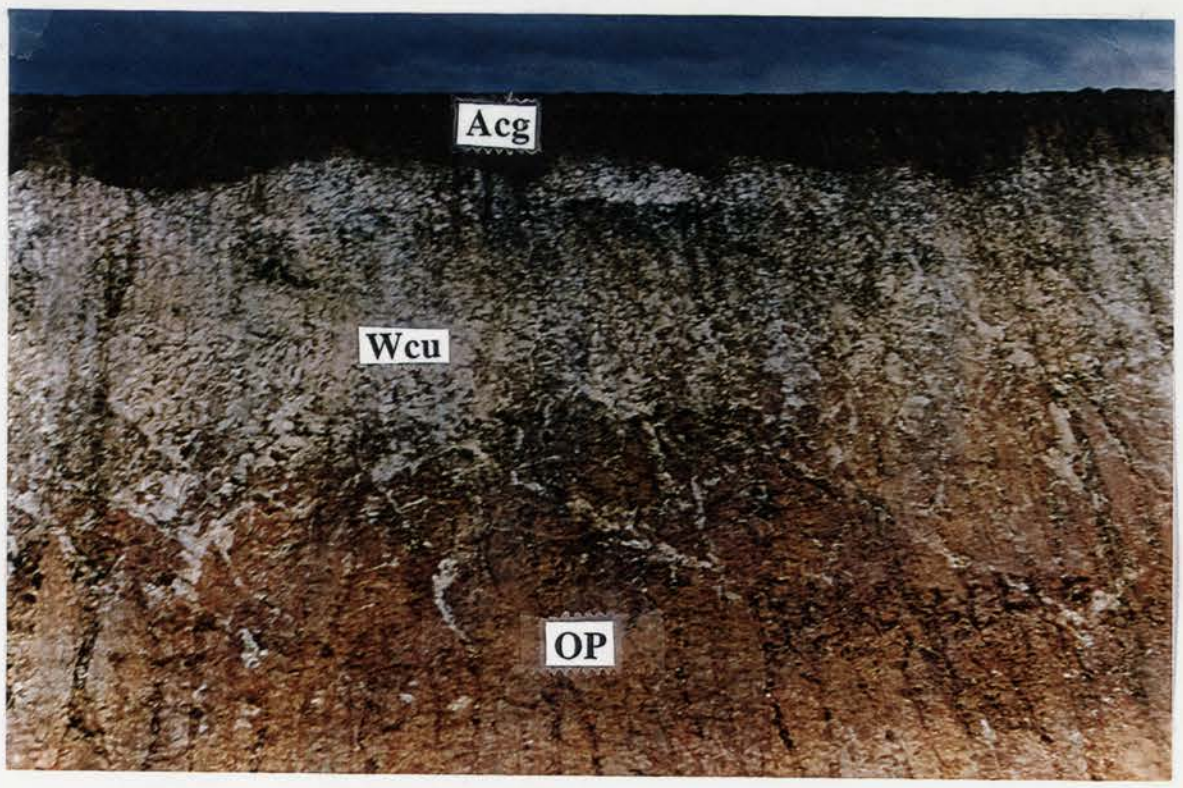

Plates 5.8. E22 P7-Orange-pink saprolite (OP)

This unit occurs between the white clay unit and greenish-grey saprolite in the E22 deposit and directly below the soil horizon in the E27 deposit. It is a soft, highly friable and clay rich saprolite with distinct orange-pink colour. The colouration is mainly due to K-feldspar matrix dusting. Overall depth is between 10 to 20 m.

Mineralogy:

Kaolin	Quartz	Hematite	Goethite	Muscovite	Orthoclase	Dolomite
64.9%	1.1%	6.4%	0.5%	8.4%	13.3%	5.5%

Geochemistry:

SiO_2	Al_2O_3	Fe_2O_3	CaO	MgO	Na_2O	K_2O	TiO_2	Au	Cu	Pb	Zn	As
33.6	24.4	4.1	4.0	1.1	0.43	7.8	0.76	34	1250	1	23	5

[Major oxides=weight %, Au-ppb; other trace elements-ppm]

Plates 5.8a and 5.8b

Very soft and friable orange-pink saprolite above and below with the thin carbonate (dolomite) stringers (Dls) within the groundmass.

Plates 5.9. E27 P7-Greenish-grey saprolite (Sgg)

This saprolite type occurs below the mottled saprolite or the orange-pink saprolite. It is the most predominant type and grades directly into the saprock below. It is soft, friable and clay rich with distinct greenish-grey colour. The greenish-grey colour is partly a result of the presence of a green smectite (nontronite) in the groundmass. Overall depth varies between 15 to 25 m.

Mineralogy:

Kaolin	Quartz	Hematite	Albite	Muscovite	Orthoclase	Smectite
21.5%	11.1%	1.2%	14.4%	17.8%	21.7%	12.2%

Geochemistry:

SiO_2	Al_2O_3	Fe_2O_3	CaO	MgO	Na_2O	K_2O	TiO_2	Au	Cu	Pb	Zn	As
50.4	23.9	7.13	1.2	1.75	1.91	5.37	0.77	78	518	48	137	26

[Major oxides=weight %, Au-ppb; other trace elements-ppm]

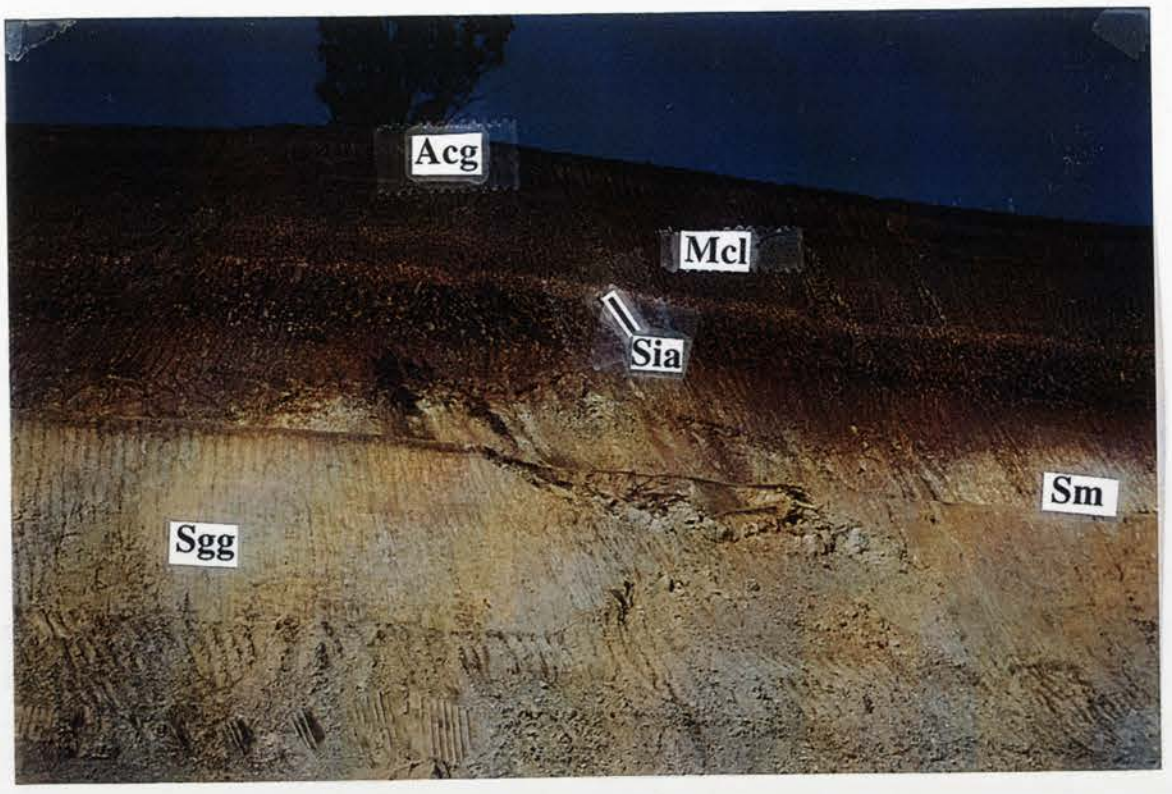

Plate 5.9a: Greenish-Grey saprolite (Sgg) underlying the mottled saprolite (Sm), tthe mottled clay (MCl) and soil horizon (ACg) above. Notice the extensive band of silica aggregates (Sia) within the mottled clay.

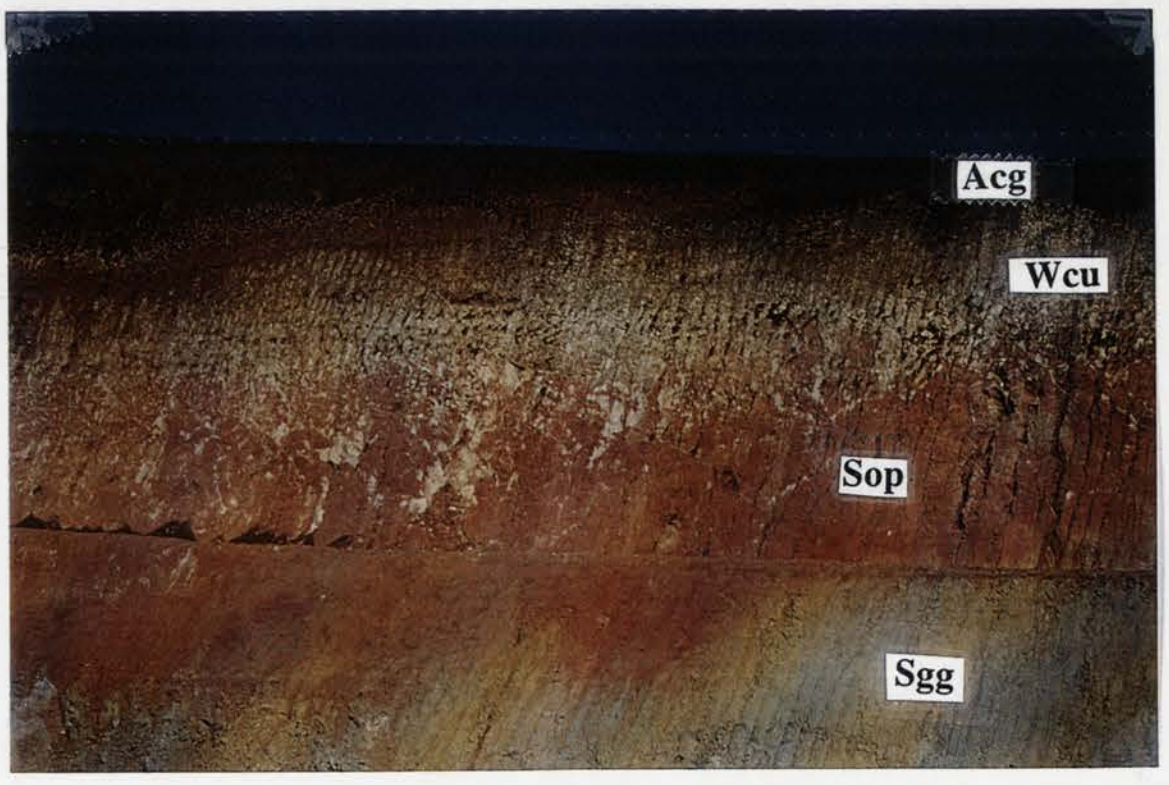

Plate 5.9b: Greenish-Grey saprolite (Sgg) underlying the Orange-Pink saprolite (Sop) and the white clay unit (Wcu) above.

Plate 5.10: Regolith profile over the trachyandesite showing the fresh rock portions (FR), saprock (Sck), greenish-grey saprolite (Sgg) and a thin soil horizon (ACg)

This unit overlies the sulphide zone or the fresh rock. It is greenish-grey, hard and jointed. The joints have been infilled by a green clay (nontronite). It is generally 5 to 8 thick. Boundary with undelying units is sharp.

Mineralogy:

Kaolin	Hematite	Muscovite	Orthoclase	Albite	Smectite	Diopside	Epidote	Chlorite
3.3%	4.8%	20.0%	22.4%	39.6%	2.7%	1.2%	1.0%	4.9%

Geochemistry:

SiO_2	Al_2O_3	Fe_2O_3	CaO	MgO	Na_2O	K_2O	TiO_2	Au	Cu	Pb	Zn	As
57.0%	20.2%	5.23%	1.11%	1.62%	4.61%	6.12%	0.63%	110ppb	1190ppm	-	34ppm	2ppm

CHAPTER 6

REGOLITH MINERALOGY: DESCRIPTION AND PARAGENETIC SEQUENCES

6.1 Introduction

The mineralogy, morphology, composition and sequential formation of weathering products in the study area have been examined using a combination of Optical Microscopy, X-ray diffraction and Scanning Electron Microscopy. This chapter deals with the identification, nature and composition of these secondary products. The next chapter deals with the distribution of these products in the regolith stratigraphy and the major profiles that are under investigation.

6.2 REGOLITH PARAGENESIS

The host trachyandesite rock in this study area is predominantly composed of feldspars (K-feldspar and plagioclase), muscovite and quartz with minor amounts of pyroxene (notably clinopyroxene), chlorite, epidote and hornblende. The pyroxenes and the accessories make up less than 10% of the rock for most of the samples (Appendices 1 and 2).

The petrographic study was made difficult by intense mineralization-related alteration, which resulted in partial, and in some cases complete destruction of the primary fabrics. This coupled with the fine-grained nature of the rocks almost made it impossible to isolate the non-feldspathic minerals from the groundmass for SEM morphological examinations. A combination of the techniques already mentioned was utilized to adequately describe the mineral paragenesis in each horizon of the profile.

6.3 Fresh rock

The rock shows effects of hydrothermal alteration associated with mineralization which has resulted in partial and in some instances total loss of fabric (Figures 6.1, 6.2, 1.7.1 and 1.7.2). The trachyandesite is an aphanitic greenish grey rock and consists of euhedral to subhedral stumpy laths of plagioclase with albite and periclase twinning. The plagioclase appears turbid with the twinning considerably diminished. The plagioclase is an albite (Table 6.1). The K-feldspar occurs as anhedral phenocrysts (0.1 to 0.3 mm) or as fine-grained groundmass as a result of hydrothermal alteration. Some crystals still

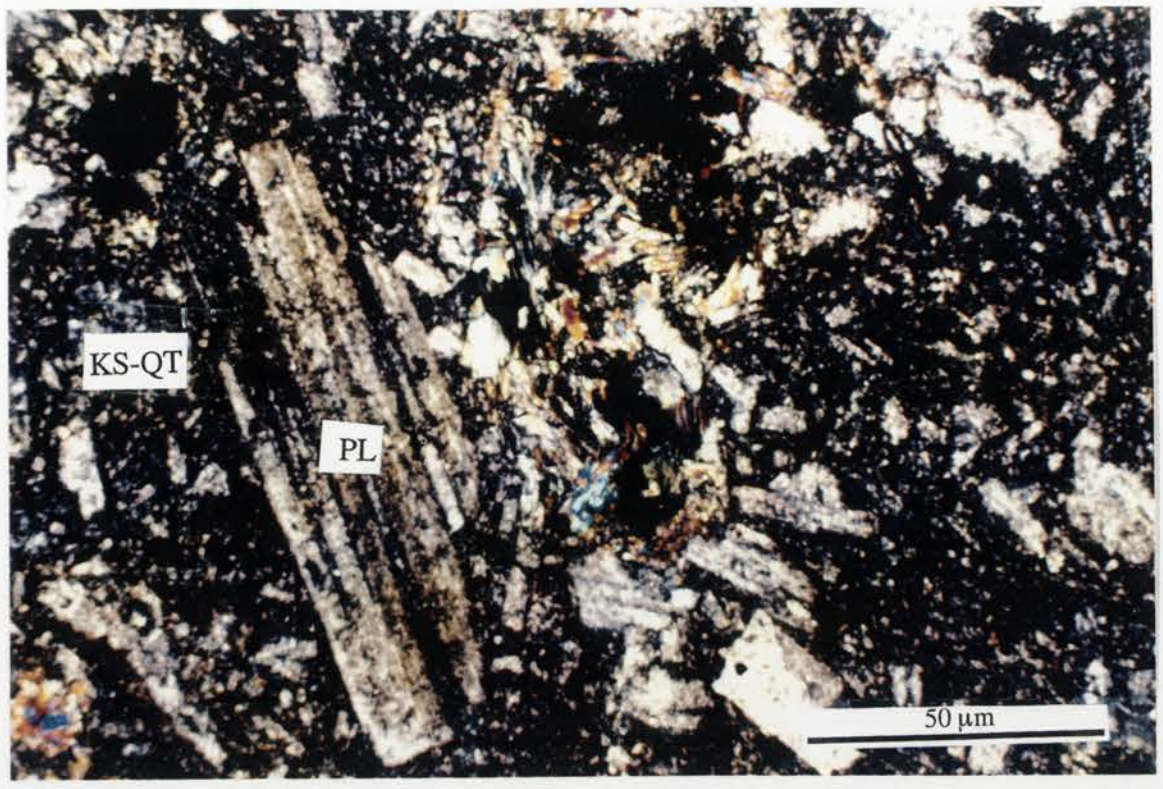

Figure 6.2.1: Trachyandesite rock showing a partially altered plagioclase lath (PL) with K-feldspar (KS) and muscovite (MS) in a groundmass of K-feldspar and quartz (KS-QT) and opaques. Hydrothermal alteration has resulted in partial destruction of rock fabric. Specimen E27 TR4. Depth (46 m). Photomicrograph with crossed polars.

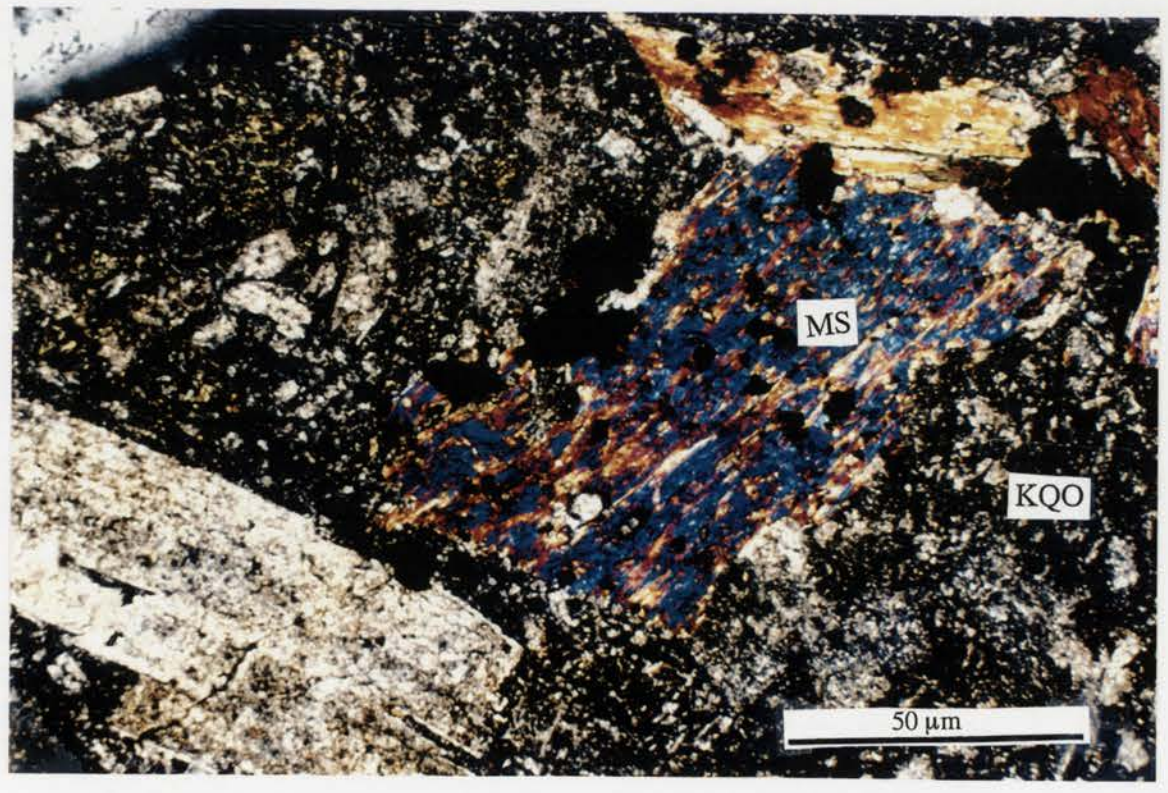

Figure 6.2.2: Muscovite (MS) pseudomorphically replacing K-feldspar within a groundmass of K-feldspar, quartz and opaques (KQO). Specimen E27 TR1 Depth (46 m). Photomicrograph with crossed polars.

retained some cross-hatched twinning though like the plagioclase the twinning is considerably clouded. The K-feldspar has the average composition shown in Table 6.1. The micas occur as bluish to yellowish brown, anhedral to subhedral equant patches within the groundmass or as pseudomorphs of the plagioclase feldspar exhibiting yellow to blue birefringence. The micas have the structural formula illustrated in Table 6.1 and are muscovites. Quartz occurs as glassy grey to white anhedral grains. Minor amounts of chlorite, epidote and apatite are also present. The apatite is enclosed within the mica cleavage.

In addition, abundant sulfides are present and they occur as dark subhedral to irregular spots. The sulfides have been identified as bornite, chalcopyrite and covellite (Chapter 1).

Table 6.1 Composition of albite, K-feldspars and muscovite from the trachyandesite (Data obtained from SEM EDXA analysis; Std. Dev.-standard deviation)

Plagioclase			**K-feldspar**			**Muscovite**		
	Mean	Std. Dev.		Mean	Std. Dev.		Mean	Std. Dev.
Si	2.951	0.002	Si	3.05	0.018	Si	3.052	0.055
Al	1.035	0.005	Al	1.015	0.005	Al	0.815	0.061
Fe^{2+}	0.000	0.000	Fe^{2+}	0.001	0.002	Fe^{2+}	0.070	0.20
Mg	0.000	0.000	Mg	0.000	0.000	Mg	0.015	0.12
Ca	0.019	0.002	Ca	0.000	0.000	Ca	0.000	0.000
Na	0.951	0.010	Na	0.030	0.007	Na	0.030	0.015
K	0.005	0.002	K	0.512	0.072	K	0.82	0.14
Ti	0.000	0.000	Ti	0.000	0.000	Ti	0.000	0.000
N = 5			N= 5			N = 5		

Nature of surrounding products [N=5]

	Mean	**Std. dev.**
Si	4.305	0.030
Al	3.521	0.000
Fe^{2+}	0.075	0.002
Mg	0.154	0.010
Ca	0.058	0.002
Na	0.010	0.010
K	0.055	0.020
Ti	0.015	0.044

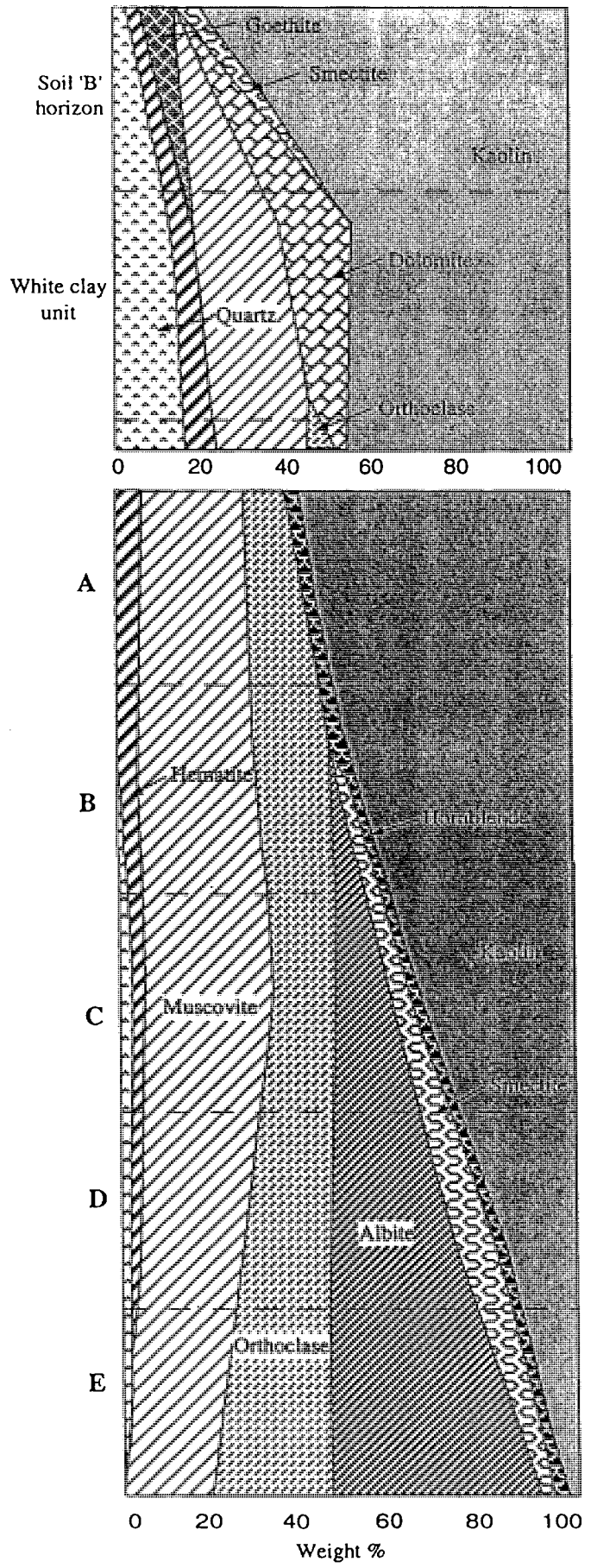

Figure 6.3.1: Mineralogical distribution in transition from the saprock (E) to the upper saprolite (A). The upper portion (whose fabrics and textures are not presented) represents the continuation of the stratigraphy into the white clay unit and soil 'B' horizon

The upper saprolite(orange pink type) showing kaolin patches(KP) an remnants of ferromagnesians in a K-feldspar stained clay plasma. Photograph of a thin section in natural light.
Specimen E22 P7 (16 m).

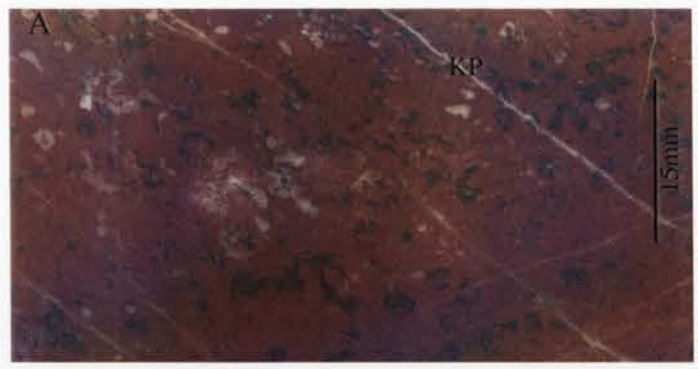

Transition between the greenish-grey and orange-pink saprolite showing the passive development of the K-feldspar stained plasma as smectite clay and plagioclase content decreases. Photograph of a thin section.
Specimen E22 P7 (18 m).

The middle saprolite (greenish grey) showing intensely altered plagioclase laths in a kaolin/ smectite/sericite plasma. Photograph of a thin section.
Specimen E22 P4 (38 m).

The lower saprolite (greenish-grey) with abundant clay infilled fractures.Some K-spar (KS) phenocrysts and abundant plagioclase(Pl) laths arepresent in the groundmass. Photograph of a thin section.
Specimen E22 P4 (44 m)

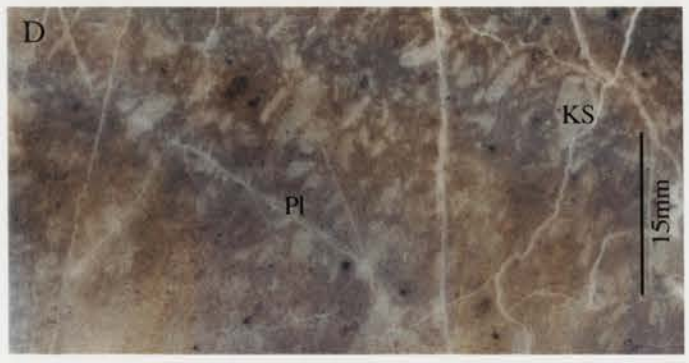

The saprock showing remnants of sulphides and opaques (OP-ferromagnesians and magnetite) and plagioclase laths in a smectite/muscovite/kaolin rich plasma. Photograph of a thin section.
Specimen E22 P4 (48 m)

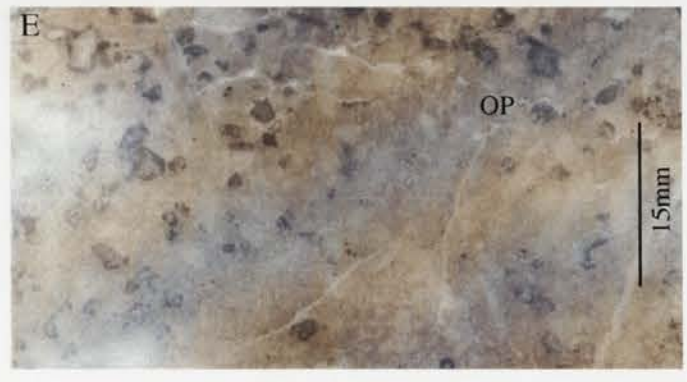

Figure 6.3.2: Fabric and textural variation in transition from the saprock to the upper saprolite

Minor amounts of opaques also occur as dark subhedral spots within the plasma. These opaques have been determined from SEM EDXA as magnetite and hematite.

6.4 SAPROCK

Distinct textural, fabric and colour changes occur in the weathered rock in transition from the saprock to the orange pink saprolite (Figure 6.3.1). The mineralogical contents of the samples representing the photomicrographs also vary with this transition (Figure 6.3.2). There is a concomitant loss of the feldspars (albite and K-feldspar) towards the upper part of the profiles while kaolin and the iron oxide content increases. Muscovite persists up to the white clay unit where it is gradually lost.

Weathering in the saprock has imparted brownish grey colour to the surface of the rock although greenish grey to blue colours of remnant sulfides and opaques are still present within the groundmass. The rock at this stage is highly jointed and slightly hard. The bulk mineralogy is dominated by K-feldspar (orthoclase), albite, muscovite and quartz.

6.4.1 Mineral paragenesis

The earliest stage of the alteration of both plagioclase and K-feldspar consists of the development of a brown, cloudy and 'turbid' patches of low birefringence which is initiated at the loci of twin planes or cross hatches within the feldspar (Figures 6.4.1 and 6.4.2). These sites could have acted as conduits for solutions to the feldspar surfaces. The net result is the development of solution pits or etch pits on the feldspar surface and formation of secondary products (Figures 6.5.1 to 6.5.8). The irregular edges of kaolinite booklets in Figures 6.5.8 and 6.5.9 indicate that the secondary products are a result of dissolution processes. Lens shaped etch pits initially develop on the surface suggesting a slow partial dissolution.

These first products of feldspar weathering develop as a result of surface dissolution of feldspar and removal of elements from the feldspar in solution. The K-fledspar exhibits both exsolution lamellae and cross-hatched patterns (Figure 6.4.1) with the development of secondary minerals following these patterns. The plagioclase displayed similar patterns following the twinning planes. This poorly crystalline material of low birefringence could not be identified from its optical properties but XRD and SEM EDXA studies suggests it is a mixture of smectite and oxyhydroxides (hematite or goethite). Intense iron staining especially along or within the twinning planes and

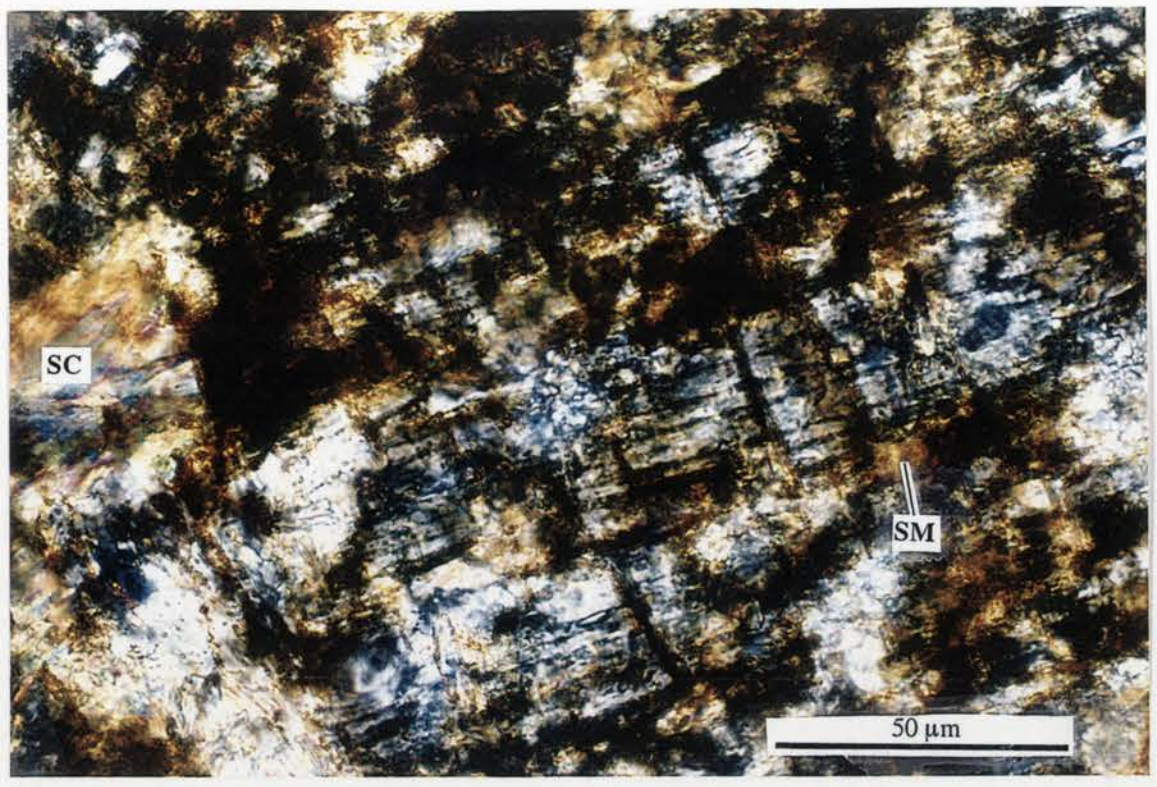

Figure 6.4.1: The development of brown cloudy 'muddy' material following cross hatch (carlsbad) twinning of K-feldspar. The smectite (SM) has developed close to the cloudy material, together with sericite flakes (SC) exhibiting yellow to blue birefringence. Sample E22 TR 3. Depth 44 m. Photomicrograph with crossed polars.

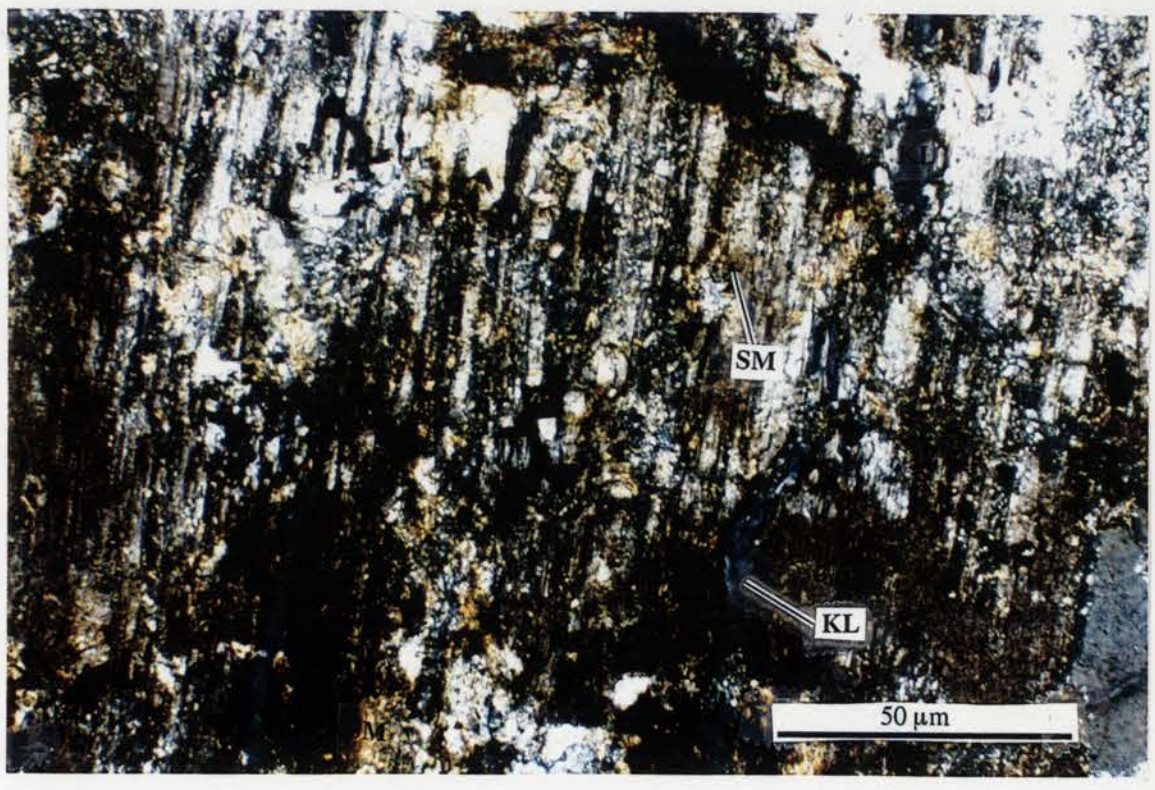

Figure 6.4.2: Development of brown cloudy 'muddy' material following the twinning planes of plagioclase. The smectite (SM) has also formed adjacent to this material with solution channels that have been infilled with very fine grained kaolinite (KL) Sample E22 TR 3. Depth 44 m. Photomicrograph with crossed polars.

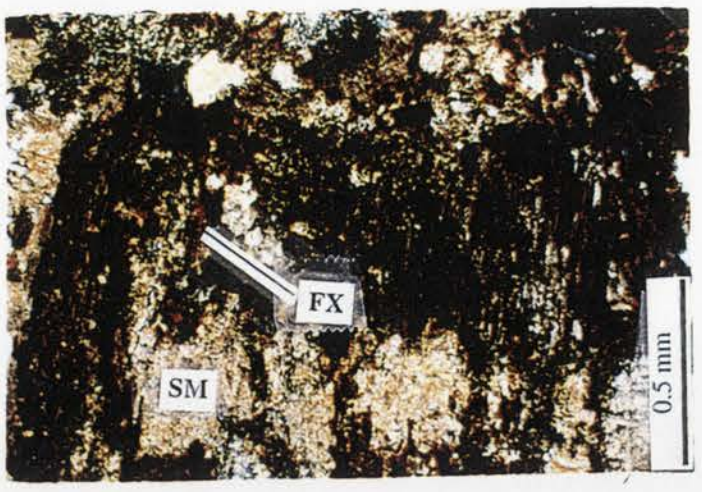

Fig. 6.4.3. The brown cloudy material is gradually replaced by smectite (SM) and iron oxide (FX). Photomicrograph with crossed polars

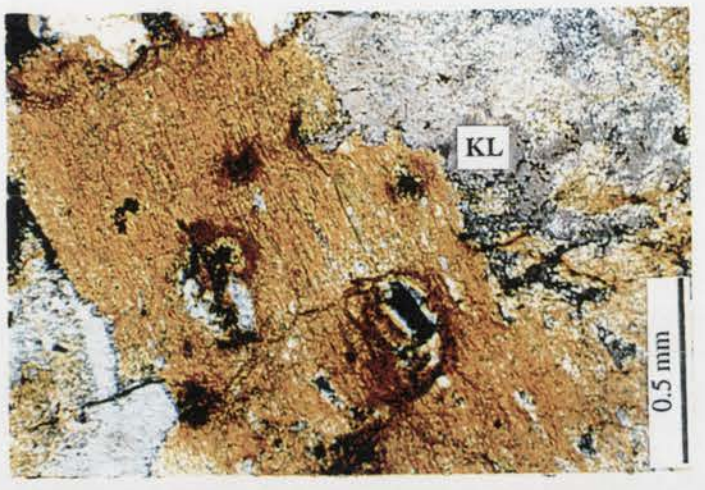

Fig.6.4.4. Muscovite (with deep yellow birefringence) after plagioclase with minor iron oxide tinges. The matrix consists of very fine grained kaolinite. Specimen E27 P7 S22 [saprock zone] Photomicrograph with crossed polars.

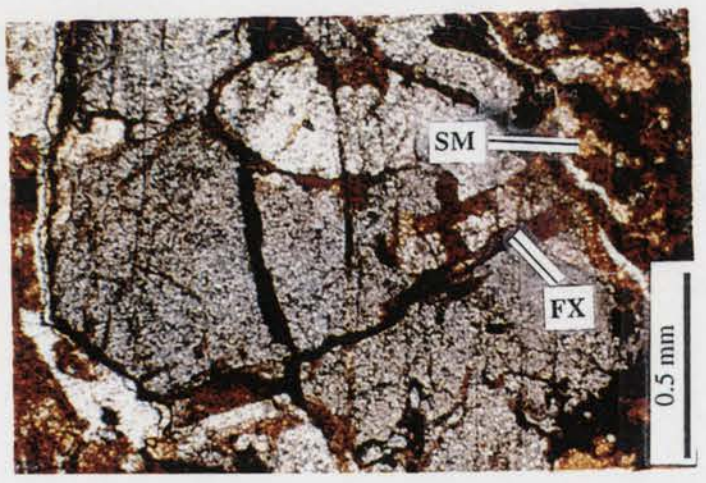

Fig.6.4.5. Iron oxide (FX) and smectite (SM) concentration within and close to fractured K-feldspar phenocryst. Specimen E27 P7 S23 [saprock zone] Photomicrograph with crossed polars.

Fig.6.4.6. Iron oxide (FX) concentration in fractures of slightly kaolinized trachyandesite. Specimen E27 P6 S23 [saprock zone]. Photomicrograph with crossed polars.

Figure 6.5.1: Etch pits developed on the 100 and 001 face of feldspar crystal
Sample from E22 P7 [saprock]. Scale bar = 2μm

Figure 6.5.2: Etch pits developed on the 100 and 001 face of feldspar crystal
Sample from E22 P7 [saprock]. Scale bar = 2 μm

Figure 6.5.3: Differential shattering, pitting and coalescence of the etch pits
Sample from E27 P7 [saprock/lower saprolite]
Scale bar = 2 μm

1

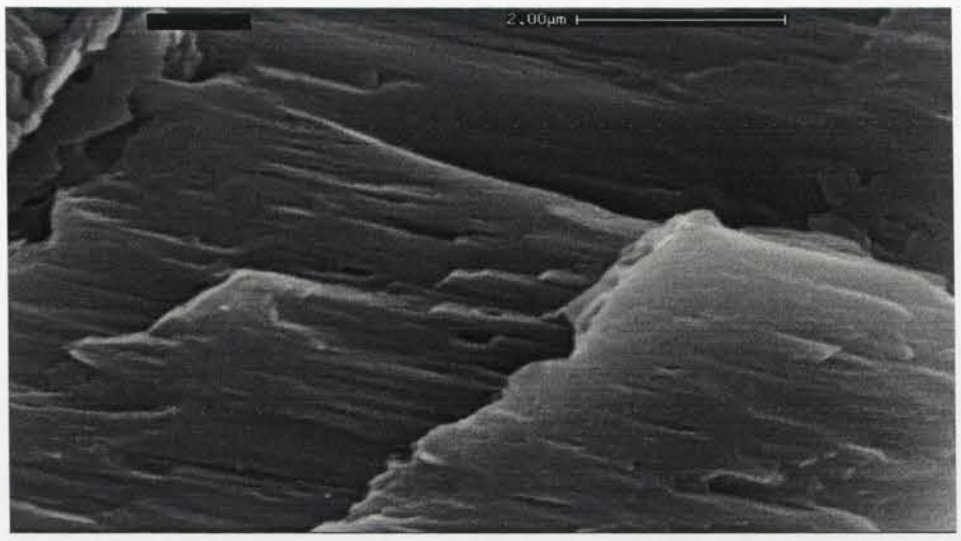

2

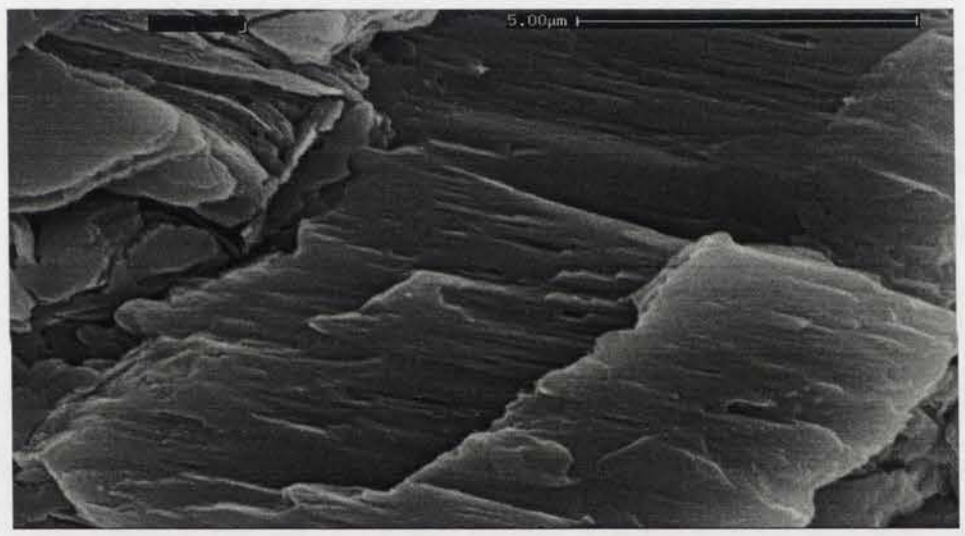

3

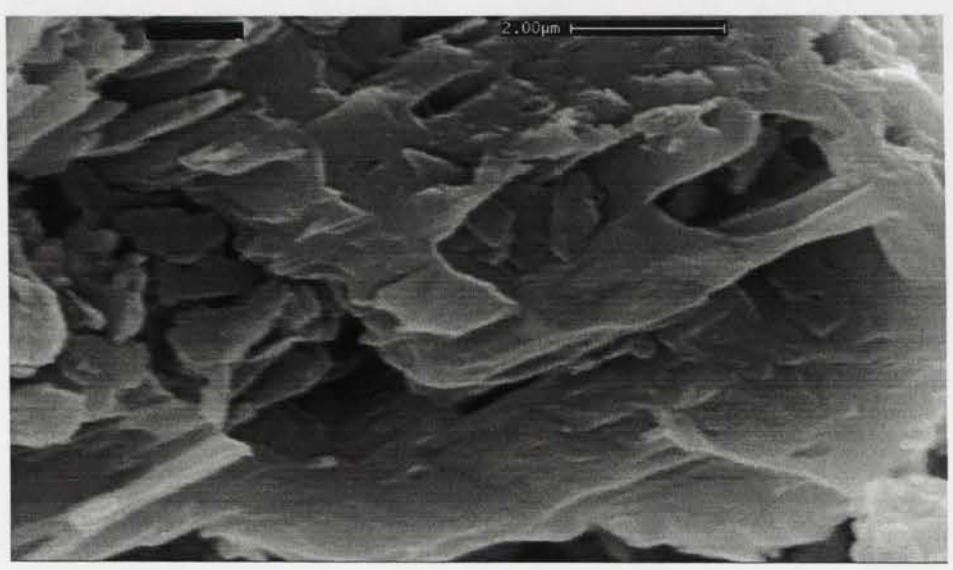

Figure 6.5.4: Kaolin plates (KP) forming randomly on shattered feldspar surface. Specimen from E22 P4 [lower saprolite]
Scale bar = 5 μm

Figure 6.5.5: Kaolin books (KB) developing randomly on shattered feldspar surface. Specimen from E22 P4 [lower saprolite]
Scale bar = 2 μm

Figure 6.5.6: 'Cotton wool' textured smectite (SM) and kaolin plates (KP) developing on shattered feldspar. Specimen from E22 P4 [lower saprolite] Scale bar = 2 μm.

4

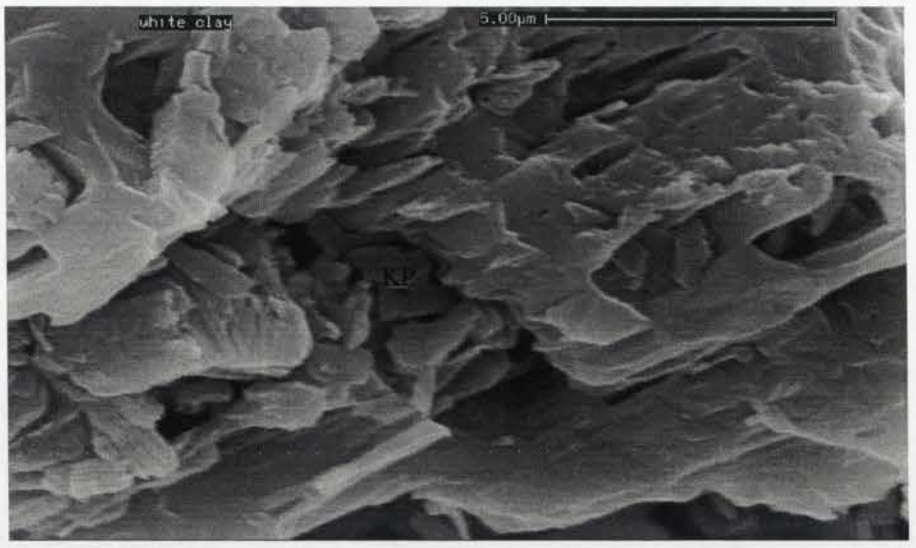
white clay
5.00μm
KP

5

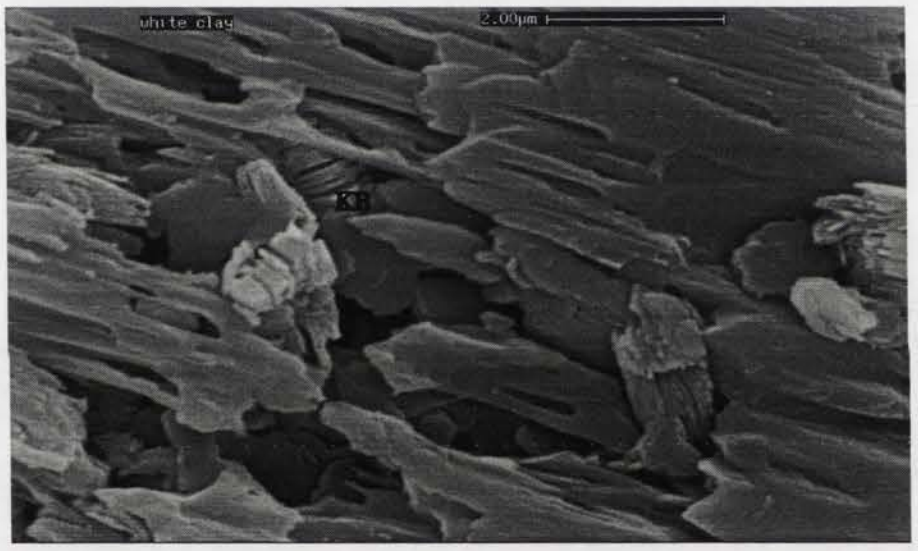
white clay
2.00μm
KP

6

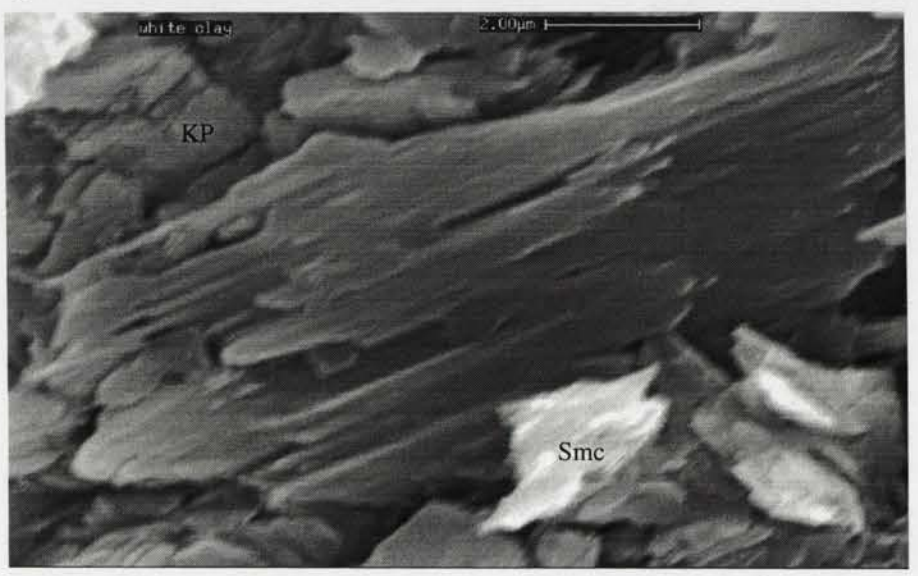
white clay
2.00μm
KP
Smc

Figure 6.5.7: Cellular 'spongy' smectite and kaolin books have replaced the shattered feldspar. Specimen from E27 P4 [lower saprolite] Scale bar = 10 μm

Figure 6.5.8: Close up view of kaolin books that have replaced the shattered feldspar. Some platy kaolin crystals occur adjacent to the books Specimen from E22 P4 [lower saprolite] Scale bar = 2 μm

Figure 6.5.9: Close up view of kaolin books that have replaced the shattered feldspar. Some platy kaolin crystals occur adjacent to the books Specimen from E22 P4 [lower saprolite] Scale bar = 2 μm

7

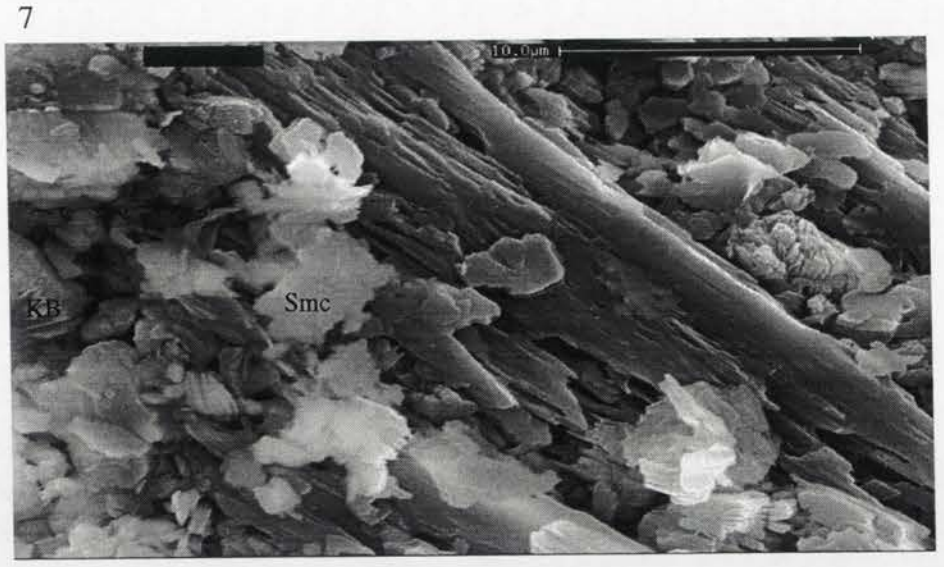

8

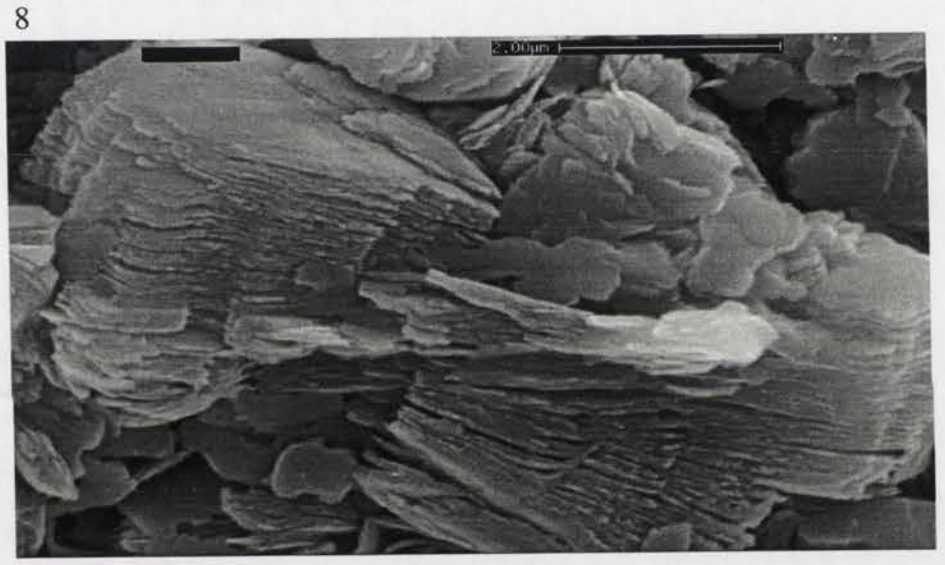

9

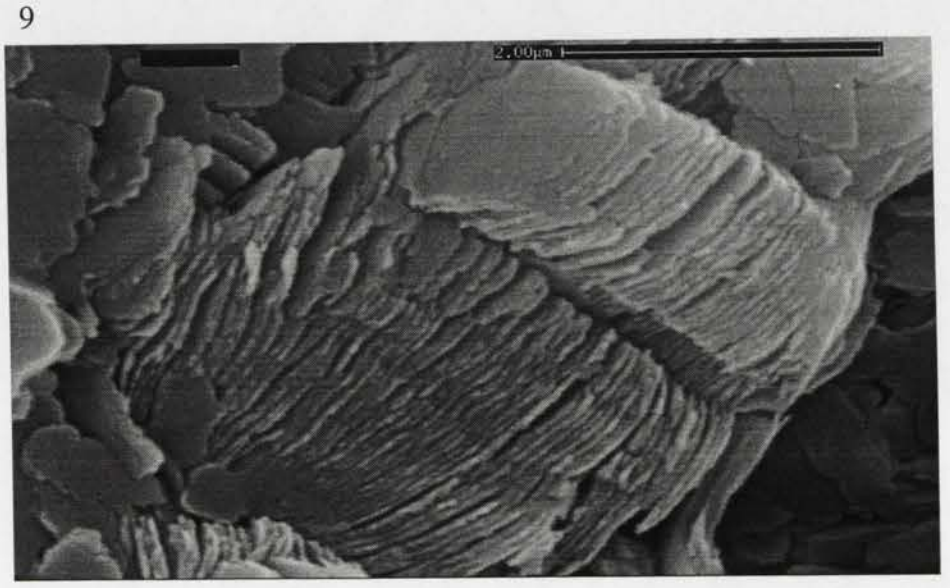

intramineral fissures is also conspicuous (Figures 6.4.3, 6.4.5 and 6.4.6). However, within or adjacent to the poorly crystalline material is light yellowish brown to yellowish green non-pleochroic material (Figures 6.4.1, 6.4.2, 6.4.3 and 6.4.5). The product is presented as relatively small (<10 μm) spongy cellular 'cotton wool' textured encrustations (Figures 6.6.1, 6.63 and 6.6.5) on the surface of the feldspar.

The composition of these spongy aggregates is characterized by a decrease in calcium and minor presence of iron as compared to the parent mineral. From these characteristics it is apparent the initial product is a smectite. The presence of small amounts of iron and high alumina allocates it as an Fe-beidellite, Fe-montmorillonite or nontronite. The characteristics of the smectites encountered in this study are discussed in Chapter 7. It is apparent that the brown, cloudy, 'turbid' material developed as a precursor to the smectite.

The <2 μm clay fraction diffraction data (Figure 6.7) confirms the dominant clay as smectite with minor amounts of kaolin and sericite. The 14 Å smectite peak is rather broad implying a moderately well crystallized clay.

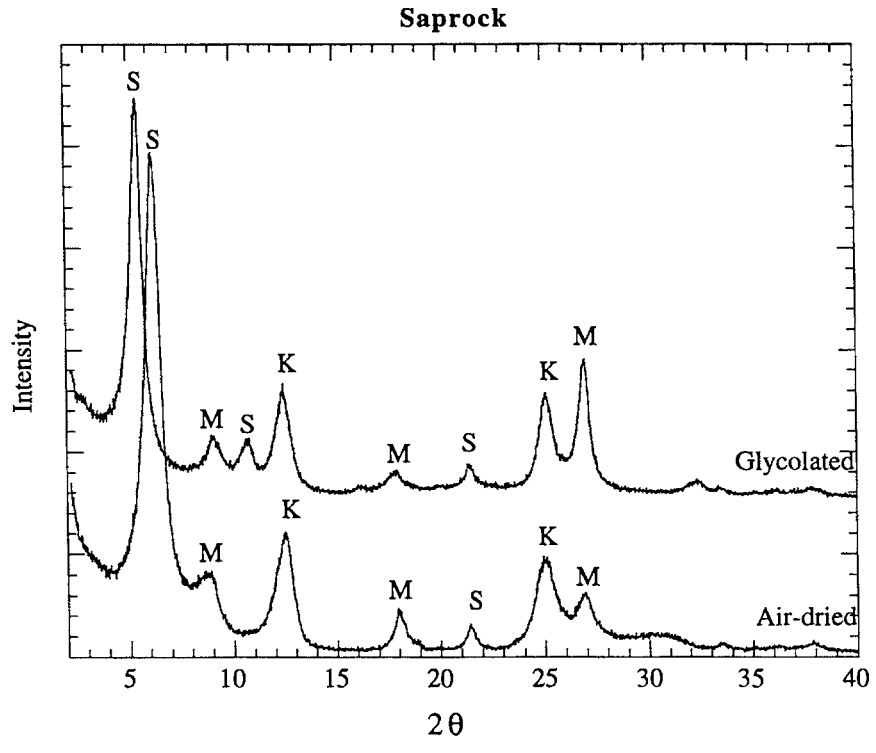

Figure 6.7: XRD traces of air-dried and ethylene glycol treated samples of the < 2 μm fractions from the saprock [Specimen E27 P9 (44 m)]: K- Kaolin; S- smectite; M- Mica

6.5 SAPROLITE

The saprolite is quite extensive in the regolith stratigraphy and occurs in most of the profiles. Locally it can extend to about 30 m. It has been subdivided into the greenish-grey and orange -pink varieties. For the purposes of this study, the terms upper, middle and lower saprolite have been employed to show the positions of these units relative to one another in the regolith stratigraphy. These terms are hence not formally defined.

The greenish-grey saprolite has been subdivided into the lower and middle saprolite respectively. The lower saprolite occurs proximal to the saprock. It is slightly hard and coherent compared to the middle saprolite. The orange-pink saprolite is situated above the greenish-grey saprolite in the regolith stratigraphy (Figure 5.1 Chapter 5) and is herein referred to as the upper saprolite.

Mineral paragenesis

6.5.1 Lower saprolite

The trachyandesite fabric is perfectly preserved in the lower saprolite (Figure 6.3.2 D). The internal destabilization of the primary minerals is much more than in the saprock. It is 3 to 5 m thick and is considered as the transient stage of weathering from the saprock to the more extensive middle saprolite.

In this horizon, feldspar alteration proceeds by differential shattering, pitting and coalescence of the etch pits of the feldspar along the main axis of the feldspar grains to irregular and elongate microfragments (Figures 6.5.3 and 6.5.4). The resulting secondary products are of two types, each with distinct morphology.

- The first and less abundant alteration product is similar to the spongy 'cotton wool' textured smectite encountered in the saprock. It generally covers the surface of the feldspar although the shattered surfaces of the feldspar grain are quite conspicuous.

- The second and more equally abundant alteration product is a platy, 'book' type variety (similar to the ones in Figures 6.5.8 and 6.5.9) that has formed in the cavities of the shattered feldspar. SEM EDXA analysis showed that this product contains equal amounts of Al and Si. The books are randomly oriented with respect to the feldspar crystallography. From these characteristics, it is apparent that this product is kaolinite.

- The third and most abundant alteration product is the development of an olive green curly and platy textured clay (Figures 6.6.2, 6.6.4, 6.6.6, 6.6.7 and 6.6.8) side by side with the spongy variety. This represents the earliest stage of the development of the 'corn flake' textured clay which is described in detail in the next horizon where the morphology becomes more pronounced. The XRD mineralogy from this horizon shows the dominant clays to be smectite and kaolin.

Petrographic observations show a smectite having two characteristics (Figure 6.9.1). One has acquired a reddish brown colour in contrast to the 'muddy' brown variety from the saprock. This colouration is due to the high content of Fe in this smectite. The other variety is a yellowish green smectite of the saprock. The smectites are smeared throughout the surfaces of the otherwise low birefringent very fine-grained 0.001-mm) kaolinite matrix.

Lower saprolite

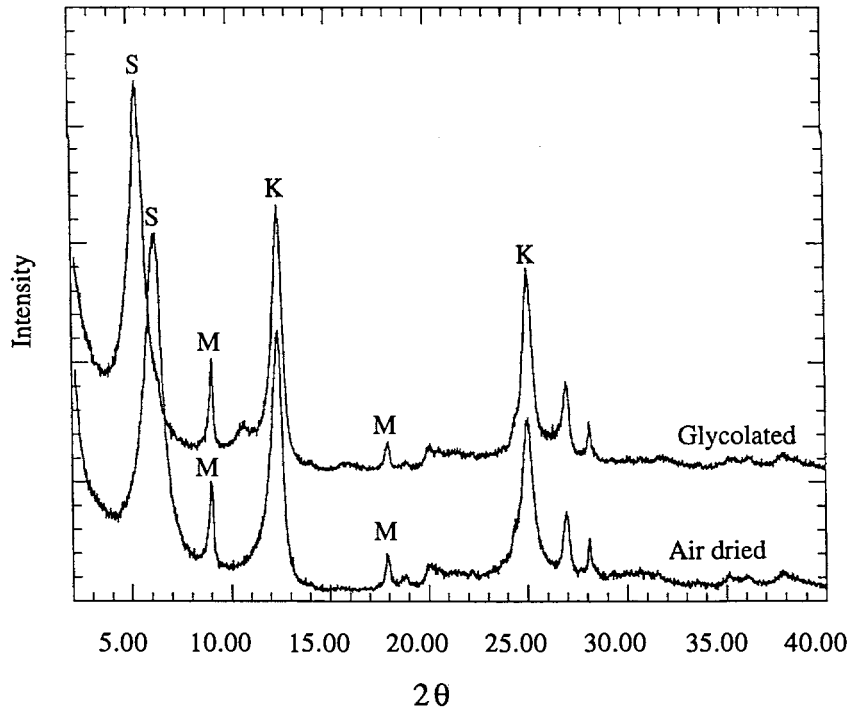

Figure 6.8: XRD traces of air-dried and ethylene glycol treated samples of <2 μm fraction from the lower saprolite [E22 P9 (18m)]: K-Kaolin; S- Smectite; M- Mica

The presence and intense iron staining of the secondary products seems to suggest that the iron plays a role in the formation and hence morphology of these products.

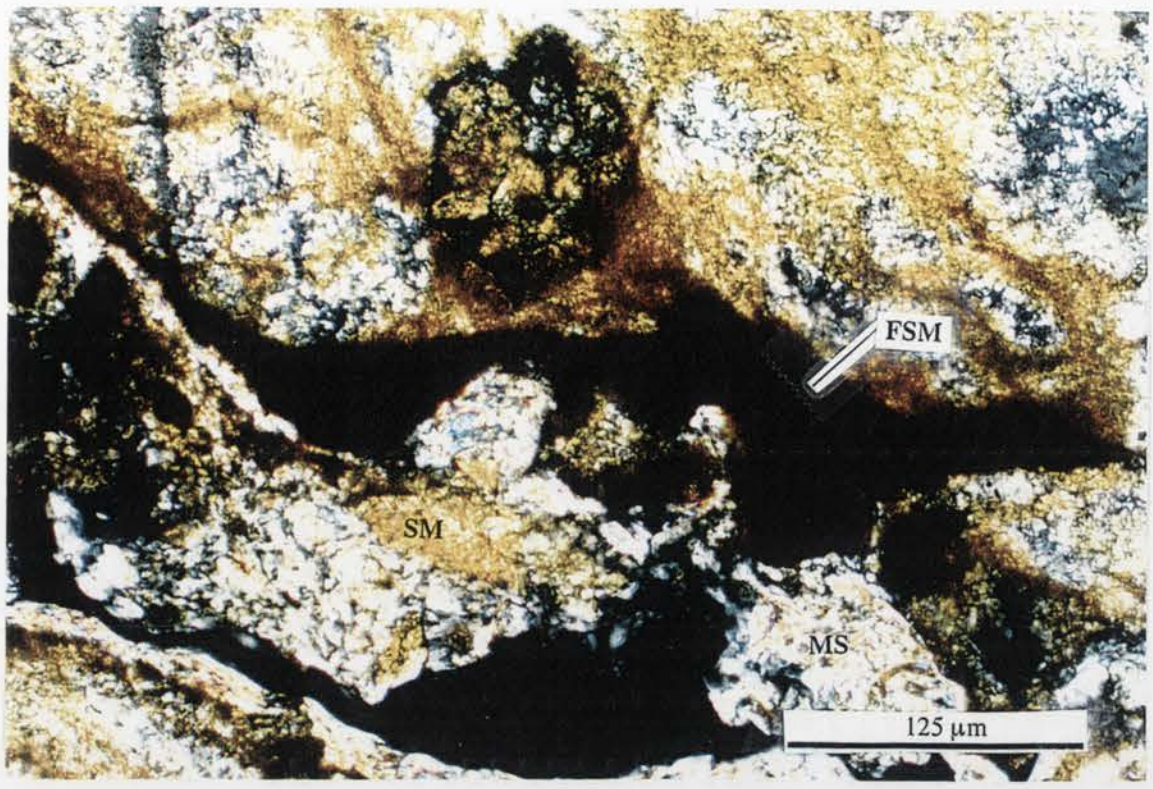

Figure 6.9.1: Reddish brown iron stained smectite (FSM) and the yellowish green smectit(SM) in a plasma of very fine-grained low birefringent kaolinite. Some muscovite plates (MS) are presnet in the plasma.

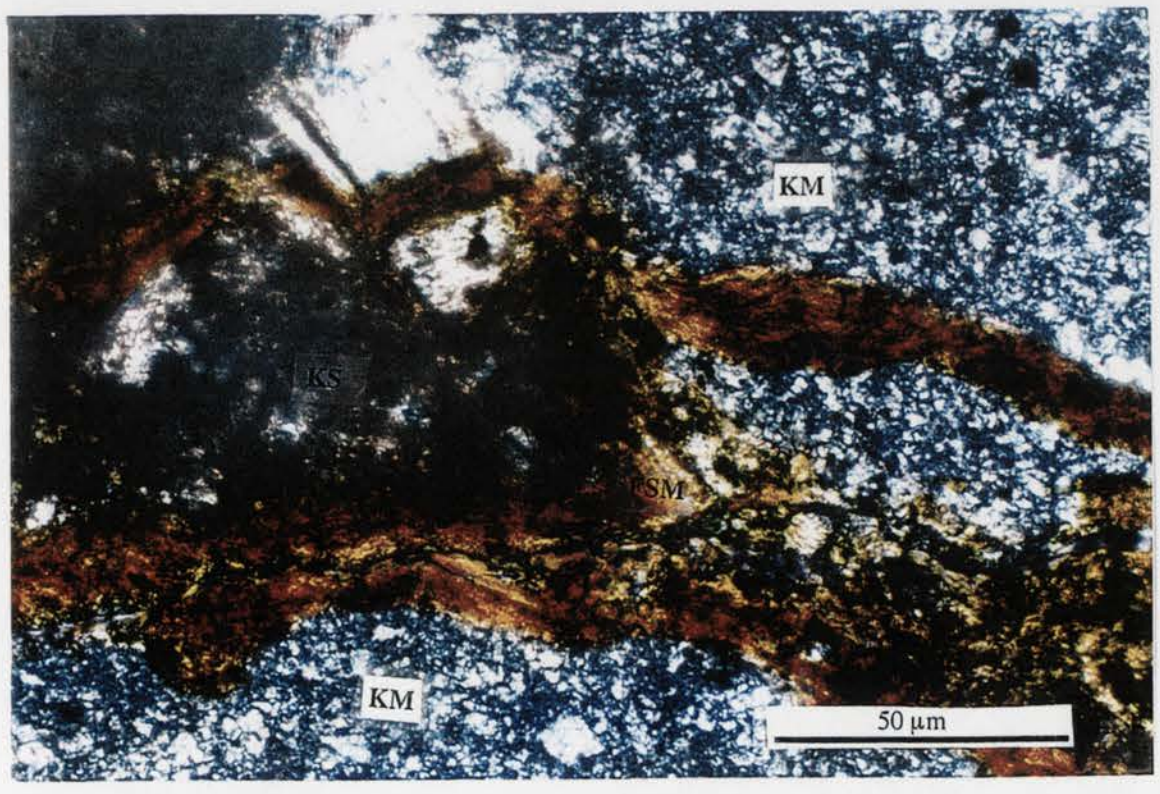

Figure 6.9.2: The plagioclase has been replaced by very fine-grained low birefringent patches of mixed kaolinite and mica (KM) while the K-feldspar has been replaced by very fine-grained 'cloudy' kaolinite (KS). Iron stained smectite (FSM) occur in fractures within the plasma.

Figures 6.6: The different morphologies of the smectites from the saprock and saprolite

Fig.ure 6.6.1: Cellular 'cotton wool' textured smectite on feldspar surface
Scale bar = 10 μm

Figure 6.6.2: Curly and striated surface of the 'cornflake' smectite during initial nucleation.
Scale bar = 10 μm

Figure 6.6.3: 'Cotton wool' textured smectite on the striated surface of 'corn-flake' textured smectite
Scale bar = 10 μm

Figure 6.6.4: Development of curly 'cornflake' texture on the smectite.
Scale bar = 10 μm

Figure 6.6.5: 'Cotton wool' textured smectite curled within tip sof the 'corn-flake' textured smectite
Scale bar = 10 μm

Figure 6.6.6: A close up view of the curls on tips of the 'corn-flake' smectite.
Scale bar = 5 μm

Figure 6.6.7: A close up view of the smectite 'cornflakes'.
Scale bar = 10 μm

Figure 6.6.8: A close up view of the smectite 'cornflakes'.
Scale bar = 5 μm

1


andesite saprolite
10.0µm

2

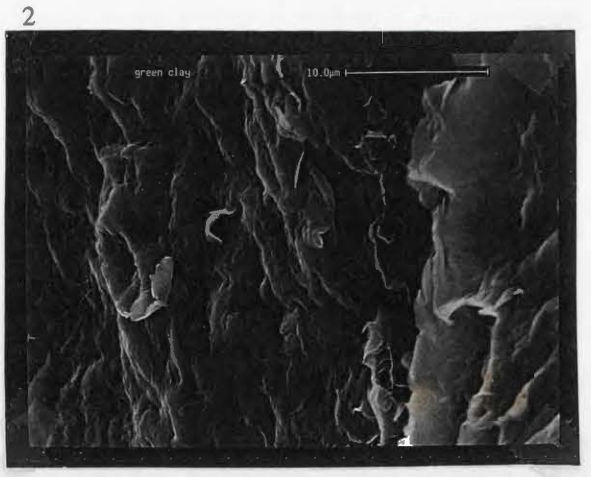
green clay
10.0µm

3

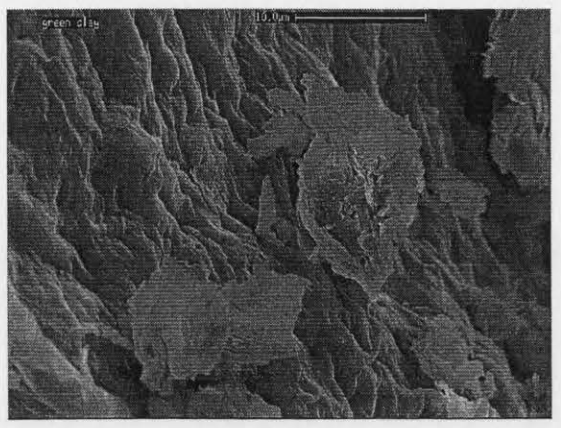
green clay
10.0µm

4

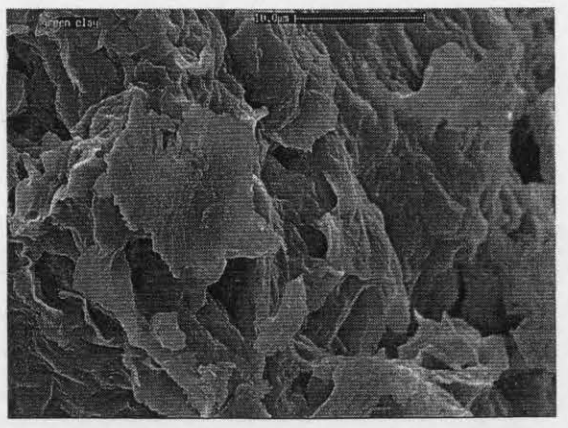
green clay
10.0µm

5

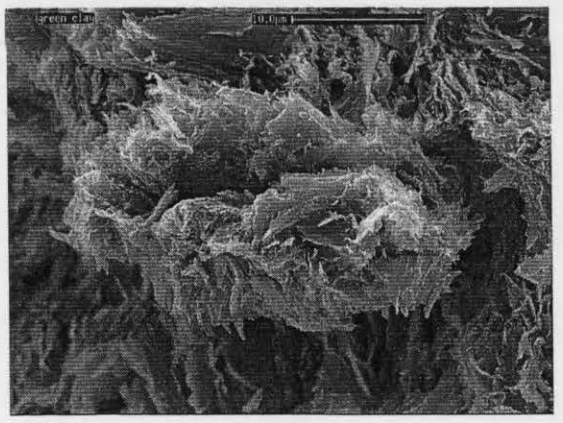
green clay
10.0µm

6

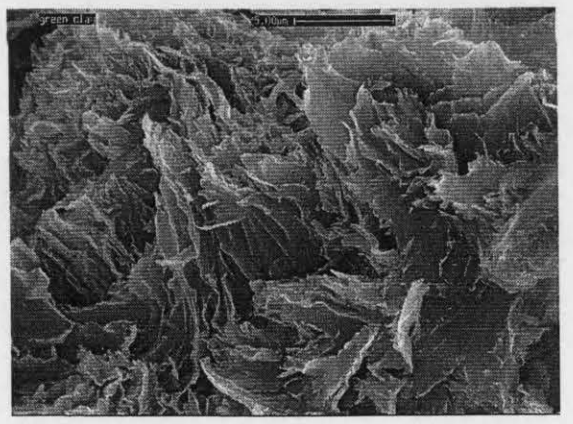
green clay
5.00µm

7

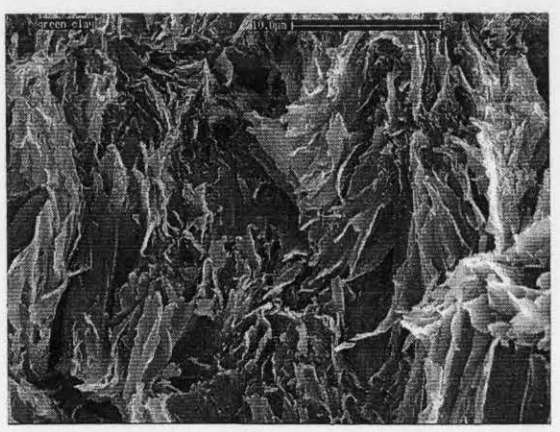
green clay
10.0µm

8


green clay
5.00µm

6.5.2 Middle saprolite

The lower saprolite grades into the middle saprolite, which is thick (15 to 25 m), more friable and softer as compared to the lower saprolite. This zone is marked by a dramatic decrease in the spongy 'cotton wool' textured clay and the predominance of the curly and platy 'corn flake' textured clay. Qualitative SEM EDXA analysis of the different 'corn flake' clays indicated that this clay has appreciable amounts of Fe and Si and low Ca. This smectite has been interpreted as nontronite (Chapter 7). SEM micrographs indicated initial nucleation as a curly and striated clay, which later develops into the diagnostic 'corn flake', texture (Figures 6.6).

XRD clay mineralogy (Figure 6.10) confirms the dominant mineralogy to be kaolinite. The kaolin content in this horizon is higher than in the lower saprolite. SEM micrographs show the kaolin to be characterized by distinct plates and books (Figures 6.12.1, 6.12.2, 6.12.3, 6.14.4) and vermiforms (6.12.7 and 6.12.8).

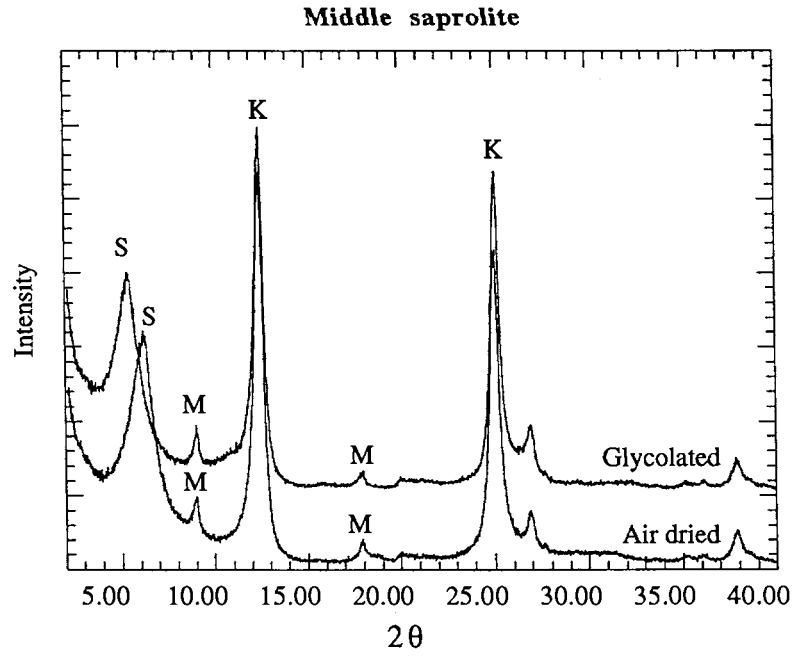

Figure 6.10: XRD traces of air-dried and ethylene-glycol treated samples of the <2μm fractions from the middle saprolite [Specimen E22 P9 (14 m)]: K-Kaolin; S- Smectite; M- Mica.

Petrographic examinations reveal that the feldspars have been extensively altered to kaolin. The plagioclase feldspars have been altered to very fine-grained (0.001-0.005 mm) low-birefringent clay kaolinite, flecked with patches of mixed kaolinite and mica (Figure 6.9.2). The K-feldspar exhibits a slight undulose extinction and is partly clouded by extremely fine-grained (< 0.001 mm) kaolinite.

The secondary clays (particularly the smectite) are also still highly stained by iron oxides. Figures 6.9.1 and 6.9.2 shows the cutanic argillans precipitating in the fractures with some pervasively intruding the groundmass outward from the fracture. The fracture seems to act as a localized redox front where iron is being reduced or oxidized and subsequently incorporated into the weathered products.

As weathering progresses, a dominant clay phase, pseudomorphing the plagioclase, consists of a mat of fine grained (0.005 - 0.10 mm), low birefringent kaolinite, set with clusters, larger flakes, plates, books and distorted stacks of a more birefringent (white to yellow) kaolinite-muscovite mixture (Figures 6.11.1, 6.11.2 and 6.11.3). SEM EDXA shows that this mixture contains Fe and K and represents weathered sericite flakes. The close association of the clay and sericite has resulted in a material with a moderate yellow to white birefringence resulting in the development of 'accordion-like' structure of mixed kaolinite and mica with birefringence varying from first order yellow to distinct grey (Figures 6.11.2 and 6.11.3). SEM micrographs also revealed the presence of these accordion fabrics (Figures 6.12.5 and 6.12.6) and showed it to consist of an intimate mixture of kaolin and muscovite plates. Intense iron staining is evident adjacent to the accordion fabrics.

Another clay phase with a streaky mat of fine-grained (0.001 mm), low birefringent clay is also set in books, stumps and plates of a white birefringent kaolinite. This variety is devoid of the iron staining. The accordion fabrics are poorly developed and the weathered sericite flakes, which occurred close to the accordion fabrics in the previous clay, are almost absent. This variety becomes more abundant as weathering progresses and is interpreted as representing the weathering of unsericiticized K-feldspar. Figure 6.11.4 distinguishes the kaolinite types resulting from the weathering of the two feldspars.

The 'corn flake' textured smectite starts to decrease in content as kaolin becomes more abundant. The kaolin has acquired pseudohexagonal platy shape with or without book or vermiform fabrics (Figures 6.12). The kaolin plates do not show any preferred orientation with respect to the other aggregates (i.e. minute plates or crystals can occur with small or large books). The plagioclase content decreases and K-feldspar and

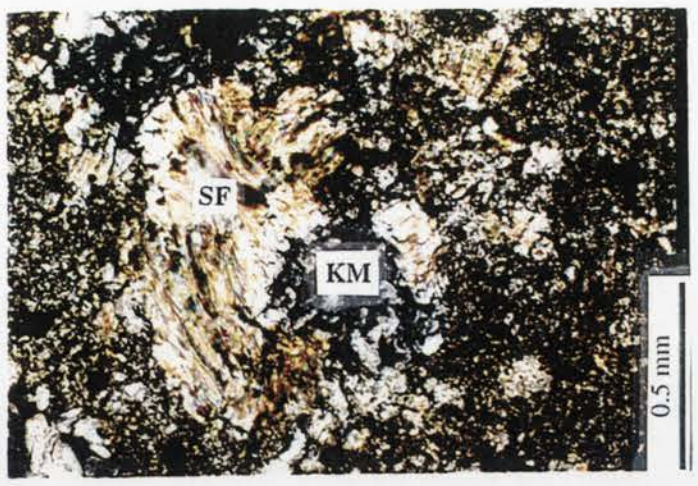

Fig.6.11.1. Sericite flakes (SF) set in fine-grained low birefringent kaolinite (KL) flecked with patches of mixed kaolinite and mica (KM). Middle saprolite. Specimen E22 TR2 S2. Photomicrograph with crossed polars.

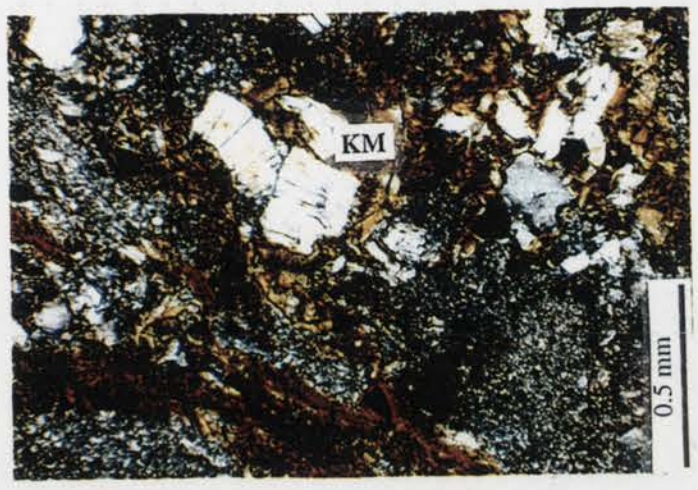

Fig.6.11.2. Stumps, books and distorted stacks of highly birefringent kaolinite-mica mixture (KM) set in a matrix of loW birefringent clay forming 'accordion' structures. Notice the iron lining the fractures in close proximity to the accordion fabrics. Middle saprolitE. Specimen E22 TR2 S2. Photomicrograph with crossed polars.

Fig. 6.11.3: Close up view of 'accordion' structures of mixed kaolinite and mica with birefringence ranging from first order white to yellowish white to grey. Middle saprolite. Specimen E22 TR2 S3. Photomicrograph with crossed polars.

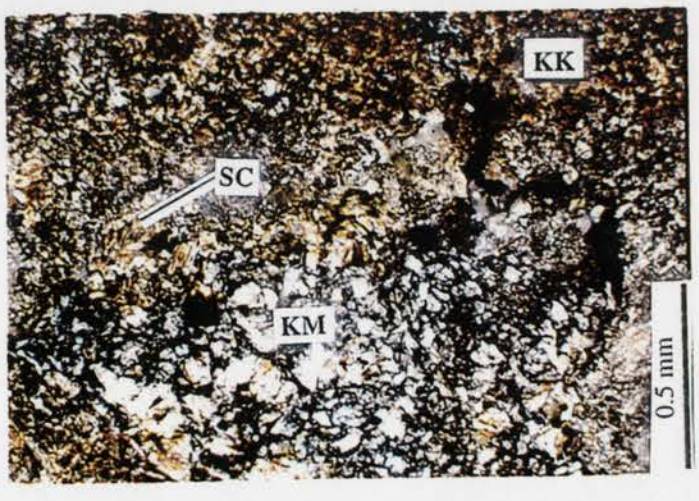

Fig. 6.11.4 Kaolinite after two types of feldspars (i) Fine-grained streaky low birefringent kaolinite (KK) from K-feldspar weathering and (ii) Coarser-grained more birefringent kaolinite (KP) from plagioclase containing remnant sericite which also occurs independent of the kaolin in the matrix (SC). Middle saprolite. Specimen E22 TR2 S3. Photomicrograph with crossed polars.

Figures 6.12: The different morphologies of the secondary products from the lower and middle saprolite

Figure 6.12.1: Kaolin plates and 'books' from the middle saprolite Scale bar = 5 μm

Figure 6.12.2: Kaolin plates and 'books' from the middle saprolite. Scale bar = 10 μm

Figure 6.12.3: Pseudohexagonal plates of kaolin with some 'books' from the middle saprolite. Scale bar = 5 μm

Figure 6.12.4: Pseudohexagonal plates of kaolin from the middle saprolite. Scale bar = 5 μm

Figure 6.12.5: Accordion oriented plates of mixed kaolinite and mica. The muscovite has larger plates than kaolin. Middle saprolite. Scale bar = 5 μm

Figure 6.12.6: Accordion plates of mixed kaolinite and mica with pseudohexagonal plates of kaolin. Middle saprolite Scale bar = 10 μm

Figure 6.12.7: Vermiform 'book' type kaolinites from the lower saprolite. Scale bar = 5 μm

Figure 6.12.8: Kaolin plates and vermiforms from the lower saprolite. Scale bar = 5μm

1

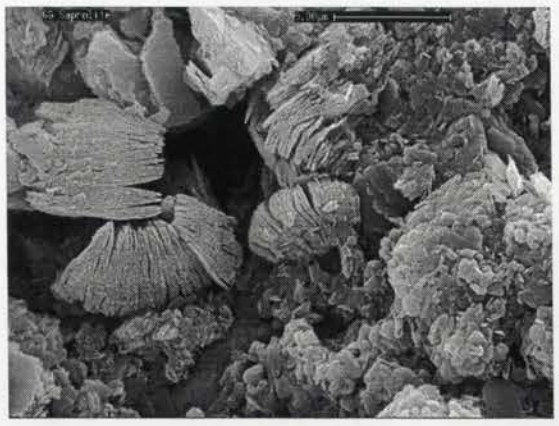

2

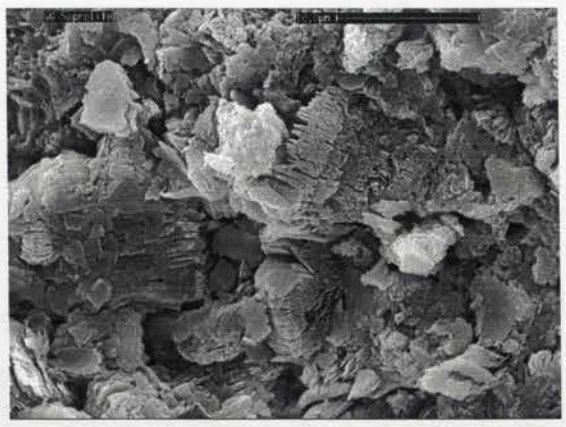

3

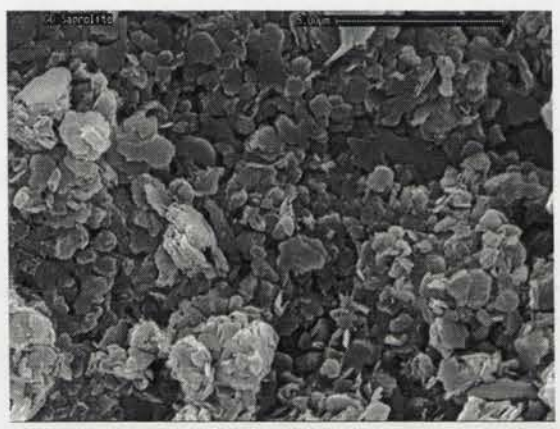

4

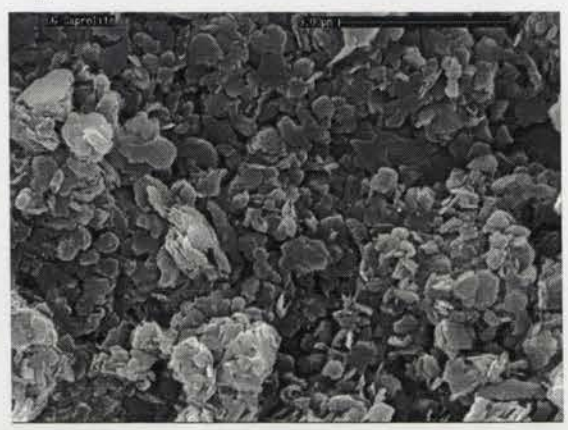

5

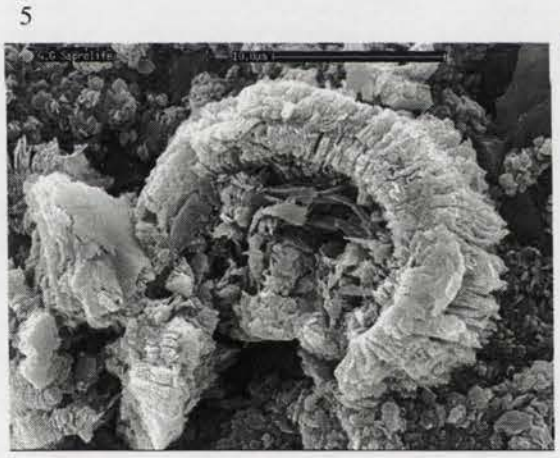

6

7

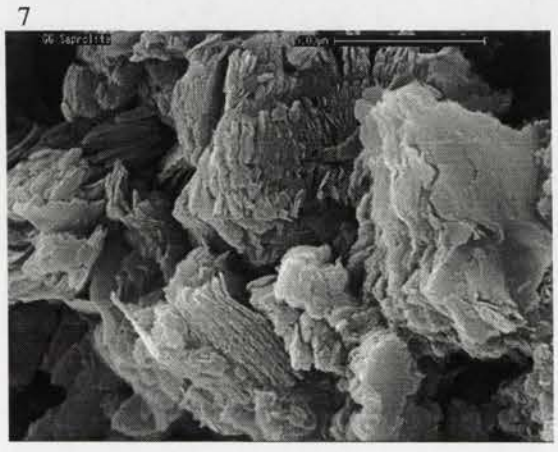

8

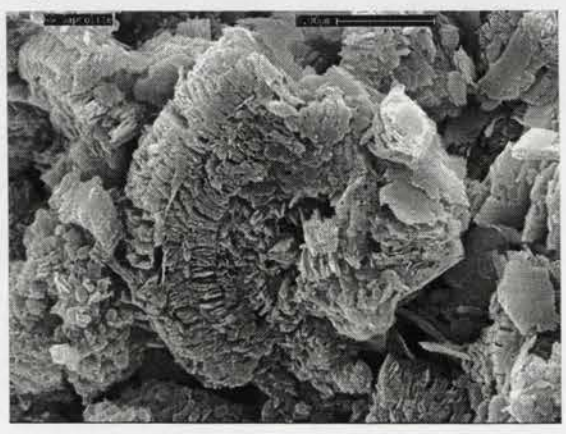

muscovite become more predominant as weathering progresses towards the upper saprolite (Figure 6.3.2) The fabric also acquires a distinct orange pink colouration.

6.5.3 Upper saprolite

This zone is marked by the disappearance of the plagioclase laths from the groundmass. The matrix is now composed of irregular spots of remnant sulfides and white clay patches in an otherwise orange pink matrix (Figure 6.3.2). The material is more friable and softer than in the middle saprolite.

XRD clay mineralogy (Figure 6.13) confirms the disappearance of the smectite clay from the matrix and the abundance of well crystalline kaolin. XRD bulk mineralogy also confirms the loss of plagioclase in this horizon. The mineralogy is now dominated by muscovite, K-feldspar, kaolin and hematite with low amounts of hornblende.

Morphologically, the secondary products consist of pseudohexagonal plates and books and vermiforms of kaolin (Figures 6.14). Relatively larger plates with slightly different morphology from the ones encountered before are present in this zone. SEM EDXA shows the presence of K within the matrix confirming these plates as muscovite crystals. These plates occurred together with the kaolin plates suggesting some of the kaolinite in this horizon to be a product of muscovite weathering. The presence of weathered sericite flakes in the middle saprolite is further evidence of the existence of this alteration mechanism.

Petrographic examinations reveal the predominance of very fine-grained low birefringent kaolin within the orange pink stained plasma (Figures 6.15). Some remnant K-feldspar phenocrysts have been almost replaced by very fine grained sericite-kaolinite mixture. The fabric is cross-cut by small channelways and void spaces many of which have been infilled with kaolinite and a mixture of a reddish brown poorly crystalline mixture of clay and iron oxide.

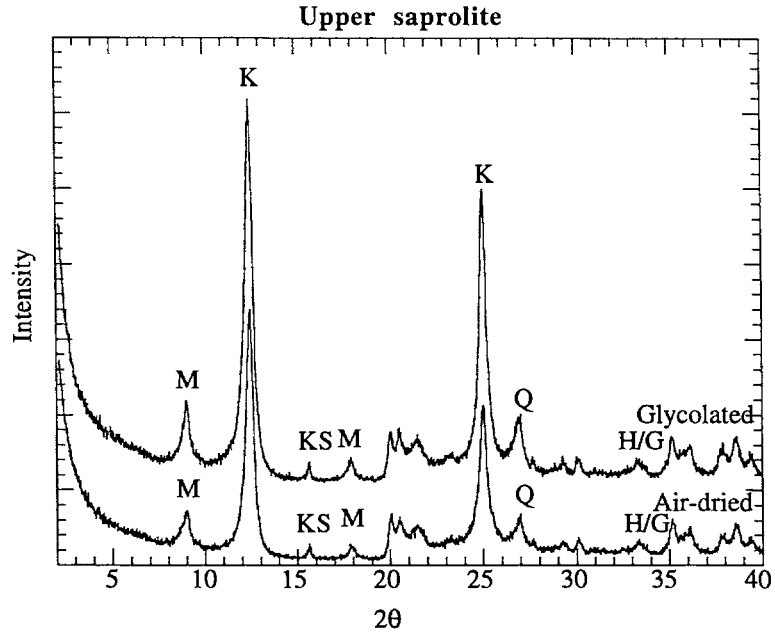

Figure 6.13: XRD traces of air-dried and ethylene-glycol treated samples of <2 μm fractions from the orange-pink saprolite [Specimen E22 P7 (16m)]: K- Kaolinite; M-Mica; KS- K feldspar; Q-Quartz; H/G- Hematite or goethite.

Intense fabric re-organization occurs towards the upper part of the profile. Small, globular blasts of very fine-grained yellow to white birefringent sericite-kaolinite mixture appear within the matrix. This progressively becomes more abundant approaching the transition zone with the overlying white clay unit. The channelways become more pervasive and many have been infilled with white to grey birefringent kaolin and iron oxides, notably hematite. The orange-pink colour of the plasma is considerably reduced as the groundmass is replaced by sericitized clay and iron oxides. This coincides with the disappearance of K-feldspar within the matrix (Figures 6.15). This reorganization has caused the loss of the original rock fabric and marks the transition from the saprolite to the white clay unit above.

6.5.4 White clay unit

The material from this unit was too soft and friable for thin-section preparation and hence most its characteristics have been mainly inferred from XRD and SEM studies. XRD clay mineralogy shows the reappearance of smectite and the persistence of muscovite and kaolin within the matrix (Figure 6.16). The smectite of this horizon is broad and shifted

Figures 6.14: Morphologies of grains from the upper saprolite

Fig. 6.14.1: Muscovite plates with clay encrustations from the upper saprolite. Specimen E22 P7 OP 1. Scale bar = 20 μm

Fig. 6.14.2: Vermiform and platy kaolin crystals from the upper saprolite. Specimen E22 P7 OP 3. Scale bar = 5 μm

Fig. 6.14.3: Kaolin plates and 'books' from the upper saprolite. Specimen E22 P7 OP 4. Scale bar = 2 μm

Fig. 6.14.4: Muscovite plates adhering closely to the quartz within the upper saprolite. Specimen E22 P7 OP 5. Scale bar = 20 μm

Fig. 6.14.5: Vermiform kaolin oriented parallel to the muscovite plates (larger size) within the white clay unit. Specimen E22 P7 OP 6. Scale bar = 5 μm

Fig. 6.14.6: Pseuodohexagonal kaolin plates within the white clay unit. Specimen E22 P7 WC 1. Scale bar = 2 μm.

1


Orange Pink saprolitee
20.0µm

2


Orange Pink saprolitee
5.00µm

3


clay saprolite
2.00µm

4


soil morphology
10.0µm

5


clay saprolite
5.00µm

6


white clay
2.00µm

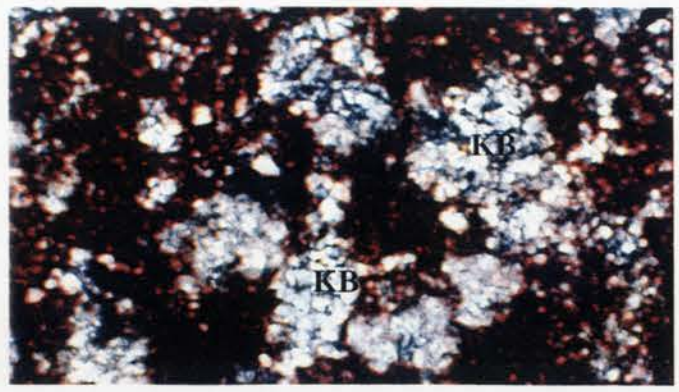

Fig.6.15.1. Globuler kaolin (KB) occurring within the orange-pink matrix. Specimen E22 P7 (16 m). Photomicrograph with crossed polars.

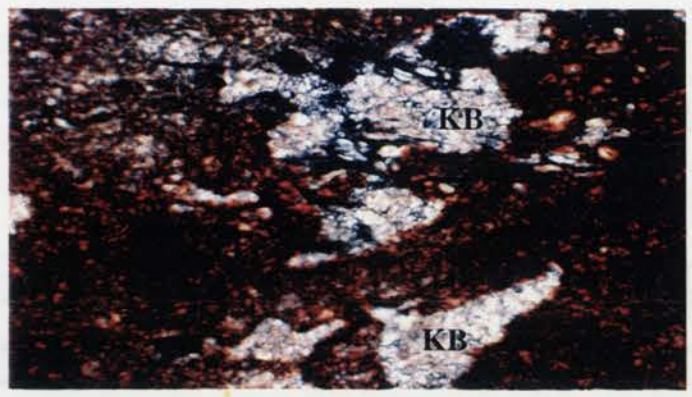

Fig. 6.15.2. Irregular blasts of mixed kaolin and mica (KB) within the orange-pink clay matrix. Specimen E22 P7 (16 m). Photomicrograph with crossed polars.

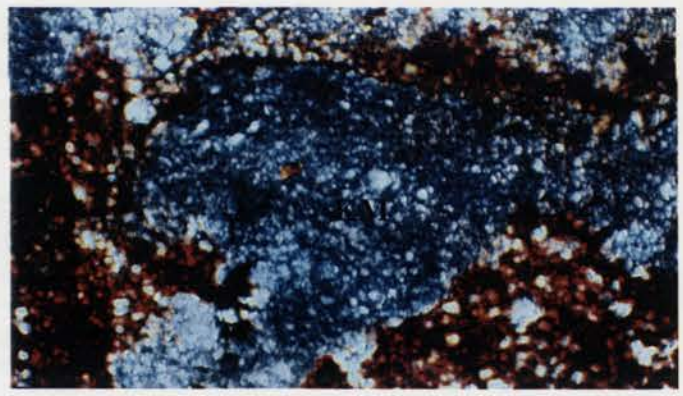

Fig. 6.15.3. A close up view of the blasts showing a mat of low birefringent kaolin (KM) with mica inclusions within the orange-pink clay plasma. Specimen E22 P7 (18 m). Photomicrograph with crossed polars.

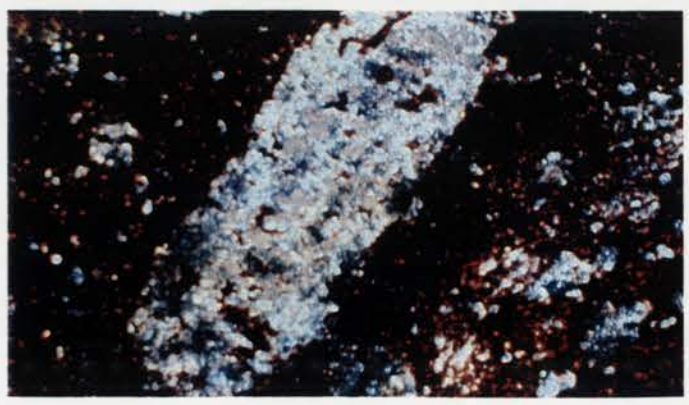

Fig.6.15.4. A K-feldspar (KSP) phenocryst which has been replaced by very fine-grained kaolin. Specimen E22 P7 (18 m). Phtomicrograph with crossed polars.

to 17Å on glycolation. It thus seems to be slightly different from the smectite of the middle and lower saprolite and is quite similar to the smectite encountered in the soil horizons (Section 6.8).

Morphological studies show the presence of pseudohexagonal plates and books of kaolin and minor amounts of muscovite plates (Figure 6.14.5 and 6.14.6). XRD bulk mineralogy also confirms the presence of hematite and goethite and dolomite although the presence of the latter was not detected by SEM examination. The loss of lithic fabric is pronounced as soil forming processes become more predominant.

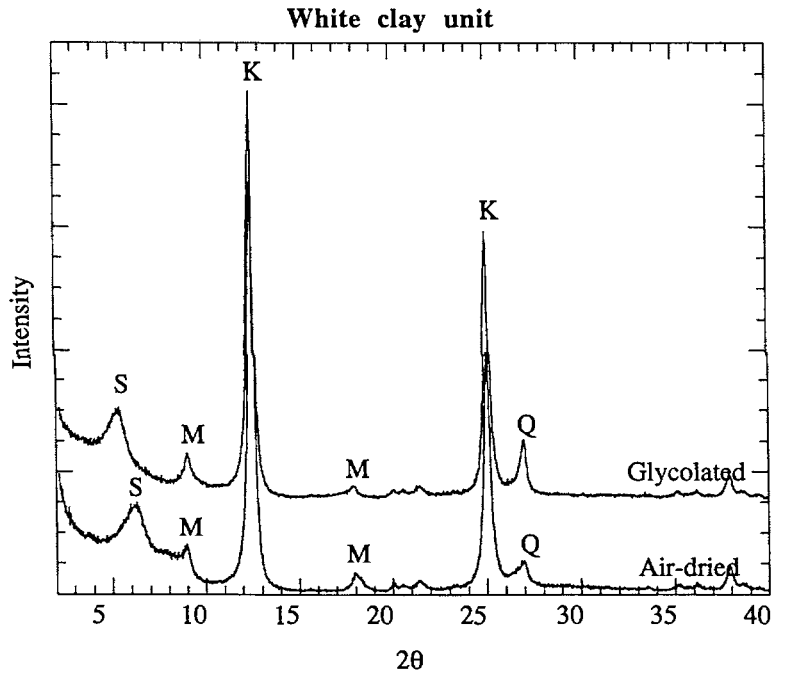

Figure 6.16: XRD traces of air-dried and ethylene-glycol treated samples of <2μm fractions from the white clay unit [Specimen E22 P7 (10 m)]: K- Kaolinite; S- Smectite; M- Mica; Q- Quartz.

The characteristics of the soils developed over the andesite and the mottled clay zone are discussed in section 6.8.

6.6 MOTTLED CLAY ZONE

This zone occurs between the soil and the saprolite in the more deeply weathered sections of the pit (Chapter 5, Figure 5.1). As already mentioned in Chapter 5, three different types of mottles have been encountered and differentiated on the basis of iron

accumulations (mottles) into mini-medium-and mega-mottles. Figures 6.18 show that the fabric of the mottled clay zone is characterized by the occurrence of intermittent or diffuse segregations of iron (mottles or nodules) in a predominantly clay rich plasma.

The mineralogy of the mottled clay zone is dominated by quartz, kaolin, hematite, goethite and dolomite and minor amounts of smectite and gypsum. Quartz, kaolin, hematite and goethite are present in all the sub-zones. Gypsum occurs in very small amounts within the mini-mottled clay zone while smectite occurs only in the mini-and-mega-mottled clay. Anatase is present in both the medium-and-mega-mottled clay while dolomite occurs only in the mega-mottled clay. Detrital rock fragments (Figure 6.27.8) rich in the primary rock minerals i.e plagioclase and muscovite are also present within the plasma although they occur in very small amounts in the predominantly clay and iron oxide rich plasma.

The mini-mottled clay has inherent characteristics of the overlying soil horizon. The plasma is traversed by numerous root channels which have been lined with pale yellowish brown to grey kaolinitic clay and yellow, cellular goethite (Figure 6.20.2). SEM EDXA of these channels also shows the presence of dark manganese rich wads. Skeletal grains of iron oxide stained lithorelics translocated from the soil horizon occur within the plasma, so too a few intercrysts of gypsum crystals and numerous sub-rounded to sub-angular quartz grains (Figure 6.20.1).

Occasionally, the root channels contain relicts of the primary minerals of the host rock i.e muscovite, plagioclase and K-feldspar. Figure 6.21.2 shows traces of muscovite with poorly defined cleavage set in fibrous to spongy goethite rich root clasts while Figure 6.21.1 shows plagioclase with poorly defined twinning also set in a fibrous to spongy goethite rich plasma. Away from these root channels, there is concentration of ultra fine-grained (< 0.001 mm) weakly anisotropic reddish brown to red hematite stained plasma. The root channels give way to void spaces which in some parts have strung together to form channelways (Figure 6.20.3). Some of these channelways are open while others have been lined with siliceous or ferruginous clay and/or goethite. The goethite has in parts permeated outwards from the channel into the clay for a short distance (Figure 6.20.4).

The fact that the interior of the channels tend to be goethitic and the exterior hematitic could be related to water access, which may either influence the equilibrium between goethite and hematite, during iron oxide precipitation, or the solid state dehydration of goethite to hematite further away from the channels. This selective distribution is more

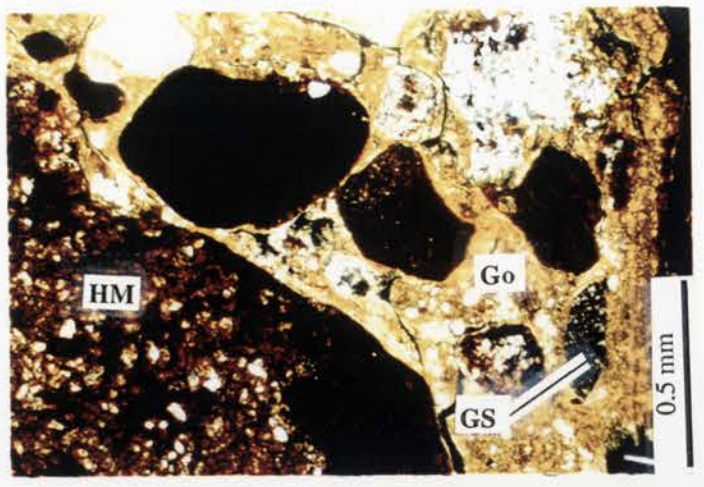

Fig.6.20.1: Translocated ferruginized lithorelicts and intercrysts of gypsum in cellular goethite infilled channel. Notice the sharp contact between the channel and the surrounding hematite-rich plasma. Specimen E22 P4 (4 m) Mini-mottled clay. Photomicrograph in crossed polars.

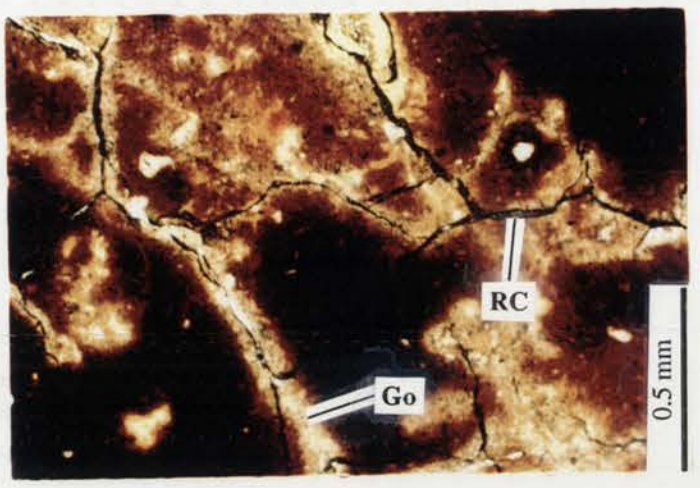

Fig. 6.20.2: Root channels that have been lined with goethite in hematite-stained plasma. Specimen E22 P4 (5 m) Mini-mottled clay. Photomicrograph in crossed polars.

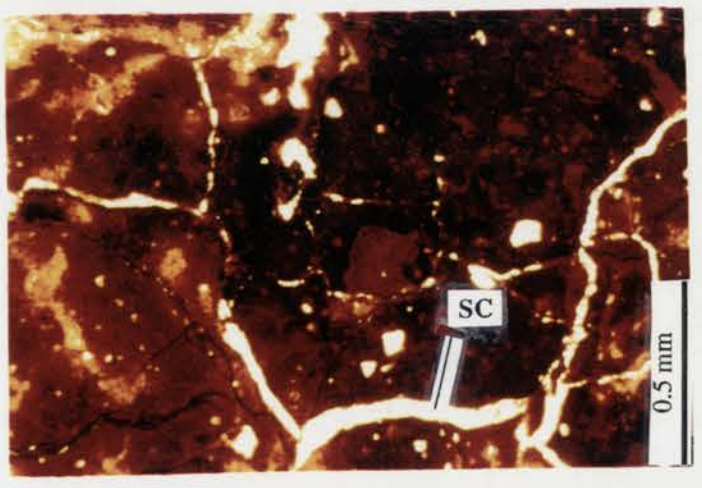

Fig. 6.20.3: Voids and channels lined with siliceous clay and cellular goethite with hematite granules in a mixed hematite/goethite rich plasma. Specimen E22 P5 (12 m)- Medium-mottled clay. Photomicrograph with crossed polars.

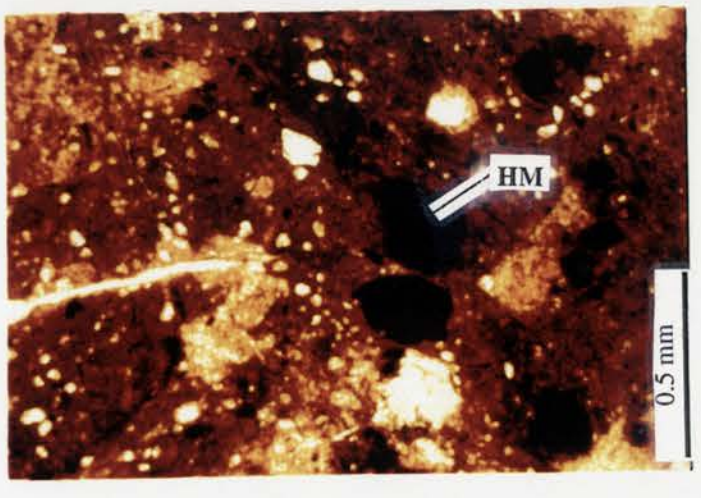

Fig. 6.20.4: Development of hematite nodules (HM) in hematite and goethite rich plasma. Detrital quartz fragments are abundant in the matrix. Specimen E22 P5 (14 m). Photomicrograph in crossed polars.

prevalent within the upper portions of the mottled clay zone than in the lower portions. XRD analysis suggests that the dominant clay within this horizon is a well crystalline (sharp peaks) kaolin with small amounts of smectite (Figure 6.22).

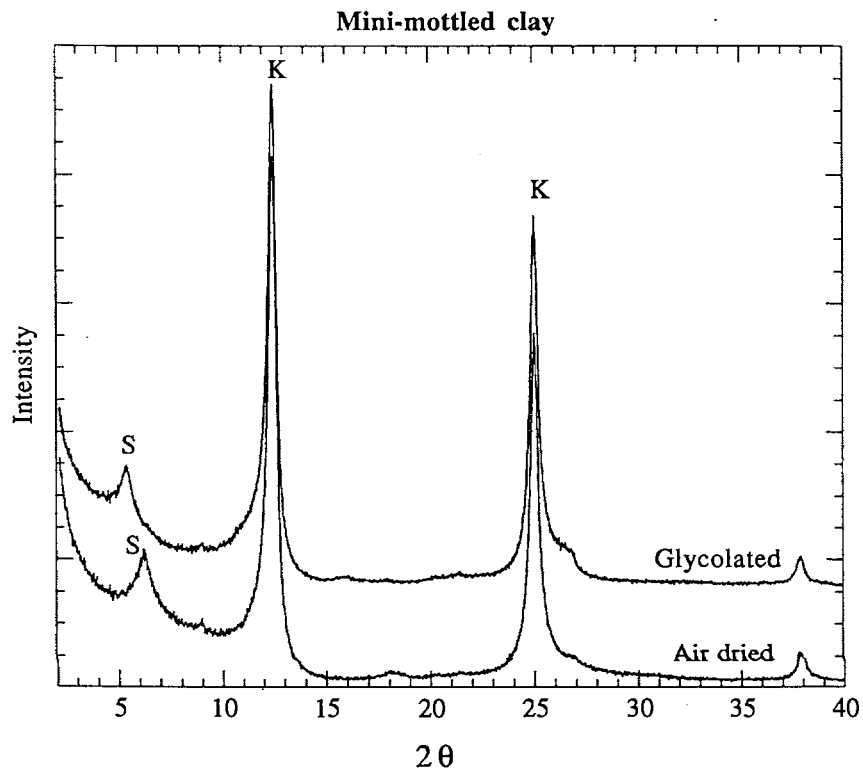

Figure 6.22: XRD traces of air-dried and ethylene-glycol treated samples of <2μm fractions from the Mini-mottled clay unit [Specimen E22 P4 (6 m)]: K- Kaolinite; S- Smectite.

As further reorganization of the fabric continues, small granules (0.5 to 1 mm) of hematite and goethite become scattered throughout the matrix (Figure 6.20.3). In some parts these have formed hematite-goethite rich nodules (Figure 6.20.4). The characteristics of these nodules are discussed in Section 6.7

The medium-mottled clay is marked by an increase in the distribution of ferruginous nodules (5 to 20 mm in size) and sub-rounded to sub-angular sand-sized (<2 mm) and pebbly quartz fragments (10 to 30 mm in size). Small ferruginous granules similar to the ones encountered before are still persistent. XRD mineralogy shows the dominant clay mineral to be a well crystalline kaolinite in this sub-zone (Figure 6.23). The distribution

of the iron oxides is more diffuse although in some places goethite is more predominant in the void spaces than hematite. The sub-zone is also marked by an increase in the concentration of voids, fractures and channelways.

Characteristic iron oxide-stained clay-filled banded channels showing a sweeping extinction under crossed polars (Figures 6.21.3) are quite common within the channelways and voids. These structures represent the settling and orientation of the eluviated clays at these channelways or voids. Some of the clay bands are poorly defined as a result of the restricted mobility of solutions within closed or restricted channelways (Figure 6.21.4) and often occur with hematite stained root stringers (6.21.5). Yellow goethite-rich cutans (argillans) forms a coating on a number of the quartz fragments (Figure 6.21.6).

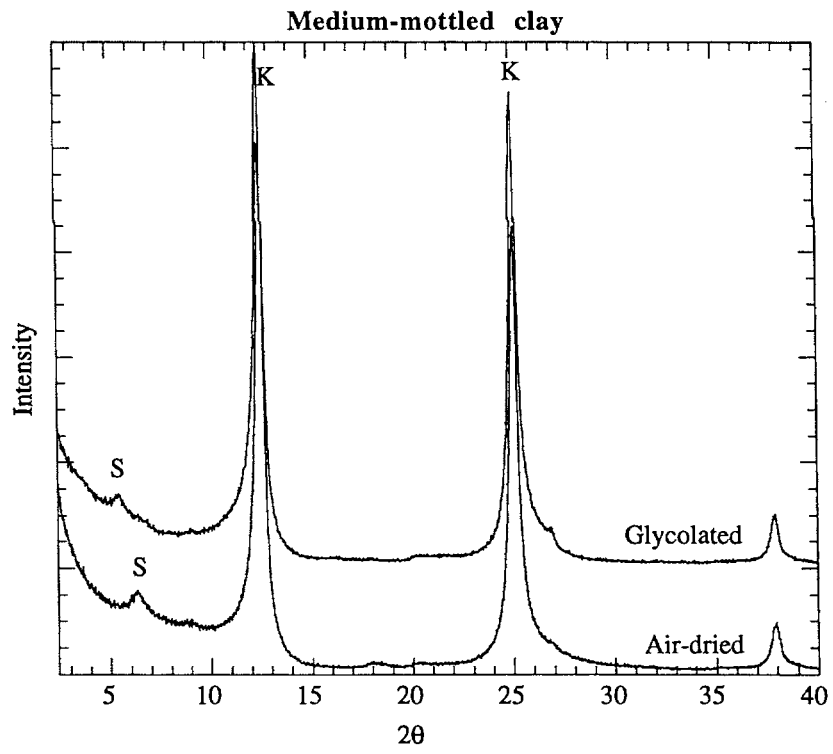

Figure 6.23: XRD traces of air-dried and ethylene-glycol treated samples of <2μm fractions from the medium-mottled clay [Specimen E22 P4 (14m)]: K- Kaolin; S- Smectite.

The mega-mottled clay is marked by a dramatic decrease in the distribution of ferruginous nodules within the plasma. Ferruginous granules are still present though in lesser amounts than in the previous sub-horizon. The quartz like in the medium-mottled

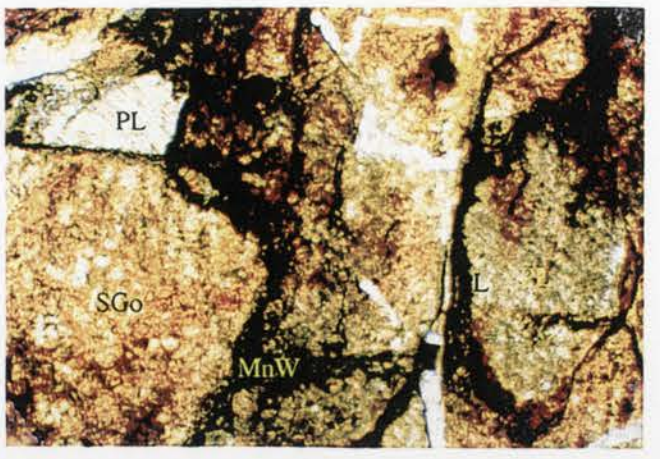

Fig. 6.21.1: Plagioclase grains (PL) with diminished twinning within root channels developed in a spongy goethite-stained clay plasma. Specimen E22 P4 (6 m). Mini-mottled clay. Photomicrograph in crossed polars.

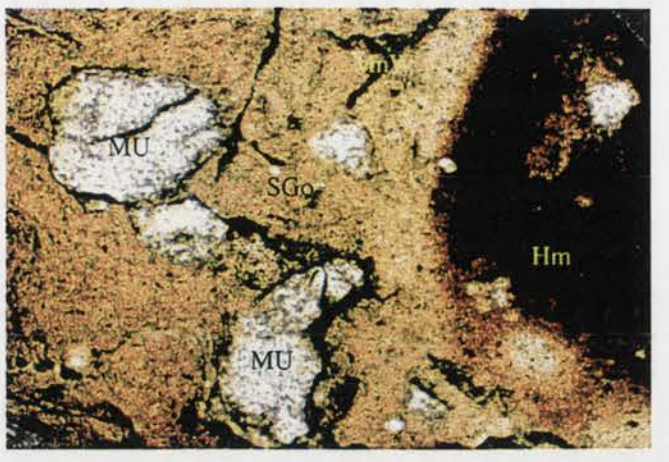

Fig. 6.21.2: Remnants of muscovite (MU) displaying poor cleavage within a root channel in a matrix of spongy goethite (SGo). The root channel is lined with undeterminable manganese wads (MNW). Specimen E22 P4 (7 m) Photomicrograph in crossed polars.

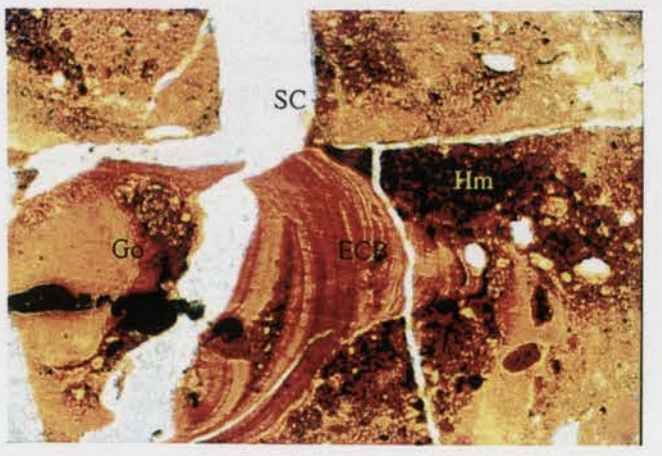

Fig. 6.21.3: Clay filled banded channel showing a sweeping extinction indicating orientation of eluviated clays during deposition. Specimen E22 P5 (12 m). Medium-mottled clay. Phtomicrograph in crossed polars.

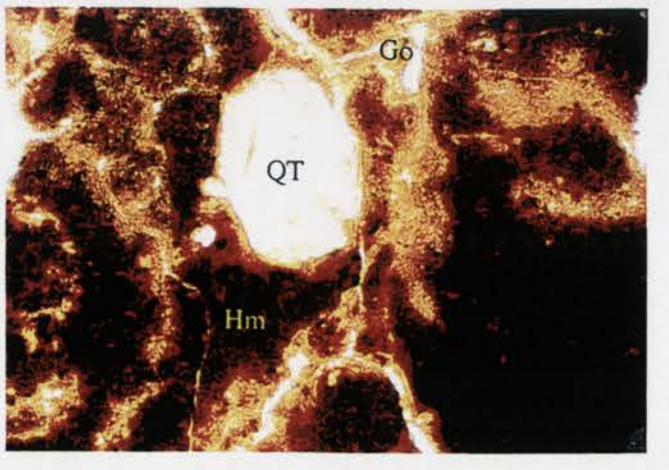

Fig. 6.21.4: Pebbly quartz (QT) coated with goethite in a hemattite-goethite rich matrix. The goethite occurs as solution channel infill. Specimen E22 P4 (16 m). Medium-mottled clay. Photomicrograph in crossed polars.

clay occur as sand sized (< 2 mm) or pebbly fragments (10 to 30 mm in size). Hematite has attained a reddish brown dull appearance in both hand specimen and thin section and mostly occurs as a clay stain as opposed to the sharp red to reddish brown colour of the mottles and nodules of the previous horizons. The goethite has acquired a characteristic dull yellowish brown colour with colloform or spongy texture. Like hematite, it occurs as a clay stain or as a void or fracture infill. The plasma is clay rich with XRD < 2 μm fraction (Figure 6.24) showing the dominant clay to be a well crystalline kaolin with some smectite.

The plasma is defined by ultra fine-grained (<0.001 mm) grey to greyish brown or pink kaolin. Root clasts, fractures and channelways are quite abundant with most of these passageways filled with a carbonate, ferruginous clay, and undeterminable manganese wads. The carbonate is quite abundant and it occurs as sugary white masses in the transition zone between the medium-and-mega mottled clay or as coatings on opaline silica rich aggregates. SEM micrographs (Figures 6.26) shows the carbonate occurring as fine sub-equant rhombohedral crystals rich in Ca and Mg with minor amounts of Al. From these characteristics, it is apparent that the carbonate is dolomite. Some of these carbonate crystals occur as small white specks (<10 mm) within the kaolin rich portions of the matrix.

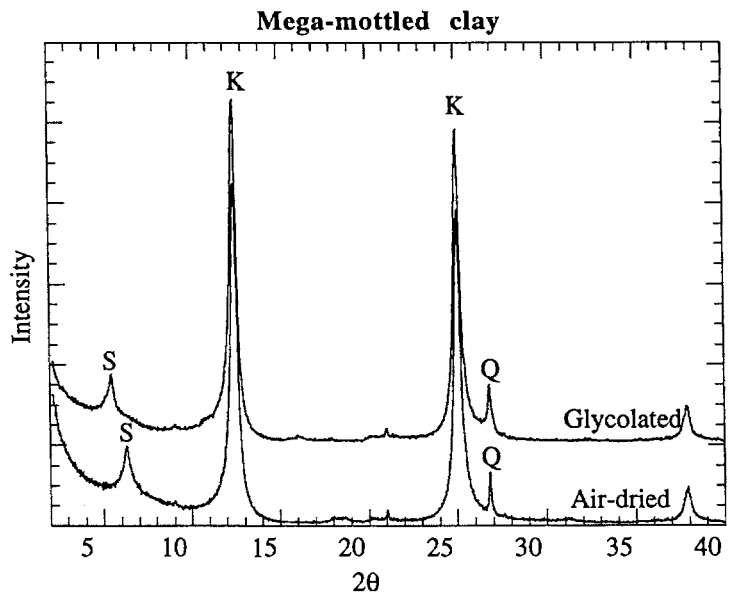

Figure 6.24: XRD traces of air-dried and ethylene-glycol treated samples of the <2 μm fractions from the mega-mottled clay [Specimen E22 P4 (22 m)]: K- Kaolin; S- Smectite.

Figures 6.25: Morphologies of the mottled clay grains

Fig. 6.25.1: Thin platy kaolin plates adhering to the quartz in the mottled clay. Specimen E22 P5 MZ 1. Scale bar = 5 μm

Fig. 6.25.2: Small dissolution pit in a quartz crystal occuring close to verm-form kaolin. Specimen E27 P6 MZ 2. Scale bar = 5 μm

Fig. 6.25.3: Slightly etched quartz crystal within the mottled clay. Specimen E27 P6 MZ 2. Scale bar = 5 μm

Fig. 6.25.4: Vermiform kaolin close to quartz grains within the mottled clay. Specimen E22 P4 MZ 2. Scale bar = 2 μm

Fig. 6.25.5: Kaolin 'books' surrounded by clay within the mottled clay. Specimen E22 P4 MZ2. Scale bar = 2 μm.

Fig. 6.25.6: Spongy smectite encrustations within the mottled clay. Specimen E22 P5 MZ 3. Scale bar = 20 μm

Fig. 6.25.7: Poorly crystalline kaolin plates from the soil horizon. Specimen E22 P9 (1m). Scale bar = 20 μm

Fig. 6.25.8: Smectite encrustations on tips of kaolin plates. Specimen E26 P5 (1m). Scale bar = 10 μm

1


mottled clay
5.00μm

2


mottled clay
5.00μm

3


mottled clay
5.00μm

4


mottled clay
2.00μm

5


mottled clay
2.00μm

6


mottled clay
20.0μm

7


soil morphology
20.0μm

8


soil morphology
10.0μm

Figures 6.26: The morphologies of dolomite

Fig. 6.26.1: Rhombohedral crystals of dolomite within the mega-mottled clay. Specimen E22 P4 QAGR 1.
Scale bar = 20 μm

Fig. 6.26.2: Rhombohedral crystals of dolomite within the mega-mottled clay. Specimen E22 P4 QAGR 1.
Scale bar = 10 μm

Fig. 6.26.3: Rhombohedral crystals of dolomite within the mega-mottled clay. Specimen E22 P4 QAGR 2.
Scale bar = 10 μm

Fig. 6.26.4: A close up view of a dolomite crystal. Specimen E22 P4 QAGR. 2. Scale bar= 10 μm

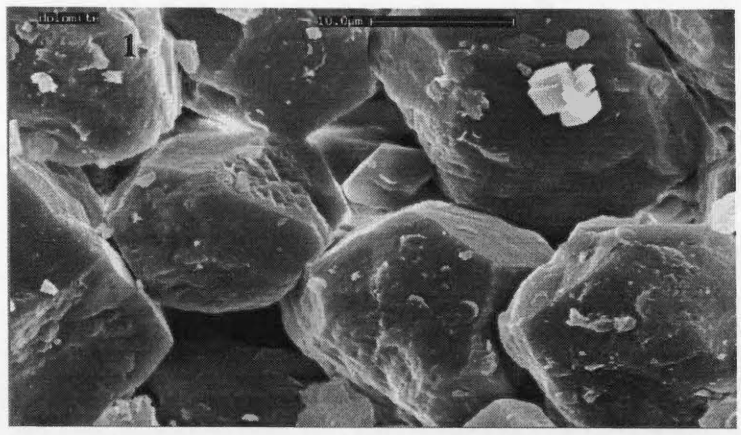
dolomite
1
20.0μm

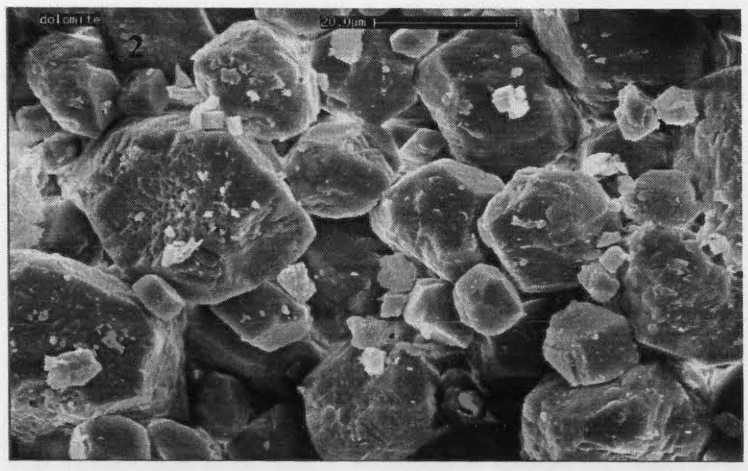
dolomite
2
20.0μm

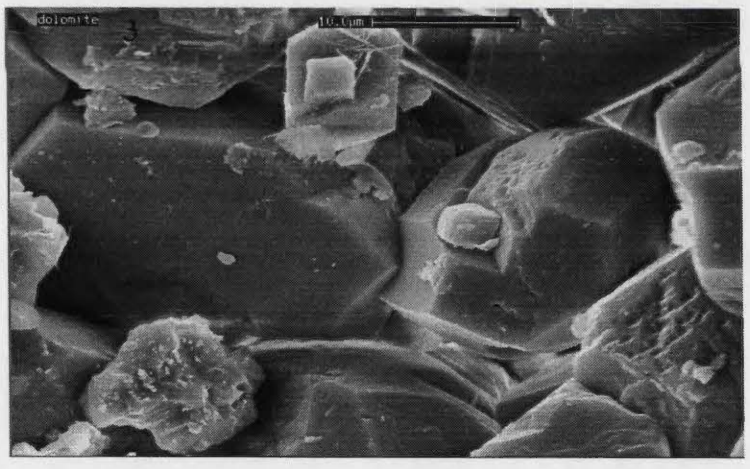
dolomite
3
10.0μm

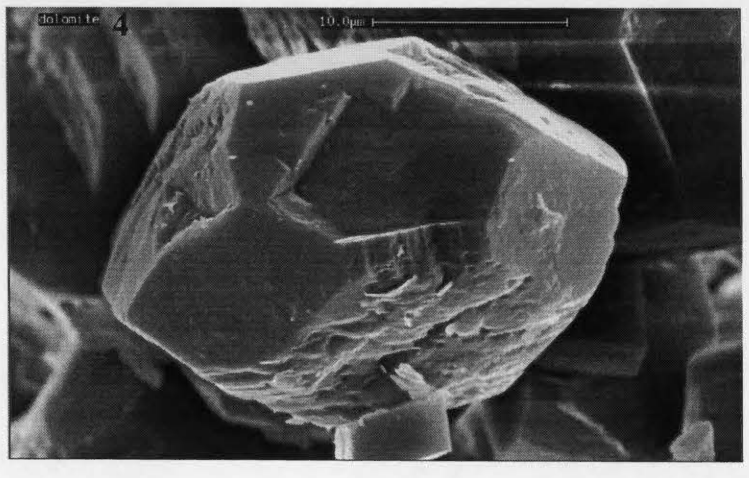
dolomite
4
10.0μm

The morphologies of the different products of the mottled clay zone are shown in Figures 6.25. The kaolin occurs as thin platy particles as opposed to the pseudohexagonal platy morphology of the saprolite. Frequently, the plates are arranged almost parallel to each other (Figure 6.25.1). The kaolin plates adhere closely to the quartz grains, which are quite abundant in this unit as opposed to the saprolite. The quartz in some specimens shows some step-like features with surfaces that are dissected by pits. These are weakly developed dissolution pits (Figures 6.25.2 and 6.25.3) on the quartz surface indicative of a moderate chemical weathering environment whereby the quartz has undergone dissolution by chemical etching.

Vermiform or book like morphology of the kaolin is also present (Figures 6.25.4 and 6.25.5) though not as abundant as in the saprolite zone. They occur close to the quartz together with the thin, platy variety (Figure 6.25.4). The smectite when present occurs as the cellular 'cotton wool' textured variety within the predominantly kaolin rich clay matrix (Figure 6.25.6).

6.7 Characteristics of nodules

The ferruginous and iron-manganese nodules also occur associated with the mottled clay units and have distinct petrographic, mineralogical and morphological features which are discussed below

6.7.1 Ferruginous nodules

The iron oxides in the mottled clay zone occur either as clay impregnations or as nodules. They also occur as dark, iron and manganese rich aggregates and nodules within the clay rich matrix in transition with the saprolite in both E22 and E27 (Chapter 5). A variety of these ferruginous nodules were recovered from the mottled clay zone and in the transition zone between the mottled clay zone and the saprolite. The size fractions, features and mineralogy of these nodules are presented in Figures 6.27.

The nodules of the mini-mottled clay zone are generally 10 to 20 mm in size. They have been subdivided into red to reddish brown hematite-goethite rich (Figure 6.27.1) and yellow to yellowish red (Figure 6.27.2) goethite-hematite rich varieties. Both varieties are sub-rounded to sub-angular in shape and are equally abundant in this horizon. The reddish brown varieties exhibit a dark shiny silvery sub-metallic lustre and the yellowish red ones a dull sub-metallic lustre. Some of the reddish brown nodules have a coating of goethite in their rims while the matrix of others have fine sand-sized (<2 mm) granules

Fig.6.26.1: A close up view of ferruginous nodules from the medium-mottled clay zone

6.26.2: Ferruginous nodules from the medium-mottled clay

Fig. 6.26.3: Fe-Mn nodules with goethite coatings

Fig. 6.26.4: Dolomite coated silica aggregates from the mega-mottled zone

Fig. 6.26.5: Detrital rock fragments from the transported regolith

Fig. 6.26.6: Gypsum crystals from the soil horizon.

5A


0
5
cm

5B


MSHN E27 P6

6


FM NOD. E27 P6
0
5
cm

7


QZAGR E27 P8

8


DRF E22 P5

9


MGC E27 P4

Figures 6.27: Characteristics of ferruginous nodules

Fig. 6.27.1: Hematite-kaolinite nodules from the mini-mottled clay. Notice the goethite coating (cutan) -GC and sand-sized rock fragments (SF) in some of the nodules. Average mineralogical contents:

Mineral	Quartz	Kaolin	Hematite	Goethite
Weight %	11.9	18.0	36.5	33.6

N=5

Fig. 6.27.2: Goethite-kaolin nodules from the mini-mottled clay zone. In some the goethite occurs as a coating on hematite-kaolin nodules or as fine stringers (FS) in the hematite rich matrix. they comprise of:

Mineral	Quartz	Kaolin	Hematite	Goethite
Weight %	6.1	27.9	30	36

N= 5

Fig. 6.27.3: Hematite-kaolinite nodules from the medium-mottled clay. the matrix is hematite rich with no cutans. They are composed of:

Mineral	Quartz	Kaolin	Hematite	Goethite
Weight %	7.9	44.9	38.5	8.7

N=5

Fig.6.27.4: Goethite -hematite-kaolinite nodules from the medium-mottled clay. The goethite occurs as a coating or as fine stringers within the matrix. Sand-sized rock fragments are also conspicuous in the matrix.

They comprise:

Mineral	Quartz	Kaolin	Hematite	Goethite
weight %	3.9	66.9	10.9	18.3

N=5

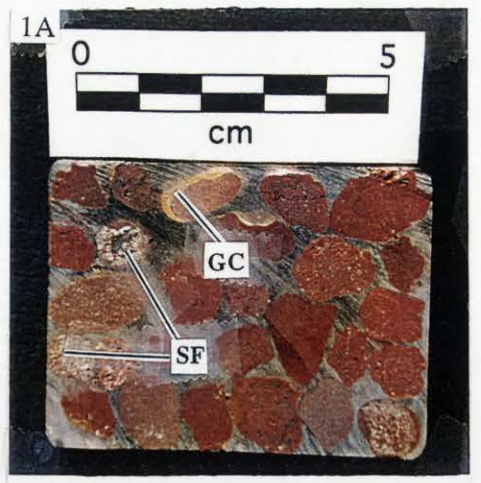
1A
0
5
cm
GC
SF


1B
MHN E22 P5


2A
0
5
cm
FS


2B
MGN E27 P7


3A
0
5
cm


3B
MMHN E22 P4


4A
0
5
cm


4B
MMGN E27 P6

which have otherwise been ferruginized. The goethite in some of the yellowish red nodules occurs as a coating on an otherwise hematite rich matrix.

The nodules of the medium mottled clay zone are 20 to 30 mm in size. They have also been sub-divided into red to reddish brown varieties (Figure 6.27.3) and yellow to yellowish red varieties (Figure 6.27.4). Like the nodules of the mini-mottled clay zone they are sub-rounded to sub-angular in shape. The red to reddish brown varieties are more abundant than the yellowish red varieties indicating that the conditions here favoured the concentration of hematite relative to the goethite. The red to reddish brown varieties in this zone also exhibit the distinct shiny silvery sub-metallic lustre. The matrix is hematite-rich with some minor tinges of goethite. The yellowish red varieties have an hematite-rich matrix with the goethite mainly occurring as coatings and as fine stringers within the matrix. Sand sized granules are also evident in hand specimen.

The nodules of Figure 6.27.5 were recovered from the iron-manganese nodule rich zone in the transition zone between the mottled clay and the saprolite. They are 20 to 40 mm in size and are red to reddish brown in colour. They are sub-rounded to sub-angular in shape and exhibit the same characteristics as the reddish-brown varieties. Yellowish varieties of the same size were also recovered.

The morphology of the crystals from the nodules is quite similar to those of the mottled clay zone as shown in Figure 6.29. The kaolin occurs as thin platy crystals (Figures 6.29.7 and 6.29.8) and like in the mottled clay is observed adhering to or closely occurring with quartz in most specimens (Figure 6.29.1 and 6.29.6). The iron oxides occur as thin plate like forms (Figures 6.29.2, 6.29,3, 6.29.4 and 6.29.5) which are quite distinct from the kaolin plates. Distinguishing between hematite and goethite using the crystal habits proved to be hard from the SEM micrographs. However, a few of the nodules have pod-like iron-rich aggregates within the matrix (Figures 6.30) which closely resembles the hematite crystal habits. The origin of these pods is unclear although their peel off skin structures suggests the action of microroganisms.

6.7.2 Nodular iron-manganese aggregates

This zone marks the transition between the mottled clay zone and the saprolite in the more deeply weathered sections of E22 and E27 deposits. A narrow band (2 to 4 m) of these nodular aggregates also occur within the mega-mottles in the E27 deposit (Chapter 5).

Figure 6.28: SEM backscattered images of Fe-Mn nodules

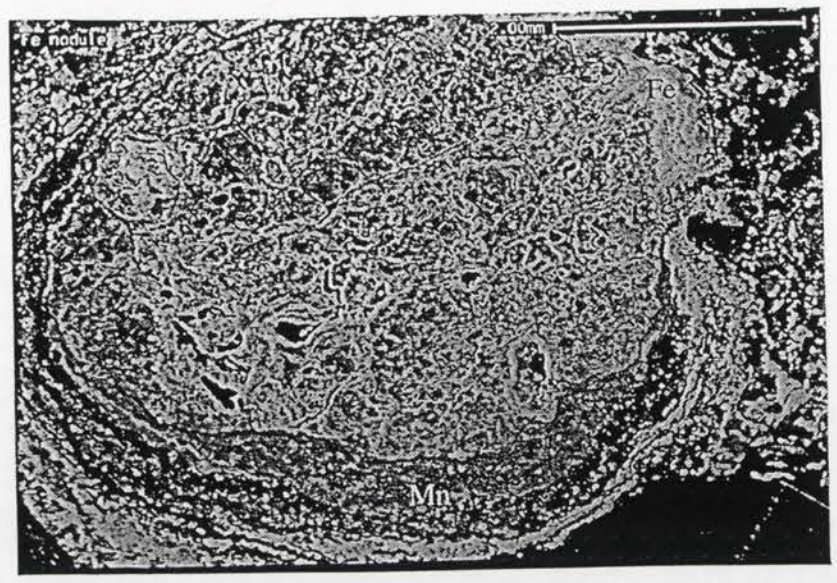

Manganese occurring as a coating on the poorly crystalline manganese nodules. Some quartz granules (FMD) occur in the matrix. Scale bar = 1 μm

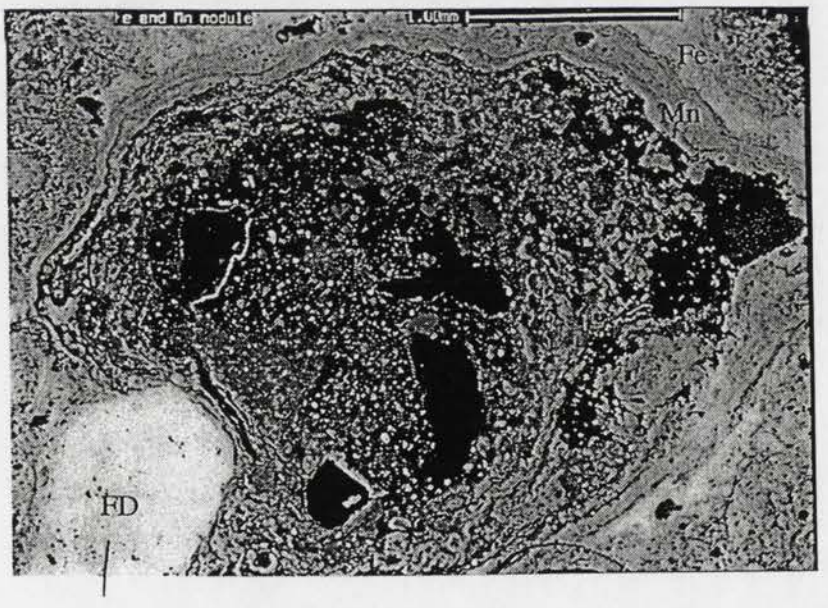

Figures 6.29: Morphologies of grains from ferruginous nodules

Fig. 6.29.1: Thin kaolin plates adhering to quartz in a ferruginous nodule. Specimen E22 FeD 1. Scale bar = 2 μm.

Fig. 6.29.2: Hematite plates on the surface of a ferruginous nodule. Specimen E22 FeD 2. Scale bar = 2 μm

Fig. 6.29.3: Hematite plates on the surface of a ferruginous nodule. Specimen E22 FeD 2. Scale bar = 2 μm

Fig. 6.29.4: Thin hematite plates sandwiched bewteen kaolin and quartz in a ferruginous nodule. Specimen E27 FeD 2 Scale bar = 2 μm

Fig, 6.29.5: A close up view of the goethite 'needles' Specimen E27 FeD 2. Scale bar = 2 μm

Fig. 6.29.6: Poorly crystalline kaolin plates with quartz in a ferruginous nodule. Specimen E27 FeD 4. Scale bar = 10 μm

Fig. 6.29.7: Thin platy kaolin within a ferruginous nodule. Specimen E27 FeD 5. Scale bar = 2 μm.

Fig. 6.29.8: Thin platy kaolin within a ferruginous nodule. Specimen E27 FeD 5. Scale bar = 2 μm.

1

2

3

4

5

6

7

8

Figures 6.30: Morphologies of ferruginous pods from the ferruginous nodules

Fig. 6.30.1: Thin platy kaolin with quartz in a ferruginous nodule. Specimen E27 P6 FP 1. Scale bar = 5 μm

Fig. 6.30.2: Ferruginous pods of..... within platy kaolin and quartz. Specimen E27 P6 FP2. Scale bar = 5 μm

Fig. 6.30.3: Ferruginous pods growing in a void close to the kaolin plates and quartz. Specimen E27 P6 FP2. Scale bar = 2μm

Fig. 6.30.4: A close up view of the ferruginous pods. Specimen E27 P6 FP2 Scale bar = 1 μm

Fig. 6.30.5: A close up view of the ferruginous pods. Specimen E27 P6 FP2. Scale bar = 1 μm

Fig. 6.30.6: Ferruginous pod forming substrate within the ferruginous nodule. Specimen E27 P6 FP3. Scale bar = 2 μm

Fig. 6.30.7: Ferruginous pods on quartz 'branches' within the ferruginous nodules. Specimen E27 P6 FP4 Scale bar = 5 μm

Fig. 6.30.8: A close up view of the Ferruginous pods on quartz 'branches' within the ferruginous nodules. Specimen E27 P6 FP4 Scale bar = 5 μm

1

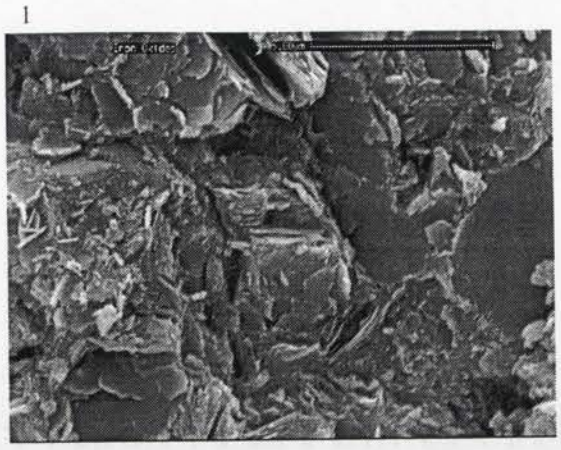

2

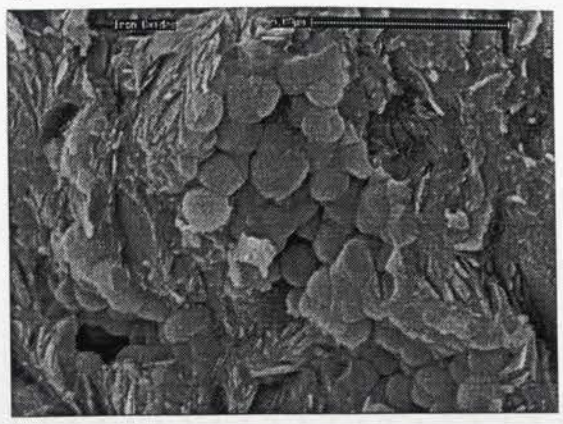

3

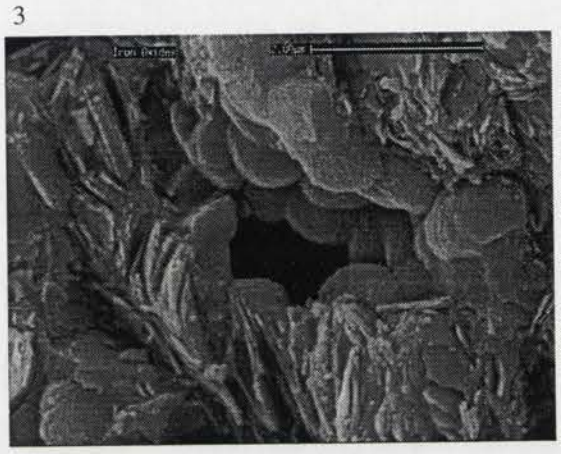

4

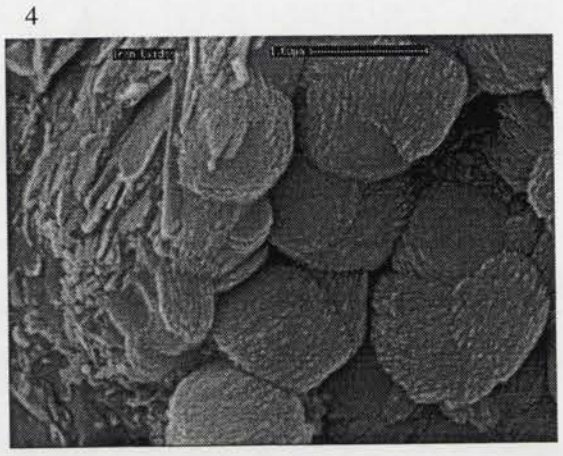

5

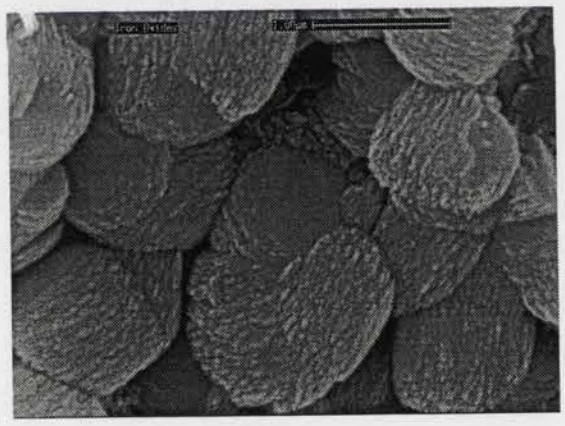

6

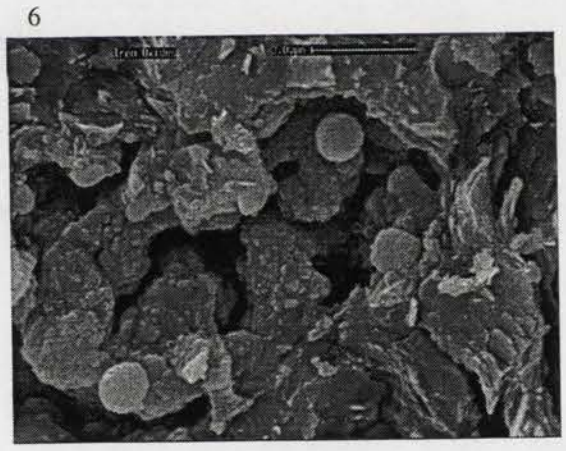

7

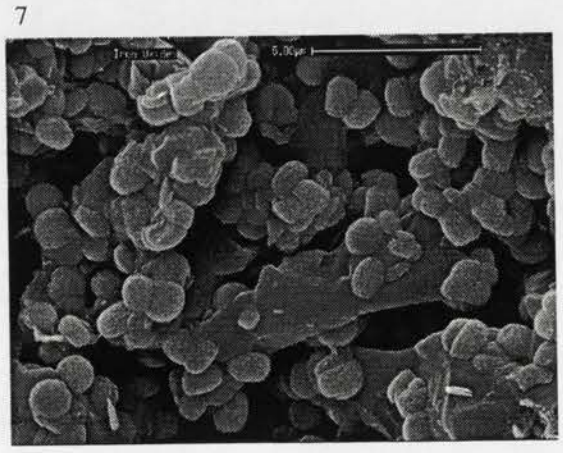

8

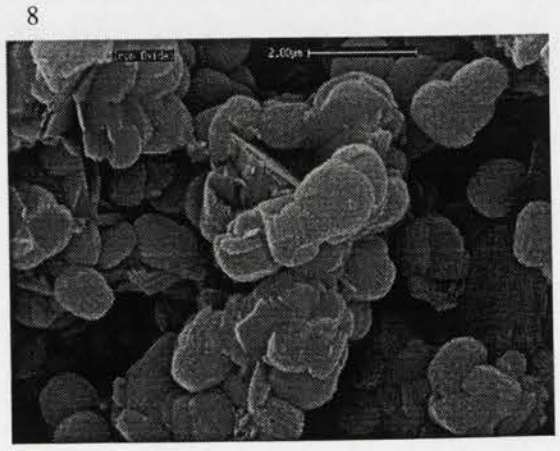

In hand specimen they appear as dark to yellowish dark (Figure 6.27.6) irregular to sub-angular nodular aggregates 30 to 50 mm in size. The matrix is composed of a whitish grey and greenish pink kaolin and smectite rich clays. Sandy quartz granules, quartz pebbles (20-50 mm in size) and detrital rock fragments (rich in muscovite) were also recovered during the separation of the nodules from the clays.

SEM backscattered electron micrographs (Figures 6.26.1 and 6.26.2) shows that these nodules are composed predominantly of iron and manganese oxides. The manganese occurs as a coating on most of the nodules while in some it has enchroached and replaced the iron in the matrix. A number of sub-angular and sub-rounded quartz fragments occur together with the iron oxides and kaolin in the matrix.

XRD analysis shows that the manganese oxides are poorly crystalline. It has poorly diffracting material contents of between 7 % and 25 % as determined by *Siroquant*t. SEM micrographs showed these aggregates as having smooth rounded surfaces confirming their poorly crystalline nature. The XRD long scan (carried out to improve resolution of the peaks) shows their mineralogical composition to be goethite, quartz and kaolin with well-developed peaks at 9.45 A° and 4.75 A° which correspond lithiophorite (Figure 6.31).

Summary statistics of SEM EDXA analyses on these aggregates (Table 6.3) shows a composition dominated by Mn (approx. 58 wt %) and Ba (approx. 9 wt %) oxides. Calculation of the structural composition provides a mostly hollandite type manganese mineral i.e BaR_8O_{16}; $R=Mn^{4+}$ mainly also Mn^{2+}, Fe, Co (Richmond and Fleisher, 1943).

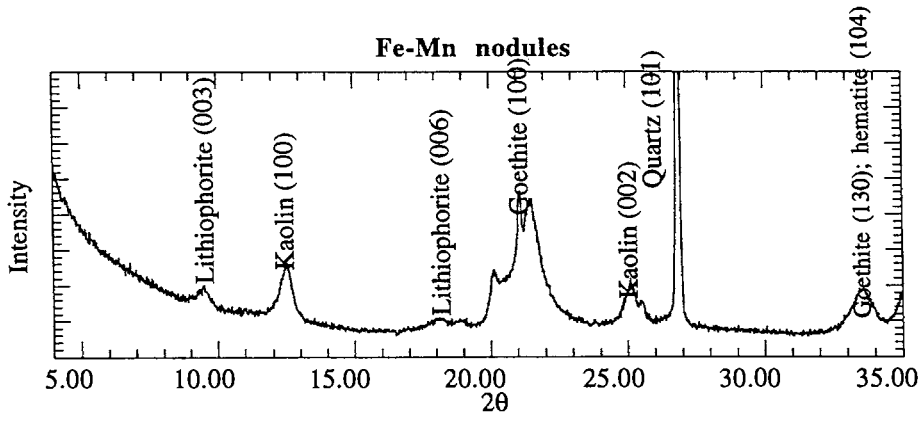

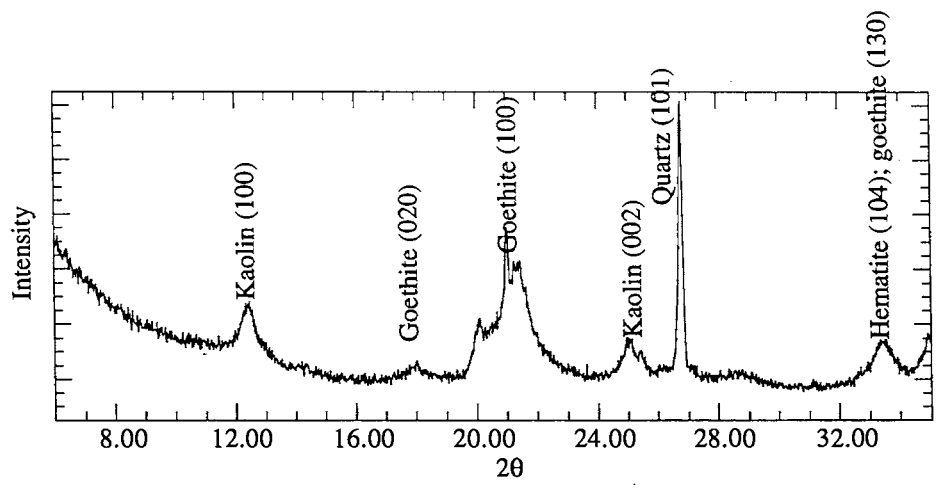

Figure 6.31: XRD traces of bulk samples from the nodular iron and manganese zone showing their mineralogical compositions [Specimen E27 P6 (30 m)]

Elements (Weight %)	Mean	No. of analyses	Minimum	Maximum
SiO_2	4.03	20	0.26	9.7
Al_2O_3	4.12	20	0.41	8.05
MgO	0.19	20	0	0.44
BaO	8.65	20	0	13.17
K_2O	0.40	20	0.11	1.24
CaO	0.42	20	0.22	0.61
MnO	57.49	20	46.62	65.72
Fe_2O_3	2.24	20	0.62	3.32

Table 6.3: Summary statistics of Fe-Mn nodule microprobe analysis

The results of this analysis are presented in Appendix 5.

6.8 SOIL

The depths of the soil horizon vary from 0-200 cm in the least weathered sections of the pit (over the weathered andesite) and 0 to 350 cm in the more deeply weathered sections of the pit (over the mottled clay zone). The soils from the two horizons exhibit minor characteristic differences which arise because they are sourced from different parent materials. XRD analysis shows the dominant clay mineralogy to be kaolin and smectite for both soils (Figures 6.33.1 and 6.33.2).

Optical microscopy shows minor differences between the two soil types. The soil developed over the mottled clay parent (Figure 6.34.1 and 6.34.3) displays a more open structure. Generally, the two soil types are composed of numerous sub-angular to sub-rounded clear to grey detrital quartz fragments with skeletal grains of ferruginized rock fragments. Root casts which have been infilled by siliceous clays and iron oxides (either goethite or hematite) and organic skeletal grains are quite pervasive within the fine grained clay rich matrix. Intercrysts of fine gypsum crystals are also quite abundant within this soil. The gypsum appears as near transparent crystals 10 to 20 mm in size (Figure 6.27.8).

The soil developed over the weathered andesite displays a more close knit structure and contains abundant detrital rock fragments derived from the andesite host rock. These include partly altered K-feldspar and muscovite grains. The quartz and gypsum is not as abundant as in the soil developed over the mottled clay. The matrix is composed of fine-grained iron stained clays. The iron staining is quite intense within the 'B' horizon of the soil developed over the mottled clay than in the soil developed over the andesite (Figure 6.34.4).

SEM micrographs shows the soils as having thin platy crystals of kaolinite which are covered by cellular encrustations of smectite (Figures 6.25.7 and 6.25.8) with equal peak heights of Al and Fe, moderate amounts of Ca and high Si adhering closely to the quartz. Diffraction data illustrates a very broad 001 peak for kaolinite implying a disordered clay.

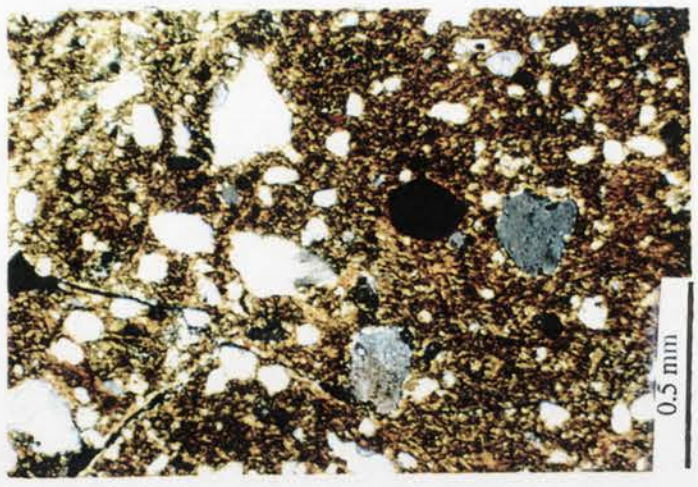

Fig. 6.34.1: Angular to sub-rounded quartz fragments and Fe-glaebules within the soil over the mottled clay. The matrix is composed of detrital rock fragments intercrysts of gypsum and very fine-grained clay. Specimen E27 P6 S1.Photomicrograph with crossed polars.

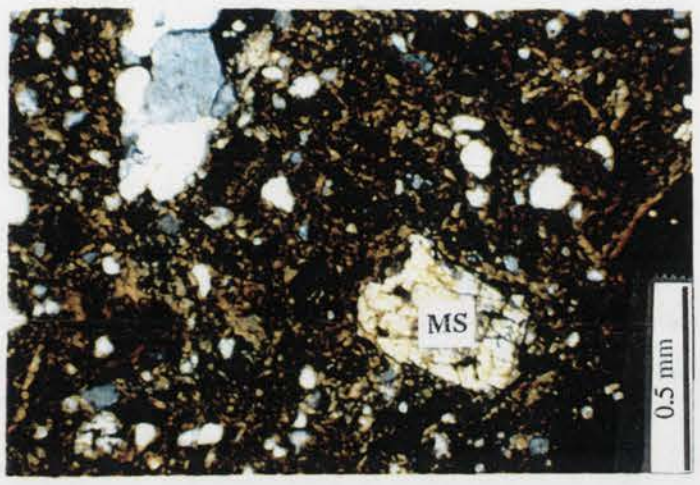

Fig. 6.34.2: Relicts of muscovite and angular to sub-rounded quartz fragments in soil developed over the andesite. The matrix is composed of very fine grained clay and skeletal bedrock fragments. Specimen E22 P11 S1. Photomicrograph with crossed polars.

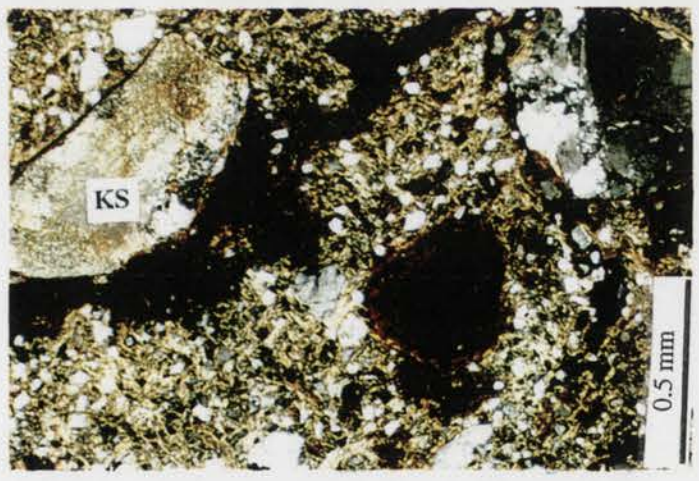

Fig. 6.34.3: Relict of K-feldspar (KS) and , Fe-glaebule and small sand-sized quartz in a clay plasma of 'B' horizon of soil over the andesite. Specimen E22 P11 S2. Photomicrograph with crossed polars.

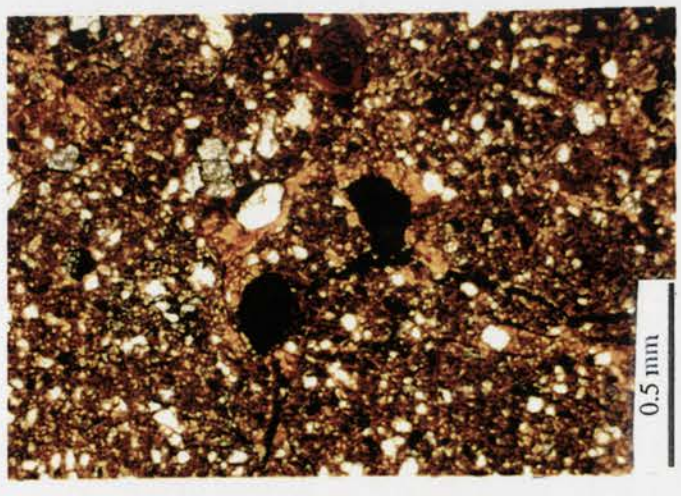

Fig. 6.34.4: Fe-glaebules and small angular to sub-rounded quartz fragments in an Fe-stained clay matrix of the soil 'B' horizon of the soil over the mottled clay. Specimen E27 P6 S2. Photomicrograph with crossed polars.

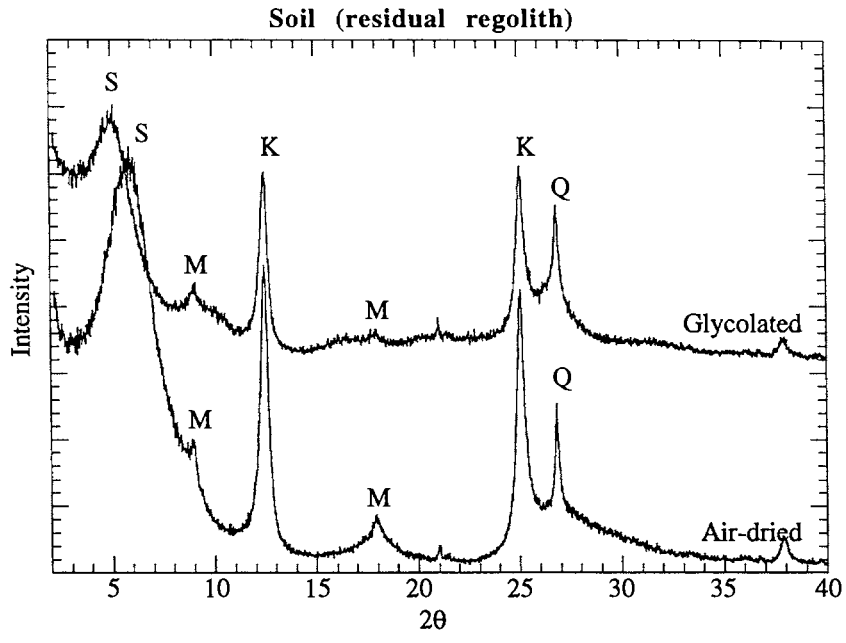

Figure 6.33.1: XRD traces of air-dried and ethylene-glycol treated samples of <2 μm fractions from the soil developed over the mottled clay zone [Specimen E27 P11 (1 m)]

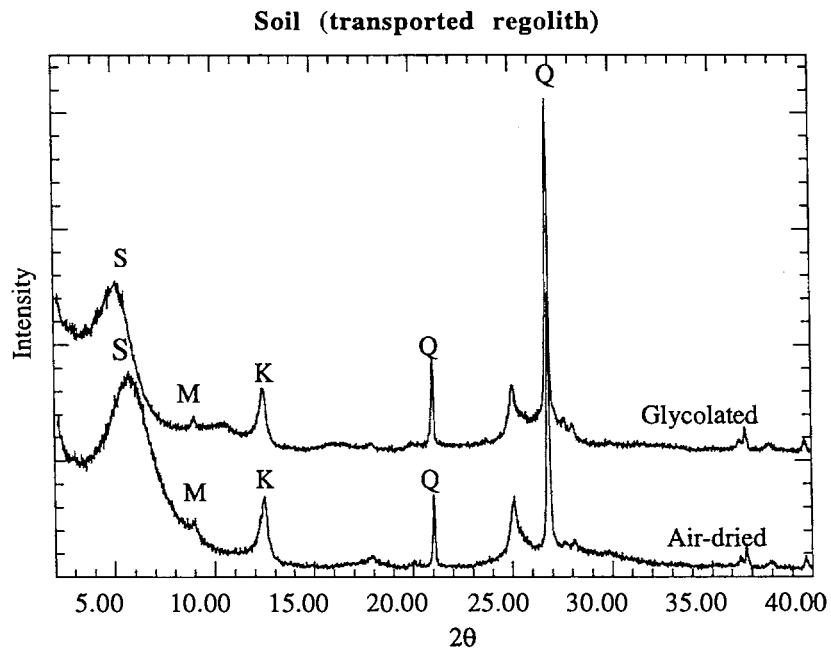

Figure 6.33.2: XRD traces of air-dried and ethylene-glycol treated samples of <2 μm fractions from the soil developed over the mottled clay zone [Specimen E22 P5 (1 m)]

6.9 SUMMARY AND DISCUSSIONS

6.9.1 Regolith paragenesis

The trachyandesite rocks of this study are predominantly composed of feldspars (K-and-plagioclase feldspars). The weathering of feldspars is a surface controlled process. Access of a solution to the feldspar surface is probably controlled by defects, cleavages, twin planes, and cracks. Dissolution appears to proceed by preferential attack at energetically favoured sites (Berner & Holdren, 1977; Nixon, 1979). Studies of surface textures of weathered minerals indicate that this mode of attack results in the formation of solution or etch pits (Siefert, 1967; Parham, 1979; Lundstrom, 1970; Berner & Holdren, 1977). Some etch pits of this type follow exsolution lamellae and twin planes (Wilson and McHardy, 1980; Rich, 1972), as in Figures 6.2.1 and 6.2.2 suggesting that the crystal structure of the feldspar controlled the nature and orientation of initial weathering products.

Considerable uncertainty still exists as to whether secondary minerals precipitate from solution or crystallize from transient, noncrystalline aluminosilicate intermediates (Banfield & Eggleton, 1990). The differential shattering, pitting and coalescence of the etch pits of the feldspar along its main axis is indicative of transport-solution mechanism operating to induce the dissolution of the mineral surfaces (Berner, 1981). Dissolution of feldspar by water in the laboratory has been shown to be incongruent i.e the solution does not have the same composition as the feldspar (Correns, 1963; Keller et al. 1963; Marshall & McDowell, 1965; Reesman & Keller, 1965; Huang & Keller, 1970). Dissolution of feldspar in nature is likewise expected to be incongruent, and it may be differential as indicated by the pitting in SEM photographs. This pitting may be due to incongruency of dissolution or in part to non-uniformity in composition of the feldspar (Keller, 1976). The access of solutions to mineral surfaces in these surfaces and hence precipitation is more pronounced, leading to ubiquitous development of phyllosilicates.

Early investigators (e.g. Fields & Swindale, 1954) stated that with the exception of micas, all primary silicates pass through a noncrystalline stage in transition to secondary phases. Views recently expressed in literature seems to favour a mechanism involving dissolution and reprecipitation. Tsuzuki & Kawabe (1983) for example suggested that the dominant transformation mechanism involving dissolution and precipitation may be responsible for the entire sequence from feldspar to kaolin. Keller (1978) stated that the most logical mechanism for the production of kaolin-group minerals is via solution. Eswaran & Bin

(1978) proposed that feldspar alters via solution to kaolinite and gibbsite via a non crystalline stage to halloysite.

There are indications in this study of the presence of an intermediate stage before the formation of smectite. Resolution of this material by optical microscopy was made difficult by its poorly crystalline nature but SEM EDXA data suggested it was a mixture of smectite and oxyhydroxides. Tazaki & Fyfe (1987) described 'primitive' clays formed during feldspar weathering which are quite similar to the ones described here. They described them as primitive clay precursors having a brownish 'muddy' appearance. They also reported (from TEM studies) the presence of Fe compounds on or adjacent to feldspar surfaces at this stage of alteration. Their unaltered feldspar grains revealed a curious, electron-dense spotting (< 50 A°), which may have represented hydrated iron-oxide precipitated on the surface. They further determined that reactive iron was later incorporated into the 'primitive' clay. However, it was not possible to determine the detailed nature of these iron compounds within the scope of this study.

However, there was a noticeable presence of Fe in the smectite over the feldspar in the present study. There have been numerous observations of secondary products containing elements not present in the parent mineral (Nahon et al. 1982; Nahon & Bocquier, 1983; Fontanaud & Meunier, 1983) but only a couple references exist, regarding the occurrence of Fe in smectite or feldspar (Banfield & Eggleton, 1990; Ildenfose, 1980). Banfield & Eggleton (1990) envisaged that Fe from adjacent solution was either adsorbed on the smectite surface or participated in the disruption of the feldspar lattice and consequently was incorporated into the smectite structure.

The presence of the Fe in this horizon has been attributed to the oxidation of sulfides from the surrounding sulfide zone, which is proximal to the saprock and from the weathering of pyroxenes and opaque oxides. The retarding effect of Al in solution or dissolution was reported by Chou & Wollast (1985). An increase in Fe concentration in solution can trigger a change in the state of Fe (Banfield & Eggleton, 1990), but the Fe can also experience oxidation by being adsorbed on the smectite surface (Gerstl & Banin, 1980). Casey et al. (1989) proposed that adsorption of a hydrated Al ion onto the feldspar surface results in the combination of two silanol groups and the elimination of a hydronium ion and water. The consequent repolymerization of the surface stabilizes the hydration layer. Banfield & Eggleton (1990), suggested that the adsorption of ferric ion may promote repolymerization in a manner similar to that suggested by Casey et al. (1989), resulting in the development of an Fe-enriched feldspar weathering product. They alternatively suggested that if Fe^{2+} is present in solution, oxidation coupled with

hydrolysis of water may provide H^+ or H_3O^+, which attacks the feldspar structure releasing K, Na, or Ca, as proposed by previous workers. The ferrolysis reaction may be written as:

$$2Fe\,(H_2O)_2{}^{2+}{}_{(aq)} + 1/2O_2 << >> 2FeO(OH)_{(s)} + 4H^+ + H_2O$$

Banfield & Eggleton (1990) also proposed that for Fe to participate in this manner, solutions in the weathering profile must have been, at least episodically reduced. The characteristics of a weathering solution (pH, oxygen content, dissolved ions) they stated, probably varied dramatically due to seasonal changes and in response to adjacent mineral weathering reactions, explaining the mobilization of Fe and its precipitation in altered feldspar crystals. In the ferric state, hydrolyzed iron may also promote feldspar weathering by buffering the pH. At pH 4-7, the most abundant Fe^{3+} species is $[Fe(OH)_2{}^{-}\,4H_2O]^+$ (Lindsay, 1979). Polymerisation of two such monomers according to Banfield & Eggleton (1990) releases a hydrogen ion according to the equation:

$$2[Fe(OH)_2.\,4H_2O]^+ << >> [Fe_2(OH)_5.\,5H_2O]^+ + H^+ + 2H_2O$$

The increase in pH resulting from K^+ - H_3O^+ exchange would promote the ion monomers to coalesce into dimers (and higher molecular-weight polymers), releasing H^+ and restoring pH. The possible participation of iron was also noted in the formation of accordion-like fabrics in the saprolite.

Although Fe was almost certainly not necessary for the weathering reactions to have proceeded, its presence probably had some effect, possibly similar to that reported for Al as mentioned above. Ildefonse (1980), Banfield & Eggleton (1990) and Wang (1988) and this study document the emergence of Fe in the smectite over feldspar while the other studies of feldspar weathering from relatively similar humid climates (Anand et al. 1985; Chittale 1986), and a temperate climate (Glasman, 1982), do not mention any such observation. This anomaly might be a consequence of different microenvironments existing between the study areas or the parent rock chemistry.

The paramount observation made from the study of the paragenetic sequences during weathering is the presence of the different morphologies of the clays. Quantitative X-ray diffraction data in combination with optical properties indicate the major secondary product in the saprolite to be the platy, vermiform and 'book' type varieties of kaolin though smectite initially occurs in appreciable amounts within the lower saprolite. The kaolin books were randomly oriented with respect o the etched or pitted feldspar surfaces.

Keller (1977), noted similar orientation of kaolin books in the pitted surfaces of feldspar in the weathering of a Missouri Precambrian granite. He envisaged that the randomness is an indication that the argillic transition was not a solid-state transformation or replacement, but that a solution in reaction with the solid phases intervened. The role of microenvironments in governing the type of the secondary mineral is quite important (Keller, 1978; Eswaran, 1979; Anand et al. 1985 and Chittale, 1986) and might be a factor responsible for the various morphologies of the clays. Intensity and amount of solution access to microcracks and fractures can regulate nucleation and crystal growth and subsequent outward appearance (Berner, 1981).

The evolution of kaolinite can be accomplished via five different mechanisms:

1) the direct transformation of plagioclase to kaolinite in proficiently leached horizons (Anand et al, 1985);

2) the alteration of tubular or spherical halloysite to kaolinite on ageing (Banfield, 1985; Anand et al. 1985 and Churchman & Gilkes, 1989);

3) the direct transformation of smectite to kaolinite (Altschuler et al. 1963 and Morgan et al. 1979);

4) the alteration of smectite via an intermediate, interstratified smectite/kaolinite stage (Herbillon et al. 1981 and Yerima et al. 1985) or amorphous stage to kaolinite; and,

5) the alteration of muscovite to kaolin during weathering or hydrothermal alteration (Stoch & Sikora, 1976; Jiang & Peacor, 1991; Robertson & Eggleton, 1991).

SEM micrographs showed a close association between feldspar and plates and books of kaolin in conjunction with smectite in the saprock and the lower saprolite. This suggests that the feldspar weathers directly to kaolin or smectite or alternatively smectite to kaolin. Keller (1976) explained that the platy book-type kaolinite mineralogically characterizes thick saprolites over feldspathic crystallines, transported sedimentary deposits derived from saprolites and certain hydrothermal, large-volume deposits. He also further explained that the book-type kaolin are products of weathering that are typical of weathering crusts and thick saprolites. These environments, he noted, were formed over notably long periods of time in widespread environments that produced deep weathering, commonly below the water table and below the zone of active erosion and denudation.

This was essential for geochemical equilibrium to be reached and maintained for a long time, between the ground-water solution and the solid, parent-daughter phases.

The weathering profiles in the study area were formed during periods of deep weathering dating back to the Carboniferous (Chapter 8) and may well explain the widespread occurrence of the platy book-type of kaolinite in the area. Several workers, among them Keller (1976), Banfield (1985), Banfield & Eggleton (1986), Anand et al. (1985) and Churchman & Gilkes (1989), have also proposed the alteration of tubular or spherical halloysite to kaolinite on ageing. The presence of halloysite in the saprock and saprolite horizons was not observed in this study despite the numerous accounts in literature of its presence in such horizons. Keller (1976) proposed that the elongate (halloysite) morphology is formed when weathering occurs in a near surface environment, or in an highland area undergoing surface erosion, in which the geochemical system is relatively more transitory in time and duration than that described for low-lying, thick saprolitization. He envisaged that the elongate kaolin mineral would be more likely to form as a product governed by kinetic processes, whereas the platy kaolinite would represent a more nearly equilibrium situation.

Aspandiar (1990) noted the presence of halloysite on the trachyandesites not far from the study area which were located in a higher landscape setting as opposed to the more flat topographic setting of the current study. However, the presence of halloysite in the other samples not covered in this study cannot be ruled out. Differences in chemical environment and alteration mechanisms as mentioned before may produce quite distinct alteration products. For example, the formation of non-crystalline compounds may be a consequence of the slow removal of dissolution products from primary minerals in poorly drained profiles or in microenvironments within individual grains.

The alteration of smectite to kaolinite transpires as a consequence of lowering of solution pH (Wilson, 1987) and improvement in drainage with landscape evolution (Borchardt, 1989). The abundance of 2:1 clay minerals (smectites) in the saprock and the lower saprolite is largely due to the poor leaching in this part of the profile. Drainage has been employed to explain the leaching intensity in weathered profiles with general consensus regarding the absence of 2:1 clays to represent macro and micro well drained profiles (Nahon & Colin, 1982; Velbel, 1989) while abundance of 2:1 phyllosilicates represents deficient leaching activity in the profile (Wilson & Farmer, 1970; Nahon & Colin, 1982). There is no doubt that drainage improved in going from the saprock to the saprolite and hence some of the smectite might have been transformed to kaolinite in the process. This

is supported by quantitative XRD results which show the amounts of smectite decreasing as the kaolin increases in transition from the saprock to the saprolite (Figure 6.3.2).

There is also evidence from optical microscopy and SEM of the weathering of muscovite to kaolinite. This was shown by the presence of a mat of fine grained (0.001-0.005 mm), low birefringent kaolinite in clusters, larger flakes, plates and books of more birefringent kaolinite-muscovite mixture containing Fe and K which represented weathered sericite flakes which resulted in the formation of accordion-like structure of mixed kaolinite and mica. The resolution of interlayer spacings to show this transformation was not possible within the scope of this study. The SEM micrographs showed this co-existence of kaolin and muscovite plates within the saprolite, which was further evidence of the existence of a weathering relationship.

The weathering sequences (using TEM techniques) of muscovite to kaolin have been studied by a number of workers (Stoch & Sikora, 1976; Sharp et al. 1990; Jiang & Peacor 1991, Robertson & Eggleton, 1991 and Chi Ma, 1996). Chi Ma (1996) in a study of weathering of muscovite to kaolinite from Weipa proposed that the mechanism involves the removal of interlayer alkali ions and octahedral Al and Fe, replacement of tetrahedral Al by Si, reorientation of the Si tetrahedra in one of two sheets and the formation of one dioctahedral sheet and gain of water and/or protons (H^+) to form OH groups coordinating Al (assuming an ideal kaolinite composition). He proposed that such major changes demanded at least a partial dissolution of octahedral and tetrahedral sheets of the mica structure and the crystallization of kaolinite. A dissolution-crystallization mechanism for transitions between phyllosilicates under low-temperature conditions has also been suggested in many other studies (e.g. Yau et al. 1984; Ahn & Peacor, 1987; Banfield & Eggleton, 1988).

A few studies document the direct transformation of one phyllosilicate to another without the formation of an intermediate phase (e.g. Veblen & Ferry, 1983; Ahn & Peacor, 1987; Banfield & Eggleton, 1988). This implies that although the alteration of muscovite to kaolinite requires major reorganization of virtually all elements of the structure, including a major change in chemistry of the tetrahedral sheets, the products and direct reactants share a common polymerization scheme. The reactant-product relationship implies that the dissolution-crystallization process may involve retention of at least part of the polymerized units, or that the general similarity in reactant and product layers provides easy pathways for change (Chi Ma, 1996). Sharp et al. (1990) proposed a mechanism involving the transition of three 2:1 layers to four 1:1 layers for phlogopite to serpentine

transition. Jiang & Peacor (1991) applied this mechanism to the dioctahedral phases for the muscovite to kaolinite transition, which may serve as the actual mechanism thus:

$$3KAl_2(Si_3Al)O_{20}(OH)_2 + 10H^+ = 4Al_2Si_2O_5(OH)_4 + Si^{4+} + Al^{3+} + 3K^+$$

Muscovite Kaolinite

The weathering of muscovite to kaolinite in the greenish-grey and orange-pink saprolite as already mentioned was marked by the presence of accordion-like structures of mixed kaolinite and mica. Very similar accordion-like structures have been described in authigenic kaolinite of argillaceous rocks (Williams et al. 1955) and in kaolin derived from granite weathering (Robertson & Eggleton, 1991). In this study, there is increased iron staining close to where these fabrics formed consistent with the view by Robertson & Eggleton (1991) that these pseudomorphs represent authigenic recrystallization of kaolinite in the saprolite that have since suffered iron replacement, preserving the accordion fabrics from saprolite re-texturing and collapse. These accordion structures took the form of fabric destroying blasts in the upper saprolite.

XRD data also suggests the presence of an interstratified kaolinite/mica phase in `two samples from E22 Profile 8 collected from the upper saprolite. The samples from the soil horizons also showed the presence of the interstratified smectite/mica phase. The presence of this clay higher up in the profile and its occurrence in very small amounts in only one profile precludes its participation as a key intermediate in the transformation of muscovite to kaolinite although it might constitute an appreciable proportion of the muscovite and kaolinite in the soil over this profile. It is apparent that most of the kaolinite in the saprolite is accounted for by the following mechanisms:-

1) the direct transformation of plagioclase to kaolinite in proficiently leached horizons (Anand et al, 1985);

2) the direct transformation of smectite to kaolinite (Altschuler et al. 1963 and Morgan et al. 1979);

3) the alteration of muscovite to kaolin during weathering or hydrothermal alteration (Stoch & Sikora, 1976; Jiang & Peacor, 1991; Robertson & Eggleton, 1991).

The mottled clay zone on the other hand shows a different set of regolith materials from the saprolite and saprock zones. The fabric in this zone has undergone intense reorganization which has resulted in iron enriched zones within the clay rich plasma.

Optical microscopy, XRD analysis and SEM microscopy confirmed the difference between the secondary products of this zone and the saprolite and saprock horizons.

The dominant mineralogy in this zone is quartz, kaolin and the iron oxides (hematite and goethite) and minor amounts of anatase, smectite and dolomite. The matrix especially in the upper portions has been traversed by numerous fractures, root channels and voids. The root channels have given way to voids which in parts have strung together to form channelways. These spaces mark zones of intense solution activity where most of the material is formed, translocated or deposited within the different parts of the zone.

In the mini-mottled clay for instance, the void spaces have been infilled with skeletal grains of iron stained lithorelics and intercrysts of gypsum which have been translocated from the soil horizon. The root channels have also been lined with goethite, siliceous clay and an undeterminable manganese wads. Within the medium-mottled clay, characteristic iron stained clay filled channels are quite pervasive within the matrix and they represent the settling and orientation of eluviated clays at channelways or voids. Carbonate (dolomite) and manganese wads also infilled the void spaces and fractures within the mega-mottled clay.

The plasma in the mottled clay zone is composed mainly of a whitish-grey kaolin with minor amounts of smectite in the mini-and-mega-mottled sub-horizons. The kaolin in some parts of the mega-mottled clay consists of pink and in some cases pale green colours, this probably a consequence of differences in chemical compositions of groundwaters and subsequent weathering cycles that formed these clays. XRD clay mineralogy showed the kaolin to be well crystalline in the mottled clay zone. Numerous sand sized or sub-rounded to sub-angular pebbly quartz fragments occurred within the clay and iron oxide rich matrix.

SEM micrographs revealed the dominant morphology of the kaolinite as the thin platy variety. The particles were observed to occur parallel to one another in some parts, with these particles in most cases adhering tightly to the quartz. Some vermiform or book-shaped kaolin also occurred though in very small amounts. A number of workers including Keller & Hanson (1975), Keller (1976) and Borst & Keller (1969) have suggested that the thin platy varieties represent sedimentary kaolins, their texture being controlled by the effects of particle size fractionation and sedimentation. According to these workers, the kaolin adheres closely to the quartz because they were deposited together in their former erosional and sedimentary environments. Their observations about pseudohexagonal and vermiform varieties showing neither preferred orientation nor

any particle size fractionation parallels the observations of the current study and hence their interpretation as these varieties representing primary kaolins.

These characteristics point to a pre-weathering detrital origin of the material that now makes up the mottled clay zone. The detrital rock fragments recovered by washing away the clays (Figure 6.27.8) are composed of rounded to sub-rounded quartz pebbles; silt and sand sized quartz granules, ferruginized rock clasts and rock fragments. The mineralogical compositions of a number of these fragments are shown in the Table 6.4 below.

Some of the rock fragments (sample numbers DR1, DR6, DR7 and DR9) have similar compositions as the Goonumbla Volcanics indicating that appreciable amounts of the detritus was derived from a local erosional regime. The presence of what is a clear boundary between this zone and the saprolite (Chapter 7 Figure 7.10), the mineralogical and geochemical differences in their compositions further exacerbated by the lack of any structures, textures and fabrics of the original rock also discounts an *in-situ* weathering origin. Chapter 11 discusses in detail the transported versus residual weathering concepts in relation to these observations.

SAMPLE	Quartz	Kaolin	Fe-oxides	Albite	Hornblende	Orthoclase	Muscovite
E22 DR 1	33.1	7.6	6.6	5.4	4.4	2.2	40.8
E22 DR 2	40.1	23.4	11.4	0.9	-	-	18.2
E27 DR 3	97.3	-	2.7	-	-	-	-
E27 DR 4	100	-	-	-	-	-	-
E22 DR 5	25.4	18.0	56.6	-	-	-	-
E27 DR 6	23.3	15.1	3.4	6.7	2.1	-	49.4
E22 DR 7	5.1	6.1	-	13.5	-	49	26.3
E27 DR 8	15.7	24.5	59.8	-	-	-	-
E22 DR 9	6.7	10.5	-	42.6	3.1	11.6	25.5

Table 6.4. Mineralogical compositions of a number of detrital rock fragments recovered from the transported regolith from both E22 and E27 deposits [All values in weight %]

6.9.2 Mechanisms of mottles and nodule formation

Tardy (1992), proposed that under contrasted tropical or near tropical climates (T= 25-30°C, rainfall = 1500 mm per year, 5 months of dry season, relative humidity of the air,

HR, = 65%) and above fine saprolites and lithomarges, iron is generally redistributed and concentrated to characterize a glaebular zone.

Brewer (1964) defined the term glaebule as being; " *a three dimensional unit within the s-matrix of the soil material, and usually approximately prolate to equant in shape; its morphology (especially size, shape and/or internal fabric) is incompatible with its present occurrence being within a single void in the present soil material. It is recognized as a unit either because of a greater concentration of some constituent and/or difference in fabric compared with the enclosing soil material or because it has a distinct boundary with the enclosing soil material".*

Nahon (1991) proposed that initial glaebular concentrations develop without significant change in the mineralogy of the host plasma. As centripetal three-dimensional glaebulization progresses, a significant change in mineralogy takes place. Within the developing glaebule, the partial or total replacement of the host material with the accumulating material takes place. These moderately differentiated glaebular accumulations are termed *nodules*. The central part of the nodules is structurally and mineralogically distinct from the enclosing plasma. Within the periphery, however, a transitional zone exists between the plasma and the glaebular accumulation.

The mechanisms responsible for mottle and nodule formation are poorly understood. In recent years much of the knowledge gained in the subject have come from French scientists, Daniel Nahon, Yves Tardy, Bruno Boulange and co-workers. This sub-section provides a summary of their observations.

Tardy (1992), mentioned that the mottled zone is characterized by a contrast between bleached domains and Fe-mottles which can be easily distinguished on a centimetre scale, in outcrops and in samples, and on a micrometer scale under the microscope. He envisaged that bleached domains consisting mainly of quartz and kaolinite and exhibiting a white or grey colour as in this study occur due to de-ferruginization of the previously associated kaolinite and iron oxyhydroxides. Original kaolinite aggregates, free of iron, can be dispersed and kaolinite particles can migrate and even be leached out. These changes according to Tardy (1992) are accompanied by a strong increase in porosity, leading subsequently to the formation of macrovoids, such as tubules and alveoles. At this stage quartz can be translocated in the generalized eluvial migration (Nahon, 1986). This is quite consistent with the characteristics of the mini-and-medium-mottled clay of this study. Eschenbrenner (1987) mentioned that quartz and kaolinite removal may be a result of termite activity.

These changes involve de-ferruginization (removal of Fe from the plasma). The de-ferruginization takes place in domains originally enriched in quartz and poor in kaolinite. Fe-mottles, mostly of a brown red colour, are diffuse glaebules according to the definition of Brewer (1964) and they result from a concentration of iron, which precipitates mainly as goethite and as hematite together with kaolinite. The domains of previous accumulation of kaolinite act as natural hosts for secondary accumulation of iron in mottles and nodules (Tardy, 1992).

Tardy (1992) proposed two situations in which kaolinite accumulation is the precursor of nodule formation:

1) Lithorelicts and pedorelicts: Lithorelictual mottles or nodules are iron accumulations in which the original structure of the parent rock can be seen. They are referred to as altorelicts by Faure (1985) and are mostly primary assemblages of aluminium and iron-rich minerals, which by alteration, give secondary stable associations of kaolinite and iron oxyhydroxides in which the pores are small. This is the case for schists, amphibolites and layers of migmatite which are rich in biotite, for example. Granitoid rocks initially poor in iron and consequently sensitive to leaching of kaolinite, are not ideal parents for the further accumulation of this element (Tardy, 1992).

2) Pedorelictual features (or pedorelicts): These are due to secondary accumulation of kaolinite, filling voids previously created in the bleached domains. They are relicts of soil forming processes. Kaolinite derived from solution or translocation from overlying upslope layers, is precipitated or deposited lower in the profile (Tardy, 1992). These secondary accumulations of kaolinite and associated quartz are generally accompanied by a secondary accumulation of iron-generating brown red coloured clays, providing a contrast with the white-grey decoloured areas, located around the tubules and channels (Nahon, 1986). Higher in the profile, these mottles evolve into nodules as accumulation progresses. They are what Nahon (1976) has called the argilomorphous nodules, which are old voids, filled by kaolinite and iron oxyhydroxide. Mottles and nodules of this kind are traces of the secondary pedogenetic activity occurring in the unsaturated zone. In the nodular zone, lithorelicts are more abundant on schists and amphibolites while pedorelicts dominate on sandstones and granitic rocks rich in quartz (Tardy, 1992).

The above observations suggest that the nodules of the mottled clay evolved from processes related to pedorelictual accumulations. The presence of numerous voids, channels and tubules and the dominance of clay eluviation and the other processes already highlighted in this section all points to the dominance of secondary pedogenic activity on

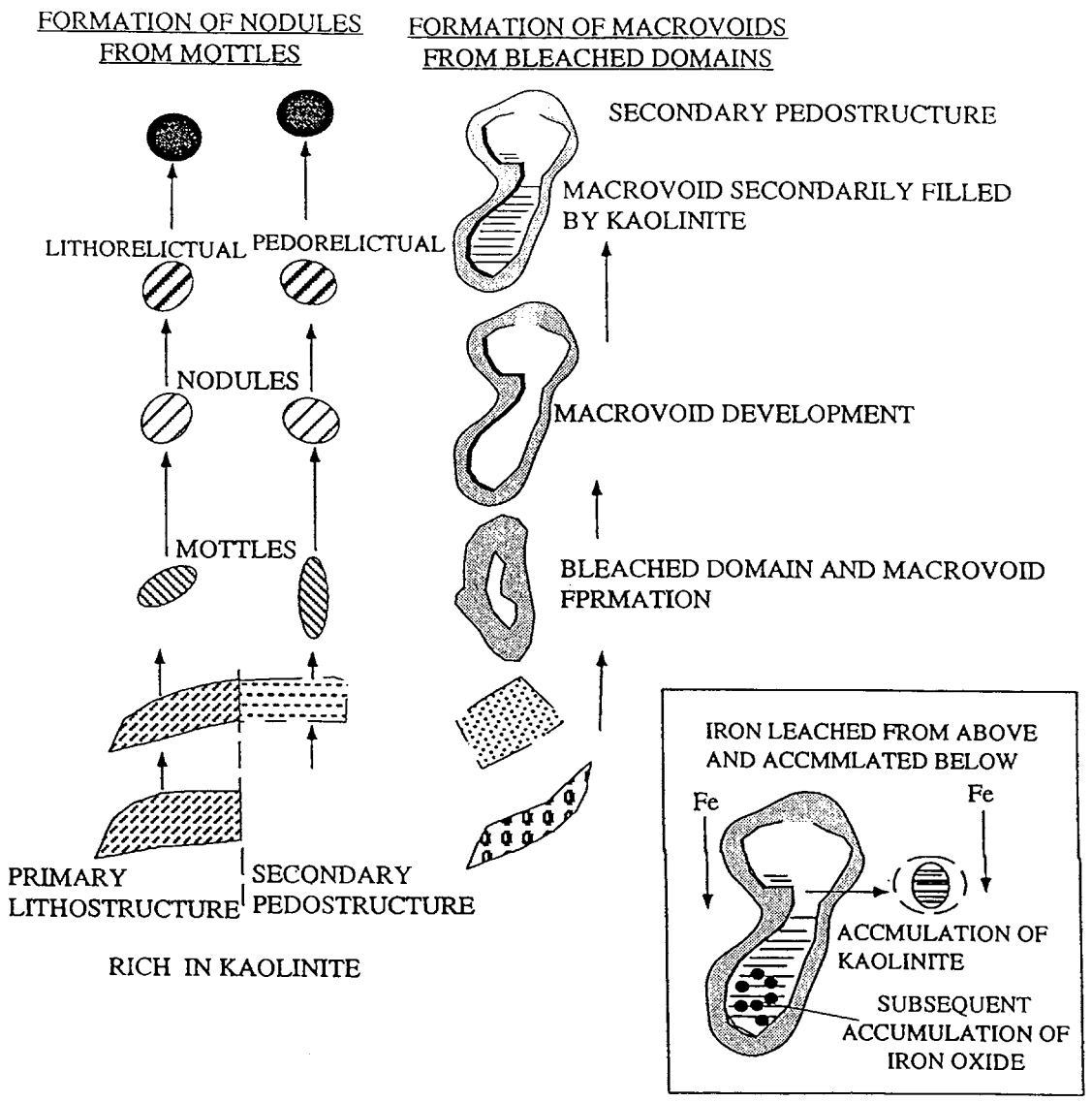

Figure 6.32: Formation of mottles and nodules, in originally kaolinite-rich domains, leading to lithorelictual features developed in primary lithostructures and pedorelictual features, developed in secondary pedostructure. Diagram also shows formation of bleached domains, macrovoids and channels from originally quartz-rich domains. and secondary formation of pedorelictual mottles in previously formed macrovoids [Adapted from Tardy (1992]

highlighted in this section all points to the dominance of secondary pedogenic activity on initially loose detrital material that gave rise to the mottles and nodules as explained by this mechanism. The nodular iron and manganese rich zone has been interpreted as representing palaeowatertable zones where redox reactions involving replacement of iron by manganese laden water and vice-versa were active. The possibility of these processes occurring at the present time cannot be discounted. The same processes gave rise to the manganese wads that infilled fractures within the mottled clay A summary of the two mechanisms responsible for nodule formation are presented in Figure 6.32.

6.9.3 Characteristics of smectites and kaolin

6.9.3.1 Smectites

Scanning electron microscopy images revealed the presence of smectites on weathered minerals and thus provided an excellent vehicle to study the surface features of these smectites. Smectites are characterized by high cation exchange capacities and hence different surfaces will affect adsorption potentials for metal ions. Güven (1989) has recently reviewed smectites in relation to their morphologies and chemical composition, and defined the basic morphological structure of smectites as a hexagonal lamella, from which other structures are derived in response to crystallization conditions (Figure 6.34).

The structural and crystal chemical characteristics of smectite provide the following criteria to differentiate the species of smectites:

1) Di- or tri-octahedral nature of the octahedral sheets, which divides the smectites into dioctahedral and trioctahedral subgroups.

2) Sources and sites of excess layer charges: the relative amounts of excess charges in tetrahedral (x_t) and octahedral (x_0) networks.
3) Predominant octahedral cation, and
4) in some instances, proxy ions in octahedra like Mg in montmorillonite, and Li in hectorite.

Obviously, the chemical and structural features of the octahedral sheets determine the identity of the smectite species (Güven, 1989). On the basis of the criteria mentioned above, a tentative classification of smectites is presented in Table 6.4.

Di-octahedral aluminous smectites are represented by the montmorillonite-beidellite series according to the structural formula:

$$(Al_{2-y}\ Mg_y^{2+})\ (Si_{4-x}\ Al_x)\ O_{10}\ (OH)_2 E^+_{x+y} \cdot nH2O$$

where the amount of E^+ represents the interlayer cation, x and y the octahedral and tetrahedral substitutions, respectively. The smectites with y>x are called montmorillonite and those with y<x beidellites. The iron analog of beidellite is called nontronite. The

Figure 6.35: Perfect hexagonal lamella and the other habits of smectite crystallites derived from it (From Güven, 1988).

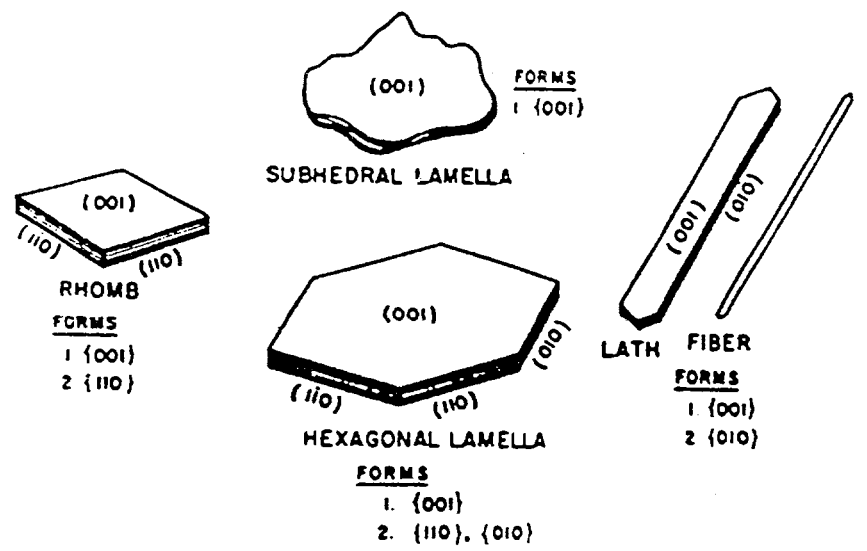

	DIOCTAHEDRAL SMECTITES		TRIOCTAHEDRAL SMECTITES	
Ratio between tetrahedral (x_t) and octahedral (x_0) charges	Predominant octahedral cation(s)	Smectite species	Predominant octahedral cation(s)	Smectite species
$x_0/x_t > 1.0$ (octahedral charges predominant)	Al (R^{2+}) *	Montmo-rillonite	Mg	Stevensite
			Mg (Li) * AlMgLi	Hectorite Swinefordite
			single or mixed transition metals	Transition metal "defect"trioc. smectites

$x_t/x_0 > 1.0$	Al	Beidellite	Mg	Saponite
(tetrahedral charges	Fe^{3+}	Nontronite	Fe^{2+}	Iron saponite
predominant)	Cr^{3+}	Volkonskoite	Zn	Sauconite
	V^{3+}	Vanadium smectite	Co	Co. smectite
			Mn	Mn. smectite
			Single or mixed transition metals	Transition metal trioc. smectites

* octahedral substitutions
Note: reasonably well-defined species (synthetic or natural) are given as separate entries.

Table 6.4: Classification of natural and synthetic smectites (Guven, 1989).

other two lesser-known species of dioctahedral smectite are volkonskite and vanadium smectite carrying Cr^{3+} and V^{3+} as the predominant octahedral cations respectively.

Trioctahedral smectites can be divided into three subdivisions considering the predominant octahedral cation(s) and the paragenetic relationships:

1) trioctahedral magnesian smectites with predominantly octahedral charges derived from monovalent Li^+ substitutions or defects (vacant octahedra). They are represented by the hectorite-stevensite series in nature as products of magnesian rich environments.

2) trioctahedral smectites of the transition metals (Ni, Co, Zn, Cu, Mn, Fe etc.) that are found around ore bodies and in laterites and saprolites of ultramafic rocks. The smectites in this group contain a transition metal as the predominant octahedral cation.

3) ferromagnesian trioctahedral smectites (saponite/iron saponite series) with Mg and Fe^{2+} as the predominant octahedral cations. They occur mainly as authigenic clay minerals produced by the alteration of oceanic and continental basalts and other basic volcanic material.

An attempt was made to characterize the smectites encountered in this study into the different species mentioned above. The smectite 00l intensities can be used to gain information on Fe substitution or, more accurately, on the scattering from the octahedral sheet (Moore & Reynolds, 1997). The intensity ratio of the 002 to the 003 increases sharply as the total number of electrons in the octahedral site increases. This intensity ratio is useful for differentiating dioctahedral from trioctahedral smectites, though moderate Fe concentration in a dioctahedral variety will produce diffraction patterns that are indistinguishable from Mg-rich trioctahedral varieties (Moore & Reynolds, 1997). As the smectites of this study had variable amounts of Fe, it was found necessary to

resolve the dilemma by measuring the spacing of the 060 peak which differentiates dioctahedral from trioctahedral species, provided that the sample does not contain other minerals that interfere with this reflection.

The 060 reflections allows this distinction because the *b* cell dimension is sensitive to the size of the cations and to site occupancy in the octahedral sheet and is unaffected by the monoclinic angle ß (Moore & Reynolds, 1997). Since the peaks are weak, step scan procedures that use long count times was utilized to improve the resolution of the peaks. Table 6.5 shows nominal values of *d* (060) and the corresponding diffraction angles. Care should be taken when identifying trioctahedral species because of the possible presence of a quartz peak at *d* = 1.542A°. When this happens, it is essential to look for another quartz reflection at *d* = 1.82A°. This reflection has about the same intensity as the peak at *d* = 1.542A°. If the peak at *d* = 1.82A° is present, allowances for the interference of quartz should be given when interpreting a peak in the 1.54A° region as evidence for a trioctahedral clay mineral in the sample (Moore & Reynolds, 1997).

Mineral	*d* (060)	2q
Kaolinite	1.490	62.31
Montmorillonite	1.492-1.504	62.22-61.67
Illite (Muscovite)	1.499	61.90
Saponite	1.520	60.95
Nontronite	1.521	60.91
Hectorite	1.530	60.51
Chlorites	1.538-1.549	60.16-59.69
Vermiculite	1.541	60.03

Table 6.5: Values of *d* (060) and 2q for micas and clay minerals. All data adapted from Bailey (1980) except for the smectites, which are taken from Brindley (1980).

Figures 6.36 shows the XRD patterns of the < 2 µm clay fractions and 060 peaks of the smectite samples from the saprock and middle saprolite of the study area. The peaks were collected by step scanning from 56 to 63° at steps of 0.02° 2q and a counting time of 0.25 seconds/step. In most cases, the smectites were identified in the field as olive-green patches within the saprolite groundmass. These patches were delicately separated from the rest of the matrix to ensure that the sample contained as much of the smectite as possible and little of the other secondary products.

The dominant smectite that formed in the saprock and saprolite was the curly and 'cornflake' textured variety, which initially formed cellular 'spongy' encrustations on the feldspar surface. This smectite displayed a composition characterised by high Si and Fe and moderate Al and low Ca. The 060 reflections, chemistry and morphology identifies this smectite as nontronite (Table 6.6). The second type of morphologically distinct smectite was the 'spongy' variety that characterized the soil, mottled clay and white clay unit. The determination of the 060 reflections of these smectites proved to be difficult because they occurred together with appreciable amounts of kaolin, mica and fine grained quartz fragments which interfered with the 060 reflection. In some cases this reflection was very broad and weak making it extremely difficult to assign it to any of the clay species. However, qualitative SEM EDXA chemistry shows it to contain high Si, moderate Al; and low Ca and Fe, which qualifies it as Fe-montmorillonites.

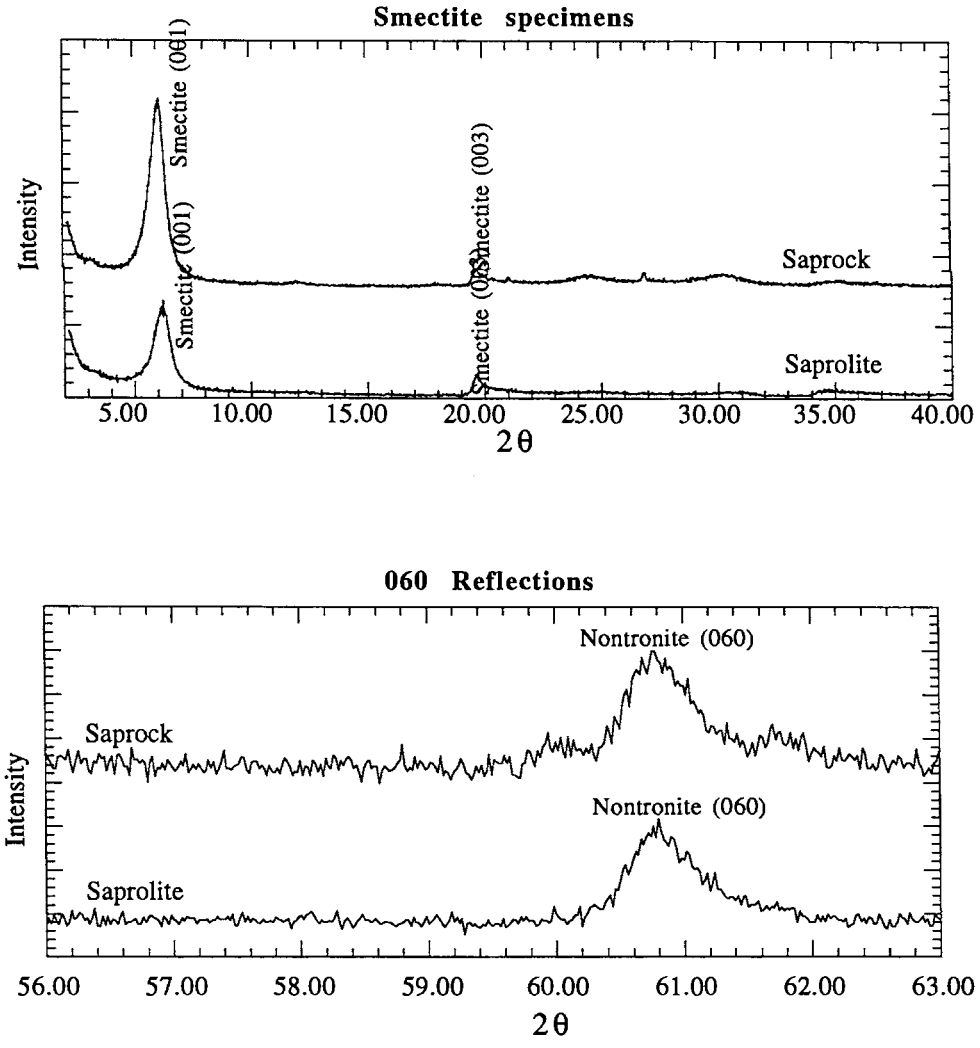

Figures 6.36: Clay mineralogy and 060 reflections of smectite specimens from the saprock and the saprolite

A summary of the results of 4 well defined 060 peaks are presented in Table 6.6:

Sample depth	*d* (060)	2q	Mineral specy
E22 P4 (46m)	1.5213	60.84	Nontronite
E22 P4 (42m)	1.5222	60.80	Nontronite
E27 P6 (40m)	1.5226	60.78	Nontronite
E22 P6 (44m)	1.5217	60.82	Nontronite

Table 6.6: *d*(060) and 2q of samples from the saprock and greenish-grey saprolite of both E22 and E27 deposits

In the soil horizons, the smectites contained similar Al and Fe, pointing to further incorporation of Fe into the initially formed Fe-montmorillonite. This composition of smectite from the upper horizons is consistent with Wilson's (1987) observations of soil smectites bearing high proportions of Fe. The influence of Fe in the formation of secondary products in solution has already been discussed in the previous chapter.

In the soil horizons and mottled clay zones, the smectites were observed to have become larger (10-20 μm) with surfaces free of undulations (Figures 6.25.7 and 6.25.7). Wetting and drying conditions are considered to affect the micro-fabric of the clays (Dalrymple & Jim, 1984) and is the prime factor that causes the characteristic swelling and shrinking of smectites. The shrink swell properties of smectites have been documented (Odom, 1984; Tazaki et al. 1990 and McEwan & Wilson, 1980), with the primary characteristics responsible for hydration being the magnitude of charge on the interlayer of the clay, the exchangeable cations which occur between the interlayers and the interactions of the water molecules with the interlayer cations (McEwan & Wilson, 1980). Intensity of swelling of smectites is dependent upon the exchangeable cation, with Na smectites inheriting high swelling capacities (Odom, 1984), with the shrinking degree being related to the exchangeable cation. In general, low exchange smectites dry out more easily and vice versa (Tazaki et al. 1990).

Apart from the interlayer cation, another factor, which may have induced different rates of swelling and shrinking in smectites of different horizons, may be the amount of precipitation and subsequent solution activity. In the relatively fresh rock, the microfractures and cleavages provide the only corridors for solution entry and hence it is possible that, only ample precipitation might have provided high surface tension and carpillarity, which is necessary for solution to gain access through the minute conduits. The length of time the material has been saturated is also critical with longer durations promoting high swelling capacities in smectites.

Conversely, in the solution dominated microsystems, primarily in the saprolite and mottled clay zone, minor amount of precipitation may provide the solution necessary to wet the horizons via abundant fissures and large cracks, thus leading to rapid crystallization and considerable reduction of wet and dry sequences as compared to the saprock. Also, the curves on the smectite surfaces may act like defects or kinks and induce further crystal growth (Berner, 1981), leading to the formation of the smooth surface.

Another factor that may provide high swelling characteristics in the smectites might be the Fe content in its structure. Fe^{3+} has been documented to replace Al^{3+} in the tetrahedral site of smectites (Egashira & Ohtsubo, 1983; Wilson, 1987) and in the soil horizons the oxidation of Fe may lead to an increase in swelling capacity of smectites (Egashira & Ohtsubo, 1983).

6.9.3.2 Kaolin

Kaolinite classification is based either on the mechanism of their formation (inheritance, neoformation, transformation) or on the environment where they were formed (hydrothermal, weathering, sedimentary) (Eberl, 1984). Although some dissimilar fabrics have been observed in sedimentary and hydrothermal kaolins (Keller & Hanson, 1975), the formation conditions of kaolinites remain largely unknown inspite of several detailed studies of structural properties (Keller, 1978; Giese, 1988; Cases et al. 1982; Jepson, 1988). Because of the mineralogical complexity of natural clays, kaolin geochemistry is often difficult.

Kaolin displays wide variations in crystallographic properties (Plancon & Tchoubar, 1977) as a result of varying modes of formation and/or subsequent transport or weathering (Keller, 1982; Muller & Calas, 1990). These include variations in crystallinity and the proportion of Fe^{3+} impurities, as well as other properties such as crystal size and shape.

The XRD traces of kaolin are mainly modified by variations in crystallinity (Brindley et al. 1986). Highly crystalline kaolin gives sharp and well-defined peaks on XRD traces. This is a result of a high degree of structural order in the kaolin crystal lattice, where the basic lattice 'building block' is repeated almost perfectly throughout the crystal. In contrast, degradation in crystallinity can be identified in XRD by poor resolution of peaks. Such degradation occurs when some domains within and between the clay layers in the

kaolinite crystal have some imperfection in them, and the kaolin pattern is not perfectly repeated throughout the crystal.

Detailed work by Plancon & Tchoubar (1977) illustrated that the dominant defect in kaolin that leads to poor crystallinity is due to a mistake in the position of the vacant octahedral site between layers. This is based on the fact that the perfect (i.e. highly crystalline) kaolinite is a dioctahedral layered clay, meaning that of the three available octahedral sites (A, B and C) in the clay only two are filled by Al, with the B site always being the vacant site between each clay layer. However, in poorly crystalline kaolin, this vacant site can occur in either the A or C sites instead of the B site. These mistakes occur within sub-layer lattice 'domains' in the clay and the more of these mistakes there are in the kaolinite, the more disordered/poorly crystalline it is.

As a result of these defects within and between the layers of a poorly crystalline kaolin, there will exist certain domains [domains imply small local changes within the clay layers that do not affect the whole layer] which are 'dickite-like'. This is because the vacant sites in dickite, in contrast to kaolin, alternate between B and C positions between layers. Consequently, poorly crystalline kaolins are typically indistinguishable from poorly crystalline dickites in XRD plots (Plancon & Tchoubar, 1977).

Another factor that has been documented in influencing the crystallinity of kaolin is the presence of Fe substitution for Al (Brindley et al. 1986). High iron contents cause crystal lattice disorders (Mestadgh et al. 1980). Although it has not been proven conclusively and is a contentious issue among experts, typically higher Fe-contents appear to correlate with lower crystallinities (Brindley et al. 1986).

Information in published literature suggests that the effects of crystallinity and Fe^{3+} content appear to be the most significant characteristics for differentiation of transported from residual kaolin. Typically residual kaolins are highly crystalline, whereas transported ones are poorly crystalline (Brindley et al. 1986; Ma Chi, 1996). Ma Chi (1996) in his study of kaolins from different environments described residual kaolin of weathering origin as displaying better crystallinity than transported kaolin and presently-formed hydrothermal kaolin. In XRD analysis, sharp kaolin peaks indicate good crystallinity whereas broad ones indicate poor crystallinity.

Recent work utilizing diffuse reflectance spectroscopy has also revealed important differences among the various types of kaolins (Malengreau, Muller & Calas, 1994, 1995). Thse inferences have been obtained using Electron Paramagnetic Resonance

(EPR) which is used to investigate point defect centres and the environment of formation. The high sensitivity of EPR to the presence of paramagnetic impurities and Radiation Induced Defects (RID's) has made it particularly useful for differentiating kaolinite formed in hydrothermal, weathering or sedimenatry environments. Details concerning the experimental conditions used for EPR investigation of kaolins have been published by Muller et al. (1992) and Muller & Callas (1993a).

These studies have shown that hydrothermal kaolinites have the lowest concentration of substituted Fe^{3+} and the highest RID content. Low levels of Fe^{3+} associated with high structural order (Meads & Malden, 1975) indicate that hydrothermal kaolinite has grown slowly from Fe-undersaturated solutions (Muller & Calas, 1993a). Kaolinites from weathering processes by comparison exhibit the highest concentration of Fe^{3+} substitution for both $Fe_{(I)}$ and $Fe_{(II)}$ sites, but the total substituted Fe^{3+} is unrelated to the substrate Fe-content (Muller, 1988). An increase in the concentration of $Fe_{(I)}$ sites leads to a decrease in crystalline order, whereas variations of $Fe_{(II)}$ have no effect (Herbillon et al. 1976; Muller & Bocquier, 1987). This type of kaolinites also have fewer RID's because radioactive element concentrations, and hence irradiation levels are low during weathering in an open hydrologic system (Muller & Calas, 1989; 1992).

Sedimentary kaolinites on the other hand are more unique in that they have RID contents three or four times that of lateritic kaolinites and close to that of hydrothermal samples with A centres being largely predominant (Muller & Calas, 1993a). The concetration of substituted Fe^{3+} is intermediate between soil and hydrothermal samples and is proportional to total Fe-content (Allard, Malengreau & Muller, 1992). Both $Fe_{(I)}$ and $Fe_{(II)}$ are related to crystalline order (Brindley et al. 1986), and the relative proportion of $Fe_{(II)}$ species is higher than in soil kaolins. The origin of sedimentary kaolionites although controversial must hence demonstrate the concept of inheritance which must be defined in relation to the parameter being considered. On the basis of lattice parameter measurements, a sedimentary kaolin might be considered to be inherited from weathering profiles whereas spectroscopic evidence might indicate transformation during sediment accumulation and evolution, which is indicative of authigenic origin (Muller et al. 1995).

The regolith in the study area has been interpreted as having evolved by *in situ* weathering on the trachyandesite and/or weathering in initially transported material. However, Figures 6.37 on the contrary shows that the mottled clay specimens, which have been interpreted as having formed on initially, transported material exhibit kaolin of good crystallinity. A study of these samples using field-portable infrared reflectance spectrometer (PIMA) also produced similar crystallinity effects and this was interpreted

as representing the *in situ* development of kaolin within the leached mottled material (Sasha Pontual pers. comm.). Her analysis of mottled clay specimens that developed over channel sequences in Western Australia produced similar results consistent with the observations of this study that poorly ordered kaolin is of transported origin.

In the weathering environment, physico-chemical conditions fluctuate widely in an open system leading to variation in reaction rates of solutes. Under these conditions, chemical equilibrium between solution and minerals is hardly ever reached. The different crystal sizes and crystallinities of kaolin may be attributed to the different conditions of crystal growth or dissolution, which are dependent on the physical and chemical states of solutions.

Growth of large kaolin crystals (e.g., more than 3 μm in thickness and 10 μm in length) may require both physically and chemically stable solution environment occurring over a long time as suggested by Keller (1977). Under these steady state conditions, the soluble species dissolved from feldspars and micas can be supplied for the growth of larger and more structurally ordered kaolin. These conditions are usually dominant in the deeper part (the saprolite and saprock zones) of a weathering profile (near or under the groundwater table) where the porosity of weathered rocks is relatively low and movement of pore-water is relatively slow. Kaolin formed in this manner would form in equilibrium with pore solution. However, in the shallow part of the weathering profile, activities of dissolved species vary greatly in the infiltrating rainwater and the relatively rapid flowing pore-water. In this condition, the activities of soluble species in the pore solution are relatively variable.

This highly variable solution environment is unfavourable for the growth of large kaolin crystals. As a result, kaolin crystals of relatively small size are formed in the mottled zone compared with larger sized kaolin crystals in the saprolite. This is the case with the kaolin from the two zones as described in this Chapter. The kaolin in the mottled zone also contained higher contents of Fe as compared to that from the saprolite. As already documented earlier in the Chapter, this is due to a relatively high Fe concentration in the pore solution of the mottled zone whereby hematite and goethite form along fissures and voids within the clay matrix. The chemical processes responsible for iron accumulation are the oxidation of the soluble Fe^{2+} to the less soluble Fe^{3+} and the subsequent precipitation of hematite or goethite:

$$Fe^{2+} <=> Fe^{3+} + e^-$$
$$2Fe^{3+} + 3H_2O <=> Fe_2O_3 \text{ (hematite)} + 6H^+$$
$$Fe^{3+} + 2H_2O <=> FeO(OH) \text{ (goethite)} + 3H^+.$$

The precipitation of hematite or goethite results in the dissolution of kaolin by means of protons liberated during hydrolysis of Fe^{3+} (Nahon, 1991).

SEM observations revealed the co-existence of quartz and kaolin in the mottled clay. From the activity diagram for the K_2O-Al_2O_3-SiO_2-H_2O system in Figure 6.38 at 25°C (Garrels & Christ, 1965), it is apparent that the solution was located within the kaolin + quartz region in this zone.

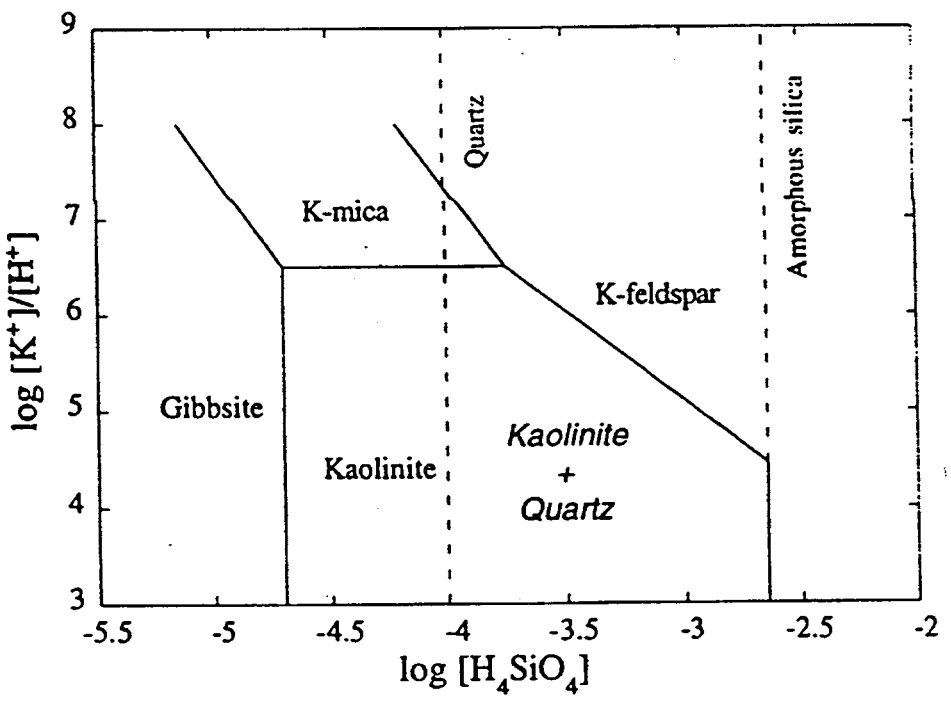

Figure 6.38. Activity diagram in the K_2O-Al_2O_3-SiO_2-H_2O system at 25°C and 1 atmosphere. Modified from Garrels & Christ (1965).

The kaolin developed in the saprolite and saprock over the trachyandesite showed moderate to poor crystallinity (Figures 6.38), consistent with the observations that

moderately to poorly crystallized kaolin occur on volcanic rocks (Koppi & Skejmstad, 1981). Chittleborough & Walker (1988) in their investigations of different aged clays, found coarse grained kaolin becoming poorly crystallized with age, suggesting older profiles would contain disordered kaolinite.

Climatic data examined points to a Late Palaeozoic age for the initiation of profile development (Chapter 8). This relatively old age itself may provide an answer to the occurrence of moderate to poorly crystallized kaolin using these observations of Chittleborough & Walker (1988).

6.9.3.3 Characteristics of kaolinite weathering

Kaolinitic weathering is not necessarily a tropical or sub-tropical phenomenon. High rainfall and efficient leaching are the prime requirements for kaolinite development, and although warm temperatures will enhance reaction rates they are not essential if the above-mentioned conditions are met. Experimental evidence on the formation of kaolinite indicates the need for extremely dilute solution that are only slightly supersaturated with respect to kaolinite (Kittrick, 1970).

The following equations represent the precipitation of kaolinite from pore water (or weathering solution) (Garrels & Christ, 1965):

$$2Al^{3+} + 2H_4SiO_4 + H_2O \text{ <=> } Al_2Si_2O_5(OH)_4 + 6H^+, \quad \text{Equation 1}$$
$$\text{(aq)} \qquad\qquad\qquad \text{kaolinite}$$

$$2H^+ + 2H_4SiO_4 + 2AlO_2^- \text{ <=> } Al_2Si_2O_5(OH)_4 + 3H_2O. \quad \text{Equation 2}$$
$$\text{(aq)} \qquad\qquad \text{kaolinite}$$

Equation 1 is generally accepted for the precipitation of kaolinite at the earth's surface (e g, Dixon, 1989). An activity diagram of the system Al2O3-SiO2-H2O at 25°C and 1 atmosphere, constructed using the thermodynamic data of Garrels & Christ (1965), Huang & Keller (1973) and Busenberg (1987), is shown in Figure 6.39.

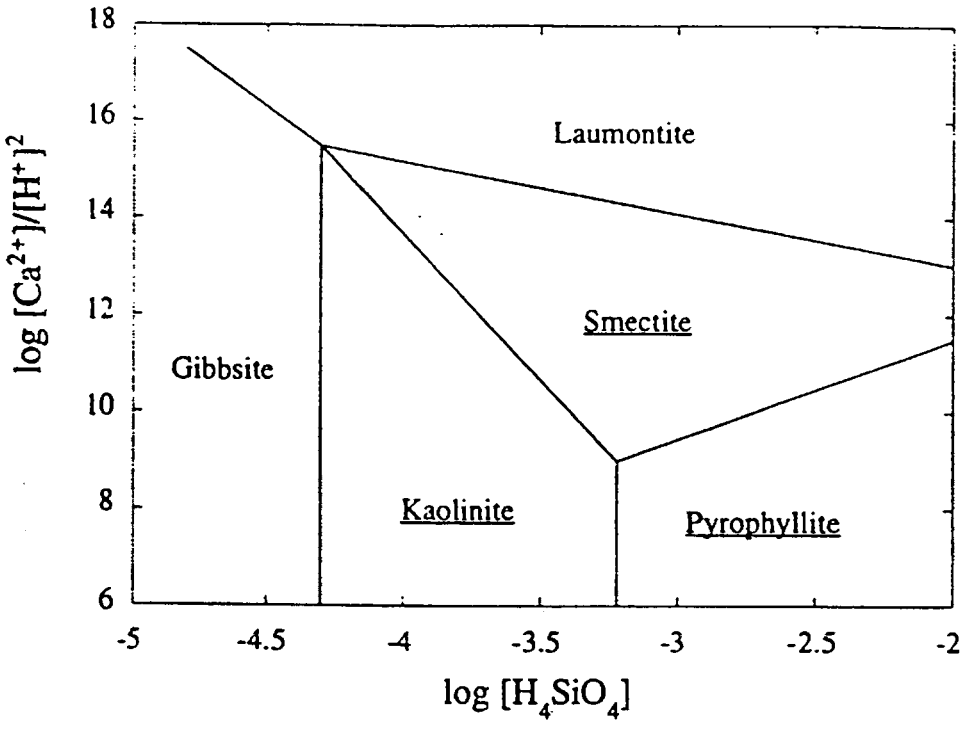

Figure 6.39: Activity diagram for phases in the $CaO-Al_2O_3-SiO_2-H_2O$ system at 25°C and 1 atmosphere (Drever, 1988).

The amount of silica in solution also affects the chemical composition of kaolinite. A relatively pure solution with a high silica content and low concentrations of other cations favours the formation of pyrophyllite. On the other hand, an impure solution with relatively high cation concentrations favours the formation of smectite. This implies that only a slight increase of silica in solution might cause a pyrophyllite cover layer on kaolinite to form, whereas an increase in dissolved cations (including silica) might result in the formation of smectitic layers on kaolinite (Drever, 1988).

6.9.4. Summary of mineral stability and alteration pathways

Broad knowledge of weathering characteristics is essential to any study of the regolith in an area. Studies of weathering susceptibility of individual minerals have been done over many years with Goldich (1938) recognizing that a simple ordering could be obtained by reversing the Bowen's Igneous Crystallization Series (Figure 6.40). The breakdown of these minerals ultimately ends up with Fe oxides, kaolinite and silica as stable phases (Table 6.7).

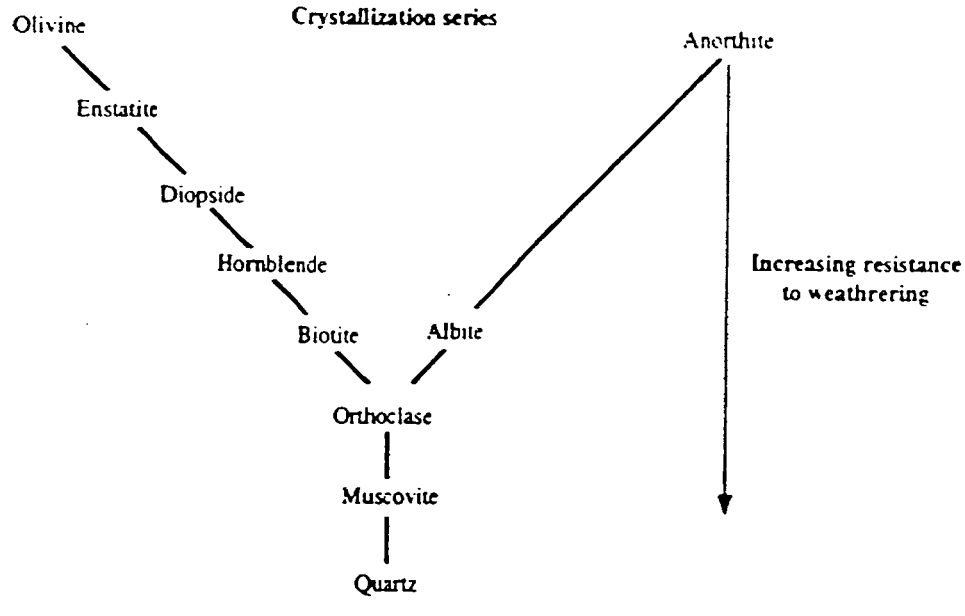

Figure 6.40: The Bowen Igneous Crystallization Series related to weathering susceptibility (Scott, 1996).

Olivine	→	Fe oxide + Si		
Plagioclase	→	Kaolinite		
K-feldspar	→	Illite	→	Kaolinite
Amphibole	→	Fe oxide	+	Kaolinite

Table 6.7: Breakdown products of some common minerals

The feldspars of the study area showed variable characteristics during weathering of the host rock. The plagioclase feldspar persisted through the saprock to the upper levels of the middle saprolite. The bulk of the K-feldspars begun to break down within the lower saprolite and they persist all through to the upper saprolite. Both these feldspars initially produced smectites and kaolin although the kaolin contents started increasing towards the upper levels of the profile (Figure 6.3).

Muscovite occurs with the feldspars within the primary rock suite although appreciable amounts also occur as pseudomorphs of plagioclase laths. Alteration of sericitized

plagioclase produced an intimate interlamination of mica and clay to give a homogenous fabric. The muscovite persisted throughout the profiles up to the white clay unit, which was marked by intense reorganization of the fabric. Quartz was the only mineral that survived throughout the profiles.

The weathering fabrics that have already been discussed are a consequence of the reactions between these weathering minerals. Some secondary minerals like muscovite replaced their plagioclase precursors, pseudomorphing and hence preserving the fabric in the process. Pseudomorphic replacements dominated the lower parts of the profile where original rock fabrics tended to be well-preserved, defining the saprock and the saprolite.

As weathering continued, mineral dissolution and fabric changes became more pronounced. Such changes involved dissolution of clays, the formation of clay accordion structures and clay blasts towards the upper saprolite. The importance of these processes increased into the mottled clay zone where segregation, concentration and cementation by iron oxide minerals occurred. This was marked by development of void structures and channelways and the appearance of root clasts, which became infilled with clays or fragments of the original rock fabric. Pockets of original fabric were also found preserved in the soil horizon.

A schematic representation of the microsystems of the residual units in transition from the saprock to the saprolite and the associated mineralogical and textural changes is outlined in Figure 6.41. The dissolution-precipitation mechanism invoked to explain secondary product formation (Keller, 1978; Berner & Schott, 1982; Glassman, 1982, Anand et al. 1985 and Velbel, 1989) certainly seems to be the paramount mechanism operating to develop and furnish the alteration products. The bulk and clay mineralogy showed a decrease in 2:1 clays up the profile with a subsequent increase in the 1:1 clays and iron oxides. The feldspar alteration paths when compared to the activity diagrams proposed for the mineral by workers such as Loughnan (1969) and Keller (1985), showed that the weathering sequences of this study is consistent with those proposed by these diagrams (Figure 6.42).

Amounts of solution exert a considerable influence on the surface morphologies of the secondary products, especially smectites. In the lower portions of the profiles, solution mobility is reduced because of the limited number of conduits present, leading to a greater frequency of wet and dry conditions and consequently the development of 2:1 clays. Higher up in the profiles, supersaturation causes change in the chemical conditions of the

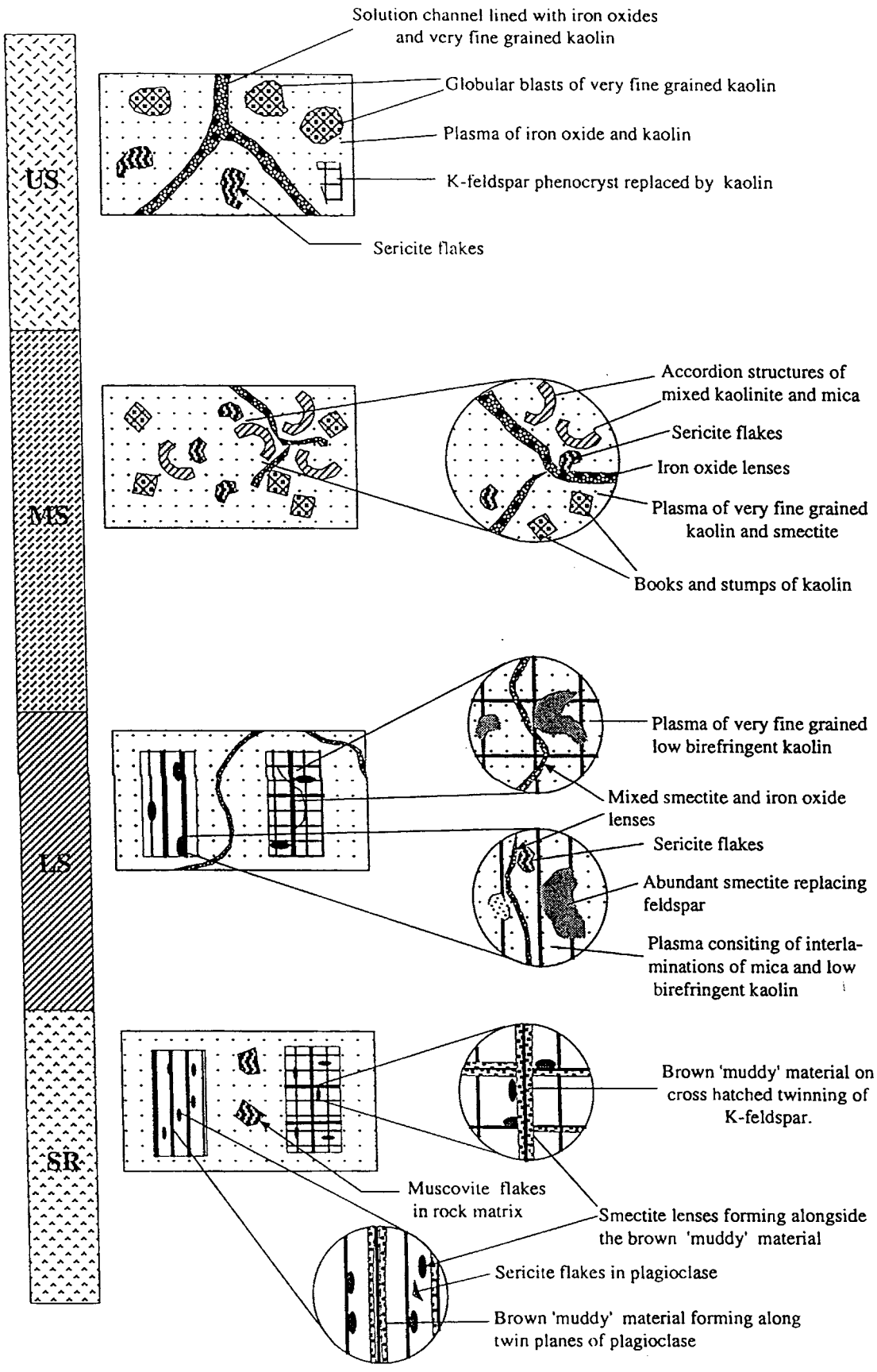

Figure 6.41 : Schematic representations of the microsystems of the residual units in transition from the saprock to the upper saprolite [SR-saprock; LS-lower greenish-grey saprolite; MS-middle greenish-grey saprolite; US-upper orange-pink saprolite]

microenvironments. Solution chemistry such as pH, affect the stability of the secondary products which is evident by the smectites experiencing dissolution higher in the profile where changes in physicochemical conditions occur. A fall in pH favours the dissolution of smectites or induce their destabilization.

Figure 6.42: Theroretical pathways for Feldspar reaction. Arrows indicate sequence of phases observed

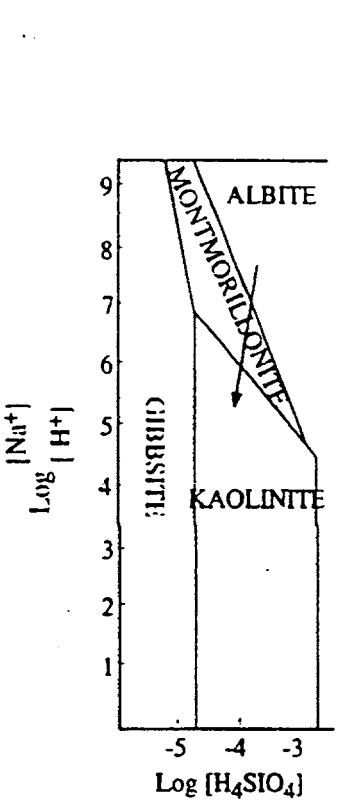

From Loughnan (1969)

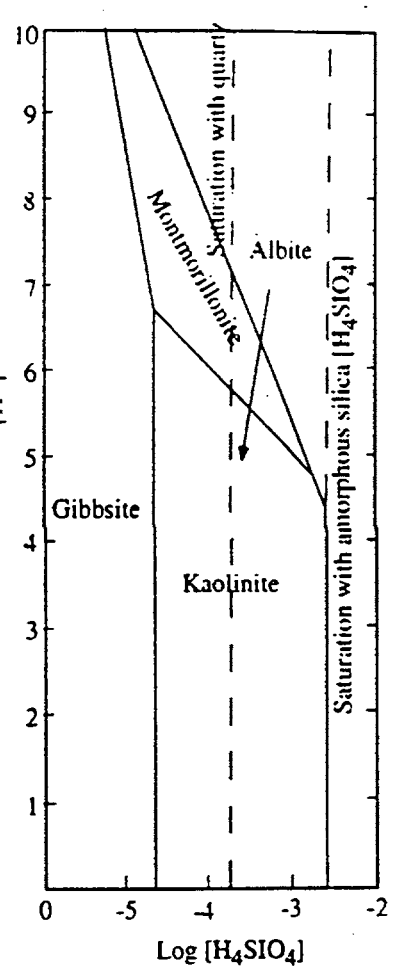

From Keller (1970)

Solution is effective on a macro-and-micro scale. Micro scale influences are observed in the saprock and saprolite where K, Ca and Al appeared in the plagioclase and K-feldspar derived smectite and the formation of iron oxides adjacent to kaolin, where Fe is supplied from the surrounding iron-rich minerals. The long-range operation of solution was demonstrated in the Fe present within the microcracks in the saprock and saprolite.

Although some of the Fe was procured from this horizon, appreciable amounts might have been translocated via solution from the higher mottled horizons of the profile. For iron to proceed on a macro-scale, it must be in the mobile ferrous state (Loughnan, 1969) which implies frequent reducing conditions in the profile (Nahon, 1986). The Fe^{2+} could have sustained a change of valence by coming in contact with the clays (Carrol, 1958; Nahon, 1986) as was suggested by the formation of iron oxides adjoining the kaolin in the lower saprolite and the saprock. The most dominant species in solution was obviously Fe and this was reflected in its appearance in all the secondary products.

A summary of the reaction equations for some of the minerals encountered in this study and their products are summarized in Table 6.8.

Table 6.8: Summary of mineral reaction equations.

Feldspar

General formula:

Plagioclase Smectite

$4Ca_{0.5}Na_{1.5}(Si_{5.5}Al_{2.5})O_{16} + 8H^+ + 16H_2O <<>> 4Ca_{0.25}Al_2[Si_{3.5}Al_{0.}O_{10}(OH)_2 + 6Na^+ + Ca^{2+} 8H_4SiO_4$

Smectite Kaolin

$4Ca_{0.25}Na_{1.5}(Si_{5.5}Al_{2.5})O_{10}(OH)_2 + 2H^+ + 13H_2O <<>> 5Al_2Si_2O_5(OH)_4 + 4H_4SiO_4 + Ca(OH)_2$

Alkali feldspar

$2KAlSi_3O_8 + 9H_2O + 2H^+ <<>> Al_2Si_2O_5(OH)_4 + 2K^+ + 4H_4SiO_4$

Orthoclase Kaolinite

Calcic plagioclase

$2NaAlSi_3O_8 + 2H_2O + 4H^+ <<>> Al_2Si_2O_5(OH)_4 + 2K^+ + 4H_4SiO_4$

Albite Kaolinite

Muscovite

$KAl_3Si_3O_{10}(OH)_2 + 8H^+ + 2H_2O <<>> 2Al_2Si_2O_5(0H)_4 + 2K^+ 2Al^{3+} + 2H_4SiO_4$

Muscovite Kaolinite

CHAPTER 7.

REGOLITH MINERALOGY: ORIGIN AND DISTRIBUTION OF PRODUCTS IN THE REGOLITH STRATIGRAPHY.

7.1 Introduction.

A diverse range of secondary products was encountered during weathering of the different host materials as reported in the previous chapter. This chapter deals with the distribution of these products in the regolith profiles and stratigraphy and the origin of the non-clay secondary products. The major diagnostic features of the different parent materials are also presented.

The quantitative mineralogy results obtained using *Siroquant* are presented in Appendix 1. The quantitative mineralogy results of the sulfides have not been presented in this text. This is because the *Siroquant* version that was used in this study did not have allowances for the refinement of these sulfides. A few other minerals such as augite, magnetite and apatite have also not been presented for the same reason despite accounts of their occurrence in XRD analysis. The different units of the mottled clay zone have also been grouped together mainly because of the close similarity in their characteristics which is reflected in their mineralogy.

7.2 Mineralogical distribution in the regolith profiles

The mineralogical distributions are shown in Figures 7.2. Most of the profiles shown in the schematic diagrams of both deposits (Chapter 5, Figures 5.2 and 5.4) have been covered in this study. These include profiles 1, 2, 3, 4, 5, 7, 9 and 10 from the E22 deposit and profiles 1, 2, 3, 4, 5, 6, 7, 8, 9, 10 and 11 from the E27 deposit.

The graphical presentations have been followed by a summary of the mineralogical trends along each profile.

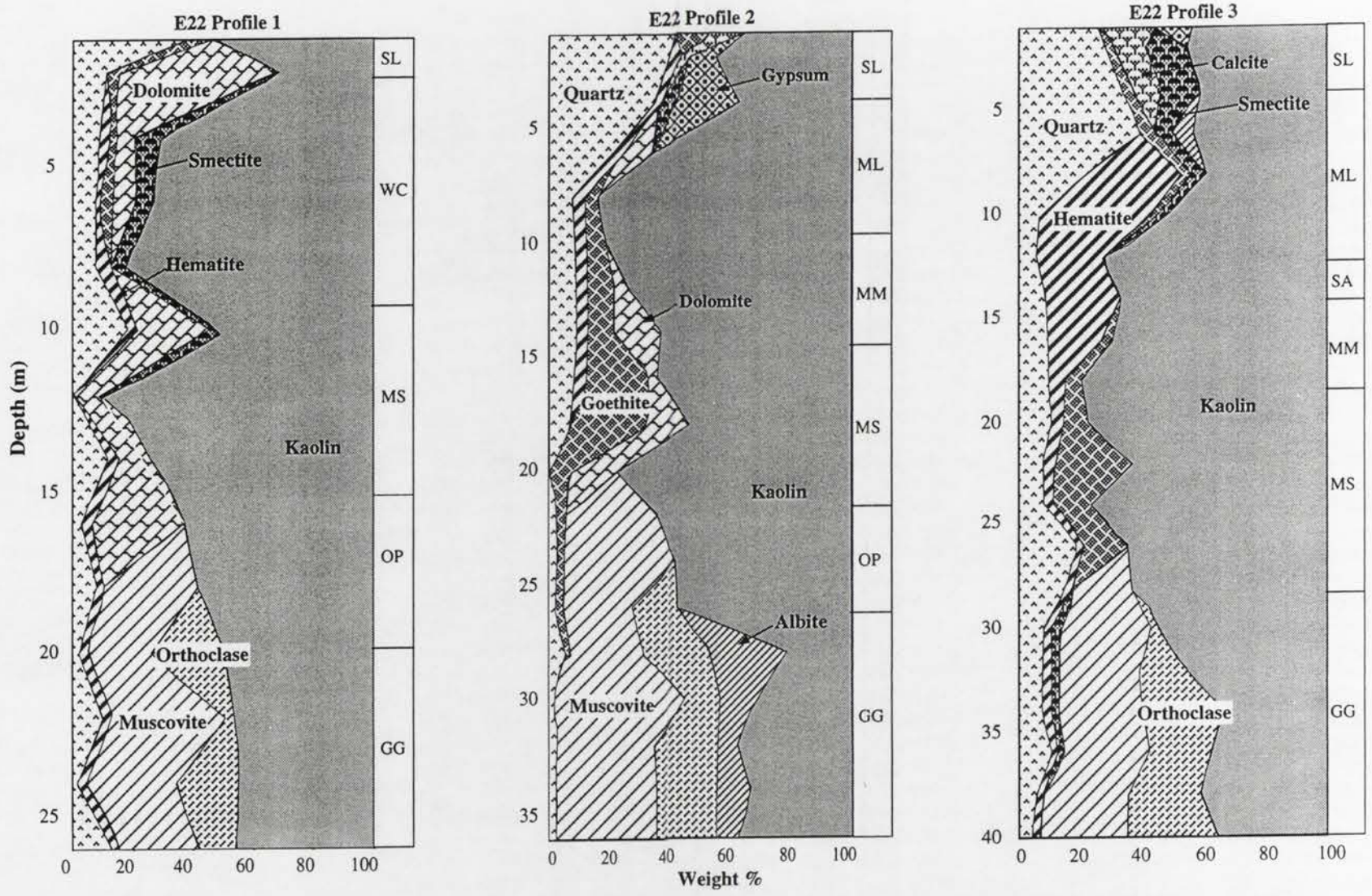

Figure 7.2.1: Mineralogical distributions along E22 Profiles 1, 2 and 3 [SL-Soil horizon; WC-white clay unit; ML- mini-and-medium-mottled clay; SA-silica aggregates; MM- mega-mottled clay; MS-mottled saprolite; OP-orange-pink saprolite; GG-greenish-grey saprolite]

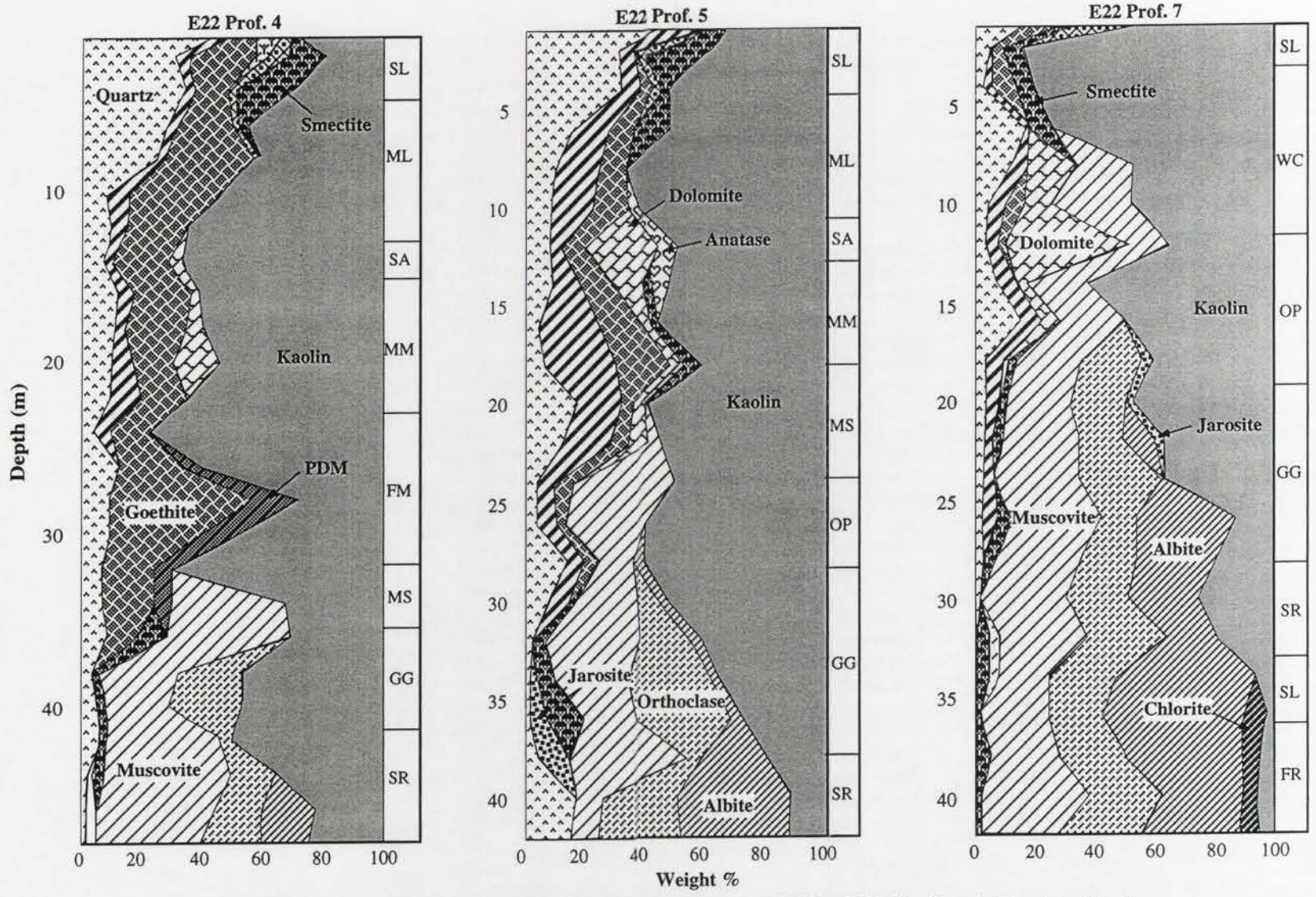

Figure 7.2.2: Mineralogical distributions along E22 Profiles 4, 5 and 7 [SL-soil horizon; WC-white clay unit; ML- mini-and-medium-mottled clay; SA-silica aggregates; MM- mega-mottled clay; FM-nodular Fe-Mn horizon; MS-mottled saprolite ; OP-orange-pink saprolite; GG-greenish-grey saprolite; SR-saprock; SL-sulfide zone; FR-fresh rock]

Profile 4

This Profile is located at the central part of the more deeply weathered section of the E22 deposit. It is defined by the soil horizon (3-4.5m), mini-and-medium mottled clay (6-8m) , band of silica aggregates (2-4m), the mega-mottled zone (5-7m), nodular iron and manganese rich zone (4-6m), mottled saprolite (5-7m), Greenish-Grey saprolite (8-10m) , saprock (4-5m) and the sulphide zone (2-4m). The weathering front occurs at depths of 42-45m. As in Profiles 2 and 3, the soil is composed of smectite (0.5-6.6%), calcite (4.5-8.1%), goethite (10-20%) and hematite (< 5%) and quartz (30-43%). Goethite is present in high amounts throughout the profile with the highest amounts (23.8-51.6%) occuring in the nodular iron and manganese aggregates zone. These aggregates have poorly diffracting material contents of between 6.6 and 15.1%. Dolomite occurs in the mega-mottled zone as coatings on silica aggregates and as void and fracture infills. Numerous green patches of nontronite smectite occurs at the Greenish-Grey saprolite. Muscovite, orthoclase and albite shows similar distributions as in the preceding profiles.

Profile 5

This profile is defined by the same regolith units as Profile 4. Calcite, smectite, gypsum and hematite occur in similar amounts in the soil as in Profile 4. Hematite and goethite occur in more or less similar proportions (4-23.9% and 4.1-18.5% respectively) within the mottled clay zones. Dolomite also occurs within the mega-mottled clay in moderate to high amounts (3-25.6%) as silica aggregate coatings and fracture and void infills . Anatase occurs within the mega-mottled clay zone and Greenish-Grey saprolite in low to moderate amounts (1.6-8.1%). Muscovite, orthoclase and albite shows similar distribution in the saprolite zones as in the previous profiles.

Profile 7

This profile is defined by the soil horizon (3-4m), white clay unit (6-8m), Orange-Pink saprolite (8-10m), Greenish-Grey saprolite (6-8m), the saprock (4-5m), sulphide zone (4-5m) and the fresh rock (12-14m). The weathering front occurs at depths of 32-34m. The soil horizon contains smectites, gypsum and goethite in more or less similar amounts as in Profiles 4 and 5 while uartz occurs in lower amounts (2.1-15.5%). The white clay unit of this profile contains muscovite in moderate to high amounts (14.2-26.5%) unlike in the white clay unit of Profile 1 where it was absent. However, the dolomite content is more or less similar (3.1-41.3%), while kaolin and smectite contents are equally high i.e 48.2-81.3% and 1.5-7.6% respectively. Jarosite occurs in the Orange-Pink saprolite in low amounts (1.2-3.6%). Albite as in the previous profiles persists up to the Greenish-Grey saprolite. Some chlorite (4.4-6.7%) occurs in the saprock, sulphide zone and the fresh rock.. Enstatite, diopside, hornblende and epidote occur with the chlorite in the saprock, sulphide zone and the fresh rock in very small amounts (<4% respectively).

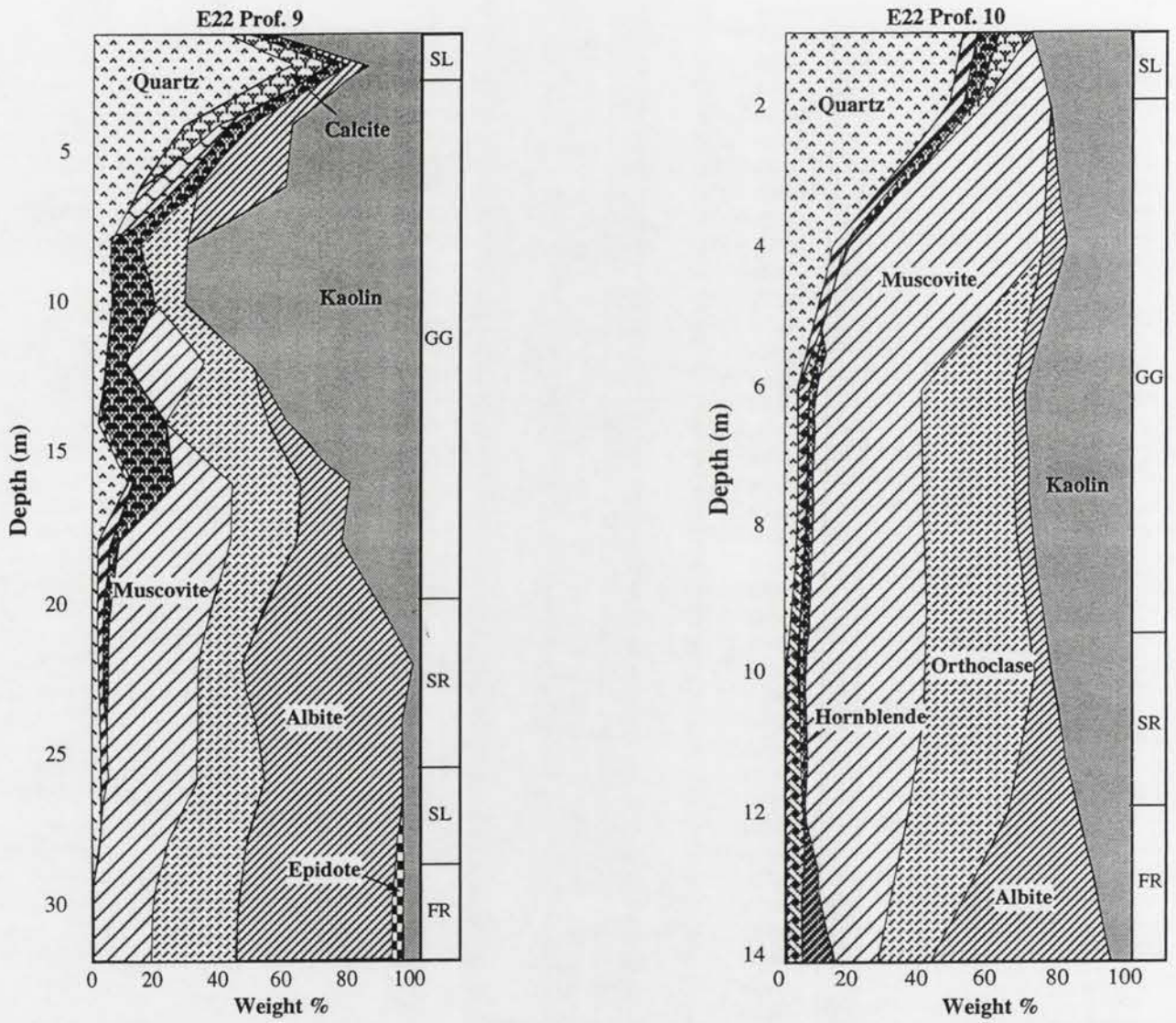

Figure 7.2.3: Mineralogical distributions along E22 Profiles 9 and 10 [SL-soil horizon; GG-greenish-grey saprolite; SR-saprock; SL-Sulfide zone; FR-fresh rock]

Profiles 9 and 10.

Profiles 9 and 10 are a direct product of *in situ* weathering of the trachyandesite. The depth to fresh rock is about 30 to 32 m in Profile 9 and 18 to 20m in Profiles 10. Both are defined by the presence of the soil horizons (1.5-2.5m), Greenish-Grey saprolite (15-20m), saprock 4-6m), the sulphide zone (4-5m) and the fresh rock (18-20m).

Profile 9

The smectite occurs throughout the profile mostly as nontronite although some occurs as montmorillonite within the soil horizon. High amounts (12.2-19.2%) occur in the middle and lower portions of the saprolite. Moderate amounts of albite (5.2-13.4) occur in the soil together with calcite (1.1-12.2%). Unlike in the other profiles the orthoclase seems to be slightly more persistent than the muscovite in the profile. Quartz occurs in increased amounts (13.6-60.8%) towards the soil horizon where it occurs as detrital fragments. Some epidote, hornblende and diopside occurs in very small amounts (<4% respectively) in the saprock, sulphide zone and the fresh rock.

Profile 10

The quartz and calcite shows similar distribution patterns as in Profile 9. Muscovite persists upto the soil horizon in this profile. It seems to be enriched as albite and orthoclase contents decrease. Albite is slightly more persistent in this profile than orthoclase. Hornblende also persists upto the upper saprolite where it is gradually lost. Moderate amounts of chlorite (84-10.7%) is present within the fresh rock.

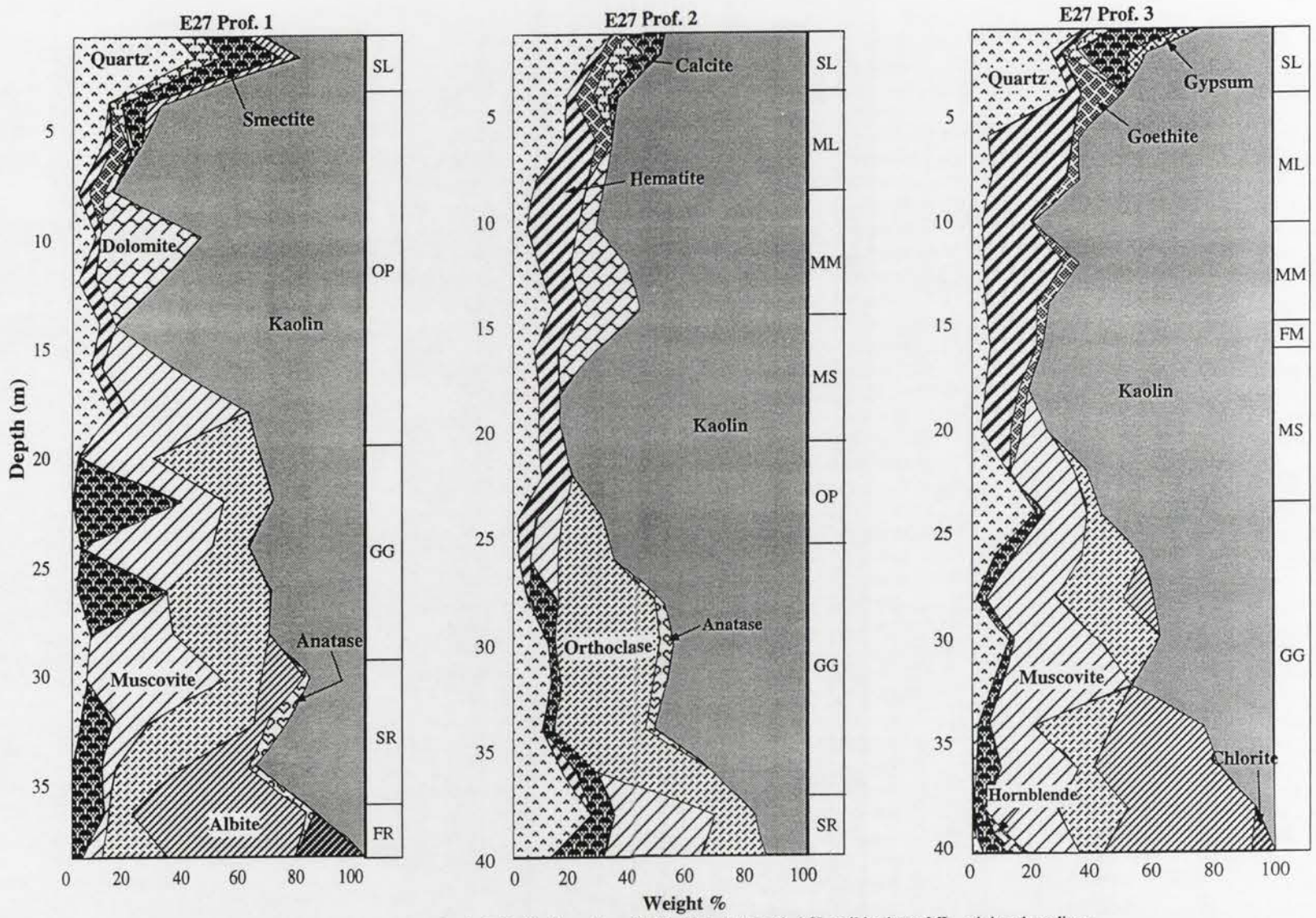

Figure 7.2.4: Mineralogical distributions along E27 Profiles 1, 2 and 3 [SL-soil horizon; ML- mini-and-medium-mottled clay; M- mega-mottled clay; MS-mottled saprolite ; FM-nodular Fe-Mn horizon; P-orange-pink saprolite; GG-greenish-grey saprolite; SR-Saprock; FR-fresh rock]

Profile 1

This profile is defined by the soil horizon (2.5-3m), the Orange-pink saprolite (15-18m), the Greenish-Grey saprolite (10-15m), the saprock (4-5m) and the fresh rock (18-20m). The weathering front occurs at depths of 38 to 40m. The soil contains moderate amounts (8.6-14.7%) of smectite and moderate amounts of calcite (2.5-6.9%) and albite (4.3-6.1%). Dolomite is concentrated at the upper levels of the Orange-Pink saprolite where it occurs as coatings on remnant quartz veins and as vein stringer infill. Quartz increases towards the soil where it occurs as detrital constituents. Increased amounts of smectite (nontronite) (9.6-36.6%) occurs in the Greenish-Grey saprolite and saprock. Hematite and goethite only occurs within the Orange-Pink saprolite where it is associated with reorganization of the fabric with some of it a product of weathering of kaolinite. Muscovite and orthoclase persists up to the Orange-Pink saprolite and albite up to the upper levels of the Greenish-Grey saprolite. Some hornblende (6.2-8.7%) and chlorite (12.6%) occur in the saprock and fresh rock respectively.

Profile 2

This profile is defined by the soil horizon (3-3.5m), the mini-and-medium- mottled clay zone (4-5m), the mega-mottled zone (4-6m), mottled saprolite (6-8m), Orange-Pink saprolite (4-5m), the Greenish-Grey saprolite (10-15m), the saprock (4-5m) and the fresh rock (12-15m). The weathering front occurs at depths of 42-45m. The soil contains low to moderate amounts of smectite (2.3-14.4) and calcite (5.5-10.7%). The dominant iron oxide within the mottled clay zones is hematite (8.2-17.5%) relative to goethite (0.3-6.1%). Some dolomite occurs within the mega-mottled zone and the mottled saprolite where it is mainly associated with silica aggregates. Low to moderate amounts of muscovite occurs within the Greenish -Grey saprolite (8.4-8.8%) and the fresh rock (33.3-34.6%). The high amounts (13-39.3%) of orthoclase in the Greenish-Grey saprolite and the saprock relative to both muscovite and albite is associated with local changes in lithological composition associated with hydrothermal alteration which gave rise to a rock with more of K-trachyte composition.

Profile 3

This profile has similar regolith units as Profile 2 although the mega-mottled zone is cross-cut by a narrow (~2m) zone of nodular iron and manganese oxide concentration. The soil contains more or less similar contents of calcite and smectite (montmorillonite) with moderate amounts of gypsum (5.3-5.9%). The dominant iron oxide within the mottled clay zone and mottled saprolite is hematite (10.1-28.9%) relative to goethite (0.3-14.9%). Minor enrichment (4.2-5.3% and 17.4-27.4% for goethite and hematite respectively) of the iron oxides occur at the nodular iron and manganese horizon. Dolomite occurs in very small amounts (<4%) in this profile despite the fact that some silica aggregates occur within the mega-mottled clay. Muscovite, orthoclase and albite shows similar distributions as Profile 1. Smectite (nontronite) is also present in the Greenish-Grey saprolite as in the other Profiles. Some chlorite (6.6-7.3%) occurs in the fresh rock.

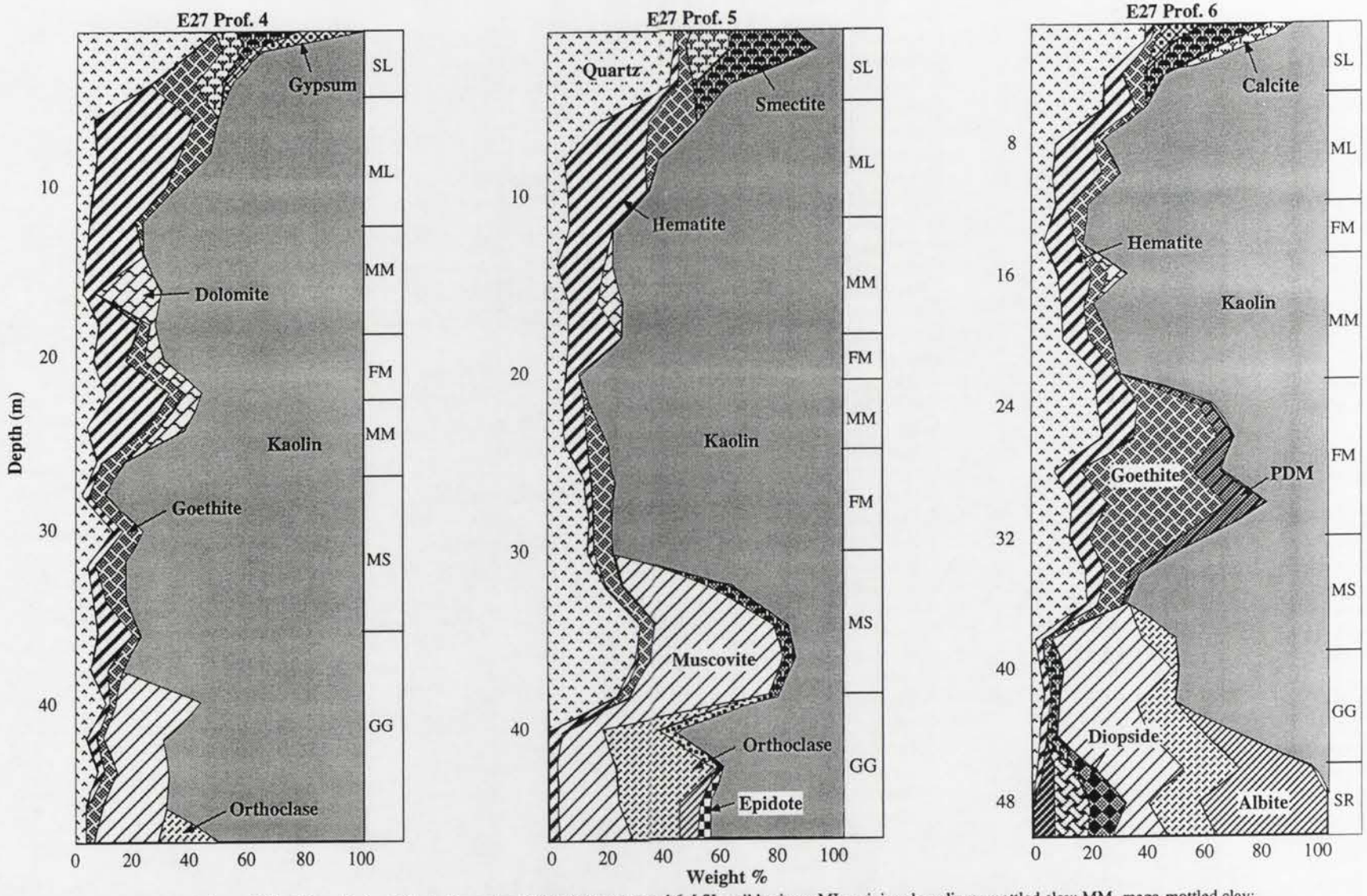

Figure 7.2.5: Mineralogical distributions along E27 Profiles 4, 5 and 6 [SL-soil horizon; ML- mini-and-medium- mottled clay; MM- mega-mottled clay; MS-mottled saprolite ; FM-nodular Fe-Mn horizon; OP-orange-pink saprolite; GG-greenish-grey saprolite; SR-saprock; FR-fresh rock; PDM-poorly diffracting material]

Profile 4

This profile is similar to Profile 3. Minor differences exist and this includes the presence of dolomite within the mega-mottled clay and the persistence of the iron oxides through to the Greenish-Grey saprolite. This is partly attributed to translocation of these iron oxides to the saprolite from the mottled zone through cracks and solution channels.

Profile 5

This profile is similar to Profile 6. They are defined by the soil horizon (3-4.5m) , the mini-and-medium-mottled clay (8-10m), the mega-mottled clay (overall depths of 10m-12m) cross-cut in the middle by an iron and manganese horizon (2-4m) , another nodular iron-manganese horizon (5-7m), the mottled saprolite (8-10m), Greenish-Grey saprolite (12-15m), the saprock (4-6m) and the fresh rock (4-6m). As is characteristic of the other soils developed over the mottled clay, this soil contains high amounts of smectites (12.3-22.6%) and calcite (12.4-15.9%). Hematite is more predominant in the mottled clay (17.3-26.9%) relative to goethite (0.6-16.8%). Minor enrichment of these iron oxides occurs towards the nodular Fe-Mn horizons. It was observed that the Mn occured more as a matrix stain with fewer nodules in this part of the profile as opposed to its predominant occurrence as nodular aggregates in Profile 6. Minor amounts of jarosite (0.9-3.9%) occur in the Greenish-Grey saprolite.

Profile 6

This profile is situated at the central part of the more deeply weathered section of the E27 pit. Two Fe-Mn rich horizons are present within the mega-mottled clay as in profile 5. The weathering front occurs at depths of 55 to 60m. In the upper horizon, the Mn occurs as stains on the iron oxide and clay rich matrix and in the lower horizon it occurs as nodular aggregates together with the iron oxides in the clay matrix. The latter horizon is about 5 to 7m while the former is 2 to 4m. Hematite is more abundant (4-16.6%) in the mini-and-medium-mottled clay relative to goethite (1.8-7%) which becomes more abundant towards the nodular Fe-Mn zone (18.2-39%). This observation was further confirmed by SEM EDXA analysis which showed goethite as the predominant iron oxide in the Fe-Mn horizons. The poorly diffracting contents of the Fe-Mn horizon ranged from 6.1 to 14.6%. As in Profile 5, the iron oxides persisted upto the saprock. The distribution of muscovite, orthoclase and albite follows the same patterns as in the other profiles. This profile also contains more diopside (0.8-5.8%) and hornblende (5.5-10.8%) as compared to the other profiles. This is attributed to local changes in chemical compositions of the trachyandesite.

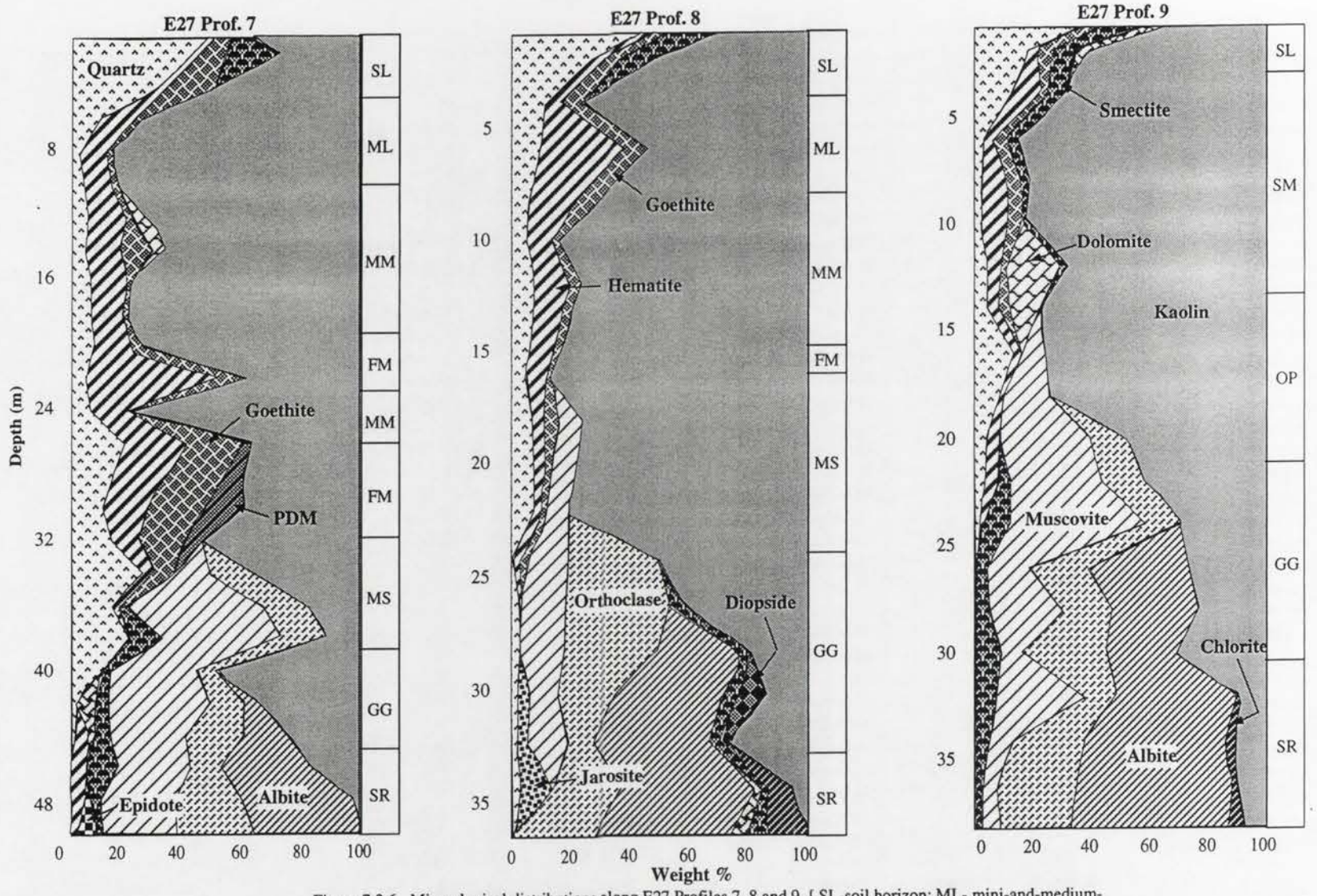

Figure 7.2.6: Mineralogical distributions along E27 Profiles 7, 8 and 9 [SL-soil horizon; ML- mini-and-medium-mottled clay; M- mega-mottled clay; MS-mottled saprolite ; SM- silica aggregates/mottled saprolite; FM-nodular Fe-Mn horizon; OP-orange-pink saprolite; GG-greenish-grey saprolite; SR-saprock; FR-fresh rock]

Profile 7

This profile contains similar distribution of regolith units as Profiles 5 and 6. The mineralogical compositions of the various units are also similar although the goethite amounts in the Fe-Mn horizons are slightly lower (14.2-25.6%) in this profile while hematite is higher (7.4-18.1%).

Profile 8

This profile is similar to Profile 2. It is defined by the soil horizon (3-4m), the mini-and-medium-mottled clay zone (4-6m), the mega-mottled clay zone (8-10m), mottled saprolite (8-10m), Greenish-Grey saprolite (10-15m), the saprock (4-5m) and the fresh rock (15-20m). The weathering front occurs at depths of 40 to 42m. The calcite and smectite contents of the soil are similar to those of the other profiles located over the mottled clay zone. The dominant iron oxide in the mottled clay is hematite (4.7-29.7%) as compared to goethite (1.6-8.5%). Low amounts of diopside (2.1-2.7%) and jarosite (0.4-1.5%) occur within the saprock/fresh rock and saprolite/saprock respectively.

Profile 9.

This profile consists of the soil horizon (3-4m), the silica aggregate rich mottled saprolite (8-10m), the Orange-Pink saprolite (12-15m), Greenish-Grey saprolite (6-8m), the saprock (4-6m), the sulphide zone (4-5m) and the fresh rock (18-20m). The weathering front occurs at depths of 38 to 40m. The soil horizon contains almost similar amounts of calcite, smectite and gypsum as Profiles 2, 3 and 8. Moderate amounts (0.5-19.5%) of dolomite occurs in the mottled saprolite where it occurs as coatings on silica aggregates. Muscovite, orthoclase, albite and nontronite smectite shows similar distribution patterns as in the other profiles. Some hornblende (2.5-7.2%) occurs in the sulphide zone and the fresh rock.

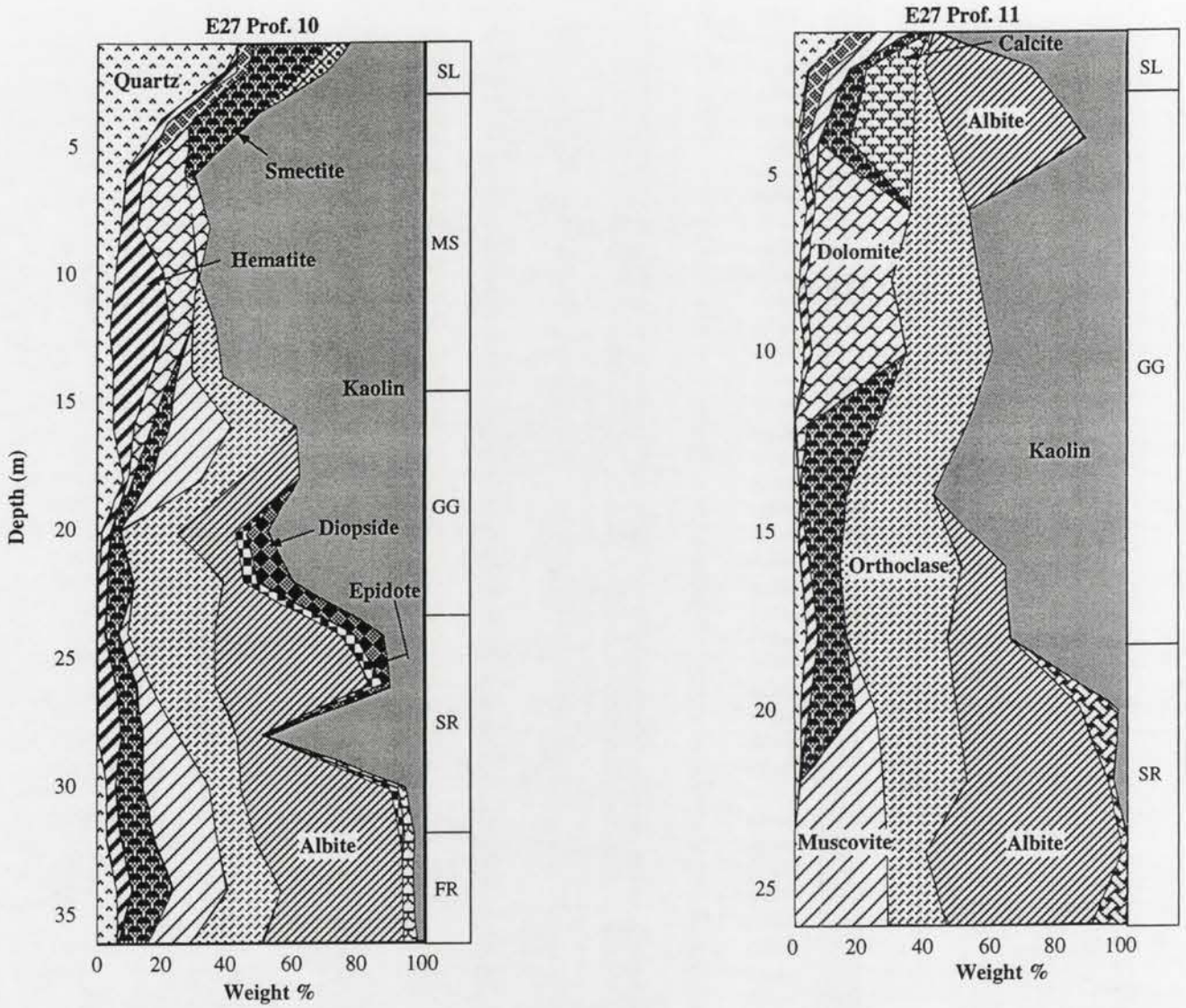

Figure 7.2.7: Mineralogical distributions along E27 Profiles 10 and 11 [SL-soil horizon; MS-mottled saprolite; OP-orange-pink saprolite; GG-greenish-grey saprolite; SR-saprock; FR-fresh rock]

Profiles 10 and 11

These two profiles are a product of *in situ* weathering of the trachyandesite. Profile 10 is similar to Profile 1 while Profile 11 is similar to Profiles 9 and 10 of E22 deposit.

Profile 10

This profile consists of the soil horizon (2.5-3m), the Orange-Pink saprolite (15-20m), the Greenish-Grey saprolite (10-15m), the saprock (4-6m), and the fresh rock (22-25m). The weathering front occurs at depths of 36 to 38m. Smectite is present in most of the horizons of this profile with high amounts occuring in the soil and upper saprolite (2.2-23.5%) as montmorillonite. It is almost absent in the lower levels of the Orange-Pink saprolite . This is consistent with the observations made in the previous chapter about the absence of smectite in the Orange-Pink saprolite. Dolomite is present in the Orange-Pink saprolite especially on the upper levels where it occurs as coatings on the silica aggregates. Hematite is also present in all the horizons of the profile with moderate amounts (1.9-16.6%) occuring in the Orange-Pink saprolite. This is evidence of the transformation of kaolin and the ferromagnesians into iron oxides in the residual profiles especially in the Orange-Pink saprolite. Muscovite, orthoclase and albite shows similar distributions as in the other profiles. Moderate to high amounts of epidote (1.5-4.2%) and diopside (0.7-11%) occur in the saprock, the sulphide zone and the fresh rock.

Profile 11

This profile is defined by the soil horizon (1.5-2.5m), the Greenish-Grey saprolite (15-20m), the saprock (4-6m) and the fresh rock (30-35m). The weathering front occurs at depths of 30 to 32m. Unlike in the other Profiles over the trachyandesite, this profile contains appreciable amounts of calcite (3.7-11.2%) and albite (31-41.4%) in the soil horizon and upper saprolite. Moderate amounts of muscovite (3.4-19.3%) is also present in this horizon. Dolomite is present in Greenish-Grey saprolite for the same reasons as Profile 10. Moderate to high amounts of nontronite smectite (4.9-20.9%) are present in the saprolite and the saprock. Orthoclase unlike muscovite, persists upto the soil horizon. As mentioned in the discussion section of this chapter, this is partly associated with the partial truncation suffered by this profile after its development.

Figures 7.3: Mineralogical distributions in the E22 and E27 Deposits

NOTES

. Mineral contents are in weight %

. Vertical axis: RL depth values in metres

Scale: 1cm = 25m

. Horizontal scale: 1cm = 25m

ENDEAVOUR 22 - K FELDSPAR

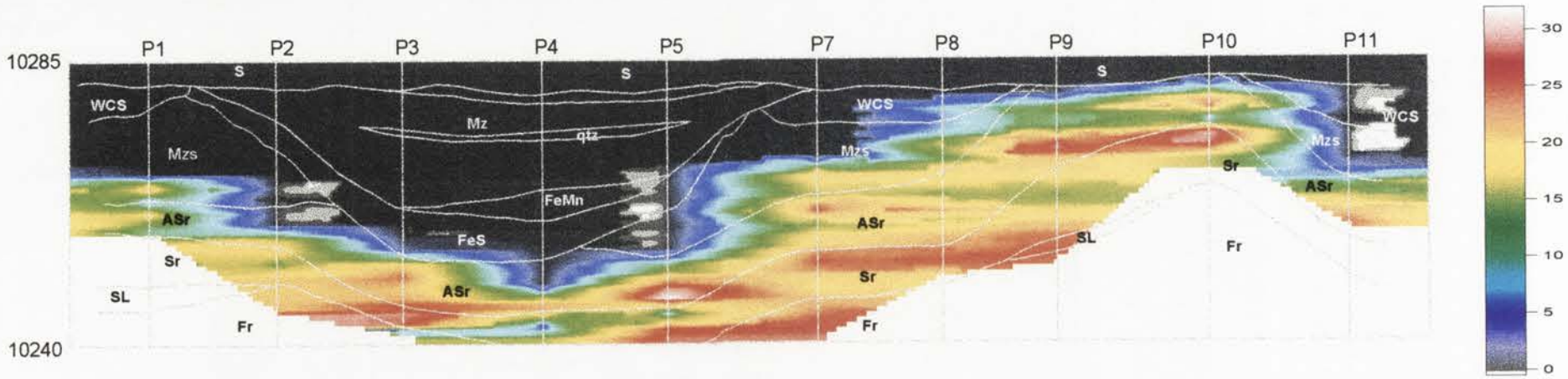

S	Soil Horizons	Osr	Orange-Pink Saprolite	SL	Sulfide Zone	FeS	Ferruginous Saprolite
WCS	White clay saprolite	FeMn	Fe - Mn nodules	Sr	Saprock	qtz	Silica nodule zone
Mz	Mottled Zones	ASr	Andesitic Saprolite	Fr	Fresh Rock		

Figure 7.3.1

ENDEAVOUR 27 - ORTHOCLASE

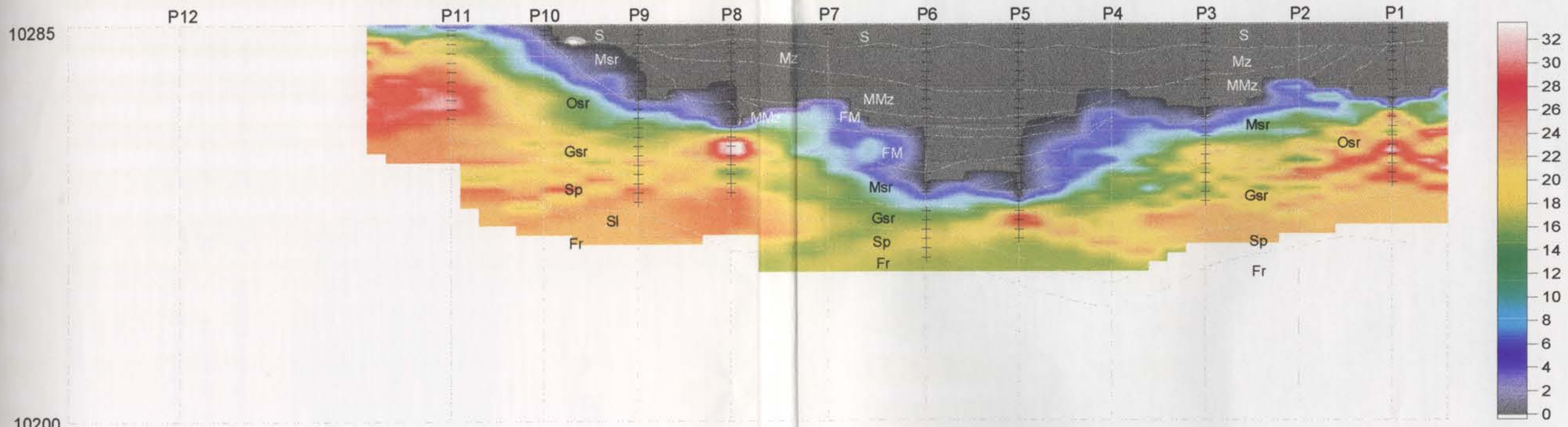

Horizontal Scale 1:2500
Vertical Scale 1:1000

S	Soil Horizons	Msr	Mottled Saprolite	Sl	Sulfide Zone
Mz	Mottled Zone	Osr	Orange-pink Saprolite	Sp	Saprock
MMz	Megamottled Zone	Gsr	Andesitic Saprolite	Fr	Fresh Rock
FM	Fe - Mn Nodules				

Figure 7.4.1

ENDEAVOUR 22 - ALBITE

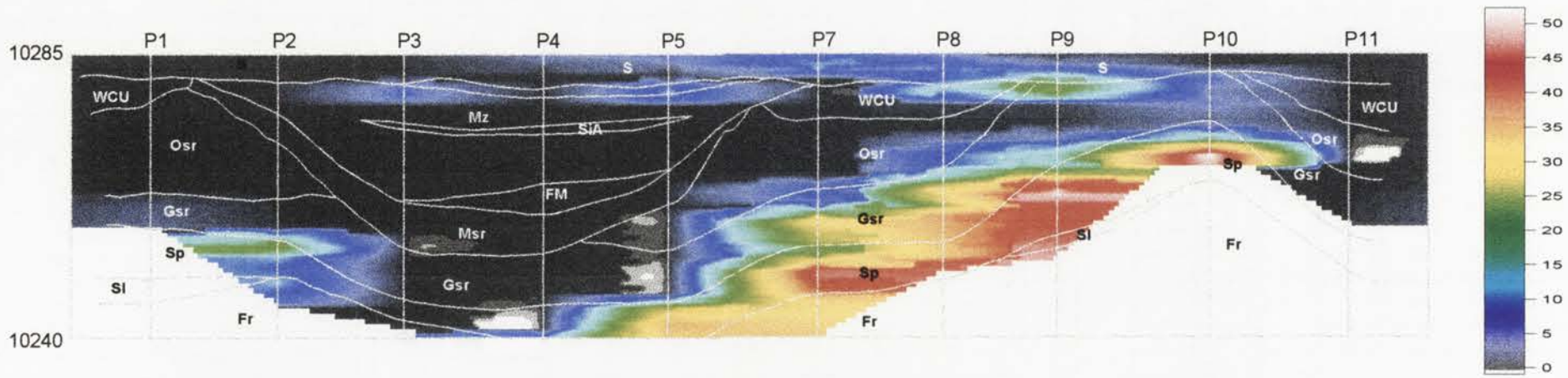

S	**Soil Horizons**	**Osr**	**Orange-Pink Saprolite**	**Sl**	**Sulfide Zone**	**Msr**	**Mottled Saprolite**
WCU	**White Clay Unit**	**FM**	**Fe - Mn Nodules**	**Sp**	**Saprock**	**SiA**	**Silica Aggregates**
Mz	**Mottled Zones**	**Gsr**	**Greenish-grey Saprolite**	**Fr**	**Fresh Rock**		

Figure 7.3.2

ENDEAVOUR 27 - ALBITE

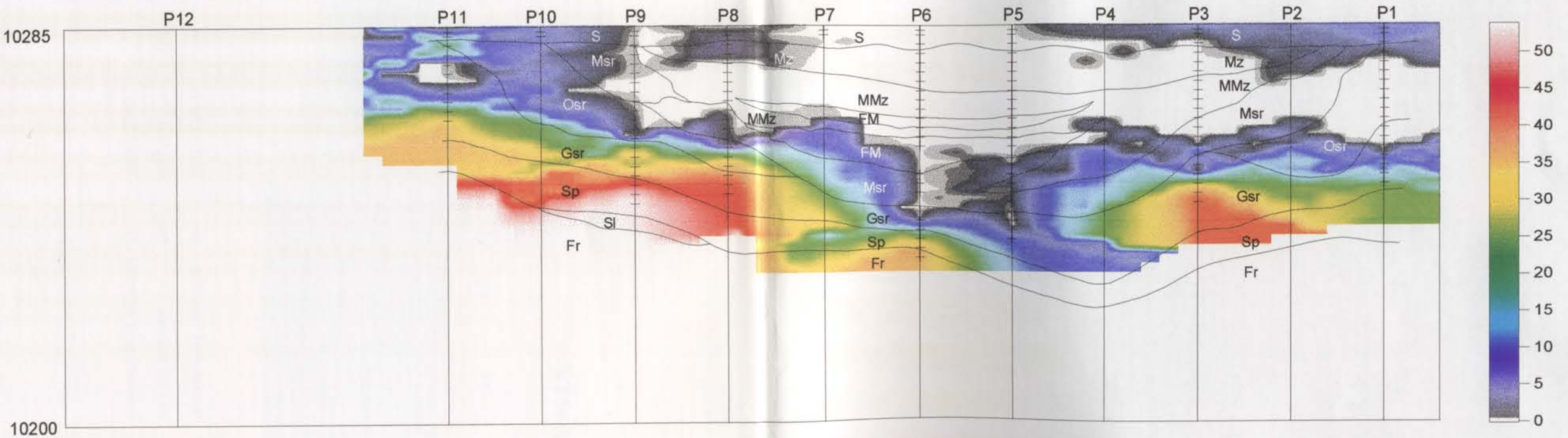

Horizontal Scale 1:2500
Vertical Scale 1:1000

S	Soil Horizons	Msr	Mottled Saprolite	Sl	Sulfide Zone
Mz	Mottled Zone	Osr	Orange-pink Saprolite	Sp	Saprock
MMz	Megamottled Zone	Gsr	Andesitic Saprolite	Fr	Fresh Rock
FM	Fe - Mn Nodules				

Figure 7.4.2

ENDEAVOUR 22 - QUARTZ

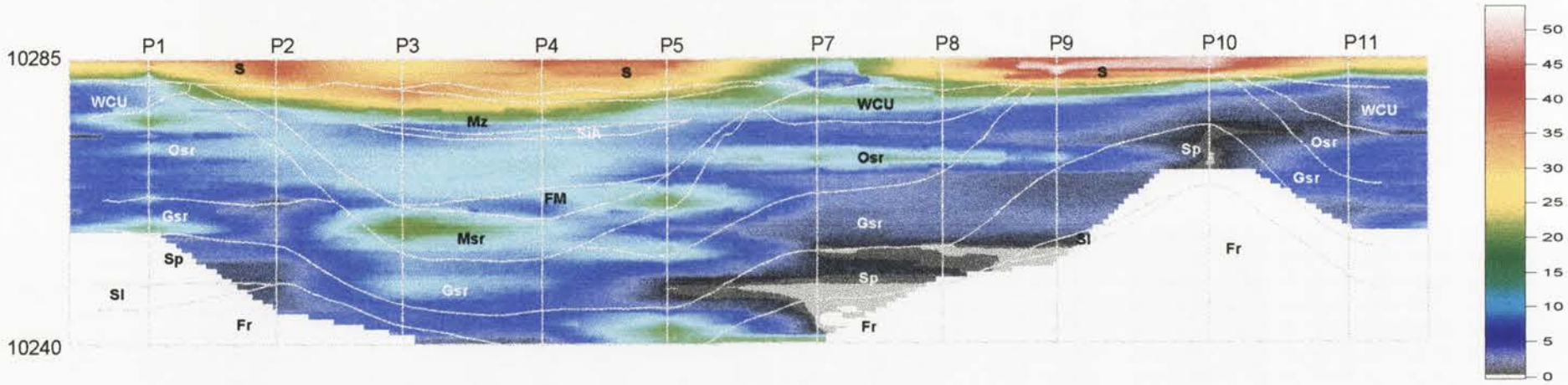

S	Soil Horizons	Osr	Orange-Pink Saprolite	Sl	Sulfide Zone	Msr	Mottled Saprolite
WCU	White Clay Unit	FM	Fe - Mn Nodules	Sp	Saprock	SiA	Silica Aggregates
Mz	Mottled Zones	Gsr	Greenish-grey Saprolite	Fr	Fresh Rock		

Figure 7.3.3

'n:\geochem\goon\eric\plots\qtz22.s

ENDEAVOUR 27 - QUARTZ

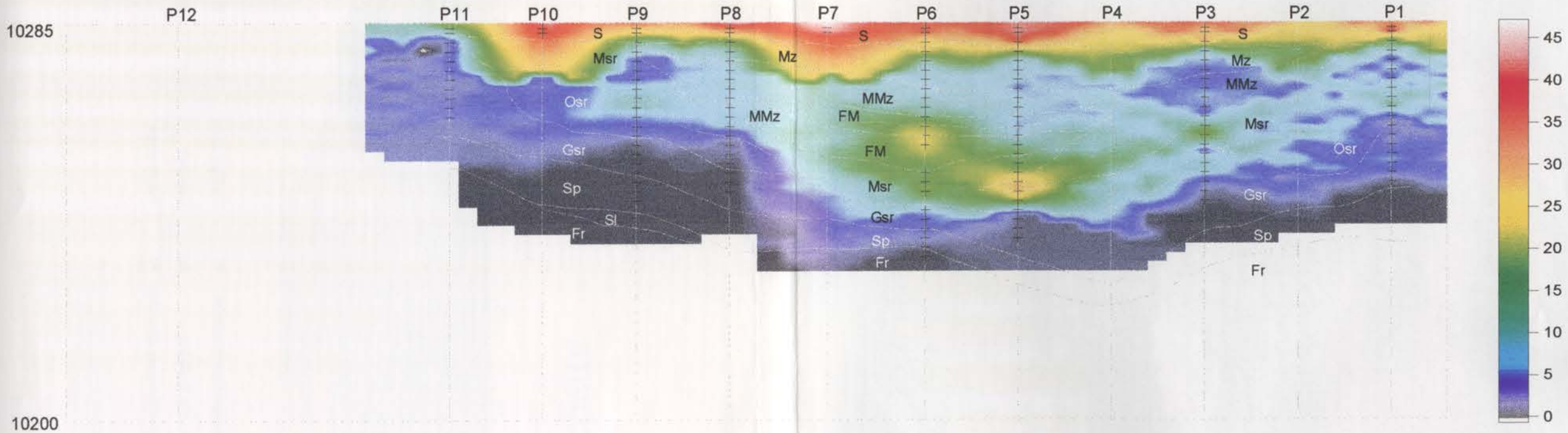

Horizontal Scale 1:2500
Vertical Scale 1:1000

S	Soil Horizons	Msr	Mottled Saprolite	Sl	Sulfide Zone
Mz	Mottled Zone	Osr	Orange-pink Saprolite	Sp	Saprock
MMz	Megamottled Zone	Gsr	Andesitic Saprolite	Fr	Fresh Rock
FM	Fe - Mn Nodules				

Figure 7.4.3

ENDEAVOUR 22 - MUSCOVITE

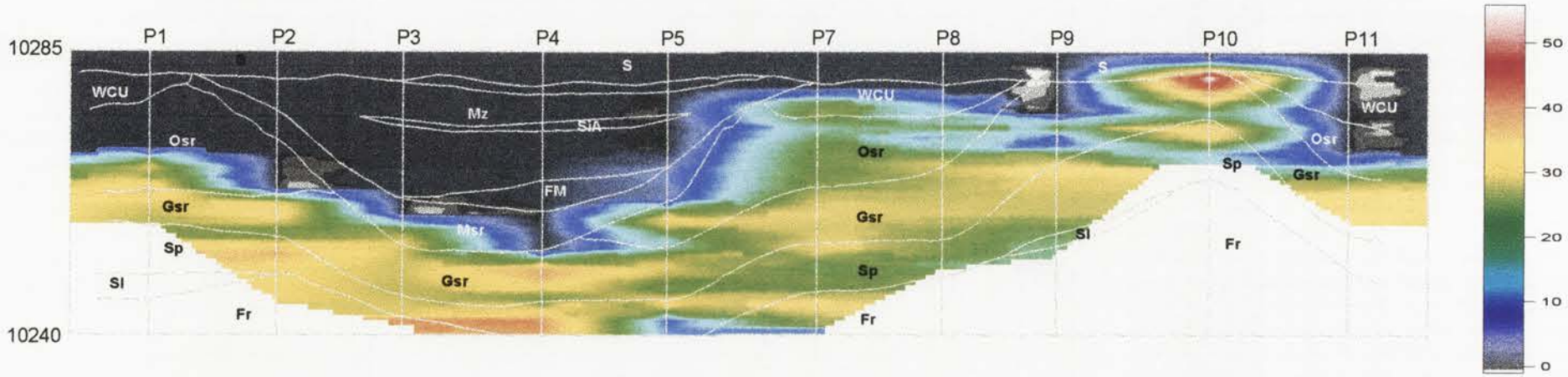

S	Soil Horizons	Osr	Orange-Pink Saprolite	Sl	Sulfide Zone	Msr	Mottled Saprolite
WCU	White Clay Unit	FM	Fe - Mn Nodules	Sp	Saprock	SiA	Silica Aggregates
Mz	Mottled Zones	Gsr	Greenish-grey Saprolite	Fr	Fresh Rock		

Figure 7.3.4

n:\geochem\goon\eric\plots\22mus.srf

ENDEAVOUR 27 - MUSCOVITE

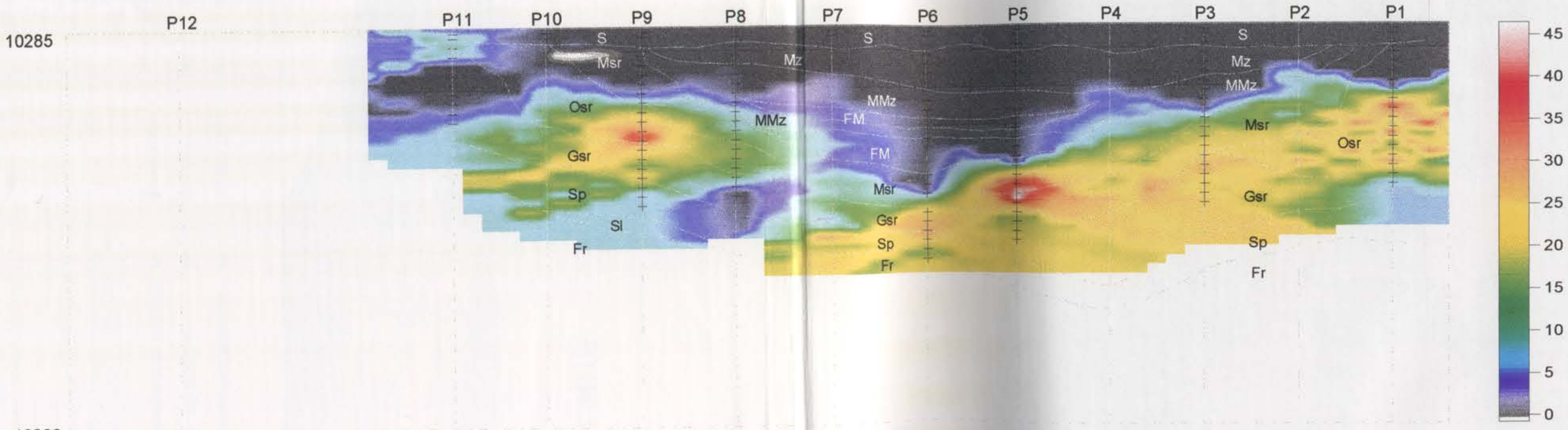

Horizontal Scale 1:2500
Vertical Scale 1:1000

S	Soil Horizons	Msr	Mottled Saprolite	Sl	Sulfide Zone
Mz	Mottled Zone	Osr	Orange-pink Saprolite	Sp	Saprock
MMz	Megamottled Zone	Gsr	Andesitic Saprolite	Fr	Fresh Rock
FM	Fe - Mn Nodules				

Figure 7.4.4

ENDEAVOUR 22 - KAOLINITE

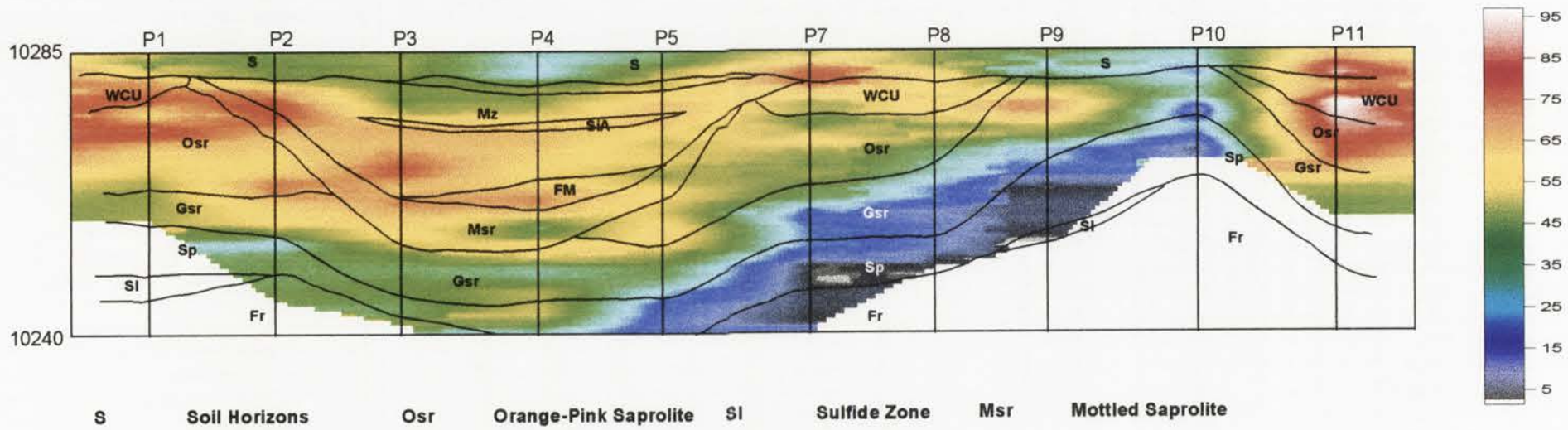

S	Soil Horizons	Osr	Orange-Pink Saprolite	Sl	Sulfide Zone	Msr	Mottled Saprolite
WCU	White Clay Unit	FM	Fe - Mn Nodules	Sp	Saprock	SiA	Silica Aggregates
Mz	Mottled Zones	Gsr	Greenish-grey Saprolite	Fr	Fresh Rock		

Figure 7.3.5

ENDEAVOUR 27 - KAOLINITE

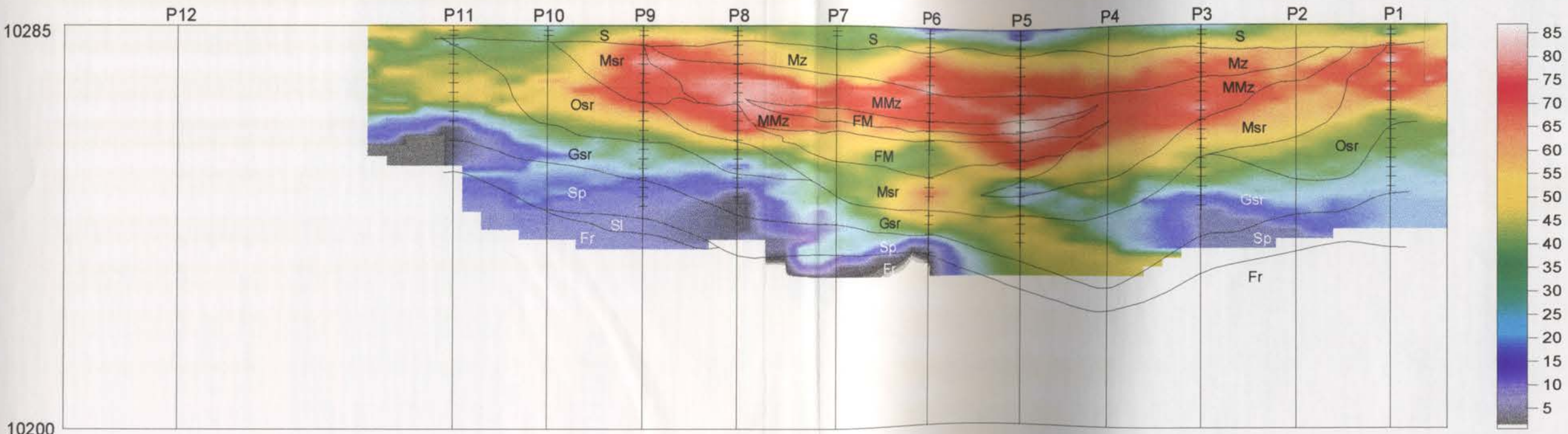

Horizontal Scale 1:2500
Vertical Scale 1:1000

S	Soil Horizons	Msr	Mottled Saprolite	Sl	Sulfide Zone
Mz	Mottled Zone	Osr	Orange-pink Saprolite	Sp	Saprock
MMz	Megamottled Zone	Gsr	Andesitic Saprolite	Fr	Fresh Rock
FM	Fe - Mn Nodules				

Figure 7.4.5

ENDEAVOUR 22 - SMECTITES

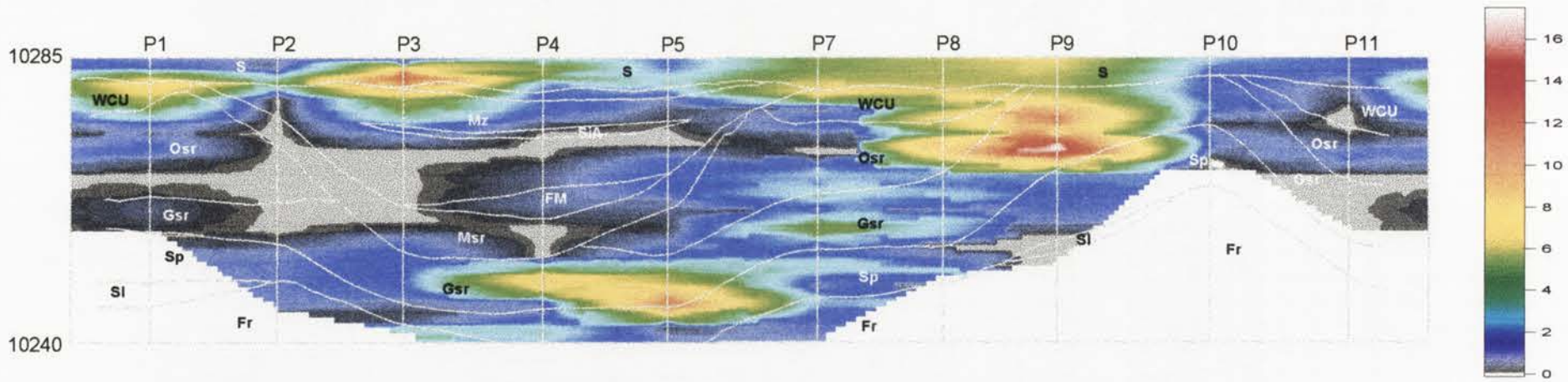

S	Soil Horizons	Osr	Orange-Pink Saprolite	Sl	Sulfide Zone	Msr	Mottled Saprolite
WCU	White Clay Unit	FM	Fe - Mn Nodules	Sp	Saprock	SiA	Silica Aggregates
Mz	Mottled Zones	Gsr	Greenish-grey Saprolite	Fr	Fresh Rock		

Figure 7.3.6

ENDEAVOUR 27 - SMECTITE

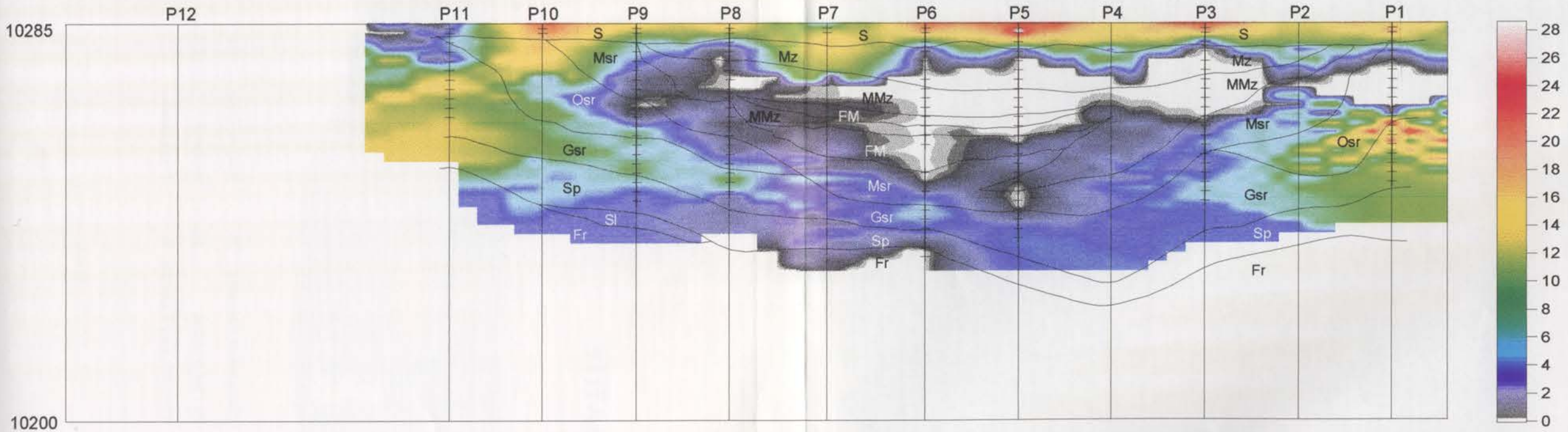

Horizontal Scale 1:2500
Vertical Scale 1:1000

S	Soil Horizons	Msr	Mottled Saprolite	Sl	Sulfide Zone
Mz	Mottled Zone	Osr	Orange-pink Saprolite	Sp	Saprock
MMz	Megamottled Zone	Gsr	Andesitic Saprolite	Fr	Fresh Rock
FM	Fe - Mn Nodules				

Figure 7.4.6

ENDEAVOUR 22 - HEMATITE

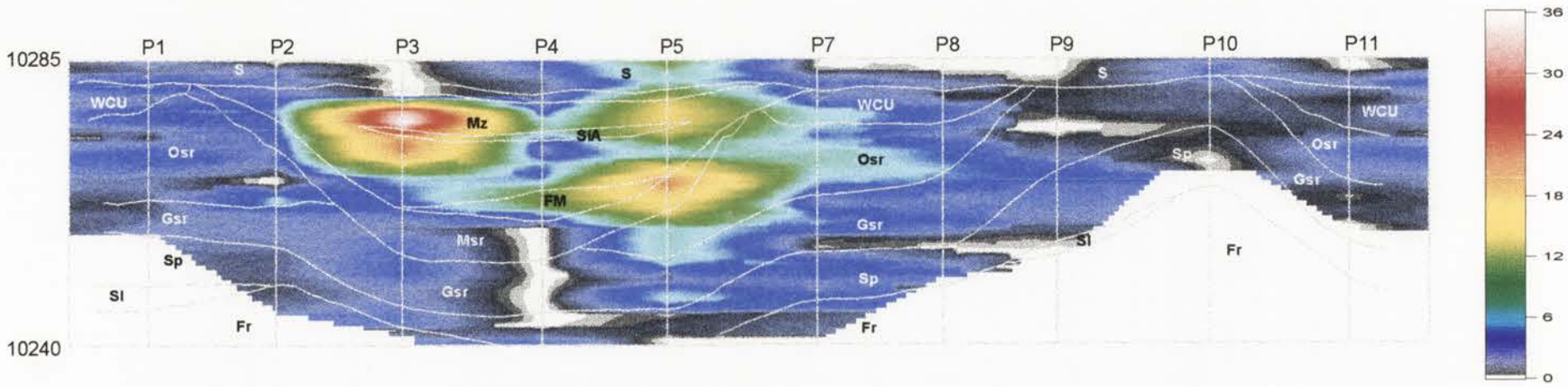

S	Soil Horizons	Osr	Orange-Pink Saprolite	Sl	Sulfide Zone	Msr	Mottled Saprolite
WCU	White Clay Unit	FM	Fe - Mn Nodules	Sp	Saprock	SiA	Silica Aggregates
Mz	Mottled Zones	Gsr	Greenish-grey Saprolite	Fr	Fresh Rock		

Figure 7.3.7

ENDEAVOUR 27 - HEMATITE

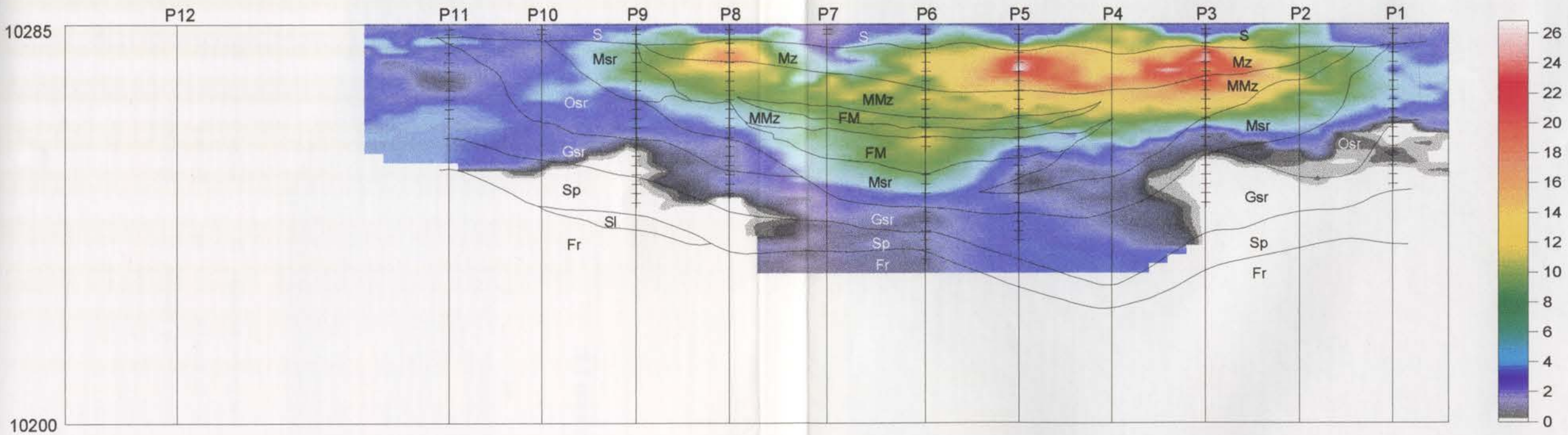

Horizontal Scale 1:2500
Vertical Scale 1:1000

S	Soil Horizons	Msr	Mottled Saprolite	Sl	Sulfide Zone
Mz	Mottled Zone	Osr	Orange-pink Saprolite	Sp	Saprock
MMz	Megamottled Zone	Gsr	Andesitic Saprolite	Fr	Fresh Rock
FM	Fe - Mn Nodules				

Figure 7.4.7

ENDEAVOUR 22 - GOETHITE

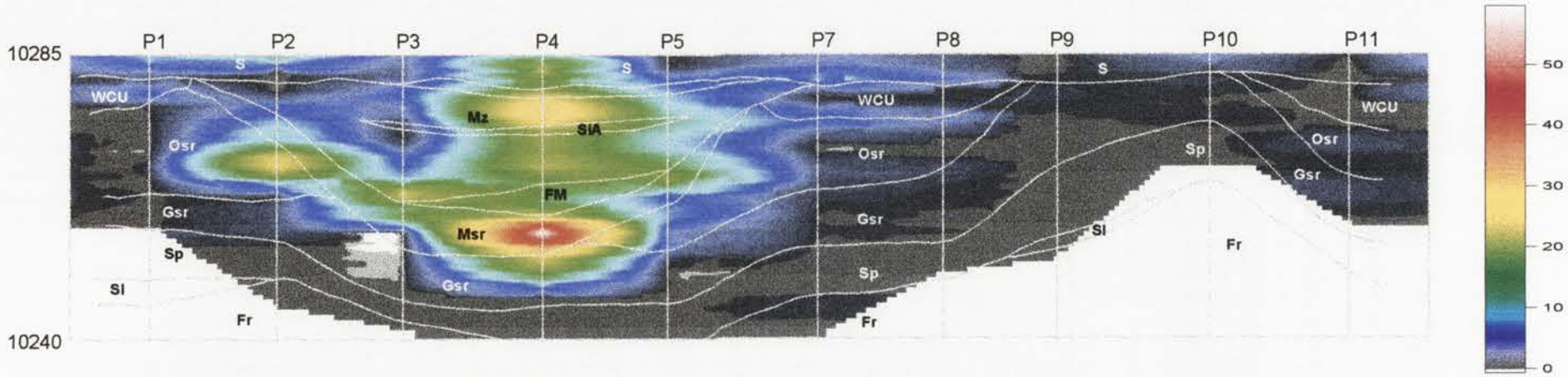

S	Soil Horizons	Osr	Orange-Pink Saprolite	Sl	Sulfide Zone	Msr	Mottled Saprolite
WCU	White Clay Unit	FM	Fe - Mn Nodules	Sp	Saprock	SiA	Silica Aggregates
Mz	Mottled Zones	Gsr	Greenish-grey Saprolite	Fr	Fresh Rock		

Figure 7.3.8

ENDEAVOUR 27 - GOETHITE

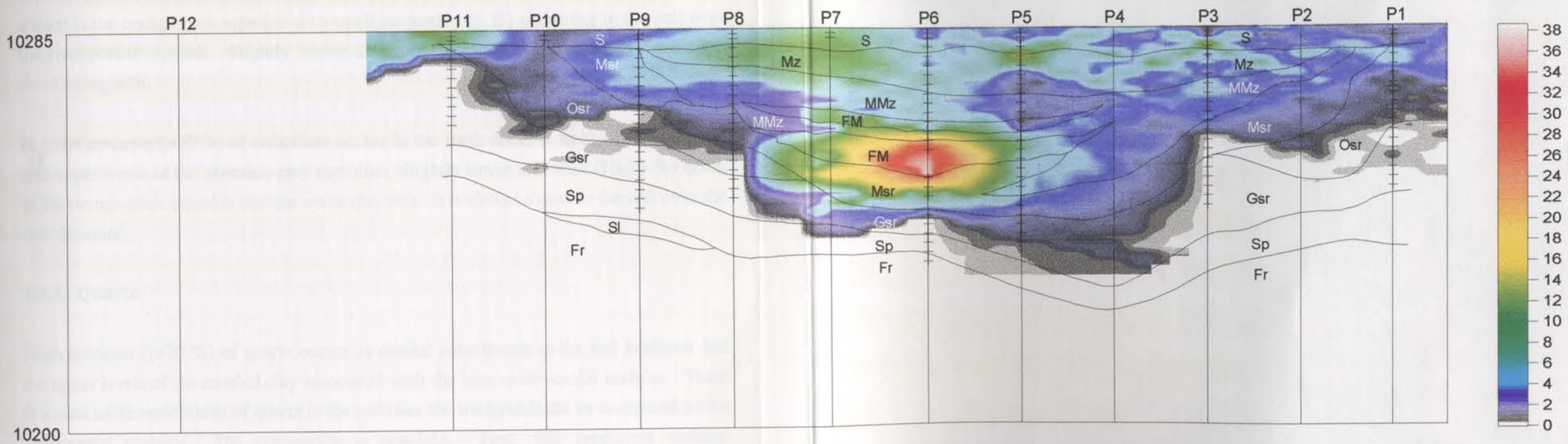

Horizontal Scale 1:2500
Vertical Scale 1:1000

S	Soil Horizons	Msr	Mottled Saprolite	Sl	Sulfide Zone
Mz	Mottled Zone	Osr	Orange-pink Saprolite	Sp	Saprock
MMz	Megamottled Zone	Gsr	Andesitic Saprolite	Fr	Fresh Rock
FM	Fe - Mn Nodules				

Figure 7.4.8

7.3 Mineralogical distribution in the regolith stratigraphy

This section provides a summary of the distribution of the secondary products in the regolith stratigraphy. The 2 dimensional plots were obtained by using a computer software package known as *'Suffer'* . The kriging and contouring was performed using an associated software known as *Gridzo*. The plots are presented in Figures 7.3.

7.3.1. Feldspars

The highest amounts (>35%) of albite in both deposits occur in the fresh rock, the saprock and the lower parts of the greenish-grey saprolite (lower saprolite). It is almost absent in the orange-pink saprolite with small amounts (<5 %) occurring in the soil over the transported regolith. Slightly higher amounts (5-10 %) occur in the soil over the residual regolith.

Highest amounts (>20 %) of orthoclase occurs in the fresh rock, saprock and the middle and upper levels of the greenish-grey saprolite. Slightly lower amounts (10-20 %) occur in the orange-pink saprolite and the white clay unit. It is almost absent in the soil over the two deposits.

7.3.2. Quartz

High amounts ((>30 %) of quartz occurs as detrital constituents in the soil horizons and the upper levels of the mottled clay associated with the iron oxide-kaolin nodules. There is a noticeable enrichment of quartz in the soil over the trachyandesite as compared to the transported regolith. The explanation is two-fold. First, this represents residual accumulation of quartz as more constituents are lost and secondly, the additional input from detrital sources. Slightly lower amounts (20-30 %) occur in the upper saprolite over the trachyandesite, which is further evidence of its residual accumulation over these units. The nodular iron and manganese horizon contains lower amounts (15-20 %) as compared to the nodular horizons of the mottled clay zone.

7.3.3. Muscovite

High amounts (>35 %) of muscovite occur in the saprock, the middle and upper levels of the greenish-grey saprolite and the orange-pink saprolite. Moderate amounts (20-35 %) occurred in the white clay unit and the mottled saprolite. Low amounts (<20%) occur in the soil horizons especially in the residual units. It is by far the most persistent of the

primary rock-forming minerals and it occurred independently or as a component of sericitized plagioclase in the saprock and lower saprolite. Some muscovite flakes also occurs in the transported regolith.

7.3.4. Kaolin

Kaolin was by far the most abundant of the secondary products. Highest amounts (>75 %) occur in the white clay unit, the mottled saprolite and the lower levels of the mega-mottled clay zone. Moderate amounts (50-65%) occurred within the mega-mottled clay zone and the orange-pink saprolite. Slightly lower amounts (35-50%) occur in the andesite saprolite, the mini-and-medium mottled clay zones and the soil horizons.

7.3.5. Smectites

High amounts (>10 %) of smectite occur in the saprock and the lower portions of the greenish-grey saprolite as nontronite. Moderate amounts (6-10 %) occur as montmorillonite in the white clay unit and the soil horizons and in the mini-and-medium mottled clay portions of some profiles (e.g. E22 Profiles 3 and 4). Moderate amounts also occur as nontronite in the middle and upper levels of the greenish-grey saprolite (middle saprolite). From this distribution it is apparent that the nontronite over the residual units is the most abundant smectite in the regolith stratigraphy.

7.3.6. Iron oxides

Because of the problems that were encountered in differentiating hematite from goethite their combined amounts as iron oxides have been presented in the regolith stratigraphy. Highest amounts (>35 %) occurred in the mini-and-medium mottled clay and the upper levels of the mottled saprolite bordering the iron-manganese nodules and in the nodular iron and manganese zone itself. Moderate amounts (20-35 %) occurred in the mega-mottled clay zone and in the soil over the mottled clay zones. Low amounts (<15 %) occurred in the greenish-grey saprolite and the orange-pink saprolite. From this distribution it is apparent that the iron oxide is most abundant in the transported regolith.

7.3.7. Carbonates

High amounts of calcite (>10 %) as expected occur in the soil horizons. This is slightly higher over the transported regolith than the residual regolith. High amounts of dolomite (>20%) occur in the white clay unit while moderate amounts (10-20%) occurring in the

mega-mottled zone and in the greenish-grey and orange-pink saprolite. This pattern is associated with the occurrence of carbonates within these units.

7.4. SUMMARY AND DISCUSSIONS

7.4.1. Distribution of the secondary products

The distribution of primary and secondary mineralogical products in the E22 and E27 deposits varied from one profile to another. In general, the two deposits contain similar regolith products with differences occurring in the position of these products in the regolith stratigraphy. The characteristics of these profiles are governed by the position in the regolith stratigraphy and the nature of the host material prior to weathering.

The significance of these changes in origin of the substrates is quite noticeable in the soil that developed over the mottled clay and the trachyandesite. The soil over the mottled clay contained high amounts of gypsum, smectite, calcite and dolomite while the soil over the trachyandesite contained lower amounts of calcite, smectite and detrital fragments of the host rock as shown by the presence of albite and muscovite in Profiles 10 and 11 respectively. The soil over the mottled clay is also more deeper (3 to 3.5 m in depth) than that over the trachyandesite (1.5 to 2.5 m in depth).

The distribution of the carbonates in both E22 and E27 deposits provided some interesting observations. The carbonate occurs as calcite in the soil horizons and dolomite within the mega-mottled clay, the white clay unit and the saprolite. Within the mega-mottled clay it occurs as coatings on silica aggregates and as fracture and void infills. Within the saprolite it occurs in the numerous vein stringers and remnant quartz veins that are conspicuously present.

Soil carbonates originate from several sources or combinations of sources (Dregne, 1976), either directly in the form of carbonates or by solution-precipitation mechanism. The most direct method is inheritance from the parent material with principal requirement being insufficient leaching to remove carbonates from the solum. Other possible mechanisms involve: -

- Dissolution of Ca-bearing minerals such as gypsum or anorthite within the immediate soil and precipitation of calcite. This distribution of dolomite is obviously related to characteristics of groundwater that gave rise to the different products of these microsystems.

-Mineralization of plant materials whereby plants recycle Ca to the surface and the Calcium released by decomposition of residues reacting with CO_2-charged H_2O to form $CaCO_3$

-Wind deposition whereby carbonate materials are transported some distance, suspended in air, and are deposited on the surface as dust or in rain. Subsequent relocation within the soil by solution is possible.

-Calcium can also enter the soil in rainwater and subsequently combine with HCO_3^- associated with CO_2^- charged H_2O (Rabenhorst et al. 1984a).

-Ground water may also move through carbonate-containing soils or strata and bring either Ca^{2+} or HCO_3^- ions into the soil, whereby they combine to form $CaCO_3$ when the soil dries or the temperature rises.

The abundance of calcite and dolomite in the inferred transported material of the mottled clay zone points to a secondary origin for these carbonates. Some of it could have been derived from the host rock but for that to occur they would have had to overcome huge diffusion or capillarity gradients in moving from the host rock to the soil horizon. The most possible mechanism might have involved groundwater moving through deposited material that contained either Ca^{2+} or HCO_3^- ions and which combined to form $CaCO_3$ as the soil dried or temperature rose. This is quite possible since the detrital rock fragments of the transported material consisted of minerals of the host rock that contained abundant calcium (e.g. plagioclase). Input from wind deposition and rainwater could have supplemented these sources.

The presence of these carbonates as vein stringer infills or as coating on quartz veins in the saprolite could also be partly attributed to carbonate alteration, which accompanied mineralization as mentioned in Chapter 1. Jones (1985) and Bowman (1987) observed calcite replacing quartz as the dominant gangue mineral away from the mineralization zone in the two deposits, which they attributed to the marked decrease in the number and thickness of veins.

In general, the occurrence of carbonates in soils depends heavily on climate, which controls leaching of constituents. In semi-arid to arid climates like those of the study area, carbonates remain in the soil and secondary carbonates may accumulate near the surface (Doner & Lynn, 1989). If other factors are considered constant, increased rainfall

means increased removal of carbonates from upper layers and deposition in deeper layers or removal from the soil. This movement can be vertical and/or lateral depending on the slope, texture and stratigraphy (Dregne, 1976).

Within the mottled clay, differences are noted in the amounts of hematite and goethite in transition from one profile to another. Part of this problem lay with the *Siroquant* quantitative mineralogy package, which had difficulty in differentiating and refining the two minerals because the major 104 and 103 *hkl* peaks of hematite and goethite both occur at 2.69Å. Resolving the dilemma partly requires the cross checking of 110 *hkl* peak of goethite at 4.183Å to confirm its presence although it still doesn't provide an adequate proof of its abundance relative to hematite. I therefore propose that the results presented here be regarded as representing relative trends rather than absolute values. However, SEM EDXA analysis of the iron oxides in the nodular and manganese rich zone did show goethite as the more abundant iron oxide in this horizon.

Appreciable amounts of gypsum crystals also occur within the soil. Soil gypsum may stem from one of several processes. Soil parent material is an important factor in its distribution in that soils formed in geologic material containing anhydrite or gypsum often contain gypsum (Watson, 1985). The amount of rainfall and the topographic setting will also strongly influence the amount and location of the gypsum in the soil (Doner & Lynn, 1989). The observation that gypsum precipitates near the maximum depth of wetting in some semi-arid soils (Nettleton et al. 1982) like those of the study area is supported by the experimental work of Krupkin (1963) with leaching soil columns. Gypsum may also accumulate from aeolian action as the result of deflation and deposition. Other sources may include surface or subsurface H_2O rich in Ca and SO_4. Being more soluble than calcite, gypsum is more sensitive to moisture conditions (Nettleton et al. 1982).

The presence of a gypsum line at 200 m has been reported at E26N underground deposit. The gypsum according to Jones (1985) has been removed by leaching leaving holes and open fractures above a deep horizontal line, which he referred to as a gypsum line. He suggested that the line pointed to the presence of a chemical interface between groundwater systems. He also offered a possible explanation that the gypsum resulted from fresh groundwater sourced from the caldera margin interacting with the hot sulfate rich hydrothermal brines. The presence of the gypsum in the host rocks seems to account for the origin of some of the gypsum in the soil over these deposits although it is difficult to explain the precise mechanisms responsible for mobilizing the gypsum to the soil from such depths. The occurrence of gypsum in soils over anomalies has also been

recently noted by Adamson (1996) who did some work on the soil landscape units in an area adjacent to these deposits. Input from the other sources mentioned above notably by aeolian action or Ca and SO_4 rich subsurface H_2O could have played an additional role.

Some jarosite occurs within the orange-pink saprolite and the greenish-grey saprolite. Jarosite is a product of the weathering of sulfides and thus is a common indicator mineral of the oxidation phase. It belongs to the non-oxide secondary alunite-jarosite group of minerals with the formula $AB_3(X_4)_2(OH)_6$, where A represents large ions in a 12-fold coordination e.g. Na^+, K^+, Ag^+ and B sites by Al^{3+}, Fe^{3+}, Zn^{2+} and Cu^{2+} and the XO_4 anions are usually SO_4^{2-}, PO_4^{3-} and ASO_4^{3-}. Jarosite is defined by the formula $KFe_3(OH)_6(SO_4)_2$. Because of the ability of this group of minerals to stabilize cations and anions in the A and B sites, the alunite-jarosite minerals may have been responsible for the retention of some of the mobile components like copper and zinc within the saprolite of this study (Chapter 10).

The origin of the silica aggregates and its association with dolomite in these units is unclear. Despite numerous accounts in literature of occurrence of secondary silica aggregates (Summerfield, 1983a, 1983b, 1983c, 1984d; Senior & Senior; Hutton et al. 1972; Gunn & Galloway, 1978; Wopfner, 1978; Callen, 1983; Ollier, 1975), their origin is poorly understood. Silcrete is a term most often used to denote "supergene accumulations of silica within pre-existing host minerals. They are normally very brittle and intensely indurated and mainly composed of quartz clasts cemented by a matrix that may be well-crystallized quartz, cryptocrystalline quartz, or amorphous (opaline silica") (Wopfner, 1978). Senior & Senior (1969), have used the term when referring to sediments cemented by secondary silica, although the term has wider applications than this.

The silica aggregates of this study are opaline in nature, angular to sub-angular and elongate in shape with lengths varying from 20 to 50 mm. Some are present within the clay as small independent sub-angular specks (< 5 mm) often with dolomite coatings. Two types of secondary silica aggregates are documented i.e. groundwater and pedogenic types. Groundwater types are characterized by a preservation of host material structures (e.g. sedimentary structures) and form at deep levels of the profile in relation to former presence of groundwater. Pedogenic types form near a former landsurface and display fabrics indicative of illuviation and other pedogenic processes (Thiry & Milnes, 1991; Milnes & Thiry, 1991).

The occurrence of the silica aggregates of this study in the general illuviation environment that characterizes the mottled clay zone suggests that this type of aggregates are classified as the pedogenic type. Several observations have been made about the conditions under which silica precipitation occurs. Williams et al. (1985) noted that silica solubility increases as a solution becomes more basic, where H_4SiO_4 (the predominant aqueous species in undersaturated silica solutions) ionizes at pH >9. Its association with Ti on the other hand indicates an acid environment as it is mobilized during weathering at pH's lower than 3.75 (Cheshire, 1977).

The solubility of silica minerals also increases with decreasing crystallinity. Quartz has the highest crystallinity and therefore the lowest solubility (Williams et al. 1985; Williams & Crerar, 1985). As a consequence of this solutions with a low silica concentration are able to precipitate quartz. At high silica concentrations other phases are able to precipitate, such as opal-CT or opal-A. These amorphous silica phases typically precipitate in colloform or overgrowth structures.

The association between the silica aggregates of this study with the carbonates is unclear. Ollier (1975) noted that silica may be precipitated near the surface or at depth within a weathering profile. The model he proposed is brief i.e. weathering releases silica, which is transported in either surface or groundwater and in the presence of bases incorporated into clay mineral formation. The precise mechanism is unclear although this may be related to the increase in solubility as solutions become more basic at pH > 9 (Williams et al. 1985). The microenvironment within the mega-mottled clay showed the carbonate influence on the pH values, which ranged here from 8 to 9.5 as opposed to the mini-and-medium-mottled clay, which showed values of 4.5 to 7. Hence the microenvironment within the regolith profile seems to play a role in the solubility of silica and hence its precipitation.

7.4.2 Influence of the parent material

The distribution of the regolith materials in both E22 and E27 deposits points to two source materials and processes i.e. *in situ* weathering on the trachyandesite and weathering on initially transported alluvial and colluvial sediments. This has been evidenced by differences in the petrography, morphology, mineralogy and as discussed in Chapters 9 and 10 by the geochemistry of the resultant products. A distinct boundary also exists between the two in the regolith stratigraphy (Figures 7.4). This section summarizes the observed features and characteristics of these two source materials.

Figure 7.4.1: Boundary between the transported and residual regolith in the Western end of E27 deposit. The disposition of this boundary shows evidence of stripping of the regolith after its formation.

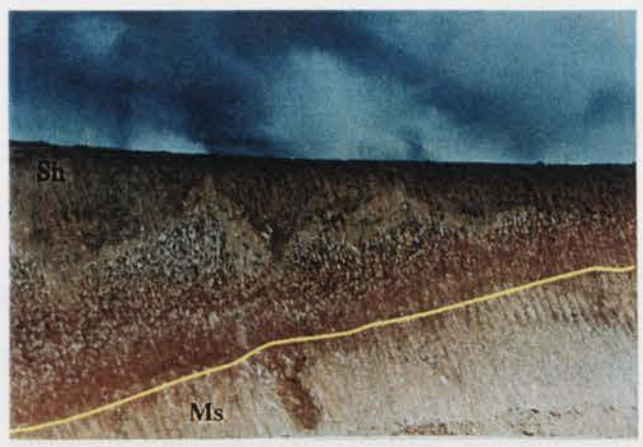

Figure 7.4.2: Sharp contact between the transported and residual regolith in the Eastern end of E22 deposit. Notice the undulating nature of the soil horizon (Sh) over the mottled clay.

Figure 7.4.3: Boundary between the transported and residual regolith in the central part of the more deeply weathered section in the E27 deposit. This boundary is defined by the presence of nodular iron and manganese aggregates within the clay.

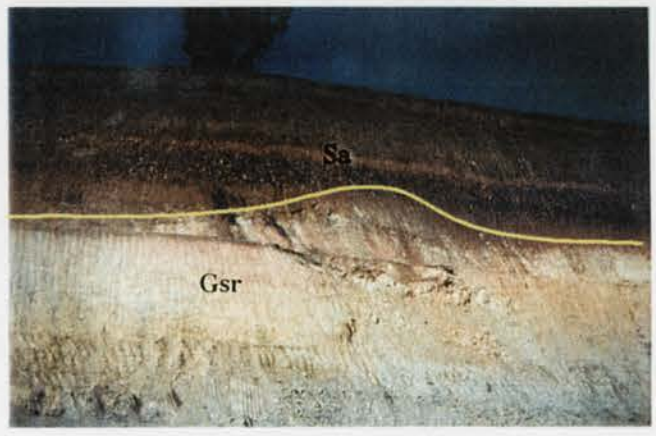

Figure 7.4.4: Extension of the sharp contact of Figure 7.9.2 into the more deeply weathered section of the E22 deposit. Notice the well defined band of silica aggregates (Sa) within the mottled clay.

Figures 7.4: The different dispositions of the boundaries between the transported and residual regolith in E22 and E27 deposits [Gsr-greenish-grey saprolite; MS-mottled saprolite; Sp- saprock; Sh- soil horizon].

The *in situ* weathering on the trachyandesite is manifested in the products that define the saprock and the two types of saprolite i.e. the orange-pink and greenish-grey varieties. The saprock and saprolite retained the fabrics of the host rock as evidenced by the presence of remnant quartz veins and numerous veinlets in their matrix, both of which have been coated and infilled by secondary carbonates. The two units also retained the mineralogy of the trachyandesite although differences occurred in quantitative amounts in different parts of the profile as dissolution of products occurred resulting in precipitation and formation of secondary oxyhydroxides i.e. clays and iron oxides. The morphology of the secondary products also provided further evidence of the primary development of these products. Kaolin, for example displayed pseudohexagonal plates, books and vermiforms that have been documented by several workers as typical of primary kaolinites. The mottled saprolite was interpreted as having formed by infusion of iron from the mottled clay horizons above it.

The weathered transported sediments were defined by the materials that formed the mottled clay horizons. The mineralogy of this sequence was dominated by quartz, kaolin, hematite and goethite with minor amounts of smectites and carbonates (notably dolomite). The plasma was defined by numerous voids and fractures that had in part strung together to form channelways. These voids and channelways had been infilled by secondary clays, iron oxides, carbonates and undeterminable manganese wads. Detrital rock fragments composed of the primary minerals notably muscovite and plagioclase was also present in the plasma. These fragments showed evidence of having been translocated from the upper parts of the soil horizon while some occurred as components of initial alluvial and colluvial materials. Microscopic examinations also showed the presence of numerous sub-rounded to sub-angular quartz fragments. Some sub-rounded quartz pebbles were also recovered from the bulk fractions.

The micromorphology also gave further evidence of the origin of these products. Kaolin for example showed the presence of thin plates, which had a close association with quartz fragments. This was interpreted as showing that the two were deposited together with the parallel orientation of the grains lending credence to this argument. Some distorted kaolin books were also present in very low amounts as compared to the saprolitic ones. XRD clay mineralogy also showed the presence of a well-crystallized kaolinite, which was interpreted as representing *in situ* development on material that was deposited on an active hydrodynamic regime.

7.4.3 Hydrothermal alteration and weathering

As already noted in Chapter 1, fingers of the quartz monzonite intrusions occur as pipe-like bodies within the fresh trachyandesite. They mostly occur at depths of between 10 to 15 m below the weathering front. As the regolith sections show, no monzonite intrusive was traced up to the regolith in either E22 or E27 open pits.

However, the effects of the monzonite intrusion were seen in the diverse hydrothermal alteration products that accompanied its emplacement. These effects were quite extensive and in some instance extended up to 200 m away from the mineralization zone. The most pronounced effect of hydrothermal alteration was that as that of partially or totally obliterating the primary rock fabrics. As a result, some of the secondary products encountered in the residual units were products of hydrothermal alteration and these included the sericitized plagioclase, iron oxides, the quartz-calcite veins and stringers and probably some of the kaolin in the lower saprolite and the saprock. Local changes in the rock compositions were also encountered in the wall rocks which could have slightly affected the chemical compositions of the regolith products.

PART 3

.Palaeomagnetic dating

.Major & trace element geochemistry

.Mineral-element host associations & distribution

.Summary & Conclusions

CHAPTER 8

PALEOMAGNETIC DATING OF THE REGOLITH

8.1 Introduction

The ages of weathered, non-fossiliferous regolith materials are notoriously difficult to determine in Australia. Dating methods such as radiocarbon, luminescence and U-series disequilibrium are generally limited to the last few hundred thousand years, while techniques such as K/Ar and electron spin resonance (ESR) are only applicable to mineral phases that are rare in regolith sequences. However, because of the common occurrence of secondary iron-rich minerals, the techniques of paleomagnetism have wide application in regolith studies. In this study, paleomagnetism is used in an attempt to establish a chronological framework for weathered regolith materials at Northparkes Mine. The study has been carried out in collaboration with Dr. Brad Pillans of the Research School of Pacific Studies, Australian National University and Matt Idnurm of the Australian Geological Survey Organization, Canberra. Dr Brad Pillans carried out the analysis. For a general introduction to the techniques and applications of paleomagnetism, readers are referred to Butler (1992).

8.2 Sample collection sites

The samples were collected from the Orange-Pink saprolite of E22 Profile 7, the mega-mottled clay of E22 Profile 5 and the valley fill (palaeotopographic low) material of E27 Profile 7. These sample collection sites are presented in Figure 8.1.

The mineralogical compositions of a couple of samples from each of these sites are presented in Table 8.1 below:

PROFILE	Qtz.	Kaol.	Hem.	Goet.	Smec.	Musc.	Orth.	Anat.	Dolm.
E22 P7-1	15.4	49.7	6.9	-	-	22.5	11.4	-	5.5
E22 P7-2	3.0	40.1	5.8	1.8	-	22.9	20.2	-	2.6
E22 P5-1	7.5	59.6	4.0	7.1	-	-	-	6.1	15.6
E22 P5-2	8.9	51.9	9.1	11.4	1.1	-	-	8.1	9.5
E27 P7-1	4.7	81.6	11.5	2.2	-	-	-	-	-
E27 P7-2	6.3	80.6	12.2	1.0	-	-	-	-	-

Table 8.1: Mineralogical compositions of samples from E22 Profiles 7 and 5 and E27 Profile 7 [Qtz.-Quartz; Kaol.-Kaolin; Hem.-Hematite; Goet.-Goethite; Smec.-Smectite; Musc.-Muscovite; Orth.-Orthoclase; Anat.-Anatase and Dol.-Dolomite].

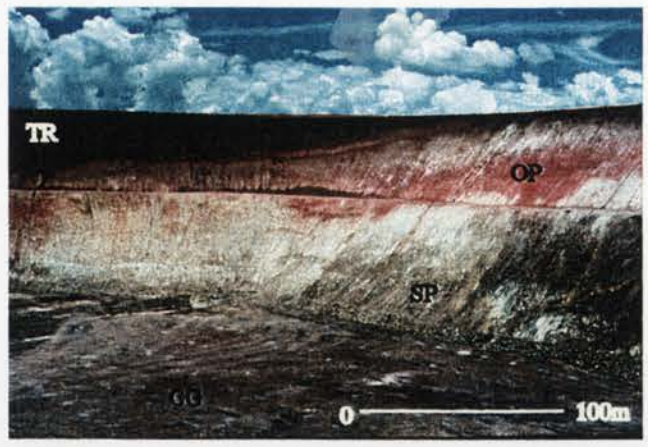

Fig.8.1.1: The orange-pink saprolite [OP 1] from sites PM-O1 and PM-02 in the E22 deposit, showing its position relative to the saprock [SP] and the greenish-grey saprolite [GG] in the regolith stratigraphy. The transported regolith [TR] occurs to the NW corner of the plate.

Fig. 8.1.2: A close-up view of the orange-pink saprolite showing carbonate stringers [CS] within its matrix. Sampling was carried out on the orange-pink portions

Fig. 8.1.3: The mega-mottled clay from site PM-03. Sampling was carried out on the iron-oxide rich portions.

Fig. 8.1.4 The valley fill [palaeotopographic low] material of site PM-09 from the E27 deposit. Sampling was also carried out on the iron-oxide rich portions.

Eighty five oriented paleomagnetic samples (NPK-01 to 85) were collected from each of nine sites in Pits E22 and E27: four sites in saprolite, and five sites in the valley fill sediments (Table 8.2). At each site, the wall of the pit was spaded back to expose a fresh, moist sub-vertical face. Small cube-shaped pedestals were carved with a sharp knife, onto which 6 cm^3 plastic boxes were carefully fitted. Before removal from the face, samples were oriented with a Brunton compass and inclinometer, and the directions corrected for local magnetic declination.

TABLE 8.2: Paleomagnetic sampling sites, Northparkes mine

Site No.	Pit	Sample Nos.	Description
PM-01	E22	NPK-01 to 06	Orange-Pink saprolite (profiles 7-8)
PM-02	E22	NPK-07 to 09	Orange-Pink saprolite (profile 7)
		NPK-46 to 63	
PM-03	E22	NPK-10 to 15	Mega-mottled zone (Profile 5)
PM-04	E22	NPK-16 to 21	Mega-mottled zone (base) -profiles 3-4)
PM-05	E27	NPK-22 to 24	Orange-Pink saprolite (profile 10)
PM-06	E27	NPK-25 to 30	Mega-mottled zone (top), profiles 5-6
		NPK-64 to 73	
PM-07	E27	NPK-31 to 36	Mega-mottle zone (profile 3)
PM-08	E27	NPK-37 to 39	Orange-Pink saprolite, profile 2
PM-09	E27	NPK-40 to 45	Mega-mottled clay, base of valley fill,
		NPK-74 to 85	(profile 7)

8.3 Laboratory measurements and results

All samples were measured on a two-axis ScT cryogenic magnetometer at the joint AGSO/ANU Paleomagnetic Laboratory, Black Mountain, Canberra. Both thermal and alternating field demagnetizations were carried out stepwise, on the samples, to isolate the Characteristic Remanent Magnetization (ChRM). From their strongly weathered appearance, it is concluded that the ChRM in the samples is a chemical remnant magnetization acquired during weathering of both the *in situ* and transported regolith materials. Resultant paleomagnetic ages thus relate to the times of weathering, not the times of deposition of the sediments or the cooling of the orebody and host rocks. In many samples, stepwise demagnetization revealed multi-component magnetic directions, which were analyzed by Principal Component Analysis (Kirschvink 1980). The results are listed in Table 8.3.

TABLE. 8.3. Paleomagnetic data from principal component analysis of samples from Northparkes Mine [Treatment level: TH = thermal demagnetization (with temperature range in °C); AF = alternating field demagnetization (with field range in mT). MAD = Mean Angular Deviation on orthogonal plots (for sites PM-02 and 09, maximum acceptable MAD was 10°; for site PM-06 maximum acceptable MAD was 15°)].

Sample No.	Treatment range	Decl. (deg)	Incl. (deg)	Long. (deg)	Lat. (deg)	MAD (deg)
SITE PM-02 - Orange-Pink saprolite						
Intermediate temperature component						
NPK-46	TH350-500	208.5	58.6	81.8E	66.2S	5.6
NPK-47	TH200-650	221.5	59.8	83.5E	56.2S	6.2
NPK-48	TH200-450	222.2	52.4	70.1E	54.8S	2.3
NPK-49	TH300-450	211.6	55.2	73.1E	63.9S	1.7
NPK-50	TH250-350	219.8	56.5	76.8E	57.4S	2.0
NPK-51	TH250-400	233.2	56.4	79.0E	46.8S	2.0
NPK-52	TH250-450	227.7	53.6	73.5E	50.6S	4.3
NPK-53	TH200-450	187.8	69.3	134.8E	69.3S	4.7
NPK-54	TH300-500	195.8	48.5	47.9E	76.1S	7.4
NPK-55	TH250-400	225.4	50.4	68.1E	51.8S	3.8
NPK-56	TH250-350	246.3	52.5	77.9E	35.4S	4.5
NPK-57	TH250-400	216.5	48.2	61.2E	58.7S	1.7
NPK-58	TH200-450	219.3	55.0	73.9E	57.6S	3.7
NPK-59	TH250-400	226.9	55.5	76.2E	51.6S	2.9
NPK-60	TH200-400	245.9	50.5	75.8E	35.1S	3.5
NPK-61	TH200-350	245.7	60.9	88.3E	38.4S	4.7
NPK-63	TH250-450	197.9	56.5	78.8E	74.8S	5.3
High temperature component						
NPK-01	TH650-700	37.5	54.7	252.9E	59.1N	8.3
NPK-02	TH650-700	55.6 -	55.0	257.6E	44.6N	7.4
NPK-03	TH570-700	60.0 -	53.7	257.2E	40.8N	4.4
NPK-04	TH660-700	65.6 -	64.8	274.4E	39.3N	7.4
NPK-05	TH650-700	42.6 -	51.6	248.9E	54.4N	5.1
NPK-06	TH620-700	44.3 -	54.0	253.2E	53.4N	2.6
NPK-07	TH650-700	13.6 -	71.9	310.8E	64.4N	5.6
NPK-08	TH620-700	37.7	-70.3	288.6E	56.0N	1.7

NPK-09	TH620-700	40.9 -	71.6	290.5E	53.5N	3.0
NPK-46	TH620-710	62.3 -	61.5	268.6E	41.0N	4.1
NPK-47	TH620-710	43.1 -	59.5	262.9E	55.0N	8.9
NPK-48	TH650-710	44.1 -	58.2	260.5E	54.2N	1.8
NPK-49	TH670-710	43.2 -	52.7	250.8E	54.1N	6.5
NPK-50	H620-710	43.8 -	59.4	262.7E	54.5N	3.0
NPK-51	TH620-710	46.5 -	58.7	261.7E	52.3N	3.9
NPK-52	TH570-710	47.2 -	55.3	256.0E	51.3N	2.8
NPK-53	TH590-710	56.1 -	50.0	251.5E	42.9N	2.1
NPK-54	TH590-690	54.7 -	61.3	267.1E	46.5N	2.3
NPK-55	TH590-700	67.8 -	54.2	260.2E	34.8N	1.6
NPK-56	TH590-690	68.2 -	57.3	264.1E	35.5N	3.2
NPK-57	TH590-700	52.5 -	62.2	268.5E	48.2N	2.3
NPK-58	TH660-710	62.2 -	64.1	272.7E	41.5N	5.3
NPK-59	TH650-700	51.4 -	54.5	255.8E	47.8N	2.5
NPK-60	TH590-710	70.7 -	51.9	258.8E	31.8N	1.8
NPK-61	TH620-710	55.5 -	59.9	264.9E	45.7N	2.3
NPK-62	TH620-700	64.4 -	49.2	253.7E	35.9N	4.3
NPK-63	TH590-680	61.4 -	57.8	262.9E	40.8N	2.8

SITE PM-06 - Mega-mottled zone

NPK-66	TH50-250	311.8	-60.6	31.0E	51.2N	14.2
NPK-67	AF50-150	350.8	-68.1	345.7E	70.6N	8.5
NPK-68	AF30-110	354.2	-54.9	29.3E	84.6N	12.6
NPK-70	AF40-130	338.5	-61.8	21.1E	70.4N	10.2
NPK-71	AF70-150	191.4	60.5	104.6E	77.6S	8.0
NPK-72	AF30-150	183.1	52.4	59.7E	87.4S	14.3

SITE PM-09 - Base of valley fill (palaeotopographic low)

NPK-74	AF7.5-150	7.7	-59.0	288.0E	80.8N	3.2
NPK-75	TH150-450	15.6 -	59.6	273.5E	75.5N	3.2
NPK-76	AF7.5-150	4.3	-62.7	312.6E	78.4N	3.9
NPK-77	AF5-130	6.3	-57.6	285.8E	82.7N	2.0
NPK-78	TH100-450	11.0 -	62.2	292.0E	76.4N	1.6
NPK-79	AF5-150	8.9	-57.1	273.8E	81.3N	2.6
NPK-80	AF5-150	12.2 -	60.9	284.6E	76.8N	3.4

NPK-82	AF5-150	7.8	-61.9	299.3E	78.1N	2.4
NPK-83	AF5-90	8.6	-66.5	308.4E	72.7N	4.8
NPK-84	AF5-130	9.8	-57.4	273.3E	80.6N	3.1
NPK-85	TH100-650	6.1	-62.0	305.0E	78.7N	4.1

Natural Remanent Magnetisation (NRM) directions (i.e. prior to demagnetization) were scattered, with a general tendency to cluster around the present field direction at the site. In some of the samples this is consistent with contemporary (e.g. mineralized bedrock-related) weathering. Eleven samples from at or just beneath the base of the valley fill sediments at Site PM-09 (Table 8.3) yielded very similar, stable magnetic directions. The resultant pole position (Table 8.4) is consistent with a Miocene age of magnetization (=weathering). However, such an age is ambiguous because:

1. All directions have the same (normal) polarity, which is unusual for a prolonged period of magnetization in the Tertiary.

2. The directional scatter is very small, suggesting again that remanence acquisition occurred over a brief interval of time (<1 Ma).

3. The mean direction (declination 9.0°, inclination -60.7° - Table 8.3) closely resembles that of the present geomagnetic field at Northparkes (declination 11.3°, inclination -64, 2°), and both have normal polarities

With progressive demagnetization many of the samples revealed a reverse polarity component, indicating remanence acquisition during weathering prior to the Brunhes/Matuyama polarity transition (0.78 Ma). Further discussions on this subject have been provided by Pillans & Bourman (1996). Samples from the weathered valley fill sediments yielded generally scattered directions; six samples from the mega-mottled zone at Site PM-06 (Table 8.2) yielded a pole position with a large (14°) uncertainty (Table 8.3) broadly consistent with remanence acquisition during Cainozoic weathering.

Principal component analysis of samples from Site 2, in the Orange-Pink saprolite, yielded 17 well defined intermediate and 27 high temperature remanence components (Table 8.4) with a combined mean pole position of 51.2°S, 81.4°E (A_{95} = 3.6°). This pole lies considerably west of the Australian Cainozoic Apparent Polar Wander Path (APWP) and appears to lie on the Carboniferous APWP (Lackie & Schmidt 1993). Although the apparent pole position will have been affected by any post-Carboniferous

tectonic deformation, the vertical orientation of the pipe-like monzonite intrusives that host the Northparkes orebody suggests that little or no tectonic correction is required.

Component	N	Remanence Direction				Pole position			
		Dec (deg)	Inc (deg)	k	α_{95} (deg)	Lat (°S)	Long (°E)	K	A_{95} (deg)
				SITE PM-02					
Intermediate	17	41.4	-56.3	58.6	4.7	56.3	77.3	31.5	6.5
High	27	52.6	-58.8	87.8	3.0	48.0	83.5	48.4	4.0
Combined (I + H)	44	48.1	-58.0	67.7	2.6	51.2	81.4	36.6	3.6
				SITE PM-06					
High	6	349.3	-61.1	47.6	9.8	187. 1	77.1	23.0	14.3
				SITE PM-09					
High	11	9.0	-60.7	628.6	1.8	111.8	78.7	389.	2.3

TABLE 8.4. Summary of paleomagnetic results from Northparkes Mine [N = number of specimens; K and k = precision parameters; α_{95} and A_{95} = semi-angles of 95% confidence]

8.4 Discussion

From the paleomagnetic results it is inferred that weathering of regolith at Northparkes Mine has been an on-going process since at least late Paleozoic time. Regional geology (e.g. Clarke & Sherwin 1990) of the Northparkes area suggests that that the area has probably been subaerially exposed since the late Devonian. Fluvial sandstone and conglomerate beds of possible Mesozoic age (Clarke & Sherwin 1990) occur to the west of Northparkes mine, but otherwise the stratigraphic record of post-Devonian times is almost entirely unknown in the area. Interpretation of apatite fission-track data in the Bathurst area, some 100 km east of Northparkes Mine, suggests kilometre-scale uplift and erosion in the mid-Cretaceous (O'Sullivan et al. 1995). If Northparkes underwent subaerial weathering in the Carboniferous, it must have undergone subsequent kilometre-scale burial, and then re-exhumation, to be consistent with the fission-track data.

The time of deposition of the valley fill sediments at Northparkes must predate the time of weathering (Cainozoic) of the sediments and postdate the truncated saprolite (Carboniferous) beneath. The valley fill sediments may relate to a system of N-S

(Carboniferous) beneath. The valley fill sediments may relate to a system of N-S trending valleys, which predate the formation of the Canobolas Divide, which was formed by downwarping of the Murray Basin. The divide was already in existence prior to 12 Ma, as evidenced by K/Ar dated lavas which flowed down valleys to the north, south and west, and may have formed by downwarping of the Murray Basin prior to the middle Eocene (Ollier & Pain 1994), i.e. prior to 45 Ma. The paleomagnetic ages from Northparkes Mine are therefore consistent with other evidence for the age of the Canobolas Divide (Chapter 2, section 2.1.3).

Unequivocal pre-Tertiary ages for weathering profiles in southeastern Australia have not previously been reported using paleomagnetic techniques: The oldest reported paleomagnetic ages for weathering profiles appear to be for the Early Tertiary Morney profile in southwest Queensland (Idnurm & Senior 1978) and Late Cretaceous-Early Tertiary profiles in the New England region (Schmidt & Ollier 1988). Stratigraphic (Daily et al. 1974) and oxygen isotopic evidence (Bird & Chivas 1989) support a pre-mid Jurassic age for a lateritic profile on Kangaroo Island, but paleomagnetic results (Schmidt et al. 1976) suggest a late Cainozoic age. Based on isotopic data from kaolinite-rich weathering profiles throughout Australia, Bird & Chivas (1989) concluded that a number of profiles with low $\delta^{18}O$ compositions (< 15 ‰) represent remnants of a once extensive regolith cover that formed in a much cooler climate than has prevailed since the late Cretaceous. Oxygen isotope analysis of kaolinite from Northparkes regolith materials is planned.

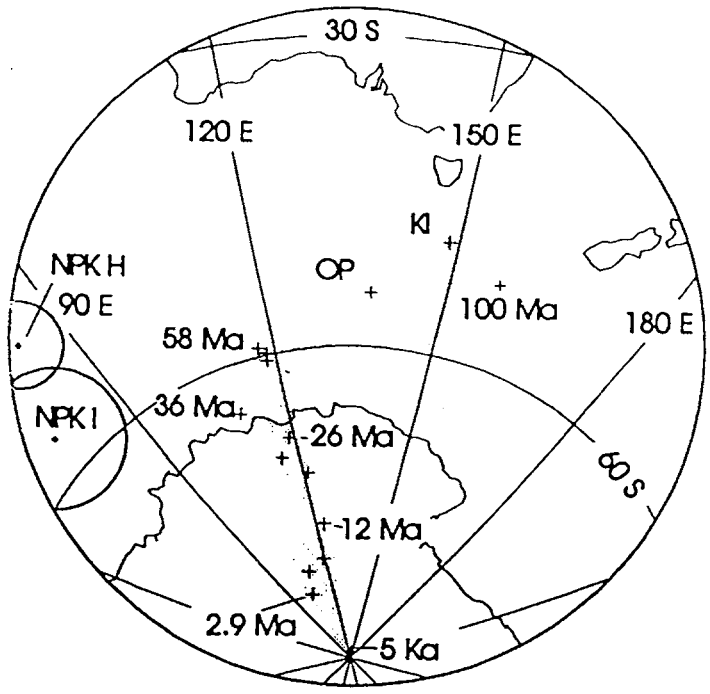

a

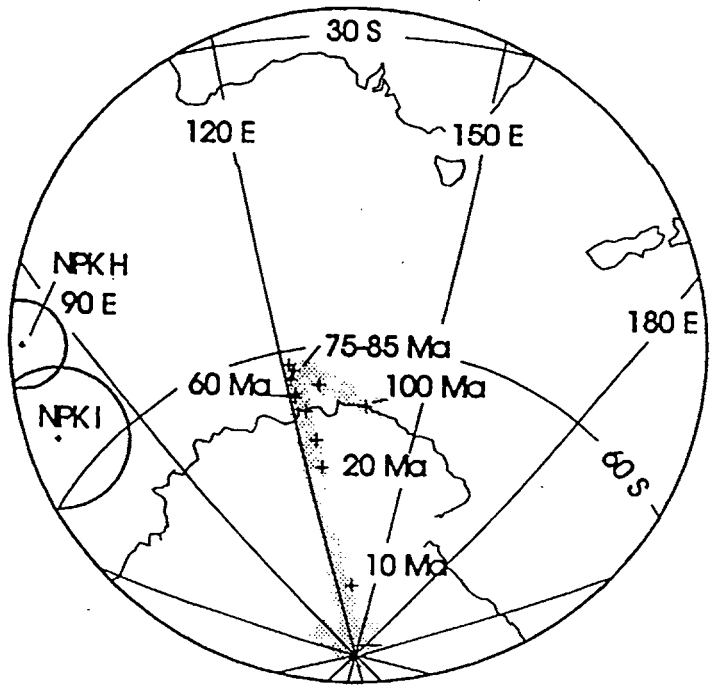

b

Figure 8.2 . Comparison of pole positions (NPK-I and NPK-H) from saprolite at Northparkes Mine, with the Australian Cainozoic polar wander path (after Idnurm 1994).

CHAPTER 9

MAJOR AND TRACE ELEMENT GEOCHEMISTRY

9.1 Introduction

Metal or non metal elements of geochemical exploration interest that are released from primary and secondary minerals through weathering processes move in solution along hydromorphic channels of geological matrices. They tend to partition into different chemical forms associated with various organic and inorganic phases depending on the chemical and geological environments. The secondary minerals that have been described in Chapters 6 and 7 are hosts to elements released and dispersed from primary mineralization in the course of weathering. An understanding of the geochemical behaviour in the weathered mantle is essential to geochemical exploration for two main reasons. Firstly, it enables an accurate interpretation of the source material's geochemistry, and secondly, it allows the development of techniques suitable for exploration in the regolith.

The processes of weathering affect the geochemical behaviour of elements differently depending on a number of factors. Firstly, the availability of an element to the processes of both physical and chemical weathering determines if the element will be affected by these processes. If an element is released from a mineral phase that is unstable in the weathering environment, it becomes available for dispersion throughout the weathered medium. If the element is not released, because of mineral stability in the surficial environment, then it is unavailable to the processes of hydromorphic dispersion, and can only be transported by physical weathering processes. Secondly, once released from a mineral phase, the mobility or immobility of an element in the surficial environment will determine its geochemical behaviour in that environment. The mobility, or immobility of an element is in turn, primarily dependent on the prevailing pH, redox, and temperature conditions, and the presence of a transporting fluid. Thus, depending on the prevailing physico-chemical conditions, the mobility of an element is extremely variable from one weathering environment to another.

Immobile elements are usually enriched in residual minerals by weathering, while mobile elements may be depleted or concentrated depending on the prevailing physico-chemical conditions. This latter type of concentration can occur as mobilized elements become immobilized in response to a change in the prevailing physico-chemical conditions. This is typically true of elements like thorium and uranium which are usually mobile under

oxidizing conditions but can be immobilized when adsorbed onto clay minerals (Boyle, 1982; Langmuir, 1978).

The main reason for carrying out geochemical exploration in the regolith is because of the large costs associated with sampling fresh rock. The variable nature of element geochemical behaviour in the weathering environment makes geochemical exploration in the regolith difficult, and in some cases unsatisfactory. In one region, an element may be residually enriched because of its immobility in the prevailing weathering environment, in another region the same element may be depleted because of its immobility under a different set of weathering conditions.

This chapter deals with the behaviour and associations of the major and trace elements in the weathering environment over the E22 and E27 deposits. Chapter 10 deals with the associations between the host minerals and ore forming elements and the distribution of these elements in the regolith stratigraphy. The sample collection and analytical techniques used and the quality control of geochemical data have already been discussed in Chapter 4. A five prong approach has been employed involving the determination of profile geochemistry; univariate and bivariate interpretation of geochemical data; the determination of depletion and enrichment of elements in the profiles utilizing the isocon technique; the determination of host minerals for ore forming elements using selective leaching techniques and 2-dimensional (computer generated) representation of the geochemical data in the regolith stratigraphy.

9.2 Data handling and statistical procedures.

All data were entered directly into *Excel 4*, a statistical spreadsheet, accessed under the *Macintosh* and *PC* operating systems and imported directly into a *PC* statistical package known as *Statistica V*. The geochemical data were further manipulated to help statistical treatment; all values below detection were assigned half the value of the lower limit of detection (LLD). Once imported into *Statistica V*, the data were handled directly for statistical processing ultimately resulting in the production of correlation matrices, scatterplots and box and whiskers plots. The line graphs utilized in interpretation of profile geochemistry were produced from *Kaleidagraph 2.0* software package accessed under the *Macintosh* operating systems. The production of the 2-dimensional representations of open cut geochemical data was carried out using the *Surfer* computer software package accessed under the PC operating systems.

Statistical processing, utilizing uni-, bivariate procedures available in *Statistica V*, was required to summarize the geochemical data. The univariate procedures employed were the commonly used; *arithmetic mean, median, standard deviation and skewness*. When statistically analyzing a distribution of elements, it is important to ascertain whether they are normally or log-normally distributed. Log-normality is a common aspect of geochemistry and generally occurs when most values of a distribution are low, with a few highs, or anomalous, values (Rock, 1988). A positive skew in the distribution usually indicates that it is log-normal.

The use of graphical procedures is perhaps one of the most important aspects of geochemical data interpretation. Many of the numerical procedures are difficult to interpret from the examination of numerical results alone. However, from the results of the numerical methods, the interrelationships between the samples and elements can be shown graphically and the nature of the relationships easily observed (Grunsky, 1991). Line graphs have been used in this study to show the changes in element concentrations with depth.

Ternary (triangular) diagrams are also an excellent means of expressing three (generally major) components (e.g. Si-Al-Fe) which are subject to closure, in two dimensions. They are most effective in comparing categories. It must be emphasized though that the ternary plot displays x: y: z ratios and the absolute values may be totally different between different triplets (e.g. major components in one and trace components in another). Ternary plots have been used in this study for a quick comparison of the distribution of SiO_2, Al_2O_3 and Fe_2O_3 in the major regolith units.

The box and whisker plots of the parent material and the regolith classes of this study proved to be useful in further description of the characteristics of geochemical data. The box and whisker plots were developed to express order statistics in a graphical form (Turkey, 1977). It provides a graphical display of the median (50^{th} percentile), left and right hinges (25^{th} and 75^{th} percentile) as well as the maximum and minimum values over the range of the data. The left and right hinges and the median are presented as a 'box' that displays the range over which 50% of the data is spread. The 'whiskers' are the lines that extend to the left and right of the box. Some plots display the values that are less than the 25^{th} and greater than the 75^{th} percentiles as points along the whisker. In these instances, the extreme ends (maximum and minimum values) of the data are marked by vertical bars at the end of the whiskers.

The location of the median line within the box gives an indication of how symmetric the distribution is within the range of the left and right hinges (midrange). The length of the whiskers on each side of the box also provides an estimate of the symmetry of the distribution. The main advantage of this technique is that its shape is independent of the interval used to present the histogram (Grunsky, 1991). Thus, providing the scale of the presentation is reasonable, the box and whisker plots provide a fast visual estimate of the frequency distribution.

Bivariate statistical analyses were employed to investigate the relationships between pairs of elements from the geochemical data. Most important was the need to ascertain correlations between elements that are geochemically related due to such processes as weathering and mineralization. The data was sub-divided into the source and regolith classes so as optimize the establishment of these processes. The Pearson's product-moment correlation coefficient (r) was found most suitable for this task. This correlation coefficient is simply the ratio of the covariance of the variables to the product of their standard deviations (Rock, 1988). The result is a measure of the correlation between the two variables, ranging from -1 to +1, with unity indicating a perfect correlation, either negatively or positively, and zero, no correlation.

The pearson's product-moment correlation coefficient procedure can only be used for estimating linear relationships between two variables; the method fails where any non-linear relationships occur. Therefore, by using this procedure alone, important geochemical correlations may be overlooked. For this reason, the visual observation of two-dimensional graphical representation is extremely beneficial when investigating the bivariate relationships of geochemical data. Here one element was plotted against another on a scatterplot so that linear and non-linear trends, possibly indicating geochemical correlations, could become apparent. Another reason for using scatterplots to check for geochemical correlations is that spurious correlations may be produced by the presence of highly anomalous outliers.

Bivariate analysis is relatively simple and veracious, but, when there is need to statistically analyze more than one variable the powerful technique of multivariate analysis can be utilized. However, the five-prong approach employed in this study proved to be more than adequate to describe the distribution and behaviour of the geochemical elements in this study and it was thus considered inappropriate to pursue any other interpretation techniques beyond the aforementioned.

9.3.1 GEOCHEMICAL RESULTS

The raw geochemical data from the two deposits are presented in Appendix 3. The results are first presented separately as major and trace elements, then later combined in a multi-element approach. Emphasis has been placed on the differentiation of the elements according to the nature of the parent material so as to enable a broad interpretation of their associations.

The geochemical data from all the data from the two deposits are summarized in Table 9.3.1. The standard deviation (s) is a measure of the spread of the population about the mean, a large s indicating a large spread, and the skew (Sk) is a measure of the symmetry of a population's spread, a negative skew Sk indicating that fewer results occur that are greater than the population's mean. A positive skew in the distribution usually indicates that it is log-normal, but the best method for checking log-normality is to compare the skewness of log-transformed and un-transformed data. The lowest skewness value indicates the transformation procedure that should be employed. The box and whisker plots are presented in Figures 9.3.1, 9.3.2, 9.3.3 and 9.3.4. The plots display the major and trace elements separately.

9.3.1 Major element geochemistry

Of the major elements, Si and Al are the only ones that have a normal distribution of concentration values; the rest are log-normally distributed. The Si content of all the data has a large standard deviation (s=9.12) and a mean value of 46.72% with a negative skew (Sk= -0.18). The standard deviation is higher (s=11.31) in the transported regolith with a positive skew (Sk=0.53) while the standard deviation in the residual regolith is (s=7.67) is lower with a negative skew (Sk=-0.88). These differences are attributed to the Si host material and its widespread occurrence in primary silicates and quartz veins or veinlets within the residual regolith causing the negative skew. Silica is present mainly as detrital constituents in the transported material.

Aluminium has a relatively uniform concentration throughout the samples though it has a moderately large standard deviation (s=5.94) and mean value of 21.96%. The negative skew is probably attributed to a few outliers of lower concentration from the two source materials. Titanium on the other hand displays a small standard deviation (s=0.24) and mean value of 0.92% for all data from the two deposits and a positive skew (Sk=0.53).

Table 9.3.1: Statistical summary of the geochemical data from E22 and E27 deposits. The data from the transported and residual regolith materials is also presented. Oxides are expressed in weight % and Au in ppb. The rest of the trace elements are presented in ppm. 229 samples were used in this computation.

Element	Minimum	Maximum	Mean	Median	Standard deviation	Skewness (untransformed)
Fe_2O_3	1.41	40.69	10.47	8.30	7.24	1.97
MnO	<0.005	8.85	0.26	0.51	0.99	6.60
TiO_2	0.20	1.70	0.92	0.88	0.24	0.53
CaO	0.06	17.62	1.57	0.26	2.94	2.99
K_2O	0.05	7.87	2.18	1.16	2.02	0.79
SO_3	0.005	16.74	0.45	0.06	1.84	7.02
P_2O_5	0.020	0.80	0.16	0.11	0.16	1.71
SiO_2	19.94	68.94	46.72	47.75	9.12	-0.18
Al_2O_3	6.99	32.03	21.96	22.60	5.94	-0.43
MgO	0.23	12.37	1.69	1.04	1.81	2.87
Na_2O	0.03	5.60	0.82	0.28	1.31	2.27
Cu	26.00	18400	1776.60	719.50	2354.13	2.68
Pb	<0.05	1880	28.02	13.00	125.46	14.31
Zn	<0.05	479.00	54.20	41.00	58.19	3.19
Ag	<0.05	3.00	-0.92	-1.00	0.47	6.37
As	<0.05	89.00	9.41	6.00	11.95	3.79
Au	<0.05	870	66.00	20.50	127.00	3.66

TRANSPORTED REGOLITH (n=77)

Element	Minimum	Maximum	Mean	Median	Standard deviation	Skewness (untransformed)
SiO_2	27.07	68.94	44.97	43.02	11.31	0.53
Al_2O_3	8.56	31.76	21.28	21.87	6.94	-0.21
TiO_2	0.44	1.70	1.07	1.03	0.27	0.14
MnO	0.003	8.85	0.36	0.03	1.43	5.01
Cu	26.00	1420.00	379.50	297.50	305.51	1.22
As	0.50	63.00	12.40	8.00	11.93	2.25
Au	0.002	0.78	0.041	0.02	0.092	7.12
Pb	3.00	66.00	29.82	27.00	15.95	0.58
Zn	<2.00	262.00	33.16	23.00	42.54	3.23

RESIDUAL REGOLITH (n=152)

Element	Minimum	Maximum	Mean	Median	Standard deviation	Skewness (untransformed)
SiO_2	19.94	65.18	47.60	48.90	7.67	-0.88
Al_2O_3	6.99	32.03	22.31	23.17	5.36	-0.54
TiO_2	0.19	1.39	0.84	0.13	0.18	-0.22
MnO	0.005	6.47	0.21	0.08	0.66	7.35
Cu	45.00	18400	2475.15	1640.00	2609.85	2.22
As	<1.00	89.00	7.91	5.00	11.71	4.89
Au	<0.001	0.87	0.078	0.021	0.14	2.98
Pb	<5.00	1880.00	27.13	9.00	153.40	11.84
Zn	6.00	479.00	64.72	51.00	62.11	3.20

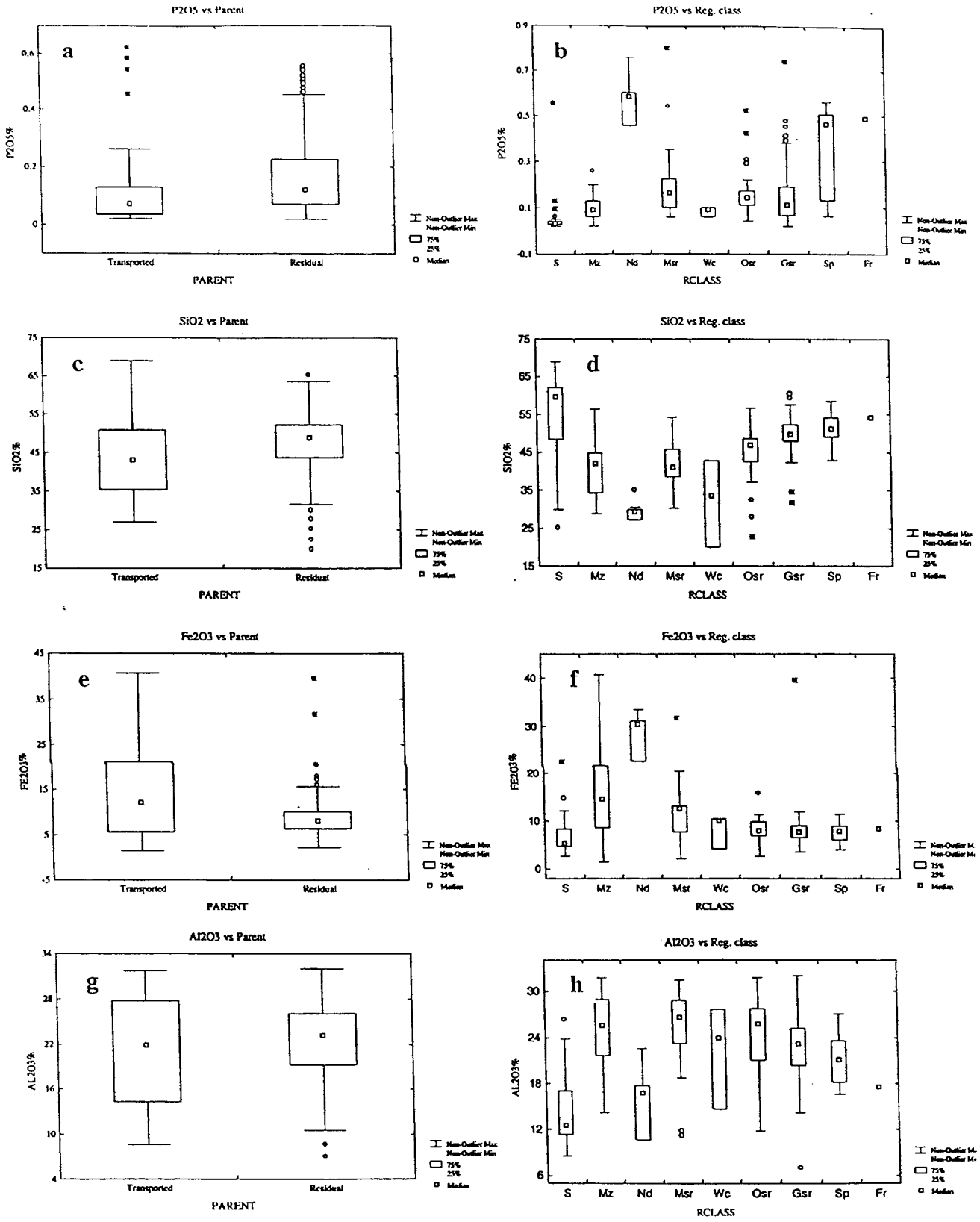

Fig. 9.3.1 : Box and whisker plots of P2O5, SiO2, Fe2O3 and Al2O3 as a function of the source material and regolith classes for both deposits. [S-soil; Mz- mottled zone; Nd- nodular Fe-Mn zone; Msr- mottled saprolite; Wc- white clay unit; Osr- orange pink saprolite; Gsr-greenish- grey saprolite; Sp-saprock; FR-fresh rock]

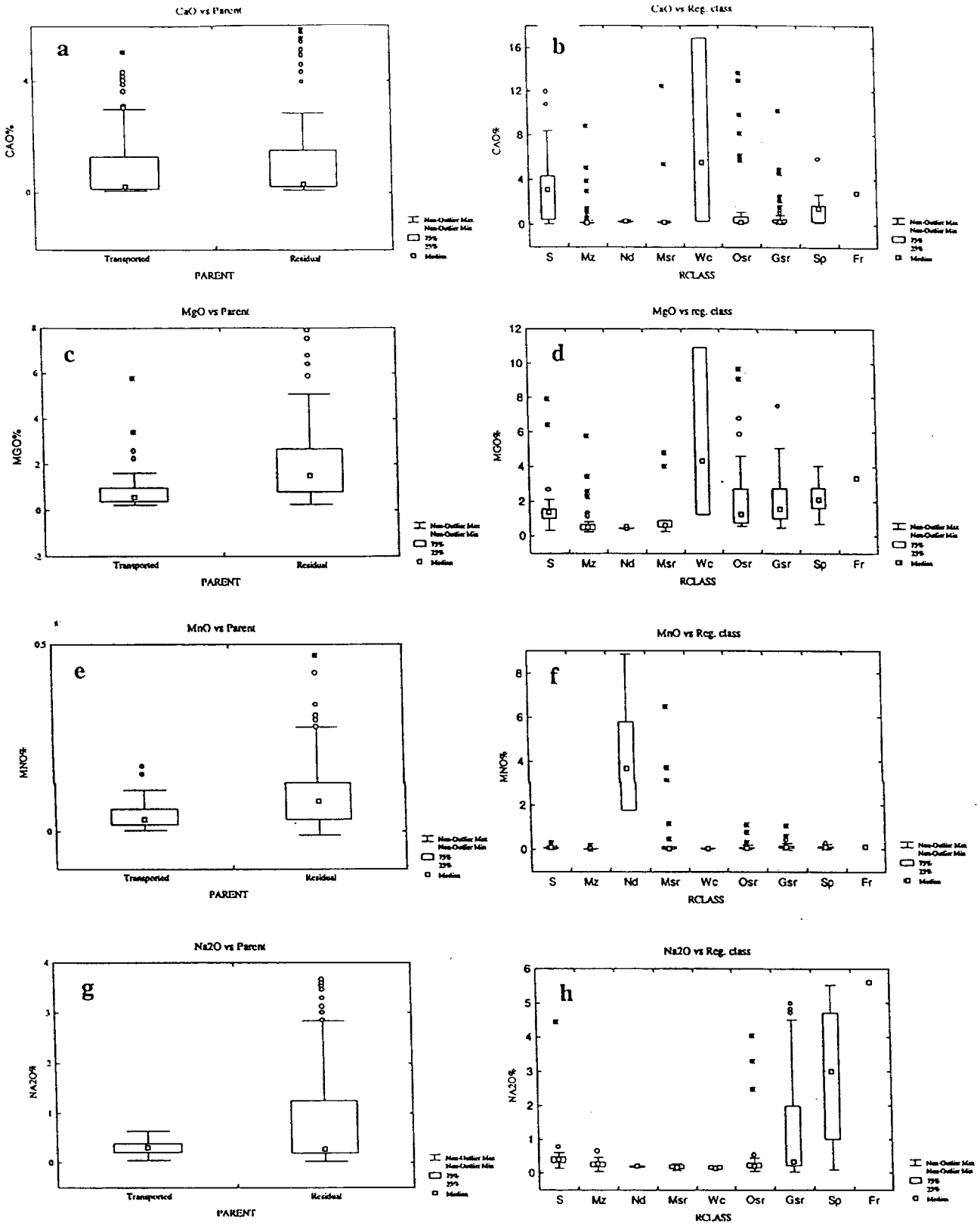

Fig. 9.3.2 : Box and whisker plots of CaO, MgO, MnO and Na2O as a function of the source material and regolith classes for both deposits. [S-soil; Mz- mottled zone; Nd- nodular Fe-Mn zone; Msr- mottled saprolite; Wc- white clay unit; Osr- orange pink saprolite; Gsr-greenish- grey saprolite; Sp-saprock; fresh rock]

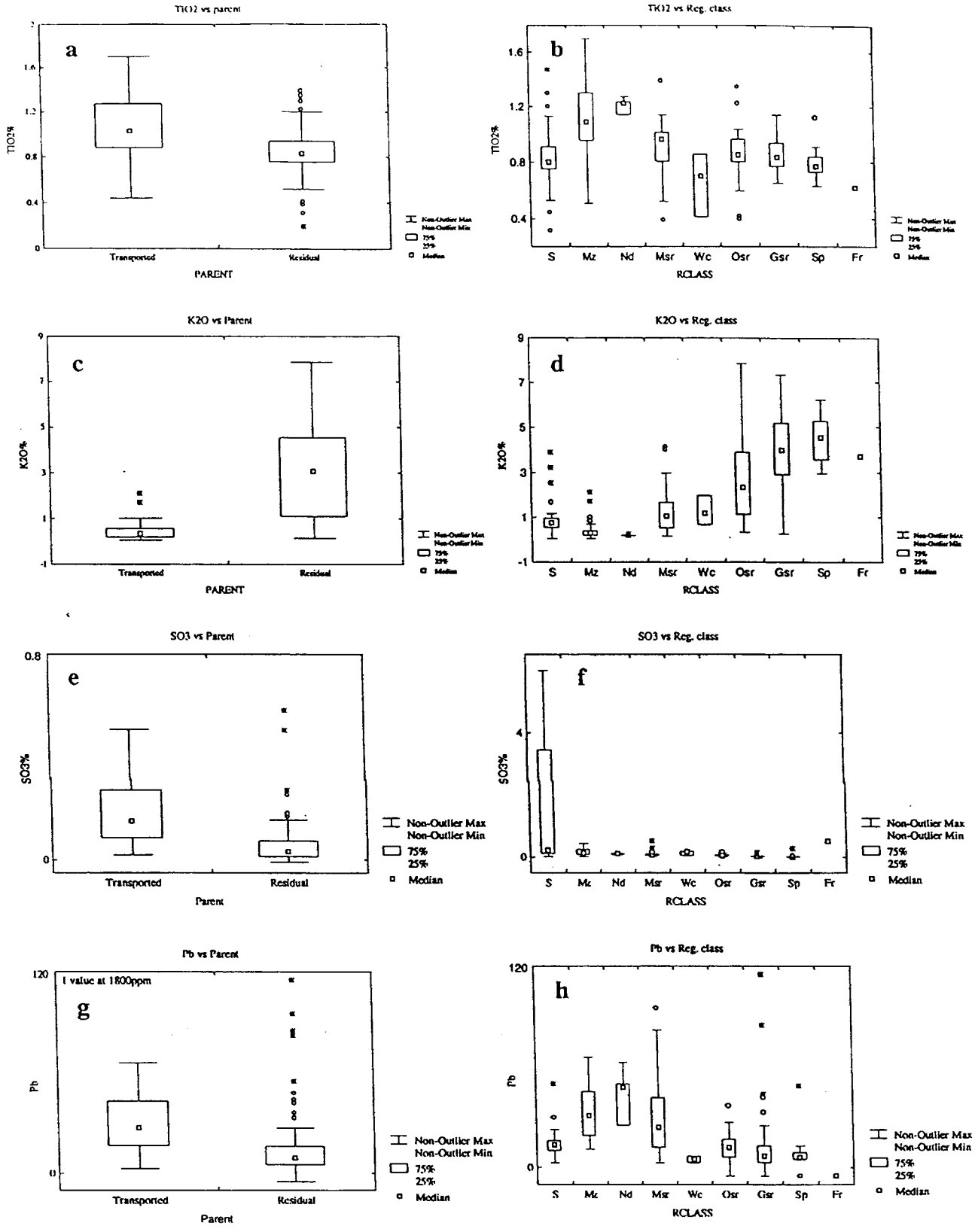

Fig. 9.3.3 : Box and whisker plots of TiO2, K2O, SO3 and Pb as a function of the source material and regolith classes for both deposits. [S-soil; Mz- mottled zone; Nd- nodular Fe-Mn zone; Msr- mottled saprolite; Wc- white clay unit; Osr- orange pink saprolite; Gsr-greenish- grey saprolite; Sp-saprock; FR-

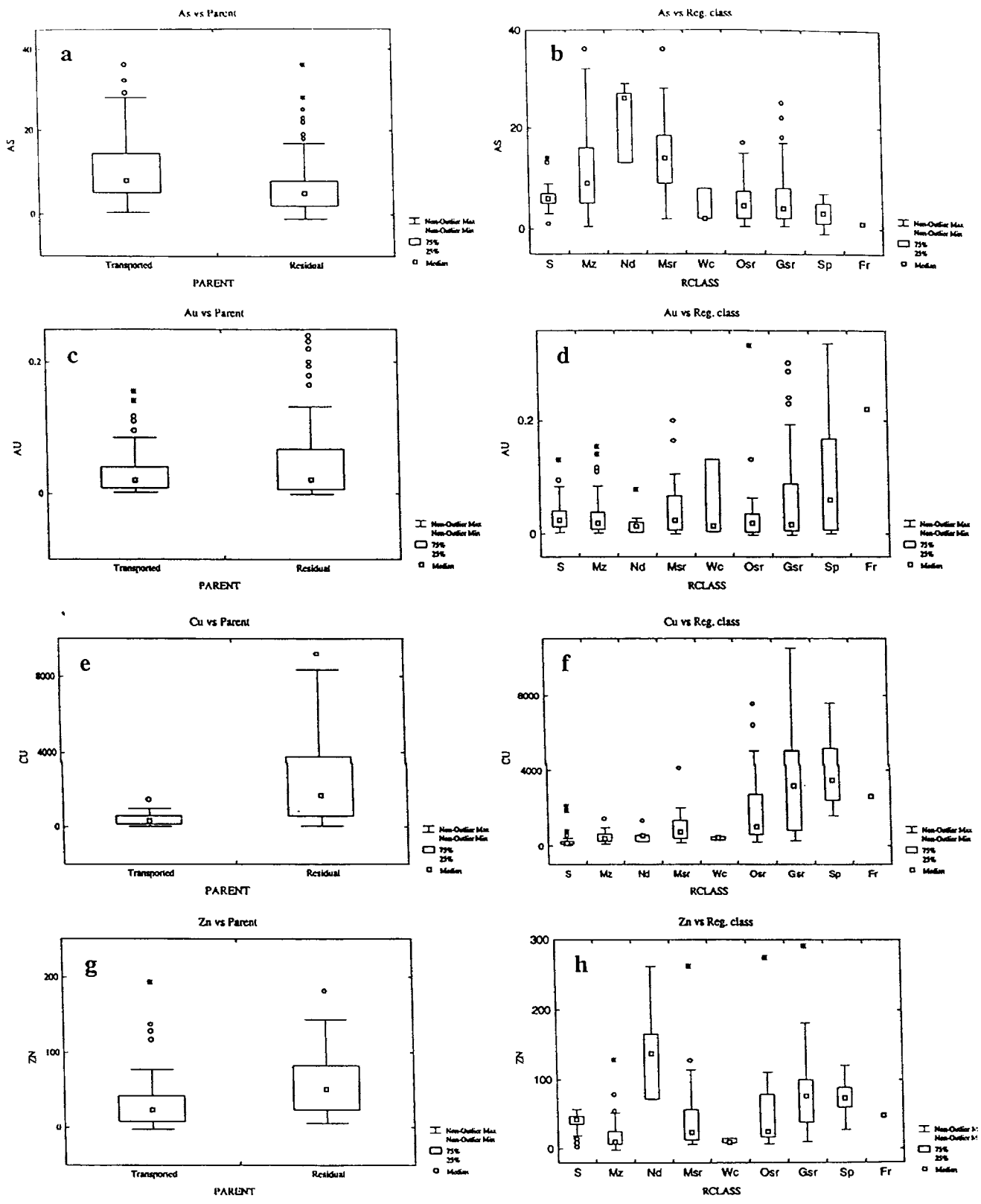

Fig. 9.3.4 : Combined box and whisker plots of As, Cu, Zn and Au as a function of the source material and regolith classes for both deposits. [S-soil; Mz- mottled zone; Nd- nodular Fe-Mn zone; Msr- mottled saprolite; Wc- white clay unit; Osr- orange pink saprolite; Gsr-greenish- grey saprolite; Sp-saprock; FR- fresh rock]

However, the residual host data shows a smaller standard deviation (s=0.18) and a negative skew (Sk=-0.22). This is also attributed to a few outliers of lower concentrations (minimum s value of 0.19 compared to 0.44 in the transported regolith) producing the low skewness.

Manganese, P, Ag and S have a small s value and a strong positive skew mainly because they either occur in very low concentrations that are quite often below the Lower Limit of Detection (LLD) or in high concentrations. Manganese in both regolith classes display small spreads and strong positive skewness because of the presence of a few outliers of high concentrations especially in the nodular iron-manganese horizons and the mottled saprolite. Magnesium, Ca, K and Na are all log-normally distributed and have relatively small s values with slight positive skews. However, Fe, which is also log-normally distributed, differs greatly from the other major elements in that it exhibits a large spread (s=7.24) and mean values of 10.47% with a relatively small positive skew (Sk=1.97). Its concentration is slightly variable with some values producing high concentration outliers.

The white clay unit and the nodular iron-manganese horizon exhibit high spreads for most of the elements as a result of the presence of samples with high concentration of elements in these units. Most affected include Mn, Si, Al, Ca, Mg and Ti (Figures 9.3.1, 9.3.2, 9.3.3 and 9.3.4). The relatively high spreads could also be a consequence of the relatively small number of sample values used in the statistical computation.

9.3.2 Trace elements

The trace elements presented here i.e Au, Cu, Pb, Zn, Ag and As have a normal distribution in concentrations. Of most interest are Cu, Pb and Zn which have extremely high spreads with Pb having a large positive skew. The large spread in Pb values is more pronounced in the residual regolith as indicated by its mean and$s$ values of 27.13 ppm and 153.40 respectively and Skewness of 11.84. Cu and Zn have small positive skews despite their large spreads (i.e s= 2354.13 and 58.29 and mean values 1776.6 and 54.20 ppm for Cu and Zn respectively). The Skewness value is higher (Sk=2.22) within the residual material as compared to the transported material (Sk=1.22). These characteristics indicate the presence of a large proportion of anomalously high value outliers in the elements with a large skew. Silver, As, Au and Cu have moderately high positive skew, and although the spread is not as large as the others, their range in values is high.

As with the major elements, the nodular iron-manganese horizon and the white clay unit exhibit high spreads for most of the elements as a result of the presence of samples with

high concentration of elements in these units (Figures 9.3.3 and 9.3.4). Most affected elements include Ag, As, Zn and Pb.

The mean and standard deviation values of both major and trace elements appears to indicate that the elements with low standard deviations relative to the mean like Ca, Mg, K, Na, Ti, Mn, P and Ag were less mobilized and locally concentrated while those with a high standard deviation and mean like Fe, Cu, Pb and Zn were highly mobilized. This may not be true in a number of cases given that the range of values could simply reflect the range of values in the original fresh rock, which was inhomogenous in some parts. Elements enriched in vein material might also be expected to exhibit a greater range of values than those spread through the more uniform host rock.

9.4 PROFILE GEOCHEMISTRY

9.4.1 Introduction

This section describes the distribution of the major and trace elements in the major profiles from both E22 and E27 deposits. Profiles 1, 4, 7 and 9 have been selected from the E22 deposit and they are representative of the major regolith units that have been encountered in this deposit. Likewise, profiles 1, 6, 9 and 11 have been selected from the E27 deposit.

Attempts have also been made in this section to compare the distribution of these elements with the profile mineralogy presented in Chapter 7 although these correlations will become clearer in subsequent sections where these relationships are discussed in more detail.

9.4.2 Major elements

Silica

Silica concentrations range from 19.94 to 68.94% with mean values that are higher in the residual regolith (47.60%) as compared to the transported regolith (44.97%). The highest concentrations (~70%) occur in the upper level of the white clay unit (E22 Profile 7) and silica aggregates/mottled saprolite (E27 Profile 9) zone. Moderate to high concentrations (55 -65%) occur in the soil horizons of most of the profiles and the mottled saprolite in both deposits. The mottled clay zones of E22 Profile 4 and E27 Profile 6 also shows enhanced concentrations (60-65%) especially in the mega-mottled

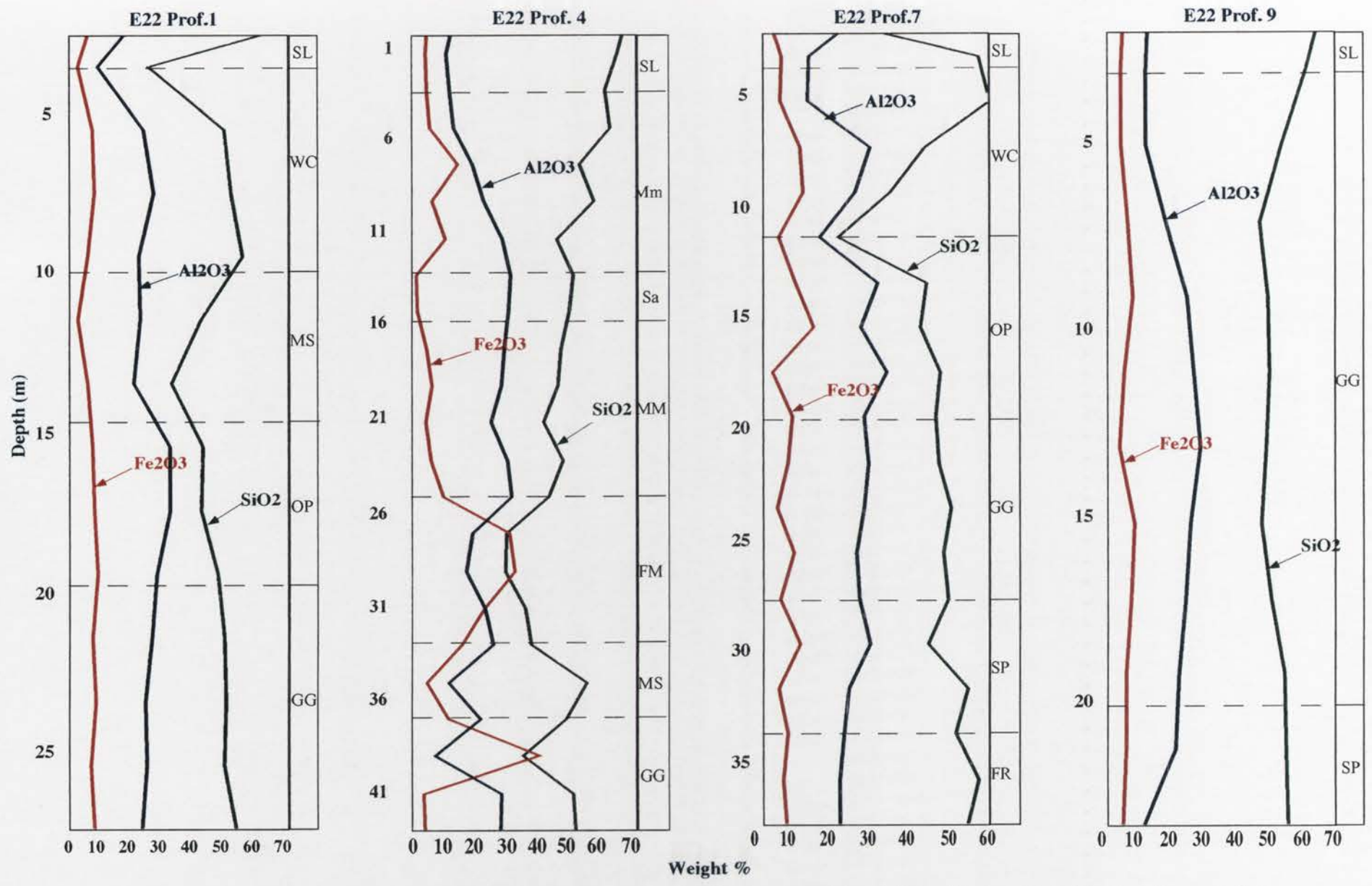

Figures 9.4.1: Plots of depth vs weight % of SiO2, Al2O3 and Fe2O3 of selected profiles from the E22 deposit [SL=soil horizon; Mm-mini-and-medium mottled clay zone; MM-mega-mottled clay; Sa-silica aggregate zone; FM-nodular Fe-Mn horizon; WC-white clay unit; MS-mottled saprolite; OP-orange-pink saprolite; GG-greenish-grey saprolite; SP-saprock; FR-fresh rock].

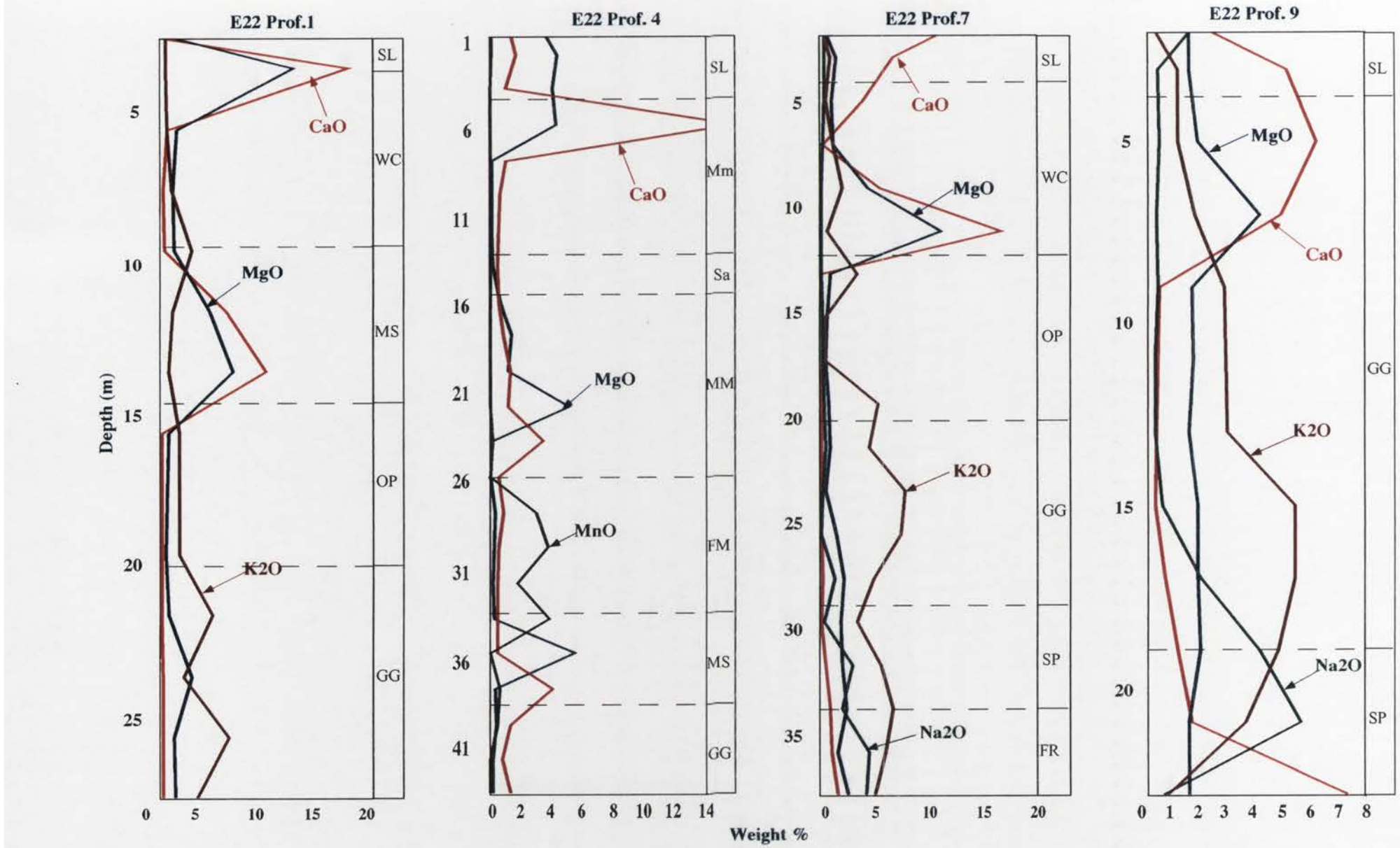

Figures 9.4. 2: Plots of depth vs weight % of CaO, MgO, MnO, Na2O and K2O of selected profiles from the E22 deposit [SL=soil horizon; Mm-mini-and-medium mottled clay; MM-mega-mottled clay; Sa-Silica aggregate zone; FM-nodular Fe-Mn horizon; MS-mottled saprolite; WC-white clay unit; MS-mottled saprolite; OP-orange-pink saprolite; GG-Greenish-Grey saprolite; SP-Saprock; FR-Fresh rock].

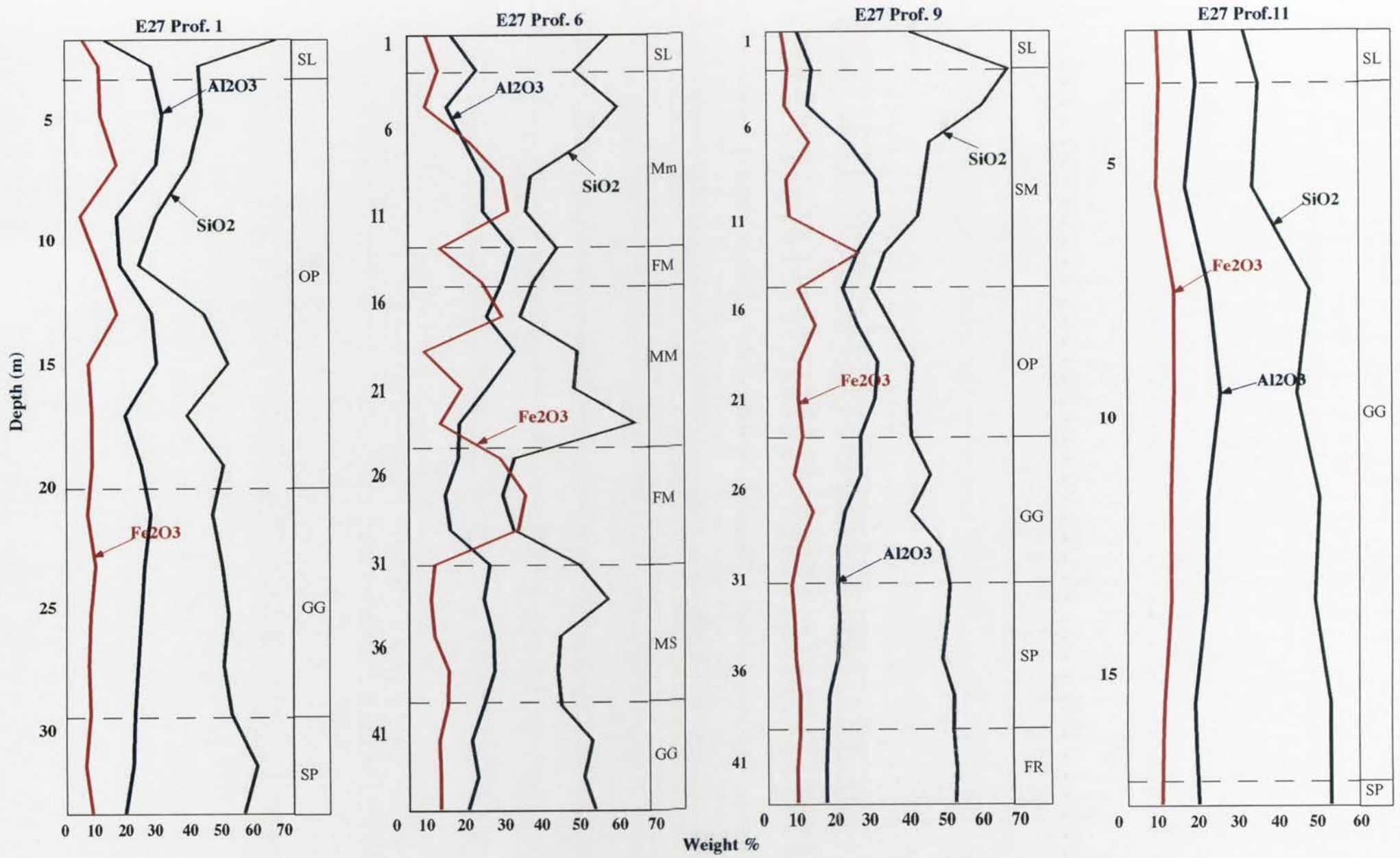

Figures 9.4.3: Plots of depth vs weight % of SiO2, Al2O3 and Fe2O3 of selected profiles from the E27 deposit [SL=Soil horizon; Mm-mini-and-medium mottled clay zone; MM-mega-mottled clay zone; SM-silica aggregates/mottled saprolite; FM-nodular Fe-Mn horizon; MS-mottled saprolite; OP-orange-pink saprolite; GG-greenish-grey saprolite; SP-saprock; FR-fresh rock].

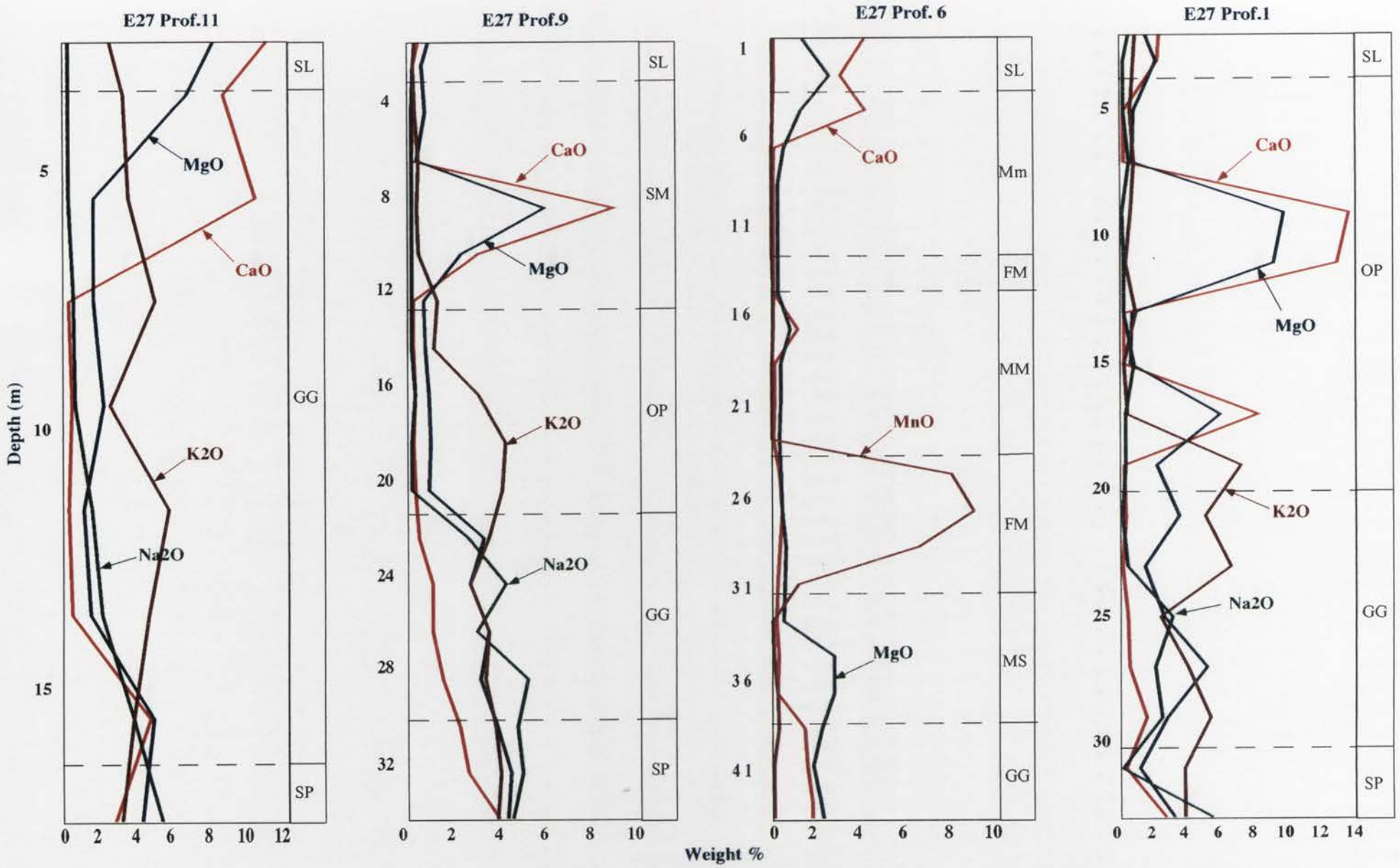

Figures 9.4.4: Plots of depth vs weight % of CaO, MgO, MnO, Na2O and K2O of selected profiles from the E27 deposit [SL=Soil horizon; Mm-Mini-and-medium mottled clay zone; MM-Mega-mottled clay zone; SM-Silica aggregates/mottled saprolite; FM-Nodular Fe-Mn horizon; MS-Mottled saprolite; OP-Orange-Pink saprolite; GG-Greenish-Grey saprolite; SP-Saprock].

sub horizons. These enrichment zones are associated with the occurrence of SiO_2 as detrital quartz fragments in the soil and silica aggregates within the mottled clay. The high concentration in the upper levels of the residual regolith units is mainly a result of residual accumulation as more soluble components are lost during weathering.

Iron

Iron oxide concentrations range from 1.41 to 40.69% with mean values that are higher in the transported regolith (14.31%) as compared to the residual units (8.53%). As anticipated, highest concentrations occur in the mottled clay (10-40%) zone and the nodular iron and manganese horizons corresponding to the high amounts of iron oxide minerals hematite and goethite in these horizons. Appreciable concentrations (~40%) also occur in the greenish-grey saprolite in E22 Profile 4 corresponding to high amounts of nontronite encountered in this zone (Chapter 7, Figure 7.7.2). Moderate concentrations (10-20%) occur in the mottled saprolite.

Aluminium

Aluminium oxide concentrations range from 6.99 to 32.03 % with mean values that are slightly higher in the residual regolith (22.31%) as compared to the transported regolith (21.28%). Highest concentrations (15-30%) occur in the mottled clay zones, mottled saprolite, white clay unit and the greenish-grey and orange-ink saprolite. Lowest concentrations (< 15%) occur in the soil and the nodular iron-manganese horizons. In general, Al_2O_3 displays a more or less uniform spread in concentration values in most of the units as compared to the other major elements. High concentrations correspond to zones of high clay (notably kaolin) contents.

Ternary (triangular) plots showing the compositions of the transported and residual regolith units in terms of SiO_2, Al_2O_3 and Fe_2O_3 are presented in Figures 9.4.5 and 9.4.6. In the transported regolith units, SiO_2 occurs as the major constituent in the soil relative to other elements while higher amounts of Fe_2O_3 occur in the nodular iron and manganese units relative to the mottled clay units. Al_2O_3 is present as kaolinitic clays mainly in the mottled clay units (Figure 9.4.5).

A few iron rich outliers occur in the white clay and mottled saprolite units of the residual regolith (Figure 9.4.6). Unlike in the transported regolith, the samples are clustered predominantly in the SiO_2 region. The plots also show that the greenish-grey saprolite contains more SiO_2 than the orange-pink and mottled saprolite with the Al_2O_3

concentrations showing the inverse relationship. The mottled saprolite as expected contains more Fe_2O_3 than the other units. The white clay unit samples contain similar compositions as those of the orange-pink saprolite.

Calcium

CaO concentrations range from 0.06 to 17.62% with mean values that are higher in the residual regolith (1.73%) as compared to the transported regolith (1.24%). Highest concentrations (10-15%) are encountered in the soil 'B' horizon, the white clay unit, the orange-pink saprolite and the upper levels of the greenish-grey saprolite in the profiles over the trachyandesite in both deposits (i.e profiles 9 and 11). Moderate to high concentrations (5-10 %) occurs in the mottled clay zones especially in the mega-mottled sub-horizon (E22 Profile 4 and E27 Profile 6). These enhanced concentrations correspond to its presence in calcite and dolomite in these units.

Magnesium

Magnesium oxide concentrations range from 0.23 to 12.37% with mean values that are higher in the residual regolith (2.13%) as compared to the transported regolith (0.84%). It shows similar distribution features as CaO in most of the profiles with the exception of a few residual units (e.g. E27 Profile 6) where enhanced concentrations (2-4%) seems to correspond to areas of high amounts (5-10%) of ferromagnesium minerals (diopside and hornblende).

Manganese

Manganese oxide concentrations range from < 0.005 to 8.85% with mean values that are higher in the transported regolith (0.36%) as compared to the residual units (0.21%). Highest concentrations (> 4%) are encountered in the nodular iron-manganese horizons of both E22 and E27 deposits (Profiles 4 and 6 respectively). Moderate to high concentrations (0.5-3%) occur in the mottled clay zone especially in the mega-mottled sub-horizon. The same level of concentrations are also encountered in the mottled saprolite especially in the units located below the nodular horizon. These enhanced concentrations are attributed to infusion with manganese from the overlying units.

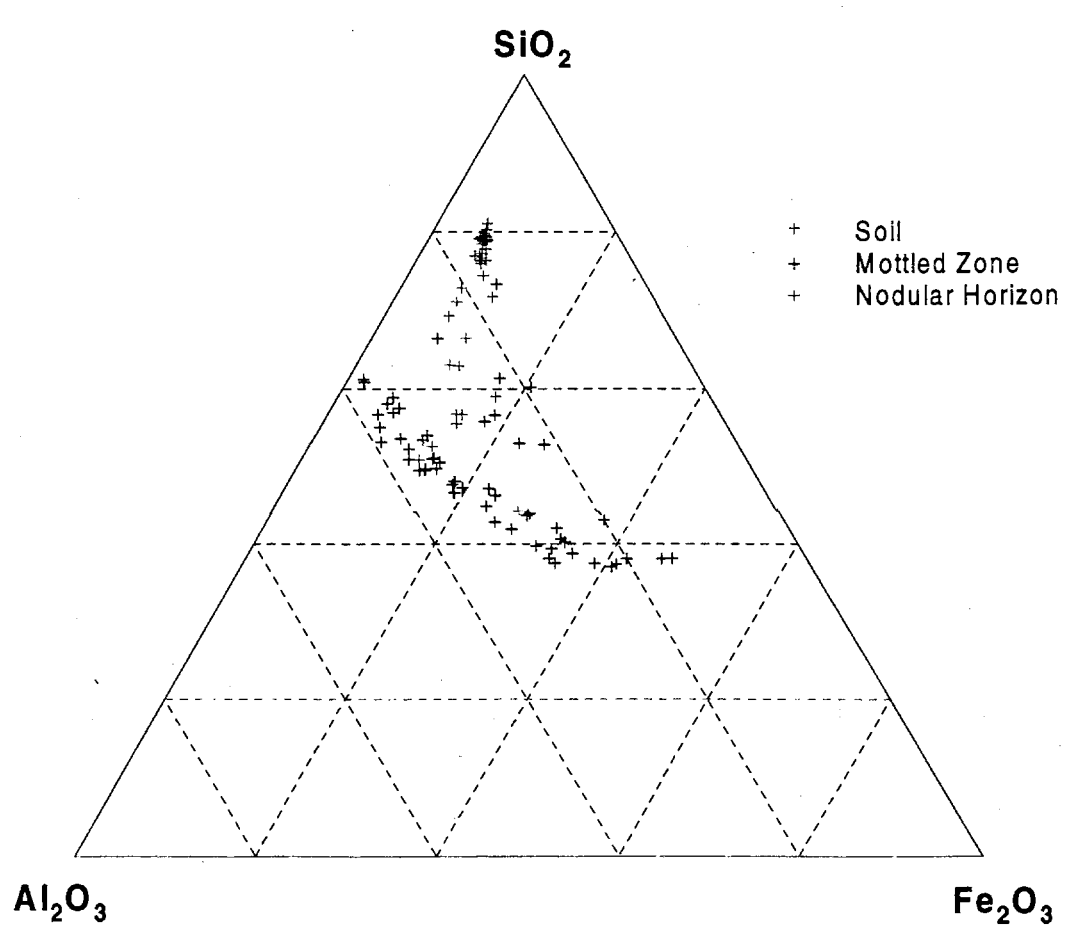

Fig.9.4.5: Ternary plots of the transported regolith in terms of SiO_2, $Al2O_3$ and Fe_2O_3

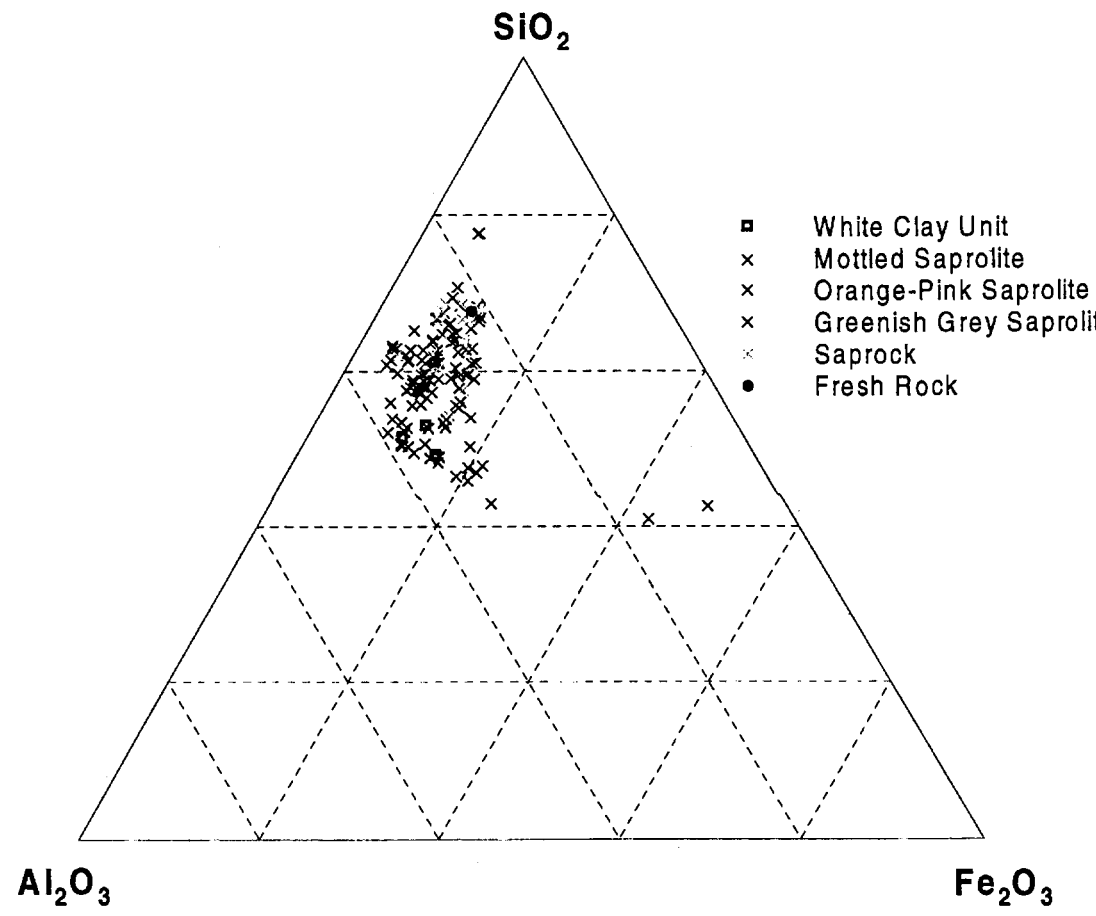

Fig.9.4.6: Ternary plots of the residual regolith in terms of SiO_2, Al_2O_3 and Fe2O3

Potassium

Potassium oxide concentrations range from 0.05 to 7.87% with mean values that are higher in residual regolith (3.06%) as compared to the transported regolith (0.43%). Highest concentrations (> 5%) occur in the orange-pink and greenish-grey saprolite, the saprock and the fresh rock. This corresponds with the high contents of K-containing silicate minerals in these units i.e muscovite and K-feldspars (chapter 7, Figures 7.7).

Sodium

Sodium oxide concentrations range from 0.03 to 5.60% with mean values that are higher in the residual regolith (1.08%) as compared to the transported regolith (0.24%). Highest concentrations (> 5%) occur in the lower parts of the greenish-grey saprolite, the saprock and the fresh rock. No significant enrichment occurs in the orange-pink saprolite showing that the enhanced concentration is associated with the high contents of plagioclase feldspars in these units.

Phosphorus

Phosphorous oxide concentrations range from 0.02 to 0.8% with mean values that are higher in the residual regolith (0.19%) as compared to the transported regolith (0.11%). Highest concentrations (> 0.4%) occur in the lower parts of the greenish-grey saprolite and the saprock and in the nodular iron-manganese horizons. Moderate to high concentrations (0.2-0.4%) occur in the mottled clay zone and the mottled saprolite. This suggests a close association with the iron and manganese oxides and possibly apatite, which was encountered in this zone.

Titanium

Titanium oxide concentrations range from 0.2 to 1.7% with mean values that are higher in the transported regolith (1.07%) as compared to the residual regolith (0.84%). Highest concentrations (> 1%) occur in the soil horizons, the mottled clay zone and the nodular iron-manganese horizon. Moderate to high concentrations (0.5-1%) occur in the upper horizons of the residual units i.e mottled saprolite and the orange-pink saprolite. The distribution in the latter suggests a residual accumulation with progressive weathering. The Ti could also be hosted by anatase, which occurred in appreciable amounts (5-10%) in the mottled clay units and the orange-pink saprolite.

Table 9.4.1 summarizes the distribution patterns of the major elements in the different regolith units from both deposits. This only applies to those zones where there is significant enrichment or depletion of the element.

Table 9.4.1: Summary of zones of enrichment and depletion of the major elements in the regolith profiles [SL-soil horizon; MZ-mottled clay zone; FM-nodular iron manganese horizon; MS-Mottled saprolite; WC-white clay unit; SM-silica aggregates/mottled saprolite; OP-orange-pink saprolite; GG-greenish-grey saprolite; SP-saprock]

Element	**Enrichment zones**	**Depletion zones**
SiO_2	WC, SM, SL, MS, MZ	OP, GG
Al_2O_3	MZ, MS, WC, GG, OP	FM, SM
Fe_2O_3	MZ, FM, GG	OP, WC, SP
CaO	SL, WC, OP, GG	FM, MZ
MgO	SL, WC, OP, GG	FM, MZ
MnO	FM, MZ, MS	SL, GG, SP
Na_2O	GG, SP	SL, MZ, OP, FM
K_2O	OP, GG, SP	SL, MZ, FM
P_2O_5	GG, SP, FM, MZ	OP, SL, WC
TiO_2	SL, MZ, FM	GG, SP, OP

9.4.3 TRACE ELEMENTS

The line plots of the element concentrations versus depth for the selected profiles are presented in Figures 9.4.7 to 9.4.12. Apart from the main target elements in this study i.e Au, Cu, Pb, Zn, Ag and As, the other trace elements were determined from approximately 120 samples. Their behaviour in the weathering profiles have been determined by a combination of distribution statistics, line graphs, mass balance calculations and selective leaching techniques. The main features of the trace element distribution patterns are outlined below:

Gold

Gold concentrations range from < 5 to 870 ppb with mean values that are higher in the residual regolith (78 ppb) as compared to the transported regolith (41 ppb). It exhibits a widespread distribution with most of the horizons containing significant amounts of the element. The highest concentrations (500-800 ppb) occur in the saprock as in E27 Profiles 6 and 9. Moderate to high concentrations occur in the greenish-grey and orange-

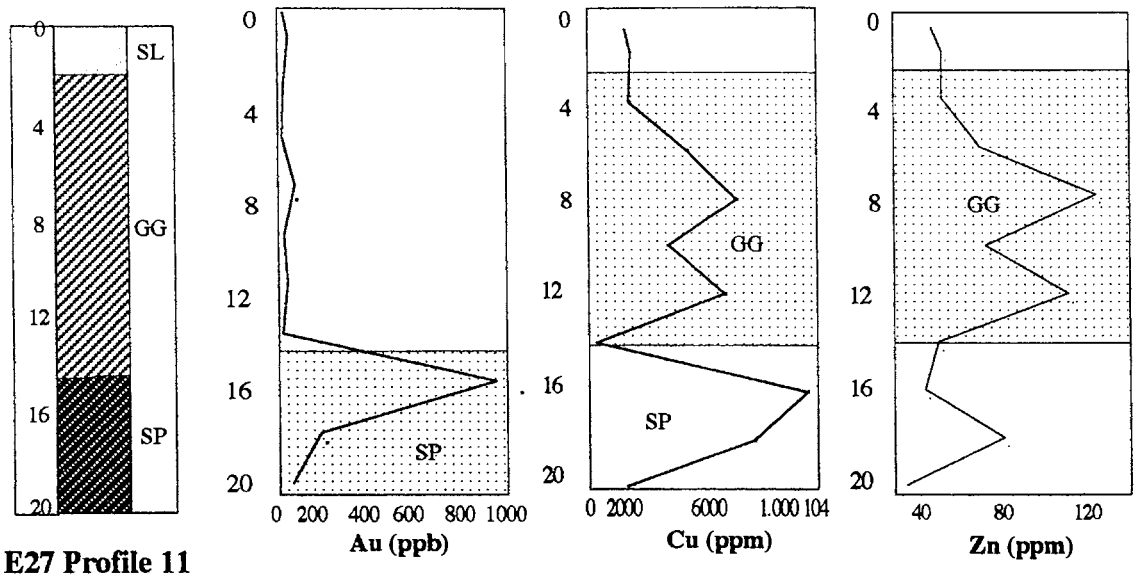

E27 Profile 11

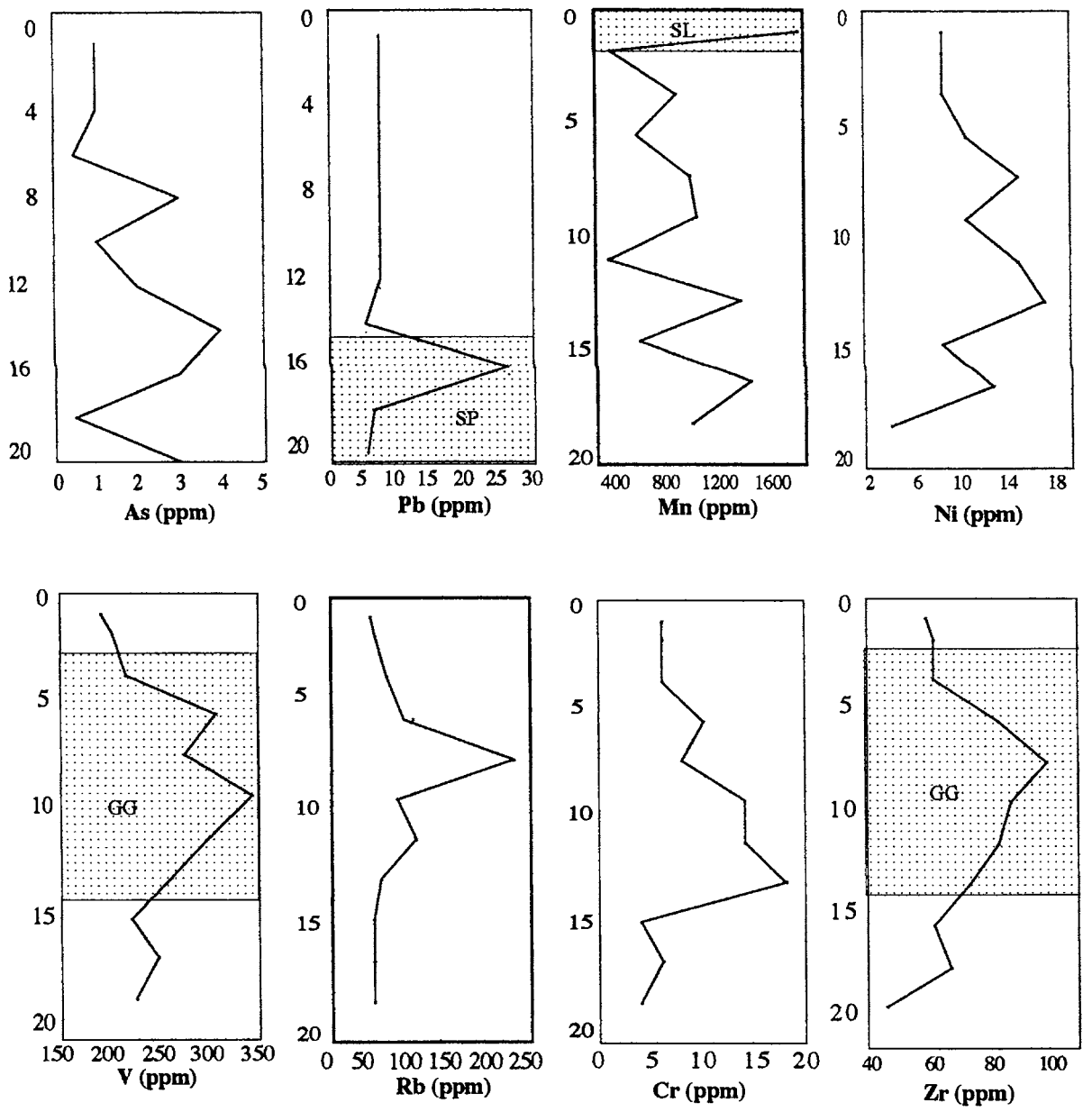

Figure 9.4.7: Line plots of depth vs ppm of selected trace elements from E27 Prof.11.
[SL- Soil horizon; GG-Greenish-Grey saprolite; SP- Saprock]

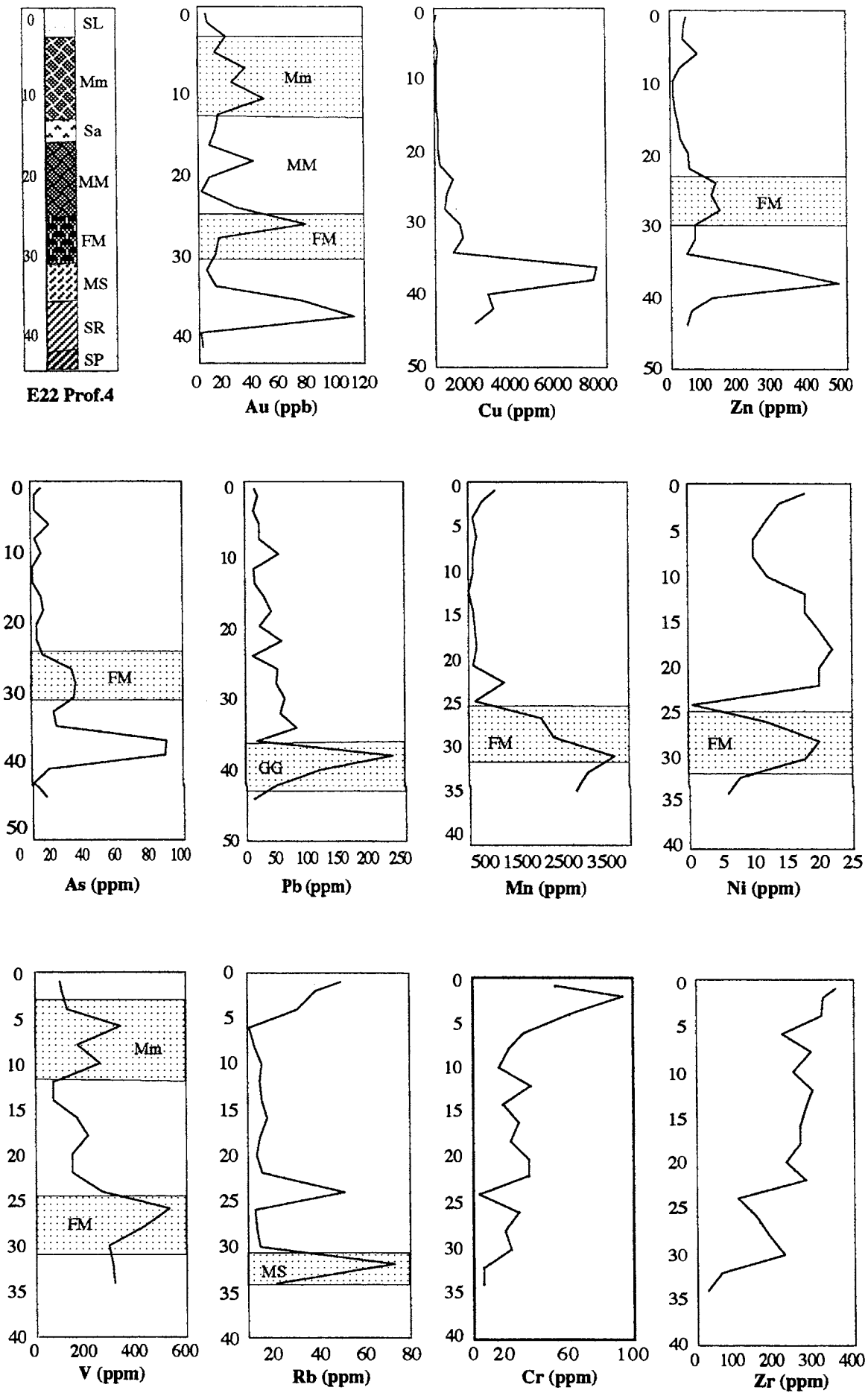

Figure 9.4.8: Line plots of depth vs ppm of selected trace elements from E22 Prof.4. [SL- Soil horizon; Mm- Mini-and-medium-mottled clay; MM-Mega-mottled clay; Sa-Silica aggregates; FM-Iron-manganese nodule zone; MS-mottled saprolite; GG-Greenish-Grey saprlolite; SP- Saprock]

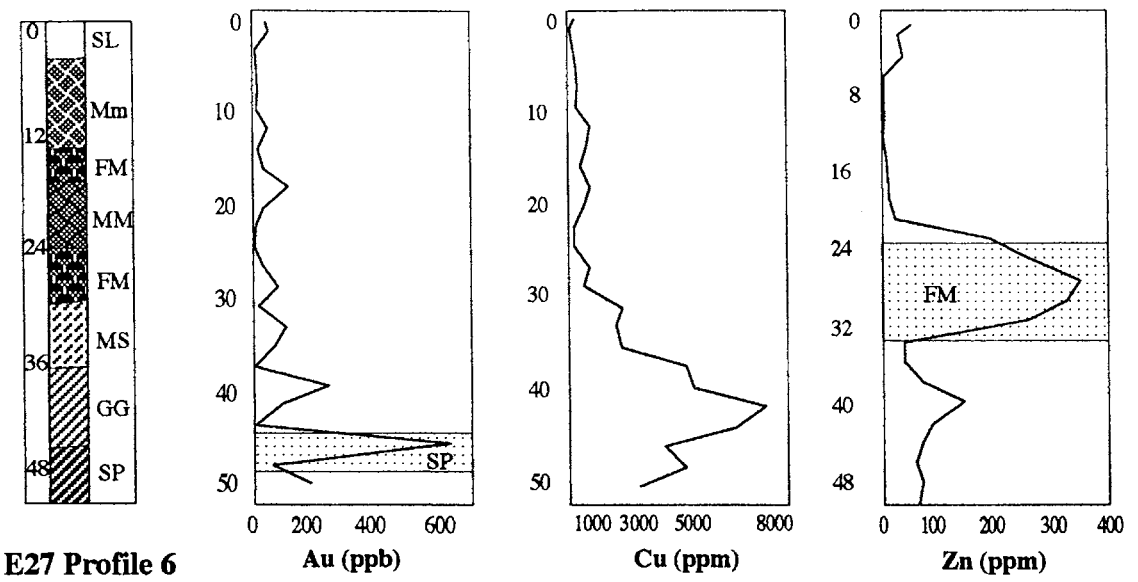

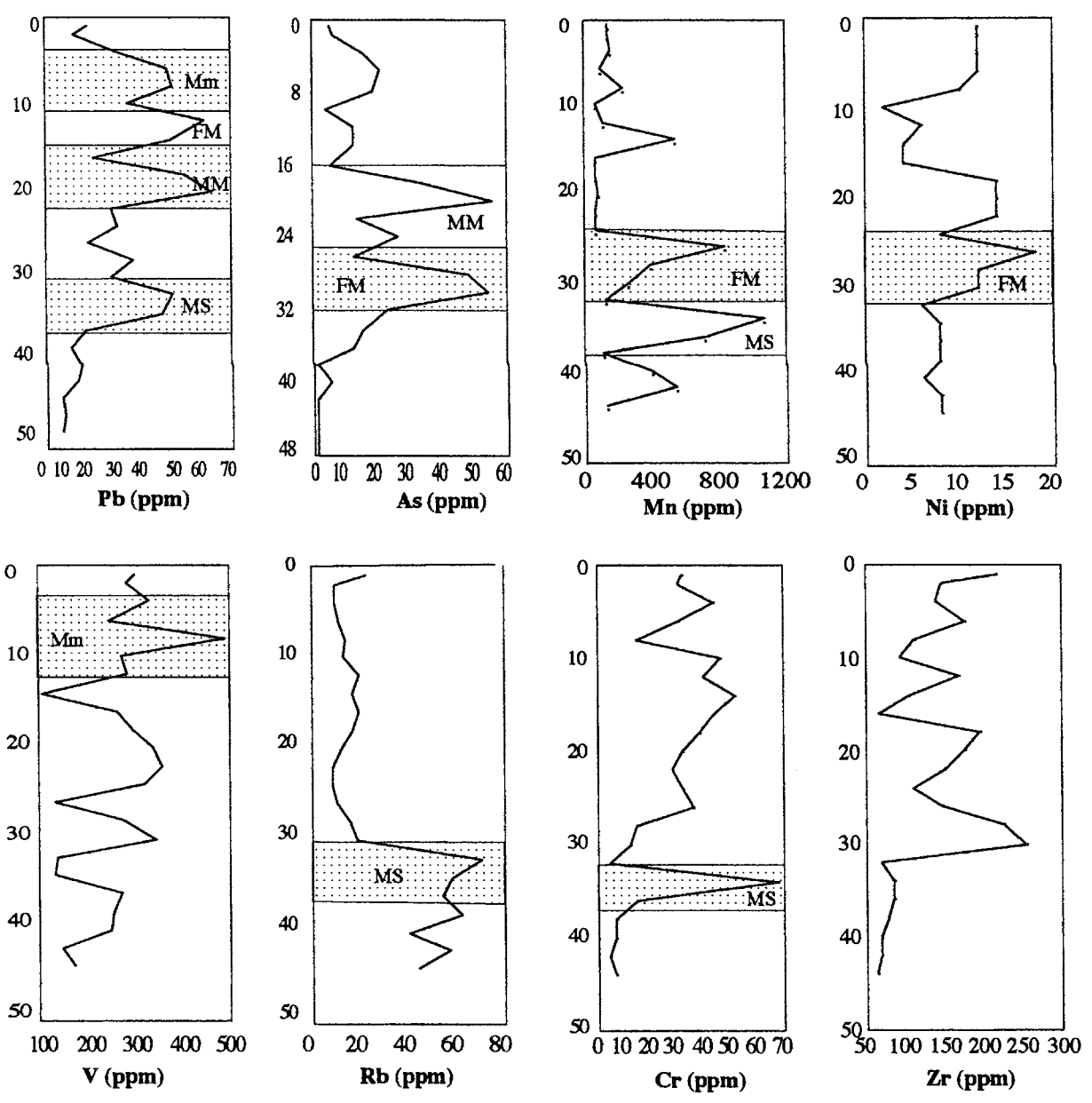

Figure 9.4.9: Line plots of depth vs ppm of selected trace elements from E27 Prof.6. [SL- Soil horizon; Mm- Mini-and-medium-mottled clay; MM-Mega-mottled clay; FM-Iron-manganese nodule zone; MS-mottled saprolite; GG-Greenish-Grey saprlolite; SP- Saprock]

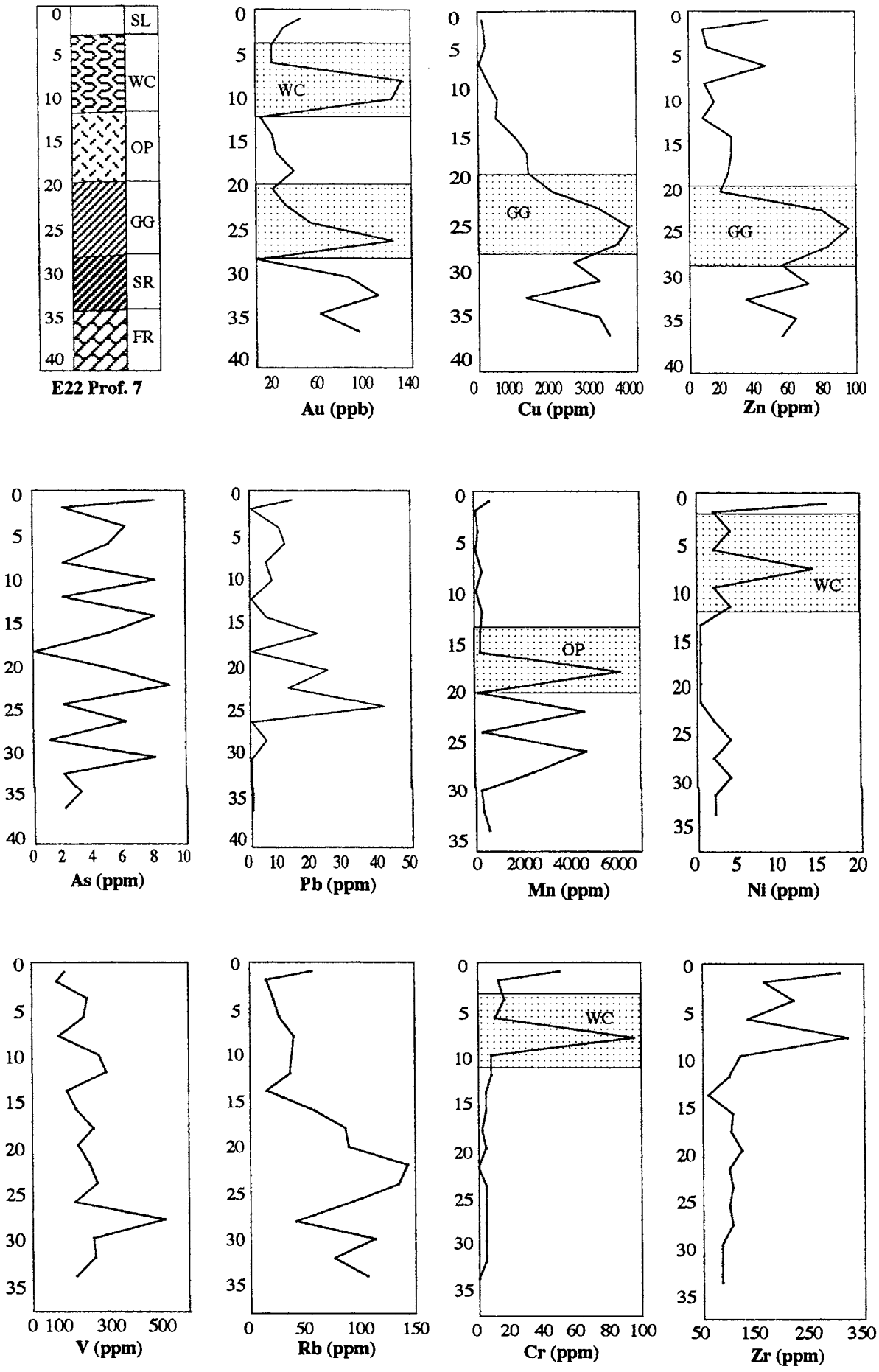

Figure 9.4.10: Line plots of depth vs ppm of selected trace elements from E22 Prof.7.
[SL- Soil horizon; WC-White clay unit; OP-Orange-Pink saprolite; GG-Greenish-Grey saprlolite; SP- Saprock; FR-Fresh rock]

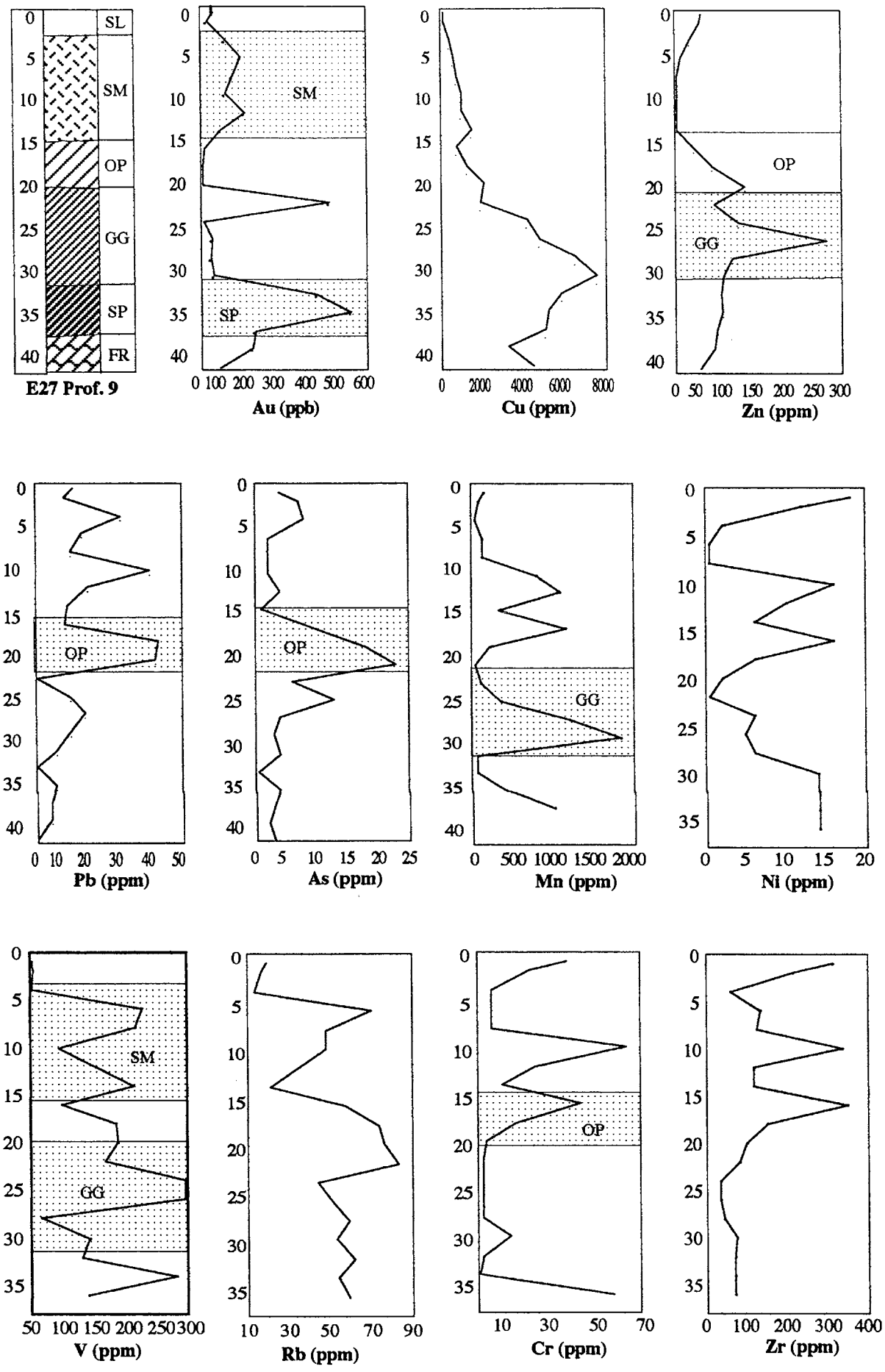

Figure 9.4.11: Line plots of depth vs ppm of selected trace elements from E27 Prof.11. [SL- Soil horizon; SM- Silica aggregates/mottled saprolite; OP-Orange-Pink saprolite; GG-Greenish-Grey saprlolite; SP- Saprock; FR-Fresh rock]

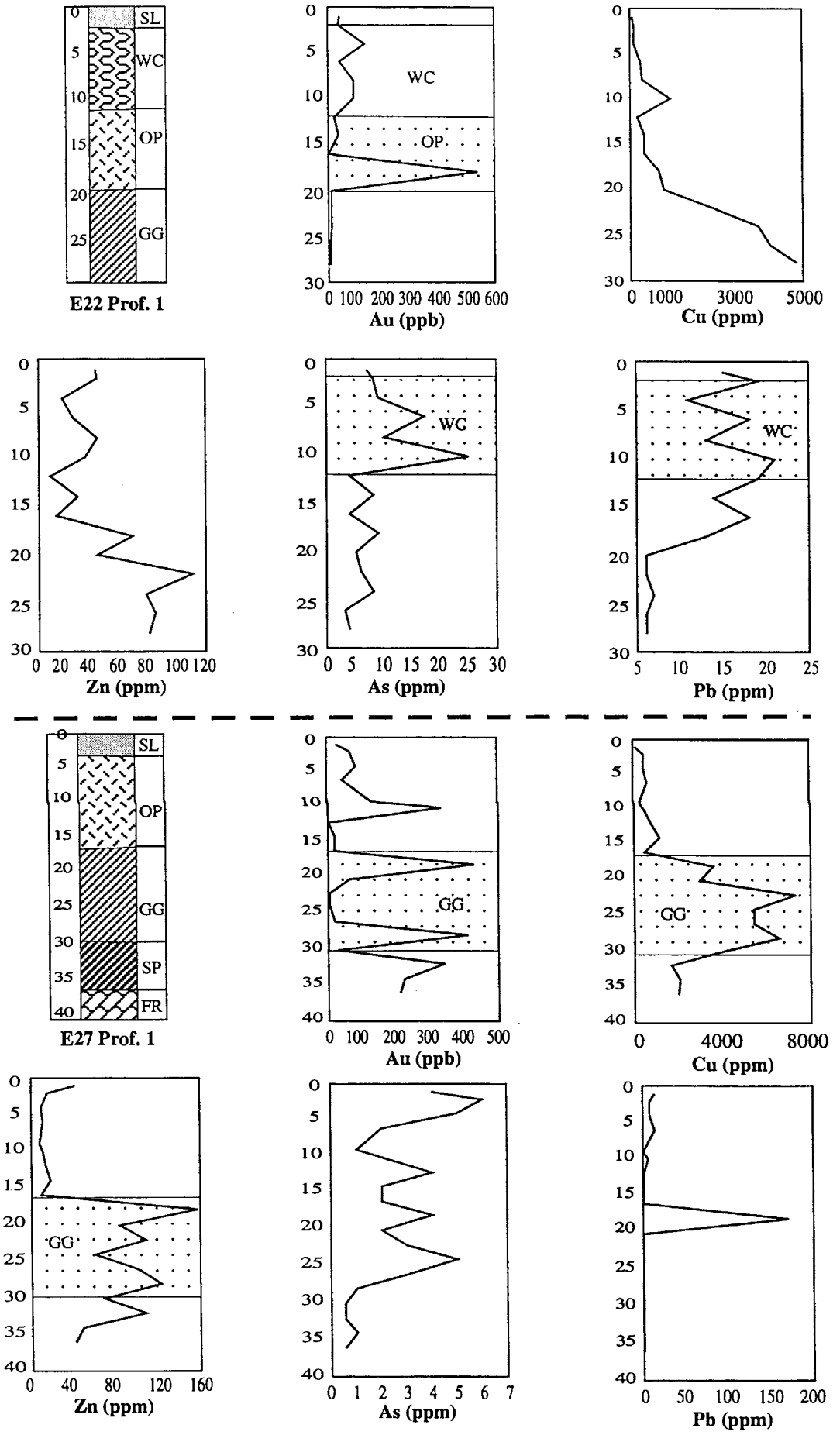

Figure 9.4.12: Line plots of depth vs ppm of selected trace elements from E22 and E27 Profiles 1.
[SL- Soil horizon; WC-White clay unit; OP-Orange-Pink saprolite; GG-Greenish-Grey saprlolite; SP- Saprock; FR-Fresh rock]

pink saprolite (100-500 ppb), the white clay units (E22 Profiles 1 and E22 Profile 7) and the mottled saprolite (100-300 ppb) of E27 Profile 9. Lower but significant concentrations (50-200 ppb) occur in the mottled clay zones and iron-manganese horizons (E22 Profile 4 and E27 Profile 6).

Because of this widespread distribution, no mineralogical associations with the gold can be discerned at this stage.

Copper

Copper concentrations range from 26 to 18400 ppm with mean values that are higher in the residual regolith (1640 ppm) as compared to the transported regolith (379.50 ppm). Most of the high concentrations (> 2000 ppm) occur in the saprock and the greenish-grey saprolite. Moderate amounts (1000-2000 ppm) occur in orange-pink saprolite and in the white clay unit of E22 Profile 1. Enrichment of this magnitude is present within the iron-manganese horizons and the mottled saprolite of both deposits.

The general trend of copper concentration is that of an increase up to the sulphide enriched zones showing that its distribution in the residual units is mainly attributed to mineralization.

Zinc

The distribution of zinc follows the same pattern as that of copper in most of the profiles. The zinc concentrations range from < 0.05 to 479 ppm with mean values that are higher in the residual units (64.72 ppm) as compared to the transported regolith (33.16 ppm). The highest concentrations (> 50 ppm) occur in the saprock, the greenish-grey saprolite and the iron-manganese aggregates. Moderate to high concentrations (20-50 ppm) occur in the white clay units, orange-pink, mottled saprolite and the mottled clay units. The other units have lower concentrations (< 20 ppm) of the element.

The most notable observation in this distribution is the enhanced concentration of Zn in transition from the mottled zone to the iron-manganese units as in E22 Profile 4 (Figure 9.4.8) and E27 Profile 6 (Figure 9.4.9), suggesting a strong association between the element and iron and manganese oxides. This association is discussed in more detail in the next Chapter.

Lead

Lead concentrations range from < 0.05 to 1880 ppm with mean values that are higher in the transported regolith (29.82 ppm) as compared to the residual regolith (27.13 ppm). One sample (sample E27 P3S15) obtained from the sulfide zone of E27 Profile 3 contains an abnormally high concentration of 1880 ppm. Apart from this high value, the other highest concentrations (150-250 ppm) of Pb occur in the greenish-grey saprolite. Moderate to high concentrations (20-150 ppm) occurs in the saprock, white clay units, orange-pink saprolite, mottled clay zones and the nodular iron-manganese zone. The distribution of lead like that of gold is thus widespread although the high concentrations in the mottled clay units and nodular iron-manganese units suggest incorporation into the Fe and Mn oxides. The high values in the sulfide zone and the lower saprolite units also suggest a strong association with the mineralization.

Arsenic

Concentrations of arsenic range from < 0.05 to 89 ppm with mean values that are higher in the transported regolith (12.40 ppm) as compared to the residual regolith (7.91 ppm). The highest concentrations (> 40 ppm) occur in the saprock (E22 Profile 4) and in the nodular iron-manganese horizons. Moderate to high concentrations (15-40 ppm) occur in the mottled clay units, mottled saprolite and the white clay units. Lower concentrations (< 15 ppm) occur in the greenish-grey and orange-pink saprolite units of most of the profiles with the exception of the orange-pink saprolite of E27 Profile 9 (Figure 9.4.10) which has moderate to high concentrations of the element.

The distribution of As suggests an association with mineralization and incorporation into the iron and manganese oxide-rich units in the transported regolith.

Silver

Most of the silver values are below the ICP-MS lower limit of detection i.e 1 ppm. Only two samples from the nodular iron-manganese horizons of E27 Profile 6 and orange-pink saprolite of E22 Profile 7 recorded values of between 1 and 2 ppm.

Manganese

Highest concentrations (> 3500 ppm) of Mn occur in the orange-pink saprolite of E22 Profile 7 and nodular iron-manganese horizon of E22 Profile 4. Moderate to high

concentrations (1000-3500 ppm) occur in the greenish-grey saprolite of some of the profiles (e.g. E27 Profiles 9 and 11) and the mottled saprolite and nodular iron-manganese horizon of E27 Profile 6. The soil samples from E27 Profile 11 (Figure 9.4.9) also recorded values in this range. Slightly lower concentrations (500-100 ppm) occur in the mottled clay units.

The distribution of Mn is related to its occurrence as fracture infills in the saprolite units and in the nodular Fe-Mn aggregates in the transported regolith units.

Nickel

Highest concentrations (> 15 ppm) of nickel occur in the nodular iron-manganese horizon and the greenish-grey saprolite. Moderate to high concentrations (10-15 ppm) occur in the mottled clay units, the white clay unit and the saprock.

The distribution of Ni is very similar to that of As with enrichment in the nodular iron-manganese horizon and the mottled clay zones indicating association the iron and manganese oxides in these zones.

Vanadium

Highest concentrations (> 500 ppm) of V occur in the mottled clay units and the nodular iron-manganese horizons. Moderate to high concentrations occur in the mottled saprolite, the saprock and the greenish-grey saprolite.

V like Ni and As distribution is associated with iron-and-manganese oxide rich portions of the transported regolith.

Rubidium

Apart from some significant enrichment in some of the residual units, rubidium shows similar distribution patterns as As, Ni and V. High concentrations (> 150 ppm) occur in the greenish-grey saprolite of E27 Profile 11, while moderate to high concentrations (50-150 ppm) occur in the mottled saprolite, nodular iron-manganese horizons and the orange-pink saprolite. This widespread distribution precludes the establishment of any mineralogical associations at this stage.

Chromium

In general, the trend in Cr distribution is one of progressive increase towards the soil horizon in most of the profiles. A few exceptions include a sharp enrichment (~60 ppm) in the saprock of E27 Profile 11 and the orange-pink saprolite of E27 Profile 6 (~70 ppm). In most of these profiles the progressive enrichment ranges from 10 ppm in the residual units to approximately 70 to 80 ppm in the top parts of the profiles.

This enrichment seems to represent residual accumulation with progressive weathering and/or association with the iron oxides in the mottled clay units of the transported regolith.

Zirconium

Like Cr, Zr shows enrichment towards the upper parts of most of the profiles. This enrichment is more pronounced in the transported regolith (100-400 ppm) as compared to the residual units (< 100 ppm). The enrichment towards the upper parts of the residual profiles suggests a residual accumulation of Zr as a result of depletion of more soluble components. The high concentrations in the transported regolith may indicate its presence in initial sediment sources.

Niobium and Lanthanum

These elements show similar distribution patterns as Zr in most of the profiles.

Barium

Highest concentrations of Ba (800-1200 ppm) occur in the orange-pink, greenish-grey saprolite and the saprock. The distribution pattern is similar to that of CaO, Sr and MgO within these units suggesting an association with the carbonates, sulfates or the primary silicates associated with these elements i.e plagioclase and ferromagnesium silicates. Some of the Ba is also been present in barite, which was detected in trace amounts in the saprolite.

Thorium

Thorium shows similar distribution patterns as Zr with enrichment occurring towards the soil horizon especially in the transported regolith (6-15 ppm) as compared to the residual

units (4-9 ppm). There is a noticeable strong depletion (< 4 ppm) in the orange-pink saprolite as compared to the other residual units.

Uranium

Uranium concentrations in most of the samples are too low (< 5 ppm) for any distribution patterns to be established.

Strontium

High concentrations (> 600 ppm) occur in the lower portions of the residual regolith mainly in the saprock. Other enrichment zones include the white clay unit, the orange-pink saprolite and the mottled clay zones (100-500 ppm). A strong local depletion (< 100 ppm) occurs in the nodular iron-manganese horizons. It shows similar distribution patterns as CaO, MgO and Ba suggesting associations with the carbonates, sulfates or the primary minerals associated with these elements.

Yttrium

Y distribution is similar to that of Zr with high concentrations (> 20 ppm) of the element occurring towards the upper parts of most of the profiles especially in the residual regolith units. Some local enrichment (40-100 ppm) occurs in the mottled saprolite and greenish-grey saprolite of some of the profiles for example E27 Profiles 9 and 11.

Cerium

Ce shows similar distribution patterns as Sr, CaO and MgO with high concentrations of the element (> 60 ppm) occurring in the soil horizon, mottled clay zones, white clay unit and the orange-pink saprolite.

Scandium

Sc concentrations are widespread with values that range from 10 to 40 ppm in most of the samples. Local enrichment (> 25 ppm) occurs in the mottled clay zones and the lower portions of the greenish-grey saprolite and the saprock in some of the profiles (e.g. E27 Profile 11). This widespread distribution precludes establishment of any mineralogical associations.

Table 9.4.2 provides a summary of the zones of enrichment and depletion of the trace elements in the regolith profiles. This only applies to the units where there has been significant enrichment or depletion of the element.

Table 9.4.2: Summary of zones of enrichment and depletion of the trace elements in the regolith profiles [SL-soil horizon; MZ-mottled clay zone; FM-nodular iron manganese horizon; MS-mottled saprolite; WC-white clay unit; OP-orange-pink saprolite; GG-greenish-grey saprolite; SP-saprock]

Element	Enrichment zones	Depletion zones
Au	SP, GG, OP, WC, MS	-
Cu	SP, GG, OP, WC	MZ, FM
Pb	GG, MZ, FM	SL
Zn	SP, GG, FM	-
As	SP, FM, MZ, MS	GG, OP
Ni	FM, GG, MZ, SP	-
Mn	FM, OP, GG	-
V	FM, MZ, MS	OP, SL
Rb	GG, MS, FM, OP	-
Cr	SP, OP, SL	-
Zr	SL, MZ	OP, GG
Nb	SL, MZ	SP, OP, GG
La	SL, MZ	SP, OP, GG
Y	SL, MZ, GG	SP, OP
Sr	SL, SP, WC, OP, MZ	FM
Ce	SL, MZ, WC, OP, GG	FM
Th	SL, MZ	OP
Sc	MZ, GG, SP	-
Ag	FM, OP	SL, GG, OP

9.5 THE STUDY OF ELEMENT DEPLETION AND ENRICHMENT IN THE REGOLITH PROFILES USING MASS BALANCE TECHNIQUES.

9.5.1 Appraisal of commonly used mass balance techniques

The chemical changes effected during weathering and regolith formation are vital to the understanding of element mobility in surficial environments, and hence in geochemical exploration (Butt & Zeegers, 1992) and to infer paleoclimate and weathering rates (Nesbitt & Young, 1982; Kirkwood & Nesbitt, 1991).

Numerous methods have been utilized to model chemical changes involved in rock weathering, and these include weathering indices (Reiche, 1943; Ruxton, 1968; Parker, 1970; Nesbitt & Young, 1982; Harnois, 1988; Chittleborough, 1991), the standard cell method (Barth, 1948), reference to an immobile element (Esson, 1983; Cramer & Nesbitt, 1983), the assumption of volumetric weathering (Millot & Bonifas, 1955;

Gardner et al. 1978) and the mass balance approach (Brimhall & Dietrich, 1987; Brimhall et al. 1991).

The existence of numerous weathering indices itself stands as evidence that no one index has appealed to workers or has been found suitable to describe chemical changes in weathering profiles. Additionally, certain assumptions made in the indices may not be valid in many weathering profiles (Chittleborough, 1991). He noted that most of the weathering indices assumed that Al was immobile during weathering, which is not necessarily true because under certain conditions common in soil zones (pH~ 4.5 and presence of organic acid), Al is susceptible to migration, and additionally, secondary Al phases (clays) are vulnerable to lateral and vertical movements in profiles. These effects may produce erroneous results if elements such as Al are assumed immobile.

Chittleborough (1991), also proposed a new index, which incorporated an element corresponding to the heavy mineral present in the rock e.g. ZrO_2 for zircon, boron for tourmaline and Ti for rutile. This index is similar to the constant element method (immobile element) which involves measuring variances of elements with respect to certain element (Zr, Ti, Al) which is assumed constant (Colman, 1982; Esson, 1983; Cramer & Nesbitt, 1983). In contrast, the Chemical Index of Alteration of Nesbitt & Young (1984) compares Al_2O_3 to alkali ratios of the parent and weathered samples.

The isovolumetric method on the other hand assumes that the unit volume of weathered rock evolves from an equal volume of fresh rock. This method employs element concentration with bulk density and has been used to model chemical changes at the early stages of weathering (Gardner et al. 1978; Colman, 1982; Eggleton et al. 1987). This method is useful only if the parent rock or source material texture is preserved in the weathered sample subjected to analysis; if the parent rock fabric is destroyed, the method is not useful. The other commonly used methods attributed Holzhauer (1985), Gardner (1980), Brimhall & Dietrich (1987), Brimhall et al. (1991), Chadwick et al. (1990) considers the mass balance approach to the study of element mobility in weathering profiles by providing relations between chemical (element concentration), volume and mechanical (deformation) properties that are likely to experience change in the progress of weathering.

The use of bulk density to determine element mobility in this study proved to be unsuitable because of the effects of mineralization which caused geochemical heterogeneity and partial to total loss of rock fabric irrespective of weathering. Thus a method had to be identified which took into account geochemical variations in the

unweathered and weathered rocks. The requirement that the parent rock characteristics had to be known discounts the use of any of these mass balance techniques in the study of transported regolith materials. Consequently the method used should serve to supplement the results of other methods utilized in this study notably the depth as a function of weathering technique and selective leaching techniques.

9.5.2 GRAPHICAL ISOCON METHOD

First Principles

Gresens (1967) compared the chemistry and specific gravity data for a group of metasomatized rocks with equivalent data for their unaltered protolith, and was able to develop mass balance equations to describe the composition-volume relationships he observed. Subsequently, Gresen's equation was modified by Grant (1986), who endeavoured to simplify interpretation of compositional changes during alteration, by presenting them graphically.

These graphical representations of the compositional data are termed 'isocon diagrams' and they enable element mobility pathways in altered rocks, to be traced. Elemental mass changes due to alteration, can be calculated relative to a unit mass of unaltered rock. Such mass balance calculations (Gresens, 1967) derived from graphical interpretations (Grant, 1986), provide a means of qualitative and quantitative evaluation of changes in rock chemistry during alteration.

If the chemical data for an unweathered rock are plotted on both axes of a graph, the resulting line will be a 1:1 line (Figure 9.5.1). As the rock weathers the element concentrations change and a new plot can be drawn where the chemical data for the weathered rock can be plotted versus the original fresh rock data (Figure 9.5.2). If an element remains immobile during weathering, the removal of other elements will cause it to be residually enriched. Hence, the ratio of the concentration of immobile element in the weathered rock to the concentration of immobile element in the fresh rock is no longer 1:1, and the data points for the immobile element will now plot above the 1:1 line (Figure 9.5.2).

The key to the isocon technique lies in these characteristics: all inferred immobile elements present in a rock during weathering will become residually concentrated in the same ratio. The assumption here is that all immobile elements are equally immobile which may not be the case in real situations. When scaled chemical data for weathered

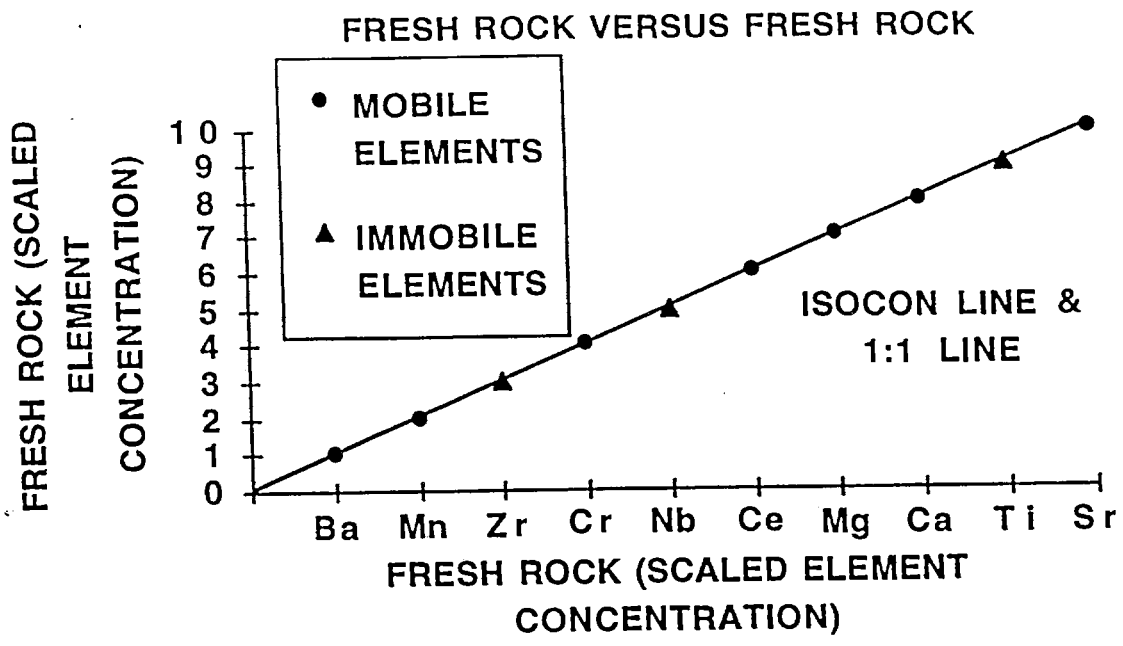

Figure 9.5.1: For a plot of fresh rock versus fresh rock, both the mobile and immobile elements lie on the 1:1 line which is also the isocon line.

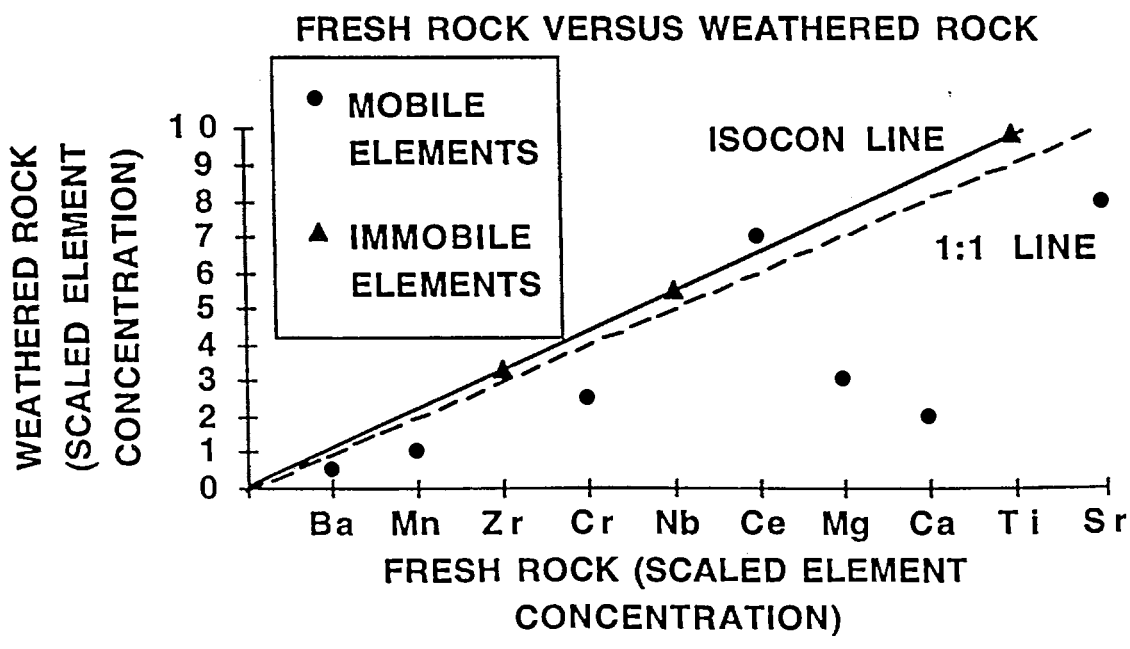

Figure 9.5.2: For a plot of fresh rock versus weathered rock, mobile elements lie above or below the isocon line. The isocon line plots through the immobile elements and is displaced from the 1:1 of fresh rock.

rocks are plotted versus similarly scaled data for unweathered protolith, relatively immobile elements plot on a straight line through the origin. The elements which lie on this line have equal (weathered rock/fresh rock) chemical concentration ratios. This line is called the isocon line.

9.5.3 Presentation of geochemical data on the isocon diagram

The major drawback when plotting geochemical concentration data for major and trace elements graphically is that many points overlap. The graphical isocon method (Grant, 1986) has been modified by Huston (1993), who recommends a scaling technique which allows clearer presentation of the graphical data. The location of any data point on the isocon is defined by the ratio:

$$C^W/C^O$$

where C^W is the concentration of an element in the weathered sample and C^O is the concentration of the same sample in fresh andesite (least weathered equivalent). If this relationship is multiplied by any number (n), the ratio remains the same.

C^W/C^O is equivalent to $(C^W/C^O).n$

Graphically, the line that plots through the origin and the point represented by the ratio: C^W/C^O is the same line that plots through the origin and the point represented by:

$(C^W/C^O).n$. Data points can therefore be scaled in such a way that they are more clearly represented on the graphical isocon plot.

In this study, elements have been allocated a position from 1 to 23 on the *x-axis* of the isocon plot (Table 9.5.1). The ratio for each element is multiplied by a factor n that allows the scaled element concentration value on the x-axis to be the same as the order number it has been assigned. The elements can be presented in any order, however, elements that are likely to show large variations with weathering cannot be assigned large factors (n values), otherwise the diagrams will become too large to work with easily (Moore, 1996). In addition, for isocon construction, it is useful to distribute the elements that are most likely to be immobile, at a regular interval across the diagram.

Table 9.5.1: Element positions allocated for isocon diagrams in this study

1	2	3	4	5	6	7	8	9	10	11	12
S	Pb	Ba	La	Fe_2O_3	Ce	Y	Cu	Zn	Nb	MgO	V
13	14	15	16	17	18	19	20	21	22	23	
MnO	SiO_2	Zr	K_2O	Na_2O	P_2O_5	Rb	Al_2O_3	CaO	Sr	TiO_2	

9.5.4 Application of the isocon technique

Net mass loss/gain for a sample

The steepness of the isocon line gives an indication of the degree of mass loss/gain of the rock as a result of weathering. If the slope of the isocon is steep, that is above the 1:1 fresh rock analysis line, then there has been a mass loss (Figure 9.5.3a). This is because most of the other elements have been removed from the rock and the immobile elements are residually enriched. If the isocon line lies below the 1:1 line of fresh andesite then there has been a mass gain (Figure 9.5.3b). In this case many other elements have been enriched with respect to the immobile elements because of secondary precipitation of phases within the weathering rock.

The slope of the isocon (m) can be determined using the relationship:

$$m = C_i^W/C_i^O.$$

where C_i^W is the concentration of immobile element in the weathered sample and C_i^O the concentration of immobile element in the least weathered equivalent.

Net mass change (ΔM) for samples can be estimated from the isocon using the equation:

$$\Delta M\ (\%) = 100\ ((1/m)-1).$$

Elemental mass changes

Data points falling on the fields above and beneath the isocon represent elemental mass gains and losses respectively (Figure 9.5.4a). That is any element that is enriched with respect to the immobile elements lies below the isocon line.

Elemental mass changes (ΔM_e) are calculated according to the equation:

$$\Delta Me\ (\%) = 100\ ((C_e^W/m.C_e^O)-1).$$

where C_e^W is the concentration of an element in the weathered sample, C_e^O is the concentration of that element in the least weathered equivalent, and m is the calculated slope of the isocon.

9.5.5 Interpretation of isocon plots

1. If the slope of the isocon is steep, that is, above the 1:1 fresh rock analysis line, then there has been a mass loss for that sample. If the isocon lies below the 1:1 line of fresh andesite, then there has been a mass gain for that sample (Figures 9.5.3 a and 9.5.3 b).

2 If there has been a net mass gain, the ΔM (%) value will be positive for that sample. If there has been a mass loss, the ΔM (%) value will be negative for that sample.

3. When the isocon diagrams for a single profile are stacked one on top of the other, the change in slope of the isocon gives an 'at a glance' indication of the pattern of weathering. For example: if the slope of the isocon lines are progressively steeper from one isocon plot to the next, up-profile, then the profile is becoming increasingly more weathered. Each fresh rock/weathered rock pair can be compared with others from the profile and stepwise changes in degree of weathering within the sequence can be examined.

4. Data points falling in the field above the isocon line represent elemental mass gains $+\Delta M_e$ (%). Data points falling in the field beneath the isocon line represent elemental mass losses $-\Delta M_e$ (%) (Figure 9.5.4a).

5. Elemental mass changes can be plotted on a histogram where losses plot in the negative direction and gains plot in the positive direction, enabling an 'at a glance' assessment of gains or losses for any elements analysed (Figure 9.5.4b).

6. When the histograms showing the relative elemental change, for a single profile, are stacked one on top of the other, detailed changes in element concentration within the profile can be observed. Each fresh rock/weathered rock pair can be compared with

others from the profile and stepwise changes in chemistry within the sequence can be examined.

A convention has been formulated for this study to describe the degree to which an element has been depleted or enriched, based on the relative mass change histograms for the elements analyzed: on or near the isocon (± 0-5% relative mass change), slight depletion/enrichment (5-30% relative mass change), moderate depletion/enrichment (30-60% relative mass change), strong depletion/enrichment (60-90% relative mass change), extreme depletion/enrichment (>90% relative mass change).

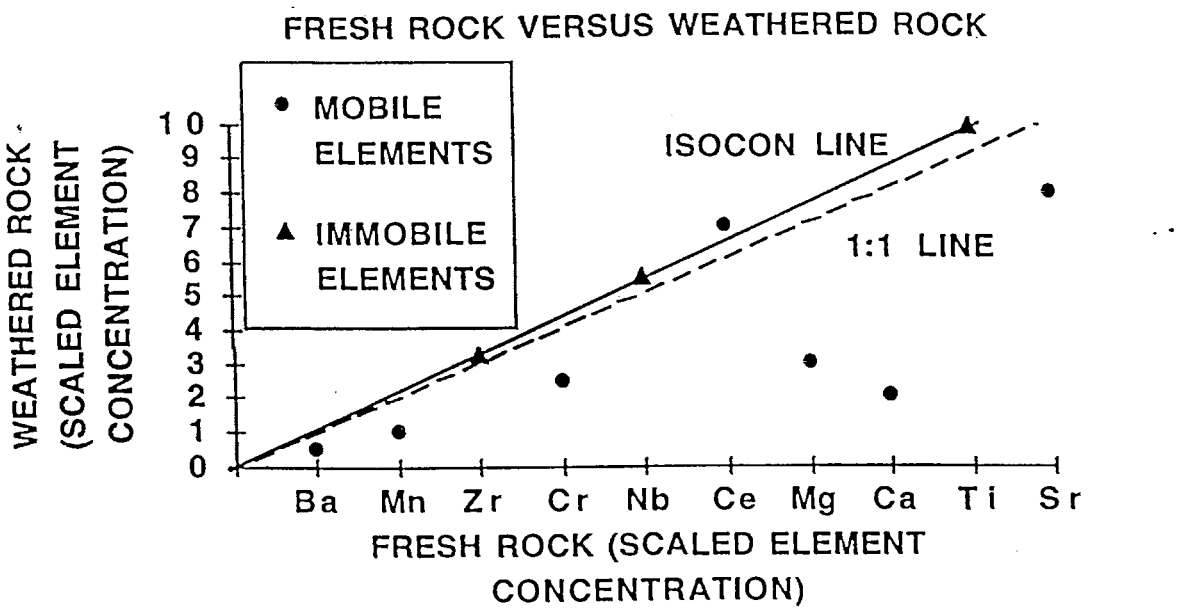

Figure 9.5.4a: The isocon line fresh versus weathered weathered rock scaled concentrations. Mobile elements that lie above the isocon line are enriched in the sample. Mobile elements that lie below the isocon line are depleted from the sample.

Once elemental changes mass changes are calculated, they can be plotted on a histogram, which enables 'at a glance' assessment of gains or losses for any elements analyzed (Figure 9.5.4b).

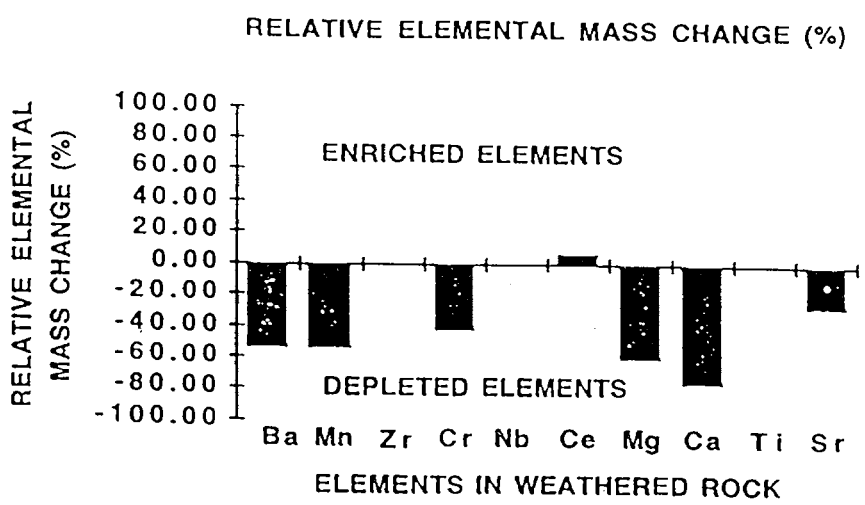

Figure 9.5.4b: Histogram showing the relative elemental mass changes. Mobile elements that have a relative mass gain have positive values on the histogram. Mobile elements that have a relative mass loss have negative values on the histogram. Immobile elements show zero relative mass change.

Selection of immobile elements

The isocon is defined by elements that are considered relatively immobile during weathering. In a study of changes in chemistry during basalt weathering, Eggleton et al. (1987) stated that Ti, V, Cr, Fe, Ni, Zr and Nb are essentially immobile as weathering proceeds. Al and Ti and some trace elements such as Y, Zr and Nb (Grant 1986; Glazner & Bartley, 1991; Tobisch et al. 1991; Marquer & Burkhard, 1992; Prochaska et al. 1992 and Streit 1994), are commonly assumed to have low mobility. In addition, many weathering indices rely on the assumption that Al (Harnois, 1988; Nesbitt & Young; 1982, Reiche, 1943; Vogel, 1975; Vogt, 1927; Roaldset, 1943; Ruxton, 1968), Nb (Price et al. 1991) and Zr, B, Y and Ti (Chittleborough, 1991) remain relatively immobile during weathering.

Specific empirical studies have also confirmed the relative immobility of groups of elements such as Al and Zr (Selverstone et al. 1991; Macquer & Burkhard, 1992), or Ti, Zr, Y, P (O'Hara, 1988; Marker & Burkhard, 1992) during alteration. However, other studies also indicated the mobility of Al (Ohara, 1988; Brimhall, 1988; Chittleborough,

1991), Ti (Serlverstone et al., 1991; Van Baalen, 1993) and Zr (Brimhall, 1992; Hutson, 1993).

For this study, isocons are constrained by a combination of two or more of Al, Ti, Zr, Y and Nb as these have been observed to be the elements most resistant to weathering in the regolith samples. It was found unsuitable to use Fe as one of the indices because the oxidation state, given by Fe^{2+}/Fe^{3+} was found to be closely associated with the mineralizing elements.

Selection of least weathered equivalents

A number of fresh rock samples were submitted for determination of the geochemistry so as to enable its use as least weathered equivalents. Where more than one analysis was available, the data was averaged as per Huston (1993).

9.5.6 Isocon method versus the other weathering indices

With the exception of Parker (1970) index and Herbillon's (1989) total reserve in bases (TRB) index, which both rely on calculating the balance of the major cations (Ca, Mg, Na and K) remaining in a weathered rock, most commonly used weathering indices assume Al to be immobile during weathering (Vogt, 1927; Reiche, 1943; Roaldset, 1943; Ruxton, 1968; Vogel, 1975; Nesbitt & Young, 1982 and Harnois, 1988), and make an evaluation of major cation depletion relative to Al. Chittleborough (1991) discussed the potential mobility of Al as a result of eluviation in weathering profiles and presented an alternative index which compares the cations Ca, Mg and Na with a single element, Zr, Y, B or Ti, believed to be immobile in the 20-90 μm fraction of the soil being studied.

In almost all cases, these weathering indices rely on the comparison of mobile elements versus a single relatively immobile element. However, it is often difficult to assess how immobile the index element really has been during the chemical and physical processes of weathering, as in the example above where Al concentration was affected by eluviation in Chittleborough's (1991) profiles. One solution to this problem lies in making the comparison relative to more than one more immobile element (Moore, 1996). This provides an internal check as all index elements must occur in the same ratio (weathered rock/unweathered rock) as each other to be truly considered immobile.

For this reason, the isocon method (Gresens, 1967; Grant, 1986; Huston, 1993 and Moore, 1996) appears the most reliable comparative method for evaluation of degree of

weathering, because at least two, and usually four or five immobile elements are used to define the isocon. If any elements do not have the same ratio of concentrations as the immobile index elements, then they have been mobilized during weathering, and they will no longer plot on the isocon.

9.5.7 RESULTS

Four representative profiles have been selected in this study. They include E22 Profiles 2 and 8 and E27 Profiles 8 and 11. Profiles 2 and 8 are sited over both transported and residual regolith units while profile 11 is sited over the trachyandesite and profile 7 over the white clay unit and the orange-pink and greenish-grey saprolite. As mentioned earlier on, the requirement that the chemistry of the parent rock had to be known was central to the success of the method, and hence this study has been carried out entirely on the residual regolith units.

The diagrammatic representations of the regolith units have been followed by description of the element depletion/gains in each profile. The use of the terms lower, middle and upper saprolite relates to the positions of the samples in the regolith i.e they are not formally defined terms. The factors responsible for these distribution patterns are presented in section 9.5.8.

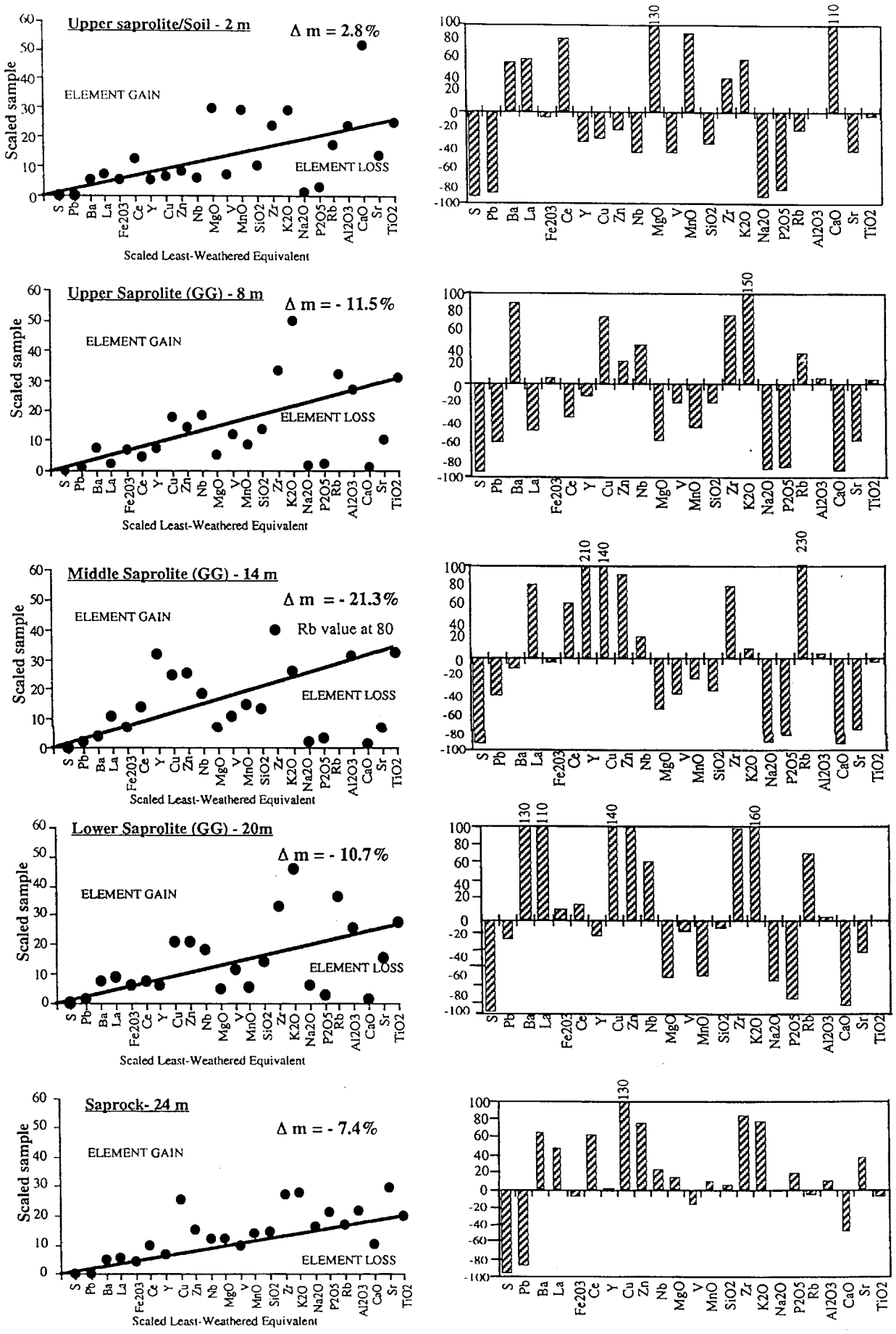

Figure 9.5.5b: Isocon diagrams and corresponding histograms for selected samples from E27 Profile 11 (GG-greenish-grey saprolite)

Figure 9.5.6b: Isocon diagrams and corresponding histograms for selected samples from E22 Profile 7 (GG-greenish-grey saprolite; OP- orange-pink saprolite)

The slopes (C_i^W/C_i^O) of the isocon lines shows variable distribution patterns in each unit of the profile. There is mass loss in most of the units of the profile except in the soil 'B' horizon where there is a mass gain.

Soil 'B' horizon	C_i^W/C_i^O =1.03	Δ m= + 8.69%
White clay unit	C_i^W/C_i^O =1.21	Δ m= - 8.26%
Upper saprolite (OP)	C_i^W/C_i^O =1.31	Δ m= - 10.7%
Middle saprolite (OP)	C_i^W/C_i^O =1.19	Δ m= - 12.91%
Middle saprolite (OP/GG)	C_i^W/C_i^O =1.12	Δ m= - 17.4%
Middle saprolite (GG)	C_i^W/C_i^O =1.09	Δ m= - 16.0%
Lower saprolite (GG)	C_i^W/C_i^O =0.92	Δ m= - 23.7%

The elements show different distribution patterns in each of the regolith units. Zirconium is the only element that shows progressive enrichment towards the upper parts of the profile. Strontium, MnO, V and Na_2O show depletion in all the units of the profile. Generally, these elements shows moderate depletion in concentration values towards the white clay units. Apart from a slight enrichment in the lower saprolite, P_2O_5 shows progressive depletion towards the soil horizon.

Copper, Zn, K_2O, and Rb show enrichment in the greenish-grey saprolite. Cu and Zn start getting depleted at the lower levels of the orange-pink saprolite while Rb and K_2O persist up to the upper saprolite where they are progressively depleted. Apart from a slight depletion at the lower levels of the middle saprolite (at depth of 24 m), Pb shows progressive enrichment towards the soil horizon, the pattern disrupted by a high anomalous enrichment at the middle saprolite (at a depth of 20m). S shows progressive depletion towards the soil horizon the pattern like for Pb disrupted by a slight enrichment in the contact zone between the orange-pink saprolite and the greenish-grey saprolite at depth of 16 m. This seems to represent progressive oxidation of the sulfides towards the upper saprolite. High enrichment occurs in the soil 'B' horizon mainly attributed to the presence of gypsum.

Calcium oxide, MgO, Fe_2O_3 and Ce show progressive depletion up to the upper saprolite where they become progressively enriched towards the soil. This is mainly attributed to input from the carbonates and iron oxides in these units. Some iron nodules (10-20 mm) in size were present in these units partly explaining the increase in Fe_2O_3 concentrations. Si on the other hand shows slight depletion towards the soil horizon. No general distribution patterns for Ba, Y, La was discerned although Ba was progressively depleted and La enriched from the upper saprolite to the soil 'B' horizon.

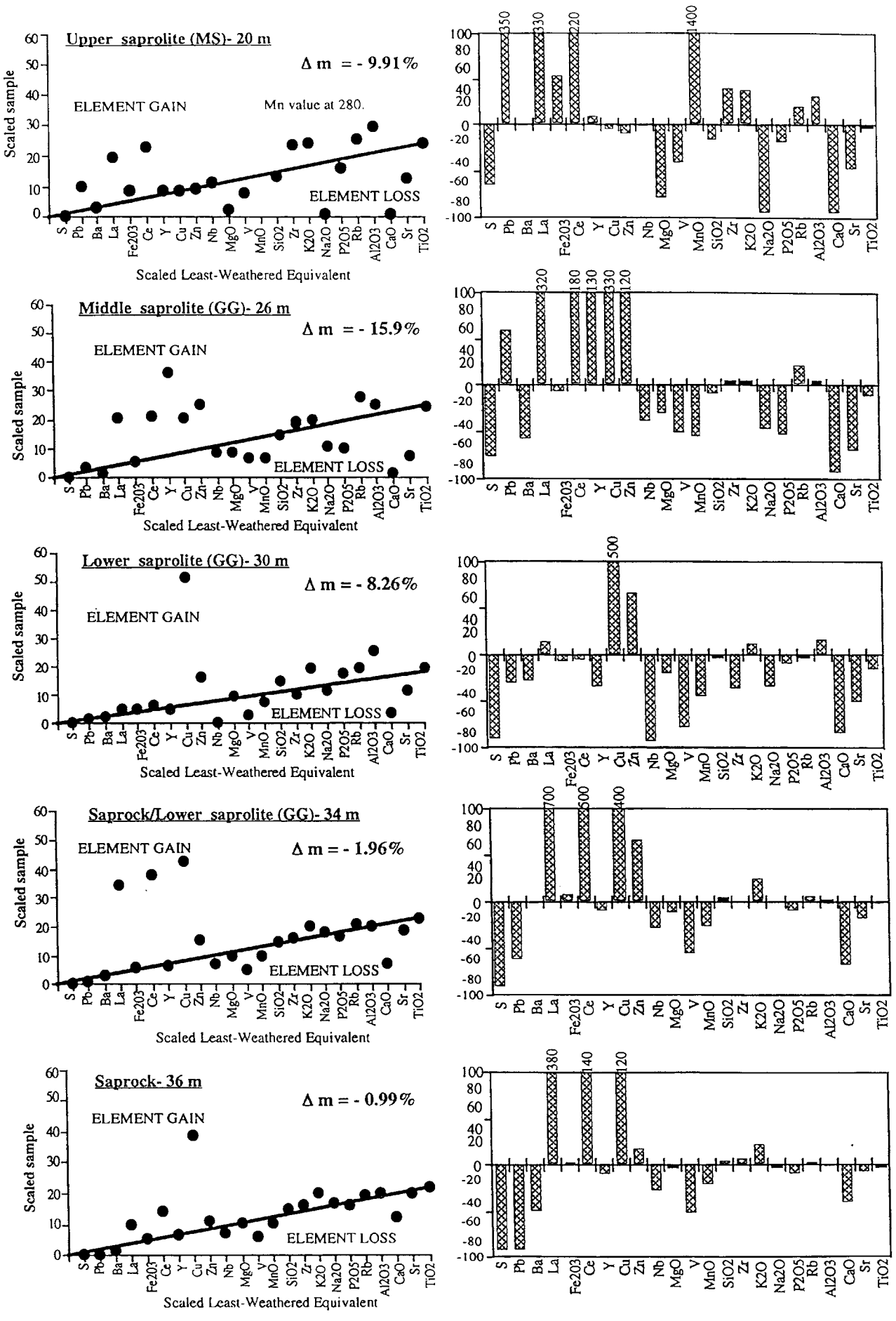

Figure 9.5.7b: Isocon plots and corresponding histograms for selected samples from E27 Profile 8 (GG-greenish-grey saprolite; MS- mottled saprolite)

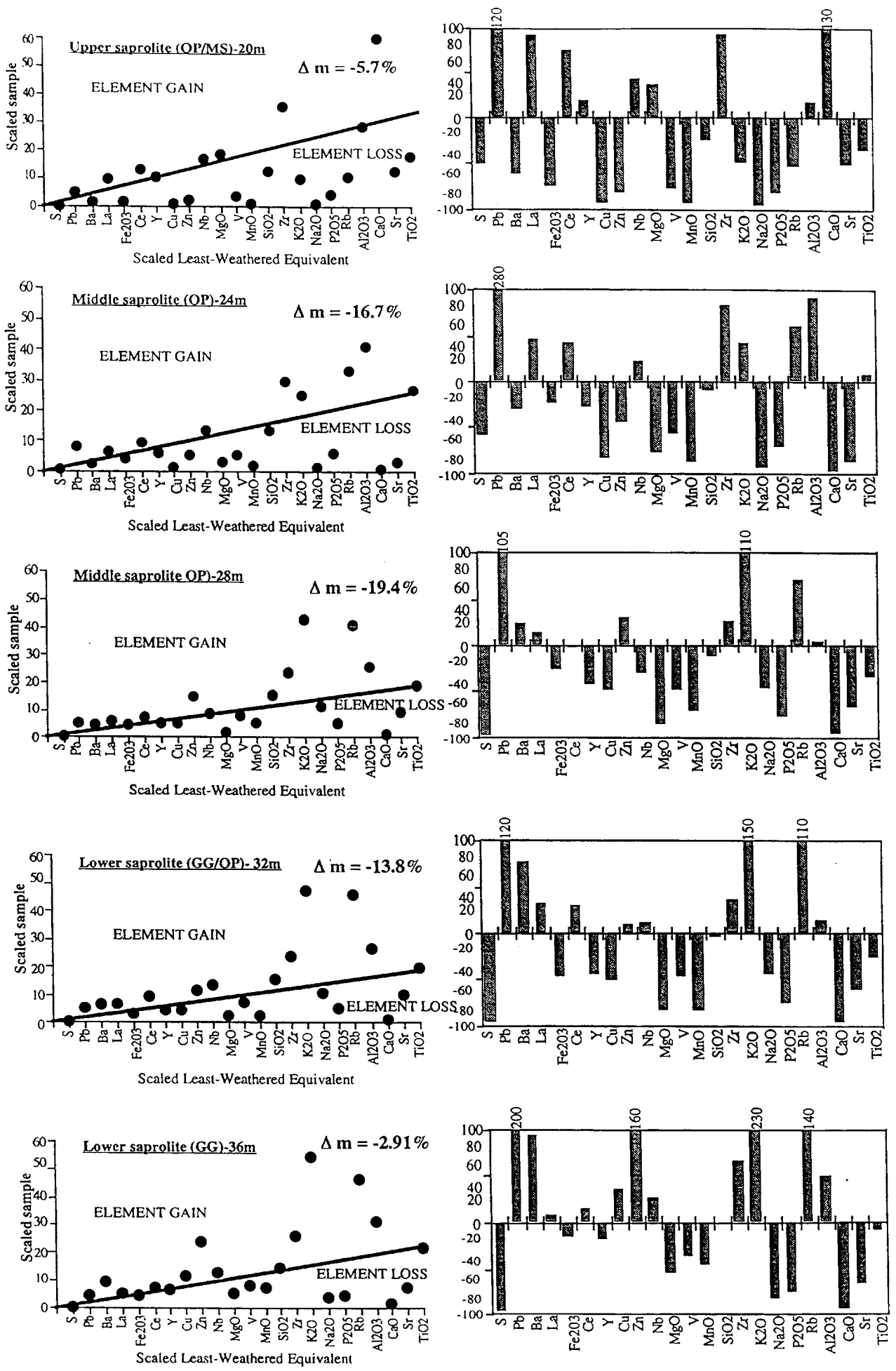

Figure 9.5.8b: Isocon plots and corresponding histograms for selected samples from E22 Profile 2
(GG- greenish-grey saprolite; OP- orange-pink saprolite; MS- mottled saprolite)

Lower saprolite (32 m)	CiW/CiO=1.19	Δ m = - 13.8%
Lower saprolite (36 m)	CiW/CiO=1.01	Δ m = - 2.91%

S, Fe_2O_3, V, MnO, Sr, SiO_2, P_2O_5 and Na_2O are depleted while Pb, La, Ce, and Zr shows enrichment in all the units of the profile. Cu, Zn and Rb shows similar distribution patterns as in profile 7 i.e enrichment in the greenish-grey saprolite and depletion in the orange-pink saprolite. CaO and MgO show progressive depletion up to the middle saprolite (at depth of 24 m) and enrichment in the upper saprolite. Ba shows moderate enrichment up to the middle saprolite (at depth of 28 m) and slight to moderate depletion afterwards. Y also shows slight enrichment and depletion in the upper saprolite and the other units respectively.

9.5.8 Discussion

The use of the graphical isocon technique has enabled the evaluation of element enrichment and depletion patterns in the regolith profiles during the weathering of the fresh trachyandesite. The distribution patterns also display some associations between these elements based on their mobility in these weathering profiles. This section summarizes the behaviour of these elements during weathering based on these inferred distribution patterns.

The major controlling factor in these distributions relates to the interaction between mineralogical and chemical agents e.g. H_2O, O_2 and CO_2 that governed profile development. Copper, Zn, Rb and K_2O for example showed similar behaviour in the two major saprolite units i.e depletion in the orange-pink saprolite and enrichment in greenish-grey saprolite. Calcium oxide, MgO, MnO and Na_2O on the other hand showed progressive depletion throughout with enrichment of CaO, MgO and MnO in the upper units related to input from secondary sources such as carbonates in the soil and the white clay unit and in the nodular iron and manganese horizons in the case of MnO. Some elements like V, S and P_2O_5 showed progressive depletion in most units of the profiles.

In order to understand these patterns, it is important to review the behaviour of these elements according to the patterns previously documented for weathering of mafic volcanic rocks and those that may show unusual behaviour during weathering and relate these characteristics with inferred patterns in this study. Processes observed for elements of the first group include: the rapid removal of the alkali and alkaline earth cations from the weathering profiles; progressive weathering of silica from the profile; oxidation of

iron during weathering resulting in its fixation, largely in secondary Fe-oxyhydroxides (goethite and hematite); similar oxidation of manganese to form coatings on weathered surfaces, the variable but limited mobility of V and the relatively high mobility of Cu once Cu-sulfide is oxidized to sulfate.

Elements that fall into the second group include: the rare earth elements (REE) cerium and lanthanum, as well as yttrium, barium and lead which may show anomalous enrichment in weathered materials when generally they might be expected to be removed from the weathering profile in a similar fashion to the alkali and alkaline earth elements. Other elements that show unusual behaviour are those that are generally considered to be immobile during weathering, but are apparently mobile under certain weathering conditions. These include Nb, Zr, Y, Al and Ti..

Calcium oxide, Na_2O, MgO and Sr show similar distribution patterns in the profiles in that they are marked by a strong depletion early in weathering and progressive depletion higher up in the profiles. Calcium and Sr partition similarly in these units and they appear to have been released at the same time during weathering. They are both products of the weathering of andesite glass, plagioclase feldspars and to a lesser extent ferromagnesium minerals. Under alkaline conditions, if the percolating fluids are carbonate rich and saturated with respect to calcite, calcite may precipitate in voids (White & Sarcia, 1978). Calcium and Sr are readily removed from the profile with progressive weathering and may be incorporated into secondary smectite clays. This explains some of the differences between the distribution of the two elements higher up in the profiles especially in the carbonate rich horizons. Whereas Ca was enriched because of the contribution from these sources, Sr was unaffected and continued to be progressively depleted.

Magnesium (Mg). As already mentioned, Mg shows similar distribution patterns as Ca. Magnesium is mobilized principally from weathering of pyroxenes and taken in as secondary smectites once mobilized (Usdowski, 1978b). The enrichment of Mg together with Ca in the higher units is attributed to its occurrence as dolomite in these units. Sodium is mobile in all the profiles studied and shows a strong depletion in the early stages of weathering. Na is released during dissolution of plagioclase feldspar and is generally mobilized out of the system. It may later be incorporated in smectites as the other alkali and alkaline earth cations.

Potassium (K). Unlike the other alkaline earth elements, K shows progressive enrichment in the greenish-grey saprolite and depletion in the orange-pink saprolite, the

white clay unit and the soil horizon. Rubidium has similar chemical properties as potassium and shows similar behaviour during weathering (Heier & Billings, 1978a). The same trend is also shown by Cu and Zn. The reason for this distribution is explained by the mineral stability of the host minerals during weathering as already explained in Chapter 7. Potassium in most of these profiles is hosted principally by micas and K-feldspar (orthoclase). The breakdown of these minerals during weathering occurs at the upper levels of the greenish-grey saprolite with most of it occurring in the orange-pink saprolite and the white clay unit. Potassium in these units also defines the K-feldspar alteration zone associated with Cu-Au mineralization thus explaining the strong association between Cu and K_2O. Some K and Rb may be taken up by smectite and retained in the secondary mineral assemblage or are lost from the weathering profile in solution. The abundance of Cu in the greenish-grey saprolite is also associated with the alteration zone although and possibly incorporation into the clay products because unlike the orange-pink saprolite (which is devoid of smectites) the greenish-grey saprolite has abundant smectites (5-20%) and kaolin (40-60%). The Zn shows similar distribution patterns as the Cu suggesting an association with the mineralization.

Silica (Si). Si shows slight depletion in most of the units of the profiles. Although Si is mobilized during the breakdown of the silicate minerals, this process progresses at a slower rate than the removal of the alkali and alkaline earth elements from the profiles studied. This slower rate of Si depletion may be explained by the fact that it is rapidly incorporated into neo formed clay minerals as fundamental part of their structure.

Vanadium (V). V exhibits moderate depletion in most of the units. It is largely enclosed in relatively resistant phases like magnetite or in ferromagnesium silicate phases like pyroxene where it substitutes for Al^{3+} or Fe^{3+} (Taylor et al. 1978; Evans, 1978). Vanadium may be released during weathering of these silicates and incorporated into smectites or may substitute for Ferric iron in hematite or goethite (Landergren, 1978). This perhaps explains its high concentrations in the mottled clay units as demonstrated by the line plots (Figures 9.4.5, 6, 7 & 8).

Manganese (Mn). Mn shows progressive depletion in most of the profiles. It is normally present in most basic rocks in ferromagnesium silicates and is progressively removed from the profile in the form of Mn^{2+} which is mobile (Paquet et al. 1987). Mn^{2+} may oxidize to Mn^{4+} which is relatively insoluble and hence precipitate within the weathering material. In this study it is noticeable as black Mn-rich coating on exposed surfaces or in fractures within the saprolite indicating that the Mn-oxide is precipitated from the weathering fluids.

The rare earth elements. The rare earth elements generally have an M^{3+} configuration, have large ionic radii and bond ionically and during weathering behave similarly to other lithophile elements of the alkali and alkaline earth groups i.e Ca, Sr, Na, K, Rb and Mg. However the rare earth elements analyzed (Y, Ce, La) and the trace elements Ba and Pb shows poorly defined enrichment or depletion patterns.

Cerium (Ce). Ce may be fixed in the profile during weathering as a result of oxidation of Ce^{3+} to Ce^{4+} and thus is expected to behave similarly to Mn (Marker & de Oliveira, 1994; Braun & Pagel, 1994). However, Ce enrichment/depletion patterns differ from those of Mn in that it may show strong anomalous enrichment, sometimes exhibiting mass gains of up to 500% (Figure 9.5.3; saprock/lower saprolite) whereas Mn does not show such mass gains. Mn does not also show enrichment in samples where Ce has elevated values. Its patterns are also unpredictable in that it may show a moderate increase in concentration followed by a progressive loss. In most of the profiles, Ce also follows enrichment patterns of La (profiles 7, 8 and 11). The reason for this distribution is unclear although it suggests that they are incorporated into a resistant phase and are being relatively enriched or they are scavenged by secondary weathering products and/or incorporated into neoformed phases during weathering.

Lead (Pb). Pb shows similar distribution patterns as the rare earth elements Ce and La although it is not as strongly enriched. Pb is largely derived from feldspar and the lanthanides from apatites and hence is not concentrated as a result of partitioning into a single resistant phase (Price et al. 1991). Cerium, La and Pb can however combine with phosphorus released from the weathering of apatite, to form the secondary resistant phosphates of the plumbogummite group (Norrish, 1957, 1968; Norrish & Rosser, 1983; Banfield & Eggleton, 1984, 1989 and Price et al. 1991). The presence of these minerals has not been documented in this study and hence the similarity in the distribution patterns cannot be clearly discerned at this stage.

Phosphorus (P). P exhibits moderate to high depletion patterns in most of the units of the profiles except profile 7. SEM EDXA analysis showed the presence of apatite in the fresh rock and it appears to be the host mineral of P in this study. Organisms are significant in the weathering of apatite, since they require P for metabolism (Banfield & Eggleton, 1989). Because the dissolution of apatite is more rapid in acid fluids there seems to be a correlation between kaolin rich deeply weathered profiles as those of this study and strong depletion of phosphate (Banfield & Eggleton, 1989).

Barium (Ba). Ba shows similar distribution patterns as Ce, La and Pb. In weathering profiles Ba is normally present in extremely fine grained $BaSO_4$ (barite) crystals (Price, 1991). Some very small amounts of barite was detected by SEM EDXA in the saprock of this study although this precludes its participation as the major host mineral. There is also no inferred correlation between Ba enrichment with S. Ba may also be fixed in weathering products in secondary carbonates or adsorbed onto clays or plumbogummite group minerals such as gorceirite (Price et al. 1991).

Sulfur (S). S shows strong depletion patterns in most of the units of the profiles except in the soils where it is strongly enriched. The depletion represents the progressive oxidation of the sulfide minerals with weathering while the enrichment in the soil is a consequence of its presence in gypsum.

Zirconium and Niobium (Zr and Nb). Nb shows constant slight enrichment or depletion patterns in most of the profiles, while Zr exhibits a general enrichment towards the upper parts of most of the profiles suggesting except in profile 8 where some moderate depletion occurred in the carbonate rich middle and upper saprolite units. This distribution was not brought about by any relative enrichment but by variable contents of Zr in the parent rock (least weathered equivalent) probably attributed to effects of mineralization. In general, Zr is concentrated by weathering processes because of the stability of the main host mineral zircon. It is commonly regarded as a very stable mineral able to survive many cycles of weathering, sedimentary transport, diagenesis, metamorphism and antexis (Speer, 1982; Milnes & Fitzpatrick, 1989). Zircon has been observed to dissolve under acid pH conditions with significant chloride concentrations as would be expected in the sulfide-rich zone, which might explain the variable contents of the Zr in the parent material of this study. Zircon may also be unstable in very acid media such as podzols (Colin et al. 1993). In addition, metamict zircons with hydrous species and disordered crystalline structure with isolated silica tetrahedra (Woodhead et al. 1991) may be sensitive to weathering. The lack of uniformity in the distribution of Zr of this study may be related to these environmental factors. This discounted its use as the immobile index in some of the profiles.

Yttrium (Y). Y shows limited mobility in most units of the profiles while in others it shows enrichment and depletion with no general distribution patterns. The principal mechanism for Y enrichment in weathering profiles is partitioning into secondary neo-formed phases in a similar fashion as the lanthanides (Moore, 1996).

Titanium (Ti). Ti like Y shows limited mobility in a most of the profiles (profiles 8, 7 and 11) and slight to moderate progressive depletion in profile 2. This differential mobility relates to the primary mineral that it is partitioned to. SEM EDXA analysis showed presence of Ti in rutile in the fresh rock. The limited mobility is attributed to the resistance of rutile to weathering processes. Higher up in the orange-pink saprolite and the mottled clay units, the Ti was fixed as anatase. This perhaps explains the depletion of Ti in the orange-pink saprolite of profile 8. However, Ti may be mobile early in weathering as a result of pyroxene weathering (Milnes & Fitzpatrick, 1989). The presence of organic acids may also enhance Ti mobility while the percolation of acid fluids as expected during the oxidation of sulfides may remobilize the Ti into secondary anatase (Correns, 1978; Dumon & Vigneaux, 1979).

9.6: ELEMENT-ELEMENT ASSOCIATIONS

Bivariate statistical treatment of the samples from the two deposits reveals a number of element associations. These associations are recognized through a combination of element correlations and their relationships when plotted on a scatterplot. A correlation matrix, using the Pearson's correlation coefficient, is supplied in Appendix 8. The positive and negative element correlations above 0.5 are listed in Table 8.6.1 for all data and transported and residual regolith. The selected scatterplots of some of the elements are shown in Figures 9.6.

Scatterplots are a means by which the association between the concentration of two elements can be visualized. Elements that increase concurrently in concentration are positively correlated and so have a trend on a scatterplot that has a positive gradient. On the other hand, elements that oppose each other in their concentration variation are negatively correlated and so have a negatively trending gradient.

Table 9.6.1: Element correlations greater than 0.5 from the E22 and E27 geochemical data. Elements with correlations less than 0.5 are not shown. The results have been extracted from the correlation matrices presented in Appendix 8.

Element	Positive correlations >0.5	Negative correlations >0.5
Fe_2O_3	-	SiO_2
MnO	P_2O_5	-
TiO_2	Al_2O_3	-
CaO	MgO	-
SO_3	CaO	-
P_2O_5	MnO, Na_2O, Zn	-
SiO_2	-	Fe_2O_3
Al_2O_3	TiO_2	CaO

MgO	CaO	-
Na_2O	P_2O_5, Cu	-
Cu	K_2O, Na_2O, Zn	-
Zn	P_2O_5, Cu	-
As	Fe_2O_3	-

N=229

Table 9.6.2: Element correlations greater than 0.5 from the transported regolith from E22 and E27 geochemical data. Elements with no correlations less than 0.5 are not shown. The results have been extracted from the correlation matrices supplied in Appendix 8.

Element	Positive correlations >0.5	Negative correlations >0.5
Fe_2O_3	MnO, P2O5, Pb, As	SiO_2
MnO	Fe_2O_3, P_2O_5, Zn, Ag, As	-
TiO_2	Al_2O_3	SO_3
CaO	SO_3, MgO	Al_2O_3
SO_3	CaO	TiO_2, Al_2O_3
P_2O_5	Fe_2O_3, MnO, Zn, As	SiO2
SiO_2	Na_2O	Fe_2O_3, P_2O_5
Al_2O_3	TiO_2	CaO, SO_3
MgO	CaO	-
Na_2O	SiO_2	Cu
Cu	-	Na_2O
Pb	Fe_2O_3, As	-
Zn	MnO, P_2O_5, Ag	-
Ag	MnO, P_2O_5, Zn	-
As	Fe_2O_3, Pb	-

N=77

Table 9.6.3: Element correlations greater than 0.5 from the residual regolith of E22 and E27 geochemical data. Elements with no correlations less than 0.5 are not shown. The results have been extracted from the correlation matrices supplied in Appendix 8.

Element	Positive correlations >0.5	Negative correlations >0.5
Fe_2O_3	MnO	-
TiO_2	Al_2O_3	MgO, CaO
CaO	MgO	TiO_2, Al_2O_3
Al_2O_3	TiO_2	CaO, MgO
MgO	CaO	TiO_2, Al_2O_3
Na_2O	P_2O_5	-
Zn	Fe_2O_3, Cu	-
As	Fe_2O_3, Zn	-

N=109

On further subdivision of the data into the transported and residual regolith of the two deposits, the following additional correlation matrices were obtained:

E22 TRANSPORTED (N=24)

Element	>0.5 (positive)	>0.5(Negative)
Cu	MnO, P_2O5	Na_2O
Na_2O	SiO_2	Fe_2O_3
Au	MnO	-
As	-	SiO_2, Na_2O

E22 RESIDUAL (N=67)

Element	>0.5 (positive)	>0.5(Negative)
Pb	Fe_2O_3, Zn, As	-
Zn	Fe_2O_3, P_2O_5	-
Zn cont'd	Pb, As, Cu	-
Cu	P_2O_5, K_2O	-

Table 9.6.4: Additional element correlations greater than 0.5 from the transported and residual regolith of E22 geochemical data. Elements with no correlations less than 0.5 are not shown. The results have been extracted from the correlation matrices supplied in Appendix 8.

E27 TRANSPORTED (N=31)

Element	>0.5 (positive)	>0.5(Negative)
K_2O	SiO_2	Fe_2O_3, TiO_2
Zn	Ag	Al_2O_3
As	Pb	-
Cu	Al_2O_3	-

E27 RESIDUAL (N=42)

Element	>0.5 (positive)	>0.5(Negative)
Au	Cu, Ag	-
As	Fe_2O_3, MnO	K_2O
Na_2O	P_2O_5, SiO_2	-
Ag	Cu	-

Table 9.6.5: Additional element correlations greater than 0.5 from the transported and residual regolith of E27 geochemical data. Elements with no correlations less than 0.5 are not shown. The results have been extracted from the correlation matrices supplied in Appendix 8.

The subdivision of the regolith into to the parent material and the different classes proved to be invaluable in the interpretation of the regolith classes responsible for each correlations in the scatterplots (Figures 9.6). An attempt has also been made to explain the reasons for each correlations.

Silica shows variable correlation patterns with a number of elements in the scatterplots. Its strong negative correlation with Fe_2O_3 (Figure 9.6.4 a) represents a process fundamental to regolith evolution in that the weathering of the primary silicates in part results in the precipitation of iron oxides, whose amounts increase with progressive Si depletion. The strong positive correlation with K_2O (Figure 9.6.1 c & d) in the residual units represents their association with muscovite and orthoclase with the progressive increase up to the orange-pink saprolite indicating the susceptibility of these minerals to weathering up to this level in the profile. The more pronounced negative correlation with TiO_2 in the residual units (Figures 9.6.1 g & h) indicates the residual accumulation of TiO_2 with progressive depletion of the silicates. Some of the Ti is hosted by the mineral anatase higher up in the residual profiles i.e in the orange-pink and mottled saprolite and in the mottled clay units of the transported regolith.

A few samples from the orange-pink saprolite, mottled clay zone and the soil horizons showed a negative correlation between CaO and SiO_2 (Figures 9.6.1 a & b) and MgO and SiO_2 (Figures 9.6.1 e & f). The reasons for this distribution relates to the weathering of ferromagnesium minerals notably hornblende which is abundant in the orange-pink saprolite. This contrasts with the strong positive correlation between CaO and MgO (Figures 9.6.6 e & f) attributed to the occurrence of carbonates in these units. The discrete clustering of concentration values along the x or y axis in the aforementioned figures and elsewhere e.g. 9.6 c & d, 9.6.2 g & h, 9.6.6 g & h, 9.6.8 g & h, 9.6.9 g & h indicates a decrease in precision as values approach the LLD (lower limit of detection). Some of the concentration values above the LLD as in Figure 9.6.9 g & h (Fe_2O_3 vs MnO) indicates a strong positive correlation between the outliers.

Some of the associations display inverted V-shaped patterns (Figures 9.6.2 c & d; 9.6.2 e & f). On cursory examination, it is apparent that the two pairs of correlation patterns arose because of the two-parent materials i.e transported and residual regolith. SiO2 in Figures 9.6.2 c & d shows a positive correlation with Al_2O_3 in the transported material (mottled clay units and nodular Fe and Mn aggregates) and a negative correlation in the residual units. The positive correlation is attributed to the abundance of Si in the kaolin-rich matrix of the mottled clay samples (chapter 6) and the negative correlation to progressive weathering of the primary silicates to kaolinite and smectitic clays. Similarly, the negative correlation between the distribution of Na_2O in Figures 9.6.2 g & h, CaO in Figures 9.6.6 g & h and MgO in Figures 9.6.2 a &b with Al_2O_3 in the residual units is attributed to the weathering of plagioclase with additional input in the lower saprolite and the saprock from chlorite, epidote and diopside.

The positive correlation between Al_2O_3 and Fe_2O_3 in the residual units of Figure 9.6.2 e & f represents their secondary accumulation as clays and iron-oxides with progressive weathering of the primary silicates. Iron oxide on the other hand exhibits relatively strong positive correlations with As (Figures 9.6.4 c & d), P_2O_5 (9.6.4 e & f), Pb (9.6.3 g & h) and Zn (9.6.9 e & f). These correlations are strongest within the mottled clay units of the transported regolith which is evidence of the strong adsorption characteristics of the iron oxide minerals in these units. Some weak correlations occurred between the Fe_2O_3 and K_2O (Figure 9.6.3 a & b), MgO (Figures 9.6.3 c & d) and Cu (Figures 9.6.3 e & f) in the residual units attributed to the weathering of muscovite or K-feldspar and some of the ferromagnesium minerals e.g. hornblende and opaques (spinels and magnetite) with additional input from the oxidation of sulfides to iron-oxides in the lower units.

Apart from the strong correlation with Fe_2O_3, P_2O_5 also correlates fairly well with Na_2O (Figure 9.6.5 c & d), Zn (9.6.5 e & f), and Cu (9.6.5 g & h). SEM EDXA analysis showed appreciable amounts of apatite (2-5%) in the saprock, sulfide zone and fresh rock with the association with Cu and Na_2O showing its association with the mineralization zone. The association with Zn mainly occurred in the mottled clay and nodular iron-manganese aggregate samples.

Copper shows a strong positive correlation with K_2O in the residual units. This association serves as an expression of mineralization in the alteration zone associated with K-feldspar and muscovite. Au shows poor correlations with most of the elements (Figures 9.6.7 b, c, d, e, f, g, h and 9.6.8 c, d, e, e, f) apart from a fairly good positive correlation with K_2O (9.6.8 g & h) and Cu (9.6.8 a & b) in the residual units and Fe_2O_3 (9.6.4 h) in the transported regolith. The former is attributed to its occurrence in the mineralized zone and the latter with the iron-oxides in the mottled clay units. Arsenic does not correlate well with a number of elements apart from Fe_2O_3 (9.6.4 c & d) and Pb (9.6.7 g &h) in the mottled clay units for reasons already mentioned.

Table 9.6.6 shows a summary of the element enrichment and depletion patterns using the techniques already covered in this Chapter. This applies only to situations where the element has been significantly enriched or depleted.

REGOLITH UNIT	DEPLETION	IMMOBILE	ENRICHMENT
Soil	As, Pb, P, V, Zn	Al, Ti, Nb	Ca, Mg, Ba, Sr, Ce, S
Mottled clay zone	Na, K	Al, Ti, Nb	Si, Ti,Pb, Zn, As, P, V, Cr, Rb
Nod. Fe-Mn units	S, Ca, Mg, Sr, Ba	Al, Ti, Nb	Cu, Ni, Pb, Zn, As, P, Ag, V, Cr, R
White clay unit	S, Ba, Cu, Zn, K, Na, Rb, Sr	Zr, Al, Ti, Nb, Fe	La, Pb, Ce, Mn, Mg, Ca
Mottled saprolite	S, Zn, Mg, Ca, Na, Sr	Al, Zr, Nb, Ti	Pb, Mn, Y, La
OP saprolite	Cu, Zn, K, Na,	Al, Fe, Nb, Ti	Mn, La, Ce, Rb, K, Pb
GG saprolite	Na, Ca, Mg, Mn, Si, Pb, S	Al, Fe, Nb, Ti	Cu, Pb, Zn, Rb, K, Y
Saprock	Na, S, Ca, V	Al, Fe, Nb, Ti, Zr	Cu, Pb, Zn, As, Rb, K, Mg, P, Sr, I

Table 9.6.6. The element enrichment and depletion patterns as a result of weathering at the Goonumbla area [GG-greenish-grey; OP-orange-pink; Nod.-nodular]- K, Na, Ca, Ti, Mg, P and Al expressed as the major oxides.

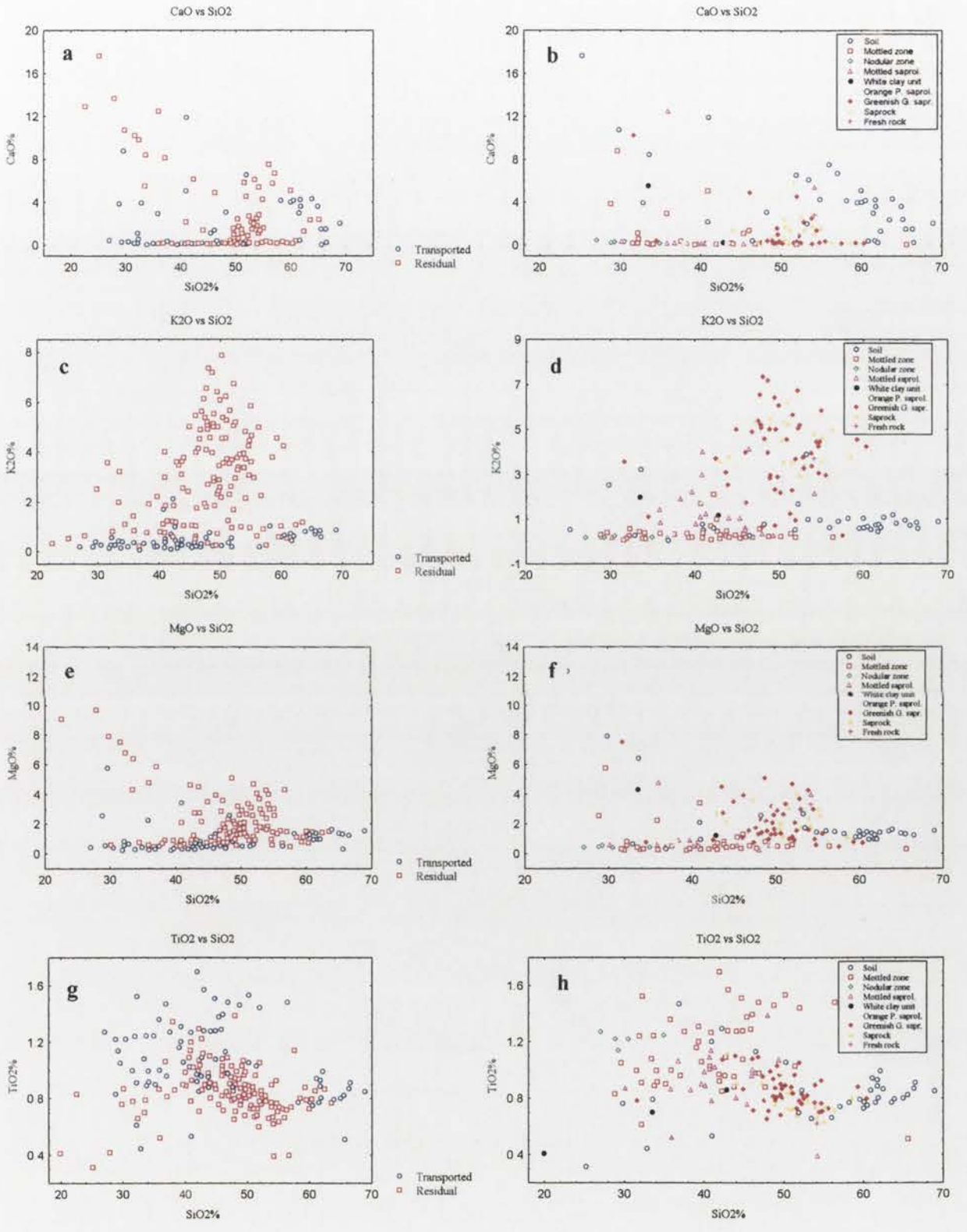

Fig.9.6.1: Scatterplots of SiO2 vs K2O, CaO, MgO and TiO2 in the parent material and the regolith classes in both deposits

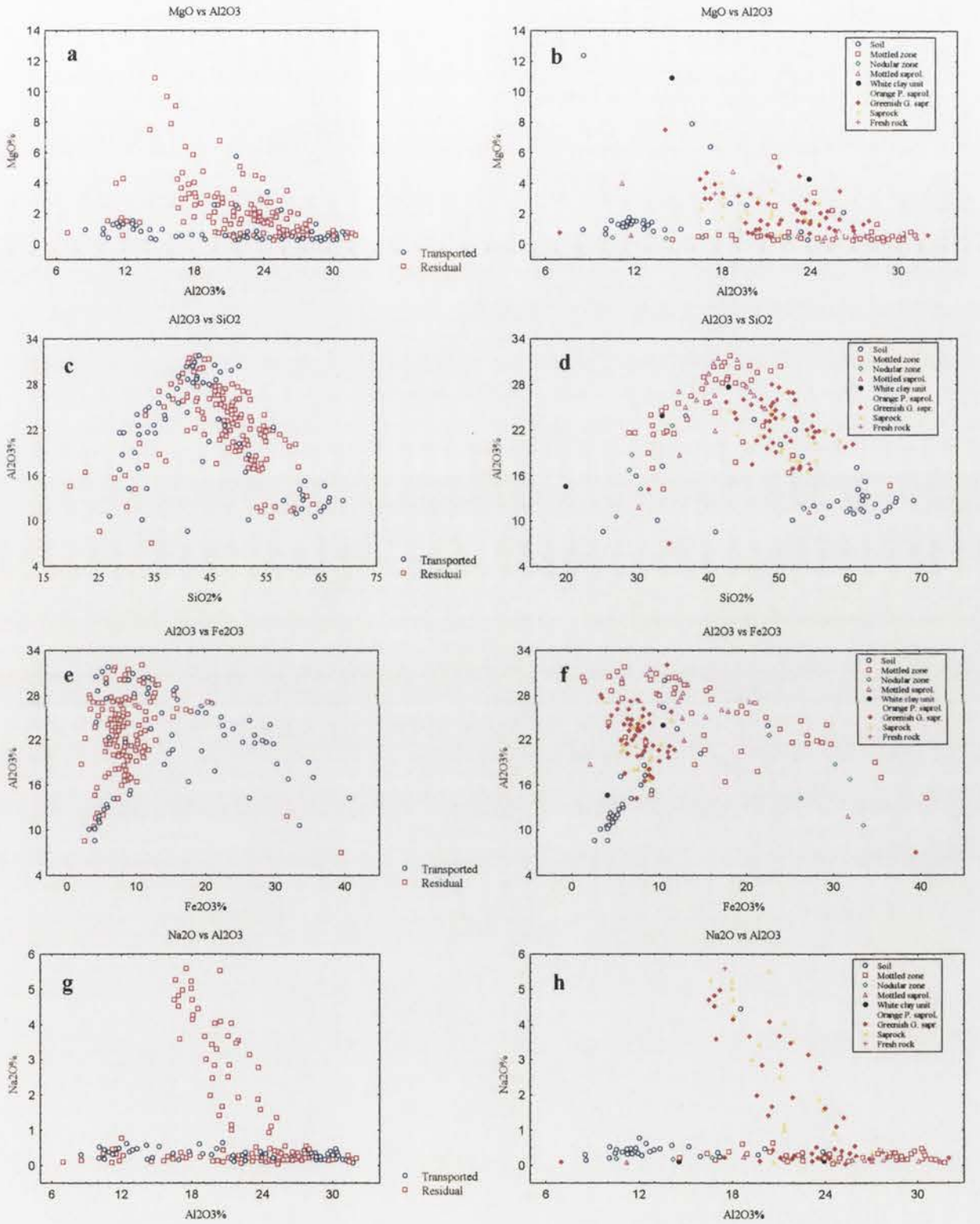

Fig.9.6.2: Scatterplots of Al2O3 vs MgO, SiO2, Fe2O3 and K2O in the parent material and the regolith classes in both deposits

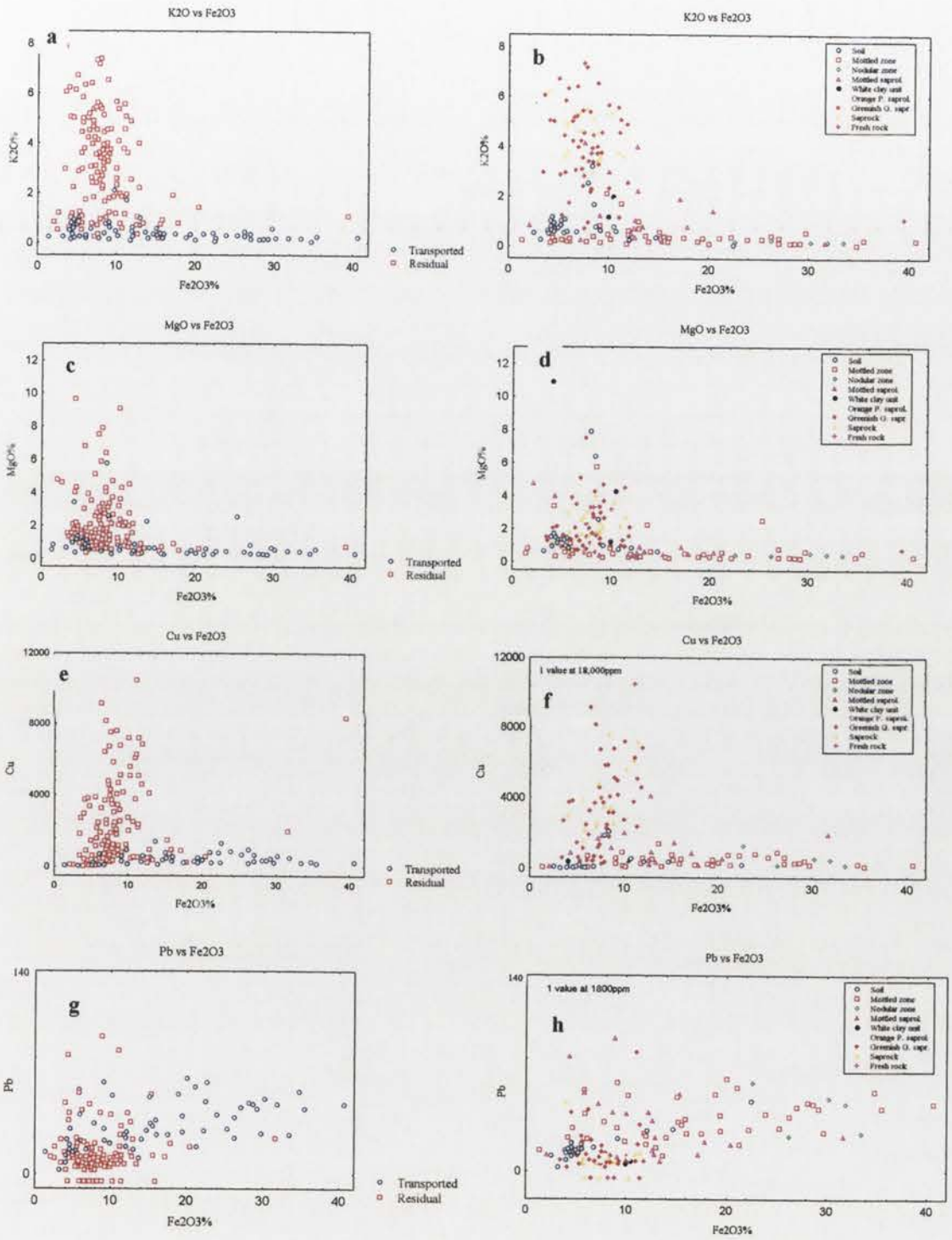

Fig.9.6.3: Scatterplots of Fe2O3 vs K2O, MgO, Cu and Pb for parent material and the regolith classes of both deposits

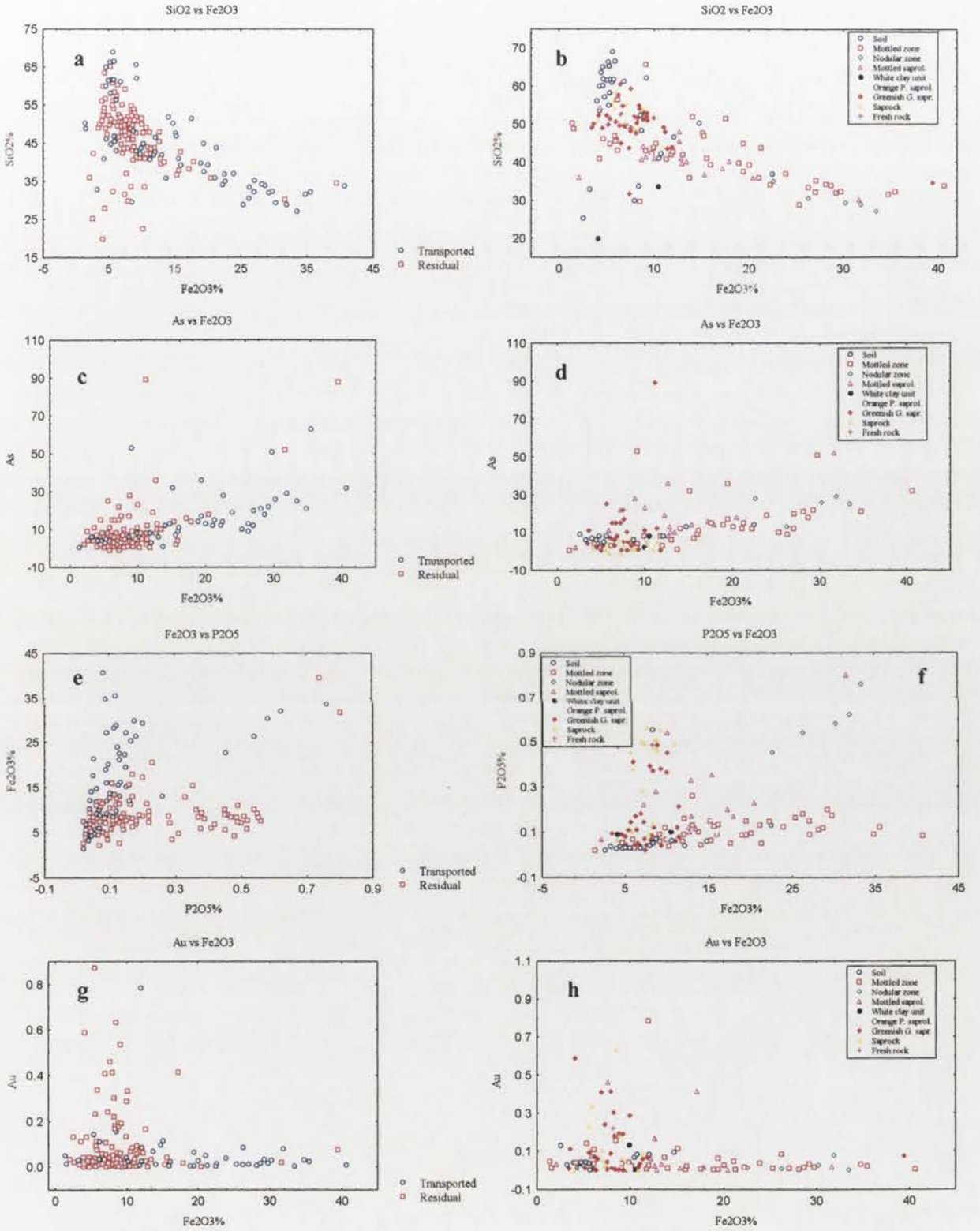

Fig.9.6.4: Scatterplots of Fe2O3 vs SiO2, As, P2O5 and Au in the parent material and the different regolith classes.

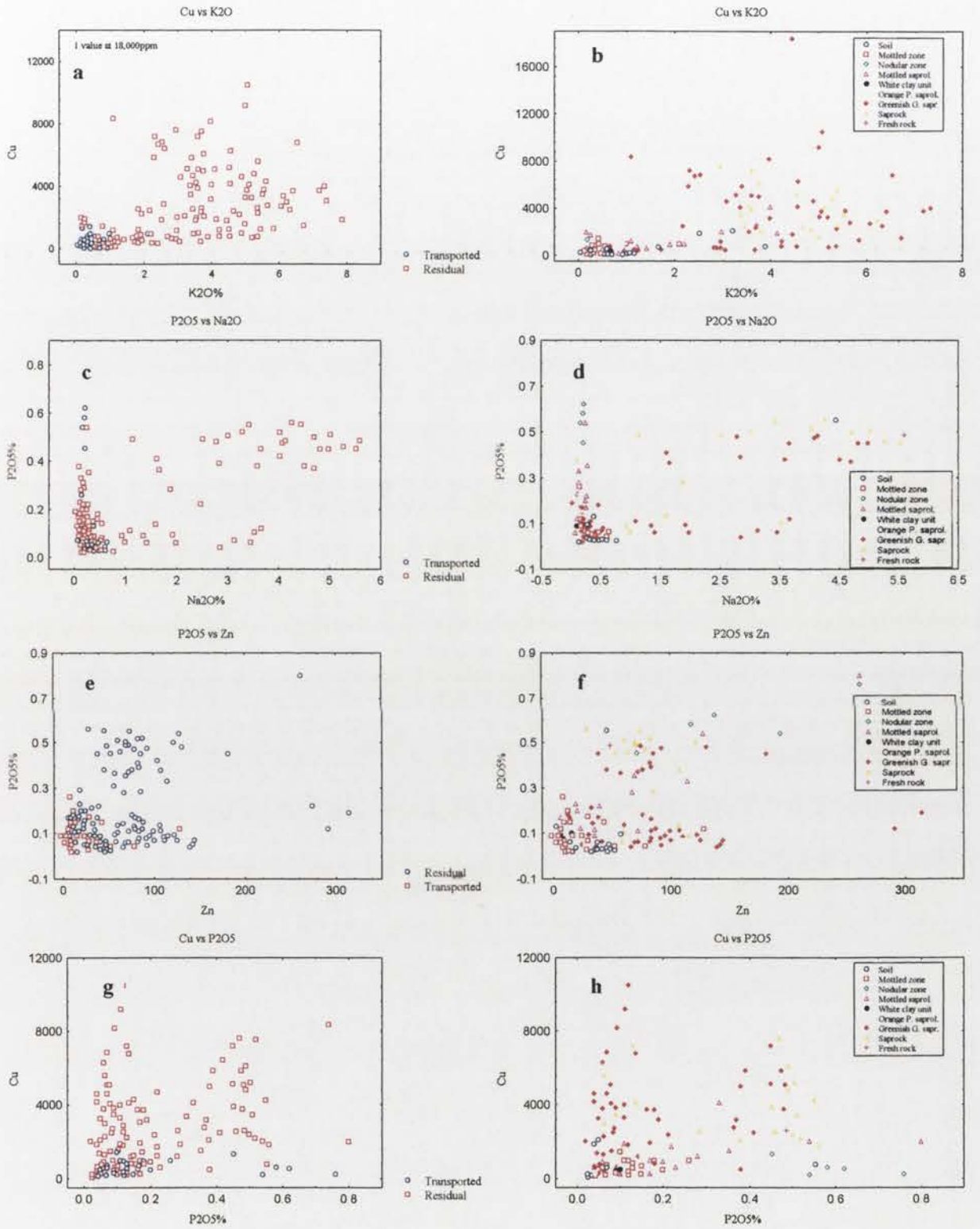

Fig.9.6.5: Scatterplots of P2O5 vs Cu, Na2O and Zn and Cu vs K2O for parent materials and regolith classes of both deposits

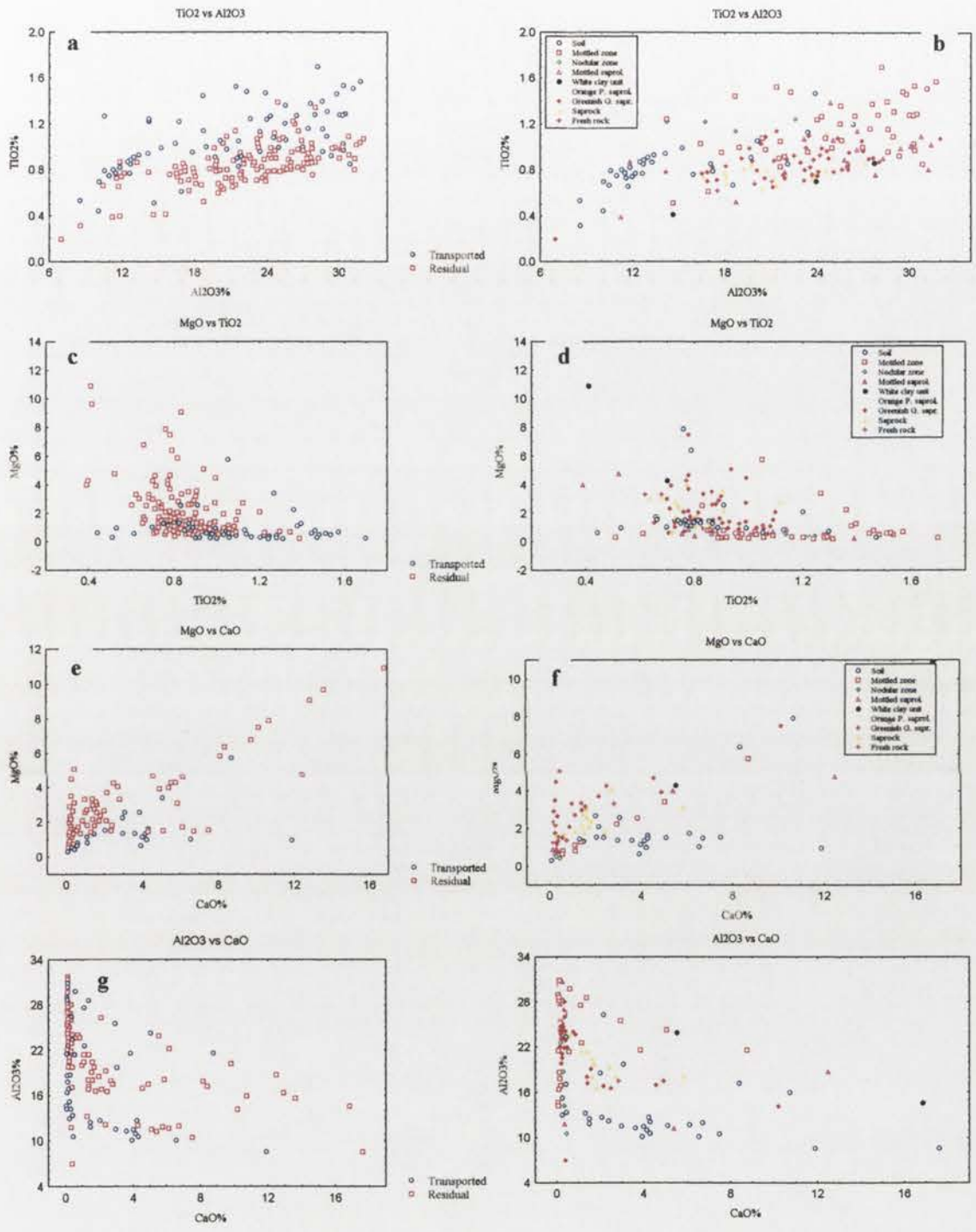

Fig.9.6.6: Scatterplots of TiO2 vs Al2O3 and MgO and CaO vs MgO and Al2O3 for the parent materials and the regolith classes in both deposits

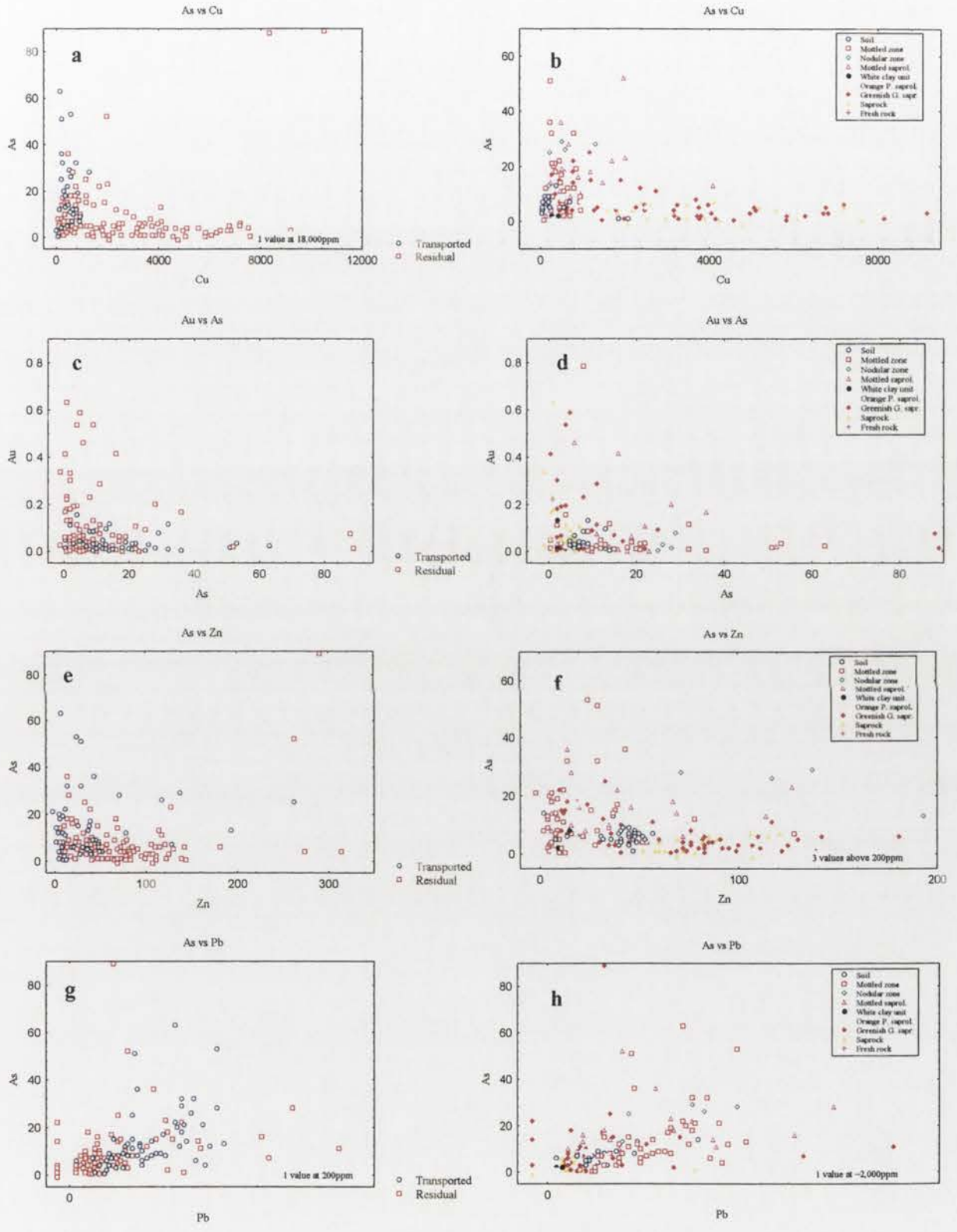

Fig.9.6.7: Scatterplots of As vs Cu, Au, Zn and Pb for parent material and the regolith classes of both deposits

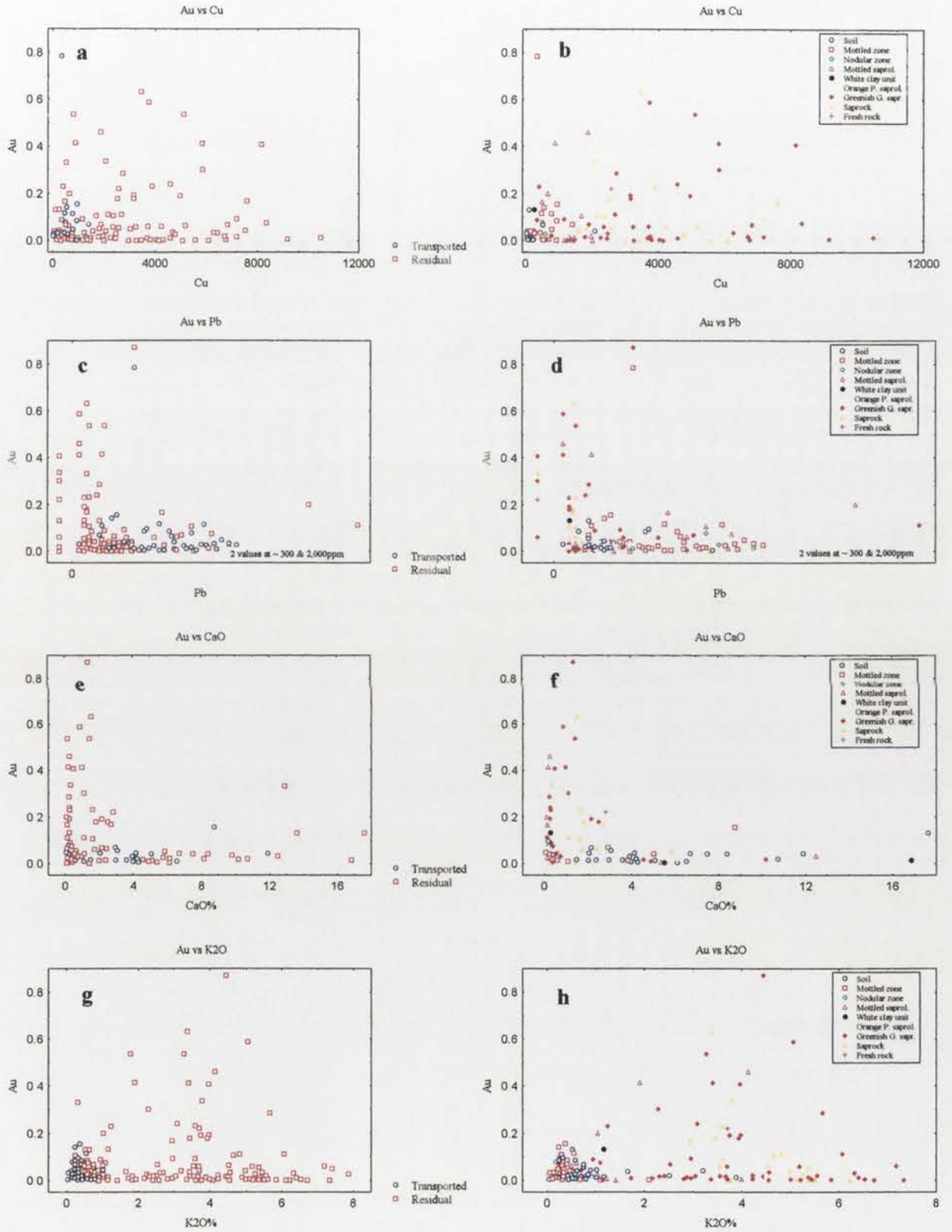

Fig.9.6.8.: Scatterplots of Au vs Cu, Pb, CaO and K2O for the parent material and regolith classes of both deposits

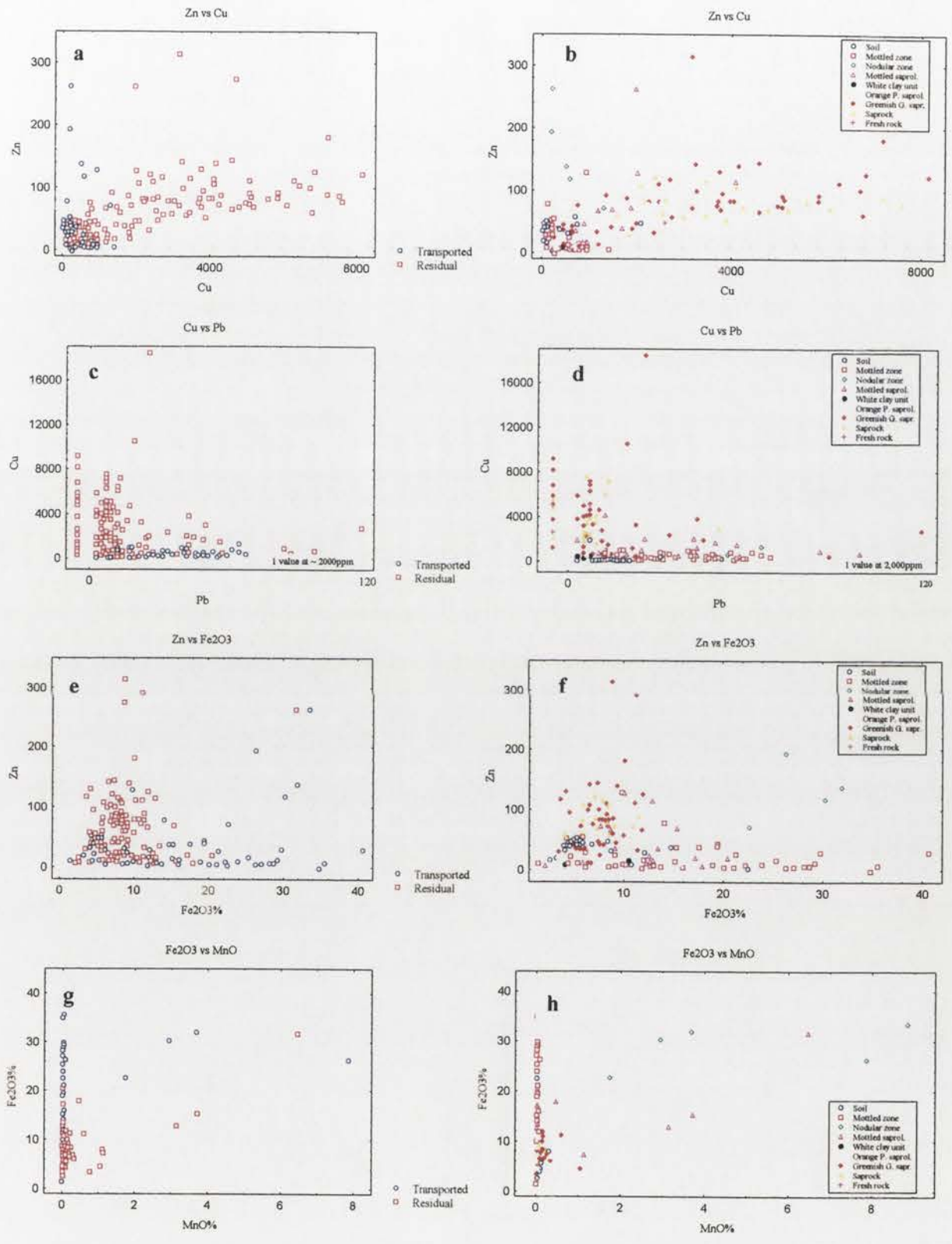

Fig.9.6.9: Scatterplots of Zn vs Cu, Pb and Fe2O3 and Fe2o3 vs Mno for the parent material and regolith classes of both deposits

CHAPTER 10

ELEMENT-MINERAL HOST ASSOCIATIONS AND DISTRIBUTION IN THE REGOLITH STRATIGRAPHY

10.1 Introduction

The aqueous solution, transport and precipitation of elements is of central importance to weathering and geochemical dispersion. The extent to which particular elements are are mobilized by groundwaters during weathering depends upon the controls of solubility in aqueous solutions and the interaction between these solutions and the complex surfaces of primary and secondary minerals. The various elements may be held within the mineral crystal lattice, loosely bound within a layer of changing potential field at the interface or may be mobile in solution either solvated by water molecules or "complexed" with one or more other soluble ions (Thornber, 1992).

During dissolution, the elements move from the mineral crystal surface through the charged layers into solution. The reverse is true of precipitation. If other elements are adsorbed at the interface, these processes tend to be hindered, and in the case of precipitation, may result in the element being coprecipitated or bound into the crystal of the precipitate. The major factors controlling the mobility of chemical elements in aqueous solutions and their behaviour during weathering have already been discussed in Chapter 2.

This chapter deals with the associations between the major and trace elements and the minerals already described in Chapters 6 and 7. These associations have been determined through statistical correlation of the mineralogy and geochemistry data and by sequential selective extraction techniques. Additional information has also been obtained by visual examination of the 2-dimensional plots of both data in the regolith stratigraphy. A summary of the element mobility and dispersion patterns in the regolith and the implications of these distribution patterns on geochemical exploration in the region is also presented. The Chapter ends with a summary of the regolith evolution features of the Goonumbla region.

10.2 MINERAL-ELEMENT ASSOCIATIONS

Bivariate statistical treatment of the mineralogy and geochemistry data yielded additional information on the associations between the minerals and the elements they host in the

weathering environment. The positive and negative element correlations above 0.5 are listed in Tables 10.1. The selected scatterplots of some of the elements are shown in Figure 10.1.

Table 10.1 a: Element-Mineral correlations greater than 0.5 from the E22 and E27 geochemical data. The correlations less than 0.5 are not shown. The results have been extracted from the correlation matrices presented in Appendix 9. 164 samples were used in this computation.

Element	Positive correlations>0.5	Negative correlations>0.5
MnO	Goethite	-
K_2O	Muscovite, Orthoclase	Kaolin, Quartz
SO_3	Gypsum	-
Al_2O_3	Kaolin	Quartz
Na_2O	Orthoclase	Kaolin
Cu	Orthoclase	-

Table 10.1 b: Element-Mineral correlations greater than 0.5 from the residual regolith of both deposits. The correlations less than 0.5 are not shown. The results have been extracted from the correlation matrices presented in Appendix 9. 109 samples were used in this computation.

Element	Positive correlations>0.5	Negative correlations>0.5
K_2O	Muscovite, Orthoclase	Kaolin
Na_2O	Albite	Kaolin
Cu	Muscovite, Orthoclase	-

Table 10.1 c: Element-Mineral correlations greater than 0.5 from the transported regolith of both deposits. The correlations less than 0.5 are not shown. The results have been extracted from the correlation matrices presented in Appendix 9. 55 samples were used in this computation.

Element	Positive correlations >0.5	Negative correlations>0.5
MnO	Goethite	-
SO_3	Gypsum	-
P_2O_5	Goethite	-
SiO_2	Quartz	-
Al_2O_3	Kaolin	Quartz, Gypsum
MgO	Smectite	-
Na_2O	Quartz	Kaolin
Cu	Kaolin	Quartz
Zn	Goethite	-

10.2.1 Summary of results

Most of the results are consistent with the predictions from the element-element associations of the previous Chapter. K_2O for example is hosted by muscovite and orthoclase with the strong association of the two minerals with Cu (Figure 10.1)

expressing the effects of mineralization in the K-feldspar alteration zone. The bulk of the Na_2O is hosted by albite. The association with orthoclase (Table 9.1a) shows it is present in the mineralization zone although it seems to play a limited role in the distribution of some of the elements in this zone i.e. Cu, Zn and Pb.

The results show that Al_2O_3 is mainly hosted by kaolin. Negative correlations also exist between kaolin and Na_2O, SiO_2, K_2O in the residual units and a positive correlation with Fe_2O_3 in most of the units apart from the mottled clay and nodular iron-manganese units. This is simply because kaolin and the iron oxides are the major secondary products from the weathering of the primary rock forming minerals. Some of the smectites seem to be derived from the Mg-containing minerals (e.g. chlorite and diopside) as expressed by their strong correlation with MgO (Table 10.1 c).

Hematite, as expected, exhibits positive correlations with Fe_2O_3 and also with Pb, As (Figure 10.1) and P_2O_5 and a negative correlation with SiO_2. Goethite is also strongly associated with Fe_2O_3, Pb, As, P_2O_5, MnO and Zn (Tables 10.1 a and c) as expressed by the strong positive correlations. This is related to the strong adsorption properties of the iron oxides in the transported regolith units. The negative correlation with SiO_2 is mainly a consequence of closure (analytical total = 100%).

The reasons for the negative correlation between Cu and quartz in the transported regolith (Table 10.1 c) is unclear. The positive correlation with kaolin in the same parent material suggests that some of it is held within the clay matrix. Additional information on these associations has been provided by the selective leaching techniques.

10.3 SEQUENTIAL SELECTIVE EXTRACTIONS

10.3.1 Background to technique

Selective extraction is a technique whereby particular soil or weathered phases are dissolved in a controlled manner, and the resulting solutions analyzed for trace elements of interest. These techniques can be used to investigate how trace elements are distributed between the phases. In addition, these extractions have been used in the past for geochemical exploration because it has been perceived that elements associated with mineralization (especially those hosted by sulfides) are more likely to be released during weathering than those in the barren rocks (hosted by silicates), more widely dispersed, and more probably held by secondary minerals and hence likely to be preferentially released by extraction solutions.

In contrast, many of the new extraction techniques currently being utilized for geochemical exploration are partial rather than selective digests: i.e., they extract part of a phase or phases rather than a selected mineral. These new methods are being claimed to have a high efficacy in the location of buried or otherwise hidden orebodies, and there has been a high degree of interest in their application. This section examines the chemistry of partial/selective extraction and their mineralogical implications.

Various phases that could be of significance in the distribution of trace elements include phyllosilicates (e.g., kaolinite), Fe oxides (e.g., goethite and hematite), Mn oxides, carbonates, or resistate minerals such as chromite, zircon or monazite. The major controls on the dispersion of the elements in the weathering environment are reaction sites in a complex chemical realm where geological materials undergo numerous chemical, physicochemical, and biological transformations (Chao, 1984; Ostwald, 1992; Parc et al. 1989). The reaction sites are oxides of iron and manganese, oxides of aluminium and silicon, organic matter, carbonates and secondary sulfides. The clay-size aluminosilicates, generally considered as the most active fraction of soils and sediments because of their surface properties, serve essentially as a vehicle for other reaction sites (Jenne, 1977). Ore metals and related pathfinder elements mobilized through weathering have to overcome various chemical barriers associated with the reaction sites in order to disperse.

10.3.2 Iron and manganese oxides as reaction sites

Iron and manganese oxides are of paramount importance in exploration geochemistry due to their ubiquitous occurrence and strong scavenging of metal ions (Chao & Theobald, 1976). Iron and manganese oxides are in general more important than aluminium and silicon oxides, because the iron and manganese oxides have greater adsorption capacities, dissolve as the redox potential decreases, and reprecipitate as the system becomes oxygenated (Jenne, 1977; Thornber, 1992; Thornber & Wildman, 1984).

Alternate dissolution and precipitation tend to maintain the oxides of iron and manganese in a highly active amorphous state or in a low degree of crystallinity. A low degree of crystallinity facilitates the non-stoichiometric incorporation of foreign elements, especially metals, into the oxides (Kuhnel et al. 1975). Although manganese oxides may precipitate less rapidly than iron oxides, isomorphic substitution and penetration by foreign ions into the extremely complex mineralogical structure of manganese oxides is much more extensive than in the iron oxides, and the oxidation state of the manganese is highly variable (Chao & Theobald, 1976; Jenne, 1977; Thornber, 1992; Thornber & Wldman,

1984). Therefore, manganese oxides usually have greater scavenging capacity for heavy metals than iron oxides on a equivalent weight basis (Chao & Theobald, 1976).

10.3.3 Role of organic matter as reaction sites

Organic matter in soils and sediments comprises a group of complex chemical components of biological origin. The active functional groups can form organometallic complexes and chelates by solubilizing metal compounds or by precipitating metal ions, depending on the solubility of complexes and chelates formed. Wherever organic matter accumulates in soils and sediments, organic related metals provide a possible indication of mineralization (Chao, 1984). Wilhem et al. (1979) suggested that if the organic carbon content in soils and sediments is less than 5%, the metal-organic matter association appears to be less important than other controls, especially iron and manganese oxides. Although some of these conjectures could be true, more research is needed on the role of organic matter in controlling metal distribution in the weathering environment.

10.3.4 Secondary carbonates as reaction sites

Carbonates of calcium and/or magnesium accumulate in arid and semi-arid regions either in the surface horizon or at a certain depth in the soil profile depending on the amount and distribution of rainfall. The control of metals in soils and sediments by the secondary carbonates is brought about by adsorption of metals on the surface, by coprecipitation, and by the formation of insoluble metal hydroxides through the capacity of the prevailing high pH to hydrolyze metal ions. The scavenging of metals by carbonates is not as effective as that by iron and manganese oxides (Patchineelam, 1978). However in arid and semiarid regions where accumulation of iron and manganese oxides is not present, carbonates as controls of the distribution of metals deserve due attention (Chao, 1984).

10.4 METHODS

Extraction schemes were chosen for this study so as to test easily extractable ions associated with carbonates, Mn oxides and/or amorphous iron oxides. This section determines the effect of carbonates, Mn oxides and amorphous Fe oxides on extractability of various base metals with the aim of enhancing our understanding of geochemical dispersion processes in the study area.

The three methods detailed below are observed to be commonly highly selective for particular mineral phases in soils (Chao, 1984). A total of 27 samples from most of the

horizons of the profiles were submitted for sequential leaching. Five grams of sample were weighed into a centrifuge tube and then sequentially extracted by the methods described below:

pH 5 acetate (extracts from carbonates and surface adsorbed metals).

The 5.00g of sample was taken with 95 mL 1 mole/litre (M) ammonium acetate at pH 5 for 6 hours. The mixture was then centrifuged (4000 rpm, 15 minutes) and the supernatant decanted. The extraction was repeated. The solid was then mixed with 10 mL 0.1 M ammonium chloride and centrifuged. The three aliquots were combined for analysis by ICPMS for Au, Ag, As, Ca, Mg, Cu, Fe, Mn, Ni, Pb and Zn.

0.1M hydroxylamine (extracts from Mn oxides).

The residual solid from the extraction was then mixed with 90.0 mL 0.1M hydroxylamine hydrochloride in 0.01M HNO3 for at least 30 minutes. The mixture was centrifuged and the supernatant decanted and analyzed by ICP-MS for the same suite of elements as the pH 5 extraction.

0.25M hydroxylamine (extracts from amorphous iron oxides)

The residual solid from the extraction was then mixed with 90.0 mL 0.25M hydroxylamine hydrochloride in 0.25M HCl at 50° C for at least 30 minutes. The mixture was centrifuged and the supernatant decanted and analyzed by ICP-MS for the same suite of elements as the pH 5 extraction.

Figure 10.5.1 provides a diagrammatic representation of the phases dissolved by selective and acid extractions.

10.5 RESULTS

The selective extraction results are presented in Appendix 10. The Au, Ag and Co values are presented in ppb while all the other values are in ppm. Most of the As values are well below the ICP-MS lower limit of detection of 1 ppm and hence have not been utilized in this study. The extraction patterns displayed by these elements in the major regolith units include:

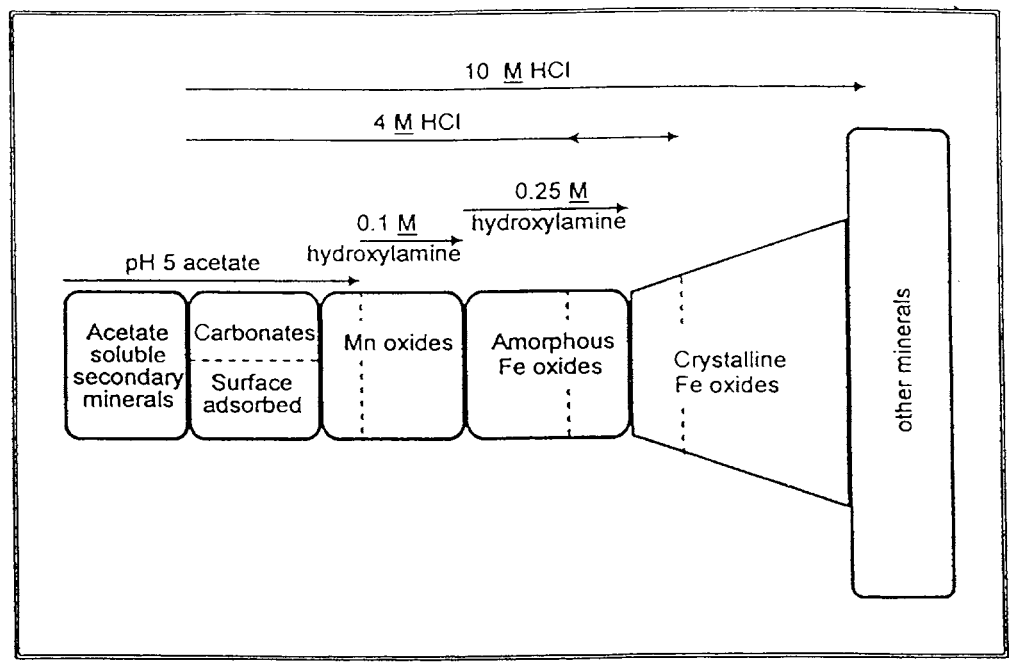

Figure 10.5.1: Diagrammatic representation of the phases dissolved by selective and acid extractions.

10.5.1 Soil horizons

The selective extraction graphs of selected regolith units are presented in Figures 10.5.2 to 10.5.6. Profile 6 soil 'B' horizon is situated over the transported regolith and that of profile 7 over residual regolith.

Most of the Ca and Mg in the soil horizons is dissolved by pH 5 acetate. Ni, Co and Pb gave high yields on 0.1M hydroxylamine extraction, indicating their association with Mn oxides. The concentration of Ni extracted in profile 6 is 6 ppm while that of Pb is 4 ppm and Co 8 ppm. The concentrations dissolved by 0.25M hydroxylamine are 2 ppm for Ni, 4 ppm for Pb and 1 ppm for Co. The total concentrations dissolved by the two reagents in this profile represent approximately 40 % of total Ni, 35 % of total Pb and 90 % of Co.

The concentration of Ni extracted by 0.1M hydroxylamine in profile 7 is 5 ppm while that of Pb is 9 ppm and Co 12 ppm. The concentration extracted by 0.25M hydroxylamine is 1.5 ppm for Ni, 4 ppm for Pb and 1.5 ppm for Co. The combined concentrations dissolved by the hydroxylamine reagents represent approximately 65% of XRF total Ni, 90% of XRF total Pb and 100 % Co. The highest concentrations of Zn (4 ppm) are extracted by the 0.25M hydroxylamine represented by 1.5 ppm in profile 6 and 3 ppm in profile 7. Slightly lower amounts (< 1 ppm) are dissolved by 0.1M hydroxylamine in

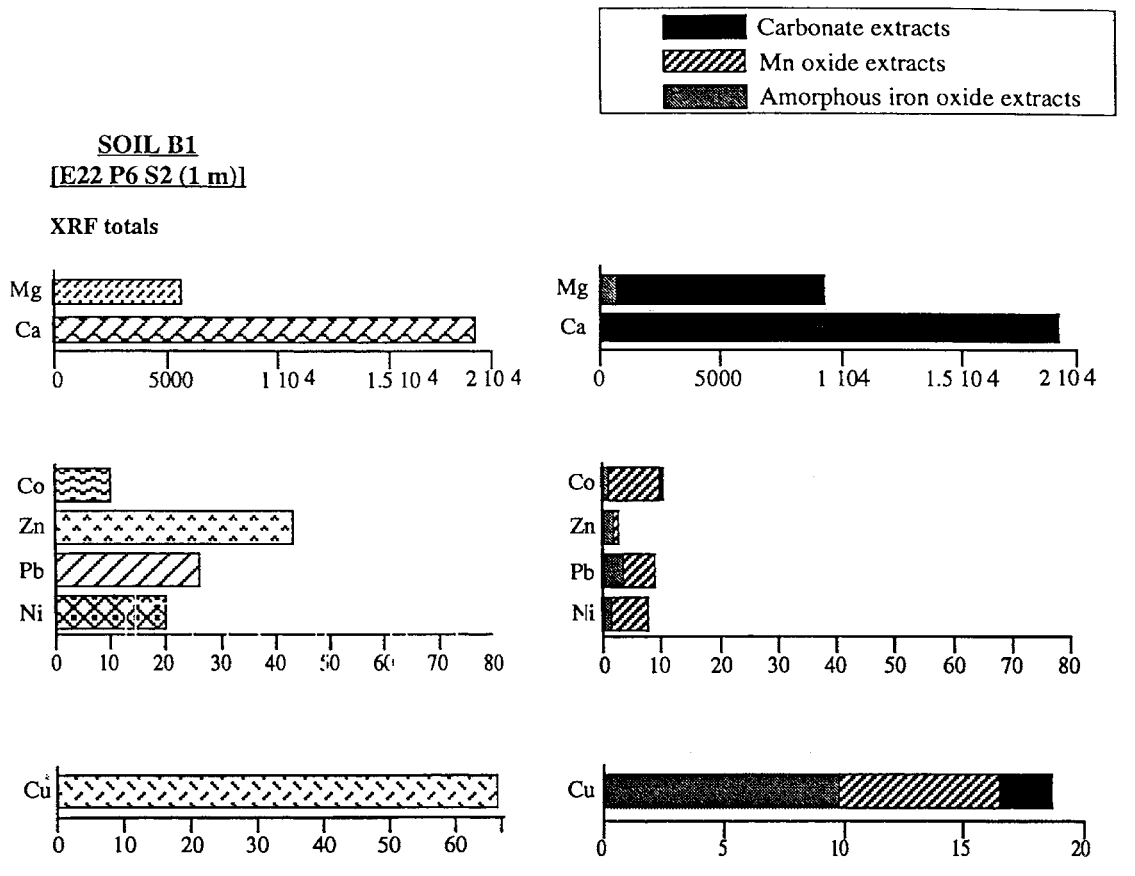

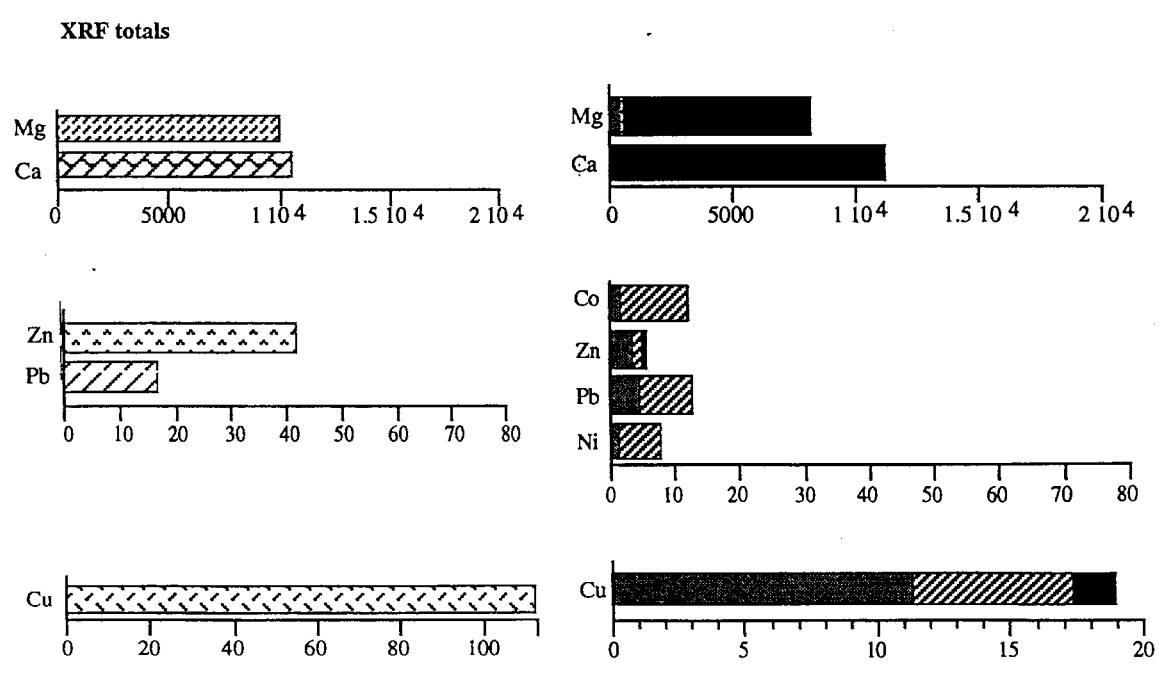

Figure 10.2: Selective extraction graphs for samples from the Soil 'B' 1 horizons
[All values are in ppm]

both profiles. The combined concentrations extracted by the three reagents represent approximately 5 % and 20% of the XRF Zn totals in profiles 6 and 7 respectively.

The highest concentrations of Cu (~ 10 ppm) are extracted by 0.25M hydroxylamine relative to the 0.1M hydroxylamine (~ 6 ppm) and pH 5 acetate (< 4 ppm) in profile 6. The same pattern is shown by profile 7 i.e ~ 12 ppm extracted by 0.25M hydroxylamine, 6 ppm by 0.1M hydroxylamine and 2 ppm by pH 5 acetate. The combined concentrations extracted by these techniques represent approximately 30 % and 18 % of the total Cu in E22 Profile 6 and E27 Profile 7 respectively. The results show that Cu is associated with the amorphous Fe oxides in the soil.

The concentrations of these elements extracted by 0.1M hydroxylamine are noticeably higher in the soil as compared to the mottled clay and white clay units. This might represent enrichment of these elements in organic matter, and degradation of Mn oxides by organic matter causing high levels of amorphous Mn oxides close to the surface. The extraction patterns are similar for the two soil types despite the differences in the parent materials.

10.5.2 Mottled clay units.

Most of the Ca and Mg is dissolved by the pH 5 acetate in both the medium-and-mega-mottled clay showing that these cations are mostly held within the carbonates in this unit. Generally, the amounts of Ni, Co, P and Zn dissolved in the two units are low (< 5 ppm). Pb and Co showed appreciable dissolution by 0.1M and 0.25M hydroxylamine in the medium-mottled clay. The combined amounts dissolved by the two reagents represent approximately 10% of the Pb totals and 80 % of the Co totals. The Zn and Pb were dissolved in equal proportions (2.5 ppm each) by the two hydroxylamine reagents in the medium-mottled clay. The combined concentrations represent approximately 8% and 45% of the Zn and Pb totals in this unit. The concentrations extracted in the mega-mottled clay are too low for any associations to be discerned. It is important to note that these elements could be present in the crystalline iron oxides whose extraction capacities using hydroxylamine were not determined.

Cu in the medium-mottled clay and mega-mottled clay is mostly dissolved by the 0.25M hydroxylamine (~ 80 and 15 ppm respectively) as compared to the pH 5 acetate (~ 25 and 10 ppm respectively) and 0.1M hydroxylamine (~ 20% and 5% respectively) indicating a stronger association with the amorphous Fe oxides in the mottled clay units.

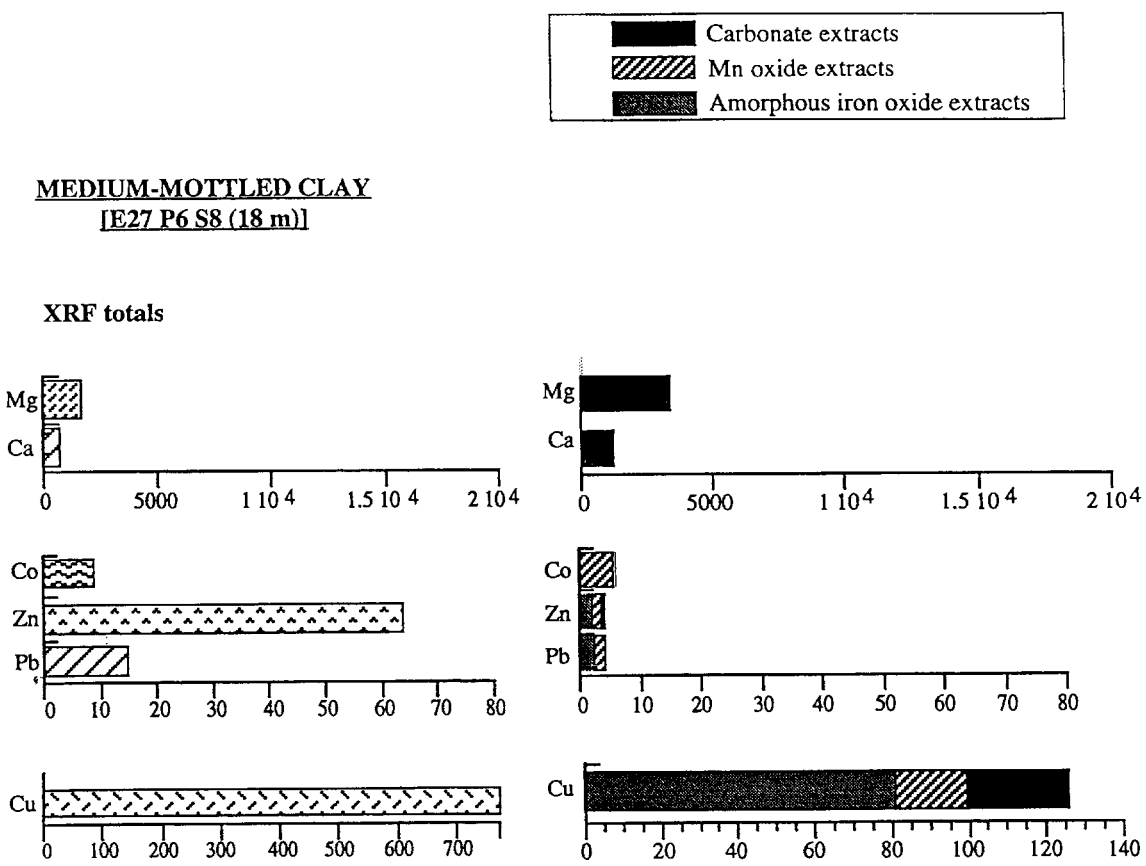

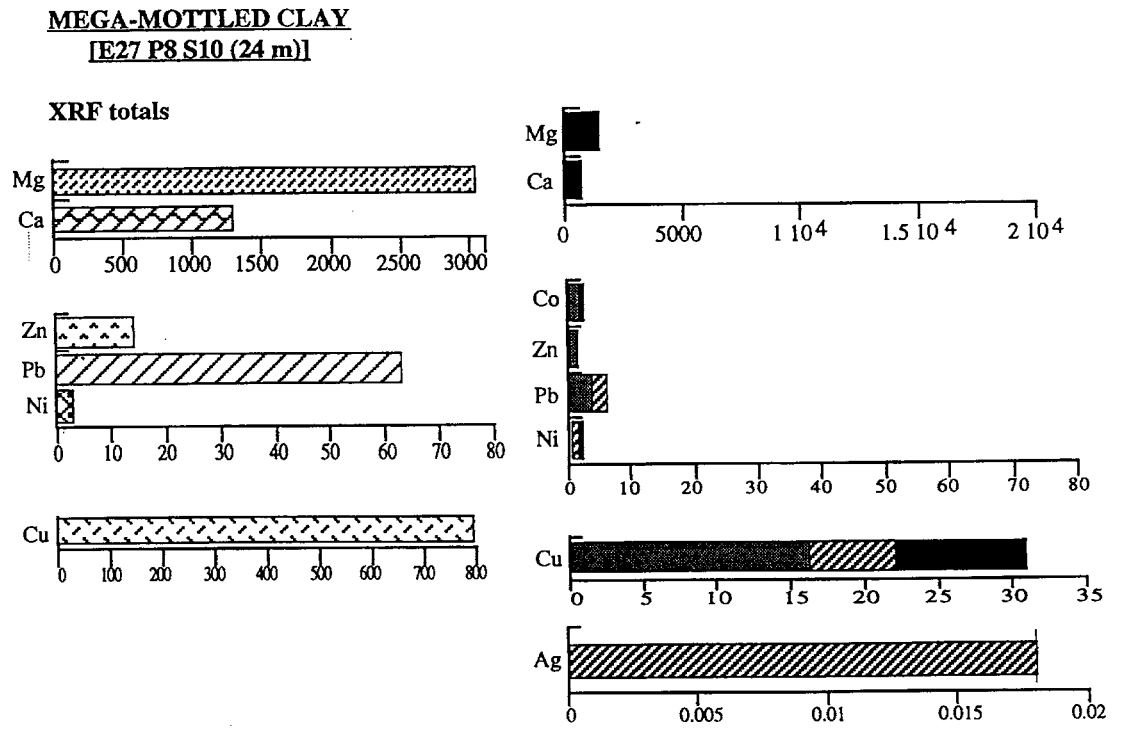

Figure 10.3: Selective extraction graphs for samples from the medium-and-mega-mottled clay unit
[All values are in ppm]

The combined XRF totals represent approximately 18 % and 4 % of the Cu in the medium-mottled clay and mega-mottled clay respectively.

10.5.3 Nodular iron-manganese aggregates

As in the other units, most of the Ca and Mg is dissolved by pH 5 acetate. All the other elements are dissolved mainly by 0.1M hydroxylamine as compared to the 0.25M hydroxylamine showing a strong association with the Mn oxides in this unit.

The Zn concentration dissolved by 0.1M hydroxylamine is 17 ppm as compared to 3 ppm by 0.25M hydroxylamine. The combined concentrations dissolved by the hydroxylamine reagents represent approximately 13 % of the XRF Zn totals (130 ppm). The concentration of Pb dissolved by 0.1M hydroxylamine is 70 ppm as compared to 22 ppm by 0.25M hydroxylamine. The combined concentrations represent approximately 80% of the Pb totals (110 ppm). Ni is mostly dissolved by 0.25M hydroxylamine (2 ppm) representing approximately 11% of its XRF total (18 ppm) while Co is mostly dissolved by 0.1M hydroxylamine (~ 85 ppm) and 0.25M hydroxylamine (~10 ppm) this representing approximately 100 % of the XRF totals (~ 95 ppm)

Some Cu (~4 ppm) is dissolved by pH 4 acetate. The rest is dissolved mainly by 0.1M hydroxylamine (~100 ppm) and 0.25M hydroxylamine (48 ppm) with the combined concentrations dissolved representing approximately 17% of the Cu XRF totals. Ag dissolved by 0.1M hydroxylamine is 0.14 ppm as compared to 0.04 ppm by 0.25M hydroxylamine. The Ag totals are not presented because it was below the XRF lower limit of detection (1 ppm).

10.5.4 White clay unit

Almost all of the Ca and Mg is dissolved by the pH 5 acetate mainly associated with the presence of carbonates and gypsum in this unit. Most of the Ag and Cu is dissolved by the 0.25M hydroxylamine (0.12 and 3.5 ppm respectively) as compared to pH 5 acetate (non for Ag and 1.8 ppm for Cu) and 0.1M hydroxylamine (0.04 and 1 ppm respectively). The Ag totals were below the XRF lower limit of detection (1 ppm). The amounts of Cu dissolved by the three reagents represent only 2% of the Cu XRF totals (350 ppm). Most of the Zn is dissolved by the pH 5 acetate although the low concentration of 2 ppm discounts the presence of any association with this phase. Co shows appreciable dissolution by the pH 5 acetate solution (~0.25 ppm) although like Zn, the relatively low concentrations precludes the presence of any association.

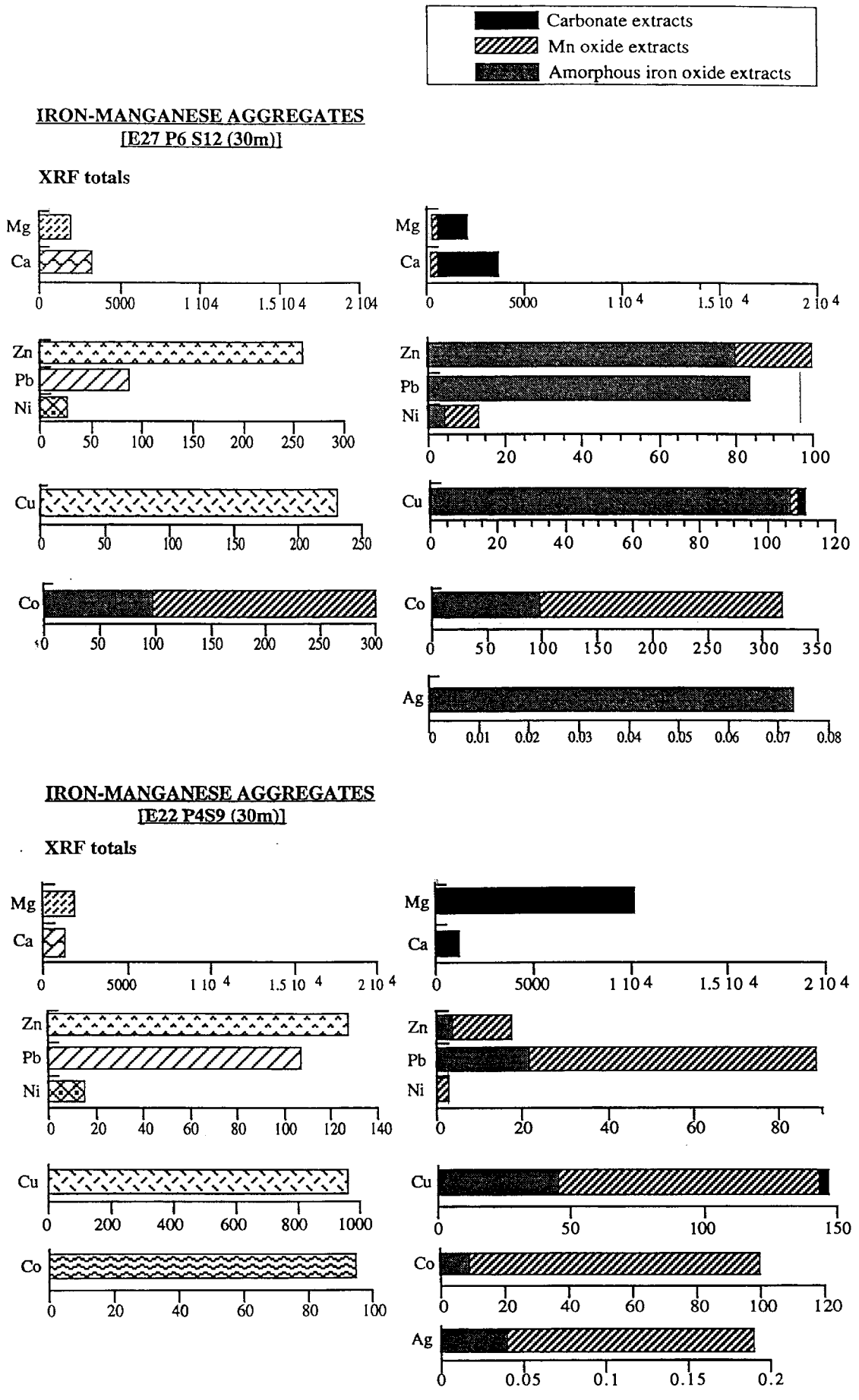

Figure 10.4: Selective extraction graphs for samples from the nodular Fe-Mn zones
[All values are in ppm]

Apart from total dissolution of Ca and Mg by pH 5 acetate, most of the other elements are dissolved to very low concentrations by the hydroxylamine reagents in this unit and hence no general partitioning characteristics can be discerned from these distributions.

10.5.5 Orange-Pink saprolite

Most of the Ca and Mg in this unit is dissolved by pH 5 acetate although unlike the other units appreciable amounts (< 2000 ppm) have also been dissolved by 0.1M hydroxylamine. All the Ni is dissolved by 0.1M hydroxylamine while the Pb is mostly dissolved by 0.1M hydroxylamine (~2 ppm). Zn on the other hand is mostly dissolved by 0.1M hydroxylamine (~ 3 ppm) as compared to pH 5 acetate (~ 2.5 ppm) and 0.25M hydroxylamine (~ 2 ppm). The combined concentrations of each of the elements represent approximately 50% of the Zn XRF totals.

Ag, Cu and Co shows appreciable dissolution in the three reagents. Ag is mostly dissolved by the 0.25M hydroxylamine (~ 5.5 ppm) as compared to 0.1M hydroxylamine (3.5 ppm). Cu is mostly dissolved by 0.1M hydroxylamine (~ 600 ppm) as compared to 0.25M hydroxylamine (~ 250 ppm) and pH 5 acetate (~ 160 ppm). The combined concentrations represent approximately 55% of the total Cu concentration (~ 1800 ppm). Co is mostly dissolved by 0.25M hydroxylamine (~ 200 ppm) and 0.1M hydroxylamine (~ 45 ppm). The combined concentrations show that all the Co was dissolved by these reagents in this unit.

These results conform to those of the isocon plots which showed the depletion of Cu in these unit associated with loss in weathering susceptibility of the host minerals i.e orthoclase and K-feldspar.

10.5.6 Greenish-Grey saprolite

Appreciable amounts of Ca and Mg is dissolved by pH 5 acetate (~ 1400 ppm and 1100 ppm respectively). This represents approximately 80% and 35% of the Ca and Mg totals respectively. This implies that unlike in the other units, the Ca and Mg is not entirely associated with the carbonates and are present in other Ca bearing mineral phases in this unit i.e albite and ferromagnesium silicates.

Zn is mainly dissolved by the pH 5 acetate acetate (~ 3 ppm) as compared to 0.1M and 0.25M hydroxylamine (~ 1% each). The combined concentrations represent

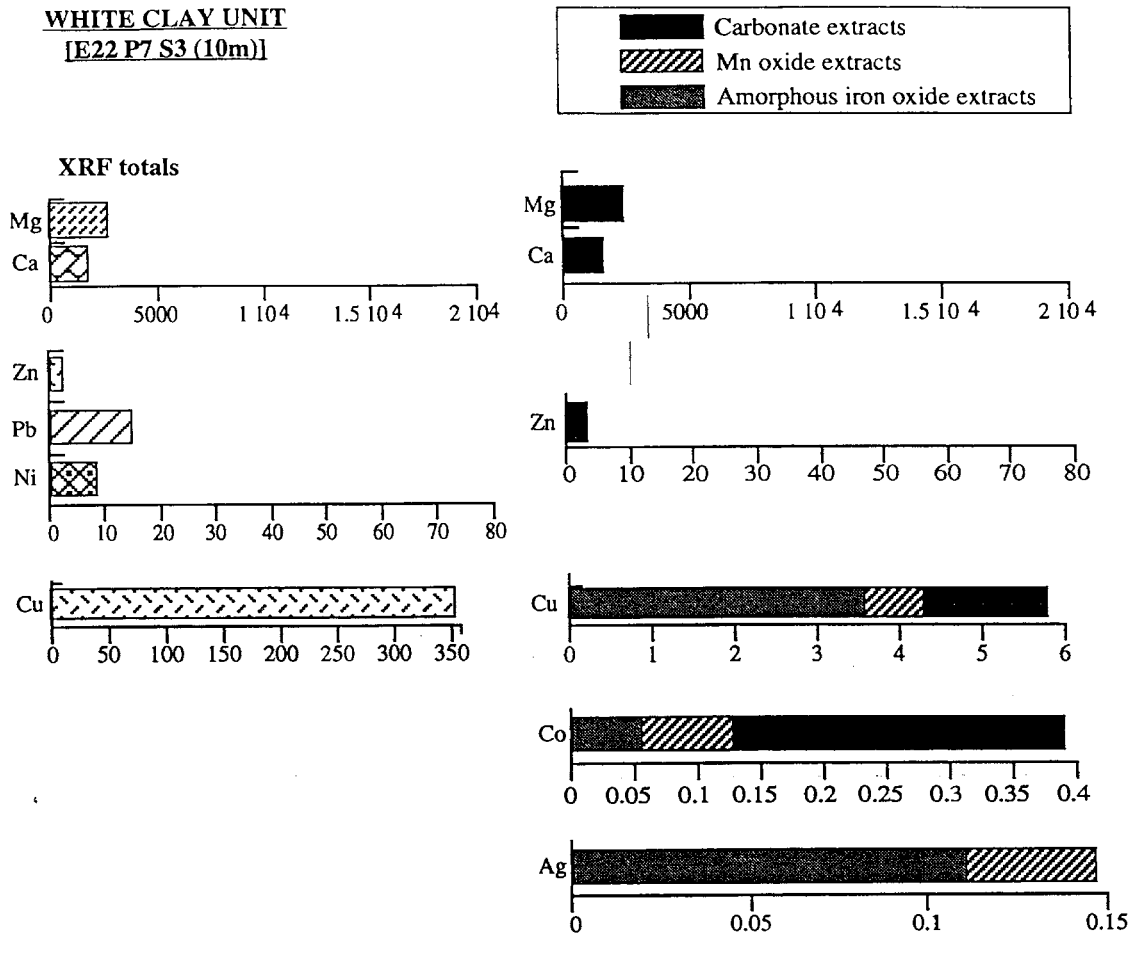

Figure 10.5: Selective extraction graphs for samples from the white clay unit and the orange-pink saprolite [All values are in ppm]

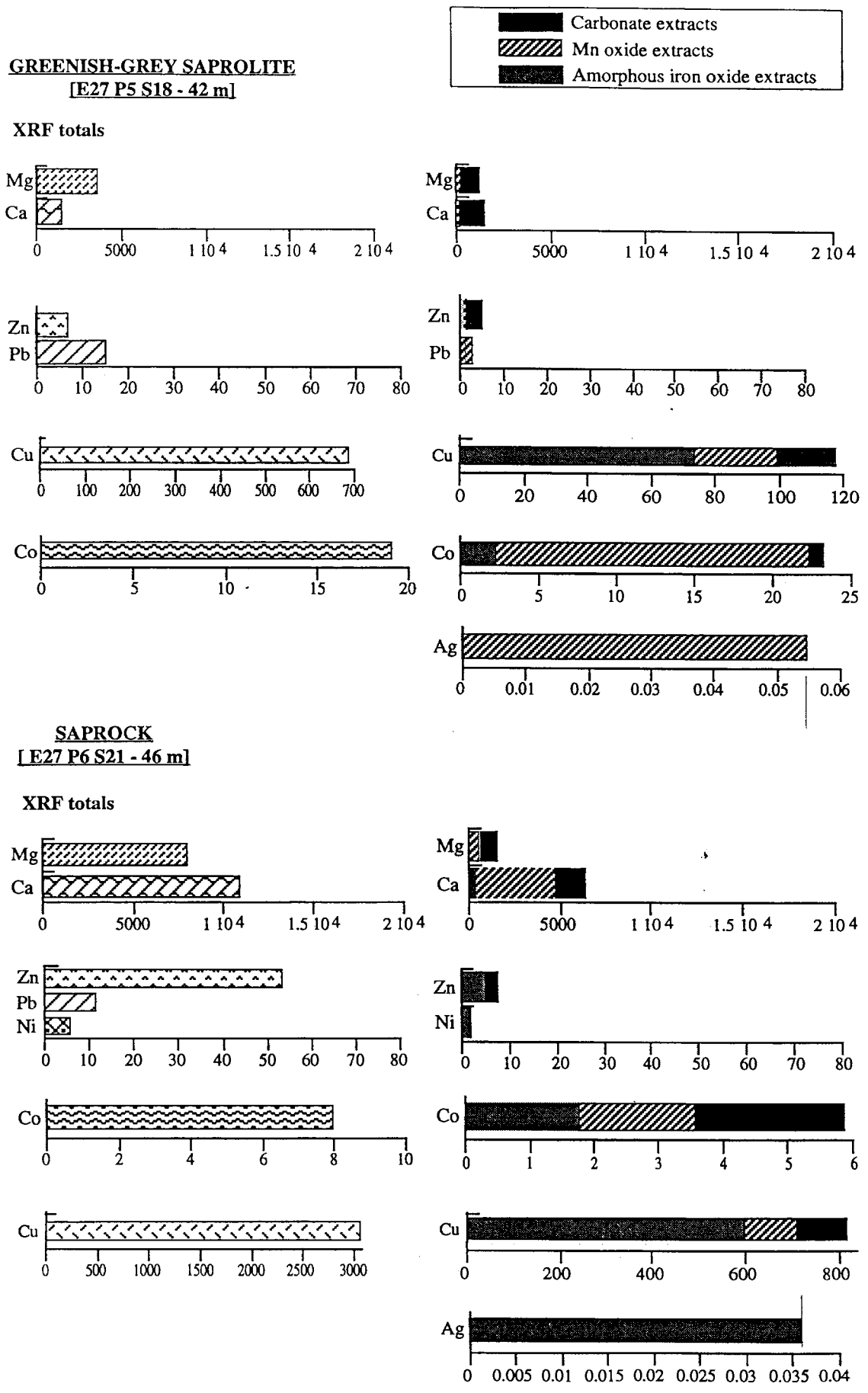

Figure 10.6: Selective extraction graphs for samples from the greenish-grey saprolite and the saprock [All values are in ppm]

approximately 70% of the Zn XRF totals. The Pb is mostly dissolved by the 0.1M hydroxylamine (~ 1 ppm) although the amount dissolved is only 7 % of the Pb totals.

Cu is mainly dissolved by 0.1M hydroxylamine (~ 75 ppm) as compared to 0.25M hydroxylamine (~ 25 ppm) and pH 5 acetate (~ 20 ppm). The combined concentrations in these reagents represent approximately 20% of the Cu totals (~ 700 ppm).

Co is mostly dissolved by the 0.1M hydroxylamine (~ 20 ppm) and 0.25M hydroxylamine (2.5 ppm). The combined concentrations imply total dissolution of Co by the two reagents.

10.5.7 Saprock

Ca and Mg shows diverse results in this unit as compared to the other units. Mg is mostly dissolved by pH 5 acetate (~ 1000 ppm) as compared to 0.25M hydroxylamine (~ 700 ppm). The combined totals represent approximately 25% of the Mg totals implying that most of the Mg is associated with other mineral phases notably the ferromagnesium silicates. Ca is mostly dissolved by 0.1M hydroxylamine (~ 4,600 ppm) as compared to pH 5 acetate (~1400 ppm) and 0.25M hydroxylamine (~ 400 ppm). The combined totals represent approximately 60% of the Ca totals (~ 10,000 ppm). The main host to the Ca in this unit is plagioclase feldspar.

Ag is entirely dissolved by 0.25M hydroxylamine (~ 0.035 ppm) while Zn is dissolved mostly by 0.25M hydroxylamine (~ 6 ppm). The combined Zn concentrations represent approximately 20% of its total concentration (55 ppm). Co is dissolved in almost similar proportions in the three reagents (~ 2 ppm each), this representing approximately 75% of the XRF totals (8 ppm).

Cu on the other hand is mostly dissolved by the 0.25M hydroxylamine (~ 6000 ppm) as compared to pH 5 acetate and 0.1M hydroxylamine (~ 100 ppm respectively). This represents approximately 27% of the Cu XRF totals (3000 ppm).

10.6 DISCUSSION

10.6.1 Interpretation

The Selective extractions are, as the name implies, designed to specifically extract certain minerals or phases, and the results indicate that the method has been very efficient for this

study. The pH 5 acetate successfully extracts all of the Ca and Mg phases from the carbonate-rich units. In contrast, in the residual units, where some of the Ca and Mg occur as non-carbonate minerals, the Ca and Mg was not entirely dissolved by pH 5 acetate. In these units, the Ca and Mg occur within plagioclase feldspars and ferromagnesium silicates (diospide, epidote and hornblende) which are more resistant to the pH 5 acetate extraction.

Other elements to be partially extracted by this reagent are Cu and Zn. In some samples these elements were appreciably dissolved by the pH 5 acetate (e.g. Zn in the greenish-grey saprolite). It should not be assumed that all these cases indicate that the elements occur within the carbonates. These elements may partially occur as soluble secondary minerals that dissolve in an acid acetate solution, which complexes most high charge (3+ or greater) ions (D.Gray pers. comm.). The dissolution involved for Cu is in the order of 100 to 200 ppm (e.g. Cu in mega-mottled clay and the saprock). This seems to be associated with the high concentrations of the element in these units although its association with the carbonate alteration zone close to mineralization in the saprock cannot be discounted.

The other extractions, namely 0.1 M hydroxylamine and 0.25 M hydroxylamine, are designed to separately dissolve Mn oxides and "amorphous" Fe oxides. These reagents were found to be good extractants for most of the elements apart from Ca and Mg. The elements were dissolved to different proportions by the two reagents. Ag for example was dissolved entirely by 0.25M hydroxylamine in the saprock and white clay unit and predominantly by 0.1M hydroxylamine in the nodular iron and manganese unit, mega-mottled clay and the greenish-grey saprolite. The general trend from all the samples analyzed favours the partitioning of the Ag into the Mn oxides.

Ni and Co are preferentially incorporated into the Mn oxides as compared to the amorphous Fe oxides. There is a general tendency for Zn to be incorporated into the iron oxides although the nodular Fe-Mn unit and the orange-pink saprolite showed some association with the Mn oxides in addition to moderate concentrations in the iron oxides. Some Zn (~ 1.5 ppm) was also dissolved by pH 5 acetate in the white clay unit. The low concentrations involved discounts the presence of any association.

Pb is preferentially partitioned into the Mn oxides in the soil and the greenish grey saprolite although the general trend in the other units favours incorporation into the iron oxides. The general trend in Cu distribution also favours partitioning into the iron oxides except in the nodular Fe-Mn unit and the orange-pink saprolite.

It is also observed that apart from total dissolution of the Ca and Mg by the pH 5 acetate, the other reagents did not dissolve most or all of the elements as shown by the disparities between the combined element concentrations and the XRF element totals. Ag showed appreciable dissolution (50-100%) by these reagents while the concentrations of the other base metals dissolved by the reagents were generally below 30%. The effect was more pronounced in the lower levels of the residual units where in general the dissolution capacity was lower than 15% especially for Pb and Cu. The explanation for this distribution seems to relate to the resistance of the host minerals of these elements. Most of these base metals are hosted by resistant mineral phases like muscovite and some of the ferromagnesium silicates. These elements appear to be tightly bound within these phases that the selective extraction could have only dissolved some and not all of the elements.

It is also important to note that amorphous and not crystalline iron oxides were utilized to extract these elements using the 0.25M hydroxylamine reagents in this study. Bivariate statistical analysis showed strong correlations between some of the elements like As, Pb and Zn with the iron oxides in the mottled clay units. Some of these associations were apparent in the extraction patterns although the generally low concentrations of these elements in the mottled clay units implies that they could be associated with the crystalline and not amorphous iron oxides in these units. It should also be born in mind that selective extractions are only operationally defined i.e there is no proof offered that they only attack carbonates, Mn oxides and amorphous Fe-oxides (Hall et al. 1996). Consequently, the results from both statistical and selective extractions have served to show the immense capacities of the oxides to incorporate the metals into their structures.

It was also observed that the dissolved concentrations of some of the elements like Ag, Ni, Co, Pb and Zn in the clay-rich units like the white clay unit were very low as compared to the other units with lower amounts of clay. This suggests that these metals were also tightly bound within the complex clay crystal structures. In general, clays tend to act as "conveyor belts" or as "sinks" to these metals although some like smectites can show some partitioning characteristics. These characteristics are not well documented although they are subjects of current intense study. Table 10.2 summarizes the partitioning affinities of these elements as observed in this study. The terms used relate to the general level of dissolution by these reagents.

Element	pH 5 acetate (from carbonates)	0.1M Hydroxylamine (from Mn oxides)	0.25M Hydroxylamine (from Fe oxides)
Ca	Strong	Mild (Mod. in saprock)	Mild
Mg	Strong	Mild	Mild (except in saprock)
Zn	Mild	Moderate	Strong
Pb	Mild	Moderate	Strong
Ni	Mild	Strong	Moderate
Co	Mild	Strong	Moderate
Cu	Mild to moderate	Moderate	Strong
Ag	Non	Moderate	Strong

Table 10.2: The general partitioning characteristics of the elements into carbonates, Mn oxides and amorphous iron oxides in the study area [Mod. -moderate]

10.6.2 Scavenging properties of iron and manganese oxides

The ability of iron and manganese oxides to scavenge metals in the secondary weathering environment has been discussed by a number of workers in recent years (Hawkes & Webb, 1962; Levinson, 1974; Chao & Theobald, 1976; Hem, 1978 and Chao, 1984, Thornber, 1992; Thornber & Wildman, 1984; Schwertmann, 1989). The iron oxides occurred as nodules and as crystalline or amorphous phases in the mottled clay samples and in the saprolite. The manganese oxides on the other hand occurred in the nodular iron-manganese aggregates and as fracture and vein infills in the mottled clay units and the saprolite. It also occurred as coatings on other mineral phases.

Historically, the scavenging properties of Fe and Mn oxides have been regarded as a negative trait in geochemical exploration because of the tendency of the oxides to concentrate metals from the background environment, thus giving rise to metal anomalies that are not related to mineralization (Chao & Theobald, 1976).

The amorphous Fe oxides are more reactive chemically than are the crystalline Fe oxides. Average soils contain greater amounts of Fe oxides than Mn oxides, but the Mn oxides exhibit greater chemical reactivity and more complex mineralogical composition than do the iron oxides. The chemical reactivity of Mn oxides is related to some specific features of Mn:

1. Mn can exist in several oxidation states

2. It forms non-stoichiometric oxides with variable valence states
3. Its higher valent oxides exist in several crystalline forms
4. The Mn oxides form coprecipitates and solid solutions with Fe oxides (Ponnanperuma et al. 1969).

Fe and Mn oxides exhibit a marked tendency to form coprecipitates or mixed oxides. Ponnamperuma et al. (1969) attributed this association to:

1. Similarities in some chemical properties of the higher oxides of Fe and Mn including reversible oxidation-reduction, insolubility, and the presence of pH dependent electric charges;
2. The closeness of the ionic radii of Mn^{2+} (0.80 Å) and Mn^{3+} (0.66 Å) to those of Fe^{2+} (0.76 Å) and Fe^{3+} (0.64 Å), respectively; and
3. Crystal-lattice-induced valence changes.

The role played by Fe and Mn oxides as scavengers in nature has been emphasized by a number of workers. Jenne (1968) proposed that Fe and Mn oxides act as 'sink' for the heavy metals in soils and sediments. Hydrous oxides of Mn and Fe are nearly ubiquitous in clays and soils both as coating on other mineral surfaces and as fine discrete particles in clusters and aggregates of colloidal dimensions. This general mode of occurrence allows the oxides to exert chemical influence on other mineral species that is far out of proportion to their concentration (Jenne, 1968).

The scavenging of metals by secondary oxides may take place by one or a combination of the following mechanisms: (1) coprecipitation, (2) adsorption, (3) surface complex formation, (4) ion exchange, (5) penetration of the crystal lattice. Coprecipitation may occur under certain conditions where Fe and Mn oxides are precipitated out of solution with other metals, for example, when underground metal-containing fluids enter an oxidative environment. Mechanisms (2), (3), (4), and (5) are listed separately only for convenience; they should be treated together because of the interrelation and interaction of one mechanism with the other (Chao & Theobald, 1976).

Mn oxides may have surface areas as much as few hundred square metres per gram (Morgan & Stumm, 1964b; Anderson et al. 1973; Loganathan & Burau, 1973) and a larger cation exchange capacity than some clay minerals (Morgan & Stumm, 1964b). The 'open structure' with both external and internal surfaces and the ready availability of sites due to crystal imperfections (Wadsley & Walkley, 1951) tend to make these oxides effective scavengers for foreign metal ions.

A general mechanism of adsorption of metal ions on hydrous oxides has been described by Loganathan and Burau (1973) as the exchange of bound H ions of the oxide surface with metal ions by the following scheme:

$$M^{n+} + x\,(=MeOH) <<>> M\,(MeO)_x^{(n-x)+} + xH^+$$

where M is the metal ion to be adsorbed and (=MeOH) and (MeO) are oxide surface sites. This model is rather attractive because it would explain the pH dependence of the adsorption of metal ions by hydrous Mn and Fe oxides and the release of H ions as a result of the adsorption, which has been observed by many investigators (McKenzie, 1970; Anderson et al. 1973; Loganathan & Burau, 1973; Gadde & Laitinen, 1974 and Murray, 1975).

The solubilities of the transition metals are pH dependent, as are also their adsorption characteristics on precipitated iron oxyhydroxides (Thornber & Wildman, 1984). Thornber (1992) provides the following sequence for the pH at which adsorption of metals begins on goethite with increasing pH:

M2+	Cu	Pb	Zn	Co	Ni	Cd	Mn
pH	4.5	5	6.2	6.5	6.7	7	7.5

Table 10.3. Adsorption of metals to goethite (Thornber, 1992)

Copper, for example, co-precipitates with goethite as tenorite or cuprite above pH 7, whereas at pH 4.5, where its solubility is 10,000 times greater, it adsorbs on precipitating iron oxides. In acid solutions the rare earth elements (REE) may be adsorbed onto precipitating ferric oxyhydroxides. Fee et al. 1992 observed that REE introduced into Lake Tyrrell in western Australia were scavenged from solution by ferric oxyhydroxides precipitated as the pH of the solution rose. Carvalho et al. (1991) found by contrast that lateritic material over gabbros had been depleted of REE-enriched in laterite formed over more basic carbonate.

Ferryhydrite is one of the most highly reactive of the amorphous Fe oxides because of its huge surface area. It slowly converts to goethite or hematite, and many of its adsorbed ions remain trapped in the better crystalline mineral. The solubilities of Cu, Ni, Zn, Co and Pb are all controlled to some degree by oxidizing Fe (II) if it is present. The amount of Fe relative to base metal is important in determining the composition of the precipitate and the oxidizing Fe also controls the pH of the environment where the precipitate is

forming (Thornber & Wildman, 1984). The association of gold with iron oxyhydroxides has been determined in this study (Section 10.7) and elsewhere (e.g. in Boddington, Mt. Gibson documented in Butt & Zeegers, 1992, p.310).

The adsorption of metal ions by hydrous Mn and Fe oxides is not limited to exchange with the surface-bound ions. Anderson et al. (1973) found that Ag adsorption maxima appeared to vary with the amount of Na and K that existed within the structure of poorly crystallized Mn oxides. The uptake of Ag by these oxides is considered to be by surface exchange for Mn, K and Na as well as exchange for structural Mn, K and Na. McKenzie (1970) studied the adsorption of Co, Cu and Ni from solution by synthetic Mn oxides and found that the initial rapid uptake of all three ions by replacement of readily exchangeable Mn^{2+}, K^{+} and H^{+} was followed by a period of slow uptake. The slow phase for the reaction was attributed to the exchange with ions in the crystal lattice which can be called 'diffusion exchange' or 'penetration of the crystal lattice'.

The study of the scavenging of metal ions by secondary oxides requires knowledge of the factors affecting the formation and reactivity of Fe and Mn oxides. Organic matter for example is a complicating factor in natural conditions. It produces periodic reducing environment, which maintains Mn and Fe oxides in a hydrous microcrystalline condition (Jenne, 1968); may solubilize these oxides under prolonged reducing conditions; and may chelate metal ions, thereby increasing their mobility and dispersion (Chao & Theobald, 1976).

In this study, Co, Ag and Ni stood out in the adsorption and scavenging by Fe and Mn oxides. Chemical analyses of Mn oxide minerals separated from some Australian soils have shown that Co is preferentially retained by Mn oxides and that it is more concentrated in the oxide minerals than in the bulk sample (Taylor & Mckenzie, 1966; Mckenzie & Taylor, 1968).

The major findings of laboratory studies on adsorption of Co are:

1). The adsorption of Co within a certain range of concentrations can be expressed by the Langmuir isotherm equation (Tewari et al. 1972; Loganathan & Burau, 1973;

2). The adsorption is strongly pH dependent (McKenzie, 1967; Mu\rray et al. 1968; Tewari et al. 1972; Loganathan & Burau, 1973);

3). The adsoprtion of Co by MnO_2 is greater than that of Zn, Ca and Na (Loganathan & Burau, 1973);

4). The initial adsorption of Cu is greater than that of Co or Ni, but extraction of the adsorbed elements using 2.5% acetic acid shows, that once adsorbed, Co is the most strongly held (Mckenzie, 1967); and

5). The adsorption of Co involves multisite reactions, interchanging with surface bound H^+, structural Mn^{++} and Mn^{3+} and other ions (McKenzie, 1970; Loganathan & Burau, 1973).

As an explanation for the stronger adsorption of Co by Mn oxides than of other transition metals, McKenzie (1970, 1972) proposed that Co^{++} is oxidized to Co^{3+} at the oxide interface which then replaces Mn^{3+} where Mn^{3+} substitutes for Mn^{4+} in the crystal lattice of the Mn oxides. The driving force of this reaction is considered to be the increased stability conferred on the Mn oxides by the high crystal-field stabilization energy (CFSE) of the low-spin Co^{3+} ion. This replacement of structural Mn3+ would not be possible with Cu^{++}, Ni^{++}, or Zn^{++} ions.

Based on the crystal chemistry of Co and Mn ions, Burns (1976) explained that the uptake of Co into Mn oxides takes place as a result of the substitution of Co for Mn^{4+} ions in the edge-shared $[MnO_6]$ octahedra in many Mn oxide mineral structures.

Although analyses of natural Mn and Fe oxides as well as laboratory adsorption studies have established the scavenging capacity of these oxides for Ag, there is lack of information for the direct quantitative relationship between Mn and/or Fe oxides and Ag and on the comparative capacity of Mn oxides versus Fe oxides to retain Ag in nature. However, a kinetic method to establish metal-oxide associations by Ellis et al. (1967) and Chao & Anderson (1974) found Mn oxides to be the major control on the scavenging of Ag in stream sediments with Fe oxides playing a secondary role.

The oxidation of Ni by MnO_2 is represented by the equation (Pourbaix, 1963):

$$2Mn_3O_4 + 3Ni^{2+} + 4H^+ >> MnO_2 + Ni_3O_4 + 2H_2O + 5Mn^{2+}$$

A number of thermodynamic studies by Van der Weijden (1975) have also shown that Ni is more soluble than Mn in oxidizing environments.

10.7 GOLD-PEDOGENIC CARBONATE AND IRON OXIDE ASSOCIATIONS

10.7.1 Introduction

Secondary carbonates, commonly referred to as calcrete, may precipitate as calcite and/or dolomite in regoliths where the average annual rainfall is less than about 600 mm. Pedogenic carbonates are those that form in unsaturated (vadose) soil horizons. In the study area, carbonates occurred as thin veneers or as friable creamy yellow to white aggregates in fine earth matrix. The carbonates concentrated in these horizons as calcite and dolomite rarely exceeding 15% of the total mineralogical composition of the rock. The depth and thickness of the carbonate rich horizons varied, but it was generally encountered within the top 1 to 2 m of the soil and was readily identified as it effervesced with dilute HCl.

A general association between Au and pedogenic carbonate has been recognized for several decades and was commonly explained as coincidental, occurring through physical entrapment of Au nuggets in a calcareous cement. In some sampling programs, carbonates were specifically avoided, for fear that they would dilute the geochemical response, as is generally the case for base metals. Au-carbonate association was investigated using selected soil samples from a few profiles in the E27 deposit. This study was carried out to supplement the works of Smith (1996) who recently completed a project on the same topic utilizing samples from the Beechmore Block which is about 5 km from this study area. The profiles covered in this study included profiles 7, 10 and 11. They represent the profiles developed over the transported regolith, the profile over the orange-pink and greenish-grey saprolite and the profile developed over the trachyandesite. The mineralogical compositions of these soils are presented in Table 10.2.

Profile	Musc.	Qtz.	Kaol.	**Goe.**	**Hem.**	**Calc.**	Dol.	Gyps.	Albite	Smec.	Orth.
P11 (0m)	2.5	38.5	30.3	**9.4**	**2.0**	**12.5**	0.5	0.5	3.7	0.5	-
P11 (0.5m)	3.4	15.3	58.0	**8.4**	**1.0**	**11.1**	-	1.4	-	0.5	1.0
P11 (1.0m)	12.5	16.2	42.3	**14.7**	**0.5**	**7.8**	-	1.7	-	1.1	1.3
P11 (1.5m)	15.0	3.8	48.0	**6.9**	**0.5**	**5.3**	-	2.2	11.0	3.3	2.7
P11 (2.0m)	19.3	6.4	22.5	**1.7**	**1.7**	**2.7**	-	-	25.1	8.7	10.2
P10 (0m)	-	42.8	34.8	**2.2**	**1.4**	**-**	-	-	5.3	13.5	-
P10 (0.5m)	-	34.9	37.2	**1.1**	**1.6**	**5.0**	0.5	-	4.1	15.7	-

P10 (1.0m)	-	41.2	22.2	**0.5**	**1.4**	**4.5**	-	1.8	4.9	23.5	-
P10 (1.5m)	-	43.4	23.6	**0.5**	**1.3**	**1.3**	-	1.6	6.1	22.4	-
P10 (2.0m)	-	41.3	29.9	**1.0**	**1.5**	**1.2**	-	1.9	4.6	18.6	-
P10 (3.0m)	-	41.5	18.9	**0.5**	**1.0**	**0.5**	-	0.6	11.3	24.0	1.7
P7 (0m)	-	38.1	23.5	**2.8**	**2.0**	**8.3**	-	0.5	11.3	13.5	-
P7 (0.5m)	-	43.5	37.3	**6.9**	**0.6**	**3.7**	0.5	2.0	-	5.4	-
P7 (1.0m)	-	47.7	38.7	**6.8**	**0.9**	**0.5**	-	2.1	-	3.3	-
P7 (1.5m)	-	41.3	39.3	**6.1**	**0.7**	**0.5**	-	8.7	-	3.4	-
P7 (2.0m)	-	42.7	44.1	**10.4**	**0.6**	**-**	-	-	-	2.2	-
P7 (3.0m)	-	30.1	50.7	**16.5**	**2.6**	**-**	-	-	-	-	-

Table 10.4: Mineralogical compositions of the soils from E27 Profiles 11, 10 and 7 [Musc.-muscovite; Qtz.-quartz; Goe-goethite; Hem.-Hematite; Calc.-calcite; Dol.-dolomite; Gyps.-gypsum; Smec.-smectite; Orth.-orthoclase]

10.7.2 RESULTS

The line plots of depth versus concentrations of Au, Calcite, goethite and hematite are presented in Figure 10.7.1. Calcite is the dominant carbonate in all the profiles. Profile 11 contains the highest amounts (2.7-12.5%) of calcite while profile 10 contains the lowest amounts (0.5-5.0%). All the profiles contain low to moderate amounts of CaO (0.2-5%) and Fe_2O_3 (4-12%). Gold in all the profiles is generally above the generally acceptable anomalous value of 5 ppb.

The results show a poor correlation between Au and calcite in all the profiles. However, a good correlation exists between Au and goethite and hematite in E27 Profile 10. Profile 11 shows a fairly good relationship between the Au and goethite and a poor correlation with hematite. No correlation exists between the iron oxide minerals and the Au in profile 7.

These results compare favourably with those of Smith (1996) who also noted the lack of an association between calcite and Au and good correlation between Au and the iron oxide minerals in samples from the nearby Beechmore Block.

10.7.3 DISCUSSION

Calcite and dolomite form in the soil by the interaction of Ca^{2+}, Mg^{2+}, bicarbonate (HCO_3^-) and water. Calcium and magnesium are derived directly or indirectly from the

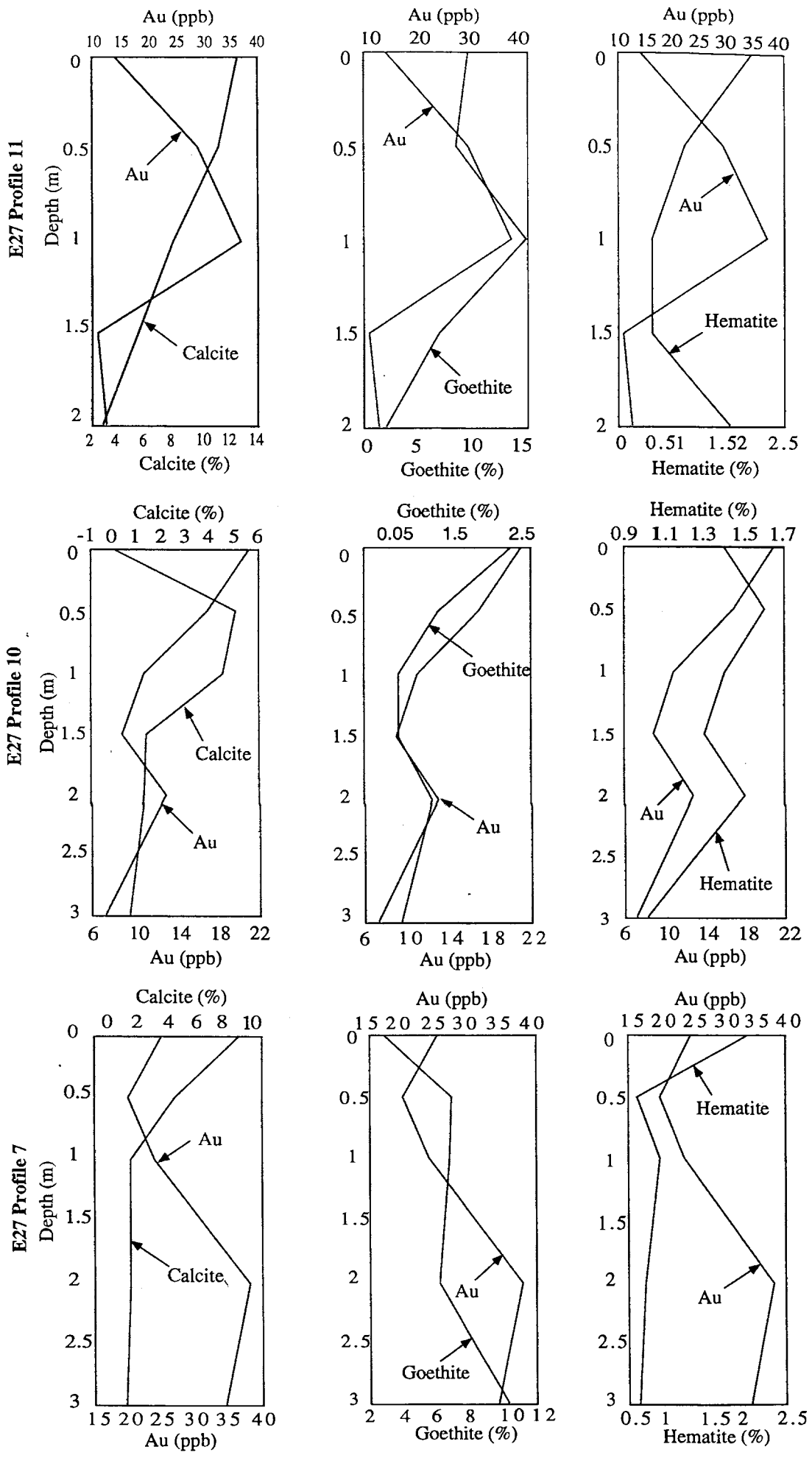

Figure 10.7.1: Association between Au and calcite, goethite and hematite in E27 Profiles 11, 7 and 10

bedrock, groundwater, vegetation, dust or rainfall. Carbon dioxide is produced by root and microbial respiration and dissolves readily in water, forming HCO_3^- which, in turn, reacts with free Ca^{2+} to precipitate as calcite as saturation is reached probably because of water being removed by evapotranspiration. Adsorption or precipitation of Au on carbonate surfaces through a pH effect from migrating soil water is improbable as it would result in a Au-enriched zone either at the top or base of the carbonate horizon.

In Western Australia, and the Gawler craton of South Australia, Au distribution within soil profiles have been observed to closely follow that of Ca and it has been assumed that it is controlled by a similar process, i.e. dissolved Au is precipitated by the removal of water from the soil (Lintern, 1997). Pedogenic carbonates in this region are widely distributed in the Gawler craton and in the Yilgarn craton south of about 30° S ('the Menzies Line') especially over basic rocks (Lintern, 1997). In the eastern parts of Australia, no such carbonate-enriched zones have been delineated. The reason for the dominant occurrence of pedogenic carbonates south of the Menzies Line is unclear, but is probably related to the region having a mainly winter rainfall and hence longer growing season and greater production of CO_2. Longer-term climatic factors related to these influences could also be of significance in the accumulation process (Milnes & Hutton, 1983).

Vegetation may play an important role in the formation of Au in carbonate anomalies. Both Au and Ca are present in plants and this suggests some involvement of vegetation in the mobility, dispersion and re-cycling of these elements in the surficial environment (Lintern, 1997). Both elements are taken up via roots, enter the plant tissue and ultimately, are returned to the soil surface as litter and released by decomposition. Gold is probably mobilized in soil solution as an organic complex which is deposited with the carbonates under evaporative conditions (Gray & Lintern, 1994).

Although this study has not addressed the reasons for the observed Au and carbonate associations in Western and Southern Australia and the absence of any association in the Parkes region, it is noted that the climates of the two districts are very different as shown in Table 10.4.

	Eyre peninsula	Yilgarn craton	Parkes region
Daily maxium temp.(¤C)	25.4	25.1	22.9
Daily minimum temp.(¤C)	12.5	11.5	11.3
Rainfall (mm)	97	257	586
Raindays (mean)	49	64	85

Table 10.5. The annual climatic indicators of the Eyre Peninsula, Yilgarn Craton and the Parkes region.

It is apparent from Table 10.4 that the Parkes region receives almost twice the rainfall, one to one and half times as many raindays and daily maximum temperatures that are 2° C less than the other two districts. These differences in climatic patterns will obviously affect the Eh and pH of the local environments and hence the distribution of the chemical species involved i.e Ca^{2+}, Mg^{2+}, H_2O and HCO_3^-.

Iron and manganese oxides are of paramount importance in the mobility and reprecipitation of Au due to their ubiquitous occurrence and strong scavenging effects (Chao & Theobald, 1976). Iron and manganese oxides are in general more important than aluminium and silicon oxides, because the iron and manganese oxides have greater adsorption capacities, dissolve as the redox potential decreases, and reprecipitate as the system becomes oxygenated (Jenne, 1977).

The preferential incorporation of Au by goethite and not hematite is related to its strong adsorption properties. This adsorption is pH dependent with many oxide surfaces including that of goethite changing from being positively charged at low pH to negatively charged at high pH. With increasing OH- concentration, such surfaces become increasingly negatively charged at high charge and thus more cations become adsorbed from solution (Thornber, 1992; Thornber & Wilman, 1984; Schwertmann, 1989).

Lateral dispersion of gold towards the top of regolith profiles particularly in the ferruginous and mottled horizons is well documented (Freyssinet et al. 1987; Michel, 1987). The chemical characteristics of an active weathering profile are such that there is an increase in Eh and decrease in pH from the weathering bed-rock interface up to the watertable (Lawrence, 1994). Implicit in the chemical model for such profiles where ferrolysis is active is that there is diffusion of ferrous ion, Fe^{2+} upward in the profile (Mann, 1983). Reprecipitation of gold occurs in conjunction with the precipitation of FeOOH (goethite) in these profiles because of the restricting effect of the presence of

Fe^{2+} in the profile (Mann, 1983). The reaction for the precipitation of gold by reduction of a acid-halide complex like $AuCl_4^-$ with Fe^{2+} can be written as:

$$AuCl_4^- + 3Fe^{2+} + 6H_2O = Au^\circ + 3FeOOH + 4Cl^- + 9H^+$$

Goethite

10.7.4 CONCLUSION

No association between Au and Carbonates has been determined from the results of this study. However, their exists a strong association between the distribution of Au and goethite in profile 10. This has been attributed to the mobility and restricting effect of Fe^{2+}, which causes reprecipitation of Au in most active weathering profiles. These results show the potential of this relationship as a major exploration tool in the region. Despite the results of this study being more or less similar to those of a recent study by Smith (1996), it is essential that more extensive regional work is carried out to decipher the extents of these relationships.

10.8.1 ELEMENT MOBILITY AND DISPERSION PATTERNS IN THE REGOLITH.

10.8.1 Introduction

This section provides a summary of the geochemical behaviour of all the elements based on the results of the techniques already discussed. The inferences described here have been supplemented by examination of the 2-dimensional plots of the elements in the E22 and E27 regolith stratigraphy (Figures 10.8 and 10.9 respectively). This section is followed by a discussion on the relationships between the distribution of the elements and regolith evolution processes in the area. The implications of these distributions on geochemical exploration in the area are also presented.

10.8.2 Fe, Si, Al

These elements are commonly the principal residual products of deep chemical weathering, occurring as the oxides (e.g. goethite, hematite and quartz) or as aluminosilicates (e.g. kaolinite and halloysite). Each is strongly enriched in the lower to mid-saprolite due to residual concentration following leaching of other components, particularly Mg and Ca. Remobilization and further concentration takes place in the upper horizons.

Figures 10.8: Distribution of elements in the E22 regolith stratigraphy

NOTES

. The major and trace elements are presented separately

. The major elements values are in weight %

. The trace element values are in ppm

. Vertical axis shows RL depth values in metres
Scale: 1 cm = 10 m

. Horizontal scale: 1 cm = 25 m

Major elements

SiO_2, Al_2O_3, Na_2O, K_2O, CaO, MgO and
TiO_2 respectively

Trace elements

Au, Cu, Pb, Zn and As

Figures 10.8: Distribution of elements in the E22 regolith stratigraphy

NOTES

. The major and trace elements are presented separately

. The major elements values are in weight %

. The trace element values are in ppm

. Vertical axis shows RL depth values in metres
Scale: 1 cm = 10 m

. Horizontal scale: 1 cm = 25 m

Major elements

SiO_2, Al_2O_3, Na_2O, K_2O, CaO, MgO and
TiO_2 respectively

Trace elements

Au, Cu, Pb, Zn and As

ENDEAVOUR 22 - SiO_2(%)

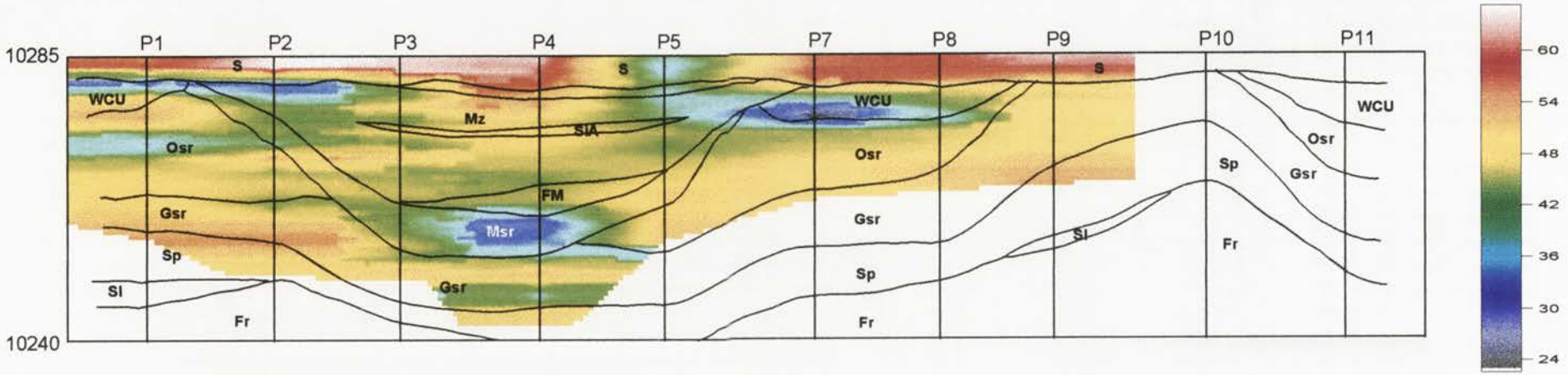

S	Soil Horizons	Osr	Orange-Pink Saprolite	Sl	Sulfide Zone	Msr	Mottled Saprolite
WCU	White Clay Unit	FM	Fe - Mn Nodules	Sp	Saprock	SiA	Silica Aggregates
Mz	Mottled Zones	Gsr	Greenish-grey Saprolite	Fr	Fresh Rock		

Figure 10.8.1

ENDEAVOUR 27 - SiO_2(%)

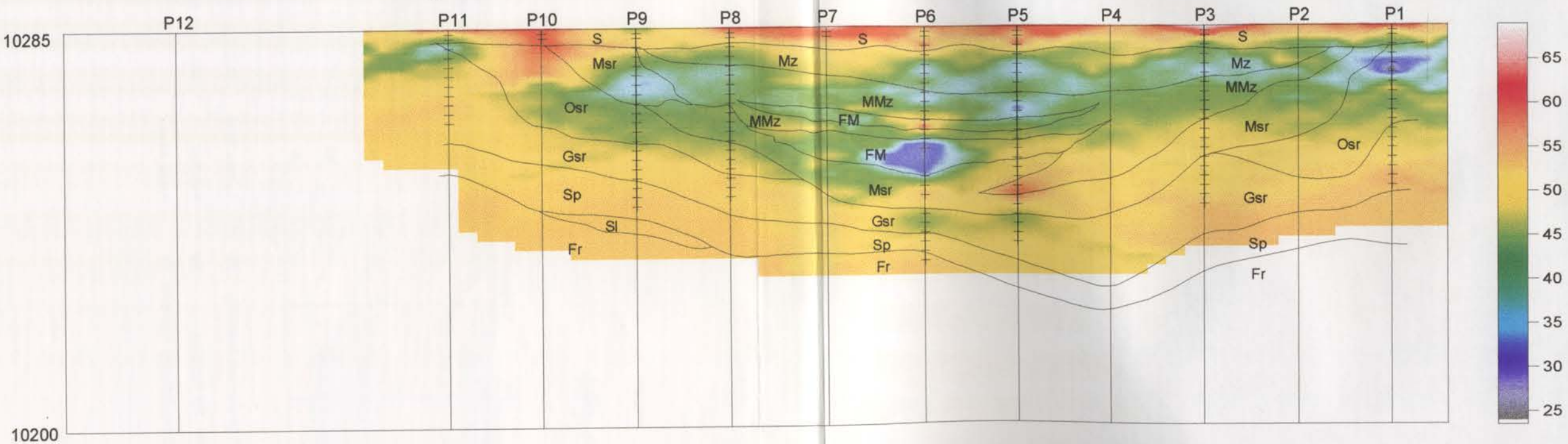

Horizontal Scale 1:2500
Vertical Scale 1:1000

S	Soil Horizons	Msr	Mottled Saprolite	Sl	Sulfide Zone
Mz	Mottled Zone	Osr	Orange-pink Saprolite	Sp	Saprock
MMz	Megamottled Zone	Gsr	Andesitic Saprolite	Fr	Fresh Rock
FM	Fe - Mn Nodules				

Figure 10.9.1

ENDEAVOUR 22 - Al_2O_3(%)

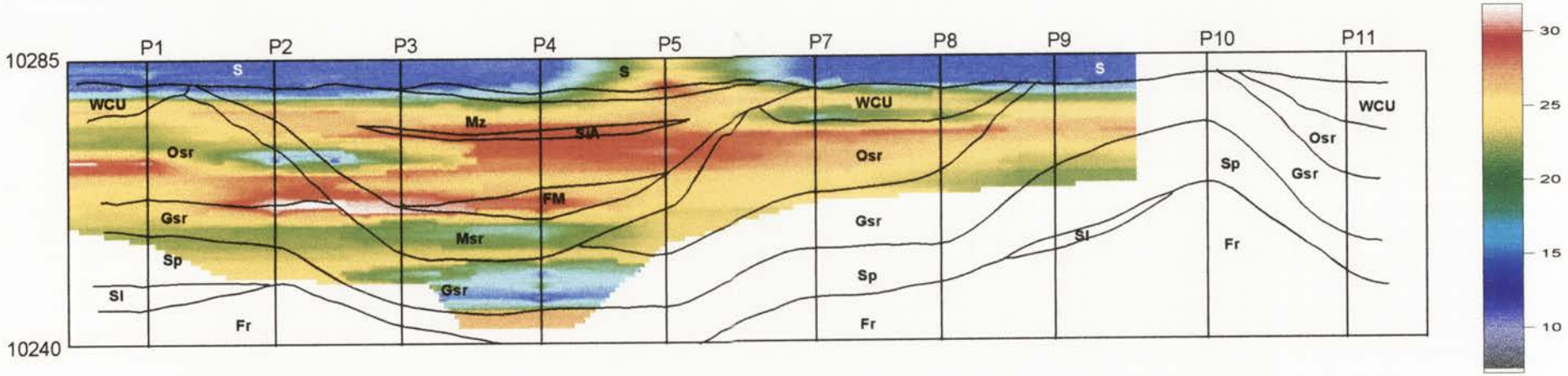

S	Soil Horizons	Osr	Orange-Pink Saprolite	Sl	Sulfide Zone	Msr	Mottled Saprolite
WCU	White Clay Unit	FM	Fe - Mn Nodules	Sp	Saprock	SiA	Silica Aggregates
Mz	Mottled Zones	Gsr	Greenish-grey Saprolite	Fr	Fresh Rock		

Figure 10.8.2

ENDEAVOUR 27 - Al_2O_3(%)

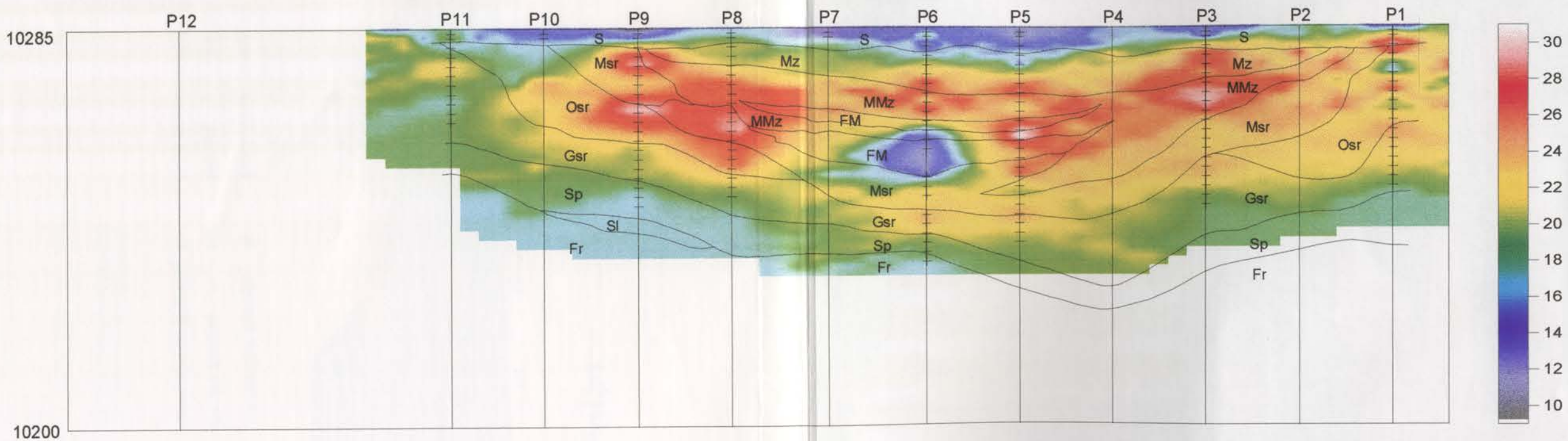

Horizontal Scale 1:2500
Vertical Scale 1:1000

S	Soil Horizons	Msr	Mottled Saprolite	Sl	Sulfide Zone
Mz	Mottled Zone	Osr	Orange-pink Saprolite	Sp	Saprock
MMz	Megamottled Zone	Gsr	Andesitic Saprolite	Fr	Fresh Rock
FM	Fe - Mn Nodules				

Figure 10.9.2

ENDEAVOUR 22 - Na_2O(%)

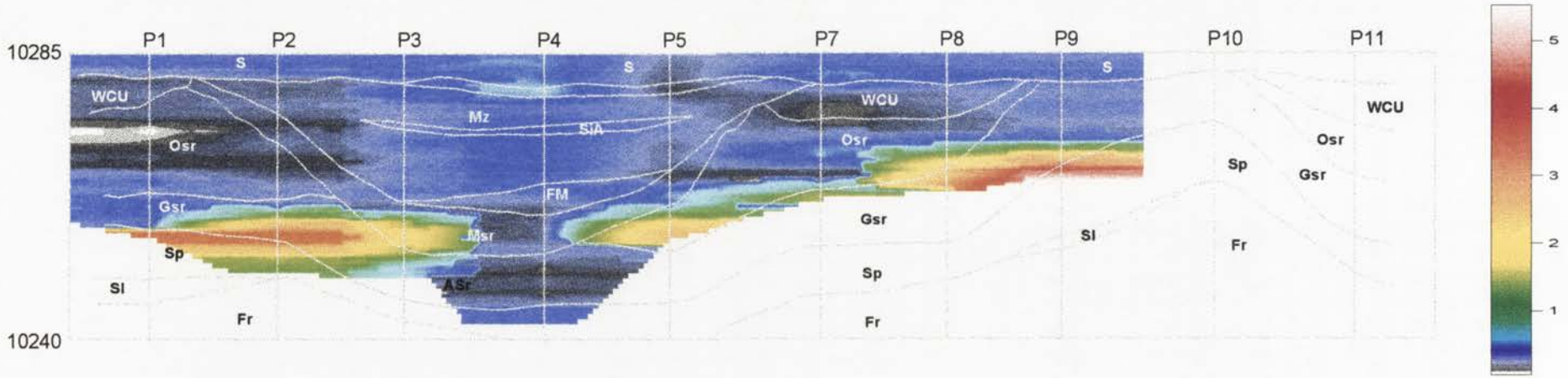

S	**Soil Horizons**	**Osr**	**Orange-Pink Saprolite**	**Sl**	**Sulfide Zone**	**Msr**	**Mottled Saprolite**
WCU	**White Clay Unit**	**FM**	**Fe - Mn Nodules**	**Sp**	**Saprock**	**SiA**	**Silica Aggregates**
Mz	**Mottled Zones**	**Gsr**	**Greenish-grey Saprolite**	**Fr**	**Fresh Rock**		

Figure 10.8.3

ENDEAVOUR 27 - Na_2O(%)

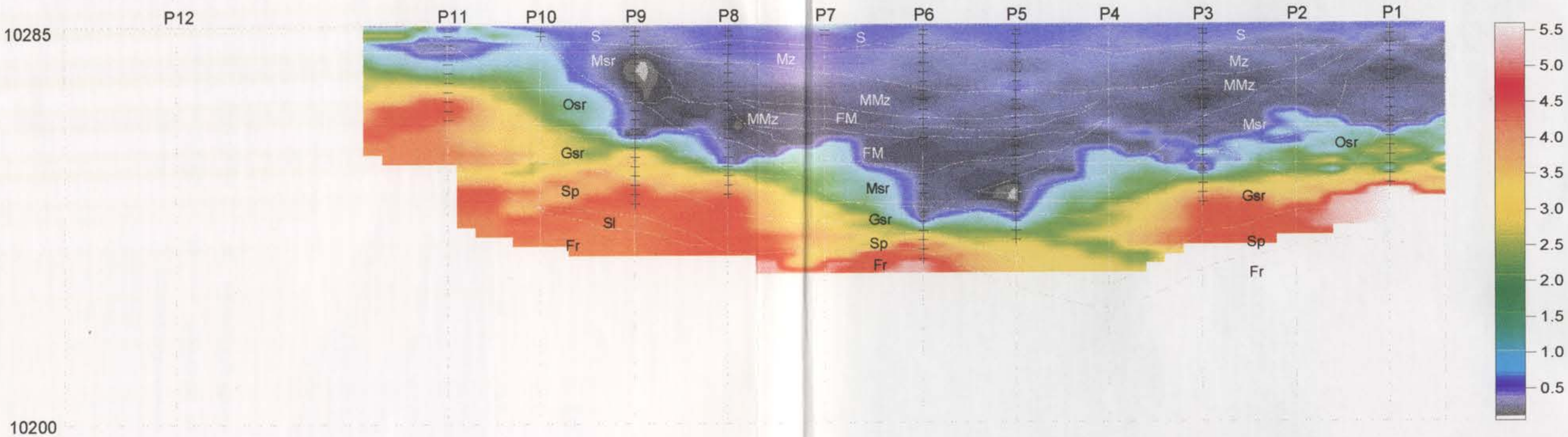

Horizontal Scale 1:2500
Vertical Scale 1:1000

S	Soil Horizons	Msr	Mottled Saprolite	Sl	Sulfide Zone
Mz	Mottled Zone	Osr	Orange-pink Saprolite	Sp	Saprock
MMz	Megamottled Zone	Gsr	Andesitic Saprolite	Fr	Fresh Rock
FM	Fe - Mn Nodules				

Figure 10.9.3

ENDEAVOUR 22 - K_2O(%)

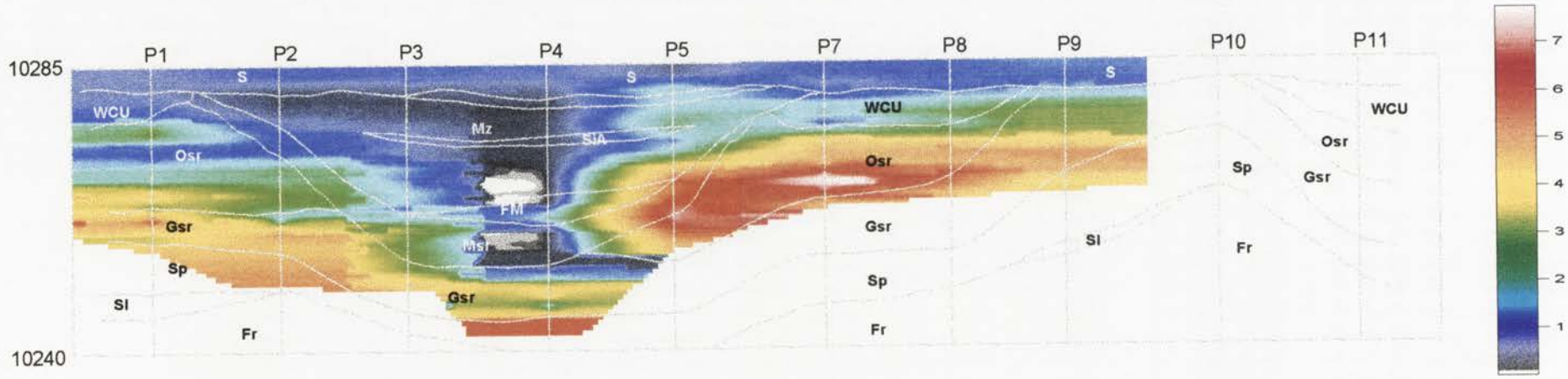

S	Soil Horizons	Osr	Orange-Pink Saprolite	Sl	Sulfide Zone	Msr	Mottled Saprolite
WCU	White Clay Unit	FM	Fe - Mn Nodules	Sp	Saprock	SiA	Silica Aggregates
Mz	Mottled Zones	Gsr	Greenish-grey Saprolite	Fr	Fresh Rock		

Figure 10.8.4

n:\geochem\goon\eric\plots\22k.srf

ENDEAVOUR 27 - K_2O(%)

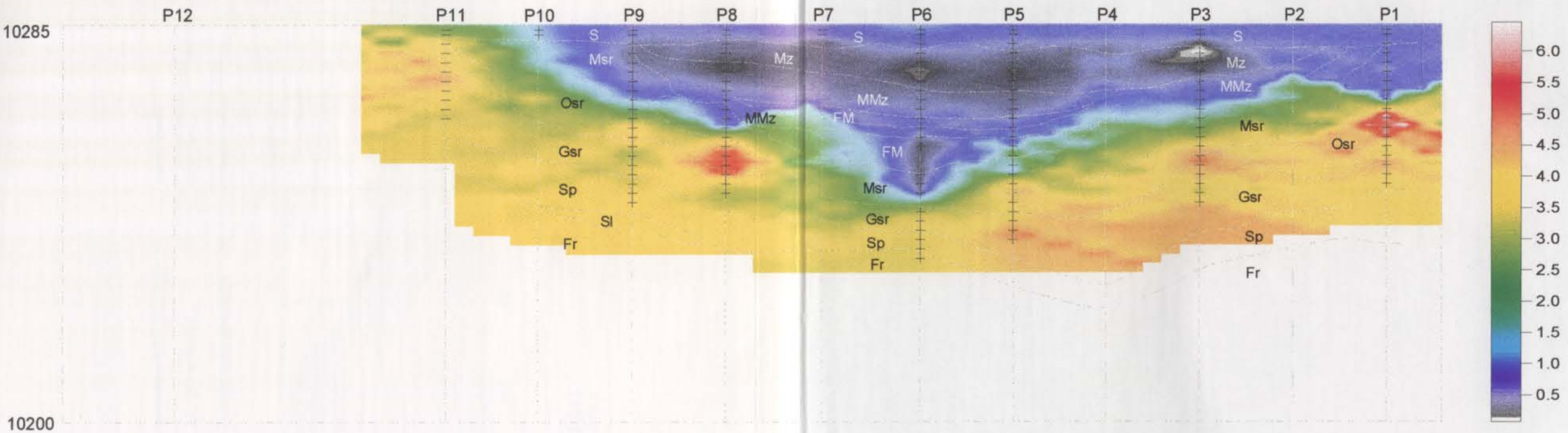

Horizontal Scale 1:2500
Vertical Scale 1:1000

S	Soil Horizons	Msr	Mottled Saprolite	Sl	Sulfide Zone
Mz	Mottled Zone	Osr	Orange-pink Saprolite	Sp	Saprock
MMz	Megamottled Zone	Gsr	Andesitic Saprolite	Fr	Fresh Rock
FM	Fe - Mn Nodules				

Figure 10.9.4

ENDEAVOUR 22 - TiO_2(%)

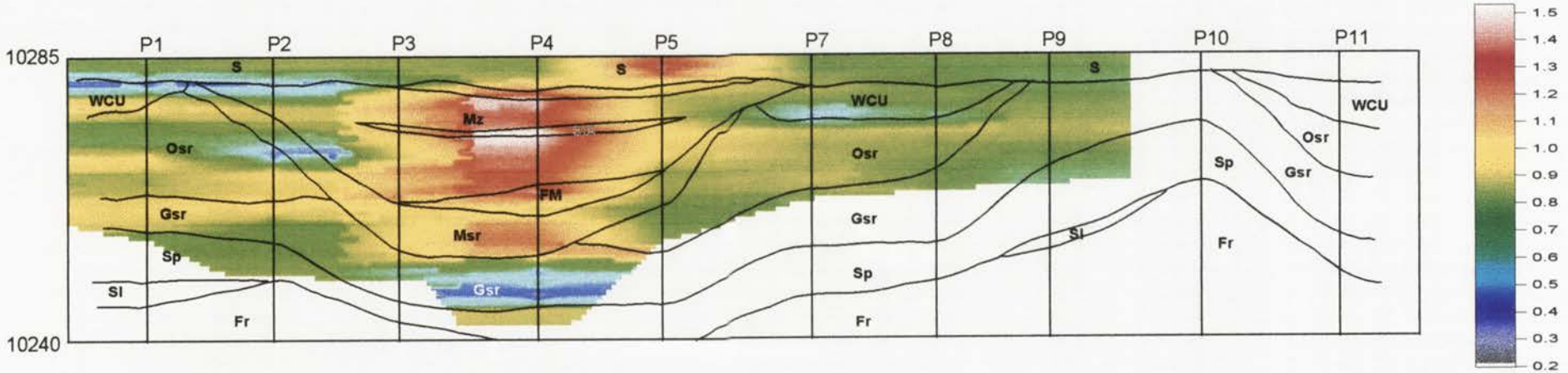

S	Soil Horizons	Osr	Orange-Pink Saprolite	Sl	Sulfide Zone	Msr	Mottled Saprolite
WCU	White Clay Unit	FM	Fe - Mn Nodules	Sp	Saprock	SiA	Silica Aggregates
Mz	Mottled Zones	Gsr	Greenish-grey Saprolite	Fr	Fresh Rock		

Figure 10.8.5

ENDEAVOUR 27 - TiO_2(%)

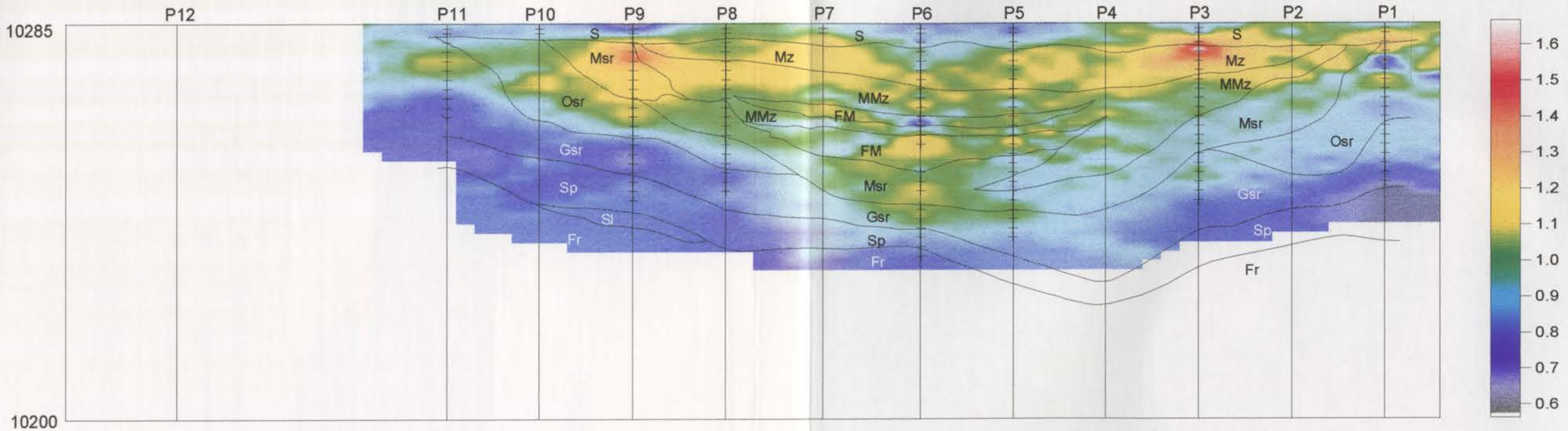

Horizontal Scale 1:2500
Vertical Scale 1:1000

S	Soil Horizons	Msr	Mottled Saprolite	Sl	Sulfide Zone
Mz	Mottled Zone	Osr	Orange-pink Saprolite	Sp	Saprock
MMz	Megamottled Zone	Gsr	Andesitic Saprolite	Fr	Fresh Rock
FM	Fe - Mn Nodules				

Figure 10.9.5

ENDEAVOUR 22 - TiO_2(%)

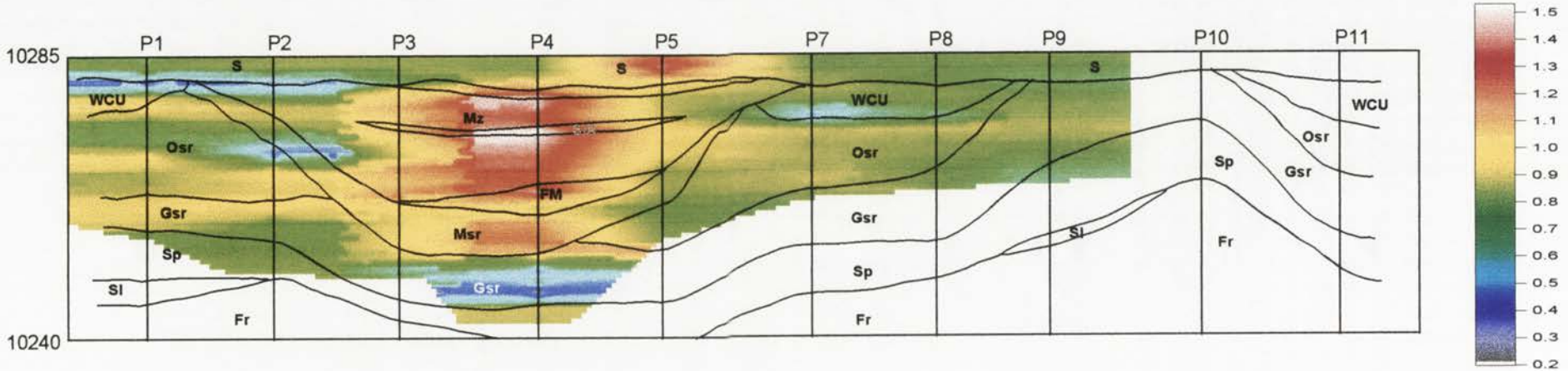

S	Soil Horizons	Osr	Orange-Pink Saprolite	Sl	Sulfide Zone	Msr	Mottled Saprolite
WCU	White Clay Unit	FM	Fe - Mn Nodules	Sp	Saprock	SiA	Silica Aggregates
Mz	Mottled Zones	Gsr	Greenish-grey Saprolite	Fr	Fresh Rock		

Figure 10.8.5

n:\geochem\goon\eric\plots\22ti.srf

ENDEAVOUR 22 - Au(ppm)

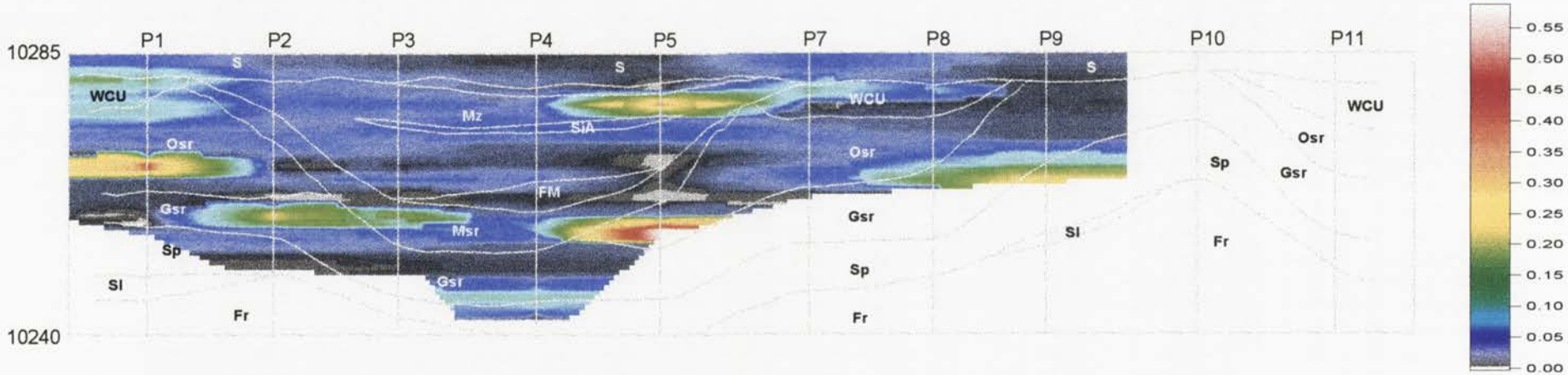

S	Soil Horizons	Osr	Orange-Pink Saprolite	Sl	Sulfide Zone	Msr	Mottled Saprolite
WCU	White Clay Unit	FM	Fe - Mn Nodules	Sp	Saprock	SiA	Silica Aggregates
Mz	Mottled Zones	Gsr	Greenish-grey Saprolite	Fr	Fresh Rock		

Figure 10.8.6

ENDEAVOUR 27 - P_2O_5(%)

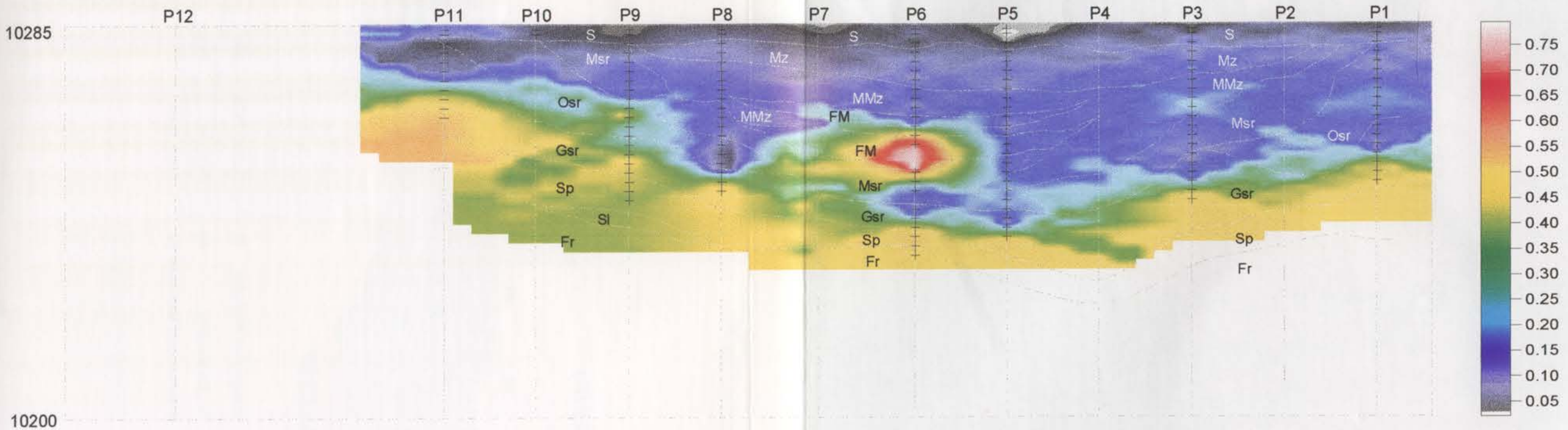

Horizontal Scale 1:2500
Vertical Scale 1:1000

S	Soil Horizons	Msr	Mottled Saprolite	Sl	Sulfide Zone
Mz	Mottled Zone	Osr	Orange-pink Saprolite	Sp	Saprock
MMz	Megamottled Zone	Gsr	Andesitic Saprolite	Fr	Fresh Rock
FM	Fe - Mn Nodules				

Figure 10.9.6

ENDEAVOUR 22 - Cu(ppm)

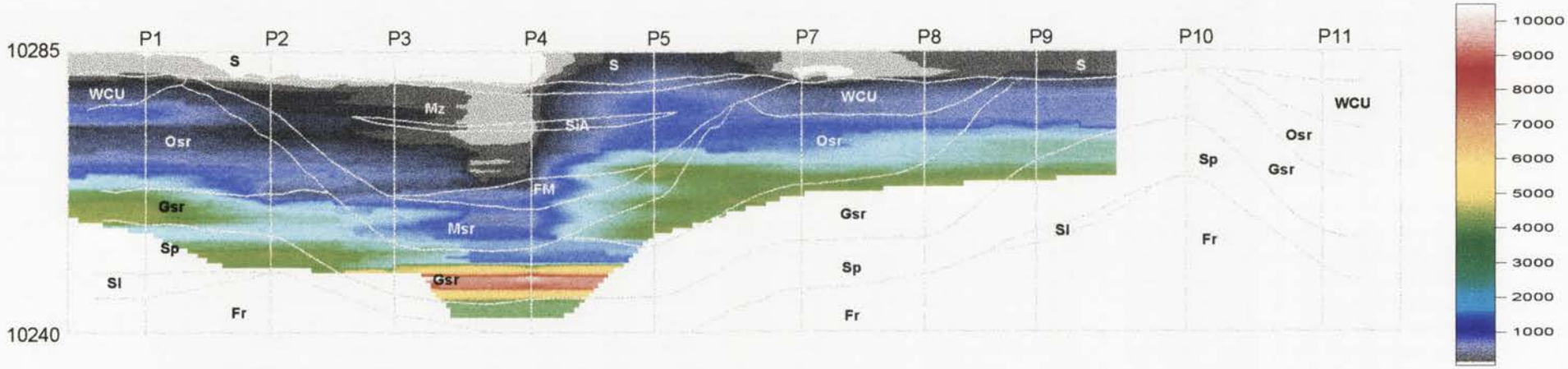

S	Soil Horizons	Osr	Orange-Pink Saprolite	Sl	Sulfide Zone	Msr	Mottled Saprolite
WCU	White Clay Unit	FM	Fe - Mn Nodules	Sp	Saprock	SiA	Silica Aggregates
Mz	Mottled Zones	Gsr	Greenish-grey Saprolite	Fr	Fresh Rock		

Figure 10.8.7

ENDEAVOUR 27 - Total Fe as Fe_2O_3(%)

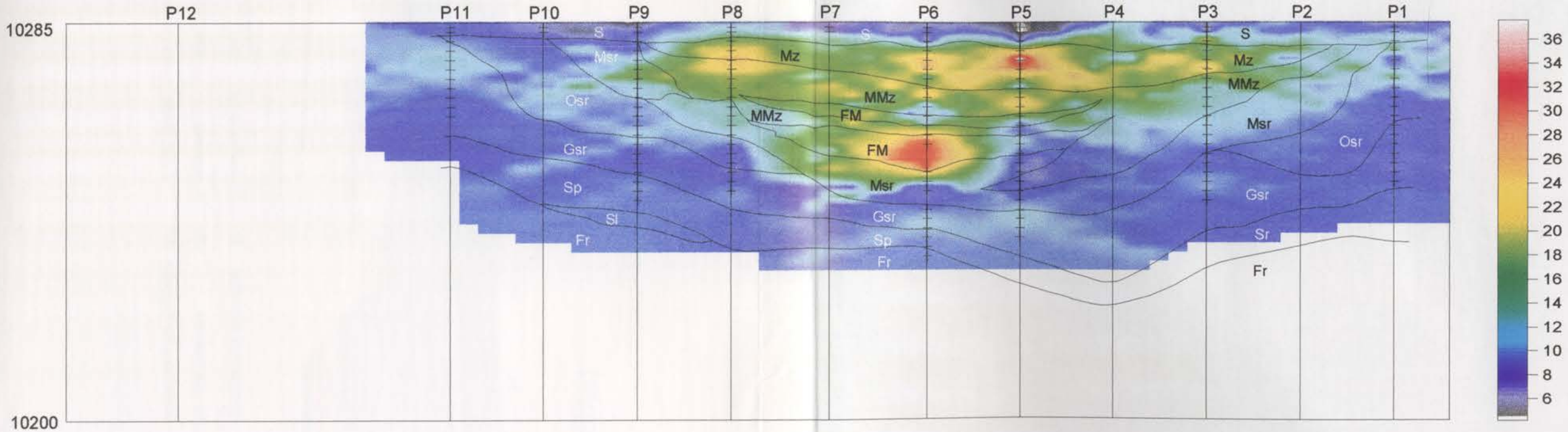

Horizontal Scale 1:2500
Vertical Scale 1:1000

S	Soil Horizons	Msr	Mottled Saprolite	Sl	Sulfide Zone
Mz	Mottled Zone	Osr	Orange-pink Saprolite	Sp	Saprock
MMz	Megamottled Zone	Gsr	Andesitic Saprolite	Fr	Fresh Rock
FM	Fe - Mn Nodules				

Figure 10.9.7

ENDEAVOUR 22 - Pb(ppm)

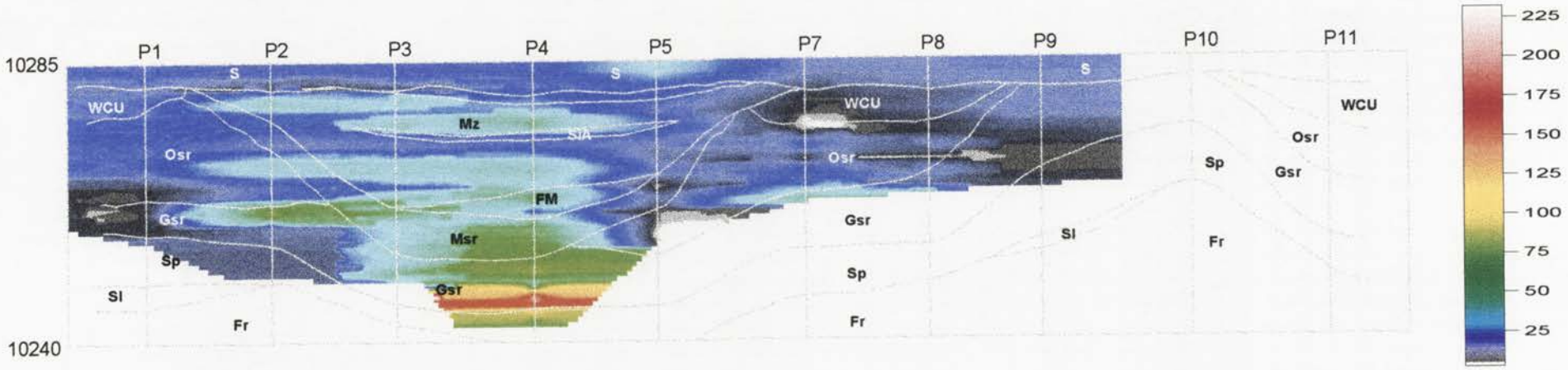

S	Soil Horizons	Osr	Orange-Pink Saprolite	Sl	Sulfide Zone	Msr	Mottled Saprolite
WCU	White Clay Unit	FM	Fe - Mn Nodules	Sp	Saprock	SiA	Silica Aggregates
Mz	Mottled Zones	Gsr	Greenish-grey Saprolite	Fr	Fresh Rock		

Figure 10.8.8

n:\geochem\goon\eric\plots\22pb.

ENDEAVOUR 27 - MgO(%)

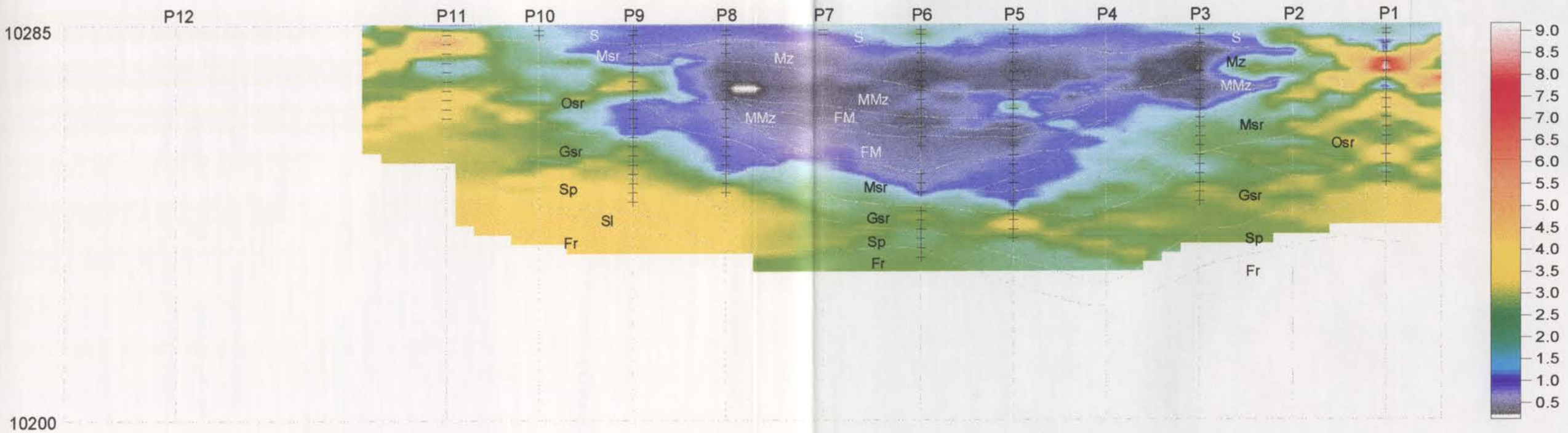

Horizontal Scale 1:2500
Vertical Scale 1:1000

S	Soil Horizons	Msr	Mottled Saprolite	Sl	Sulfide Zone
Mz	Mottled Zone	Osr	Orange-pink Saprolite	Sp	Saprock
MMz	Megamottled Zone	Gsr	Andesitic Saprolite	Fr	Fresh Rock
FM	Fe - Mn Nodules				

Figure 10.9.8

ENDEAVOUR 22 - Zn(ppm)

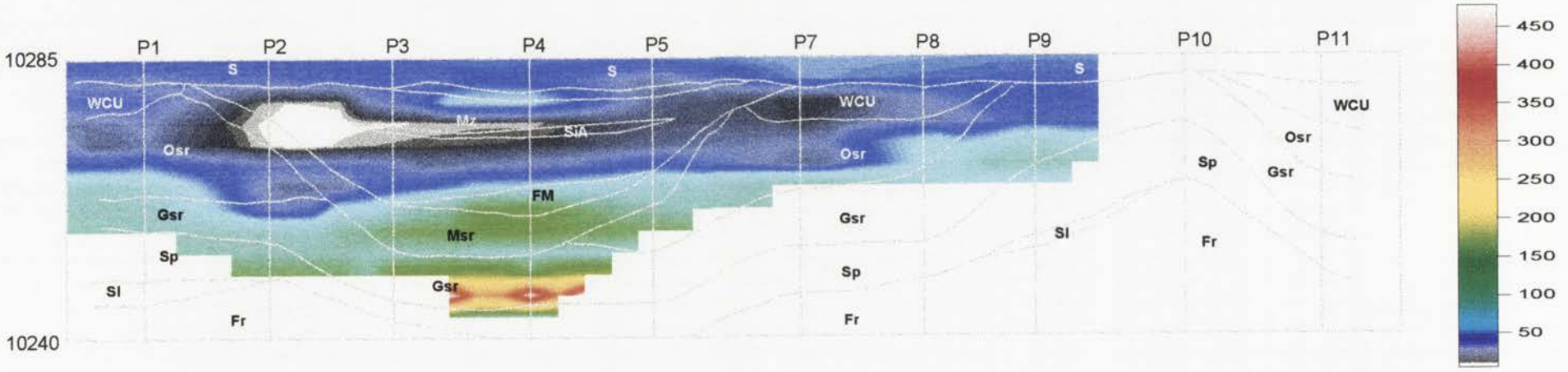

S	**Soil Horizons**	**Osr**	**Orange-Pink Saprolite**	**Sl**	**Sulfide Zone**	**Msr**	**Mottled Saprolite**
WCU	**White Clay Unit**	**FM**	**Fe - Mn Nodules**	**Sp**	**Saprock**	**SiA**	**Silica Aggregates**
Mz	**Mottled Zones**	**Gsr**	**Greenish-grey Saprolite**	**Fr**	**Fresh Rock**		

Figure 10.8.9

ENDEAVOUR 27 - Au (ppm)

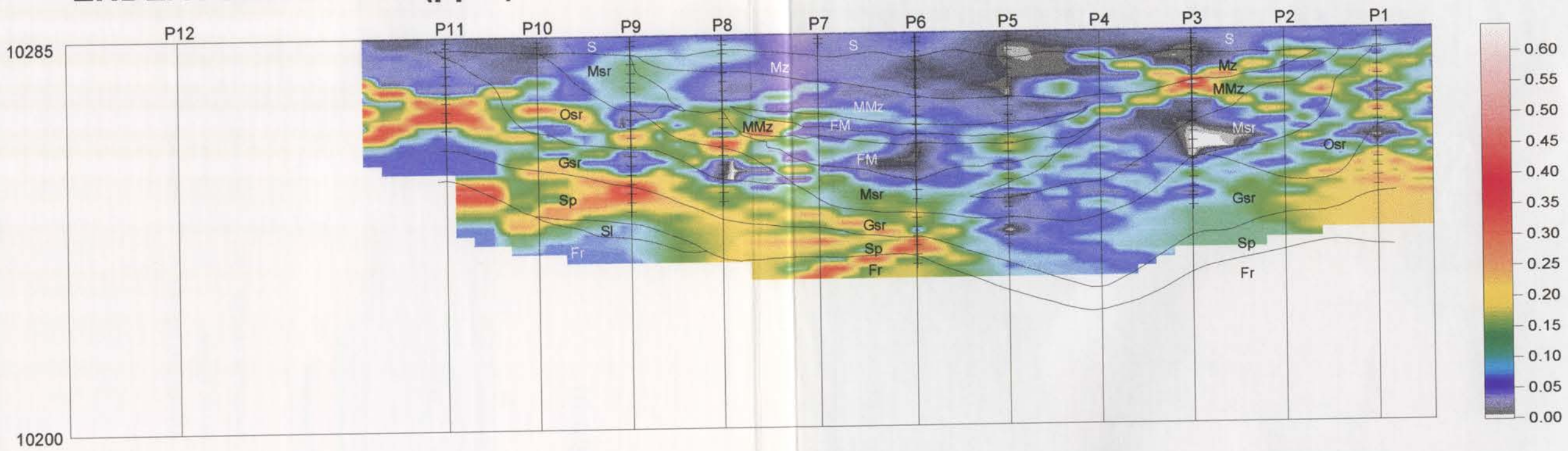

Horizontal Scale 1:2500
Vertical Scale 1:1000

S	Soil Horizons	Msr	Mottled Saprolite	Sl	Sulfide Zone
Mz	Mottled Zone	Osr	Orange-pink Saprolite	Sp	Saprock
MMz	Megamottled Zone	Gsr	Andesitic Saprolite	Fr	Fresh Rock
FM	Fe - Mn Nodules				

Figure 10.9.9

ENDEAVOUR 22 - As(ppm)

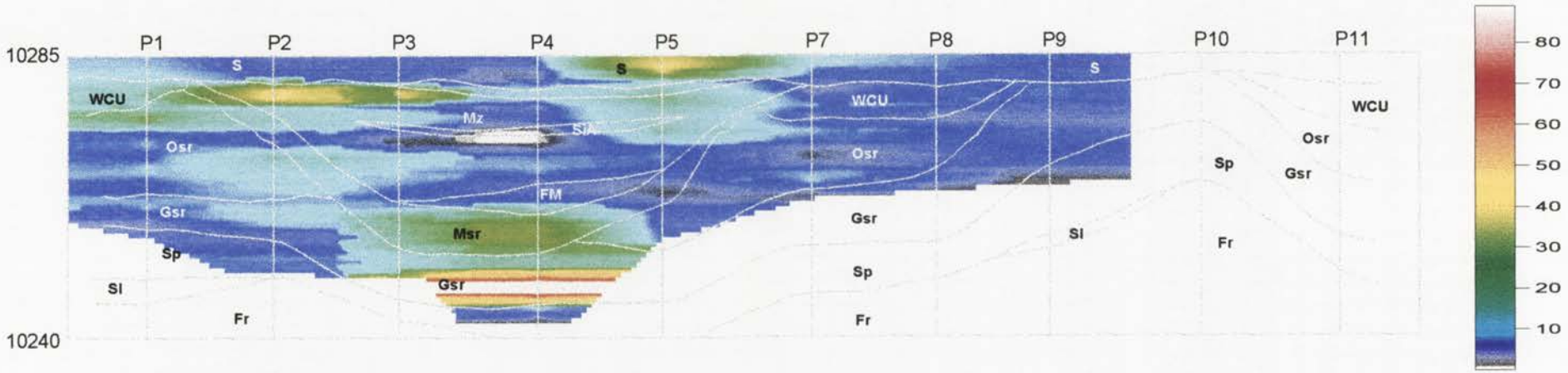

S	Soil Horizons	Osr	Orange-Pink Saprolite	Sl	Sulfide Zone	Msr	Mottled Saprolite
WCU	White Clay Unit	FM	Fe - Mn Nodules	Sp	Saprock	SiA	Silica Aggregates
Mz	Mottled Zones	Gsr	Greenish-grey Saprolite	Fr	Fresh Rock		

Figure 10.8.10

ENDEAVOUR 27 - Cu (ppm)

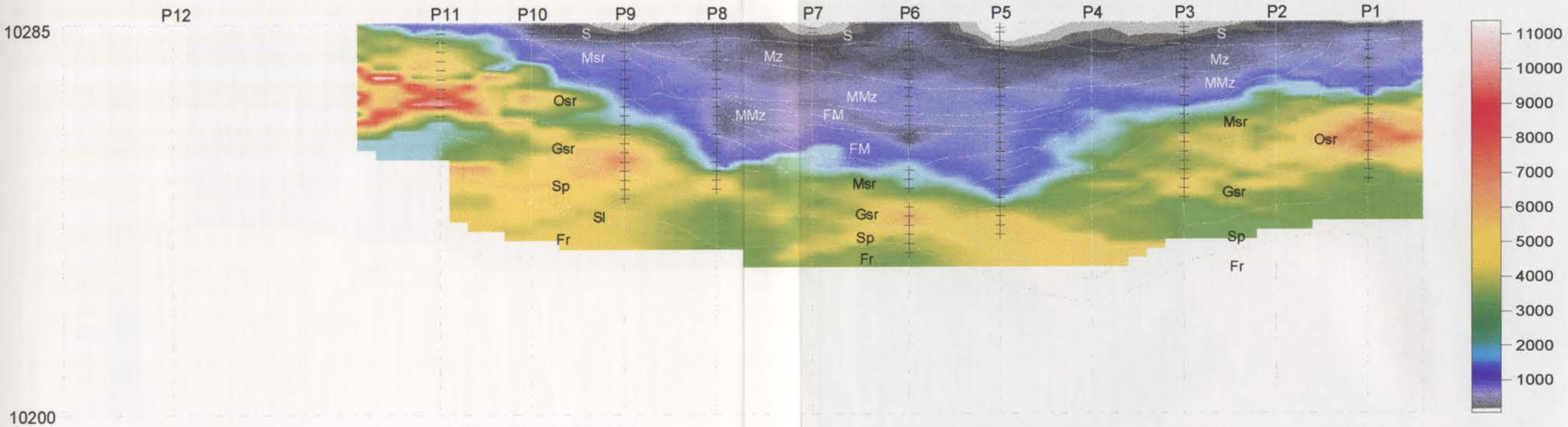

Horizontal Scale 1:2500
Vertical Scale 1:1000

S	Soil Horizons	Msr	Mottled Saprolite	Sl	Sulfide Zone
Mz	Mottled Zone	Osr	Orange-pink Saprolite	Sp	Saprock
MMz	Megamottled Zone	Gsr	Andesitic Saprolite	Fr	Fresh Rock
FM	Fe - Mn Nodules				

Figure 10.9.10

ENDEAVOUR 27 - Pb (ppm)

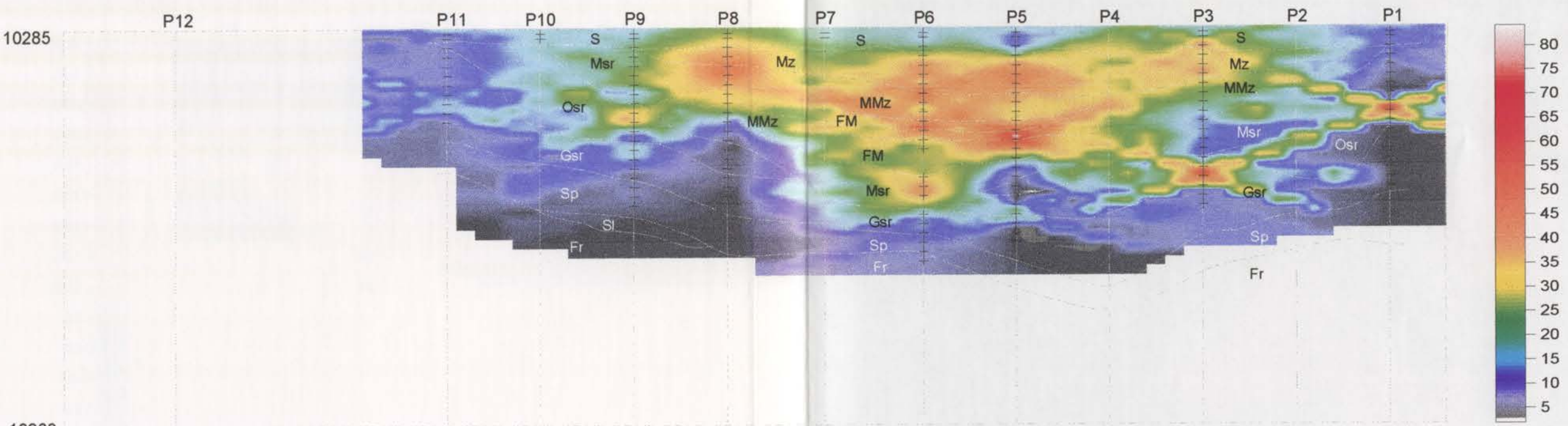

Two extreme values (171 and 1880 ppm) trimmed to 100 ppm.

Horizontal Scale 1:2500
Vertical Scale 1:1000

S	Soil Horizons	Msr	Mottled Saprolite	Sl	Sulfide Zone
Mz	Mottled Zone	Osr	Orange-pink Saprolite	Sp	Saprock
MMz	Megamottled Zone	Gsr	Andesitic Saprolite	Fr	Fresh Rock
FM	Fe - Mn Nodules				

Figure 10.9.11

ENDEAVOUR 27 - Zn (ppm)

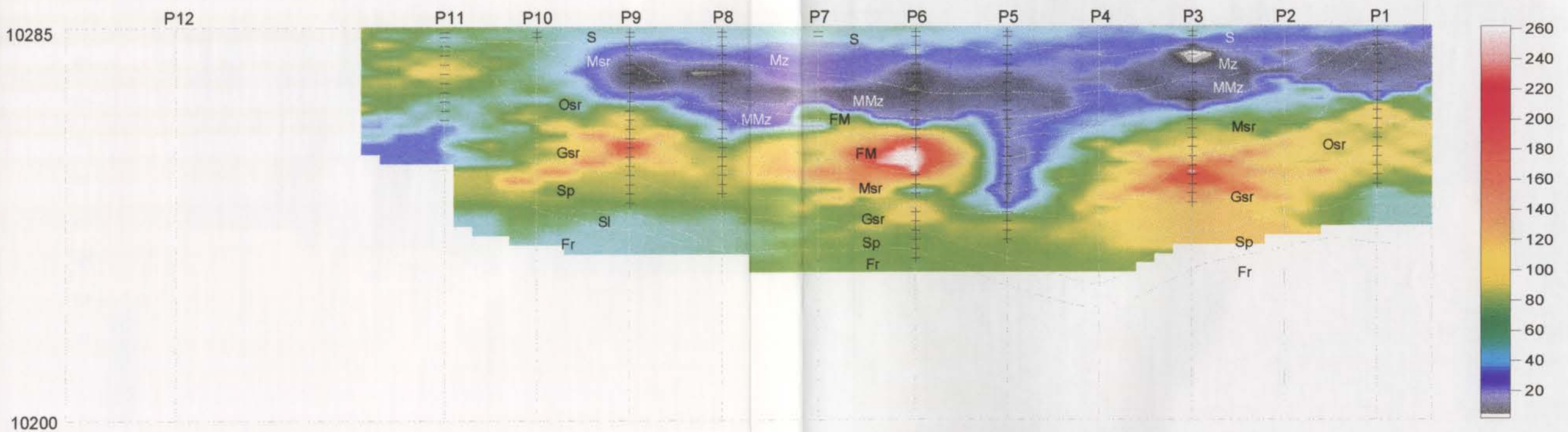

Horizontal Scale 1:2500
Vertical Scale 1:1000

S	Soil Horizons	Msr	Mottled Saprolite	Sl	Sulfide Zone
Mz	Mottled Zone	Osr	Orange-pink Saprolite	Sp	Saprock
MMz	Megamottled Zone	Gsr	Andesitic Saprolite	Fr	Fresh Rock
FM	Fe - Mn Nodules				

Figure 10.9.12

ENDEAVOUR 27 - As (ppm)

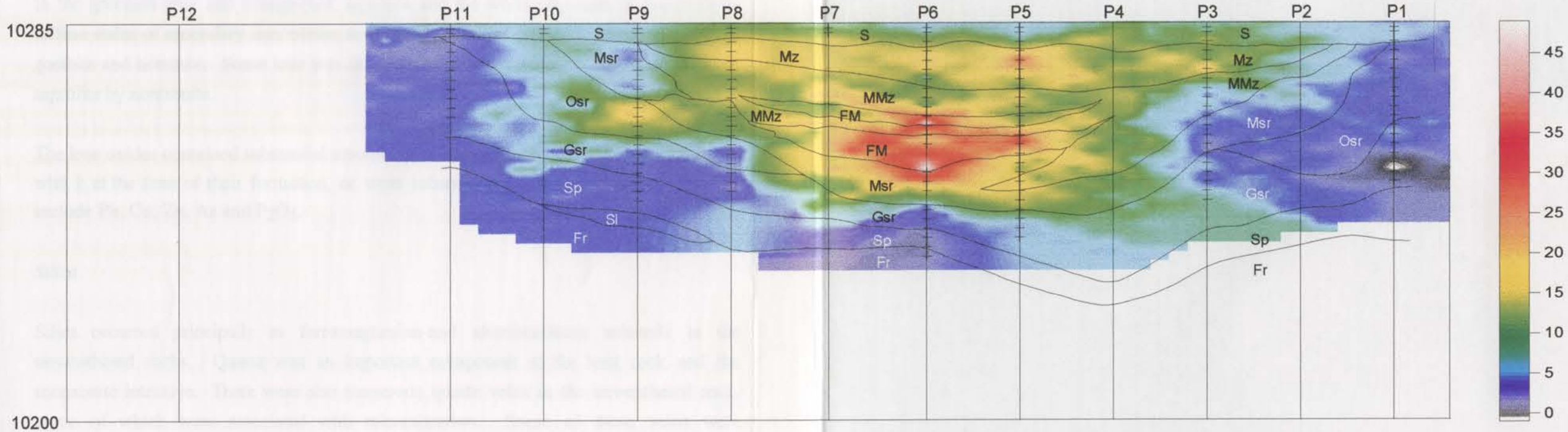

Horizontal Scale 1:2500
Vertical Scale 1:1000

S	Soil Horizons	Msr	Mottled Saprolite	Sl	Sulfide Zone
Mz	Mottled Zone	Osr	Orange-pink Saprolite	Sp	Saprock
MMz	Megamottled Zone	Gsr	Andesitic Saprolite	Fr	Fresh Rock
FM	Fe - Mn Nodules				

Figure 10.9.13

Aluminium

Aluminium is present in the host rock as aluminosilicate minerals (i.e feldspars and mica). It was enriched in all the regolith units after the onset of weathering. As these minerals decompose during weathering, Al_2O_3 is precipitated largely in the form of clay minerals notably kaolin. Highest concentrations (> 28 %) in the regolith stratigraphy occur in the orange-pink saprolite and the mottled clay units (Figure 10.8 and 10.9, Al_2O_3). The progressive increase up to the orange-pink saprolite in the residual units is partly a result of relative enrichment, attributable as in the case of Si to leaching of more soluble components.

10.8.2 Alkaline earth elements

Mg, Ca, Ba and Sr displayed a number of similarities in their weathering behaviour, namely that they are strongly leached at the onset of weathering and re-concentrated in the saprolite, mottled clay units and soil horizons as secondary carbonates. The slight increase in the abundance of carbonates in the orange-pink saprolite in some of the profiles was probably a function of greater porosity and friability of the host horizon than of lateral dispersion.

Magnesium

Magnesium occurred as dolomite and in ferromagnesian silicates (i.e. chlorite) and pyroxenes i.e. diopside and augite. Augite is not included in the profile mineralogy although it was observed in a number of fresh rock samples because *Siroquant* did not have allowances for its refinement. The presence of MgO in these minerals explains its greater abundance in the lower units of the residual units in the profile geochemistry than CaO. Highest concentrations (> 8 %) of MgO occur in the regolith stratigraphy in the white clay unit and the orange-pink saprolite (Figure 10.8 and 10.9, MgO) where it was precipitated with CaO as dolomite.

Calcium

Calcium is hosted predominantly by calcite or dolomite and is enriched (10-16%) in the soil, white clay unit and orange-pink saprolite in the regolith stratigraphy (Figures 10.8 CaO). Ca appears to have been leached more strongly than Mg, which was present in the minerals mentioned above at concentrations above 0.2 % CaO. At the surface, Ca was

precipitated in pedogenic carbonates, as calcite and, less commonly, dolomite, at concentrations of up to 8-18 % CaO. This explains the general depletion of MgO in the soil horizons. Some of the CaO was also hosted by gypsum in the soil horizons.

Strontium

Ca and Sr partitioned similarly in the isocon plots and appeared to have been released together during weathering. There was also a strong association between the element and Ca and Ba. Ca and Sr are also both products of the weathering of the plagioclase feldspars and to a lesser extent ferromagnesium minerals. Highest concentrations (> 600 ppm) occurred in the saprock and the fresh rock. In general, Sr had a distribution pattern similar to that of Ca in the regolith. Local depletion (< 100 ppm) occurred in the nodular iron-manganese units.

The distribution of Sr in igneous rocks is controlled by its size, intermediate between Ca and K as it can substitute for both, but will preferentially substitute for Ca. In plagioclase feldspars, there is an increase in Sr content with decrease in Ca content (Fischer, 1978b).

Barium

The distribution patterns of Ba are very similar to those of Ca and Sr. It also showed similar distribution patterns with Ce, La and Pb in the isocon plots. SEM EDXA showed traces of barite in a few samples from the slightly weathered rock although this precludes its participation as the major host mineral. Like Sr, the plagioclase feldspars appear to be host to the Ba in the unweathered rock.

Ba^{2+} has a large ionic radius and is commonly replaced by, and substitutes for, Pb^{2+} and Sr^{2+} and less commonly for K^{+} and Ca^{2+}. Ba is usually enclosed in feldspars in igneous rocks (Fischer, 1978a). Apatite is also an important non-silicate Ba-bearing phase (Puchelt, 1978). The presence of apatite in the host rocks suggests that some of the Ba could have been derived from it. Slight enrichment (250-500 ppm) of Ba occurred in the mottled clay units and nodular Fe-Mn units. Ba is adsorbed from solutions by clays and organic matter, Fe-oxides and Mn oxyhydroxides (Puchelt, 1978)

10.8.3 Alkali metals: Na, K and Rb

The isocon plots showed similarity in the distribution of K with Rb in most of the regolith units. Strong enrichment occurred in the lower levels of the regolith units

implying an association between these elements and the alteration zone. Rb showed some association with Fe in the units higher up in the profile. There was no obvious Na enrichment associated with mineralization although a few samples showed positive correlations between albite and K_2O.

Sodium

Sodium was present in albite in unweathered rocks to concentrations of between 3-5%. These concentrations were retained in the saprock and the lower portions of the greenish-grey saprolite. Above this level the Na is leached with total depletion occurring in the orange-pink saprolite. The distribution is a bit similar to that of Sr, which was also hosted by albite. Some positive correlation occurred between albite and K_2O in some of the units showing that some of the Na enrichment was associated with mineralization.

Potassium

The K distribution in the regolith stratigraphy was controlled by the presence of K-feldspars and micas (Figures 10.8 and 10.9, K_2O). The presence of these two minerals characterized the alteration zone associated with mineralization as shown by its positive correlations with Cu, Au and K_2O. The muscovite persisted up to the white clay unit and the K-feldspar (orthoclase) while the K-feldspar persisted up to the orange-pink saprolite. The distribution of the two minerals is indicated throughout the regolith up to these levels by concentrations of 2-7% K_2O.

The K_2O contents of the upper saprolite units in transition with the soil over the trachyandesite is much lower (0.5-1.0%), but nevertheless appears to give near surface expression to the alteration.

Rubidium

Rubidium concentration closely follows that of K, As and V with highest concentrations (> 150 ppm) occurring in the greenish-grey saprolite and the saprock. Slightly higher concentrations (50-150 ppm) occurred in the nodular iron-manganese units, mottled saprolite and orange-pink saprolite. Association with K suggests occurrence in the alteration zone. Enrichment in the mottled clay units and nodular iron-manganese horizons attests to adsorption on the surfaces of iron and manganese oxides.

A number of studies have confirmed that Rb is generally enclosed in K-bearing minerals (Cocco, 1978b). K and Rb have similar ionic radii which allows mutual substitution but Rb is generally scarce (Heier & Billings, 1978a). Adsorption plays an important role in the concentration of Rb relative to K in the late stages of weathering, as Rb is held more firmly in adsorption positions than K because it has similar ionic radii to H_3O^{3+} (Heier & Billings, 1978b).

10.8.4 Elements associated with the mineralization: Au, S, As and Ag

The primary gold mineralization in this study is mainly associated with the potassic alteration that accompanied the intrusion of the trachyandesite by the quartz monzonite porphyry. Other less common alteration patterns involved sericite and carbonates. S, As and Ag accompanied the gold although there is no close correlation between gold and these elements. Each of them behaved differently during weathering and had distinctive dispersion patterns.

Gold (Au)

Au exhibits a widespread distribution in the regolith stratigraphy (Figure 10.8 and 10.9, Au) with most of the units containing significant amounts of the element. The highest concentrations (500-800 ppb) occur in the saprock, moderate to high concentrations in the greenish-grey saprolite (100-500 ppb), and the white clay units and mottled saprolite (100-300 ppb). A zone of depletion containing lower but still significant concentrations (50-200 ppb) occurs in the mottled clay units and the nodular iron-manganese zones. The principal features of this distribution patterns are:

1. A progressive depletion from the fresh rock to the upper levels of the residual units. These patterns in most of the units are patchy although lateral dispersion is quite evident in a number of units in the E27 stratigraphy (Figure 10.9, Au). This suggests that the Au is either getting depleted with progressive weathering and/or further away from the mineralization.

2. Within the mottled clay units, the Au is preferentially enriched (100-150 ppb) in the upper nodular sections of the mini-and-medium mottled clay and the mega-mottled clay portions. Similar concentrations also occur in the nodular Fe and Mn horizons. Selective extractions did not show the partitioning of the gold into any of the mineral species in these units although correlation matrices showed a mild positive correlation (r=0.55) with MnO.

Lateral dispersion of gold has elsewhere been documented higher up in the ferruginous and mottled horizons of profiles (Freyssinet et al. 1987; Michel, 1987). This has been attributed partly to mobility, either in solution or as colloids complexed by humic acids or organic matter from the soil or to residual concentration and surface wash during landsurface reduction (Butt, 1992). Mechanical illuviation of gold during weathering is also possible in these horizons. Reduction of the complexes by ferrous iron results in the incorporation of gold within the iron oxides. The relative contributions of the physical and chemical mechanisms during the ferruginization process and subsequent climatic episodes are uncertain.

3. The white clay units also contain significant amounts (100-300 ppb) of Au relative to the underlying orange-pink saprolite. This unit as previously mentioned contains high amounts of smectitic clays, carbonates (dolomite) and iron oxides. It is also located below the soil in the truncated residual units. The evolution of this unit has been attributed to continuous leaching and loss of material to reduce the competence of the upper saprolite zone so that settling of the clays occurred at the same time as the rock fabrics were being destroyed. This destruction of the fabric may have also been aided by the shrinking and swelling of smectitic clays with subsequent infusion by carbonates and iron oxides. Although the Au has not been connected to any specific mineral host and the enrichment mechanisms unclear, the features of this unit suggest localized mechanical entrapment and retention within the dense clays.

Arsenic (As)

The highest concentrations of As (> 40 ppm) occur in the saprock and the nodular iron and manganese units while moderate concentrations (15-40 ppm) occur in the mottled clay units, mottled saprolite and the white clay units. Zones of depletion occur in the middle and upper portions of the greenish-grey saprolite and the orange-pink saprolite.

Arsenic is probably present as a component of sulfides within the primary ore. It is normally found within pyritic ores as arsenopyrite. There is however no association between the gold and As in most of the units. High associations between As and iron and manganese oxides occurred in the transported regolith units indicating that the Fe and Mn oxides account for most of the As. Arsenic in its oxidized form is present largely as arsenate anions, which tend to be strongly adsorbed by goethite because goethite has an excess of positive charges at pH values below 8 (Hingston et al. 1972). As also showed

moderate associations with P_2O_5 and Zn, which was also, incorporated into the Fe and Mn oxides.

Sulphur (S)

Sulfur in the unweathered mineralized rock is present mainly as bornite, chalcopyrite, pyrite, chalcocite, covellite, galena and sphalerite. The sulfide minerals are very susceptible to weathering as shown by progressive depletion up to the upper levels of the profile. There is some enrichment (0.25 - 0.75%) in the soil units associated with the presence of gypsum. Moderate amounts (0.10 - 0.25%) occur in the upper portions of the mottled clay units.

Silver (Ag)

Most of the Ag values were below the ICP-MS lower limit of detection i.e. 1 ppm. A few samples from the nodular iron and manganese units and orange-pink saprolite recorded values of between 1 and 2 ppm. Selective extraction confirmed the strong adsorption of Ag by Mn oxides in a similar fashion to that of Co and Ni.

10.8.5 Base and transition metals: Pb, Cu, Zn, Ni, Mn

These elements are considered together because the base metals (Pb, Zn, and Cu) are associated with primary Au mineralization and because the transition metals (Mn, Ni, Cu and Zn) have many similarities in chemical behaviour in the weathering environment. The distribution patterns of Mn, Co, Ni, Cu and Zn are similar. They all tend to be leached under acid, reducing conditions and precipitated under more alkaline, oxidizing conditions, with the behaviour of Mn being the most strongly influenced by redox changes (Butt, 1990). In this study, these elements were patchily enriched, together or separately deeper in the regolith. The closest associations involved Zn, Ni, Mn and Pb in the mottled clay units and Cu, Zn and Pb in the residual units.

Lead

Highest concentrations (> 150 ppm) of Pb occurred in the sulfide zone (one sample gave a value of 1880 ppm) and the greenish-grey saprolite. Moderate to high concentrations (50-150 ppm) occurred in the orange-pink saprolite, mottled saprolite and the mottled clay units. This shows that Pb is associated with the alteration zone with the high concentrations in the mottled clay units associated with adsorption into the iron oxides.

Some of the Pb could be hosted by galena which occurred in low amounts in the sulfide zone. Association with the alteration zone conforms with observations that K-feldspars and micas are host minerals for Pb in igneous rocks (Wedepohl, 1978c).

Copper

Copper was mainly hosted by the sulfides namely bornite, chalcopyrite, chalcocite and covellite. This explains the high concentrations (> 1200 ppm) of the element with depth in the regolith stratigraphy (Figures 10.8 and 10.9, Cu). During weathering, Cu is released when the sulfides are oxidized. Selective extractions showed that some of the Cu was incorporated into the smectites and kaolin in the clay-rich portions. The concentration of Cu in solution is controlled by adsorption onto clays and Fe-oxides and the presence of anions in solution (Wedepohl, 1978a).

The transported regolith contains low concentrations of Cu with minor enrichment (500-800 ppm) in the mottled clay and nodular iron and manganese horizons. The low concentrations in the transported regolith is still regarded as highly anomalous in most regional geochemical surveys. Selective extractions confirmed its incorporation into the iron and manganese oxides.

Zinc

Zinc is also associated with the alteration zone as shown by positive correlations with Cu and K_2O. Its distribution patterns closely followed that of Cu. Some of the zinc could have been hosted by sphalerite which occurred in small amounts in the sulfide zone.

Zinc can occur in magnetite and chromite with lesser amounts in the pyroxenes (Wedepohl, 1978f). Hence, the ferromagnesian silicate minerals and spinels of this study could have also been host to Zn in the unweathered rocks. Zn^{2+} substitutes for Fe^{2+} and Mg^{2+} in silicates and oxides (Wedepohl, 1878f). Zn was also strongly adsorbed by manganese oxides in the nodular iron and manganese units.

Nickel

The host minerals of Ni in the regolith stratigraphy is unclear with the highest concentrations (> 15 ppm) occurring in the nodular iron-manganese units and the greenish-grey saprolite. Its distribution pattern closely followed that of As. Like Zn it

was observed to have been strongly adsorbed into the surfaces of manganese and iron oxides.

Nickel is usually taken into olivine in early magmatic crystallization. Spinels (magnetite and chromite) are also important sites for Ni incorporation (Turekian, 1978). Ni^{2+} may be released from the weathering silicate into solution and subsequently incorporated into secondary Fe-Mg-layer silicates, probably nontronite and saponite (Paquet et al. 1987) and as already confirmed by selective extractions, in Fe-oxyhydroxides i.e goethite and hematite. The low contents of olivine in the host rock suggests that the Ni was probably hosted by the other ferromagnesium silicates.

Manganese

Highest concentrations (> 3500 ppm) occurred in the orange-pink saprolite and nodular iron-manganese aggregates. It showed no direct correlations with any of the host rock forming elements although the fresh rocks contained moderate amounts (0.05-0.2 %) of the element. Mn may be present in pyroxenes and feldspars in igneous rocks (Peacor, 1978). Hence, it might have been present in this study in the feldspars and the pyroxenes (enstatite and/or augite).

The distribution of the Mn oxides during the evolution of the regolith was governed by redox reactions associated with fluctuating water tables. Mn^{2+} may oxidize to Mn^{4+} which is relatively insoluble and hence precipitate within the weathering material. Because of some similarities in chemical properties of Mn^{2+} with Fe^{2+} and Mg^{2+}, Mn substitutes for these minerals in igneous minerals (Paquet et al. 1987). Selective leaching confirmed the scavenging abilities of Mn for a number of elements which included Pb, Ni, Zn and As.

10.8.6 Lithophile elements: Cr, Sc, Ti, V

Chromium

No specific Cr minerals were observed in the host rock. Highest concentrations (> 60 ppm) were encountered in the saprock and the orange-pink saprolite suggesting association with muscovite and K-feldspars. Chromium usually occurs as a minor component in ferromagnesium silicates and fuchsitic muscovite in ultramafic and some basic rocks (Nickel, 1984). Chromite is also one of the major host minerals of chromium although it was not present in the unweathered rocks of this study.

Possible host minerals in this study include muscovite and chlorite. The increase in concentrations of the element towards the upper parts of the profiles is attributed to residual accumulation as more soluble components are lost. Moderate amounts (35-50%) of Cr were encountered in the mottled clay units. Because Cr^{3+} resembles Al^{3+} and Fe^{3+} in its crystallographic properties, it behaves similarly to those ions during weathering and ultimately concentrates in secondary products. Cr was also adsorbed onto the surfaces of Fe and Mn-oxides. This is partly explained by the fact that under progressive oxidation, Cr goes to the chromate $(CrO_4)^{2-}$ which is a readily soluble anion (Shiraki, 1978).

Scandium

Scandium concentrations in igneous rocks generally increase with decreasing contents of SiO_2, with the exceptions of olivine- (and nepheline-) rich rocks (Frondel, 1978). This is partially evident in the two deposits as shown by the Sc contents of the unweathered rocks (mean 16 ppm) and in the greenish-grey saprolite (mean 25 ppm). High concentrations occurred in the mottled clay units and the greenish-grey saprolite. There was also a close similarity between the distribution of Sc and Cr suggesting that they are probably hosted by the same minerals.

The high concentrations in the mottled clay (> 25 ppm) may be due to sorption of Sc by Fe-oxides and the replacement of the Fe^{3+} ion by Sc^{3+} as ScO (OH) has been determined to form structural analogues of goethite and lepidocrocite (Frondel, 1972). Hence Sc becomes more firmly bound to the Fe-oxides than Cr.

Titanium

Rutile is present in the unweathered rocks, although Ti may also be hosted by ferromagnesium minerals. Isocon plots confirmed the restricted mobility of Ti during weathering as many of its host minerals are resistant and Ti is chemically mobile only in very acid environments (pH < 4.0) (Baes & Mesmer, 1976). Ti may also be mobile early in weathering as a result of pyroxene weathering (Milnes & Fitzpatrick, 1989). Ti thus tends to accumulate residually in the regolith as was confirmed by the isocon plots. Slightly enhanced enrichments (1.0-3 %) occurred in some samples in the mottled clay units and the saprolite probably as a result of incorporation into anatase which was encountered in these units. The presence of organic acids may also enhance Ti mobility

while the percolation of acid fluids as expected during the oxidation of sulfides may remobilize the Ti into secondary anatase (Correns, 1978; Dumon & Vigneaux, 1979).

Vanadium

Vanadium showed similar distribution patterns as Ti with the isocon plots showing the steady increase in V contents towards the upper levels of the profile. No specific V mineral was identified in the unweathered rocks. It is normally enclosed in relatively resistant phases like magnetite or in ferromagnesium silicate phases like pyroxene where it substitutes for Al^{3+} or Fe^{3+} (Taylor et al. 1978; Evans, 1978).

Highest concentrations (> 500 ppm) occurred in the mottled clay units and the nodular iron and manganese horizons showing a strong association with the Fe and Mn oxides. V has been observed to substitute for Ferric iron in hematite or goethite or to be incorporated into smectites (Landergren, 1978). Mobility is also possible as vanadate ions in solution.

10.8.7 Immobile elements: Zr, Th, Nb

These elements generally exhibit little chemical mobility in the weathering environment. Zr and Nb are members of the second and third transition series together with Hafnium (Hf) and Tantulum (Ta) and have very similar chemical characteristics. In particular, the chemical behaviours of Zr and Hf are almost identical, and Nb and Ta invariably occur together. Th is an actinide element but it has chemical characteristics similar to Hf.

The most important Zr-bearing mineral is zircon. Amongst the oxides, the highest concentrations of Zr are found in minerals containing Ti, Y, Nb and Ta, i.e titanomagnetite and ilmenite (Bayer, 1978). Zr showed a general enrichment towards the top levels of the saprolite suggesting residual accumulation. It is commonly regarded as a very stable mineral able to survive many cycles of weathering, sedimentary transport, diagenesis, metamorphism and antexis (Speer, 1982; Milnes & Fitzpatrick, 1989). It has however been observed to dissolve under acid pH conditions with significant chloride concentrations (Colin et al. 1993) and may also become soluble under alkaline (in the presence of carbonates) weathering conditions (Moore, 1996; Carrol, 1953).

Niobium showed slight enrichment or depletion patterns in most of the profiles. In general, it displayed similar distribution patterns as Zr in the isocons. Nb and Ta may form a solid solution and because of the geochemical similarity, they commonly co-exist

in pyroxene, magnetite and titanite (Wedepohl, 1978d). Niobium is unique in that most of its compounds are almost insoluble in acid and alkaline media, hence the soluble Nb compounds require high concentrations of acid or alkali for their formation and stabilization. It is also normally depleted in proportions intermediate between Al and Si. Once released it may occur in clay minerals (Heinrich, 1978).

Thorium (Th) showed similar distribution patterns as Zr with enrichment (6-9 ppm) towards the upper parts of the residual units. Some strong enrichment (9-15 ppm) occurred in the mottled clay units. It is usually abundant in apatite, titanite and zircon. The observation that it may accumulate in hydroxide minerals and clays when mobilized during weathering (Rogers & Adams, 1978b) may explain the enrichment in the mottled clay units. This enrichment has also been observed to be enhanced by the presence of P_2O_5 within the mottled clay units (Keith Scott, pers. comm.).

10.8.8 Rare earth elements: Y, La, Ce

Yttrium (Y) is considered with the rare earths elements (REE) because of its similar chemical behaviour, particularly to the "heavier" REE (Yb, Eu and Lu). The distribution of these elements has a number of general characteristics in common, although in general the behaviour of the REE during weathering is not well understood.

The distribution patterns of Ce and La were very similar in the isocon and line plots. There was no distinct pattern in the distribution in most of the units i.e. moderate loss could be followed by a sharp enrichment although in general there was a noticeable enrichment of both in the soil horizons and upper saprolite of profiles 2, 8 and 7. Because of these unpredictable patterns, it was also difficult to tie the enrichment zones with the mineralogy. Y showed limited mobility in most of the units and like Ce and La displayed unpredictable patterns.

The "light" lanthanides (La, Ce and Sm) have been observed to partition into plagioclase and "heavy" lanthanides (Yb, Eu and Lu) into pyroxene. The accessory phase apatite may also be rich in REE. La and Ce may also be present in pyroxenes with very minor amounts of Ce in olivine (Herrmann, 1978). Y may be fixed in a resistant phase as it remains relatively immobile during weathering. Ce fractionates from the balance of the REE during weathering because it oxidizes from Ce^{3+} to Ce^{4+} and is thereby fixed, while other REE are readily removed from the profile (Marker & de Oliveira; Braun & Pagel, 1994).

10.8.9 Other elements: Ga

The distribution pattern of Gallium (Ga) generally followed that of Al and Fe in the line plots. It is normally concentrated in the unweathered rocks in feldspars, some amphiboles, chlorites and micas and substituting for Fe^{3+} in magnetite (Braun & Pagel, 1994). Its concentrations increase towards the upper parts of the profiles, with a marked enrichment (25-35 %) in the mottled clay units.

10.9 ELEMENT DISTRIBUTIONS, WEATHERING HISTORY AND REGOLITH EVOLUTION

10.9.1 Evolution of deeply weathered regolith profiles

Weathering profiles can be considered to develop progressively, with each horizon formed from a progenitor which resembles that currently underlying it. The full sequence of horizons is thus not present until a considerable interval of time has passed. The effect of continued chemical weathering with little erosion of the insoluble products is the development of a saprolite i.e material from which mobile constituents have been lost but in which original rock textures are preserved by stable primary minerals and neo-formed secondary minerals.

An effect of the loss of mobile constituents is to give a relative accumulation of the less mobile ones. This process continues further in the upper zones of saprolite, in which the most resistant primary minerals, like muscovite in this study, persist and some secondary minerals are destroyed. Loss of primary fabric, which defined the top of the saprolite in the white clay unit, usually occurs close to the watertable (Fitzpatrick, 1980). This is a site of considerable chemical activity, particularly for elements such as Fe and Mn, whose aqueous chemistry is influenced by redox reactions. Iron and Al-oxyhydroxides are precipitated close to the water table as replacements and as secondary deposits such as coatings or as nodular aggregates as in the case of Fe-Mn oxides of this study. The material may be contributed from above, below or laterally, as absolute enrichments (Butt, 1992).

With the dissolution of primary and secondary minerals and the growth of new structures, the original rock fabric is destroyed. In time a full regolith profile is developed which comprises the fresh rock merging gradually with the saprolite and at the top of the saprolite, the mottled zone with irregular Fe-oxide accumulations with secondary

structures such as nodules. The mottled zone developed from initially transported sediments.

The development of a deep weathering profile is not a continuous process. Interruptions occur due mainly to climatic changes which, although not necessarily very marked, would tend to cause erosion of the upper parts of the profile at least. In Goonumbla, this took the form of partial truncation of the upper saprolite units. Deep weathering continues to date and is marked by reorganization of the upper mottled clay units as shown by formation of mega-mottles and secondary structures such as nodules.

The mineralogical, geochemical and palaeomagnetic data presented in this study have provided an insight into the evolution of the regolith in the Goonumbla area. From the palaeomagnetic data it was inferred that weathering of the regolith at the area has been an on-going process since the late Palaeozoic time. Regional geology suggests that the area has probably been subaerially exposed since the late Devonian.

The distribution of each element in the regolith is related to the different weathering processes that prevailed during the principal climatic regimes during this period. Many of the dominant mineralogical and geochemical characteristics of the regolith can be related to the development of the profiles under wet conditions of high water-tables, whereas others are due to later events related to more arid conditions which still persist to date. The features produced by later events appear as modifications of the pre-existing profiles and tend to be reflected more by the minor components of the regolith.

10.9.2 Weathering in past wet climates

The weathering characteristics associated with periods of past wet climates of intense leaching that are recognizable in the regolith in this area include:

1. Strong leaching of alkali and alkaline earth metals.

These include Na, Ca and Sr, which are hosted mainly by the readily weatherable minerals like albite, which are reduced to very low concentrations throughout most of the regolith. The other alkali metals i.e K and Rb are generally less strongly leached because they are hosted principally by very resistant mineral muscovite and slightly less resistant orthoclase. The weathering of these minerals occurred at the upper levels of the saprolite. Mg is also leached in a similar manner although it was retained up to the upper saprolite

because it was present in more resistant ferromagnesium minerals such as diopside and hornblende.

2. Oxidation of sulfide minerals.

Progressive depletion of sulfur occurs towards the upper parts of the residual regolith. This observation is consistent with conclusion that sulfides are some of the most unstable minerals in wet oxidizing environments, rarely persisting into the weathering zone except as supergene phases such as marcasite and violarite (Butt, 1992) none of which have been observed in these deposits. Some chalcocite was present in the sulfide zone but even then its distribution did not extend up to the weathering environment. The other elements released by the oxidation of the sulfides (Fe, Cu, Zn and Pb) were either leached or retained in iron and manganese oxides.

3. Retention of Si, Fe and Al as stable secondary minerals.

The mineralogical and chemical compositions of most of the regolith units was dominated by the three elements Si, Al and Fe in the form of kaolinite, quartz and hematite, goethite and partly in the structures of smectites. The distribution of several minor and trace elements (e.g. Cr, V, Rb, Sc, Ga, As, Pb and Au) are controlled in part by the distributions of these major elements. The immobiles for example Ti, Zr and Nb also accumulate with the iron oxides residually with little chemical interaction.

The kaolin contents increase towards the upper parts of the profiles as weathering progresses. This increase seems to be related to the introduction of Al as an iterative accumulation that occurs as kaolinite is replaced during the precipitation of the iron oxides that form the mottled clay. The smectites occur in the lower units over the greenish-grey saprolite and the saprock as nontronite and higher up in the profiles towards the soil as montmorillonite. Quartz is present as a detrital constituent within the mottled clay and soil horizons and in the residuals as quartz veins and primary silicates. Secondary quartz is also present within the mottled clay and mottled saprolite as nodular aggregates.

4. Accumulation of immobile elements and stable minerals

The distributions of K, Zr, Nb, Ti, Th and V in the regolith profiles are in part related to their inertness during weathering which is due to their chemical immobility (e.g. V, Ti) and/or to the stability of their host minerals (e.g. Ti in anatase or Zr in Zircon). Their abundances tend to increase upwards through the profile due to the gradual loss of other

components. The high concentrations in the mottled clay zones of this study are due to their presence in the initially transported sediments and may not be attributed to the relative accumulation. Vanadium and Ti are released during weathering but may become immobilized by precipitation with iron oxides. Co, Cu, Pb and Ni are also released during weathering and later incorporated into the Fe or Mn oxides.

10.9.2 Weathering under semi-arid and arid conditions

Characteristics commonly associated with weathering under arid conditions are those related to excess of evaporation over precipitation, which result in the accumulation of otherwise soluble weathering products within the regolith (Butt, 1992). The most important of these are the alkali and alkaline earth metals, which concentrate in groundwaters and precipitate as carbonates, sulfates and other salts. This is exemplified in this study by the marked concentration of Ca and Mg as pedogenic carbonates and gypsum in the near surface horizons and as dolomite in the other units.

The presence of smectitic clays as intermediate weathering products is also typical of semi-arid environments. Smectites tend to form in environments where leaching is at a minimum in poorly drained environments. The type of smectite formed is partially determined by the parent rock. Basic rocks like the trachyandesite containing high Fe and low Al often weather to form iron smectite like nontronite. Beidellite tends to form as a weathering product of rocks containing micas and chlorite because they already have tetrahedral substitution required for the beidellite structure. Montmorillonite on the other hand tends to form pedogenically from solutions high in Si, Al and Mg (Borchardt & Hill, 1985).

The nodular iron and manganese aggregate formation has also been attributed to fluctuations in groundwater levels in response to change to drier climates. They are present in the E27 deposit as cones of depressions which seem to mark palaeoredox fronts associated with palaeowatertables. They also tend to mark the transition zones between the transported and residual regolith in these palaeotopograhic lows as these could have once been sites of water still-stands.

The distribution of gold has some characteristics that can also be attributed to processes occurring in response to change to drier climates. This includes the presence of zones of leaching and depletion in some zones of the profiles for example enrichment in the white clay unit and depletion in the orange-pink saprolite.

The general preservation of the regolith at Goonumbla implies that there has been little erosion at site. Such truncation as has occurred may be attributed to the units being soft and friable especially towards the upper levels of the greenish-grey and orange-pink saprolite. The soils over these truncated units appear to have partly developed from the underlying residium with some input from later transported alluvial and colluvial material. The soils over these truncated units are also shallow relative to those over the transported sediments. The deeper nature of the latter is probably attributed to soil forming processes keeping pace with the development of the palaeotopograhic low and appears to have developed well after the truncation of the residual units. The soils also show distinct cones of depression probably attributed to large trees using up water after the onset of aridity. The most likely way for the anomalies to be reflected is by bio-pumping with the trees cycling the trace elements from the lower to the upper levels of the regolith.

The evolution of the regolith at Goonumbla points to a multiplicity of events related to a sequence of erosional and depositional events occurring during and after the deep weathering that has affected the mineralogical and chemical compositions of the substrates. The palaeomagnetic dating of the regolith has enabled a number of inferences to be made regarding these events.

The paleomagnetic results showed that the weathering of the regolith has been an on-going process since the late Paleozoic. Regional geology suggests that the area has been subaerially exposed since the late Devonian although the stratigraphic record of post-Devonian times is almost entirely unknown in the area. However, interpretation of apatite fission-track data in the Bathurst area, some 100 km east of Goonumbla suggest kilometre-scale uplift and erosion in mid- Cretaceous, suggesting that the area underwent subsequent kilometre-scale burial and then re-exhumation to be consistent with subaerial weathering in the Carboniferous.

The time of deposition of the initially transported sediments must predate the time of weathering (probably Cainozoic) of the sediments and postdate the truncated saprolite (Carboniferous) beneath. These materials may relate to a system of N-S trending valleys which predate the formation of Canobolas Divide, which has formed by downwarping of the Murray Basin. The divide was already in existence prior to 12 Ma, as evidenced by K/Ar dated lavas which flowed down valleys to the north, south and west, and may have formed by downwarping of the Murray Basin prior to the middle Eocene (Ollier & Pain, 1994) i.e prior to 45 Ma. Evidence of continued weathering lies in the development of weathering profiles in the transported material which are characterized by strong mottling

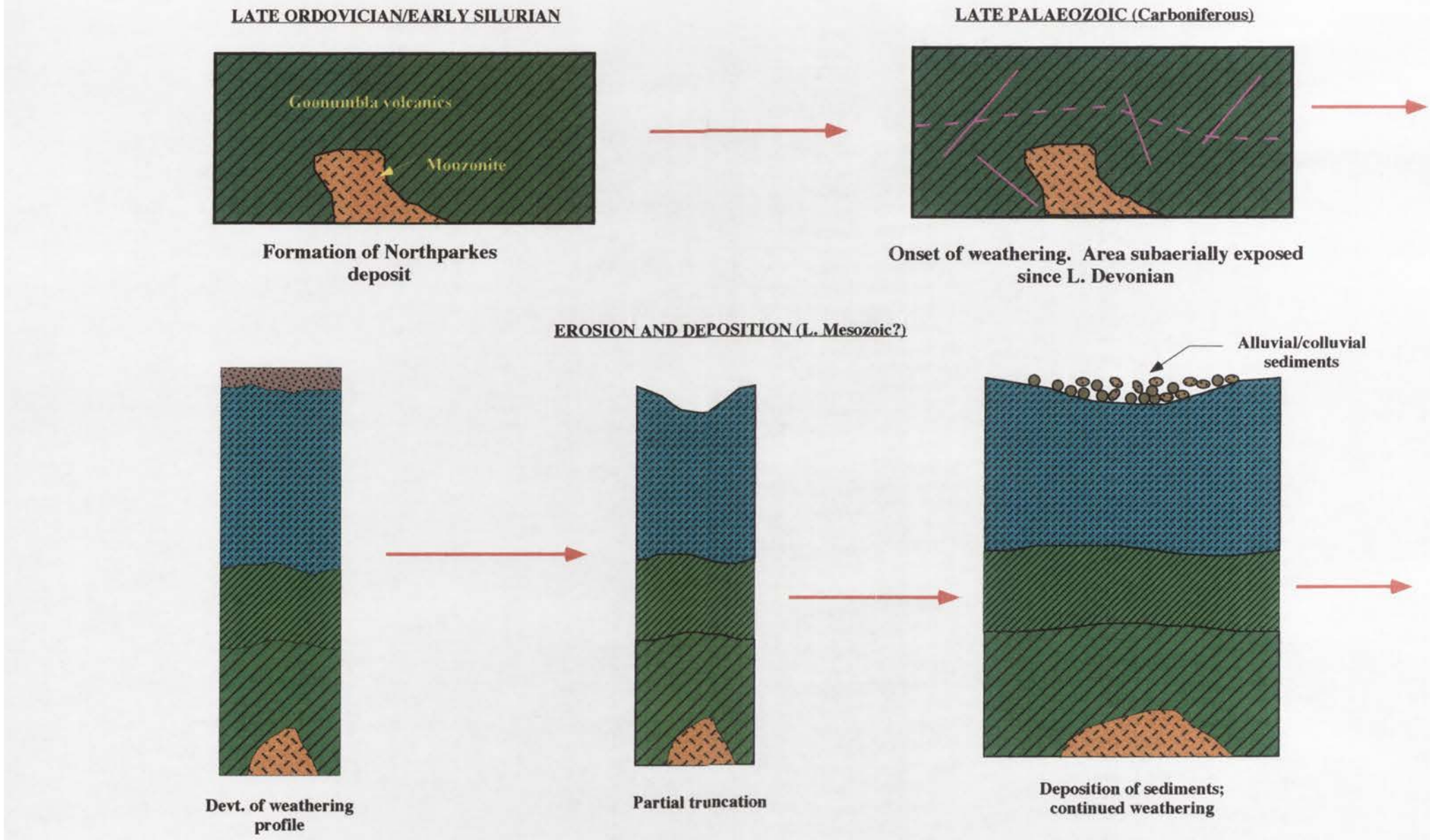

Figure 10.10: Schematic diagram showing the weathering history of the Goonumbla Cu-Au deposits

[continued next page]

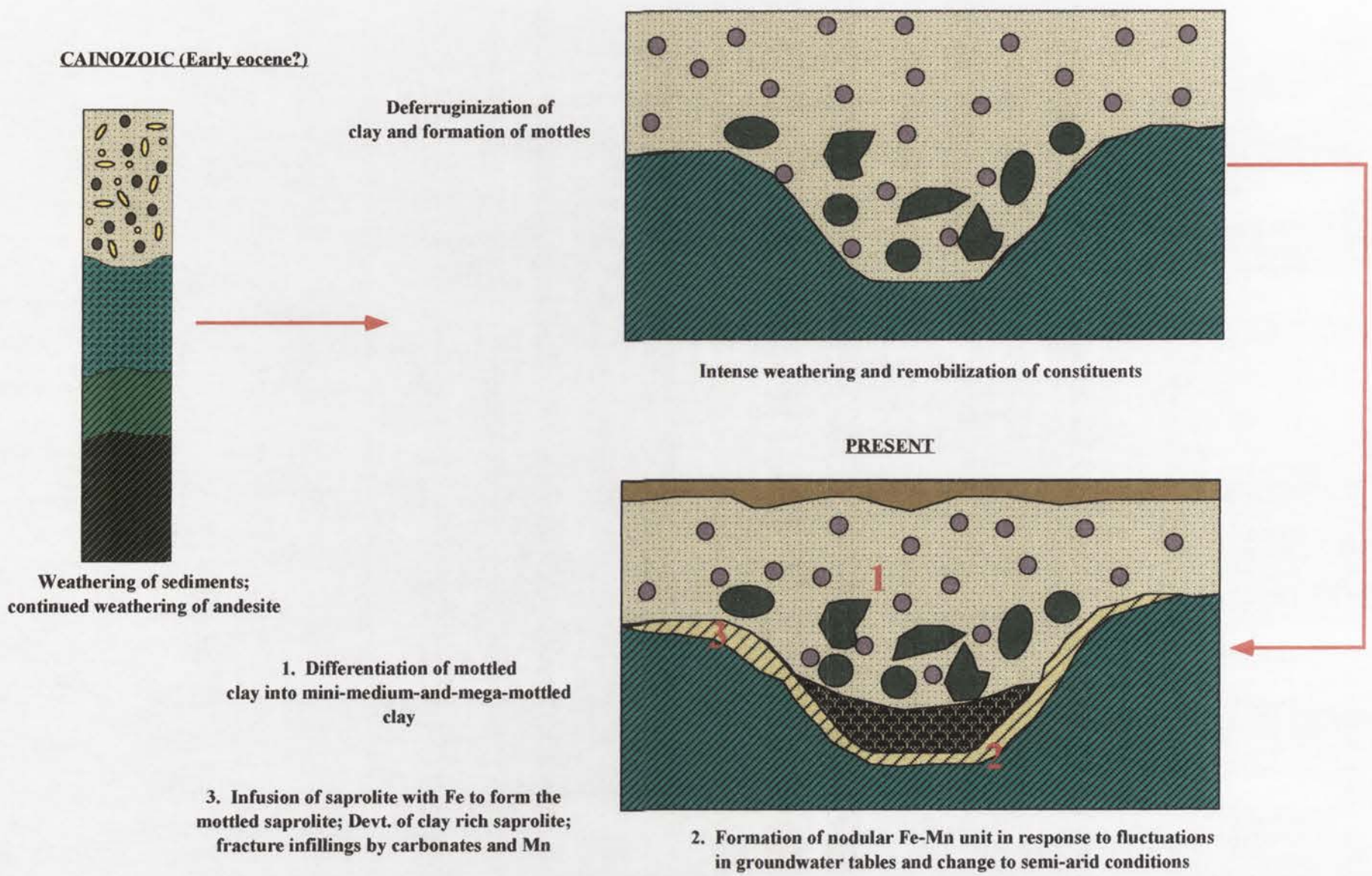

Figure 10.10: Schematic diagram showing the weathering history of the Goonumbla Cu-Au deposits
[continued from last page]

and the development of nodular horizons. A summary of the weathering history is provided in Figure 10.10.

10.10 IMPLICATIONS FOR GEOCHEMICAL EXPLORATION

The dispersion patterns revealed by this study have several implications for exploration for gold and other elements, as well as providing pertinent data of relevance to exploration for other commodities. The most obvious impact of weathering on exploration is the masking of ore deposits by the products of weathering. Besides tending to mask the appearance of most bedrock hosted mineral deposits, regolith-forming processes can give rise to large, though often weak, dispersion patterns. Use of these dispersion patterns can provide great advantages in exploration for concealed deposits in regolith-dominated terrains by increasing the likelihood of success and, at the same time, substantially reducing exploration costs.

Understanding the nature and distribution of regolith helps to develop geochemical sampling strategies for weathered terrain. Apart from the use of regolith-landform mapping and establishing of the regolith stratigraphy, studies of profile mineralogy and geochemistry in pit faces and open cuts is invaluable when this understanding is extended to areas where there are less exposures and one has to utilize drilling as the major sample collection tool.

The determination of the nature of the regolith parent material can also aid in the understanding of the processes that occurred during regolith development. An important early step in exploration of transported cover is to try to first detect, and then determine the extent of areas where full profiles occur. Within the mottled clay for example, nodules with angular irregular shapes and diffuse external borders, and those with similar framework grains within matrix materials appear to form in situ (Anand, 1991). Indicators of the transported origin of the regolith in this study include the numerous presence of sub-angular to sub-rounded quartz grains, detrital rock fragments of the parent material, laminar or cellular goethite cutans on nodules with quartz grains between them, the presence of numerous voids and channel spaces which have been infilled by illuviated clays and carbonates from horizons higher up in the profile and the presence of obvious boundaries between the transported and regolith materials. The mineralogical and geochemical data also demonstrated different origins of units in which separate parts of the weathering profiles developed.

Conversely, areas where the weathering profile is partly or extensively truncated should be delineated during the course of regolith mapping. Where this has occurred, mottled saprolite and the higher levels of the white clay unit for example are suitable sampling media although much closer sampling is required since these units can show variable characteristics over a very small areal extent. The different characteristics of the regolith units at Goonumbla and their use as sample media include:

10.10.1 Soils

Primary Au mineralization is indicated by anomalous concentrations (25- 100 ppb) of Au in the soils associated with Fe oxides. The distribution is related to the weathering processes that led to the development of the mottled clay and the later to change to arid phases which continues to the present. Mineralization is also indicated by the presence of other ore-associated elements i.e Cu, Zn and As.

Most of the soil horizons highly elevated values of Au (between 50 to 100 ppb) even above the transported regolith (above 10 ppb) and this has significant implications for geochemical exploration in the region. Soil sampling at 200 m spacings and 25 m composites could easily delineate areas of mineralization in the region.

10.10.2 Mottled clay units

These are the units with lowest though still significant Au contents (40-200 ppb). The different units of this zone had variable Au contents. Local enrichments (100-200 ppb) occurred at the nodular horizons of the mini-and-medium mottled clay and the mega-mottled clay. The iron oxides showed correlations with As, Pb, Zn, Ag, P_2O_5, V, Cr and Rb as a result of its strong adsorption characteristics. Of these elements, As, Pb and Zn are significant because they are associated with the mineralization. The presence, however, of the depletion zones in these units illustrates that care should be taken when sampling the top 5 to 25 m of the regolith.

10.10.3 Nodular iron and manganese aggregates

The Au concentrations were slightly higher (80-200 ppb) in this unit as compared to the mottled clay. The unit also showed strong adsorption for the base metals i.e Co, Ni, Cu, Pb, Zn and Ag. Apart from a mild association in a few samples, no general association was detected between the Au and MnO. Recognition of these zones in the regolith

stratigraphy should serve as avenues for recognition of anomalies in the base metals and other pathfinder elements.

10.10.4 Mottled saprolite

This unit showed broad anomalies of Au mainly associated with the presence of iron oxides and its association with the ore-forming elements in the residual units. The unit also contained appreciable amounts of the manganese oxides and carbonates. The variable contents of the Fe and Mn oxides, clays and the carbonates in this unit necessitates close spaced sampling if a broad interpretation of the geochemical anomalies is to be discerned. High concentrations of Cu and the ore-related elements i.e As, Zn and Pb also occurred in this unit.

The fact that the unit extensively occurs below the mottled clay units even in areas of partial truncation makes it the most suitable sample media in the study area. Its relatively shallow depths i.e 5 to 25 m in the regolith stratigraphy also makes it cost-effective in terms of drilling.

10.10.5 White clay unit

The unit also showed high concentrations of Au probably related to its high clay and carbonate contents and moderate amounts of Fe oxides. Its occurrence directly below the soil horizons in the truncated residual units makes it an appealing sampling media although unlike the mottled saprolite it occurs in restricted pockets at the margins of the transported regolith materials.

The recognition of this unit in drilled material may also be difficult because apart from colour it has no other outstanding physical properties. It is also important to recognize that some clay-enriched portions occur in the units although unlike in this unit, these clays tend to be grey to green in colour and have lower contents of carbonates and smectites. Its occurrence at the upper levels of the orange-pink saprolite is associated with fabric reorganization and swelling and shrinkage of the clays in transition with the soil.

10.10.6 Saprolite

Gold is present throughout the saprolite in abundances broadly similar to those in the fresh rock. The high concentrations and localized lateral dispersions enhances the weathering expression of the primary mineralization. The distribution of the other ore-

associated elements generally show greater consistency in the saprolite than in the fresh, mineralized bedrock, the homogenization attributed to chemical dispersion during weathering. Progressive depletion of Au occurred towards the upper saprolite away from mineralization with dispersion being greatest in the lower and mid saprolite.

The concentrations of Cu and Zn followed the same patterns with the enrichment defined by K_2O throughout. Depletion occurred in the upper levels of the orange-pink saprolite corresponding to the loss of susceptibility of weathering of the host minerals muscovite and K-feldspars.

In general, the consequence of weathering and secondary mobilization is to reduce grain sizes and to homogenize gold distributions, although sampling problems, particularly the "nugget effect", remain of great significance. The use of pathfinder elements reduces bias and variability due to sampling and potentially enhances the expression of mineralization. Carefully documented orientation studies should generally improve understanding of element behaviour in deeply weathered environments and also be of benefit to exploration for commodities other than gold.

CHAPTER 11

SUMMARY & CONCLUSIONS

The aim of this thesis has been to achieve a better understanding of the regolith evolution processes in the Goonumbla area in terms of its mineralogy and geochemistry. Specific aims included the establishment of the classification system for the description of the regolith, the elucidation of regolith paragenetic sequences and processes of rock alteration and the determination of element mobility and geochemical dispersion patterns in the regolith. The influence of these regolith processes on landscape evolution has also been studied. In this Chapter, the results are summarized and combined in order to present a generalization of the regolith evolution processes.

The diverse range of techniques utilized and the general approach to the study have resulted in some fresh findings and significant contributions to the study of regolith evolution processes which include:

. Formulation of a broad classification system for the description of the regolith in the region, which takes into account genetic attributes, related to the nature of parent material and physical attributes such as colour, texture and nature of secondary structures.

. Paragenetic sequences associated with the weathering of the different components of the trachyandesite, mineral reaction processes in intially transported alluvial and colluvial materials and the microsystems in the different parts of the profiles that resulted from these processes.

. The existence of originally undefined palaeotopographic lows in the landscape whose origin is linked to palaeodrainage systems in the area and the implications of the distribution of their components on geochemical exploration in the region.

. An evaluation of the element enrichment and depletion patterns during weathering in the different units of the profile. The isocon method, which has found new applications in the study of weathered rocks, was used to supplement the results of other applications.

. The determination of mineral host associations and applications of the techniques to mineral exploration in the region. The use of the relatively new quantitative mineralogy

package known as *siroquant* has enabled good correlations to be made between the mineralogy and geochemical data and hence better interpretation of inherent associations.

. The originally undocumented old age of weathering (Late Paleozoic) has provided new insights into the study of regolith and landscape evolution processes in the area in addition to changing the dimension of thinking with regard to the subject in the south eastern Australian region.

. Regolith evolution and classification

Regolith evolution is governed by processes that involve interactions between the primary minerals and chemical agents such as water, oxygen and carbondioxide that circulate below the earth's surface. Rocks that were initially coherent, dense and composed of anhydrous or weakly hydrated minerals alter progressively during weathering to friable material composed principally of strongly hydrated and microcrystalline phyllosilicates and hydroxides. The resultant secondary minerals are significant in that they are host to elements released and dispersed from primary mineralization by weathering.

One of the initial challenges posed by this study was the need to identify or adopt a classification system for the description of the regolith materials in the field, which could then be used to assign genetic links between the units or profiles. The challenge, however, is global in that there is a lack of a universally accepted system for the terminology of deeply weathered regolith, whether for whole profiles or individual horizons. This is because there is a wide range of materials within the regolith, with great variations in mineralogical and chemical composition, fabric and origin, even within a single profile or toposequence. Many of the existing terms are also used in different senses by different authors and comparisons of like situations are greatly hindered by either the lack or inadequacy of existing terminology.

The scheme that has been formulated for this study conforms as much as possible with established and currently available national and international usage. The terms used have taken into account the nature of the regolith parent material, physical attributes such as colour, texture, friability of component materials and the presence of secondary structures (i.e modules, concretions, laminations etc). The physical attributes have been emphasized because they are readily identifiable in the field and are therefore useful for first hand description of materials.

The determination of the nature of the parent material has been central to the description and hence classification of the regolith materials. The regolith materials in the area have been determined to have evolved from two parent materials; firstly, weathering of the trachyandesite host rock and hence the use of the term residual regolith materials in describing them, and secondly, transported regolith used to describe the material that developed on initially transported alluvial and colluvial sediments. The residual regolith materials are defined by the materials that form saprock and saprolite (which together constitute the "saprolith") and the soil that formed from it. The transported regolith materials are defined by the regolith materials that constitute the mottled clay units and the soil that formed from it (both constitute the "pedolith").

Some pertinent field attributes were employed to differentiate the regolith materials that had similar characteristics under their broad definitions. Two of the three main types of saprolite for example were differentiated in the field by their distinct colours i.e the orange-pink (2.5 YR 8/4) and greenish-grey saprolite (8/5 GY) and the third by its mottled nature. The orange-pink saprolite is situated on top of the greenish-grey saprolite in the regolith stratigraphy and was interpreted to have formed by loss of nontronite and plagioclase feldspars that imparted the green colour to greenish-grey saprolite. The orange-pink saprolite contains higher contents of the K-feldspar and muscovite. The decomposition of the two minerals occurred mainly in this unit corresponding to the loss in their weathering susceptibility. The mottled saprolite has been interpreted to have formed by infusion of the other saprolite units with iron oxides as shown by its higher contents of goethite (10-20%) and hematite (5-10%). This saprolite unit was also slightly harder and more massive as compared to the other two.

Colour was also utilized to describe and distinguish the regolith unit that occurs between the orange-pink saprolite and the soil in the flanks of the mottled clay portions of the E22 pit. This unit consists of massive white (7.5 YR 8/1) to whitish-grey (7.5 YR 7/1) clays with mesoscopically homogenous fabrics. The evolution of the unit has been attributed to continuous leaching and loss of material to reduce the competence of the upper saprolite zone so that settling of the clays occurred at the same time as the rock fabrics were being destroyed. The unit also contains high contents of smectite (10-15%), kaolin (50-70%), dolomite (5-10%) and muscovite (10-15%). The shrinking and swelling of smectitic clays may have hence aided the destruction of the fabric with subsequent infusion by carbonates. Because of these distinct properties highlighted by the white colour of the clays the term white clay unit was adopted to describe it.

The different horizons of the mottled clay have also been distinctively subdivided on the basis of the size of iron segregations or accumulations (mottles) into mini, medium and mega-mottles. The mini-mottled clay has iron oxide segregations of 2 to 5 mm, the medium-mottled clay, 5 to 30 mm and the mega-mottled clay 50 to 300 mm. These subdivisions were necessary when carrying out detailed descriptions because these mottles had subtle differences in their fabrics, texture, mineralogy and geochemistry.

. Mineral paragenetic sequences

1) Residual regolith units

The saprolith (the saprock and saprolite) is dominant in the regolith profiles and constitute over 60% of the entire regolith of the area. The chemical, mineralogical and textural evolution of the regolith, especially the residual units, is strongly dependent on the texture and mineralogy of the parent rock. Joints and cracks in the trachyandesite presented sites of rapid solution and matter movement and subsequently represented a zone of enhanced kinetics and alteration as compared to the rest of the rock. The presence of accelerated reactions within microcracks or fissures have led to the formation of two distinct microsystems i.e contact and rock solution microsystems. In contact microsystems, the alteration is host mineral dependant while rock-solution microsystems operate in minerals adjoining the fissures where primary mineral and solution activity and chemistry exerted roughly equal influence on the production of secondary assemblages. These microsystems were represented in the weathering of the different components of the trachyandesite.

The trachyandesite mineralogy of this study is dominated by feldspars (albite and orthoclase), muscovite, quartz and minor amounts of pyroxenes, ferromagnesium silicates and opaque oxides (magnetite, hematite and sulfides). The weathering of feldspars is a surface controlled process with access of solutions controlled by defects, cleavages, twin planes and microcracks. Dissolution proceeded by preferential attack at energetically favoured sites which resulted in formation of etch pits which followed the twinning planes of plagioclase and crossed hatched twinning of K-feldspar. This was represented petrographically by the formation of an intermediate stage marked by a brown "cloudy" poorly crystalline material of low birefringence, which appeared from SEM EDXA studies to be a mixture of smectite and oxyhydroxides. Thus the crystal structure of the feldspar appears to have controlled the nature and orientation of initial weathering products.

Their was a noticeable presence of secondary products containing elements not present in the parent material in this study as was shown by the presence of iron in the poorly crystalline material over the feldspar. Rock-solution microsystem reactions often involve introduction of secondary products from fissures into the active sites with fissure microsystems prevailing and solution chemistry dictating the type of secondary product. The occurrence of iron in the smectite of this study and its role in the weathering of feldspar was not properly understood. Other studies have documented the same observations workers (Casey et al. 1989; Chou & Wollast and Wollast, 1985; Ildenfose, 1980) with the most plausible explanation offered by Banfield & Eggleton (1990) who suggested that if Fe^{2+} is present in solution, oxidation coupled with hydrolysis of water may provide H^+ or H_3O^+, which attacks the feldspar structure releasing K, Na or Ca with the ferrolysis reaction written as:

$$2Fe(H_2O)_2^{2+}{}_{(aq)} + 1/2O_2 \;<\!\!>\!\!>\; 2FeO(OH)_{(s)} + 4H^+ + H_2O.$$

For Fe to have participated in this manner, it was concluded that solutions in the weathering profile must have been episodically reduced with characteristics of the weathering solution (pH, oxygen content, dissolved ions) varying due to seasonal changes in response to adjacent mineral weathering reactions, explaining the mobilization of Fe and its precipitation in altered feldspar surfaces. The Fe was probably sourced from the oxidation of sulfides and weathering of pyroxenes.

Continued weathering of the feldspars in the saprolite was marked by differential shattering, pitting and coalescence of the etch pits along which was further evidence of transport-solution mechanism operating to induce the dissolution of the mineral surfaces. This resulted in the precipitation of clays of different morphologies which included platy, vermiform and "book" type varieties of kaolin and cellular "cotton wool' or "corn flake" textured smectite with striated surfaces. The main product was kaolin which was interpreted to have evolved by direct transformation of the feldspars, smectite and alteration of muscovite.

Random orientation of kaolin books with respect to the etched or pitted surfaces of feldspar was also noted and was interpreted as indicating that the argillic transition was not a solid-state transformation or replacement, but rather the intervention of a solution in reaction with the solid phases. The book-type kaolinites were concluded to be products of weathering of the thick residual units i.e saprolites and saprock. These units were formed over notably long periods of time in different climatic conditions that produced deep weathering below the active zone of erosion and denudation. These conditions are

essential for geochemical equilibrium to be reached and maintained for a long time, between the ground-water solution and the solid, parent-daughter phases.

The alteration of smectite to kaolinite transpired as a consequence of lowering of solution pH and improvement in drainage in going from the saprock to the saprolite. The abundance of 2:1 clay minerals (smectites) in the saprock and the lower saprolite was largely due to poor leaching in this part of the profile. Drainage governs leaching intensity in weathered profiles with the absence of 2:1 clays representing macro and micro well-drained profiles and abundance to deficient leaching activity in the profiles. This led to the important conclusion that microenvironments governed the type of secondary mineral in any part of the profile. Intensity and amount of solution access to microcracks regulated nucleation and crystal growth and was responsible for the outward appearance of the secondary products.

2) Weathered transported alluvial/colluvial sediments

The fabrics of the mottled clay zone varied from those of the saprolite. The fabric was defined by the occurrence of diffuse or intermittent segregations of iron (mottles or nodules) in a predominantly clay plasma. The mineralogy of this zone was dominated by quartz, kaolin, hematite and goethite with minor amounts of anatase, smectite and dolomite. The plasma, especially in the upper levels, was traversed by numerous fractures, root channels and voids. The root channels in some parts had strung together to form channelways. These spaces mark zones of intense solution activity where most of the material was formed, translocated or deposited within the different parts of the zone.

The void spaces in the mini-mottled clay for instance had been infilled with skeletal grains of iron stained lithorelicts and intercrysts of gypsum, which had been translocated from the soil horizon. The root channels were also lined with goethite, siliceous clay and undeterminable manganese wads. Within the medium-mottled clay, characteristic iron-stained clay filled channels were quite pervasive within the plasma and they were interpreted as representing the settling and orientation of eluviated clays at these passageways. Carbonate (dolomite) and manganese wads had subsequently infilled these spaces. The diverse colours of the clay in the different parts of the mottled clay zone as defined for example by the white, pale green, pink and grey colours of kaolin was attributed to the differences in groundwater compositions and its influence on the weathering processes and resulting products.

Scanning electron microscopy confirmed the differences between this material and that which that which comprised the residual regolith. Kaolin in the mottled clay occurred as the thin platy variety with the particles observed occurring parallel to one another and in most cases adhering tightly to quartz. These differences were attributed to the fact that thin platy varieties represent sedimentary kaolins whose texture is controlled by the effects of particle size fractionation and sedimentation. The kaolin adheres to the quartz because they were deposited together in the former erosional and sedimentary environments.

Secondary structures of different morphologies and characteristics were present in the clay plasma in the mottled clay zone. Ferruginous nodules occurred mainly in the mini-and-medium mottled clay. The bleached (Fe-poor) domains of the mottled clay consisted mainly of quartz and kaolinite and exhibited a white or grey colour. The mechanism of formation of mottles or nodules is poorly understood with general conscensus favouring de-ferruginization in the bleached domains already mentioned (Nahon ,1986; Tardy, 1992, Brewer, 1964). Original kaolin aggregates, free of iron, can be dispersed and kaolin particles can migrate and even be leached out. The changes were accompanied by a strong increase in porosity that led to the formation of macrovoids and channelways.

The secondary accumulation of kaolin was attributed to solution or translocation from overlying layers as relicts of soil forming processes. These secondary accumulations of kaolin and associated quartz are generally accompanied by a secondary accumulation of iron-generating brown red coloured clays, providing a contrast with the white-grey decoloured areas, located around the channels. Nodules and nodules formed this way are hence traces of the secondary pedogenetic activity occurring in the unsaturated zone.

The petrography and micromorphological studies hence provided evidence of the differences in the origin of substrates that constitute the pedolith and saprolith. From these observations, it was concluded that the material that consitute the pedolith resulted from weathering on initially transported alluvial/colluvial sediments. Additional evidence was provided by the geochemistry (to be discussed later) of their constituents.

Transported regolith and palaeotopograhic lows

A distinct boundary exists between the transported and regolith materials through the entire sequence in the regolith stratigraphy. The transported material of this study occupy a distinct U-shaped position in the present landscape and has been interpreted as having formed in localized palaeotopographic hollows or lows in the landscape. These features

seem to be widespread in this region although their occurrence had hitherto not been well documented.

Similar sequences on mottled clay zones have been reported on the depositional regimes of the Yilgarn craton of Western Australia (Anand et al. 1993; Clarke, 1994 and Dusci, 1995). These workers have interpreted these sequences as having developed through weathering of sediments deposited in palaeochannels. They describe this material as composed of variable thicknesses of alluvium (up to 100 m) which has buried the channels cut into saprolite. They further observed that the weathering of the basement is deepest beneath the palaeo-drainage system, with the weathering front closer to the present day surface with increased distance away from the palaeochannels.

A typical profile over the channels (Figure 7.3) in the Yilgarn craton shows some similarities with the sequence over this study. These channels are composed of extensive mega-mottled sequences characterized by extensive bleaching and development of evenly spaced, irregular, vertical hematite and goethite-rich, 10-25 cm long mottles or septa (Dell, 1992; Anand et al. 1993). They also recognized two zones within the mottled zone as opposed to the three in this study; that is the mini-mottled zone (4-8 m thick) and mega-mottled zone (6-10 m thick). They also described the presence of black ferruginous granules and root systems with intimate relationships with Fe accumulations, which they suggested was evidence that these units once supported abundant vegetation. Anand et al. (1993) attributed the greater depth of weathering in the palaeochannels to a combination of factors which favour weathering. These include incision of palaeochannels along a structural weakness, salinity of groundwaters and abundant water during and after deposition of sediments.

The mineralogy of the detrital rock fragments that were recovered from the weathered matrix in this study was compatible with those of the host rock showing that this material was sourced from a localized drainage basin. The boundary between the transported and residual regolith units can be traced through the entire regolith sequence. This 2-dimensional feature could represent a palaeotopographic low in the landscape where a channel might have once traversed. However, it is difficult to assign a genetic origin to this feature because the material within it has been extensively weathered and hence total obliteration has occurred of inherent sedimentary features that could have provided more clues as to the actual nature of alluvial/colluvial environment of the depositional basin. From a geochemical point of view, the recognition of the transported origin of these materials was invaluable in the design of exploration programs characterization of the sample media.

Figure 11.1: A regolith profile over a paleochannel sequence in Kanowna Belle, Western Australia (Anand et al. 1993)

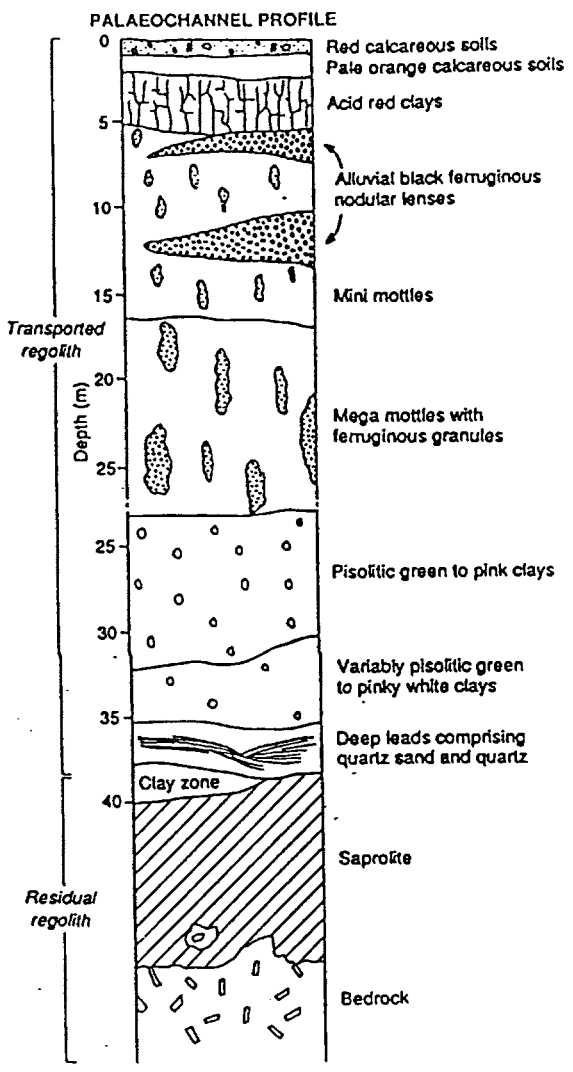

One other significant observation of the mottled clay sequence of this study was the presence and disposition of the nodular iron and manganese rich zone. This occurred at the bottom of the most extensively weathered sequence in E22 marking the transition between transported and residual regolith and as two cones of depression in E27 deposit that followed the general topographic setting of the basin. These zones seem to represent palaeo-redox fronts associated with positions of palaeo-watertables.

A second significant aspect concerned the depth and occurrence of cones of depression within the soil over the transported material. The soils over this material are quite deep (up to 4.5m in some parts). The possible explanation for this is that the deposition of the material in the basin was slow enough to allow soil forming processes to keep pace. The development of the cones of depression is probably related to large trees using up water in the sediments during an arid climatic phase.

. Element mobility and dispersion processes

An understanding of the geochemical behaviour in the weathered mantle facilitated a better interpretation of the source material's geochemistry and the development of techniques suitable for exploration. A number of techniques were utilized to show the distribution and mobilities of the various elements during weathering.

The use of statistical measurements like standard deviation (s) and skew (Sk) gave a measure of the spread of the element concentrations about the mean and the symmetry of the population spreads respectively. A positive skew in the distribution for example indicated that it was log-normal. Of all the elements, Si and Al were the only ones that had a normal distribution of concentration values. It was inferred from the mean and standard values that the elements with a low standard deviation relative to the mean such as Ti, Mn, P, Ag and Ag were not mobilized and locally concentrated while those with a high standard deviation like Fe, Cu, Pb and Zn were highly mobilized. Some regolith units like the white clay unit and the nodular iron and manganese zone exhibited high spreads for most of the elements as a result of the presence of samples with high concentration outliers related to the characteristics of this unit.

The major elements associated with most of the secondary products were Si, Fe and Al which occurred as the oxides i.e hematite, goethite and quartz or as aluminosilicates notably kaolinite. Ternary plots showed that SiO_2 in the transported regolith units occurred as a major constituent in the soil relative to the other elements while higher amounts of Fe_2O_3 occurred in the nodular Fe-Mn units relative to the mottled clay units. Al_2O_3 was mainly clustered around the mottled clay units mainly associated with kaolin. A few Fe-rich outliers occurred in the white clay unit and mottled saprolite units. Unlike in the transported regolith units the samples from the residual regolith units were clustered around SiO_2 mainly associated with its occurrence in primary rock-forming silicate minerals such as muscovite and feldspars.

The line plots of element concentrations in relation to depth provided a general idea on the distribution of these elements in the different regolith units. Of the major elements, CaO and MgO were enriched in the soil horizons and the white clay units in the form of calcite, dolomite and gypsum while MnO showed enrichment in the nodular Fe-Mn units and the mottled clay units particularly in the mega-mottled clay. High amounts of K_2O occurred in the saprolite units associated with muscovite and K-feldspars while high amounts of Na_2O occurred in the saprock and greenish-grey saprolite associated with plagioclase feldspars. P_2O_5 amounts were highest in the saprock and nodular Fe-Mn units associated with apatite and adsorption into the Fe and Mn oxides respectively.

Among the trace elements, Au occurred in appreciable amounts (50-800 ppb) in all the regolith profiles with enrichments in the saprock, white clay unit and the mottled saprolite. Copper, Zn and Pb concentrations on the other hand showed progressive enrichment with depth showing that their distribution was associated with mineralization. High concentrations of Zn and Pb occurred in the mottled clay units and nodular Fe-Mn units associated with the strong adsorption properties of Fe and Mn oxides. Arsenic, Ni, V, Cr, Sc and Rb were mainly enriched in the mottled clay units and nodular Fe-Mn units for the same reasons. The enrichment and depletion patterns of the other elements could not be clearly discerned from the line graphs.

Mass balance techniques were used to monitor element mobility and chemical changes during regolith formation and to infer weathering rates. The isocon technique although developed for the study of alteration enabled the evaluation of the enrichment and depletion patterns during the weathering of the trachyandesite. Isovolumetric methods which assumes that the unit volume of weathered rock evolves from an equal volume of fresh rock by utilizing the rock densities could not be utilized because of the effects of mineralization which caused geochemical heterogeneity and partial loss of rock fabric irrespective of weathering. The requirement that the parent rock characteristics had to be known discounted the use of the mass balance techniques in the study of the transported regolith materials.

The calculated net mass change ΔM (%) for each sample, generally a net loss in weathering, from the isocon, was used to estimate the degree of weathering which then acted as a weathering index for inter-and intra-profile comparisons. Most other mass balance techniques (Reich, 1943; Roaldset, 1943; Ruxton, 1968; Parker, 1970; Vogel, 1975; Nesbitt & Young, 1982; Harnois, 1988; Price et al. 1991; Brimhall et al. 1992) rely on the comparison of mobile element concentrations versus the concentration of a single relatively immobile element. Generally it is difficult to assess how immobile this index

element has really been during the chemical and physical processes of weathering and hence the limitations of these methods.

The isocon technique also provides an internal check as all index elements must occur in the same ratio (weathered rock/unweathered rock) as each other to be considered truly immobile. Other elements, which lack the same ratio as the immobile index elements, have been mobilized by weathering and lie off the isocon. The fact that four index elements are required to define the isocon also makes it more reliable than the other techniques. Because the technique relies on the use of ratios (element concentration in the weathered sample compared with element concentration in the unweathered protolith), data can be used independent of units (weight %, ppm) and major and trace element data from a regolith sample represented on the same isocon diagram.

Some general observations regarding the mobility of elements were made from the stacked isocon plots. Calcium oxide, Na_2O, MgO and Sr showed similar distribution patterns in the profiles in that they were marked by a strong depletion early in weathering and progressive depletion higher up in the profiles. Calcium and Sr partitioned similarly in these units and appeared to have been released at the same time during weathering suggesting a common source i.e plagioclase feldspars and ferromagnesium silicates. The Ca and Sr were later incorporated into secondary smectite clays. Magnesium oxide behaved similarly to Ca and they were enriched together in the higher units because of occurrence in dolomite. Sodium oxide was released during dissolution of plagioclase feldspars and later incorporated into smectite clays or completely leached out of the system.

Unlike the other alkaline earth elements, K showed progressive enrichment in the greenish-grey saprolite and depletion in the orange-pink saprolite, the white clay unit and soil horizons. Rubidium, Cu and Zn partitioned in a similar fashion the reason for the distribution explained by the fact that K_2O was hosted principally by micas and K-feldspar whose breakdown during weathering occurred in the upper levels of the greenish-grey saprolite with most of it sustained in the orange-pink saprolite and the white clay units. The K_2O also defined the alteration zone explaining its strong association with Cu and Zn. Rubidium has similar chemical properties as K_2O and showed similar behaviour during weathering.

The depletion of Si occurred at a slower rate than the removal of the alkalies because it was incorporated into neoformed clay minerals as a fundamental part of their structure. Cerium showed variable distribution patterns in that depletion could be followed by

strong mass gains of up to 500%. It showed similar distribution patterns as La and Pb. This distribution suggested incorporation into a resistant mineral phase resulting in the enrichment or scavenging by secondary weathering products or incorporation into neoformed phases explaining the depletion. The fact that Pb is largely derived from feldspar and the lanthanides from apatite precludes their concentration as a result of partitioning into a resistant phase.

Sulfur showed strong depletion patterns in most units of the profile except in the soils where it was enriched. This depletion represented the progressive oxidation of the sulfides with the enrichment in the soil a consequence of its presence in gypsum. Yttrium showed no general distribution patterns with its enrichment in weathering profiles related to partitioning into secondary neo-formed phase in much the same way as lanthanides. The relatively high anomalous concentrations of Zr in some profiles was attributed to its varied composition in the parent rock associated with mineralization effects on pH and Eh which influenced its mobility. This discounted its use as an immobile index in a number of profiles.

- **Mineral-element host associations**

The secondary minerals are host to elements released and dispersed from primary mineralization in the course of weathering. The association between the secondary minerals and trace elements were further investigated using selective leaching techniques. This technique involves a dissolution of a particular soil or weathered phases in a controlled manner, and the resulting solutions analyzed for trace elements of interest. Secondary Fe and Mn oxides ubiquitously present in soils and regolith units as stains and concretions or as discrete particles of colloidal dimensions, are strong scavengers for many heavy metals released in the weathering processes.

The scavenging action is a manifestation of the solid-liquid interfacial phenomenon related to mineralogical structure and physicochemical properties of these oxides. Extraction schemes are selected to test extractable ions associated with carbonates and the Fe and Mn oxides utilizing pH 5 acetate (extracts carbonates), 0.1M hydroxylamine (extracts Mn oxides) and 0.25M hydroxylamine (extracts amorphous Fe oxides). The elements chosen for this study were Ca, Mg, As, Pb, Zn, Co, Ag, Ni, Fe and Mn.

The pH 5 acetate successfully extracted all of the Ca and Mg phases from the carbonate-rich units. In contrast, in the residual units where some of the Ca and Mg occurred as non-carbonate minerals, the Ca and Mg was not entirely dissolved. This is because, the

Ca and Mg occurred within plagioclase feldspars and ferromagnesium silicates which were more resistant to the pH 5 acetate. Copper and Zn were also partially extracted by the reagent although it was not assumed that this indicated occurrence within the carbonates because they can occur as soluble secondary minerals that dissolve in an acid acetate solution, which complexes most high charge cations except Cu^{2+} and Zn^{2+}.

The hydroxylamine reagents were found to be good extractants for most of the other elements apart from Ca and Mg. The general trends showed the partitioning of Ag, Co, Ni and Pb into the Mn oxides and Cu into the iron oxides. Apart from the total dissolution of the Ca and Mg by the pH 5 acetate, the other reagents did not dissolve most or all of the elements. The effect was more pronounced in the lower levels of the residual units where the dissolution capacity was lower than 15% for Pb and Cu. This phenomenon was attributed to their host minerals i.e muscovite and the ferromagnesium silicates being resistant to weathering and the elements being so tightly bound within their structures that selective extraction could not extract most of them. The low dissolved concentrations of some of the elements like Ag, Ni, Pb and Zn in the clay-rich units like the white clay unit was for similar reasons linked to their being tightly bound within the complex clay crystal structures.

The scavenging of metals by Fe and Mn oxides involves coprecipitation, adsorption, surface complex formation, ion exchange and penetration of crystal lattice. Iron and Mn oxides exhibit a marked tendency to form coprecipitates or mixed oxides because of similarities in some chemical properties of the higher oxides of Fe and Mn including reversible oxidation-reduction, insolubility and the presence of pH dependent electric charges and the closeness of ionic radii of Mn^{2+} (0.80 Å) and Mn^{3+} (0.66Å) to those of Fe^{2+} (0.76Å) and Fe^{3+} (0.64Å). The chemical reactivity of Mn oxides is related to some inherent specific features such as its ability to exist in several oxidation states and form non-stoichiometric oxides with variable valence states and the existence of its valent oxides in several crystalline forms. Mn can also form coprecipitates and solid solutions with Fe oxides. Because of its high charge ratio, amorphous Fe oxides are also more chemically reactive than are crystalline Fe oxides.

In using secondary oxides as a sample medium for geochemical exploration, attention should be paid to 'false' or 'apparent' metal anomalies that are not related to mineralization but are caused by scavenging action of varying amounts of Fe and Mn oxides. Ratios of metal (s)/Mn, metal (s)/Fe, or metal (s)/ (Fe + Mn), or increased threshold levels with increasing concentrations of Fe and Mn oxides in the sample should be considered in analyzing and interpreting experimental data under such circumstances.

This study has shown that Fe and Mn oxides and their relationships to the geochemistry of heavy metals provide one of the promising avenues to the study of mineral-element host associations and detection of metal anomalies in the weathering zone and hence it's use should be strengthened.

The general association between Au and carbonates which has been recognized for several decades also provides another tool for the study of anomalies associated with the element and also its behaviour in the weathering environment. This association has commonly been explained as coincidental, occurring through physical entrapment of Au nuggets in a calcareous cement. This phenomenon has been encountered in the Yilgarn craton of Western Australia and recently in the Gawler craton in South Australia. The reason for this distribution is unclear although it relates to these regions having a mainly winter rainfall and hence longer growing season and greater production of CO_2. Long-term climatic factors seem to be of significance in the accumulation process.

No association between the Au and carbonates was observed in this study although there was a strong association between goethite and Au. Although this study has not addressed the reasons for the observed Au and carbonate associations in Western and South Australia and the absence of any association in this study, it is noted that the climates of these regions are different. Parkes region receives almost twice the rainfall of the other regions and one to one and a half times as many raindays and daily maximum temperatures that are 2° C less. The differences in climate will obviously impact on leaching, Eh and pH of the local environments and hence the distribution of Au.

The preferential incorporation of Au by goethite is related to its strong adsorption properties and its mobility in the weathering environment. The chemical characteristics of an active weathering profile are such that there is an increase in Eh and pH from the weathering bedrock interface up to the watertable (Mann, 1984; Lawrence, 1994). Implicit in the chemical model for such profiles where ferrolysis is active is the diffusion of ferrous iron, Fe^{2+} upward in the profile with reprecipitation of Au usually occurring in conjunction with precipitation of goethite because of the restricting effect of the presence of Fe^{2+} in the profile (Mann, 1983).

A number of observations were made concerning the distribution of Au in the regolith. Gold exhibited a widespread distribution in the regolith stratigraphy with most of the units containing significant amounts of the element. The highest concentrations (500-800 ppb) occurred in the saprock, with moderate concentrations (200-500 ppb) in the greenish-grey saprolite, mottled saprolite and the white clay unit. Lower but still

significant concentrations (50-200 ppb) occurred in the mottled clay and nodular Fe-Mn units. Progressive depletion of Au was noted from the fresh rock to the upper levels of the residual regolith units with some lateral dispersion in the E27 deposit. This pattern represents depletion of Au with progressive weathering and/or further away from the mineralization.

Within the mottled clay units, Au was preferentially enriched in the upper nodular horizons of the mini-and-medium mottled clay. The enrichment in the white clay units appears to be related to the characteristic features of this unit. It was interpreted to have evolved by continuous leaching and loss of material to reduce the competence of the upper saprolite zone so that settling of the clays occurred at the same time as the rock fabrics were being destroyed. This destruction was probably aided by the shrinking and swelling of smectite clays with infusion by carbonates and iron oxides. Although the Au has not been connected to any mineral host and enrichment mechanisms unclear, the features of the unit suggested localized mechanical entrapment and retention within the dense clays. The moderate concentrations in the mottled saprolite have been associated with a dual input from the Fe-oxides and expression of mineralization in the residual units.

- **Climate, element distribution and old age of weathering**

The distribution of the elements in the regolith is related to the different weathering processes that prevailed during the principal climatic regimes during this period. Many of the dominant mineralogical and geochemical characteristics of the regolith can be related to the development of the profiles under wet conditions of high watertables, whereas others are due to later events related to more arid conditions which still persist to date. The former are related to periods of past wet climates of intense leaching that are expressed in the regolith by the strong leaching of alkali and alkaline earth metals, oxidation of the sulfide minerals, retention of Fe, Si and Al as stable minerals (goethite, hematite, kaolin and quartz) and accumulation of immobile elements and stable minerals related to their chemical immobility.

Characteristics associated with weathering under arid conditions are those related to excess of evaporation over precipitation which resulted in the accumulation of otherwise soluble weathering products within the regolith. This was expressed in the regolith by marked concentration of Ca and Mg as pedogenic carbonates and gypsum and the presence of smectitic clays (formation is linked to poor drainage and minimum leaching). The nodular Fe-Mn units were also interpreted to have formed by fluctuations in

groundwater levels in response to change to drier climates and they were expressed in the regolith by cones of depressions defining palaeoredox fronts.

The general preservation of the regolith at Goonumbla showed that there has been limited erosion in the region. Such truncation as has occurred may be attributed to the units being soft and friable especially towards the upper levels of the saprolite. The soils over the truncated units are shallow relative to those over the transported regolith. The deeper nature of the soils in the latter was attributed to soil forming processes keeping pace with the development of the palaeotopographic basin and appears to have developed well after the truncation of the residual units.

The oldest palaeomagnetic ages for weathering profiles in southeastern Australia appear to be the Ealry Tertiary Morney profile in southwest Quuensland (Idnurm & Senior) and the Late Cretaceous-Early Tertiary profiles in the New England region (Schmidt & Ollier, 1988). The palaeomagnetic data shows that the weathering of the regolith in the Goonumbla region has been an on-going process since the Late Palaeozoic. This is the oldest age of weathering that has yet been documented using this technique and has led to a number of inferences to be made regarding the landscape evolution processes in this region.

Regional geology suggests that the area has been subaerially exposed since the Late Devonian although the stratigraphic record of post-Devonian times is relatively unknown in the area. The time of deposition of the initially transported sediments predates the time of the weathering (Cainozoic) of the sediments and postdate the truncated saprolite (Carboniferous) beneath. These materials may relate to a system of N-S trending valleys, which predate the formation of Canobolas Divide, which was formed by downwarping of the Murray Basin prior to Middle Eocene (Ollier & Pain, 1994). Evidence of continued weathering lies in the development of weathering profiles in the transported material characterized by strong mottling and development of nodular horizons.

The relatively old age of weathering determined by this study provided a challenge to the dimensions of thinking regarding the landscape evolution processes in the southeastern highlands. Thus, the evolution of the regolith at Goonumbla points to a multiplicity of events related to a sequence of erosional and depositional events occurring during and after the deep weathering that has affected the mineralogical and chemical compositions of the substrates.

• Implications on geochemical exploration

The geochemical dispersion patterns revealed by the study has several implications for exploration for gold and other elements and provides pertinent data of relevance to exploration for other commodities. The mottled saprolite showed the greatest potential as a sample medium because of its relatively shallow depths and its uniform and anomalously high distribution of the elements. The white clay unit showed equal potentials although it occurred in restricted pockets in the regolith stratigraphy.

The delineation of the nodular Fe-Mn units in the regolith stratigraphy serves as avenues for recognition of anomalies in the base metals and other pathfinder elements. Soil sampling should take into account the strong Au and goethite associations while careful sampling should be carried out in the mottled clay units because of the presence of element depleted zones despite the strong adsorption properties of the Fe-oxides. The presence of depletion zones in the mottled clay units illustrates that care should be taken when sampling the top 5 to 25 m of the regolith.

Understanding the nature and distribution of regolith helps to develop geochemical sampling strategies for weathered terrain. Studies of profile mineralogy and geochemistry in pit surfaces and open cuts is invaluable when this understanding is extended to areas where there are less exposures and one has to utilize drilling as the major sample collection tool. The delineation of areas of transported cover can help in the detection and determination of the extent of areas where full profiles occur. Conversely, areas where the weathering profile is partly or extensively truncated should be delineated during the course of regolith mapping. Carefully documented orientation studies should generally improve understanding of element behaviour in deeply weathered environments and also be of benefit to exploration for commodities other than gold.

REFERENCES

References

Adamson, S. (1996). "Exploration Geochemistry and regolith stratigraphy of the Beechmore Block, Parkes, NSW." The Australian National University, Honours thesis

Ahn, J. H. and Peacor, D. R. (1986)."Transmission and analytical electron microscopy of the smectite-to-illite transition." *Clays and Clay Minerals* **34**: 165-179.

Ahn, J. H. and Peacor, D. R. (1987)."Kaolinization of biotite: TEM data and implications for an alteration mechanism."*Amer. Mineral* **72**: 353-356.

Altschuler, Z. S., Dwornik, E. and Kramer, H. (1963)."Transformation of montmorillonite to kaolinite during weathering."*Science* **141**: 148-152.

Ambrosi, J. and Nahon, D. (1986)."Petrological and geochemical differentiation of lateritic iron crust profiles."*Chem. Geol.* **57**: 371-393.

Anand, R., Gilkes, R. J., Aritage, T. and Hillyer, J. (1985)."Feldspar weathering in lateritic saprolite."*Clays and Clay Min.* **33**: 31-43.

Anand, R. R., Smith, R. E., Innes, J., Churchward, H. M., et al. (1989). "Laterite types and associated ferruginous materials, Yilgarn Block, WA Terminology, classification and atlas." CSIRO Australia, Division of Exploration Geoscience, Restricted Report 60R.

Anderson, B. J., Jenne, E. A. and Chao, T. T. (1973)."The sorption of silver by poorly crystallized manganese oxides."*Geochim. et Cosmochim. Acta.* **37**: 611-622.

Aspandair, M.F. (1990). "Geology and regolith evolution at Parkes, NSW". The Australian National University, Honours Thesis.

Augustithus, S. and Vgenopoulous, A. (1981). Geochemical and mineralogical studies of alteration (Laterite) cover of alkali-trachyandesites. *Proc. Inter. Sem. Lat. processes*, : 139-143.

Baker, W. E. (1978)."The role of humic acid in the transport of gold." *Geochimica et Cosmochimica Acta* **42**: 645-649.

Banfield, J. F. (1985). "Mineralogy and chemistry of granite weathering". The Australian National University, MSc thesis.

Banfield, J.F. and Eggleton, R.A. (1988). Transmission electron microscope study of biotite weathering. *Clays and Clay Minerals* **40**, 273-279.

Banfield, J.F. and Eggleton, R.A (1990). Analytical transmission electron microscope studies of plagioclase, muscovite, and K-feldspar weathering. *Clays and Clay Minerals* **38**, 77-89.

Barshad, I. (1957). Factors affecting soil formation, *Proc. 6th Natl. Conf. Clays and Clay Min.*, **6**: 110-113.

Barth, T. F. W. (1948)."Oxygen in rocks: a basis of petrographic calculations." *Jour. Geol.* **56**: 50-61.

Barton, D. (1916)."The disintegration of granite in Egypt." *Jour. Geol.* **24**: 382-393.

Bayer, G. (1978). "Zirconium, Handbook of Geochemistry." In Wedepohl, K. H. (ed.), Berlin, Springer-Verlag, : 40A.

Berner, R. A. (1981). "Kinetics of weathering and diagenesis." In Lasaga, A. and Kirkpatrick, R. (eds.), Kinetics of Geochemical Processes, Reviews in Mineralogy, **8**.

Berner, R. A. and Holdren, G. J. (1979)."Mechanism of Feldspar Weathering I. Some Observational Evidence." *Geology* **5**: 369-372.

Berner, R. A. and Holdren, G. J. (1979)."Mechanism of feldspar weathering II. Observations of feldspars from soils." *Geochim. Cosmochim. Acta.* **43**: 1173-1186.

Berner, R. A. and Schott, J. (1982)."Mechanism of pyroxene and amphibole weathering II. Observations from soil grains." *Am. Journ. Sci.* **282**: 1214-1231.

Bird, M. I. and Chivas, A. R. (1988)."Stable-isotope evidence for low-temperature kaolinitic weathering and post-formational hydrogen-isotope exchange in Permian kaolinites." *Chemical Geology (Isotope Geoscience Section)* **72**: 249-265.

Bird, M. I., Fyfe, A. R. and Longstaff (1990b). "Deep weathering at extratropical latitudes: a response to increased atmospheric CO_2." In Bourman, A. F. (ed.), Soils and the Greenhouse Effect, New York and London, Wiley, 283-289.

Birkeland, P. (1964)."Pleistocene glaciation of the northern Sierra Nevada north of lake Tahoe, California." *Jour. Geol.* **72**: 810-825.

Birman, J. (1964)."Glacial geology across the crest of the Sierra Nevada, California." *Geol. Soc. Amer. Spec. Pap.* **75**: 80.

Bishop, P., Young, R. W. and McDougall, I. (1985)."Stream profile change and long term landscape evolution: Early Miocene and modern rivers of the east Australian highland, central New South Wales, Australia." *Jour. Geol.* **93**: 455-474.

Bowman, H. N., Hobbs, J. J. and Barron, L. M. (1977). "The Goonumbla copper district northwest of Parkes, central New South Wales." Geol. Surv. N.S.W. Rep., GS1977/095 (unpublished).

Boyle, R. W. (1982). "Geochemical prospecting for thorium and uranium deposits." Developments in Economic Geology, Amsterdam, The Netherlands, Elsevier Scientific Publishing Company, **16**.

Braun, J. J. and Pagel, M. (1994)."Geochemical and mineralogical behaviour of REE, Th and U in the Akongo lateritic profile (SW Cameroon)." *Catena* **21**: 173-177.

Brewer, R. (1964). "Fabric and Mineral Analysis of Soils." New York, Wiley, 470.

Brid, M. I. and Chivas, A. R. (1989)."Stable-istope geochronology of the Australian regolith." *Geochimica et Cosmochimica Acta* **53**: 3239-3256.

Brimhall, G. H., Chadwick, O. A., Lewis, C. H., Compston, W., et al. (1992)."Deformational mass transport and invasive processes in soil evolution." *Science* **255**: 695-702.

Brimhall, G. H. and Dietrich, W. E. (1987)."Constitutive mass balance relations between chemical composition, volume, density, porosity and strain in metasomatic hydrothermal systems." *Geochim. Cosmochim. Acta* **51**: 567-587.

Brindley, G. W. and Brown, G. (1984). "Crystal structures of clay minerals and their x-ray identification." Miner. Soc., London, Spottiswoode Ballantyne Ltd, 495.

Brindley, G. W., Kao, C. C., Harrison, J. L., Lipsica, M. and Raythatha (1986)."Relation between structural disorder and other characteristics of kaolinites and dickites." *Clays and Clay Minerals* **34**: 239-249.

Burns, R. G. (1976)."The uptake of cobalt into ferromanganese nodules, soils and synthetic manganese (IV) oxides." *Geochim. Cosmoschim. Acta.* **40**: 95-102.

Butler, R. F. (1992). "Paleomagnetism: magnetic domains to geologic terranes." Blackwell, Boston.

Butt, C. R. M. (1981). "The nature and origin of the lateritic weathering mantle, with particular reference to Western Australia." In Doyle, H. A., Glover, J. A. and Grovers, D. I. (eds.), Geophysical Prospecting in Deeply Weathered terrains. Special Publications Geology Department and Extension Service, University of Western Australia, **6**: 11-29.

Butt, C. R. M. (1982). "History and characteristics of weathering in Australia." In Smith, R. E. (ed.), Geochemical Exploration in Deeply Weathered Terrain, Australia. CSIRO Division of Mineralogy, Floreat Park: 9-18.

Butt, C. R. M. (1987). "Geomorphology and climatic history-keys to understanding geochemical dispersion in deeply weathered terrain." Paper presented at Exploration 87, Toronto, Canada. : .

Butt, C. R. M. (1991). "Dispersion of gold and associated elements in the lateritic regolith, Mystery zone." Mt. Percy, Kalgoorlie, Western Australia. CSIRO Exploration Geoscience Restricted Report, , 156R.

Butt, C. R. M. and Zeegers, H. (1992). "Regolith exploration geochemistry in tropical and subtropical terrains." Govett, G. J. S. e. (ed.), Handbook of Exploration Geochemistry, B.V. Amsterdam, Elsevier Science Publishers, **4**: 607.

Callen, R. A. (1983)."Late tertiary 'grey billy' and the age and origin of surficial silicifications (silcrete) in South Australia." *Journal of the Geological Society of Australia* **30**: 393-410.

Carr, R. G., Rodgers, K. A. and Black, P. M. (1980)."The chemical and mineralogical changes accompanying the laterization of basalt at Keri Keri, North Auckland." *Journal of the Royal Society of New Zealand* **10/3**: 247-258.

Carrol, D. (1953)."Weatherability of zircon." *Jour. of Sed. Petrology* **23**: 106-116.

Carrol, D. (1958)."Role of clay minerals in the transportation of iron." *Geochim. Cosmochim. Acta.* **14**: 1-27.

Carvalho, I. G., Metsrinho, S. S., Fontes, V. M., Goel, O. P. and Souza, F. A. (1991)."Geochemical evolution of laterites from two areas of the semi-arid region in Bahia State, Brazil." *Jour. of Geochem. Explor.* **40**: 385-411.

Casey, W. H., Westrich, H. R. and Arnold, G. W. (1989)."Surface chemistry of labradorite feldspar reacted with aqueous solutions at pH=2,3 and 12." *Geochim. Cosmochim. Acta.* **52**: 2795-2807.

Cawsey, D. C. and Mellon, P. (1983). "A review of experimental weathering of basic igneous rocks." In Wilson, R. C. L. (ed.), Residual deposits: Surface related weathering, processes and materials, Oxford, Blackwell Scientific Publications.

Chadwick, O. A., Brimhall, G. H. and Hendricks, D. N. (1990)."From a black box to grey box-a mass balance interpretation of pedogenesis." *Geomorphology* **3**: 369-390.

Chan, S. (1996). The drainage evolution in the Bathurst Region. , *The 13th Australian Geological Convention*, Canberra, (February 19-23) Abstracts No.41.

Chao, T. T. (1972)."Selective dissolution of manganese oxides from soils and sediments with acidified hydroxylamine hydrochloride." *Soil. Soc. America Proc.* **36**: 764-768.

Chao, T. T. (1984)."Use of partial extraction techniques in geochemical exploration." *Jour. Geoch. Explor.* **20**: 101-135.

Chao, T. T. and Theobald, P. K. (1976)."The significance of secondary iron and manganese oxides in geochemical exploration."*Economic Geology* **71**: 1560-1569.

Chesire, M. V., Benbow, M. L., Goodman, B. A. and Mundie, C. M. (1977)."Metal distribution and nature of some Cu, Mn and V complexes in humic and fulvic acid fractions of soil organic matter."*Geochim. et Cosmochim. Acta* **41**: 1131-1138.

Chi, M. (1996). "The ultra-structure of kaolin." The Australian National University, PhD thesis

Chittale, D. (1986). "Bauxites, Laterites and Associated clays from western India." Texas Tech. Uni. 146 PhD thesis

Chittleborough, D. and Walker, P. (1988)."Crystallinity of Soil Kaolinites in relation to Clay Particle size and soil age."*Journ. Soil Sci.* **39**: 81-86.

Chittleborough, D. J. (1991)."Indices of weathering for soils and paleosols formed on silicate rocks."*Australian Journal Earth Science* **38**: 115-120.

Chou, L. and Wollast, R. (1985)."Steady-state kinetics and dissolution mechanisms of albite."*Amer. J. Sci.* **285**: 963-993.

Churchman, G. and Gilkes, R. J. (1989)."Recognition of intermediates in the possible transformation of halloysite to kaolinite in weathering profiles."*Clay Min.* **24**: 579-590.

Churchman, G. and Gilkes, R. J. (1989)."Recognition of intermediates in the possible transformation of halloysite to kaolinite weathering profiles."*Clay Min.* **24**: 579-590.

Clarke, I. (1985). "Primary mineralisation in the Forbes-Parkes-Peak Hill-Tomingley gold belt." Geol. Surv. N.S.W. Rep., GS1985/123 (unpublished).

Clarke, I. and Sherwin, L. (1990)."Geological setting of gold and copper deposits in the Parkes area, New South Wales."*Records of the Geological Survey of New South Wales* **23**: 196.

Cline, G. R., Powell, P. E., Staniszlo, P. J. and Reid, C. P. P. (1983)."Comparison of the abilities of hydroxamic and other organic acids to chelate iron and other ions in soils."*Soil Sci.* **136**: 145-157.

Cloke, P. L. and Kelly, W. C. (1964)."Solubility of gold under inorganic supergene conditions."*Economic Geology* **59**: 259-270.

Cloud, P., Gustafon, L. B. and Watson, J. A. L. (1980)."The works of living social insects as pseudofossils and the age of the oldest known metazoa."*Science* **210**: 1013-1015.

Colman, S. M. (1982)."Chemical weathering of Basalts and Andesites: Evidence from Weathering Rinds."*Geol. Surv. Prof. Pap.* **1246**: 51.

Coohey, J. C., Edwards, A., Hine, R., Morrison, F. and Windrim, D. (1990)."The regional tectonics of the Tasman Orogenic System, Eastern Australia."*Journal of Structural Geology* **12**(No. 5/6): 519-534.

Cooper, R. A. and Grindley, G. W. (1982 (Eds)). "Late Proterozoic to Devonian sequences of southeastern Australia, Antarica and New Zealand and their correlation, Geol. Soc.", Aust. Spec. Publ. 9.

Correns, C. W. (1961)."The experimental weathering of silicates."*Clay Min. Bull.* **4**: 249-265.

Correns, C. W. and Engelhardt, W. V. (1941)."Rontgeographissche untersuchungen uber den mineralbestand sedimentarer eisenerze."*Nachr. Akad. Wiss. Gottingen Math. Phys. Kl* **213**: 131-137.

Cox, K. G., Bell, J. D. and Pankhurst, R. J. (1979). "The interpretation of igneous rocks." George Allen and Unwin: London.

Cramer, J. J. and Nesbitt, H. W. (1983)."Mass-balance relations and trace element mobility during continental weathering of igneous rocks."*Sci. Geol. Mem.* **72**: 57-68.

D'Orey, F. L. C. (1975)."Contribution of termite mounds to locating hidden copper deposits."*Trans. Inst. Min. Metall. Sect. B, Appl. Earth Sci.* **84**: 150-151.

Daily, B., Twidale, C. R. and Milnes, A. R. (1974)."The age of the lateritized summit surface on Kangaroo Island and adjacent areas of South Australia."*Journal of the Geological Society of Australia* **21**: 387-392.

Dalrymple, J. and Jim, C. (1984)."Experimental study of soil microfabric induced by isotropic stresses of wetting and drying."*Geoderma* **34**: 43-68.

Dell, M. R. (1982). "Regolith-landform relationships and geochemical dispersion about the Kanowna-Belle Au Deposit." University of Tasmania, WA Honours Thesis

Delmas, A. B. (1979). "Etude experimentale des phenomenes de dissolution des sels et des silicates approche kinetique." Paris (unpublished), Institute National de la Recherche Agronomique, 256 PhD Thesis

Delvigne, J., Nahon, D. and Noack, Y. E. (1983)."Micromorphology of the alteration and weathering of pyroxenes in the Koua Bocca ultramafic intrusion, Ivory Coast, West Africa: In *pedologie des Alterations et des Sols*, Vol 2."*Sci Geol. Mem.* **72**: 57-68.

Doner, H. E. and Lynn, W. C. (1989). "Carbonates, halides, sulfates and sulfide minerals." In Bailey, S. (ed.), Hydrous Phyllosilicates (excluding micas): 279-324.

Dregne, H. E. (1976). "Soils of arid regions." Develop. In Soil Sci., New York, Elsevier North Holland Inc., **6**.

Dumon, J. C. and Vigneaux, M. (1979)."Evidence for some mobility of titanium in podzols and under laboratory conditions as a result of the organic agents."*Physicaal Chemistry of the Earth* **11**: 331-337.

Dusci, M. E. (1994). "Regolith-landform evolution of the Black Flag area with emphasis on upper reaches of the Roe palaeodrainage system, Western Australia." Perth, Western Australia, Curtin University of Technology, 134 Honours thesis

Egashira, K. and Ohtsubo, M. (1983)."Swelling and mineralogy of smectites in paddy soils derived from marine alluvium, Japan."*Geoderma* **29**: 119-127.

Eggleton, R. A. (1975)."Nontronite topoaxial after hedenbergite."*Amer. Min.* **60**: 1063-1068.

Eggleton, R. A. (1986). "The relation between crystal structure and silicate mineral weathering rates." In Colman, S. M. and Dethier, D. P. (eds.), Rates of Chemical Weathering of Rocks and Minerals, New York, Academic Press: 21-40.

Eggleton, R. A. and Boland, J. N. (1982)."Weathering of enstatite to talc through a sequence of transitional phases."*Clays and Clay Mineral* **33**: 161-169.

Eggleton, R. A., Foudoulis, C. and Verkevisse, D. (1987)."Weathering of basalt: change in rock chemistry and mineralogy."*Clays and Clay Mineral* **35**: 161-169.

Elliss, A. J., Tooms, J. S. and Bicknell, J. V. (1967)."Application of solution experiments in geochemical prospecting."*Am. Inst. Mining. Metall. Petroleum Engineers Trans.* **76**: B25-B33.

Esson, J. (1983). "Geochemistry of a nickeliferous laterite profile, Liberdade, Brazil." In Wilson, R. C. L. (ed.), Residual Deposits: Surface related weathering processes and materials, London, Geological Society of London Special Publications: 91-99.

Eswaran, H. (1979)."The alteration of plagioclases and augites under differing pedoenvironmental conditions."*Journal Soil Sci.* **30**: 547-555.

Eswaran, H. and Bin, W. C. (1978)."A study of deep weathering profile on granite in Peninsular Malaysia III Alteration of feldspars."*Soil Sci.* **42**: 154-158.

Eswaran, H. and De Coninck, F. (1971)."Clay mineral formations and transformations in basaltic soils in tropical environments."*Pedologie* **21**: 181-210.

Evans, H. T. (1978). "Vanadium." In Wedepohl, K. H. (ed.), Handbook of Geochemistry, Berlin, Springer-Verlag, 23A.

Fee, J. A., Gaudette, H. E., Lyons, W. S. and Long, D. T. (1992)."Rare-earth element distribution in Lake Tyrrel groundwaters, Victoria, Australia."*Chemical Geology* **84**: 68-69.

Fieldes, M. and Swindale, L. D. (1954)."Chemical weathering of silicates in soil formation."*J. Sci. Tech. New Zealand* **56**: 140-154.

Fischer, K. (1978a). "Barium, Handbook of Geochemistry." In Wedepohl, K. H. (ed.), Berlin, Springer-Verag: 56A.

Fischer, K. (1978b). "Strontium, Handbook of Geochemistry." In Wedepohl, K. H. (ed.), Berlin, Springer-Verlag: 38A.

Fitzpatrick, E. A. (1980). "Soils, their formation, classification and distribution." London, Longman: 353.

Fleischer, M. and Richmond, W. (1943)."The manganese minerals: a preliminary report."*Econ. Geol.* **38**: 269-286.

Fletcher, R. J. (1985). "Geochemical exploration for gold in the Red Sea Hills, Sudan." Prospecting in Areas of Desert Terrain, London. Institution of Mining Metallurgy: 79-84.

Fontanaud, A. and Meunier, A. (1983)."Mineralogical facies of weathered serpentinized lherzolite from Pyrenees, France."*Clay Miner.* **18**: 77-88.

Freyssinet, P., Edimo, E., Lecomte, P. and Vairon, J. (1987). Dispersion of trace elements through lateritic profiles of East Cameroon. , *The 12th International Geochemical Exploration Symposium*, Orleans, France, : 69-70.

Frondel, C. (1978). "Scandium, Handbook of Geochemistry." In Wedepohl, K. H. (ed.), Berlin, Springer-Verlag, **II-1, Section 21.**

Gadde, R. R. and Laitinen, H. A. (1974)."Studies of heavy metal adsorption by hydrous iron and manganese oxides."*Anal. Chemistry* **46**: 2022-2026.

Gardner, L. R. (1980)."Mobilization of Al and Ti during weathering-isovolumetric geochemical evidence."*Chem. Geol.* **30**: 151-166.

Gardner, L. R., Kheoruenromne, I. and Chen, H. S. (1978)."Isovolumetric geochemical investigation of a buried granite near Columbia, S.C."*Geochim. Cosmochim. Acta* **43**: 417-424.

Glassman, J. R. (1982)."Alteration of andesite in wet, unstable soils of Oregon's Western Cascades."*Clays and Clay Mineral* **30**: 253-263.

Glazner, A. F. and Bartley, J. M. (1991)."Volume loss, fluid flow and state of strain in extensional mylonites from the central Mojave desert, California."*Jour. Structural Geology* **13**: 587-594.

Goldich, S. S. (1938)."A study of rock weathering."*Jour. Geol.* **46**: 17-58.

Grant, J. A. (1986)."The isocon diagram-a simple solution to Gresens equation for metasomatic alteration."*Economic Geology* **81**: 1976-1982.

Gray, D., Butt, C. R. M. and Lawrance, L. M. (1992). "The geochemistry of gold in laterite terrains." In Butt, C. R. M. and Zeegers (eds.), Regolith Geochemistry in Tropical and Subtropical Terrains, Handbok of Exploration Geochemistry. Elsevier Science Publishers 3, 406.

Gray, D. J. and Lintern, M. J. (1984). "The solubility of gold in from semi-arid areas of Western Australia." CSIRO Australia, Division of Exploration and Mining, Exploration and Mining Research News, 1.

Gray, D. J. and Lintern, M. J. (1984). "The solubility of gold in soils from semi-arid areas of Western Australia." Exploration and Mining News 1, CSIRO Australia Division of Exploration and Mining: 8-9.

Gresens, R. L. (1967)."Composition: volume relationships of metasomatism."*Chemical Geology* **2**: 47-65.

Grunsky, E. C. (1986)."Recognition of alteration in volcanic rocks using statistical analysis of lithogeochemical data."*Jour. Geoch. Explor* **25**: 157-183.

Grunsky, E. C. (1991). "Laterite geochemistry in the CSIRO-AGE Database for the Albany-Fraser Region." CSIRO/AMIRA Laterite Geochemistry Project P240, Exploration Geoscience Restricted Report, 161.

Gunn, R. H. and Galloway, R. W. (1978). "Silcretes in south-central Queensland." In Langford, S. T. (ed.), Silcrete in Australia, Armidale, University of New England: 51-57.

Güven, N. (1989). "Smectites: In Hydrous Phyllosilicates (excluding micas)." In Bailey, S. 497-559.

Harnois, L. (1988)."The CIW index: a new chemical index of weathering."*Sedim. Geol.* **55**: 319-322.

Hawkes, H. E. and Webb, J. S. (1962). "Geochemistry in mineral exploration." New York, Harper and Row: 415.

Heier, K. S. and Billings, G. K. (1978a). "Potassium." In Wedepohl, K. H. (ed.), Handbook of Geochemistry, Berlin, Springer-Verlag, 19B-19N.

Heier, K. S. and Billings, G. K. (1978b). "Rubidium." In Wedepohl, K. H. (ed.), Handbook of Geochemistry, Berlin, Springer-Verlag, 37B-37N.

Heier, K. S. and Billings, G. K. (1978c). "Sodium." In Wedepohl, K. H. (ed.), Handbook of Geochemistry, Berlin, Springer-Verlag, 11B-11O.

Heinrich, E. W. (1978). "Niobium." In Wedepohl, K. H. (ed.), Handbook of Geochemistry, Berlin, Springer-Verlag, 41D.

Heithersay, P. S. (1986). Endeavour 26 North copper-gold deposit Goonumbla N.S.W.-paragenesis and alteration zonation, *13th Congress of the Council of Mining and Metallurgical Institutions and the Australasian Institute of Mining and Metallurgy*, Melbourne: Publications of the 13th CMMI Congress, **2**: 181-189.

Hendricks, D. M. and Whittig, L. D. (1968)."Andesite weathering, part II. Geochemical changes from andesite to saprolite."*Soil Sci.* **19**: 147-153.

Herbillon, A., Frankart, R. and Veilvoye, L. (1981)."An occurrence of interstratified kaolinite-smectite minerals in a red-back soil toposequence."*Clays and Clay Min.* **16**: 195-201.

Hingston, F. J., Posner, A. M. and Quirk, J. P. (1972)."Anion adsorption by goethite and gibbsite, I. The role of the proton in determining adsorption envelopes."*Jour. Soil Sci.* **23**: 177-192.

Holzhauer, C. C. (1985). "Weathering of Fe-Ti minerals." Canberra, The Australian National University, MSc Thesis

Hough, D. (1982). "The influence of parent rocks on the nature of surficial materials in the Eden region." The Australian National University, MSc. Thesis

Huang, W. H. and Keller, W. D. (1973)."Gibbs free energies of formation calculated from dissolution data using specific mineral analysis. III. Clay minerals."*Amer. Mineral.* **58**: 1023-1028.

Hume-Rothery, W. and Raynor, G. V. (1958). "The structure of Metals and Alloys Monograph and Report Series, 1." London, The Institute of Matals,

Hutson, D. L. (1993)."The effect of alteration and metamorphism on wall rocks to the Balcooma and Dry River South volcanic-hosted massive sulfide deposits, Queensland, Australia."*Jour. Geoch. Explor.* **48**: 277-307.

Hutton, J. T., Twidale, C. R., Milnes, A. R. and Rosser, H. (1972)."Composition and genesis of silcretes and silcrete skins from the Beda Valley, Southern Arcona Plateau, South Australia."*Journal of the Geological Society of Australia* **19**: 31-39.

Idnurm, M. (1994)."New Late Eocene pole of Australia, time-averaging of remanence direction, and palaeogeographic reference systems."*Geophysical Journal International* **117**: 827-833.

Idnurm, M. and Senior, B. (1978)."Palaeomagnetic dating of weathered profiles in the Eromanga Basin, Queensland."*Palaeogeography, Palaeoclimatology, Palaeoecology* **24**: 263-277.

Ildenfose, P. (1980)."Mineral fabrics developed by weathering of meta-gabbro Loire-Atlantique (France)."*Geoderma* **24**: 257-274.

Jenne, E. A. (1968)."Controls on Mn, Co, Ni, Cu and Zn concentrations in soils and water: the significant role of hydrous Mn and Fe oxides."*Advances Chemistry series* **73**: 337-388.

Jiang, W. T. and Peacor, D. R. (1991)."Transmission electron microscopic study of the kaolinization of muscovite."*Clays and Clay Minerals* **39**: 1-13.

Jones, G. J. (1985)."The Goonumbla porphyry copper deposits."*New South Wales Econ. Geol.* **80**: 591-613.

Joplin, G. A. (1968)."The shoshonite association: a review."*Jour. Geol. Soc. Aust.* **15**: 275-294.

Keller, W. D. (1970)."Environmental aspects of clay minerals."*Jour. Sed. Petrol* **40**: 788-813.

Keller, W. D. (1976)."Scanning electron micrographs of kaolins collected from diverse environments of origin-I."*Clays and Clay Minerals* **24**: 107-113.

Keller, W. D. (1977a)."Scanning electron micrographs of kaolins collected from diverse environments of origin-IV. Georgia kaolin and kaolinizing source rocks."*Clays and Clay Minerals* **25**: 311-345.

Keller, W. D. (1977b)."Scanning electron micrographs of kaolins collected from diverse environments of origin-V. Kaolins collected in Australia and Japan on trips of the 6th and 7th conference."*Clays and Clay Minerals* **25**: 347-364.

Keller, W. D. (1978)."Kaolinization of feldspar as displayed in scanning electron micrographs."*Geology* **6**: 184-188.

Keller, W. D. (1982)."Kaolin-A most diverse rock in genesis, texture, physical and properties and uses." *Geol. Soc. Amer. Bull.* **93**(27-36).

Kirkwood, D. E. and Nesbitt, H. W. (1991)."Formation and evolution of soils from an acidified watershed: Plastic Lake, Ontario, Canada."*Geochim. Cosmochim. Acta* **55**: 1295-1308.

Kirschvink, J. L. (1980)."The least-squares line and plane and analysis of palaeomagnetic data." *Geophysical Journal of the Royal Astronomical Society* **45**: 699-718.

Koppi, I. and Skjemstad, J. (1981)."Soil kaolins and their genetic relationships in South East Queensland, Australia." *Jour. Soil Sci.* **32**: 661-672.

Krauskopf, K. B. (1951)."The solubility of gold."*Economic Geology* **46**: 858-870.

Krinsley, D. H. and Doornkamp, J. C. (1973). "Atlas of quartz sand surface textures." Cambridge University Press, 91.

Krynen, J. P. (1984). "Geological setting of mineralisation in the Parkes area." Geol. Surv. N.S.W. Report.

Lackie, M. A. and Schmidt, P. W. (1993)."Remagnetisation of strata during the Hunter-Bowen Orogeny." *Exploration Geophysics* **24**: 269-274.

Lakin, H. W., Curtin, G. C., Hubert, A. E., Shacklette, H. T. and Doxtader, G. (1974)."Geochemistry of gold in the weathering cycle."*U.S. Geol Survey Bull* **1330**: 80.

Lambeck, K. and Stephenson, R. (1986)."The Post-Palaeozoic uplift history of south-eastern Australia."*Australian Journal of Earth Sciences* **33**: 253-270.

Landergren, S. (1978). "Handbook of Geochemistry." In Wedepohl, K. H. (ed.), Berlin, Springer-Verlag, 22B-23O.

Langmuir, D. (1978). "Uranium solution-mineral equilibria at low temperatures with applications to sedimentary ore deposits." In Kimberley, S. J. (ed.), Uranium deposits, their mineralogy and origin. Mineralogical Society of Canada, Short course handbook, Toronto, Canada, University of Toronto Press, 17-55.

Langmuir, D. (1988)."Techniques of estimating thermodynamic properties for some aqueous complexes of geochemical interest. In Jenne, E.A. (ed.)," *Chemical modelling in Aqueous Systems: Specification, Solubility and Kinetics. American Chemical Society Symposium Seriers* **93**: 353-387.

Lawrance, L. M. (1988a). The morphology and geochemistry of supergene gold at Hannan South gold mine. , *Bicentenial Gold 88*, Western Australia, Geol. Soc., **1**: 360-364. Australia Abstracts No. 23

Lawrence, L. M. (1994). Exploration Geochemistry: A review of element mobility. , *Proceedings of the 12th Australian Geological Convention Perth*, Perth, : 242-243. Abstracts No. 37

Lecomte, P. and Colin, F. (1987). Gold dispersion and size fraction distribution in a tropical rainforest weathering profile at Dondo-Mobi, Gadbon. , *The 12th International Geochemical Exploration Symposium*, Orelans, France, : 72.

Leneuf, N. (1959). "Lalteration des granites calco-alcalins et des granodiorites en Cote d'Ivore forestiere et les sols qui en sont derives." Paris, These Sci., 210.

Leprun, J. C. (1979). "Les cuirasses ferrugineuses des pays cristallins de l'Afrique Occidentale seche genese- transformation-degradation." *Sci. Geol. Mem.* Strasbourg, **58**: 224.

Levinson, A. A. (1974). "Introduction to Exploration Geochemistry." Calgary Canada, Applied Publishing Ltd., 412.

Lindsay, L. (1979). "Chemical equilibrium in soils." New York, Wiley, 449.

Lintern, M. J. (1997). Calcrete sampling for gold exploration. , *The AUSIMM annual Conference extended abstracts*, Ballarat Victoria, : . (12-15 March)

Lock, N. (1985). "Kimberlite exploration in the Kalahari region of southern Botswana with emphasis on the Jwaneng kimberlite province." Prospecting in Areas of Arid Terrain, London, Institute of Mining and Metallurgy, 183-190.

Lodding, W. (1972)."Conditions for the direct formation of gibbsite from K-feldspar. Discussion."*Amer. Mineral* **57**: 292-294.

Loganathan, P. and Burau, R. G. (1973)."Sorption of metal ions by a hydrous manganese oxide."*Cosmochim. et Cossmochim. Acta.* **37**: 1277-1293.

Loughnan, F. C. (1969). "Chemical weathering of silicate minerals." American Elsevier Publishing Company Inc., 169.

Lunderstrom, I. (1970)."Etch pattern and albite twinning in two plagioclases."*Ark Mineral Geol.* **5**: 63-91.

Mabbut, J. A. (1980)."Weathering history and landform development: In Conceptual Models in Exploration Geochemistry."*Jour. Geoche. Explor.* **12**: 96-106.

Macewan, D. M. and Wilson, M. J. (1980). "Interlayer and intercalation complexes of Clay Minerals." In Brindley, G. W. and Brown, G. (eds.), In Crystal structures of clay minerals and X-ray Identification.

Mackenzie, R. M. (1967)."The sorption of cobalt by manganese minerals in soils."*Australian Jour. Soil Research* **5**: 235-246.

Mackenzie, R. M. (1970)."The reaction of cobalt with manganese dioxide minerals."*Australian Journal of Soil Research* **5**: 235-246.

Mackenzie, R. M. (1972)."The sorption of some heavy metals by the lower oxides of manganese."*Geoderma* **8**: 29-35.

Maignien, R. (1966). "Review of research on laterites." UNESCO, natural resources research, IV.

Mann, A. W. (1984a)."Mobility of gold and silver in weathering profiles: Some observations from Western Australia."*Economic Geology* **79**: 38-49.

Mann, A. W. (1984b). Redistribution of gold in the oxidized zone of some Western Australia deposits: In Gold-mining, Metallurgy and Geology. , *Institute of Mining and Metallurgy, Perth and Kalgoorinal Regional Conference Proceedings*, : 1-12. (October)

Markeer, A. and de Oliveira, J. (1994)."Climatic and morphological control of rare earth element distribution in weathering mantles on alkaline rocks."*Catena* **21**: 179-193.

Marquer, D. and Burkhard, M. (1992)."Fluid circulation, progressive deformation and mass transfer processes in the upper crust: the example of basement cover relationships in the External Crystalline Massifs, Switzerland." *Jour. Struc. Geol.* **14**: 1047-1057.

Marshall, C. E. (1962)."III. Reactions of feldspars and micas with aqueous solutions." *Econ. Geol.* **57**: 1219-1227.

Mc Caughey, W. J. (1990)."The solvent effect of ferric and cupric salt solutions upon gold." *Am. Che. Soc. Jour.*: 1261-1271.

Mestdagh, M. M., Vielvoye, L. and Herbillon, A. (1980)."Iron in kaolinite. The relationship between kaolinite crystallinity and iron content." *Clay Miner.* **15**: 1-14.

Michel, D. (1987)."Concentration of gold in *in situ* from Marto Grosso." *Mineralium Deposita* **22**: 185-189.

Millot, G. (1964). "Geologie des argiles." Paris, Masson, 499.

Millot, G. and Bonifas, M. (1955)."Transformations isovolmétriques dans les phénomènes de latéritisation et de bauxitisation." *Bull Serv. Carte Géol. Alsace-Lorraine* **8**: 3-10.

Milnes, A. R. and Fitzpatrick, R. W. (1989). "Titanium and zirconium minerals; In minerals in soil environments." Soil Science Society of America book series, Madison, WI, USA, Soil Science Society of America. : 1131-1205.

Milnes, A. R. and Hutton, J. T. (1983). "Calcretes in Australia." Soils: an Australian viewpoint, CSIRO/Academic Press, 119-162.

Milnes, A. R. and Thiry, M. (1992). "Silcretes." In Martini, I. P. and Chesworth, W. (eds.), Developments in Earth Surface Processes 2, Weathering, Soils and Palaesols, Amsterdam, Elsevier, 618.

Moore, C. L. (1996). "Processes of chemical weathering of selected Cainozoic Eastern Australian Basalts." Canberra, Australian National University, PhD Thesis

Moore, D. M. and Reynolds, R. C. J. (1997). "X-ray diffraction and the identification and analysis of clay minerals." Oxford University Press, 332.

Morgan, D., Highley, D. and Bland, D. (1979). A montmorillonite-kaolinite association in the Lower Cretaceous of South-east England. In Mortland, M. and Farmer, V. (eds.), *Proc. Int. Clay Conf. (1978)*, : 301-310.

Morgan, J. J. and Stumm, W. (1964a.)."Colloid-chemical properties of manganese oxides." *Jour. Coll. Sci.* **9**: 347-359.

Morgan, J. J. and Stumm, W. (1964b.). The role of multivalent metal oxides in limnological transformations as exemplified by iron and manganese. , 2^{nd} *International Conference on water Pollution Research*, Tokyo 1964, : 103-118.

Morrison, G. W. (1980)."Characteristics and tectonic setting of the shoshonite rock association." *Lithos* **13**: 97-108.

Muller, J.P. and Bocquier, G. (1986). Dissolution of kaolinites and accumulation of iron oxides in lateritic-ferruginous nodules. Mineralogical and microstructural transformations. *Geoderma* **37**, 113-136.

Muller, J.P. and Calas, G. (1989). Tracing kaolinites through their defect centers. Kaolinite paragenesis in laterite (Cameroon). *Economic Geology* **84**: 694-707.

Muller, J.P., Manceau, A., Hazemann, J.L., Allard, T., Ildenfose, P., Calas, G. (1995). Crystal chemistry of clays and associated oxides: constraints for modeling element transfer at the Earth's surface. *American Journal of Science*, **295**: 115-1155.

Murray, J. W. (1975)."The interaction of metal ions at the manganese dioxide-solution interface."*Geochim. et Cosmochim. Acta.* **39**: 505-519.

Nahon, D. (1986). "Evolution of iron crusts in tropical landscapes." In Colman, S. M. and Dethier, D. P. (eds.), Rates of Chemical Weathering of Rocks and Minerals, London, Academic Press, 169-191.

Nahon, D. and Bocquier, G. (1983). "Petrology of elements transfers in weathering and soil systems." In Peterologie des Alterations et des Sols, **2**.

Nahon, D. and Colin, F. (1982)."Chemical weathering of orthopyroxenes under lateritic conditions."*Amer. Jour. Sci.* **282**: 1232-1243.

Nahon, D. and Tardy, Y. (1992). "The ferruginous laterites." In Butt, C. R. M. and Zeegers, H. (eds.), Handbook of Exploration Geochemistry: Regolith Exploration Geochemistry in Tropical and Subtropical Terrains, **4**: 40-55.

Nakamura, M. T. and Sherman, G. D. (1965)."The genesis of halloysite and gibbsite from mugearite on the island of Maui."*Hawaii Agric Stat. Tech. Bull.* **62**.

Nesbitt, H. W. and Young, G. M. (1982)."Early Proterozoic climates and plate motions inferred from major elemental chemistry of lutites."*Nature* **199**: 715-717.

Nesbitt, H. W. and Young, G. M. (1984)."Prediction of some weathering trends of plutonic and volcanic rocks based on thermodynamic and kinetic considerations."*Geochim. Cosmochim. Acta* **48**: 1523-1534.

Nettleton, W. D., Nelson, R. E., Brasher, B. R. and Derr, P. S. (1982). "Gypsiferous soils in the western United States." In Kittrick, J. A. (ed.), Acid sulfate weathering spec. Publ., SSSA Madison WI, **10**: 147-168.

Nickel, E. H. (1984)."The mineralogy and geochemistry of the weathering profile of the Teutonic Bore Cu-Pb-Zn sulfide deposit."*Jour. of Geoch. Explor.* **22**: 239-364.

Nissenbaum, A. and Serban, A. (1987)."Enzymatic activity associated with humic substances in deep sediments from the Cariaco Trench and Wlaivas Ridge."*Geochim. Cosmochim. Acta.* **51**: 373-378.

Nixon, R. A. (1979)."Differences in incongruent weathering of plagioclase and microcline-Cation leaching versus precipitates."*Geology* **7**: 221-224.

Norrish, K. (1957). Some phosphate minerals in soils. , *Proceeding 2nd Australian Conference of Soil Science*, : 1-15.

Norrish, K. (1968). Some phosphate minerals in soils. , *Translations of the 9th Conference of the International Soil Society*, : 713-723.

Norrish, K. and Pickering, J. (1983). "Clay minerals: in Soils: An Australia Viewpoint." London, CSIRO, Melbourne and Academic Press, 281-308.

Norrish, K. and Rosser, H. (1983). "Mineral phosphate, in Soils: An Australian viewpoint (CSIRO)." In Division of Soils, C. (ed.), Melbourne, Academic Press. : 281-308.

Novikoff, A. (1974). "L'alteration des roches dans le Massif du Chaillu (Republique Populaire du Congo)." These Doct. Sci., Strasbourg, Universite Louis Pasteur, 298.

Novikoff, A., Tsawlassou, G., Gac, J. Y., Bourgeat, F. and and Tardy, Y. (1972)."Alteration des biotites dans les arenes des pays temeperes tropicaux et equatoriaux." *Sci. Geol. Bull.* **25**: 287-305.

O'Hara, K. (1988)."Fluid flow and volume loss during mylotinization: an origin for phyllonite in an overthrust setting, North Carolina."*Tectonophysics* **156**: 21-36.

O'Sullivan, P. B., Kohn, B. P., Foster, D. A. and Gleadow, A. J. W. (1995)."Fission track data from the Bathurst batholith: evidence for rapid mid-Cretaceous uplift and erosion within the Eastern Highlands of Australia." *Australian Journal of Earth Sciences* **42**: 597-607.

Odom, I. E., Fowden, L., Barrer, R. and Tinker, P. (1984)."Smectite clay minerals: properties and uses." *In Clay Minerals: Their structure, behaviour and use. Philosophical Transactions of The Royal Society of London* **311**: 391-410.

Ollier, C. D. (1981). "Tectonics and Landforms." In Clayton, K. M. (ed.), London and New York, Longman, 161-163.

Ollier, C. D. (1982)."The great escarpment of eastern Australia: tectonic and geomorphic significance." *Journal of the Geological Society of Australia* **29**: 13-23.

Ollier, C. D. and Pain, C. F. (1994)."Landscape evolution and tectonics in southeastern Australia." *AGSO Journal of Australian Geology & Geophysics* **15**: 335-345.

Ollier, C. D. and Pain, C. F. (1996). "Regolith, soils and landforms." Wiley, J., Joneschild, Boffins Lane and Chichester (eds.), England, West Sussex P 019 UD.

Ostwald, J. (1992)."Genesis and paragenesis of the tetravalent manganese oxides of the Australian continent." *Economic Geology* **87**: 1237-1252.

Paquet, H., Colin, F., Durplay, J., Nahon, D. and Millot, G. (1987). "Ni, Mn, Zn, Cr smectites, early and effective traps for transition elements in supergene ore deposits." In Rodrigez-Clemente, R. and Tardy, Y. (eds.), Geochemistry and mineral formation in the earth surface. Consejo superior de Investigaciones, Cientificas Centre National de la Recherche Scientifique, 221-229.

Parc, S., Nahon, D., Tardy, Y. and Vieelard, P. (1989). "Estimated solubility products and fields of stability for cryptomellane, nsutite, birnessite and lithiphorite based on natural lateritic weathering sequences."

Parham, W. E. (1969)."Formation of halloysite from feldspar: Low temperature artificial weathering versus natural weathering." *Clays and Clay Minerals* **17**: 13-22.

Parker, A. (1970)."An index of weathering for silicate minerals." *Geology Mag.* **107**: 501-504.

Pedro, G. (1961)."An experimental study of the geochemical weathering of crystalline rocks by water." *Clay Mineral Bulletin* **4**: 266-281.

Pickering, R. J. (1962)."Some leaching experiments on three quartz-free silicate rocks and their contribution to an understanding of laterization." *Economic Geology* **57**: 1185-1206.

Picket, J. W. (1985). "Plant fossils from Milpose." Geol. Surv. NSW. Palaeontolog. Rep.1985/05, GS1985/124 (unpublished).

Pillans, B. and Bourman, R. (1996)."The Brunhes/Matuyama polarity transition (0.78Ma) as a chronostratigraphic marker in Australian regolith studies." *AGSO Journal of Australian Geology & Geophysics* **16**: 289-294.

Plancon, A. and Tchoubar, C. (1977a)."Determination of structural defects in phyllosilicates by X-ray diffraction I-Principle of calculation of the diffraction phenomenon." *Clays and Clay Minerals* **25**: 430-435.

Plancon, A. and Tchoubar, C. (1977b)."Determination of structural defects in phyllosilicates by X-ray diffraction II-Nature and proportion of defects in natural kaolinites." *Clays and Clay Minerals* **25**: 436-450.

Ponnamperuma, F. N., Tianco, E. M. and Loy, T. (1967)."Redox equlibria in flooded soils: I. The iron hydroxide systems."*Soil Sci.* **103**(373-382).

Ponnamperuma, F. N., Tianco, E. M. and Loy, T. (1969)."Redox equlibria in flooded soils: II. The manganese oxide systems."*Soil Sci.* **108**(48-57).

Price, R. C., Gray, C. M., Wilson, R. E., Frey, F. A. and Taylor, S. R. (1991)."The effects of weathering of rare-earth elements, Y and Ba in Tertiary Basalts from southeastern Australia." *Chemical Geology* **93**.

Prochaska, W., Bechtel, W. A. and Kloezli, U. (1992)."Phyllonite formation and alteration of gneisses in shear zones (Gleinalmkristallin, Eastern Alps, Austria)."*Mineralogy and Petrology* **45**: 195-216.

Puchelt, H. (1978). "Barium, Handbook of Geochemistry." In Wedepohl, K. H. (ed.), Berlin, Springer-Verlag, 56B-56O.

Rabenhost, M. C., Wilding, L. P. and Girdner, C. L. (1984)."Airbone dusts in the Edwards Plateau region of Texas."*Soil Sci. Soc. Am. J.* **48**: 621-627.

Rahn, P. (1971)."The weathering of tombstones and its relationship to the topography of New England."*Jour. Geol. Educ.* **19**: 112-118.

Reiche, P. (1943)."Graphic representation of chemical weathering."*Journal of Sed. Petrology* **13**: 58-68.

Rich, C. I. (1972). "Potassium in soil minerals, edited by International Potash Institute." In Potassium in Soil, Proc. 9th Coll. Intern. Potassium Inst., Federal Republic of Germany, Landshut, 15-31.

Roaldset, E. (1943)."Mineralogy and geochemistry of Quaternary clays in the Numedal area, southern Norway."*Norsk Geolisk Tidsskrift* **52**: 335-369.

Robertson, I. D. and Eggleton, R. A. (1991)."The weathering of granitic muscovite to kaolinite and halloysite and of plagioclase-derived kaolinite to halloysite." *Clays and Clay Minerals* **39**: 113-126.

Rock, N. M. S. (1988). "Lecture notes in earth sciences." Numerical Geology, Germany, Springer-Verlag, **18**.

Rogers, J. J. and Adams, A. S. (1978b). "Uranium, Handbook of Geochemistry." In Wedepohl, K. H. (ed.), Berlin, Springer-Verlag, 92D-92O.

Ruhe, R. (1965). "Quaternary paleopedology." In Wright, H. E. J. and Frey, D. G. (eds.), The Quaternary of the United States, Princeton, Princeton University Press, 755-764, 922.

Ruhe, R. (1967a)."Geomorphology of parts of the Greenfield quadrungle, Adair Country Iowa."*U.S. Dept. Agri. Tech. Bull.* **1349**: 93-161.

Ruxton, B. P. (1968)."Measures of the degree of weathering of rocks."*Journal Geology* **76**: 518-527.

Scheibner, E. (1975). "Definition and review of structural elements." In Markham, N. L. and Basden, H. (eds.), The Mineral Deposits of New South Wales, Geological Survey of New South Wales: Sydney, 108-113.

Schmidt, P. W., Currey, D. T. and Ollier, C. D. (1976)."Sub-basaltic weathering, damsites, palaeomagnetism, and the age of lateritization."*Journal of the Geological Society of Australia* **23**: 367-370.

Schmidt, P. W. and Ollier, C. D. (1988)."Palaeomagnetic dating of Late Cretaceous to Early Tertiary weathering in New England, NSW, Australia."*Earth-Science Reviews* **25**: 363-371.

Schwertmann, U. and Kampf, N. (1985)."Properties of goethite and hematite in kaolinitic soils of southern and central Brazil."*Soil Sci.* **139**: 344-350.

Scott, K. M. (1996)."Composition of white micas in weathered rocks."*Indicators of rock-type and proximity to gold mineralization, western Australia* **Explore No.93**: 3-5.

Selverston, J. G., Morteani, G. and Stoud, J. M. (1991)."Fluid channeling during ductile shearing: transformation of granodiorite into aluminous schist in the Tauern Window, Eastern Alps."*Journal of Metamorphic Geology* **9**: 419-431.

Senior, B. R. and Senior, D. A. (1972)."Silcrete in southwest Queensland."*BMR Bulletin* **125**: 23-28.

Seward, T. M. (1984). "The transport and deposition of gold in hydrothermal system." In Foster, R. P., Gold'82 (ed.), The Geology, Geochemistry and Genesis of Gold deposits, 165-181.

Shannon, R. D. (1976)."Revised effective ionic radii and systematic studies of interatomic distance in halides and chalcogenides."*Atca Crystallogr. Sect. A* **32**: 751.

Sharp, T. G., Otten, M. T. and Buseck, P. R. (1990)."Serpentinization of phlogopite phenocrysts from a micaceous kimberlite."*Contrib. Mineral Petrol* **194**: 530-539.

Sherwin, L. (1973)."Stratigraphy of the Forbes-Bogan Gate district."*Geo. Surv. NSW. Rec.* **15**(1): 47-101.

Sherwin, L. (1979)."Age of the Nelungaloo Volcanics, near Parkes."*Geol. Surv. NSW. Q.* **35**: 15-18.

Sherwin, L., Clarke, I. and Krynen, J. P. (1987)."Revision of stratigraphic units in the Forbes-Parkes-Tomingley district."*Geol. Surv. NSW. Q.* **67**: 1-23.

Shiraki, K. (1978). "Chromium, Handbook of Geochemistry." In Wedepohl, K. H. (ed.), Berlin, Springer-Verlag, 24B-24O.

Siefert, K. E. (1967)."Electron microscopy of etched plagioclase feldspars."*Amer. Ceramics Soc.J.* **50**: 660-661.

Siefferman, G. and Millot, G. (1969). Equatorial and tropical weathering of recent basalts from Cameroon: allophane, halloysite, metahalloysite, kaolinite and gibbsite. In Heller, L. (ed.), *Proc. Int. Clay. Conf.*, Tokyo, Japan, Israel University Press, Jerusalem, 417-430.

Silleen, L. G. and Martell, A. E. (1964)."Stability constants of metal ion complexes, London."*Chem. Soc. Spec. Pub.* **17**: 754.

Smith, B. (1996). "The association between gold and carbonates in Broken Hill and Parkes area." Canberra, The Australian National University, Honours thesis

Smith, B. H. and Keele, R. A. (1984)."Some observations on the geochemistry of gold mineralisation in the weathered zone at Norseman, Western Australia."*Jour. of Geochem. Explor.* **22**: 1-20.

Smith, F. G. (1943)."The alkali sulfide theory of gold deposition."*Economic Gelogy* **38**: 561-590.

Smith, R. E. (1983). "Generalized model for secondary dispersion haloes in transported overburden in weathered terrain." In Smith, R. E. (ed.), Geochemical exploration in Deeply Weathered Terrain. CSIRO Division of Mineralogy, Floreat Park, Western Australia, 153-154.

Smith, R. E., Campbell, N. A. and Litchfield, R. (1984)."Multivariate statistical techniques applied to pisolite laterite geochemistry at Golden Grove, Western Australia." *Jour. Geochem. Explor.* **22**: 193-216.

Smith, R. E. and Pedrix, R. L. (1983)."Pisolitic laterite geochemistry in the Golden Grove massive sulfide district, Western Australia." *Jour. Geochem. Explor* **18**: 131-164.

Speer, J. A. (1982). "Zircon." In Ribbe, P. H. (ed.) reviews in mineralogy-Orthosilicates. Washington, DC., Mineralogical Society of America, : 67-112.

Stoch, L. and Sikora (1976)."Transformation of micas in the process of kaolinization of granites and gneisses." *Clays and Clay Minerals* **31**: 357-366.

Stoffregan, R. (1986)."Observations on the behaviour of gold during supergene oxidation at Summitville, Colorado, U.S.A., and implications for electrum stability in the weathering environment." *Applied Geochemistry* **1**: 549-558.

Stoops, G., Altemuller, H. J., Bisdom, F. B. A., Delvigne, J., et al. (1979)."Guidelines for the description of mineral alterations in soil micromorphology." *Pedologie* **29**: 121-125.

Strakhov, N. M. (1967). "Principles of lithogenesis." Edinburgh, Oliver and Boyd Ltd, **1**: 245.

Streit, J. (1994). "The effects of fluid rock interaction on shear zone evaluation in Proterozoic granites on King Island, Tasmania." Canberra, Australian National University, Unpublished PhD Thesis

Summerfield, M. A. (1983a)."Petrography and diagenesis of silcrete from the Kalahari Basin and Cape Coastal Zone, Southern Africa." *Jour. of Sed. Petrology* **53**: 895-909.

Summerfield, M. A. (1983b)."Silcrete as palaeoclimatic indicator: evidence from Southern Africa." *Palaeogeography, Palaeoclimatology, Palaeoecology* **41**: 65-79.

Summerfield, M. A. (1983c). "Silcrete: Chemical sediments and geomorphology: Precipitates and residual in the near surface environment." In Goudie, A. S. and Pye, K. (eds.), London, Academic Press, 59-91.

Summerfield, M. A. (1983d). "Geochemistry of weathering profiles silcretes, southern Cape Province, South Africa, residual deposits." In Wilson, R. C. L. (ed.), London, Special Publication of the Geological Society of London, **11**: 167-168.

Tardy, Y. (1992). "Diversity and terminology of lateritic profiles." In Martini, I. P. and Chesworth, W. (eds.), Weathering, soils and palaeosols; Developments in earth science processes, **2**: 379-405.

Tardy, Y., Bocquier, G., Paquet, H. and Millot, G. (1973)."Formation of clay from granite and its distribution in relation to climate and topography." *Geoderma* **10**: 271-284.

Tardy, Y. and D., N. (1985)."Geochemistry of laterites, stability of Al-goethite, Al-hematite and Fe-kaolinite in bauxites and ferricretes: an approach to the mechanism of concretion formation." *Am. Jour. Sci.* **285**: 865-903.

Taylor, G., Truswell, McQueen, K. G. and Brown, M. C. (1989)."Major geomorphic features of the Kosciusko-Bega region-Discussion." *BMR Journal of Australian Geology and Geophysics* **11**: 123-124.

Tazaki, K. (1981). Analytical electron microscope studies of halloysite formation processes- Morphology and composition of halloysite. In Van Olphen, H. and Veniale, F. (eds.), *In Proc. Int. Clay Conf., Bologna, Pavia 1981*, Amsterdam, Elsevier, : 573-584.

Tazaki, K. and Fyfe, W. S. (1987)."Primitive clay precursors formed on feldspar."*Canadian Jour. Earth Sci.* **24**: 506-527.

Tension Woods, K. (1983). "Interpretation of regional aeromagnetic and gravity data for the Forbes and Narromine 1: 250,000 sheets." Geol. Surv. NSW. Rep., GS1983/200 (unpublished).

Thiry, M. and Milnes, A. R. (1991)."Pedogenic and groundwater silcretes at Stuart Creek Opal Field, South Australia."*Jour. of Sed. Petrology* **61**: 11-127.

Thornber, M. R. (1979)."Supergene alteration of sulfides, V. Laboratory studies on the dispersion of Ni, Cu, Co and Fe."*Chemical Geology* **26**: 135-149.

Thornber, M. R. and Nickel, E. H. (1976)."Supergene alteration of sulfides, III. The composition of associated carbonates."*Chemical Geology* **17**: 45-72.

Thornber, M. R. and Taylor, G. F. (1992)."The mechanisms of sulfide oxidation and gossan formation."*Regolith Exploration Geochemistry in Tropical and Subtropical Terrains* **4**: 119-137.

Thornber, M. R. and Wildman, J. E. (1979)."Supergene alteration of sulfides, IV. Laboratory study of the weathering of nickel ores."*Chemical Geology* **24**: 97-110.

Thornber, M. R. and Wildman, J. E. (1984)."Supergene alteration of sulfides, VI. The binding of Cu, Ni, Zn, Co and Pb with gossan (iron-bearing) minerals."*Chemical Geology* **44**: 399-434.

Tipping, E. and Cooke, D. (1962)."The effect of adsorbed humic substances on the surface change of goethite (alpha-FeOOH) in freshwaters."*Geochim. Cosmochim. Acta.* **46**: 75-80.

Tobisch, O. T., Barton, M. D., Vernon, R. H. and Paterson, S. R. (1991)."Fluid enhanced deformation: transformation of granitoids to banded mylonites, western Sierra Nevada, California and south eastern Australia."*Jour. Struc. Geol.* **17**: 1137-1156.

Trescasses, J. J. (1992)."Chemical weathering."*Regolith Exploration Geochemistry in Tropical and Subtropical Terrains* **4**: 25-38.

Tsuzuki, Y. and Kawabe, I. (1983)."Polymorphic transformations of kaolin minerals in aqueous solutions."*Geochim. Cosmochim. Acta* **47**: 56-66.

Turekian, K. K. (1978). "Nickel, Handbook of Geochemistry." In Wedepohl, K. H. (ed.), Berlin, Springer-Verlag, 28B-20O.

Turkey, J. W. (1977). "Exploratory data analysis." Addisson-Wesley, Mass., 506.

Usdowski, H. E. (1978a). "Calcium." In Wedepohl, K. H. (ed.), Handbook of Geochemistry, Berlin, Springer-Verlag, 20B-20O.

Usdowski, H. E. (1978b). "Magnesium." In Wedepohl, K. H. (ed.), Handbook of Geochemistry, Berlin, Springer-Verlag, 12G-12L.

Van Baalen, M. R. (1993)."Titanium mobility in rocks."*Chemical Geology* **110**: 233-249.

Veblen, D.R. and Ferry, J.M. (1983). A TEM study of the biotite-chlorite reaction and comparison with petrologic observations. *Amer. Mineral.* **68**, 1160-1168.

Velbel, M. A. (1983)."Weathering processes of rock-forming minerals." *In Environmental Geochemistry. MAC short course handbook* **10**: 67-111.

Velbel, M. A. (1989)."Weathering of Hornblende to Ferruginous products by a dissolution reprecipitation mechanism: Petrography and Stoichiometry." *Clays and Clay Minerals* **37**: 515-524.

Velde, B. (1985)."Clay minerals: A physico-chemical explanation of their occurence."*Developments in Sedimentology* **40**: 427.

Velde, B. (1985)."Clay Minerals: A physico-chemical explanation of their occurrence."*Developments in Sedimentology* **40**: 427.

Vogel, D. E. (1975)."Precambrian weathering in acid volcanic rocks from the Superior Province, Villebon Township, south central Quebec."*Canadian Journal of Earth Sciences* **12**: 2080-2085.

Vogt, T. (1927)."Sulitjelmafeltes geologi og petrografi." *Norges Geologiske Undersokelse* **121**: 1-560.

Wadsley, A. D. and Walkley, A. (1951)."The structure and reactivity of the oxides of manganese." *Rev. Pure Applied Chemistry* **1**: 203-213.

Wahrhaftig, C. (1965)."Stepped topography of the southern Sierra Nevada, California."*Geol. Soc. Amer. Bull.* **76**: 1165-1190.

Wang, Q. (1988). "Mineralogical aspects of monzonite weathering." The Australian National University, PhD thesis

Watson, A. (1985)."Structure, chemistry and origins of gypsum crusts in southern Tunisia and the Central Namid desert." *Sedimentology* **32**: 855-875.

Webster, J. G. (1986)."The solubility of gold and silver in the system Au-Ag-S-O_2-$H_2$0 at 25°C and 1atm." *Geochimica et Cosmochimica Acta* **50**: 1837-1845.

Wedepohl, K. H. (1978a). "Copper, Handbook of Geochemistry." Berlin, Springer-Verlag, 29B-29O.

Wedepohl, K. H. (1978b). "Lead, Handbook of Geochemistry." Berlin, Springer-Verlag, 82C-82O.

Wedepohl, K. H. (1978c). "Manganese, Handbook of Geochemistry." Berlin, Springer-Verlag, 25B-25O.

Wedepohl, K. H. (1978d). "Niobium, Handbook of Geochemistry." Berlin, Springer-Verlag, 41E.

Wedepohl, K. H. (1978e). "Strontium, Handbook of Geochemistry." Berlin, Springer-Verlag, 38G.

Wedepohl, K. H. (1978f). "Zinc, Handbook of Geochemistry." Berlin, Springer-Verlag.

Wellman, P. (1979a)."On the Cainozoic uplift of the southeastern Australian highlands." *Journal of the Geological Society of Australia* **26**: 1-9.

Wellman, P. (1987)."Eastern Highlands of Australia; their uplift and erosion BMR."*Journal of Australian Geology and Geophysics* **10**: 277-286.

White, R. W. and Sarcia, C. (1978)."Natural and artificial weathering of basalt."*Bulletin Bureau Rech. Geology Mineralogy* **2**: 3-29.

White, R. W. and Sarcia, C. (1978)."Natural and artificial weathering of basalt: Bulletin Bureau Rech."*Geology Mineralogy* **2**: 3-29.

Williams, L. A. and Crerar, D. A. (1985)."Silica diagenesis, II. General Mechanism."*Jour. of Sed. Petrology* **55**: 312-321.

Williams, L. A., Parks, G. A. and Crerar, D. A. (1985)."Silica diagenesis, I. Solubility Controls."*Jour. of Sed. Petrology* **55**: 301-311.

Wilson, A. (1981). The economic significance of non-hydrothermal transport of gold, and of the accretion of large gold nuggets in laterite and other weathering profiles in Australia. , *Interat. Conf. Appl. Mineralogy*, Johannesburg, 1-15.

Wilson, M. J. (1975)."Chemical weathering of some primary rock-forming minerals."*Soil. Sci.* **119**: 349-355.

Wilson, M. J. (1987). Soil smectites and related interstratified minerals; recent developments. In Schultz, L. G., Van Olphen, H. and Mumpton, F. A. (eds.), *Proc. Inter. Clay Conf. Denver*, Denver, Clay Minerals Soc. Bloomington, Indiana, : 167-183.

Wilson, M. J. and Farmer, V. (1970)."A study of weathering in soil derived from biotite-hornblende rock II. The weathering hornblende."*Clay Mineral* **8**: 435-444.

Wilson, M. J. and McHardy, W. J. (1980)."Experimental etching of a microcline perthite and implications regarding natural weathering."*Jour. Microscopy* **120**: 291-302.

Wollast, R. (1967)."Kinetics of the alteration of K-feldspar in buffered solutions at low temperature."*Geochim. et Cosmochim. Acta.* **31**: 635-648.

Wood, F. A., Rossman, G. R. and Thomas, A. P. (1991)."Hydrous species in zircons."*Am. Mineralogist* **76**: 74-82.

Wopfner, H. (1978). "Silcretes of northern South Australia and adjacent regions." In Langford Smith, T. (ed.), Silcrete in Australia, Armidale, University of New England, 93-142.

Wyborn, D. (1977)."Discussion: the Jindabyne thrust and its tectonic, physiographic and petrogenetic significance."*Jour. Geol. Soc. Aust.* **24**: 233-236.

Yau, Y. C., Anovitz, L. M., Essene, E. J. and Peacor, D. R. (1984)."Phlogopite-chlorite reaction mechanisms and physical conditions during retrograde reactions in the Marble Formation, Franklin, New Jersey."*Contrib. Mineral Petrol* **88**: 299-306.

Yerima, B. P., Calhoun, F. G., Senkayi, A. L. and Dixon, J. B. (1985)."Occurrence of interstratified kaolinite-semectite in E1 Salvador Vertisols."*Soil Sci. Soc. Am. J.* **49**: 462-466.

APPENDICES

APPENDIX 1: E22 Mineralogical data

APPENDIX 2: E27 Mineralogical data

APPENDIX 3: Major element geochemistry data

APPENDIX 4: XRF Trace element geochemistry data

APPENDIX 5: Fe-Mn nodules SEM EDXA data

APPENDIX 6: Trace element ICP MS data

APPENDIX 7: Descriptive statistics

APPENDIX 8: Element-element correlation matrices

APPENDIX 9: Mineral-element correlation matrices

APPENDIX 10: Partial/selective leaching data

Appendix 1

E22 Mineralogical data

PROFILE	Eastings	Northings	Kaolin	Quartz	Hematite	Goethite	Muscovite	Orthoclase	Microcline	Albite	Smectite	Dolomite	Gypsum	Other
E22 P1S1 (1m)	56992	9795	52.5	37.7	1.8	7.2	_	_	_	_	0.7	_	_	
E22 P1S2 (2m)	56992	9795	31.9	11.2	0.4	3.2	_	_	_	_	1.9	51.5	_	
E22 P1S3 (4m)	56992	9795	70.8	8.8	5.2	0.1	_	_	_	_	8.7	6.4	_	
E22 P1S4 (6m)	56992	9795	73.2	7.9	_	5.9	_	_	_	_	5.8	7.3	_	
E22 P1S5 (8m)	56992	9795	83.1	7.9	4.2	0.2	_	_	_	_	4.7	_	_	
E22 P1S6 (10m)	56992	9795	52.3	18.5	2.8	0.1	_	_	_	_	1.7	24.7	_	
E22 P1S7 (12m)	56992	9795	91.5	0.4	_	_	_	_	_	_	0.2	7.9	_	
E22 P1S8 (14m)	56992	9795	75	12.1	3.3	_	_	_	_	_	1.5	8.1	_	
E22 P1S9 (16m)	56992	9795	62.9	3	3.4	_	_	_	_	_	0.5	30.2	_	
E22 P1S10 (18m)	56992	9795	58	8.4	1.1	0.9	31.5	_	_	_	_	_	_	
E22 P1S11 (20m)	56992	9795	49.1	2	1.5	_	22.1	24.5	_	_	_	_	_	Dps. 0.8
E22 P1S12 (22m)	56992	9795	45.8	10.5	0.8	0.1	39.9	2.6	_	_	0.2	_	_	
E22 P1S13 (24m)	56992	9795	44.3	2.1	0.8	_	30.4	20.6	_	1.3	0.4	_	_	
E22 P1S14 (26m)	56992	9795	46.4	13.9	1.6	_	26.8	9.6	_	1.5	0.2	_	_	
E22 P2S1 (1m)	57000	9820	35.5	41.5	_	11.8	_	_	_	_	0.6	_	_	Calc.-10.7
E22 P2S2 (2m)	57000	9820	44.9	40.1	3.2	_	_	_	_	_	0.5	_	7.5	Calc.-3.2
E22 P2S3 (4m)	57000	9820	37.2	34.6	1.5	_	_	_	_	_	4.6	_	22.2	_
E22 P2S4(6m)	57000	9820	65	21.8	2.6	_	_	_	_	_	_	9.7	0.8	_
E22 P2S5 (8m)	57000	9820	84.1	7.6	4.6	3.5	_	_	_	_	_	_	_	_
E22 P2S6 (10m)	57000	9820	81.8	8.6	3.3	6.3	_	_	_	_	_	_	_	_
E22 P2S7 (12m)	57000	9820	74.2	9	3.6	8.9	_	_	_	_	_	4.2	_	_
E22 P2S8 (14m)	57000	9820	63.2	9.8	1.6	10.1	_	_	_	_	_	15.2	_	_
E22 P2S9 (16m)	57000	9820	64.7	8.4	2.6	22.8	_	_	_	_	_	1.5	_	_
E22 P2S10 (18m)	57000	9820	53.2	7.3	0.1	24.7	_	_	_	_	_	14.6	_	_
E22 P2S11 (20m)	57000	9820	70.7	8.6	_	11.1	_	_	_	_	_	9.7	_	_
E22 P2S12 (22m)	57000	9820	77.8	0.6	6.5	_	_	_	_	_	_	15	_	_
E22 P2S13 (24m)	57000	9820	64.7	2.4	1.9	1.3	29.8	_	_	_	_	_	_	_

PROFILE	Eastings	Northings	Kaolin	Quartz	Hematite	Goethite	Muscovite	Orthoclase	Microcline	Albite	Smectite	Dolomite	Gypsum	Other
E22 P2S14 (26m)	57000	9820	58.1	3	1.6	1	36.2	_	_	_	_	_	_	_
E22 P2S15 (28m)	57000	9820	57.6	2	1.5	1	23.1	14.8	_	_	_	_	_	_
E22 P2S16 (30m)	57000	9820	21.7	5.3	1.1	_	23.7	22.1	_	25.6	0.5	_	_	_
E22 P2S17 (32m)	57000	9820	31.8	1.4	1	_	42.2	11.4	_	11.4	0.8	_	_	_
E22 P2S18 (34m)	57000	9820	38.1	1.5	1.1	_	31.1	21.5	_	6	0.8	_	_	_
E22 P2S19 (36m)	57000	9820	33.3	1.1	0.5	_	32.5	20.6	_	11.4	0.8	_	_	_
E22 P2S20 (38m)	57000	9820	38.1	1.5	1.1	_	31.1	21.5	_	6	0.8	_	_	_
E22 P3S1 (1m)	56940	9975	43.7	26	_	1.9	_	_	_	_	_	_	12.2	Calc.16.2
E22 P3S2 (2m)	56940	9975	46.5	28.5	_	1.9	_	_	_	_	13.5	_	_	Calc.10.6
E22 P3S3 (4m)	56940	9975	41	35.1	_	1.3	_	_	_	_	12.8	_	_	Calc.9.8
E22 P3S4 (6m)	56940	9975	43.1	39.1	_	5.3	_	_	_	7.3	5.2	_	_	_
E22 P3S5 (8m)	56940	9975	39.1	21.4	31.9	3	_	_	_	_	4.6	_	_	_
E22 P3S6 (10m)	56940	9975	52.2	6.7	37.3	1.5	_	_	_	_	2.4	_	_	_
E22 P3S7 (12m)	56940	9975	71.9	5.5	21.4	_	_	_	_	_	1.2	_	_	_
E22 P3S8 (14m)	56940	9975	66.7	8.4	24.4	0.5	_	_	_	_	_	_	_	_
E22 P3S9 (16m)	56940	9975	69.4	9.6	17.3	3.7	_	_	_	_	_	_	_	_
E22 P3S10 (18m)	56940	9975	79.9	9.5	5.6	5.1	_	_	_	_	_	_	_	_
E22 P3S11 (20m)	56940	9975	77.4	10.5	4.2	7.9	_	_	_	_	_	_	_	_
E22 P3S12 (22m)	56940	9975	62.7	7.9	3.8	25.5	_	_	_	_	_	_	_	_
E22 P3S13 (24m)	56940	9975	77.9	7.9	2.9	12.3	_	_	_	_	_	_	_	_
E22 P3S14 (26m)	56940	9975	64.8	20	0.9	14.3	_	_	_	_	_	_	_	_
E22 P3S15 (28m)	56940	9975	62.9	15.5	2	0.3	18.9	_	_	_	0.4	_	_	_
E22 P3S16 (30m)	56940	9975	55.8	8.1	2.4	_	30.9	_	1.6	_	1.2	_	_	_
E22 P3S17 (32m)	56940	9975	44.5	8	2.6	_	27.6	14.3	1.8	_	1.2	_	_	_
E22 P3S18 (34m)	56940	9975	32.3	7.4	2.8	_	28.4	26.6	_	_	1.4	_	_	tit. 1.1
E22 P3S19 (36m)	56940	9975	37.4	11	1.5	_	28.2	20.5	_	_	1.5	_	_	_
E22 P3S20 (38m)	56940	9975	40	5.9	1.7	_	26.7	23.8	_	_	0.7	_	_	jar. 1.2
E22 P3S21 (40m)	56940	9975	34.7	3.6	2.2	_	28.7	29.5	_	_	0.2	_	_	jar 1.1

PROFILE	Northings	Eastings	Kaolin	Quartz	Hematite	Goethite	Muscovite	Orthoclase	Microcline	Albite	Smectite	Dolomite	Gypsum	Other
E22 P4S1 (1m)	56935	9930	29.2	43	3.2	11	–	–	–	2.5	3	–	–	Calc. 8.1
E22 P4S2 (2m)	56935	9930	20.5	30.9	1.5	24.7	–	–	–	–	6.6	–	11.3	Calc. 4.5
E22 P4S3 (4m)	56935	9930	28.7	34.6	1	12	–	–	–	–	2.1	–	20.6	–
E22 P4S4 (6m)	56935	9930	47.2	28.1	1.4	20.2	–	–	–	–	1.2	–	1.9	–
E22 P4S5 (8m)	56935	9930	41.5	24.8	2	30	–	–	–	–	1.7	–	–	–
E22 P4S6 (10m)	56935	9930	53.7	7.6	7.7	30.6	–	–	–	–	0.4	–	–	–
E22 P4S7 (12m)	56935	9930	64.8	9.6	5.3	19.3	–	–	–	–	–	1.1	–	–
E22 P4S8 (14m)	56935	9930	67.9	9	0.6	18.2	–	–	–	–	–	4.2	–	–
E22 P4S9 (16m)	56935	9930	62.9	11.1	5.3	19.3	–	–	–	–	–	2.3	–	–
E22 P4S10 (18m)	56935	9930	59.9	10.7	2.7	21	–	–	–	–	0.5	5.1	–	–
E22 P4S11 (20m)	56935	9930	54.7	9.3	7.5	13.1	–	–	–	–	0.3	15.1	–	–
E22 P4S12 (22m)	56935	9930	65.2	9.3	10.6	14.4	–	–	–	–	0.5	–	–	–
E22 P4S13 (24m)	56935	9930	77.7	3.8	5.9	12.1	–	–	–	–	0.5	–	–	–
E22 P4S14 (26m)	56935	9930	61.4	11.8	–	26.8	–	–	–	–	–	–	–	–
E22 P4S15 (28m)	56935	9930	29.3	9.1	–	61.6	–	–	–	–	–	–	–	–
E22 P4S16 (30m)	56935	9930	49.6	8.9	–	41.5	–	–	–	–	–	–	–	–
E22 P4S17 (32m)	56935	9930	70	6.3	–	23.8	–	–	–	–	–	–	–	–
E22 P4S18 (34m)	56935	9930	32.4	6.6	–	17.1	37.4	–	–	–	6.4	–	–	–
E22 P4S19 (36m)	56935	9930	31	8.2	–	9.8	41.8	–	–	–	9.2	–	–	–
E22 P4S20 (38m)	56935	9930	47.8	3.3	–	–	27	20.3	–	–	1.7	–	–	–
E22 P4S21 (40m)	56935	9930	48.6	5.1	–	–	21.1	24.8	–	–	0.3	–	–	–
E22 P4S22 (42m)	56935	9930	51.6	5.8	–	–	40.3	0.4	–	–	2	–	–	–
E22 P4S23 (44m)	56935	9930	35.8	1.9	1.8	–	41.8	15.1	–	–	3.5	–	–	–
E22 P4S24 (46m)	56935	9930	21.9	1.3	3.4	–	38.1	15.5	–	18.2	0.6	–	–	–
E22 P4S25 (48m)	56935	9930	25	0.8	4.6	–	32.9	19.9	–	15.7	0.4	–	–	hrn. 0.7
E22 P5S1 (1m)	57200	10995	33.1	43.8	9.3	0.1	–	–	–	4.9	1.4	–	0.7	Calc. 6.7
E22 P5S1 (2m)	57200	10995	37.7	30.3	5.2	0.6	–	–	–	–	1.8	–	24.6	–
E22 P5S3 (4m)	57200	10995	53.9	32	6.2	4.1	–	–	–	–	3.4	–	0.5	–

PROFILE	Eastings	Northings	Kaolin	Quartz	Hematite	Goethite	Muscovite	Orthoclase	Microcline	Albite	Smectite	Dolomite	Gypsum	Other
E22 P5S4 (6m)	57200	10995	51.6	15	12.6	7.5	–	–	–	12.6	0.7	–	–	–
E22 P5S5 (8m)	57200	10995	67	9.4	15	8.3	–	–	–	–	0.4	–	–	–
E22 P5S6 (10m)	57200	10995	65.8	8.5	13.6	11.9	–	–	–	–	0.1	–	–	–
E22 P5S7 (12m)	57200	10995	66	7.1	12.9	10.5	–	–	–	–	–	–	–	Ana. 3.5
E22 P5S8 (14m)	57200	10995	49.6	7.5	4	7.1	–	–	–	–	–	25.6	–	ana. 6.1
E22 P5S9 (16m)	57200	10995	51.9	8.9	9.1	11.4	–	–	–	–	1.1	9.5	–	ana. 8.1
E22 P5S10 (18m)	57200	10995	55.7	3.9	20.7	14.4	2.8	–	–	–	1.2	1.3	–	–
E22 P5S11 (20m)	57200	10995	41	6	23.9	18.5	4.4	–	–	–	1.5	4.8	–	–
E22 P5S12 (22m)	57200	10995	58.7	17	14.6	4.1	1.9	–	–	–	0.6	3	–	–
E22 P5S13 (24m)	57200	10995	54.6	12.5	15.5	6.2	4.5	–	–	–	0.4	6.3	–	–
E22 P5S14 (26m)	57200	10995	50.4	3.3	5.6	6.9	33.6	–	–	–	0.2	–	–	–
E22 P5S15 (28m)	57200	10995	59.8	3.4	6.6	3	26.9	–	–	–	0.3	–	–	–
E22 P5S16 (30m)	57200	10995	61.4	13.6	6.1	3.8	11.1	0.1	–	–	1.1	–	–	ana. 2.9
E22 P5S17 (32m)	57200	10995	52.4	7.8	6.3	1.1	20.9	7	–	–	1.4	–	–	ana. 3
E22 P5S18 (34m)	57200	10995	37.2	1.5	–	–	31.8	17.4	–	–	5.1	–	verm. 3.8	ana. 3.2
E22 P5S19 (36m)	57200	10995	35.4	–	3.7	0.2	24.4	28.7	–	–	5.9	–	–	ana. 1.6
E22 P5S20 (38m)	57200	10995	27.4	1	6.2	–	18.1	32.5	–	–	12	–	–	ana. 2.7
E22 P5S21 (40m)	57200	10995	15.3	3.7	–	–	39.8	4.7	–	21.5	10.7	–	–	jar. 2.8
E22 P5S22(42m)	57200	10995	12.4	16.3	1	–	8.2	18.4	6.7	36.8	–	–	–	–
E22 P5S23 (44m)	57200	10995	11.6	13.9	–	–	8.9	23.8	5.2	35	0.7	–	–	–
E22 P7S2 (1m)	56675	9860	46.5	15.5	–	2.3	–	–	–	5.2	4.7	–	15.7	Calc. 10.1
E22 P7S3 (2m)	56675	9860	72.3	4.5	0.4	3.6	–	–	–	13.3	4.4	–	1.7	–
E22 P7S4 (4m)	56675	9860	81.3	2.1	3.2	7.7	–	–	–	–	5.7	–	–	–
E22 P7S5 (6m)	56675	9860	74.9	17	0.5	–	–	–	–	–	7.6	–	–	–
E22 P7S6 (8m)	56675	9860	47.5	11.9	4.9	0.4	18.5	–	–	–	0.2	16.6	–	–
E22 P7S7 (10m)	56675	9860	48.2	3.5	6.3	6.1	26.5	–	–	–	1.5	7.9	–	–
E22 P7S8 (12m)	56675	9860	34.6	3.4	3.3	2.6	14.2	–	–	–	0.6	41.3	–	–
E22 P7S8 (14m)	56675	9860	63	6.9	6.2	–	20.4	–	–	–	–	3.1	–	–

PROFILE	Northings	Eastings	Kaolin	Quartz	Hematite	Goethite	Muscovite	Orthoclase	Microcline	Albite	Smectite	Dolomite	Gypsum	Other
E22 P7S9 (16m)	56675	9860	49.7	15.4	6.9	_	22.5	_	_	_	_	5.5	_	_
E22 P7S10 (18m)	56675	9860	40.1	3	5.8	1.8	22.9	20.2	_	_	2.6	_	_	jar. 3.6
E22 P7S11 (20m)	56675	9860	48	2.9	4.6	0.9	21.5	18.4	_	_	1.5	_	_	jar. 2.2
E22 P7S12 (22m)	56675	9860	36.7	3	1.4	0.6	25.7	14.3	_	11	3.7	0.2	_	jar. 3.5
E22 P7S14 (24m)	56675	9860	35.9	2.4	2.7	0.4	28.4	29	_	_	0.1	_	_	jar.1.2
E22 P7S15 (26m)	56675	9860	11.5	1.5	5.3	_	30.4	11.9	_	33.3	4.6	_	_	_
E22 P7S16 (28m)	56675	9860	17.7	1.8	0.9	0.3	27.8	19.1	_	27.4	4.3	_	Ens. 0.5	hrn. 0.2
E22 P7S17 (30m)	56675	9860	18.7	_	_	_	29.9	20.5	_	24	_	_	Ens. 0.7	Verm. 6.3
E22 P7S18 (32m)	56675	9860	18.8	0.7	3.7	_	30.5	27.4	_	16.7	2.3	_	_	_
E22 P7S19 (34m)	56675	9860	3.8	0.6	3.8	_	17.7	22.3	_	46.2	2.8		Ens. 2.6	
E22 P7S20 (36m)	56675	9860	2.3	_	0.5	_	24.3	11.4	6.4	47	_	Dps. 1.0		Chlr. 6.7
E22 P7S21 (38m)	56675	9860	3.3	_	4.8	_	20	22.4	_	39.6	2.7	Dps. 1.2	Epd. 1	Chlr. 4.9
E22 P7S22 (40m)	56675	9860	4.7	_	0.7	0.5	35.4	23.2	_	28.5	1.6	Dps. 3.7	Epd. 0.6	Hrn.1.0
E22 P7S23 (42m)	56675	9860	2.7	_	1.1	_	25.5	27.8	Hrn. 0.6	32.9	0.9	Dps. 2.1	Epd. 1.4	Chlr. 4.4
											6.7			Calc. 5.7
E22 P9S1 (1m)	57235	10800	47.2	40.5	_	_	_	_	_	_	5.5	_	_	Calc.12.2
E22 P9S2 (2m)	57235	10800	16.3	60.8	_	_	_	_	_	5.2	5.3	3.9	_	Calc.10.8
E22 P9S3 (4m)	57235	10800	39	27	0.4	0.2	_	_	_	13.4	5.5	10.8	_	Calc. 1.1
E22 P9S4 (6m)	57235	10800	41.6	13.6	0.5	0.5	_	_	_	26.4	8.5	_	_	_
E22 P9S5 (8m)	57235	10800	71.1	4.9	0.8	0.3	_	13.9	_	0.5	13.2	_	_	_
E22 P9S6 (10m)	57235	10800	72.2	5.5	_	_	_	9.1	_	_	6.3	_	_	_
E22 P9S7 (12m)	57235	10800	51.8	3.4	_	_	24.6	14	_	_	19.2	_	_	_
E22 P9S8 (14m)	57235	10800	40.8	1.5	1.4	_	_	31.6	_	5.5	12.2	_	_	_
E22 P9S9 (16m)	57235	10800	21.5	11.1	1.2	_	17.8	21.7	_	14.4	1.8	_	_	hrn. 1.2
E22 P9S10 (18m)	57235	10800	22.9	1.6	4.5	_	34.6	19.9	_	13.5	1.7	_	_	hrn. 0.1
E22 P9S11 (20m)	57235	10800	12.7	1.2	2.3	_	30.8	17.5	_	33.6	1.1	_	_	_
E22 P9S12 (22m)	57235	10800	1.9	1.5	2	_	28	12.6	_	52.8	1	_	_	_
E22 P9S13 (24m)	57235	10800	5.2	1.7	1.8	_	28	17	_	45.3				

PROFILE	Northings	Eastings	Kaolin	Quartz	Hematite	Goethite	Muscovite	Orthoclase	Microcline	Albite	Smectite	Dolomite	Gypsum	Other
E22 P9S14 (26m)	57235	10800	5	2.8	1.2	_	27.6	20.2	_	42.6	0.7	_	_	_
E22 P9S15 (28m)	57235	10800	4.8	1.3	0.5	_	21.3	24.2	_	45.6	_	Dps. 1.3	Epd. 1.0	
E22 P9S16 (30m)	57235	10800	2.3	_	_	_	18.4	26.3	_	47.1	_	Dps. 2.1	Epd. 1.3	Hrn. 2.5
E22 P9S17 (32m)	57235	10800	1.5	_	_	_	17.3	25.7	_	48.6	_	Dps. 2.1	Epd. 2.2	Hrn. 2.6
E22 P10S1 (1m)	56815	9660	28.6	51.1	1.2	3.1	_	_	_	_	2.3	_	7.4	Calc. 6.3
E22 P10S2 (2m)	56815	9660	23.1	47.7	3.5	_	19.7	_	_	_	1.1	_	1.6	Calc. 3.3
E22 P10S3 (4m)	56815	9660	19.3	13.9	1.5	0.5	56.4	_	_	5.7	1.5	_	_	Calc. 1.2
E22 P10S4 (6m)	56815	9660	31.8	3.4	0.7	0.2	40.5	18.1	_	1.9	0.9	_	_	hrn. 2.5
E22 P10S5 (8m)	56815	9660	28.4	2.3	1.3	_	31.9	27	_	4.8	2	_	_	Hrn.2.4
E22 P10S6 (10m)	56815	9660	4	0.5	0.3	0.5	11.3	3.1	_	0.9	0.1	78.7	_	hrn. 0.7
E22 P10S7 (12m)	56815	9660	24.2	0.3	0.5	_	37.2	30.5	_	3.7	0.8	_	_	Hrn. 2.8
E22 P10S8 (14m)	56815	9660	15.9	0.4	0.4	_	29.9	28.3	_	20.7	1.2	_	_	Hrn. 3.5
E22 P10S9 (16m)	56815	9660	5.6	_	_	_	12.1	15.6	_	52.6	_	_	Chlr. 10.7	Hrn. 3.4
E22 P11S1 (1m)	56905	9705	63.4	35.2	_	_	_	_	_	_	1.4	_	_	_
E22 P11S2 (2m)	56905	9705	81.5	17	_	_	_	_	_	_	1.5	_	_	_
E22 P11S3 (4m)	56905	9705	94.5	35	2.1	_	_	_	_	_	0.4	_	_	_
E22 P11S4 (6m)	56905	9705	60.8	1.8	0.4	_	_	_	_	_	0.4	36.5	_	_
E22 P11S5 (8m)	56905	9705	97.1	1.2	0.6	_	_	_	_	_	_	0.5	_	_
E22 P11S6 (10m)	56905	9705	95.6	1.5	1.1	_	_	_	_	_	_	1.8	_	_
E22 P11S7 (12m)	56905	9705	90.6	0.4	0.5	_	_	_	_	_	_	8.5	_	_
E22 P11S8 (14m)	56905	9705	86.4	3.5	2.6	1.3	_	_	_	_	0.5	5.7	_	_
E22 P11S9 (16m)	56905	9705	81.9	5.2	2.1	0.5	_	_	_	_	1.2	9.1	_	_
E22 P11S10 (18m	56905	9705	77.1	5.6	1.5	_	12.3	3.5	_	_	_	_	_	_
E22 P11S11 (20m	56905	9705	63.3	4.4	1.2	0.5	21.7	8.9	_	_	_	_	_	_
E22 P11S12 (22m	56905	9705	48.5	3.3	_	0.9	31.5	15.8	_	_	_	_	_	_
E22 P11S13 (24m	56905	9705	43	1.5	1.1	0.5	34.5	14.9	4.5	_	_	_	_	_
E22 P11S14 (26m	56905	9705	38.9	2.2	_	_	33.6	15.2	10.1	_	_	_	_	_

Appendix 2

E27 Mineralogical data

PROFILE	Northings	Eastings	Kaolin	Quartz	Hematite	Goethite	Muscovite	Orthoclase	Albite	Smectite	Dolomite	Epidote	Chlorite	Other
E27 P1S1 (1m)	56780	10900	37.2	32.7	1.3	1.7	_	_	4.3	14.7	1.2	_	_	Calc.6.9
E27 P1S2 (2m)	56780	10900	22.6	42.4	1.3	0.5	_	_	6.1	21.3	_	_	_	Calc. 5.8
E27 P1S3 (4m)	56780	10900	69.9	11.3	1.5	1	_	_	5.2	8.6	_	_	_	Calc. 2.5
E27 P1S4 (6m)	56780	10900	77	9.8	3.5	5.5	_	_	_	2.3	1.9	_	_	_
E27 P1S5 (8m)	56780	10900	86.8	1.2	4.7	4.5	_	_	_	_	2.9	_	_	_
E27 P1S6 (10m)	56780	10900	56.3	7.7	1.9	_	_	_	_	_	34.1	_	_	_
E27 P1S7 (12m)	56780	10900	69.8	1.7	4.4	1.2	_	_	_	_	22.9	_	_	_
E27 P1S8 (14m)	56780	10900	85.6	9.3	5.1	_	_	_	_	_	_	_	_	_
E27 P1S9 (16m)	56780	10900	65.8	6.1	2.5	1.3	24.3	_	_	_	_	_	_	_
E27 P1S10 (18m)	56780	10900	39.8	14	4.9	_	41.4	_	_	_	_	_	_	_
E27 P1S11 (20m)	56780	10900	35.9	1	_	0.7	25	37.3	_	_	_	_	_	_
E27 P1S12 (22m)	56780	10900	31.5	0.8	_	_	14.4	16.7	_	36.6	_	_	_	_
E27 P1S13 (24m)	56780	10900	38.9	2.8	_	_	44.9	12.5	_	_	_	_	_	verm. 0.7
E27 P1S14 (26m)	56780	10900	32.2	0.6	_	_	_	35	_	32.1	_	_	_	_
E27 P1S15 (28m)	56780	10900	33	4.4	0.6	0.6	28.8	32.4	0.3		_	_	_	_
E27 P1S16 (30m)	56780	10900	18.1	5.3	_	_	33	12	15.4	13.7	_	_	_	anat. 2.4
E27 P1S19 (32m)	56780	10900	26.7	2.7	_	_	11.2	37.1	5.2	10.9	_	_	_	6.2
E27 P1S18 (34m)	56780	10900	19.3	_	_	_	5.1	22.4	22.6	9.6	_	_	anat. 2.4	hrn.18.7
E27 P1S19 (36m)	56780	10900	16.7	_	_	_	_	9.4	60.7	10.8	_	_	2.4	_
E27 P1S20 (38m)	56780	10900	_	_	1.8	_	6.4	22.8	43.3	1.3	Dps. 6	0.8	chlor. 12.6	neph. 4.8
E22 P2S1 (1m)	56825	10950	48.2	34.1	1.4	1.9	_	_	_	14.4	_	_	_	_
E22 P2S2 (2m)	56825	10950	49.9	28.2	1.3	3.2	_	_	_	6.7	_	_	_	Calc. 10.7
E22 P2S3 (4m)	56825	10950	65.4	18.3	2.4	6.1	_	_	_	2.3	_	_	_	Calc. 5.5
E22 P2S4 (6m)	56825	10950	66.3	17.6	10.5	5.6	_	_	_	_	_	_	_	_
E22 P2S5 (8m)	56825	10950	69.1	7.8	17.5	_	_	_	_	_	5.6	_	_	_
E22 P2S6 (10m)	56825	10950	72	4.6	16.1	0.5	_	_	_	_	6.8	_	_	_
E22 P2S7 (12m)	56825	10950	60.4	8.3	10.4	_	_	_	_	_	20.9	_	_	_
E22 P2S8 (14m)	56825	10950	56.9	13.3	9.3	0.3	_	_	_	_	20.4	_	_	_

PROFILE	Northings	Eastings	Kaolin	Quartz	Hematite	Goethite	Muscovite	Orthoclase	Albite	Smectite	Dolomite	Epidote	Chlorite	Other
E22 P2S9 (16m)	56825	10950	73.2	6.5	8.3	0.5	_	_	_	_	11.5	_	_	_
E22 P2S10 (18m)	56825	10950	83.2	8.7	6.6	1.5	_	_	_	_	_	_	_	_
E22 P2S11 (20m)	56825	10950	83.5	8.4	8.2	_	_	_	_	_	_	_	_	_
E22 P2S12 (22m)	56825	10950	79.7	9.9	10.4	_	_	_	_	_	_	_	_	_
E22 P2S13 (24m)	56825	10950	70.4	1.1	6.4	0.5	8.4	13.3	_	_	_	_	_	_
E22 P2S14 (26m)	56825	10950	65.9	1.1	4.5	_	8.8	19.7	_	_	_	_	_	_
E22 P2S15 (28m)	56825	10950	48	5.2		_	_	29.5	3.6	9.8	_	_	_	anat. 3.9
E22 P2S16 (30m)	56825	10950	45.1	11.1	0.5	_	_	36.1	_	2.7	_	_	_	anat. 4.6
E22 P2S17 (32m)	56825	10950	48.3	12.4	0.7	_	_	31.2	_	2.9	_	_	_	anat.4.4
E22 P2S18 (34m)	56825	10950	52.9	9.7	0.5	_	_	31.4	_	3.3	_	_	_	anat.2.4
E22 P2S19 (36m)	56825	10950	31.4	15.6	5.2	_	_	39.3	_	7.1	_	_	_	anat. 1.4
E22 P2S20 (38m)	56825	10950	17.3	26	1	_	34.6	13	_	7.3	_	_	_	anat.0.7
E22 P2S21 (40m)	56825	10950	13.9	11.3	_	_	33.3	22.9	_	18.6	_	_	_	_
E27 P3S1 (1m)	56890	10995	20.3	37.5	1.8	0.5	_	_	4.5	23.8	Calc.6.3	_	_	Gyps. 5.3
E27 P3S2 (2m)	56890	10995	42.2	26.6	2.1	0.3	_	_	_	18.5	Calc. 4.7	_	_	Gyps. 5.9
E27 P3S3 (4m)	56890	10995	48.8	32.1	4.2	14.9	_	_	_	_	_	_	_	
E27 P3S4 (6m)	56890	10995	65.3	5.2	28.9	0.5	_	_	_	_	_	_	_	_
E27 P3S5 (8m)	56890	10995	64	6.3	25	4.7	_	_	_	_	_	_	_	_
E27 P3S6 (10m)	56890	10995	80.6	3.2	16	0.3	_	_	_	_	_	_	_	_
E27 P3S7 (12m)	56890	10995	64.4	2.9	27.4	5.3	_	_	_	_	_	_	_	_
E27 P3S8 (14m)	56890	10995	74.2	4.1	17.4	4.2	_	_	_	_	_	_	_	_
E27 P3S9 (16m)	56890	10995	76.5	5.8	15.4	2.3	_	_	_	_	_	_	_	_
E27 P3S10 (18m)	56890	10995	82	4.1	11.4	2.6	_	_	_	_	_	_	_	_
E27 P3S11 (20m)	56890	10995	75.3	2.8	10.1	3.7	8.1		_		_	_	_	_
E27 P3S12 (22m)	56890	10995	62.9	12.3	0.6	0.4	19.9	3.8	_	0.4	_	_	_	_
E27 P3S13 (24m)	56890	10995	57.9	20.4	1.1	_	15.1	4	_	1.6	_	_	_	_
E27 P3S14 (26m)	56890	10995	43.1	7	0.8	_	23.2	20.5	_	5.4	_	_	_	_
E27 P3S15 (28m)	56890	10995	40.2	1.3	_	_	23.7	22.3	10.2	2.3	_	_	_	_
E27 P3S16 (30m)	56890	10995	37.1	11.9	_	_	28.1	20.5	_	2.1	_	_	_	_

PROFILE	Northings	Eastings	Kaolin	Quartz	Hematite	Goethite	Muscovite	Orthoclase	Albite	Smectite	Dolomite	Epidote	Chlorite	Other
E27 P3S17 (32m)	56890	10995	47.2	6.5	–	–	31.6	12.5	–	2.2	–	–	–	–
E27 P3S18 (34m)	56890	10995	24.2	2	–	–	15.3	26.2	29.6	2.8	–	–	–	–
E27 P3S19 (36m)	56890	10995	18	1.1	–	–	25.4	5.4	41.8	8.3	–	–	–	–
E27 P3S20 (38m)	56890	10995	5.3	–	–	–	25.3	23.5	42.8	3	–	–	–	–
E27 P3S21 (40m)	56890	10995	–	–	0.8	–	19.3	7	49.9	2.2	5.5	2.3	7.3	hrn.5.6
E27 P3S22 (42m)	56890	10995	–	–	0.5	–	18.5	13.9	49.9	2	Dps4.4	1.5	6.6	hrn.2.3
E27 P4S1 (1m)	57000	11020	18.1	45.9	1.7	0.3	–	–	4.3	20.7	Dol. 0.8	–	Calc. 6.6	Gyps. 1.6
E27 P4S2 (2m)	57000	11020	35.9	39.6	1.4	10	–	–	–	3.5	–	–	Calc. 6.6	Gyps.2.9
E27 P4S3 (4m)	57000	11020	46.6	24.4	1.1	15.3	–	–	–	–	–	–	Calc. 10.6	Gyps. 2.1
E27 P4S4 (6m)	57000	11020	51.2	5.8	34.7	8.3	–	–	–	–	–	–	–	–
E27 P4S5 (8m)	57000	11020	53.3	6.9	28.6	11.1	–	–	–	–	–	–	–	–
E27 P4S6 (10m)	57000	11020	65.3	5.8	25.3	3.5	–	–	–	–	–	–	–	–
E27 P4S7 (12m)	57000	11020	77.6	4.3	16.2	1.9	–	–	–	–	–	–	–	–
E27 P4S8 (14m)	57000	11020	76.8	3	20.2	–	–	–	–	–	–	–	–	–
E27 P4S9 (16m)	57000	11020	70.6	2	3.5	–	–	–	–	–	23.9	–	–	–
E27 P4S10 (18m)	57000	11020	72.3	8.2	14.7	2.3	–	–	–	–	2.4	–	–	–
E27 P4S11 (20m)	57000	11020	69.4	5.5	11	7	–	–	–	–	7.2	–	–	–
E27 P4S12 (22m)	57000	11020	55.5	10.3	22.3	5.8	–	–	–	–	6.2	–	–	–
E27 P4S13 (24m)	57000	11020	63	4	20.9	3.6	–	–	–	–	8.9	–	–	–
E27 P4S14 (26m)	57000	11020	83.4	7.6	1.5	7.4	–	–	–	–	–	–	–	–
E27 P4S15 (28m)	57000	11020	89.5	1.8	2.6	6.1	–	–	–	–	–	–	–	–
E27 P4S16 (30m)	57000	11020	76.3	13.1	3.2	7.4	–	–	–	–	–	–	–	–
E27 P4S17 (32m)	57000	11020	83	4.3	2.1	10.7	–	–	–	–	–	–	–	–
E27 P4S18 (34m)	57000	11020	82.4	6.6	2.9	8	–	–	–	–	–	–	–	–
E27 P4S19 (36m)	57000	11020	77.7	7.6	12.3	2.3	–	–	–	–	–	–	–	–
E27 P4S20 (38m)	57000	11020	83.9	5.4	6.2	4.4	–	–	–	–	–	–	–	–
E27 P4S21 (40m)	57000	11020	56	10.7	1.7	1.9	29.7	–	–	–	–	–	–	–
E27 P4S22 (42m)	57000	11020	69.7	4.1	2.8	1.8	20.7	–	–	–	–	–	–	Jar. 1
E27 P4S23 (44m)	57000	11020	67.1	7.9	2.3	2.8	18.7	–	–	–	–	–	–	Jar.1.1

PROFILE	Northings	Eastings	Kaolin	Quartz	Hematite	Goethite	Muscovite	Orthoclase	Albite	Smectite	Dolomite	Epidote	Diopside	Other
E27 P4S24 (46m)	57000	11020	68.5	3.3	1.3	3.6	22	0.5	–	–	–	–	–	0.8
E27 P4S25 (48m)	57000	11020	46.5	3.2	2	–	22.4	22.1	–	0.6	–	Dps. 1.6		hrn. 0.9
E27 P5S1 (1m)	57110	11025	15.6	43.2	2.3	3.6	–	–	–	22.6	Calc. 12.4	–	–	Gyps. 0.3
E27 P5S2 (2m)	57110	11025	6.2	43.2	1.4	0.4	–	–	–	30.4	Calc. 15.9	–	–	Gyps. 2.4
E27 P5S3 (4m)	57110	11025	38.7	42.1	2.4	4.5	–	–	–	12.3	–	–	–	–
E27 P5S4 (6m)	57110	11025	49.1	16.8	17.3	16.8	–	–	–	–	–	–	–	–
E27 P5S5 (8m)	57110	11025	62.4	5.6	26.5	5.6	–	–	–	–	–	–	–	–
E27 P5S6 (10m)	57110	11025	66.6	6.5	26.9		–	–	–	–	–	–	–	–
E27 P5S7 (12m)	57110	11025	76.4	7.1	14.8	1.7	–	–	–	–	–	–	–	–
E27 P5S8 (14m)	57110	11025	80.2	3.5	15.7	0.6	–	–	–	–	–	–	–	–
E27 P5S9 (16m)	57110	11025	74.5	6.9	9.6	2.5	–	–	–	–	6.5	–	–	–
E27 P5S10 (18m)	57110	11025	74.6	6.4	17.5	0.9	–	–	–	–	0.6	–	–	–
E27 P5S11 (20m)	57110	11025	89.8	6.3	3.4	0.6	–	–	–	–	–	–	–	–
E27 P5S12 (22m)	57110	11025	85.9	4.8	8.1	1.2	–	–	–	–	–	–	–	–
E27 P5S13 (24m)	57110	11025	79.7	5.5	7.5	7.3	–	–	–	–	–	–	–	–
E27 P5S14 (26m)	57110	11025	77.5	11.9	2.8	7.8	–	–	–	–	–	–	–	–
E27 P5S15 (28m)	57110	11025	77.8	13.7	1.7	4.6	–	–	–	2.2	–	–	–	–
E27 P5S16 (30m)	57110	11025	77.8	13.2	2.4	4.9		–		1.7	–	–	–	–
E27 P5S17 (32m)	57110	11025	39	19.5	0.3	5	30.5	–	4.8	0.8	–	–	–	–
E27 P5S18 (34m)	57110	11025	19.6	30.5	0.9	4.5	40.5	–	–	0.3	–	–	–	Jar. 3.5
E27 P5S19 (36m)	57110	11025	16	30.1	0.7	4	44.7	–	0.6	–	–	–	–	Jar. 3.9
E27 P5S20 (38m)	57110	11025	21.2	23.1	1.9	2.1	47.5	–	0.7	–	–	–	–	Jar. 3.4
E27 P5S21 (40m)	57110	11025	57.8	0.9	3	1.4	12.9	19.1	–	–	–	1.1	2.5	Jar. 1.3
E27 P5S22 (42m)	57110	11025	40.2	0.5	2.1	1.1	17.4	35.9	–	1.4	–		0.7	Jar. 0.9
E27 P5S23 (44m)	57110	11025	51.2	0.4	2.2	1.1	16.9	21.7	–	2.7	–	1	2.8	–
E27 P5S24 (46m)	57110	11025	45.8	0.5	3	0.3	20.9	15.4	6.4	3.5	–	1.4	2.9	–

PROFILE	Northings	Eastings	Kaolin	Quartz	Hematite	Goethite	Muscovite	Orthoclase	Albite	Smectite	Dolomite	Epidote	Chlorite	Other
E27 P6S1 (1m)	57210	10995	11.3	38.5	3.3	2.7	–	–	–	22.6	0.8	–	Calc. 13.5	Gyps. 7.3
E27 P6S2 (2m)	57210	10995	25.5	38.3	2.1	0.5	–	–	–	18.7	–	–	Calc. 7.1	Gyps. 7.7
E27 P6S3 (4m)	57210	10995	55.8	24.5	6	7.4	–	–	–	6.3	–	–	–	–
E27 P6S4 (6m)	57210	10995	61	24.3	11.2	3.4	–	–	–	–	–	–	–	–
E27 P6S4 (8m)	57210	10995	77.2	7.9	12.2	2.7	–	–	–	–	–	–	–	–
E27 P6S5 (10m)	57210	10995	70.4	6.7	16.6	6.3	–	–	–	–	–	–	–	–
E27 P6S6 (12m)	57210	10995	81.5	8.1	4	6.4	–	–	–	–	–	–	–	–
E27 P6S7 (14m)	57210	10995	83.8	4.2	9.6	2.5	–	–	–	–	–	–	–	–
E27 P6S8 (16m)	57210	10995	67.9	8.8	12.2	7	–	–	–	–	3.9	–	–	–
E27 P6S9 (18m)	57210	10995	79.3	9.8	7.7	3.3	–	–	–	–	–	–	–	–
E27 P6S10 (20m)	57210	10995	73.2	10.8	9.5	6.5	–	–	–	–	–	–	–	–
E27 P6S11 (22m)	57210	10995	70.2	21.4	6.6	1.8	–	–	–	–	–	–	–	–
E27 P6S12 (24m)	57210	10995	39.4	22	13.4	25.2	–	–	–	–	–	–	–	–
E27 P6S13 (26m)	57210	10995	30.9	24	10.5	34.6	–	–	–	–	–	–	–	–
E27 P6S14 (28m)	57210	10995	36.9	7.5	8.9	46.6	–	–	–	–	–	–	–	–
E27 P6S15 (30m)	57210	10995	21	13.7	11.7	53.6	–	–	–	–	–	–	–	–
E27 P6S16 (32m)	57210	10995	41.7	12.5	6.5	39.2	–	–	–	–	–	–	–	–
E27 P6S17 (34m)	57210	10995	66.5	17.3	6.6	9.6	–	–	–	–	–	–	–	–
E27 P6S18 (36m)	57210	10995	68.1	18.8	3.2	9.1	–	–	–	0.9	–	–	–	–
E27 P6S19 (38m)	57210	10995	41.1	1.3	2.2	–	30.6	11.7	–	3.1	–	–	–	–
E27 P6S20 (40m)	57210	10995	50.5	3.8	0.8	–	26.7	12.3	–	5.9	–	–	–	–
E27 P6S21 (42m)	57210	10995	52.7	4.7	0.5	–	25.6	13.3	–	3.3	–	–	–	–
E27 P6S22 (44m)	57210	10995	30.7	2.5	1.5	–	31.6	17.9	11.8	4	–	–	–	–
E27 P6S23 (46m)	57210	10995	5.5	2.1	1	–	30.6	19.5	23.9	1.5	–	Dps. 4.3	6.1	hrn. 5.5
E27 P6S24 (48m)	57210	10995	3.4	–	1.3	–	7.7	17.7	39.5	Neph. 0.8	–	Dps. 5.8	12.6	hrn. 10.8
E27 P6S25 (50m)	57210	10995	0.6	–	0.8	–	19.8	16	37.4	Neph. 1.7	Dps. 4.6	0.8	10.1	hrn. 8.1
E27 P7S1 (1m)	57235	10900	38.7	47.7	0.9	6.8	–	–	–	3.3	Calc. 0.5	–	–	Gyps. 2.1
E27 P7S2 (2m)	57235	10900	28.1	42.7	0.6	10.4	–	–	–	18.2	–	–	–	–
E27 P7S3 (4m)	57235	10900	50.7	30.1	2.6	16.5	–	–	–	–	–	–	–	–

PROFILE	Northings	Eastings	Kaolin	Quartz	Hematite	Goethite	Muscovite	Orthoclase	Albite	Smectite	Dolomite	Epidote	Chlorite	Other
E27 P7S4 (6m)	57235	10900	76.1	10.1	12.6	1.3	–	–	–	–	–	–	–	–
E27 P7S5 (8m)	57235	10900	86.6	2.3	9.9	1.2	–	–	–	–	–	–	–	–
E27 P7S6 (10m)	57235	10900	85.2	3.9	9.8	1.1	–	–	–	–	–	–	–	–
E27 P7S7 (12m)	57235	10900	34.1	5.3	14	0.4	–	–	–	–	46.1	–	–	–
E27 P7S8 (14m)	57235	10900	72.6	4.2	11.2	1.3	–	–	–	–	10.7	–	–	–
E27 P7S9 (16m)	57235	10900	80.2	6.5	12.7	1.1	–	–	–	–	–	–	–	–
E27 P7S10 (18m)	57235	10900	82.4	6.8	10.7	–	–	–	–	–	–	–	–	–
E27 P7S11 (20m)	57235	10900	80	7.9	12.2	–	–	–	–	–	–	–	–	–
E27 P7S12 (22m)	57235	10900	81.6	4.7	11.5	2.2	–	–	–	–	–	–	–	–
E27 P7S13 (24m)	57235	10900	80.6	6.3	12.2	1	–	–	–	–	–	–	–	–
E27 P7S14 (26m)	57235	10900	37.7	18.7	22	21.7	–	–	–	–	–	–	–	–
E27 P7S15 (28m)	57235	10900	41.2	13.8	18.6	26.4	–	–	–	–	–	–	–	–
E27 P7S16 (30m)	57235	10900	41	10.8	23.5	24.6	–	–	–	–	–	–	–	–
E27 P7S17 (32m)	57235	10900	53.2	13.8	11.4	20.2	–	–	–	1.5	–	–	–	–
E27 P7S18 (34m)	57235	10900	37.2	25.9	3.1	5.4	11	15.6	–	1.8	–	–	–	–
E27 P7S19 (36m)	57235	10900	13.7	13.9	1.5	1.4	47.8	14.5	–	7.2	–	–	–	–
E27 P7S20 (38m)	57235	10900	16.2	20.5	–	4.5	39.9	14.4	2.3	2.2	–	–	–	–
E27 P7S21 (40m)	57235	10900	43.6	11.5	–	–	29	6.3		2.1	–	–	Ens. 0.5	Hrn. 7
E27 P7S22 (42m)	57235	10900	40	0.3	–	–	35	11.9	4.7	4.6	–	–	–	Hrn. 3.4
E27 P7S23 (44m)	57235	10900	29.1	1	4.1	–	26.1	20.3	14.9	4.5	–	–	–	–
E27 P7S24 (46m)	57235	10900	16.8	–	4.2	–	25.7	10.4	31.6	11.1	–	–	–	–
E27 P7S25 (48m)	57235	10900	2.7	–	3.9	–	26.2	22.6	38.4	3.7	–	Ens. 1.5	Dps. 1	–
E27 P7S26 (50m)	57235	10900	2.7	–	1.1	–	25.5	27.8	32.9	0.9	Dps. 2.2	1.4	4.4	Hrn. 0.6
E27 P8S1 (1m)	57235	10800	30.9	45.2	1.9	3.2	–	–	–	18.2	–	–	–	Calc. 0.5
E27 P8S2 (2m)	57235	10800	51.1	27.3	3	7	–	–	–	10.9	–	–	–	Calc. 0.8
E27 P8S3 (4m)	57235	10800	71.2	11.1	4.7	7	–	–	4.5	1.5	–	–	–	–
E27 P8S4 (6m)	57235	10800	53.5	8.9	29.4	8.3	–	–	–	–	–	–	–	–
E27 P8S5 (8m)	57235	10800	68.3	6	17.3	8.5	–	–	–	–	–	–	–	–
E27 P8S6 (10m)	57235	10800	83.9	4.8	8.4	2	–	–	–	–	–	–	–	–

PROFILE	Northings	Eastings	Kaolin	Quartz	Hematite	Goethite	Muscovite	Orthoclase	Albite	Smectite	Dolomite	Epidote	Chlorite	Other
E27 P8S7 (12m)	57235	10800	77.1	7.3	11.5	4.2	_	_	_	_	_	_	_	_
E27 P8S8 (14m)	57235	10800	81.8	6.7	9	2.5	_	_	_	_	_	_	_	_
E27 P8S9 (16m)	57235	10800	87.1	5.1	6.3	1.6	_	_	_	_	_	_	_	_
E27 P8S10 (18m)	57235	10800	76.3	6.8	4.1	1.9	8	_	_	2.8	_	_	_	_
E27 P8S11 (20m)	57235	10800	78.7	7.1	4.6	0.8	8.4	_	_	0.4	_	_	_	_
E27 P8S12 (22m)	57235	10800	79.6	7.2	3.4	0.5	7.8	_	_	0.5	_	_	_	_
E27 P8S13 (24m)	57235	10800	47.6	0.7	1.9	0.8	14.2	30.1	0.4	1	Dps. 1.2	Epd. 0.7	_	Jar. 1.5
E27 P8S14 (26m)	57235	10800	44.8	1	1	0.4	14.4	35.2	1	1.3	_	_	_	Jar. 1.0
E27 P8S15 (28m)	57235	10800	18.9	0.9	1.4	_	14.1	31.6	30.6	1	_	0.5	_	Jar. 1
E27 P8S16 (30m)	57235	10800	13.7	_	1.2	_	9.5	19.3	37.1	4.7	Dps. 2.5	1.4	9.4	Jar. 1.2
E27 P8S17 (32m)	57235	10800	26.5	_	1	_	13.6	8.8	38.7	4.1	Dps. 2.4	1.1	3.4	Jar. 0.4
E27 P8S18 (34m)	57235	10800	5.3	_	2.5	_	_	22.9	45.1	11.6	Dps. 2.1	_	8	Hrn. 2.6
E27 P8S19 (36m)	57235	10800	2.1	_	_	_	_	26.2	46.2	1.5	Dps. 2.7	4.2	12.1	Hrn. 5.2
E27 P9S1 (1m)	57215	10710	37.1	34.9	1.6	1.1	_	_	_	15.7	Calc. 5	_	_	Gyps. 4.6
E27 P9S2 (2m)	57215	10710	63.3	18.8	2.1	5.7	_	_	_	8	_	_	_	Gyps. 2.1
E27 P9S3 (4m)	57215	10710	68.5	13.4	9	2.7	_	_	_	6.4	_	_	_	_
E27 P9S4 (6m)	57215	10710	85.6	2.7	3.6	4.1	_	_	_	4.1	_	_	_	_
E27 P9S5 (8m)	57215	10710	81.3	2.4	8.1	4.8	_	_	_	3.4	_	_	_	_
E27 P9S6 (10m)	57215	10710	82.5	1.7	9.7	5.4	_	_	_	0.7	_	_	_	_
E27 P9S7 (12m)	57215	10710	68.7	4.3	4.2	2.1	_	_	_	1.2	19.5	_	_	_
E27 P9S8 (14m)	57215	10710	77.4	4.1	4	3.9	_	_	_	0.9	9.7	_	_	_
E27 P9S9 (16m)	57215	10710	76.2	13.1	2.7	_	7.5	_	_	_	0.5	_	_	_
E27 P9S10 (18m)	57215	10710	74.4	8.1	1.8	_	15.8	_	_	_	_	_	_	_
E27 P9S11 (20m)	57215	10710	47.9	4.4	3.2	_	31.3	12.5	_	_	0.7	_	_	_
E27 P9S12 (22m)	57215	10710	42.1	3.6	3	0.8	30.5	15.4	_	3.8	0.8	_	_	_
E27 P9S13 (24m)	57215	10710	29.6	1.4	0.8	_	46.4	12.4	_	9.5	_	_	_	_
E27 P9S14 (26m)	57215	10710	25.6	_	_	_	14.2	19.7	35.4	5	_	_	_	_
E27 P9S15 (28m)	57215	10710	24.5	_	_	_	24.8	17.3	29.4	4.1	_	_	_	_

PROFILE	Northings	Eastings	Kaolin	Quartz	Hematite	Goethite	Muscovite	Orthoclase	Albite	Smectite	Dolomite	Epidote	Chlorite	Other
E27 P9S16 (30m)	57215	10710	31	_	_	_	7.4	28.6	24	9	_	_	_	_
E27 P9S17 (32m)	57215	10710	9.5	_	_	_	30.7	10.2	42.3	7.4	_	_	_	_
E27 P9S18 (34m)	57215	10710	11.1	_	_	_	7.1	25.1	48.1	5.3	_	_	_	Hrn. 3.2
E27 P9S19 (36m)	57215	10710	9.1	_	_	_	5	27.3	52.9	2.3	_	_	_	Hrn. 2.5
E27 P9S20 (38m)	57215	10710	6.8	_	_	_	6.9	23	53.8	2.3	_	_	_	Hrn. 7.2
E27 P10S1 (1m)	57125	10640	22.2	44.7	1.4	0.5	_	_	4.9	23.5	Calc. 1	_	_	Gyps. 1.8
E27 P10S2(2m)	57125	10640	29.9	41.3	1.5	1	_	_	4.6	18.6	Calc. 1.2	_	_	Gyps. 1.9
E27 P10S3 (4m)	57125	10640	53.4	19.8	2.1	6.7	_	_	_	18.1	_	_	_	_
E27 P10S4 (6m)	57125	10640	71.1	8.3	5.6	0.4	_	_	_	2.2	12.3	_	_	_
E27 P10S5 (8m)	57125	10640	66.8	7.4	4.2	0.3	_	_	_	3.7	17.7	_	_	_
E27 P10S6 (10m)	57125	10640	69.6	5	14.9	0.3	_	_	_	_	10.1	_	_	_
E27 P10S7 (12m)	57125	10640	63.5	4.1	16.6	1.2	_	7.8	_	_	6.8	_	_	_
E27 P10S8 (14m)	57125	10640	61.8	4.5	11.5		4.9	9.3	_	1.4	6.6	_	_	_
E27 P10S9 (16m)	57125	10640	38.8	4.7	6.6	_	19	20	_	5.5	5.2	_	_	_
E27 P10S10 (18m	57125	10640	38.4	7.6	1.9	_	15.5	12	18.2	5.7	0.7	_	_	_
E27 P10S11 (20m	57125	10640	47.8	1.4	2.8	0.8	_	18.3	18.4	1.4	_	2.6	Dps. 6.5	
E27 P10S12 (22m	57125	10640	7	_	3.3	1.6	_	26.8	37.7	6.6	_	3.9	Dps. 11	Hrn. 2.1
E27 P10S13 (24m	57125	10640	12.5	_	1.7	_	2.6	27.4	37.3	4.6	_	4.2	Dps. 9.7	_
E27 P10S14 (26m	57125	10640	10.3	_	6.2	_	4.1	20.3	48	5.6	_	2.5	Dps. 3	_
E27 P10S15 (28m	57125	10640	14.6	_	7.1	_	10.3	18.8	39.8	6.8	_	1.5	Dps. 1	_
E27 P10S16 (30m	57125	10640	6	2.6	2.8	_	19.7	10.1	46.1	8.7	_	2	Dps. 2	_
E27 P10S17 (32m	57125	10640	3.7	2.8	4.3	_	19.3	11.6	45	9.8	_	1.5	Dps. 1.9	_
E27 P10S18 (34m	57125	10640	3.9	6	4.2	_	16.3	16.6	37.4	13	_	_	Dps. 0.7	Ens. 1.9
E27 P10S19 (36m	57125	10640	1.5	5.1	1	_	14.4	21.3	40.9	8.1	_	2.3	Dps.2.1	Ens.3.4
E27 P11S1 (1m)	57055	10625	58	15.3	1	8.4	3.4	1.3	_	_	Calc. 11.2	_	_	Gyps. 1.4
E27 P11S2 (2m)	57055	10625	29.5	3.8	_	7.1	15	2.7	31	3.3	Calc. 5.3	_	_	Gyps. 2.2

PROFILE	Northings	Eastings	Kaolin	Quartz	Hematite	Goethite	Muscovite	Orthoclase	Albite	Smectite	Dolomite	Epidote	Chlorite	Other
E27 P11S3 (4m)	57055	10625	12.5	_	1.7	1.7	19.3	10.3	41.4	9.4	Calc.3.7	_	_	_
E27 P11S4 (6m)	57055	10625	47.5	3.3	2.5	_	_	17.3	_	_	29.3	_	_	_
E27 P11S5 (8m)	57055	10625	44.3	0.8	1.5	_	_	26.1	_	_	27.3	_	_	_
E27 P11S6 (10m)	57055	10625	35.2	3.1	1.6	_	_	25.5	_	4.9	29.6	_	_	_
E27 P11S7 (12m)	57055	10625	47.8	0.9	_	_	_	27.6	_	20.9	2.8	_	_	_
E27 P11S8 (14m)	57055	10625	58.4	1.3	_	_	_	26.1	_	14.2	_	_	_	_
E27 P11S9 (16m)	57055	10625	36.1	1.3	3.1	_	_	36.7	13.1	9.5	_	_	_	_
E27 P11S10 (18m)	57055	10625	35.1	3.2	3.6	_	_	30.9	18.2	9	_	_	_	_
E27 P11S11 (20m)	57055	10625	1.7	1.3	3.5	_	6.1	24.7	36.5	13.5	_	_	_	Hrn. 12.7
E27 P11S12 (22m)	57055	10625	5.6	1.6	_	_	24.9	25.3	42.5	_	_	_	_	_
E27 P11S13 (24m)	57055	10625	_	0.6	_	_	27	11.3	59.4	_	_	_	_	Hrn. 1.8
E27 P11S14 (26m)	57055	10625	_	_	_	_	27.3	18.7	42.6	_	_	_	Act. 8.3	Hrn. 3.3

Appendix 3

Major element geochemistry data

-ID-	Fe2O3	MnO	TiO2	CaO	K2O	SO3	P2O5	SiO2	Al2O3	MgO	Na2O	Total
etp001	22.53	0.01	1.46	0.08	0.05	0.25	0.13	36.78	24.15	0.30	0.42	86.16
etp002	11.88	0.07	1.70	0.10	0.08	0.18	0.06	41.92	28.71	0.31	0.38	85.40
etp003	16.01	0.05	1.31	0.07	0.18	0.08	0.09	39.24	29.23	0.23	0.22	86.71
etp004	29.25	0.02	1.22	0.09	0.13	0.15	0.20	31.87	24.35	0.23	0.23	87.75
etp005	12.03	0.02	1.08	0.14	0.47	0.08	0.09	42.67	29.48	0.48	0.32	86.85
etp006	13.06	0.02	0.91	0.11	0.71	0.07	0.13	41.90	29.65	0.32	0.20	87.06
etp007	12.02	0.01	0.95	0.10	0.62	0.06	0.16	41.81	30.56	0.29	0.17	86.75
etp008	13.06	0.02	0.93	0.11	0.97	0.07	0.26	42.37	28.89	0.38	0.21	87.27
etp009	11.38	0.23	1.03	0.22	1.92	0.06	0.13	47.56	23.58	2.04	0.35	88.50
etp010	10.66	0.06	0.83	0.19	1.84	0.04	0.12	48.99	23.13	1.98	0.26	88.10
etp011	10.08	0.08	0.89	0.26	2.57	0.04	0.12	49.92	22.91	2.07	0.24	89.17
etp012	10.26	0.08	0.93	0.34	4.08	0.01	0.07	47.72	22.08	2.39	0.26	88.23
etp013	6.36	0.04	0.88	0.28	5.00	0.01	0.11	49.43	24.88	2.10	1.11	90.19
etp014	6.59	0.09	0.79	0.22	5.19	0.00	0.05	52.49	23.42	1.55	0.18	90.57
etp015	8.85	0.02	1.07	0.25	4.01	0.00	0.20	45.84	25.59	1.10	0.07	87.00
etp016	9.33	0.13	0.88	0.35	4.57	-0.01	0.05	50.86	21.42	2.67	2.90	93.15
etp017	10.06	0.13	0.90	1.58	2.31	0.00	0.46	49.49	19.31	3.24	3.72	91.21
etp018	7.06	0.09	0.73	1.65	4.63	0.00	0.49	55.07	18.31	2.62	4.76	95.41
etp019	17.58	0.01	1.02	0.11	0.34	0.27	0.05	51.49	16.60	0.54	0.37	88.39
etp020	27.15	0.00	0.89	0.08	0.14	0.44	0.09	35.18	21.91	0.29	0.32	86.50
etp021	28.68	0.01	0.87	0.07	0.13	0.43	0.12	33.68	22.00	0.28	0.33	86.60
etp022	9.17	0.00	1.27	0.08	0.13	0.26	0.05	42.97	30.43	0.26	0.34	84.98
etp023	21.18	0.04	0.98	0.06	0.35	0.15	0.14	35.87	27.51	0.25	0.25	86.77
etp024	27.16	0.02	0.90	1.13	0.33	0.10	0.15	32.63	23.29	0.82	0.18	86.73
etp025	4.44	0.01	1.29	0.11	0.35	0.10	0.06	46.98	31.64	0.36	0.32	85.67
etp026	15.16	0.02	0.85	0.09	0.57	0.12	0.15	47.86	22.97	0.38	0.40	88.57
etp027	9.16	0.01	0.51	0.07	0.81	0.08	0.09	66.12	15.08	0.31	0.26	92.50
etp028	26.32	7.88	1.18	0.33	0.24	0.07	0.54	30.37	14.51	0.41	0.21	82.06
etp029	33.46	8.87	1.24	0.44	0.18	0.09	0.77	26.87	10.70	0.44	0.24	83.31
etp032	31.79	6.47	0.84	0.35	0.16	0.07	0.80	30.11	12.11	0.59	0.20	83.50
etp033	7.28	1.13	1.08	0.23	0.26	0.07	0.22	50.10	23.90	0.57	0.30	85.14
etp034	6.28	0.01	1.12	0.18	0.25	0.03	0.17	57.74	21.68	0.50	0.23	88.22
etp036	7.40	0.07	0.96	0.27	3.09	0.03	0.07	43.92	24.89	2.80	0.24	83.74
etp037	11.46	0.19	1.13	0.24	3.56	0.01	0.13	42.90	24.83	2.78	0.17	87.40
etp038	10.99	0.28	0.91	1.44	3.77	0.01	0.50	44.61	21.95	2.21	1.23	87.91
etp039	8.56	0.06	0.80	1.52	3.36	0.01	0.53	54.14	18.70	1.87	5.24	94.79

-ID-	Fe2O3	MnO	TiO2	CaO	K2O	SO3	P2O5	SiO2	Al2O3	MgO	Na2O	Total
etp040	9.19	0.08	0.84	1.74	3.56	0.00	0.54	50.79	20.24	2.13	3.49	92.61
etp041	8.93	0.09	0.75	1.86	3.46	0.00	0.48	55.13	17.20	2.43	5.54	95.86
etp042	12.12	0.04	1.11	0.40	0.26	0.06	0.04	46.97	24.03	0.86	0.30	86.22
etp043	5.41	0.01	1.50	0.22	0.24	0.03	0.07	45.06	31.77	0.61	0.19	85.11
etp044	6.21	0.05	1.57	0.20	0.31	0.02	0.07	43.45	32.33	0.71	0.11	85.03
etp045	26.32	0.08	1.07	0.16	0.42	0.03	0.19	33.50	24.80	0.39	0.11	87.07
etp046	8.54	0.02	1.05	8.79	0.38	0.05	0.10	29.82	22.11	5.81	0.14	76.81
etp047	13.73	0.04	1.34	2.97	0.42	0.05	0.11	36.06	25.98	2.27	0.17	83.14
etp048	9.11	0.11	1.01	0.19	1.23	0.05	0.09	41.42	31.99	0.67	0.14	86.03
etp049	8.74	0.07	1.09	0.25	1.09	0.27	0.28	40.95	31.41	0.72	0.17	85.07
etp050	10.07	0.11	1.14	0.31	2.97	0.53	0.54	41.31	27.39	0.90	0.29	85.55
etp051	7.71	0.06	0.97	0.24	4.11	0.05	0.11	46.50	26.95	0.95	0.18	87.86
etp052	12.94	3.16	0.75	0.31	4.00	0.04	0.33	40.98	22.17	0.89	0.17	85.73
etp053	8.73	0.10	0.79	0.43	3.44	0.03	0.22	49.84	20.06	3.22	2.55	89.39
etp054	6.85	0.31	0.58	1.00	2.58	0.01	0.42	52.03	20.37	2.58	4.05	90.78
etp056	8.06	0.11	0.68	0.99	3.40	0.01	0.39	49.99	20.45	3.42	2.91	90.41
etp057	9.01	0.13	0.83	1.43	3.27	0.00	0.46	53.36	17.53	3.06	5.07	94.15
etp058	9.34	0.15	0.80	2.16	3.73	0.01	0.38	53.12	17.23	3.76	4.64	95.31
etp059	8.42	0.16	0.78	2.51	3.93	0.04	0.37	54.14	16.83	4.33	4.84	96.36
etp060	8.90	0.16	0.78	3.94	3.69	0.00	0.38	52.95	17.09	4.10	4.33	96.34
etp061	7.98	0.30	0.75	10.78	2.50	0.02	0.05	29.96	16.30	7.97	0.29	76.89
etp062	8.43	0.07	0.79	8.45	3.18	0.02	0.05	33.90	17.73	6.57	0.29	79.48
etp063	7.43	0.13	0.77	10.24	3.53	0.02	0.03	32.19	14.75	7.74	0.23	77.07
etp064	11.85	0.10	1.08	0.30	4.87	0.01	0.04	46.85	20.90	1.57	0.48	88.05
etp065	11.91	0.17	1.09	0.35	2.51	0.01	0.07	43.68	23.75	2.09	0.56	86.19
etp066	11.04	0.16	1.03	0.28	5.57	0.02	0.07	49.48	20.70	1.02	1.46	90.81
etp067	10.98	0.07	0.96	0.42	4.47	0.01	0.06	48.14	19.85	1.42	2.00	88.38
etp068	9.29	0.17	0.78	4.57	3.68	0.00	0.38	51.96	17.14	4.75	3.65	96.38
etp070	8.44	0.18	0.76	2.71	2.96	0.01	0.46	52.36	18.27	4.10	5.33	95.59
etp072	4.46	0.10	0.78	2.38	1.16	0.05	0.04	63.71	12.35	1.52	0.32	86.87
etp073	4.23	0.09	0.74	5.13	1.02	0.11	0.03	60.82	11.93	1.52	0.38	86.02
etp074	4.26	0.10	0.66	6.16	0.99	2.32	0.03	53.36	11.84	1.75	0.37	81.84
etp075	6.13	0.34	0.70	4.94	1.73	0.08	0.04	46.48	17.94	4.01	0.27	82.66
etp076	7.62	0.12	0.77	0.39	2.80	0.14	0.05	49.01	24.37	1.59	0.35	87.22
etp077	5.20	0.05	0.80	0.35	2.85	0.07	0.04	49.70	26.21	1.65	0.28	87.22
etp078	3.45	0.02	0.87	0.34	2.94	0.04	0.10	48.86	28.41	1.51	0.24	86.78

-ID-	Fe2O3	MnO	TiO2	CaO	K2O	SO3	P2O5	SiO2	Al2O3	MgO	Na2O	Total
etp079	8.14	0.03	0.77	0.24	5.37	0.02	0.06	47.35	25.33	1.78	0.45	89.54
etp080	7.13	0.03	0.73	0.64	5.36	0.03	0.28	50.41	23.86	1.75	1.91	92.14
etp081	5.84	0.05	0.67	1.12	4.84	0.01	0.52	54.10	21.61	1.87	4.08	94.71
etp082	5.62	0.06	0.63	1.63	3.58	0.03	0.45	54.97	20.57	3.05	5.60	96.19
etp086	3.99	0.09	0.66	7.52	0.62	1.56	0.02	55.80	10.61	1.52	0.36	82.75
etp087	5.61	0.12	0.85	0.41	0.53	0.12	0.03	60.79	17.35	1.49	0.39	87.69
etp087b	5.59	0.12	0.83	0.42	0.53	0.12	0.03	60.28	17.18	1.48	0.38	86.96
etp088	2.62	0.03	0.31	17.67	0.52	0.06	0.02	25.17	8.80	12.50	0.17	67.88
etp088b	2.60	0.04	0.32	17.55	0.53	0.05	0.02	25.05	8.80	12.40	0.16	67.50
etp089	7.60	0.08	0.80	0.57	0.72	0.08	0.05	49.35	23.80	1.52	0.23	84.82
etp090	7.96	0.01	1.04	0.32	0.95	0.07	0.07	51.82	27.04	1.15	0.20	90.65
etp091	5.69	0.04	0.71	0.37	2.96	0.06	0.14	55.37	22.22	1.34	0.22	89.14
etp092b	2.67	0.08	0.69	6.17	1.19	0.05	0.13	42.11	22.54	4.65	0.13	80.42
etp093	5.68	0.02	0.65	9.86	0.81	0.05	0.05	32.35	20.53	6.84	0.15	76.98
etp094	7.17	0.02	1.00	0.12	1.83	0.06	0.13	42.46	32.19	0.75	0.21	85.94
etp094b	7.85	0.01	1.00	0.11	1.82	0.06	0.14	42.26	32.15	0.70	0.20	86.31
etp095	9.21	0.16	0.85	0.14	1.79	0.07	0.14	47.62	27.75	0.53	0.17	88.44
etp096	7.16	0.19	0.80	0.12	4.92	0.02	0.09	49.37	26.39	0.80	0.44	90.30
etp097	8.18	0.05	0.88	0.19	2.15	0.01	0.08	50.11	24.19	2.99	0.23	89.07
etp098	6.92	0.25	0.97	0.17	6.38	0.02	0.18	49.58	24.90	1.32	0.49	91.17
etp099	8.48	0.04	0.89	0.15	3.33	0.01	0.08	53.76	22.36	1.63	0.32	91.04
etp100	4.62	0.10	0.79	3.61	0.92	0.08	0.04	64.76	11.52	1.37	0.34	88.16
etp101	4.70	0.16	0.82	1.50	0.70	1.77	0.03	65.45	12.05	1.36	0.53	89.07
etp102	3.25	0.01	0.45	3.96	0.26	16.66	0.02	32.81	10.23	0.61	0.21	68.46
etp103	35.65	0.04	0.59	0.18	0.24	0.27	0.12	32.16	17.13	0.59	0.23	87.19
etp103b	35.68	0.03	0.59	0.18	0.25	0.25	0.12	31.79	17.02	0.58	0.20	86.70
etp104	9.94	0.01	0.87	0.22	0.47	0.10	0.07	43.79	28.51	0.80	0.28	85.05
etp105b	17.88	0.48	0.86	0.17	0.78	0.09	0.17	39.98	26.18	0.49	0.23	87.31
etp106	12.72	0.01	0.74	0.15	1.04	0.05	0.11	45.31	28.10	0.55	0.19	88.96
etp107	2.12	0.01	0.52	12.45	0.83	0.16	0.07	35.92	19.01	4.80	0.26	76.15
etp107b	2.10	0.01	0.52	12.64	0.84	0.16	0.07	36.15	19.16	4.90	0.25	76.80
etp108	4.57	0.02	0.39	5.76	2.22	0.05	0.06	56.60	11.90	4.26	0.16	85.99
etp108b	2.22	0.01	0.55	13.30	0.87	0.16	0.07	37.70	20.11	5.12	0.28	80.39
etp109	11.34	0.02	0.97	0.13	1.93	0.13	0.17	42.18	29.98	0.68	0.18	87.71
etp110	8.24	0.02	0.93	0.17	2.70	0.07	0.16	47.79	27.58	1.04	0.22	88.94
etp111	7.00	0.02	0.91	0.13	2.38	0.14	0.11	44.67	31.64	0.78	0.31	88.09

-ID-	Fe2O3	MnO	TiO2	CaO	K2O	SO3	P2O5	SiO2	Al2O3	MgO	Na2O	Total
etp112	11.08	0.02	1.07	0.10	1.15	0.09	0.16	42.28	32.32	0.58	0.22	89.08
etp113	9.99	0.14	0.73	0.25	5.64	0.01	0.37	51.77	20.92	1.07	1.72	92.61
etp114	8.44	0.06	0.70	0.24	4.44	0.01	0.11	54.78	21.36	0.59	3.71	94.45
etp115	5.79	0.03	0.73	0.24	4.95	0.02	0.11	56.26	22.22	0.69	3.58	94.61
etp116	8.43	0.24	0.76	0.29	5.12	0.00	0.14	48.82	24.07	1.57	1.61	91.05
etp117	7.86	0.09	0.78	0.26	5.49	0.00	0.09	48.83	24.79	1.61	0.99	90.79
etp118	4.25	0.09	0.78	4.31	0.80	0.19	0.02	63.86	10.73	1.59	0.47	87.11
etp119	4.63	0.04	0.78	3.98	0.58	5.56	0.02	59.91	11.57	1.14	0.50	88.73
etp120	5.43	0.01	0.90	4.25	0.44	6.00	0.02	61.63	12.77	0.95	0.44	92.83
etp121	14.05	0.02	1.42	0.11	0.19	0.31	0.05	51.76	18.79	0.61	0.65	87.95
etp122	6.15	0.02	1.45	0.09	0.19	0.31	0.03	56.38	22.47	0.51	0.31	87.91
etp122b	6.02	0.01	1.44	0.09	0.19	0.32	0.03	56.16	22.46	0.51	0.31	87.53
etp123	10.21	0.01	1.26	0.10	0.28	0.21	0.04	44.84	28.22	0.47	0.37	86.03
etp124	1.42	0.00	1.53	0.13	0.23	0.17	0.02	50.16	30.69	0.51	0.41	85.27
etp125	1.57	0.00	1.46	0.60	0.23	0.15	0.02	48.66	29.96	0.80	0.42	83.89
etp126	4.69	0.02	1.38	1.37	0.20	0.12	0.05	45.95	28.75	1.28	0.39	84.23
etp127	5.96	0.03	1.37	1.10	0.15	0.19	0.07	45.41	27.78	1.14	0.46	83.67
etp128	4.26	0.01	1.27	5.09	0.15	0.14	0.05	40.88	24.42	3.37	0.35	79.99
etp129	5.88	0.17	1.46	0.12	0.19	0.11	0.06	46.75	29.76	0.54	0.37	85.42
etp130	9.81	0.02	0.84	0.12	2.10	0.06	0.12	42.09	31.05	0.79	0.18	87.20
etp131	30.28	2.93	1.11	0.29	0.18	0.13	0.58	29.18	18.91	0.54	0.24	84.36
etp132	31.85	3.68	1.19	0.20	0.18	0.13	0.62	28.87	16.93	0.43	0.27	84.37
etp133	22.67	1.76	1.23	0.16	0.18	0.08	0.45	34.92	23.06	0.43	0.26	85.22
etp134	15.32	3.72	1.02	0.21	0.20	0.09	0.35	36.61	25.37	0.46	0.31	83.67
etp135	29.92	0.52	0.49	0.26	2.61	0.05	0.72	33.22	16.56	1.15	0.20	85.69
etp135b	4.36	0.03	0.39	5.40	2.13	0.05	0.06	54.00	11.41	4.00	0.16	81.98
etp136	11.26	0.60	0.65	0.27	5.03	0.03	0.13	47.90	21.42	1.32	0.26	88.86
etp136	11.20	0.59	0.64	0.28	5.07	0.03	0.12	47.58	21.39	1.31	0.24	88.44
etp137	39.41	0.41	0.19	0.39	1.10	0.02	0.75	34.27	7.20	0.76	0.15	84.65
etp137b	39.61	0.40	0.18	0.38	1.09	0.02	0.74	34.18	7.17	0.76	0.15	84.69
etp138	3.62	0.03	0.89	0.13	6.05	0.03	0.09	49.92	27.92	1.32	0.36	90.34
etp139	4.04	0.08	0.84	0.20	6.19	0.01	0.07	50.63	27.40	1.20	0.38	91.04
etp142	19.45	0.03	1.24	0.36	0.32	0.08	0.15	37.37	26.86	0.49	0.26	86.60
etp143	29.68	0.03	1.51	0.56	0.56	0.11	0.18	32.14	21.75	0.66	0.23	87.41
etp144	11.22	0.03	1.01	0.12	1.67	0.08	0.16	40.51	30.69	0.70	0.21	86.39
etp145	20.48	0.02	0.84	0.17	1.42	0.08	0.23	35.69	27.40	0.60	0.21	87.14

-ID-	Fe2O3	MnO	TiO2	CaO	K2O	SO3	P2O5	SiO2	Al2O3	MgO	Na2O	Total
etp146	17.19	0.01	0.85	0.18	1.91	0.10	0.20	38.38	26.61	0.93	0.29	86.66
etp147	12.96	0.03	0.89	0.16	2.22	0.11	0.17	40.04	29.20	0.92	0.30	86.98
etp148	8.76	0.01	1.00	0.11	1.03	0.07	0.10	46.22	28.69	0.70	0.33	87.02
etp149	9.68	0.03	0.93	0.12	1.82	0.06	0.22	41.11	31.45	0.76	0.20	86.37
etp150	7.85	0.04	0.96	0.13	3.61	0.08	0.13	43.74	30.56	0.79	0.21	88.09
etp151	4.79	0.08	0.76	0.16	6.12	0.02	0.30	47.07	27.42	2.01	0.20	88.93
etp152	8.67	0.10	0.92	0.23	6.35	0.01	0.16	53.21	29.14	3.36	0.20	102.34
etp152b	7.59	0.09	0.81	0.20	5.63	0.01	0.14	46.79	25.77	2.84	0.20	90.07
etp153	5.03	0.01	0.82	0.19	6.70	0.01	0.08	52.24	26.56	0.95	0.57	93.15
etp154	7.57	0.09	0.70	0.20	7.36	0.00	0.10	48.50	23.69	2.40	0.38	90.99
etp155	6.04	0.03	0.73	0.77	6.30	0.01	0.41	50.77	24.46	1.35	1.68	92.57
etp156	4.18	0.02	0.75	0.86	5.08	0.01	0.48	52.24	24.24	2.12	2.84	92.82
etp157	4.79	0.08	0.73	6.70	0.90	0.19	0.03	57.08	12.26	1.49	0.37	84.63
etp158	4.61	0.04	0.76	3.96	0.58	5.52	0.02	59.81	11.61	1.12	0.49	88.55
etp159	9.93	0.01	0.85	0.27	1.15	0.16	0.06	42.90	28.35	1.26	0.25	85.18
etp160	10.45	0.04	0.70	5.53	1.96	0.06	0.10	33.55	24.36	4.39	0.14	81.27
etp161	4.08	0.03	0.40	16.86	0.66	0.18	0.09	19.92	14.92	11.15	0.13	68.42
etp162	8.66	0.04	0.88	0.15	3.45	0.05	0.20	43.27	30.62	0.90	0.17	88.41
etp163	7.94	1.11	0.81	0.16	5.42	0.07	0.14	45.73	26.83	0.80	0.41	89.42
etp164	6.61	0.03	0.85	0.22	4.50	0.17	0.15	46.55	27.98	0.95	0.57	88.57
etp165	3.51	0.78	0.80	0.11	7.83	0.04	0.28	50.03	26.60	0.62	0.23	90.84
etp166	8.06	0.05	0.90	0.18	7.39	0.01	0.17	48.02	24.72	1.46	0.11	91.06
etp167	4.53	1.06	0.75	0.27	4.99	0.03	0.08	48.97	25.64	2.21	1.36	89.89
etp168	9.68	0.04	0.82	0.21	3.52	0.02	0.10	43.71	28.20	1.86	0.43	88.60
etp169	8.50	0.20	0.78	6.67	2.92	0.11	0.43	50.89	17.56	4.17	4.44	96.67
etp170	9.34	0.17	0.86	5.41	1.67	0.33	0.40	51.71	17.29	3.64	5.76	96.57
etp180	4.06	0.06	0.54	11.91	0.51	16.63	0.02	40.75	8.72	0.90	0.37	84.47
etp182	5.64	0.09	0.85	2.07	0.89	0.19	0.03	68.68	12.92	1.56	0.54	93.46
etp183	4.99	0.10	0.76	2.97	0.74	3.45	0.03	61.36	11.78	1.37	0.51	88.06
etp184	5.88	0.03	0.89	0.26	0.59	0.17	0.03	66.16	13.16	1.25	0.51	88.93
etp185	5.32	0.10	0.73	4.13	1.01	3.73	0.04	57.82	12.88	1.30	0.54	87.61
etp186	8.68	0.10	0.90	3.07	0.75	0.12	0.07	48.16	20.02	2.59	0.38	84.85
etp187	4.71	0.07	0.74	4.13	0.65	3.71	0.02	60.33	11.12	1.31	0.48	87.30
etp188	8.23	0.05	1.03	0.41	0.47	0.12	0.03	59.70	16.19	1.08	0.36	87.67
□												

-ID-	ZnO	Cr2O3
etp001	0.002	0.007
etp002	0.000	0.003
etp003	0.001	0.006
etp004	0.000	0.009
etp005	0.003	-0.001
etp006	0.002	0.002
etp007	0.002	0.009
etp008	0.005	0.003
etp009	0.009	0.001
etp010	0.009	0.000
etp011	0.009	0.004
etp012	0.013	-0.003
etp013	0.012	0.004
etp014	0.020	0.001
etp015	0.040	0.007
etp016	0.014	0.003
etp017	0.022	0.002
etp018	0.015	-0.002
etp019	0.007	0.011
etp020	0.001	0.005
etp021	0.003	0.011
etp022	0.002	0.008
etp023	0.002	0.006
etp024	0.004	0.006
etp025	0.001	0.004
etp026	0.003	0.006
etp027	0.005	0.009
etp028	0.023	0.005
etp029	0.035	0.003
etp032	0.034	0.009
etp033	0.006	0.004
etp034	0.004	0.007
etp036	0.017	0.004
etp037	0.010	0.001
etp038	0.006	0.000
etp039	0.007	0.001

-ID-	ZnO	Cr2O3
etp040	0.009	-0.002
etp041	0.010	0.005
etp042	0.005	0.012
etp043	0.003	0.002
etp044	0.003	0.002
etp045	0.002	0.009
etp046	0.001	0.005
etp047	0.002	0.007
etp048	0.006	0.010
etp049	0.010	0.009
etp050	0.008	0.003
etp051	0.009	0.020
etp052	0.018	0.002
etp053	0.041	-0.001
etp054	0.013	0.001
etp056	0.012	0.006
etp057	0.012	0.003
etp058	0.011	0.003
etp059	0.010	0.003
etp060	0.009	0.006
etp061	0.008	0.001
etp062	0.006	-0.001
etp063	0.009	0.005
etp064	0.010	0.000
etp065	0.019	0.001
etp066	0.010	0.000
etp067	0.025	0.000
etp068	0.006	0.006
etp070	0.011	0.001
etp072	0.006	0.006
etp073	0.006	0.008
etp074	0.006	0.000
etp075	0.005	0.007
etp076	0.005	0.001
etp077	0.009	0.004
etp078	0.006	-0.001

-ID-	ZnO	Cr2O3
etp079	0.011	-0.003
etp080	0.012	-0.001
etp081	0.011	0.005
etp082	0.006	-0.003
etp086	0.006	0.005
etp087	0.005	0.013
etp087b	0.005	0.009
etp088	0.005	0.005
etp088b	0.006	-0.004
etp089	0.007	0.007
etp090	0.009	0.006
etp091	0.007	0.005
etp092b	0.004	-0.003
etp093	0.025	0.001
etp094	0.004	0.001
etp094b	0.002	0.003
etp095	0.011	0.002
etp096	0.009	-0.001
etp097	0.020	0.002
etp098	0.009	0.000
etp099	0.014	0.004
etp100	0.007	0.008
etp101	0.006	0.013
etp102	0.002	-0.020
etp103	0.003	0.010
etp103b	0.001	0.012
etp104	0.000	0.001
etp105b	0.000	0.004
etp106	0.001	0.003
etp107	0.002	0.001
etp107b	0.002	-0.003
etp108	0.007	0.000
etp108b	0.002	-0.005
etp109	0.003	0.008
etp110	0.004	0.001
etp111	0.006	0.002

-ID-	ZnO	Cr2O3
etp112	0.003	0.003
etp113	0.011	-0.002
etp114	0.017	0.001
etp115	0.013	0.000
etp116	0.016	-0.002
etp117	0.014	-0.001
etp118	0.007	0.007
etp119	0.003	0.012
etp120	0.006	0.010
etp121	0.012	0.004
etp122	0.004	0.002
etp122b	0.004	0.004
etp123	0.001	0.006
etp124	-0.001	0.008
etp125	0.001	0.004
etp126	0.005	0.007
etp127	0.005	0.002
etp128	0.007	0.007
etp129	0.008	0.009
etp130	0.002	0.004
etp131	0.022	0.010
etp132	0.021	0.005
etp133	0.009	0.012
etp134	0.017	0.006
etp135	0.041	0.001
etp135b	0.007	0.000
etp136	0.018	0.002
etp136	0.016	0.001
etp137	0.063	-0.001
etp137b	0.063	0.002
etp138	0.008	0.000
etp139	0.012	0.001
etp142	0.004	0.009
etp143	0.004	0.005
etp144	0.000	-0.001
etp145	-0.001	0.006

	ETP230	ETP231	ETP232	ETP233	ETP234	ETP235	ETP236	ETP237	ETP238	ETP239
SiO2	55.03	47.96	54.64	39.07	41.23	40.43	40.42	0.00	0.00	65.18
TiO2	0.75	0.65	1.08	1.35	1.11	1.15	1.12	0.00	0.00	0.81
Al2O3	9.71	9.21	16.74	16.14	25.09	26.04	26.69	0.00	0.00	11.97
Fe2O3	4.39	3.96	12.58	29.87	18.12	16.16	16.47	0.00	0.00	5.28
MnO	0.08	0.06	0.04	0.07	0.05	0.71	0.13	0.00	0.00	0.09
MgO	1.38	1.04	1.07	0.45	0.35	0.42	0.38	0.00	0.00	1.51
CaO	3.80	9.45	0.22	0.11	0.07	0.07	0.09	0.00	0.00	2.39
Na2O	0.46	0.39	0.59	0.49	0.29	0.42	0.37	0.00	0.00	0.53
K2O	0.70	0.55	0.32	0.24	0.10	0.16	0.19	0.00	0.00	0.85
P2O5	0.02	0.02	0.03	0.10	0.05	0.06	0.07	0.00	0.00	0.03
S	1.11	5.23	0.07	0.11	0.08	0.10	0.05	0.00	0.00	0.10
	77.44	78.52	87.38	87.99	86.54	85.72	85.97	0.00	0.00	88.74

	ETP240	ETP241	ETP242	ETP243	ETP244	ETP245	ETP246	ETP247	ETP248	ETP249
SiO2	40.95	42.27	38.01	27.92	22.62	42.74	49.70	37.10	0.00	48.71
TiO2	1.20	1.29	1.35	0.42	0.83	1.22	0.99	0.81	0.00	0.81
Al2O3	26.32	29.98	28.02	15.61	16.39	26.15	27.74	17.89	0.00	23.17
Fe2O3	10.53	10.77	15.65	4.39	10.16	15.90	6.93	7.72	0.00	7.83
MnO	0.05	0.03	0.05	0.02	0.03	0.07	0.04	0.01	0.00	0.05
MgO	2.09	0.75	0.71	9.67	9.08	0.67	0.57	5.87	0.00	2.07
CaO	2.15	0.16	0.21	13.63	12.90	0.17	0.21	8.15	0.00	0.20
Na2O	0.23	0.20	0.45	0.13	0.18	0.15	0.25	0.28	0.00	0.29
K2O	0.76	0.59	0.75	0.64	0.33	0.91	0.79	0.35	0.00	7.19
P2O5	0.06	0.07	0.16	0.04	0.10	0.11	0.18	0.17	0.00	0.16
S	0.04	0.02	0.05	0.03	0.05	0.01	0.03	0.05	0.00	0.00
	84.38	86.13	85.41	72.50	72.66	88.09	87.42	78.40	0.00	90.48

	ETP250	ETP251	ETP252	ETP253	ETP254	ETP255	ETP256	ETP257	ETP258	ETP259
SiO2	44.95	47.75	49.78	48.69	51.07	58.54	54.19	0.00	61.85	51.91
TiO2	0.87	0.93	0.87	0.94	0.73	0.80	0.62	0.00	0.80	0.70
Al2O3	26.05	24.19	22.93	21.94	21.10	20.67	17.54	0.00	11.27	10.12
Fe2O3	6.55	8.90	7.47	6.97	7.30	5.92	8.27	0.00	4.64	4.08
MnO	0.21	0.10	0.09	0.06	0.06	0.01	0.11	0.00	0.09	0.08
MgO	3.50	1.41	2.59	5.09	2.78	1.11	3.32	0.00	1.27	1.02
CaO	0.25	0.14	0.39	0.49	1.48	0.32	2.82	0.00	3.59	6.54
Na2O	0.12	0.39	3.13	1.92	2.51	0.10	5.60	0.00	0.48	0.51
K2O	5.01	6.54	2.42	3.97	5.27	3.79	3.71	0.00	0.74	0.53
P2O5	0.11	0.14	0.07	0.09	0.49	0.38	0.49	0.00	0.03	0.02
S	0.00	0.00	0.00	0.00	0.00	0.02	0.20	0.00	1.63	3.63
	87.62	90.49	89.74	90.16	92.79	91.66	96.87	0.00	86.38	79.14

ETP260	ETP261	ETP262	ETP263	ETP264	ETP265	ETP266	ETP267	ETP268	ETP269
61.73	43.79	33.72	34.18	39.74	44.10	37.04	28.86	39.11	46.06
0.93	0.95	1.24	0.92	1.06	1.28	0.96	0.83	1.16	1.00
13.37	17.80	14.21	21.87	25.57	30.28	23.40	21.62	27.44	30.28
5.78	21.31	40.69	28.16	18.94	7.85	23.93	25.35	16.11	5.87
0.01	0.01	0.04	0.02	0.02	0.00	0.02	0.01	0.01	0.01
0.84	0.61	0.32	0.30	0.34	0.43	0.43	2.55	0.36	0.36
0.43	0.15	0.07	0.08	0.09	0.12	0.25	3.85	0.13	0.12
0.46	0.39	0.24	0.26	0.38	0.47	0.27	0.15	0.33	0.27
0.46	0.26	0.24	0.13	0.20	0.19	0.28	0.29	0.35	0.61
0.03	0.05	0.08	0.11	0.09	0.06	0.12	0.17	0.13	0.07
0.20	0.12	0.18	0.16	0.10	0.09	0.05	0.04	0.05	0.04
84.24	85.44	91.04	86.19	86.52	84.88	86.75	83.72	85.19	84.68

ETP270	ETP271	ETP272	ETP273	ETP274	ETP275	ETP276	ETP277	ETP278	ETP279
44.08	48.03	54.73	48.04	51.35	59.31	60.38	54.69	42.53	43.56
0.80	1.39	0.76	0.90	0.97	0.88	0.80	0.93	1.06	0.99
31.27	24.87	23.98	27.36	27.00	19.80	20.11	22.50	25.71	23.28
8.87	12.67	6.72	7.68	5.37	7.55	6.43	7.24	11.40	11.42
0.01	0.01	0.01	0.01	0.00	0.07	0.18	0.21	0.12	0.13
0.42	0.27	0.74	0.73	0.89	0.79	0.73	0.98	0.94	4.49
0.10	0.14	0.18	0.25	0.29	0.20	0.16	0.28	0.20	0.29
0.18	0.12	0.22	0.20	0.20	0.12	0.09	0.10	0.16	0.52
1.04	0.34	3.06	0.66	1.25	4.55	4.23	4.24	3.70	3.61
0.10	0.16	0.13	0.13	0.11	0.18	0.18	0.14	0.21	0.08
0.03	0.01	0.01	0.01	0.01	0.00	0.00	0.00	0.00	0.00
86.91	88.01	90.54	85.97	87.44	93.45	93.29	91.31	86.02	88.37

ETP280	ETP281	ETP282	ETP283	ETP284	ETP285	ETP286	ETP287	ETP288	ETP289
47.24	50.36	52.40	0.00	0.00	0.00	0.00	0.00	0.00	62.10
0.90	0.81	0.77	0.00	0.00	0.00	0.00	0.00	0.00	0.99
21.39	19.25	17.78	0.00	0.00	0.00	0.00	0.00	0.00	15.22
10.27	8.88	8.38	0.00	0.00	0.00	0.00	0.00	0.00	9.21
0.12	0.13	0.17	0.00	0.00	0.00	0.00	0.00	0.00	0.05
3.58	1.82	4.40	0.00	0.00	0.00	0.00	0.00	0.00	0.98
0.36	2.43	4.46	0.00	0.00	0.00	0.00	0.00	0.00	0.26
1.00	3.01	4.28	0.00	0.00	0.00	0.00	0.00	0.00	0.52
5.38	4.53	3.82	0.00	0.00	0.00	0.00	0.00	0.00	0.62
0.06	0.50	0.45	0.00	0.00	0.00	0.00	0.00	0.00	0.03
0.00	0.00	0.09	0.00	0.00	0.00	0.00	0.00	0.00	0.07
90.30	91.72	97.00	0.00	0.00	0.00	0.00	0.00	0.00	90.05

	ETP290	ETP291	ETP292	ETP293	ETP294	ETP295	ETP296	ETP297	ETP298	ETP299
SiO2	50.24	46.91	44.90	31.57	39.34	41.02	34.06	45.98	0.00	40.79
TiO2	1.05	0.98	1.08	1.00	1.20	1.16	1.00	0.96	0.00	1.01
Al2O3	20.13	20.65	20.45	18.95	25.50	28.64	24.95	27.08	0.00	30.09
Fe2O3	14.75	15.27	19.43	34.81	20.07	15.58	22.27	12.28	0.00	12.56
MnO	0.03	0.03	0.03	0.01	0.01	0.02	0.03	0.01	0.00	0.04
MgO	0.64	0.56	0.51	0.32	0.31	0.30	0.26	0.38	0.00	0.54
CaO	0.19	0.18	0.15	0.17	0.13	0.08	0.09	0.14	0.00	0.19
Na2O	0.47	0.64	0.38	0.32	0.32	0.24	0.20	0.23	0.00	0.12
K2O	0.34	0.31	0.32	0.06	0.10	0.37	0.38	0.51	0.00	0.72
P2O5	0.06	0.06	0.09	0.09	0.09	0.13	0.15	0.10	0.00	0.12
S	0.09	0.11	0.11	0.06	0.05	0.03	0.03	0.02	0.00	0.02
	87.99	85.71	87.45	87.36	87.13	87.57	83.41	87.69	0.00	86.20

	ETP300	ETP301	ETP302	ETP303	ETP304	ETP305	ETP306	ETP307	ETP308	ETP309
SiO2	40.09	0.00	47.42	47.86	49.14	55.04	51.59	51.16	51.83	53.44
TiO2	0.99	0.00	0.95	0.87	0.80	0.76	0.74	0.83	0.80	0.75
Al2O3	29.43	0.00	26.06	27.13	25.62	21.80	20.45	18.07	18.45	17.07
Fe2O3	13.44	0.00	8.22	6.86	7.42	5.70	8.29	8.89	9.38	8.31
MnO	0.04	0.00	0.05	0.11	0.27	0.30	0.08	0.19	0.12	0.12
MgO	0.63	0.00	0.75	0.85	0.98	0.68	2.71	3.35	3.26	3.36
CaO	0.17	0.00	0.16	0.13	0.17	0.22	1.11	1.40	2.31	2.39
Na2O	0.10	0.00	0.25	0.25	0.33	3.46	4.08	4.14	5.01	4.72
K2O	0.79	0.00	5.37	5.21	5.45	5.85	2.29	3.72	2.30	4.02
P2O5	0.12	0.00	0.05	0.04	0.05	0.06	0.47	0.48	0.51	0.46
S	0.02	0.00	0.01	0.00	0.01	0.00	0.00	0.00	0.00	0.00
	85.82	0.00	89.30	89.31	90.24	93.87	91.81	92.23	93.97	94.64

	ETP310	ETP311	ETP312	ETP313	ETP314	ETP315	ETP316	ETP317	ETP318	ETP319
SiO2	64.18	50.30	52.25	54.78	53.27	67.75	67.46	66.37	61.14	53.63
TiO2	0.95	0.86	0.86	0.68	0.67	0.88	0.87	0.87	0.94	1.22
Al2O3	14.69	22.83	22.08	20.94	18.56	12.62	12.08	12.47	14.14	17.73
Fe2O3	7.61	9.28	8.57	7.35	8.31	5.44	5.67	5.22	6.83	13.40
MnO	0.15	0.06	0.03	0.13	0.13	0.11	0.09	0.11	0.02	0.01
MgO	0.53	0.70	0.77	1.88	2.67	1.39	1.27	1.27	0.96	0.59
CaO	0.48	0.36	0.36	0.92	2.02	0.33	0.57	1.49	0.22	0.16
Na2O	0.56	0.15	0.27	4.47	4.44	0.77	0.74	0.61	0.57	0.46
K2O	2.17	1.68	1.67	2.52	3.89	0.90	0.89	0.84	0.57	0.24
P2O5	0.12	0.11	0.09	0.33	0.55	0.03	0.03	0.03	0.03	0.04
S	0.02	0.01	0.00	0.00	0.01	0.12	0.23	0.73	0.07	0.12
	91.45	86.34	86.96	94.00	94.52	90.33	89.90	90.01	85.48	87.60

	ETP320	ETP321	ETP322	ETP323	ETP324	ETP325	ETP326	ETP327	ETP328	ETP329
SiO2	63.44	60.38	62.46	62.79	54.89	62.49	32.62	41.74	47.07	54.31
TiO2	0.81	0.86	0.87	0.85	0.77	0.96	0.70	0.91	1.02	0.73
Al2O3	12.20	14.18	13.25	13.20	12.05	16.14	19.91	25.78	32.84	22.63
Fe2O3	5.53	6.02	5.69	5.56	5.25	7.18	2.83	13.35	2.26	4.06
MnO	0.10	0.09	0.10	0.11	0.10	0.14	0.00	0.02	0.01	0.04
MgO	1.03	1.39	1.43	1.39	1.47	1.49	0.65	0.72	0.61	2.02
CaO	0.46	1.64	1.31	2.21	4.29	0.39	10.74	0.26	0.25	0.56
Na2O	0.28	0.42	0.55	0.56	0.77	0.69	0.35	0.29	0.30	3.11
K2O	0.93	1.03	1.07	1.05	0.96	1.13	0.39	0.50	0.59	5.55
P2O5	0.04	0.04	0.03	0.04	0.03	0.05	0.05	0.09	0.06	0.25
S	0.00	0.04	0.50	0.49	0.23	0.09	6.03	0.09	0.15	0.00
	84.82	86.09	87.26	88.24	80.80	90.74	74.27	83.75	85.15	93.26

	ETP330	ETP331	ETP332	ETP333
SiO2	51.12	57.04	53.77	57.08
TiO2	0.67	0.63	0.63	0.65
Al2O3	21.46	20.23	20.25	20.54
Fe2O3	6.26	5.23	6.38	5.52
MnO	0.07	0.06	0.17	0.05
MgO	2.47	1.62	2.75	2.56
CaO	0.91	1.11	1.76	1.62
Na2O	2.08	4.61	4.14	4.14
K2O	6.68	6.12	4.96	5.57
P2O5	0.44	0.54	0.49	0.49
S	0.00	0.00	0.00	0.00
	92.16	97.19	95.29	98.22

Appendix 4

XRF Trace element geochemistry data

SC	V	CR	MN	NI	CU	ZN	GA	AS	RB	SR	Y	ZR	NB	BA	LA	CE	PB	TH	U
26	94	48	1420	24	138	76	14	9	63	156	44	336	10	575	30	65	28	11	2
22	172	64	%10230	22	515	84	14	13	53	144	47	304	10	1120	24	115	38	9	4
24	162	68	2370	34	194	84	15	14	58	151	81	312	10	725	32	95	36	11	2
28	138	58	270	12	328	80	13	10	57	144	22	376	10	740	16	30	30	9	3
24	126	12	500	4	780	290	19	9	95	226	34	152	8	920	18	25	24	6	3
26	102	8	7780	4	1040	290	20	6	84	495	32	134	6	725	78	110	26	4	4
30	102	4	200	<2	122	34	13	8	107	221	13	128	6	585	10	15	166	4	1
26	86	82	335	14	44	52	12	6	41	312	17	318	10	420	14	40	20	9	6
34	108	58	95	12	30	46	14	6	31	140	13	302	12	400	14	25	12	10	5
28	356	32	220	10	160	108	21	16	11	99	10	212	12	340	12	15	26	11	3
30	172	22	110	10	120	40	23	7	12	111	11	296	14	1020	14	20	22	7	3
30	276	20	135	14	142	14	28	8	17	144	12	240	14	305	16	25	54	8	8
22	72	44	35	20	100	14	28	2	15	158	18	292	18	145	16	20	14	14	3
20	80	22	120	18	126	18	28	2	16	63	12	280	16	90	16	25	14	10	2
34	168	30	175	18	172	30	25	5	18	71	12	258	16	75	20	20	32	9	2
26	358	36	175	10	4220	156	22	4	65	670	13	66	2	760	14	20	6	2	<1
36	384	36	160	14	8180	218	21	8	43	1020	13	62	2	500	12	15	4	3	<1
24	268	42	135	8	2500	136	17	8	55	980	12	62	2	520	14	20	2	3	<1
24	302	32	140	12	228	48	21	16	23	76	10	218	10	515	10	15	22	12	3
28	286	30	130	12	312	14	30	22	9	43	7	146	6	545	12	15	36	13	3
26	332	44	155	12	376	14	28	19	9	33	6	138	6	340	10	20	40	12	3
32	246	30	85	12	310	10	28	7	11	32	7	176	10	275	10	15	28	7	3
38	492	14	220	10	855	12	29	13	14	83	20	112	6	110	38	90	68	5	5
40	272	46	60	2	710	16	29	12	13	94	8	94	4	80	10	10	46	4	2
38	284	40	100	6	452	14	32	6	20	73	8	168	10	235	10	20	18	6	1
42	108	52	540	4	850	16	25	31	17	124	11	104	4	390	18	50	52	4	1
30	262	44	65	4	520	18	18	44	20	68	8	66	4	250	12	15	64	2	1
16	294	38	60	14	170	176	13	34	17	550	18	196	10	295	8	15	64	7	4
14	338	32	80	14	176	230	9	42	12	595	20	176	12	220	8	10	64	7	4

SC	V	CR	MN	NI	CU	ZN	GA	AS	RB	SR	Y	ZR	NB	BA	LA	CE	PB	TH	U
10	318	32	65	8	410	276	7	49	8	310	16	110	8	255	8	10	52	4	3
14	136	36	830	18	1610	238	10	63	10	293	21	146	8	405	20	55	56	5	4
14	276	14	385	12	1550	44	26	25	16	149	18	226	12	190	22	35	58	8	2
14	344	12	255	12	1850	44	21	16	19	106	18	254	12	115	26	45	42	8	2
24	140	4	115	6	4750	90	21	16	71	525	17	70	4	35	12	25	6	2	<1
34	136	68	1070	8	4800	166	25	4	58	196	18	84	4	480	24	70	2	3	2
38	272	14	705	8	7740	106	25	6	55	374	34	86	6	345	20	45	4	2	1
30	254	6	100	8	6400	86	22	4	62	895	22	78	4	155	32	55	6	2	<1
24	252	6	390	6	3620	70	17	4	40	770	19	68	6	330	52	110	<2	2	1
28	146	4	540	8	4730	84	21	2	57	1090	21	70	2	495	58	130	4	3	1
26	172	6	125	8	2750	74	17	4	44	625	19	64	2	90	22	50	<2	2	1
20	52	38	170	18	130	56	28	1	19	78	13	314	20	85	28	30	22	10	2
14	56	22	95	12	108	50	28	1	17	182	12	214	14	140	30	45	22	8	2
6	54	6	40	2	106	14	13	<1	13	374	5	60	4	535	16	30	10	2	1
18	230	6	140	<2	630	16	31	4	70	262	16	134	8	470	34	70	22	4	2
16	218	6	140	<2	660	18	30	4	48	271	13	126	8	490	36	75	20	5	<1
14	96	64	800	16	64	52	12	5	48	270	27	334	10	475	26	60	14	9	3
12	154	24	1100	10	194	26	23	6	34	238	14	116	6	115	18	35	12	4	4
26	214	10	330	6	720	16	28	5	21	135	19	116	8	155	36	45	24	3	3
12	100	44	1160	16	124	48	11	5	58	216	40	350	10	525	34	75	18	9	3
16	186	16	235	6	800	46	21	4	74	388	26	150	8	945	58	105	14	6	3
16	190	4	55	2	1040	60	16	4	76	735	24	100	6	1160	54	110	26	3	2
16	170	2	110	<2	2590	170	22	4	83	458	103	82	4	525	58	105	10	2	1
24	298	2	355	6	6970	140	30	5	44	630	18	34	<2	680	18	45	12	1	<1
8	8270	116	23	5	66	990	15	44	2	8	4	1							
22	68	2	1840	6	6560	112	22	2	59	695	14	44	<2	815	14	30	4	<1	<1
34	144	14	60	14	5820	116	19	3	53	940	18	74	4	950	42	80	4	2	<1
34	132	2	70	14	5340	104	17	3	62	1090	18	68	4	1060	96	185	2	2	1
34	282	<2	435	14	3700	108	18	4	54	890	17	70	4	315	36	70	<2	2	2
34	142	58	1000	14	4910	74	17	3	59	1200	18	70	4	540	28	70	<2	1	1

SC	V	CR	MN	NI	CU	ZN	GA	AS	RB	SR	Y	ZR	NB	BA	LA	CE	PB	TH	U
28	190	6	1770	8	1890	54	16	2	49	515	13	60	2	1120	18	40	<2	2	2
32	202	6	500	8	2170	58	17	2	57	510	14	62	4	1050	24	45	2	3	1
26	216	6	940	8	2380	60	16	3	72	293	12	62	4	1000	6	15	<2	3	<1
30	306	10	685	10	5300	94	23	4	92	377	19	84	6	1560	6	15	2	4	<1
40	276	8	1040	14	7440	168	26	4	228	260	79	100	6	815	26	45	4	4	2
30	344	14	1080	10	3790	86	23	4	82	461	57	88	6	1860	10	35	4	2	<1
32	300	14	485	14	6250	138	22	3	105	595	16	84	6	1550	22	25	4	3	<1
34	262	18	1370	16	440	68	18	3	63	1430	18	74	4	1020	14	25	<2	1	1
22	220	4	700	8	%18090	64	18	3	52	398	16	62	2	635	12	30	22	<1	1
26	248	6	1430	12	7700	102	18	2	52	1100	17	68	4	1020	14	30	<2	2	<1
16	226	4	1040	4	1580	46	18	3	53	1660	18	46	<2	1280	14	30	4	2	1
16	110	50	860	18	52	52	12	6	52	180	26	366	10	450	28	65	16	10	1

SC	V	CR	MN	NI	CU	ZN	GA	AS	RB	SR	Y	ZR	NB	BA	LA	CE	PB	TH	U
16	106	54	1240	24	50	58	13	6	49	150	21	358	10	430	22	90	18	11	4
14	122	32	110	12	180	52	26	17	19	%106630	16	2790	4	1070	26	50	28	7	<1
16	855	36	185	8	214	24	21	68	9	525	13	160	6	720	24	35	34	16	14
18	218	10	105	8	260	20	27	17	15	114	20	206	12	130	28	45	22	8	6
20	316	12	2970	6	368	14	26	19	16	145	35	200	10	255	58	220	22	9	2
16	216	6	120	<2	326	12	24	11	19	100	20	192	10	100	28	40	14	8	1
12	78	4	75	2	202	12	18	3	19	735	29	128	8	160	34	70	10	5	2
12	142	4	220	4	358	62	14	21	51	166	9	94	4	90	14	25	38	3	1
22	300	4	145	<2	645	30	27	8	51	164	16	124	8	180	32	70	26	4	<1
20	236	4	130	<2	955	38	27	15	74	117	18	112	6	155	20	40	10	4	<1
14	128	2	115	<2	458	32	25	4	60	175	15	106	6	260	22	50	16	4	<1
22	308	6	85	<2	800	24	30	13	36	179	14	130	8	270	38	95	100	4	<1
20	286	4	900	4	3100	90	19	17	100	505	11	98	4	755	20	40	8	2	<1
16	178	4	450	2	1670	90	20	6	75	520	14	86	6	550	20	40	10	4	2
16	174	2	135	2	1540	72	20	5	84	570	13	86	6	730	22	50	10	2	<1
18	220	4	1090	4	4670	152	22	11	117	303	14	98	4	855	16	30	8	3	1
18	184	2	530	4	3770	146	24	5	86	426	17	94	6	1080	16	40	8	4	2
12	92	52	650	18	44	50	12	6	50	199	29	356	10	605	26	60	14	11	2
14	100	94	345	14	42	50	13	6	40	309	17	322	10	445	16	50	18	10	6
14	116	60	90	12	28	44	14	6	31	141	13	316	12	405	16	25	12	11	4
28	336	32	190	10	158	108	21	16	11	100	11	216	12	300	12	15	24	9	2
30	162	22	90	10	118	40	23	6	13	115	11	290	14	850	12	15	24	6	3
22	254	16	110	12	138	16	28	8	16	144	12	244	14	260	16	20	52	8	8
22	66	36	25	18	98	14	28	2	15	165	18	294	18	120	14	15	12	14	2
22	66	18	90	18	122	18	27	2	16	66	12	278	16	75	16	20	14	9	2
18	154	28	140	20	164	30	26	6	18	76	12	264	16	65	18	20	30	10	2
22	204	24	215	22	198	40	28	7	15	79	12	264	16	170	22	30	42	11	2
20	140	34	120	20	226	64	25	7	14	129	23	226	14	160	22	15	24	11	2
22	142	34	865	20	282	70	29	5	16	74	14	278	16	190	24	50	52	10	2
18	258	4	150	<2	1210	20	26	5	52	97	12	106	8	225	12	25	6	4	1

SC	V	CR	MN	NI	CU	ZN	GA	AS	RB	SR	Y	ZR	NB	BA	LA	CE	PB	TH	U
16	212	16	145	4	284	20	31	6	22	244	11	164	8	360	28	50	16	5	8
18	192	10	90	2	398	14	34	5	26	6560	12	218	8	490	32	60	14	6	7
16	54	4	70	<2	362	10	30	1	17	158	7	132	8	240	24	35	8	5	7
22	505	10	2510	2	620	18	30	8	42	238	14	104	6	830	36	95	16	4	4
16	230	<2	275	4	2880	78	18	2	114	720	15	86	4	1230	24	35	10	3	<1
16	164	<2	555	2	3650	96	21	5	107	960	16	84	6	2630	16	35	8	3	1

Appendix 5

Fe-Mn nodule SEM EDXA data

Sample No	MnO	SiO2	Al2O3	Fe2O3	BaO	K2O	CaO	MgO
1	46.62	9.7	8.05	2.58	8.96	0.41	0.48	0.44
2	51.27	6.1	5.47	1.68	11.52	0.23	0.48	0.2
3	55.15	3.67	3.8	2.46	11.57	0.22	0.56	0.35
4	59.37	0.26	0.41	0.62	13.17	0.23	0.61	0.25
5	58.39	0.49	1.66	2.63	8.81	0.78	0.33	0.28
6	57.58	2.15	2.44	1.34	12.19	0.21	0.57	0.33
7	58.32	7.47	6.86	3.27	6.19	0.44	0.33	0.15
8	59.34	0.33	0.95	1.12	11.85	0.24	0.52	0.35
9	64.26	0.36	1.01	2.51	7.46	1.24	0.48	0.17
10	59.79	3.84	3.77	2.38	8.36	0.61	0.41	0.11
11	64.03	4.44	4.15	2.37	3.91	0.35	0.24	0
12	58.84	7.41	6.76	3.31	0	0.44	0.34	0.14
13	65.72	5.08	4.32	1.9	2.66	0.33	0.29	0
14	56.94	5.53	5.14	2.69	9	0.51	0.38	0
15	55.88	3.21	4.68	1.35	8.7	0.34	0.22	0.05
16	54.34	0.95	4.55	2.34	10.61	0.33	0.56	0.31
17	52.36	6.7	3.9	1.51	9.65	0.11	0.36	0.15
18	56.31	5.8	3.66	2.16	8.79	0.43	0.41	0.29
19	55.68	2.9	4.57	3.32	11.65	0.26	0.38	0
20	59.61	4.23	6.21	3.27	7.93	0.33	0.47	0.25

Appendix 6

Trace element ICP MS data

AUSTRALIAN LABORATORY SERVICES P/L

A.C.N. 009 936 029

ANALYTICAL REPORT

CONTACT: MR E TONUI
CLIENT: NORTH LTD
ADDRESS: GEOLOGY DEPT.
ANU
ACT 0200

LABORATORY: ORANGE
BATCH NUMBER: OR5437
SUB BATCH: 0
No. OF SAMPLES: 186
DATE RECEIVED: 30/01/96
DATE COMPLETED: 07/02/96

No.: NSW0706 SAMPLE TYPE: REGOLITH PROJECT:

LE NUMBER	ELEMENT UNIT METHOD L.O.R.	Cu ppm IC580 2	Pb ppm IC580 5	Zn ppm IC580 2	Ag ppm IC580 1	As ppm IC580 1	Au ppm PM204 0.001
ETP001		236	50	2	<1	14	0.003
ETP002		294	27	2	<1	8	0.008
ETP003		302	37	4	<1	9	0.004
ETP004		458	45	12	<1	22	0.033
ETP005		353	25	16	<1	8	0.784
ETP006		542	24	7	<1	6	0.004
ETP007		606	19	5	<1	3	0.025
ETP008		966	17	8	<1	7	0.008
ETP009		2230	9	78	<1	2	0.011
ETP010		2530	14	79	<1	5	<0.001
ETP011		2880	11	79	<1	2	<0.001
ETP012		5080	9	111	<1	<1	<0.001
ETP013		3280	8	99	<1	1	<0.001
ETP014		3250	22	142	<1	6	0.058
ETP015		3170	1880	314	<1	4	0.193
ETP016		4160	7	139	<1	1	<0.001
ETP017		7200	7	181	<1	6	0.015
ETP018		2390	7	121	<1	7	0.106
ETP019		233	27	38	<1	15	0.008
ETP020		317	46	5	<1	20	0.011
ETP021		369	48	6	<1	18	0.016
ETP022		301	31	6	<1	4	0.011
ETP023		801	60	4	<1	12	0.048
ETP024		661	47	9	<1	12	0.016
ETP025		467	18	10	<1	5	0.034
ETP026		790	53	14	<1	32	0.114
ETP027		586	63	24	<1	53	0.033
ETP028		203	25	193	<1	13	0.010
ETP029		220	27	262	1	25	0.003
ETP030		783	16	354	2	12	0.031

ITS:

Extra gold check on sample number ETP036: 1.54ppm.

he Final Report which supersedes any preliminary reports with this batch number. • Results apply to sample(s) as submitted by client.

s Laboratory
52 6020 Fax: (089) 52 6028
oratory
46 1390 Fax: (054) 46 1389
boratory
243 7222 Fax: (07) 3243 7218
vers Laboratory
87 4155 Fax: (077) 87 4220

Cloncurry Laboratory
Phone: (077) 42 1323 Fax: (077) 42 1685
Kalgoorlie Laboratory
Phone: (090) 21 1457 Fax: (090) 21 6253
Mt Isa Laboratory
Phone: (077) 49 5545 Fax: (077) 49 5546
New Zealand Laboratory
Phone: (07) 575 7654 Fax: (07) 575 7641

Orange Laboratory
Phone: (063) 63 1722 Fax: (063) 63 1189
Perth Laboratory
Phone: (09) 249 2988 Fax: (09) 249 2942
Townsville Laboratory
Phone: (077) 79 9155 Fax: (077) 79 9729

All pages of this report have been checked and approved for release.

AUSTRALIAN LABORATORY SERVICES P/L
A.C.N. 009 936 029

ANALYTICAL REPORT

CONTACT: MR E TONUI
CLIENT: NORTH LTD
ADDRESS: GEOLOGY DEPT.
ANU
ACT 0200

LABORATORY: ORANGE
BATCH NUMBER: OR5437
SUB BATCH: 0
No. OF SAMPLES: 186
DATE RECEIVED: 30/01/96
DATE COMPLETED: 07/02/96

lo.: NSW0706 SAMPLE TYPE: REGOLITH PROJECT:

LE NUMBER	ELEMENT UNIT METHOD L.O.R.	Cu ppm IC580 2	Pb ppm IC580 5	Zn ppm IC580 2	Ag ppm IC580 1	As ppm IC580 1	Au ppm PM204 0.001
ETP061		1860	7	42	<1	1	0.019
ETP062		2090	7	47	<1	1	0.041
ETP063		2000	7	47	<1	1	0.017
ETP064		4600	7	66	<1	<1	0.011
ETP065		6840	7	125	<1	3	0.067
ETP066		3780	7	69	<1	1	0.019
ETP067		6280	7	111	<1	2	0.034
ETP068		467	5	45	<1	4	0.015
ETP069		1.84%	25	38	3	3	0.870
ETP070		7600	6	78	<1	<1	0.168
ETP071		1830	5	28	1	3	0.051
ETP072		145	14	45	<1	6	0.014
ETP073		124	14	41	<1	5	0.012
ETP074		164	13	40	<1	5	0.004
ETP075		469	12	36	<1	7	0.009
ETP076		649	14	42	<1	5	0.005
ETP077		636	11	35	<1	3	0.012
ETP078		628	8	30	<1	4	0.009
ETP079		2270	6	82	<1	5	0.012
ETP080		2600	5	85	<1	6	0.054
ETP081		2180	5	82	<1	4	0.112
ETP082		3890	7	52	<1	1	0.231
ETP083		1.14%	7	49	<1	4	2.30
ETP084		2880	7	60	<1	2	0.299
ETP085		3300	5	46	<1	<1	0.380
ETP086		66	15	40	<1	7	0.041
ETP087		92	19	41	<1	8	0.037
ETP088		117	11	16	<1	9	0.131
ETP089		275	18	24	<1	17	0.042
ETP090		358	13	41	<1	10	0.088

ITS:

he Final Report which supersedes any preliminary reports with this batch number. • Results apply to sample(s) as submitted by client.

Laboratory
52 6020 Fax: (069) 52 6028
oratory
46 1390 Fax: (054) 46 1389
oratory
243 7222 Fax: (07) 3243 7218
vers Laboratory
87 4155 Fax: (077) 87 4220

Cloncurry Laboratory
Phone: (077) 42 1323 Fax: (077) 42 1685
Kalgoorlie Laboratory
Phone: (090) 21 1457 Fax: (090) 21 6253
Mt Isa Laboratory
Phone: (077) 49 5545 Fax: (077) 49 5546
New Zealand Laboratory
Phone: (07) 575 7654 Fax: (07) 575 7641

Orange Laboratory
Phone: (063) 63 1722 Fax: (063) 63 1189
Perth Laboratory
Phone: (09) 249 2988 Fax: (09) 249 2942
Townsville Laboratory
Phone: (077) 79 9155 Fax: (077) 79 9729

AUSTRALIAN LABORATORY SERVICES P/L

A.C.N. 009 936 029

ANALYTICAL REPORT

CONTACT: MR E TONUI
CLIENT: NORTH LTD
ADDRESS: GEOLOGY DEPT.
ANU
ACT 0200

LABORATORY: ORANGE
BATCH NUMBER: OR5437
SUB BATCH: 0
No. OF SAMPLES: 186
DATE RECEIVED: 30/01/96
DATE COMPLETED: 07/02/96

No.: NSW0706 SAMPLE TYPE: REGOLITH PROJECT:

LE NUMBER	ELEMENT UNIT METHOD L.O.R.	Cu ppm IC580 2	Pb ppm IC580 5	Zn ppm IC580 2	Ag ppm IC580 1	As ppm IC580 1	Au ppm PM204 0.001
ETP121		134	24	78	<1	12	0.012
ETP122		100	23	28	<1	3	0.034
ETP123		114	54	8	<1	6	0.024
ETP124		90	15	10	<1	<1	0.048
ETP125		112	16	13	<1	<1	0.014
ETP126		158	31	22	<1	6	0.012
ETP127		181	41	29	<1	8	0.008
ETP128		214	24	52	<1	4	0.040
ETP129		266	58	54	<1	4	0.008
ETP130		940	12	128	<1	7	0.002
ETP131		599	52	117	<1	26	0.028
ETP132		518	48	137	<1	29	0.078
ETP133		1310	63	71	<1	28	0.014
ETP134		1490	55	69	<1	14	0.012
ETP135		900	82	46	<1	16	0.006
ETP136		1.05%	19	291	<1	89	0.012
ETP137		8350	232	479	<1	88	0.074
ETP138		2710	115	117	<1	11	0.112
ETP139		2980	49	58	<1	1	<0.001
ETP140		2020	12	48	<1	9	0.002
ETP141		191	25	38	<1	11	0.010
ETP142		228	29	43	<1	36	0.004
ETP143		241	28	29	<1	51	0.016
ETP144		491	18	16	<1	7	0.002
ETP145		589	19	19	<1	18	<0.001
ETP146		905	12	20	<1	16	0.414
ETP147		963	24	16	<1	10	<0.001
ETP148		644	17	19	<1	17	0.064
ETP149		1230	11	19	<1	5	0.018
ETP150		1000	11	16	<1	7	<0.001

NTS:

he Final Report which supersedes any preliminary reports with this batch number. • Results apply to sample(s) as submitted by client.

s Laboratory
52 6020 Fax: (089) 52 6028
oratory
46 1390 Fax: (054) 46 1389
boratory
243 7222 Fax: (07) 3243 7218
wers Laboratory
87 4155 Fax: (077) 87 4220

Cloncurry Laboratory
Phone: (077) 42 1323 Fax: (077) 42 1685
Kalgoorlie Laboratory
Phone: (090) 21 1457 Fax: (090) 21 6253
Mt Isa Laboratory
Phone: (077) 49 5545 Fax: (077) 49 5546
New Zealand Laboratory
Phone: (07) 575 7654 Fax: (07) 575 7641

Orange Laboratory
Phone: (063) 63 1722 Fax: (063) 63 1189
Perth Laboratory
Phone: (09) 249 2988 Fax: (09) 249 2942
Townsville Laboratory
Phone: (077) 79 9155 Fax: (077) 79 9729

AUSTRALIAN LABORATORY SERVICES P/L

A.C.N. 009 936 029

ANALYTICAL REPORT

CONTACT: MR E TONUI
CLIENT: NORTH LTD
ADDRESS: GEOLOGY DEPT.
ANU
ACT 0200

LABORATORY: ORANGE
BATCH NUMBER: OR5437
SUB BATCH: 0
No. OF SAMPLES: 186
DATE RECEIVED: 30/01/96
DATE COMPLETED: 07/02/96

lo.: NSW0706 SAMPLE TYPE: REGOLITH PROJECT:

.E NUMBER	ELEMENT UNIT METHOD L.O.R.	Cu ppm IC580 2	Pb ppm IC580 5	Zn ppm IC580 2	Ag ppm IC580 1	As ppm IC580 1	Au ppm PM204 0.001
ETP151		3370	16	56	<1	5	<0.001
ETP152		4300	<5	88	<1	4	0.004
ETP153		1470	13	41	<1	<1	<0.001
ETP154		3980	5	83	<1	6	<0.001
ETP155		2480	5	82	<1	4	0.030
ETP156		3760	<5	130	<1	5	0.588
ETP157		93	13	48	<1	8	0.042
ETP158		45	11	46	<1	5	0.026
ETP159		267	5	9	<1	2	0.132
ETP160		472	7	15	<1	8	0.004
ETP161		428	<5	8	<1	2	0.014
ETP162		941	5	25	<1	8	0.018
ETP163		1240	21	25	2	5	0.034
ETP164		1250	<5	23	<1	1	0.014
ETP165		1850	24	19	<1	5	0.026
ETP166		3050	12	79	1	9	0.050
ETP167		3820	42	95	<1	2	0.004
ETP168		3520	<5	82	<1	6	0.010
ETP169		1090	<5	47	<1	7	0.086
ETP170		3500	<5	41	<1	4	0.292
ETP171		641	10	189	3	10	0.042
ETP172		34	<5	9	<1	3	0.020
ETP173		634	46	9	<1	21	0.020
ETP174		737	57	7	<1	22	0.020
ETP175		338	59	6	<1	26	0.024
ETP176		260	29	4	<1	12	0.100
ETP177		407	61	5	<1	17	0.044
ETP178		369	59	7	<1	22	0.016
ETP179		155	6	26	<1	4	0.136
ETP180		100	13	49	<1	4	0.042

TS:

ıe Final Report which supersedes any preliminary reports with this batch number. • Results apply to sample(s) as submitted by client.

i Laboratory
i2 6020 Fax: (089) 52 6028
ıratory
l6 1390 Fax: (054) 46 1389
ıratory
243 7222 Fax: (07) 3243 7218
ıers Laboratory
37 4155 Fax: (077) 87 4220

Cloncurry Laboratory
Phone: (077) 42 1323 Fax: (077) 42 1685
Kalgoorlie Laboratory
Phone: (090) 21 1457 Fax: (090) 21 6253
Mt Isa Laboratory
Phone: (077) 49 5545 Fax: (077) 49 5546
New Zealand Laboratory
Phone: (07) 575 7654 Fax: (07) 575 7641

Orange Laboratory
Phone: (063) 63 1722 Fax: (063) 63 1189
Perth Laboratory
Phone: (09) 249 2988 Fax: (09) 249 2942
Townsville Laboratory
Phone: (077) 79 9155 Fax: (077) 79 9729

AUSTRALIAN LABORATORY SERVICES P/L

A.C.N. 009 936 029

ANALYTICAL REPORT

CONTACT: MR E TONUI
CLIENT: NORTH LTD
ADDRESS: GEOLOGY DEPT.
ANU
ACT 0200

LABORATORY: ORANGE
BATCH NUMBER: OR5437
SUB BATCH: 0
No. OF SAMPLES: 186
DATE RECEIVED: 30/01/96
DATE COMPLETED: 07/02/96

lo.: NSW0706 SAMPLE TYPE: REGOLITH PROJECT:

.E NUMBER	ELEMENT UNIT METHOD L.O.R.	Cu ppm IC580 2	Pb ppm IC580 5	Zn ppm IC580 2	Ag ppm IC580 1	As ppm IC580 1	Au ppm PM204 0.001
ETP181		279	18	53	<1	6	0.064
ETP182		114	16	48	<1	7	0.044
ETP183		106	15	50	<1	7	0.014
ETP184		71	10	45	<1	7	0.020
ETP185		228	16	53	<1	5	0.044
ETP186		563	11	31	<1	6	0.054

TS:

ıe Final Report which supersedes any preliminary reports with this batch number. • Results apply to sample(s) as submitted by client.

ı Laboratory
12 6020 Fax: (089) 52 6028
ıratory
16 1390 Fax: (054) 46 1389
ıratory
143 7222 Fax: (07) 3243 7218
ers Laboratory
87 4155 Fax: (077) 87 4220

Cloncurry Laboratory
Phone: (077) 42 1323 Fax: (077) 42 1685
Kalgoorlie Laboratory
Phone: (090) 21 1457 Fax: (090) 21 6253
Mt Isa Laboratory
Phone: (077) 49 5545 Fax: (077) 49 5546
New Zealand Laboratory
Phone: (07) 575 7654 Fax: (07) 575 7641

Orange Laboratory
Phone: (063) 63 1722 Fax: (063) 63 1189
Perth Laboratory
Phone: (09) 249 2988 Fax: (09) 249 2942
Townsville Laboratory
Phone: (077) 79 9155 Fax: (077) 79 9729

AUSTRALIAN LABORATORY SERVICES P/L

A.C.N. 009 936 029

ANALYTICAL REPORT

CONTACT: MR E TONUI
CLIENT: NORTH LTD
ADDRESS: GEOLOGY DEPT.
ANU
ACT 0200

LABORATORY: ORANGE
BATCH NUMBER: OR5437
SUB BATCH: 0
No. OF SAMPLES: 186
DATE RECEIVED: 30/01/96
DATE COMPLETED: 07/02/96

lo.: NSW0706 SAMPLE TYPE: REGOLITH PROJECT:

.E NUMBER	ELEMENT UNIT METHOD L.O.R.	Au PM204 ppm CHECKS 0.001					
ETP001							
ETP002							
ETP003							
ETP004							
ETP005							
ETP006							
ETP007							
ETP008							
ETP009							
ETP010		<0.001					
ETP011							
ETP012							
ETP013		<0.001					
ETP014							
ETP015							
ETP016							
ETP017							
ETP018							
ETP019							
ETP020							
ETP021							
ETP022							
ETP023							
ETP024							
ETP025							
ETP026							
ETP027							
ETP028		0.012					
ETP029							
ETP030							

TS:

ıe Final Report which supersedes any preliminary reports with this batch number. • Results apply to sample(s) as submitted by client.

Laboratory
2 6020 Fax: (089) 52 6028
ratory
6 1390 Fax: (054) 46 1389
oratory
43 7222 Fax: (07) 3243 7218
ers Laboratory
7 4155 Fax: (077) 87 4220

Cloncurry Laboratory
Phone: (077) 42 1323 Fax: (077) 42 1685
Kalgoorlie Laboratory
Phone: (090) 21 1457 Fax: (090) 21 6253
Mt Isa Laboratory
Phone: (077) 49 5545 Fax: (077) 49 5546
New Zealand Laboratory
Phone: (07) 575 7654 Fax: (07) 575 7641

Orange Laboratory
Phone: (063) 63 1722 Fax: (063) 63 1189
Perth Laboratory
Phone: (09) 249 2988 Fax: (09) 249 2942
Townsville Laboratory
Phone: (077) 79 9155 Fax: (077) 79 9729

AUSTRALIAN LABORATORY SERVICES P/L

A.C.N. 009 936 029

ANALYTICAL REPORT

CONTACT: MR E TONUI
CLIENT: NORTH LTD
ADDRESS: GEOLOGY DEPT.
ANU
ACT 0200

LABORATORY: ORANGE
BATCH NUMBER: OR5437
SUB BATCH: 0
No. OF SAMPLES: 186
DATE RECEIVED: 30/01/96
DATE COMPLETED: 07/02/96

o.: NSW0706 SAMPLE TYPE: REGOLITH PROJECT:

.E NUMBER	ELEMENT UNIT METHOD L.O.R.	Au PM204 ppm CHECKS 0.001					
ETP031							
ETP032							
ETP033							
ETP034							
ETP035							
ETP036		3.03					
ETP037							
ETP038							
ETP039							
ETP040							
ETP041							
ETP042							
ETP043							
ETP044							
ETP045							
ETP046							
ETP047							
ETP048							
ETP049							
ETP050							
ETP051							
ETP052		0.006					
ETP053							
ETP054							
ETP055							
ETP056							
ETP057		0.546					
ETP058							
ETP059							
ETP060							

TS:

ıe Final Report which supersedes any preliminary reports with this batch number. • Results apply to sample(s) as submitted by client.

Laboratory
i2 6020 Fax: (089) 52 6028
ratory
6 1390 Fax: (054) 46 1389
oratory
43 7222 Fax: (07) 3243 7218
ers Laboratory
7 4155 Fax: (077) 87 4220

Cloncurry Laboratory
Phone: (077) 42 1323 Fax: (077) 42 1685
Kalgoorlie Laboratory
Phone: (090) 21 1457 Fax: (090) 21 6253
Mt Isa Laboratory
Phone: (077) 49 5545 Fax: (077) 49 5546
New Zealand Laboratory
Phone: (07) 575 7654 Fax: (07) 575 7641

Orange Laboratory
Phone: (063) 63 1722 Fax: (063) 63 1189
Perth Laboratory
Phone: (09) 249 2988 Fax: (09) 249 2942
Townsville Laboratory
Phone: (077) 79 9155 Fax: (077) 79 9729

AUSTRALIAN LABORATORY SERVICES P/L

A.C.N. 009 936 029

ANALYTICAL REPORT

CONTACT: MR E TONUI
CLIENT: NORTH LTD
ADDRESS: GEOLOGY DEPT.
ANU
ACT 0200

LABORATORY: ORANGE
BATCH NUMBER: OR5437
SUB BATCH: 0
No. OF SAMPLES: 186
DATE RECEIVED: 30/01/96
DATE COMPLETED: 07/02/96

lo.: NSW0706 SAMPLE TYPE: REGOLITH PROJECT:

.E NUMBER	ELEMENT UNIT METHOD L.O.R.	Au PM204 ppm CHECKS 0.001					
ETP061		0.024					
ETP062							
ETP063							
ETP064							
ETP065							
ETP066							
ETP067							
ETP068							
ETP069		0.873					
ETP070							
ETP071		0.053					
ETP072							
ETP073							
ETP074							
ETP075							
ETP076							
ETP077							
ETP078							
ETP079							
ETP080							
ETP081		0.100					
ETP082							
ETP083		1.48					
ETP084							
ETP085							
ETP086							
ETP087							
ETP088							
ETP089							
ETP090							

TS:

ıe Final Report which supersedes any preliminary reports with this batch number. • Results apply to sample(s) as submitted by client.

Laboratory
ż 6020 Fax: (089) 52 6028
ratory
6 1390 Fax: (054) 46 1389
oratory
43 7222 Fax: (07) 3243 7218
ers Laboratory
7 4155 Fax: (077) 87 4220

Cloncurry Laboratory
Phone: (077) 42 1323 Fax: (077) 42 1685
Kalgoorlie Laboratory
Phone: (090) 21 1457 Fax: (090) 21 6253
Mt Isa Laboratory
Phone: (077) 49 5545 Fax: (077) 49 5546
New Zealand Laboratory
Phone: (07) 575 7654 Fax: (07) 575 7641

Orange Laboratory
Phone: (063) 63 1722 Fax: (063) 63 1189
Perth Laboratory
Phone: (09) 249 2988 Fax: (09) 249 2942
Townsville Laboratory
Phone: (077) 79 9155 Fax: (077) 79 9729

AUSTRALIAN LABORATORY
SERVICES P/L
A.C.N. 009 936 029

ANALYTICAL REPORT

CONTACT: MR E TONUI
CLIENT: NORTH LTD
ADDRESS: GEOLOGY DEPT.
ANU
ACT 0200

LABORATORY: ORANGE
BATCH NUMBER: OR5437
SUB BATCH: 0
No. OF SAMPLES: 186
DATE RECEIVED: 30/01/96
DATE COMPLETED: 07/02/96

o.: NSW0706 SAMPLE TYPE: REGOLITH PROJECT:

.E NUMBER	ELEMENT UNIT METHOD L.O.R.	Au PM204 ppm CHECKS 0.001					
ETP091							
ETP092							
ETP093							
ETP094							
ETP095		0.528					
ETP096							
ETP097							
ETP098							
ETP099							
ETP100							
ETP101							
ETP102							
ETP103							
ETP104							
ETP105							
ETP106							
ETP107							
ETP108							
ETP109							
ETP110							
ETP111							
ETP112							
ETP113							
ETP114							
ETP115							
ETP116							
ETP117							
ETP118							
ETP119							
ETP120							

TS:

e Final Report which supersedes any preliminary reports with this batch number. • Results apply to sample(s) as submitted by client.

AUSTRALIAN LABORATORY
SERVICES P/L
A.C.N. 009 936 029

ANALYTICAL REPORT

CONTACT: MR E TONUI
CLIENT: NORTH LTD
ADDRESS: GEOLOGY DEPT.
ANU
ACT 0200

LABORATORY: ORANGE
BATCH NUMBER: OR5437
SUB BATCH: 0
No. OF SAMPLES: 186
DATE RECEIVED: 30/01/96
DATE COMPLETED: 07/02/96

o.: NSW0706 SAMPLE TYPE: REGOLITH PROJECT:

.E NUMBER	ELEMENT UNIT METHOD L.O.R.	Au PM204 ppm CHECKS 0.001					
ETP121							
ETP122							
ETP123							
ETP124							
ETP125							
ETP126							
ETP127							
ETP128							
ETP129							
ETP130							
ETP131							
ETP132							
ETP133							
ETP134							
ETP135							
ETP136							
ETP137							
ETP138							
ETP139							
ETP140							
ETP141							
ETP142							
ETP143							
ETP144							
ETP145							
ETP146							
ETP147							
ETP148							
ETP149							
ETP150							

TS:

ıe Final Report which supersedes any preliminary reports with this batch number. • Results apply to sample(s) as submitted by client.

Laboratory
12 6020 Fax: (089) 52 6028
ratory
16 1390 Fax: (054) 46 1389
oratory
143 7222 Fax: (07) 3243 7218
ers Laboratory
17 4155 Fax: (077) 87 4220

Cloncurry Laboratory
Phone: (077) 42 1323 Fax: (077) 42 1685
Kalgoorlie Laboratory
Phone: (090) 21 1457 Fax: (090) 21 6253
Mt Isa Laboratory
Phone: (077) 49 5545 Fax: (077) 49 5546
New Zealand Laboratory
Phone: (07) 575 7654 Fax: (07) 575 7641

Orange Laboratory
Phone: (063) 63 1722 Fax: (063) 63 1189
Perth Laboratory
Phone: (09) 249 2988 Fax: (09) 249 2942
Townsville Laboratory
Phone: (077) 79 9155 Fax: (077) 79 9729

AUSTRALIAN LABORATORY SERVICES P/L

A.C.N. 009 936 029

ANALYTICAL REPORT

CONTACT: MR E TONUI
CLIENT: NORTH LTD
ADDRESS: GEOLOGY DEPT.
ANU
ACT 0200

LABORATORY: ORANGE
BATCH NUMBER: OR5437
SUB BATCH: 0
No. OF SAMPLES: 186
DATE RECEIVED: 30/01/96
DATE COMPLETED: 07/02/96

o.: NSW0706 SAMPLE TYPE: REGOLITH PROJECT:

.E NUMBER	ELEMENT UNIT METHOD L.O.R.	Au PM204 ppm CHECKS 0.001					
ETP181							
ETP182							
ETP183							
ETP184							
ETP185							
ETP186							

TS:

ıe Final Report which supersedes any preliminary reports with this batch number. • Results apply to sample(s) as submitted by client.

Laboratory
2 6020 Fax: (089) 52 6028
ratory
6 1390 Fax: (054) 46 1389
oratory
43 7222 Fax: (07) 3243 7218
ers Laboratory
7 4155 Fax: (077) 87 4220

Cloncurry Laboratory
Phone: (077) 42 1323 Fax: (077) 42 1685
Kalgoorlie Laboratory
Phone: (090) 21 1457 Fax: (090) 21 6253
Mt Isa Laboratory
Phone: (077) 49 5545 Fax: (077) 49 5546
New Zealand Laboratory
Phone: (07) 575 7654 Fax: (07) 575 7641

Orange Laboratory
Phone: (063) 63 1722 Fax: (063) 63 1189
Perth Laboratory
Phone: (09) 249 2988 Fax: (09) 249 2942
Townsville Laboratory
Phone: (077) 79 9155 Fax: (077) 79 9729

NORTH LTD

Attention: MR E TONUI
YourOrder: PK 02320
SampleType:PULP
Project:

ORANGE

Page-no: 3

Batch-no: 7861
Sub-batch:0
No-samples:104
Received: 07/03/97
Checked: 10/03/97

Element Unit Method	Cu ppm IC580	Pb ppm IC580	Zn ppm IC580	Ag ppm IC580	Au ppm PM204	Au PM204 ppm CHECKS
ETP320	184	16	49	6	0.021	
ETP321	196	15	50	5	0.017	
ETP322	202	16	50	7	0.011	
ETP323	204	15	51	6	0.009	
ETP324	228	15	52	6	0.013	0.012
ETP325	420	16	56	7	0.007	
ETP326	132	<5	8	2	0.015	
ETP327	201	9	11	6	0.014	
ETP328	312	7	7	3	0.123	
ETP329	2400	5	55	1	0.001	
ETP330	3090	<5	71	8	0.084	
ETP331	1190	<5	34	2	0.110	0.103
ETP332	3020	<5	64	3	0.058	
ETP333	3300	<5	55	2	0.093	
Limit of Detection	2	5	2	1	0.001	0.001

NORTH LTD

ORANGE

Page-no: 1

Attention: MR E TONUI
YourOrder: PK 02320
SampleType:PULP
Project:

Batch-no: 7861
Sub-batch:0
No-samples:104
Received: 07/03/97
Checked: 10/03/97

Element	Cu	Pb	Zn	Ag	Au	Au PM204
Unit	ppm	ppm	ppm	ppm	ppm	ppm
Method	ICP90	ICP90	ICP90	ICP90	PM204	CHECK
ETP230	47	17	43	5	0.006	
ETP231	38	8	36	3	0.007	
ETP232	101	28	73	17	0.002	
ETP233	173	87	120	30	0.012	0.013
ETP234	109	61	21	13	0.008	
ETP235	140	103	18	11	0.007	
ETP236	113	80	16	12	0.010	
ETP237	S.N.R.	S.N.R.	S.N.R.	S.N.R.	S.N.R.	
ETP238	S.N.R.	S.N.R.	S.N.R.	S.N.R.	S.N.R.	
ETP239	96	13	41	4	0.025	
ETP240	533	7	14	6	0.067	
ETP241	567	8	8	5	0.084	
ETP242	731	13	10	2	0.042	
ETP243	307	<5	7	1	0.131	
ETP244	545	6	10	2	0.332	0.244
ETP245	957	<5	13	4	<0.001	
ETP246	1430	<5	18	2	0.017	
ETP247	606	<5	9	2	0.019	
ETP248	4510	171	157	4	0.428	0.491
ETP249	3730	<5	83	2	0.060	
ETP250	9180	<5	107	3	0.006	
ETP251	6780	<5	60	5	0.003	
ETP252	6720	<5	100	3	0.018	
ETP253	8160	<5	122	1	0.408	0.441
ETP254	4790	<5	69	<1	0.026	
ETP255	2080	<5	107	<1	0.337	0.316
ETP256	2600	<5	48	1	0.220	
ETP257	S.N.R.	S.N.R.	S.N.R.	S.N.R.	S.N.R.	
ETP258	65	16	36	5	0.012	
ETP259	61	8	32	5	0.008	
ETP260	75	9	37	7	0.003	
ETP261	233	19	26	15	0.006	
ETP262	267	48	29	32	0.008	
ETP263	354	49	6	21	0.007	
ETP264	303	55	8	14	0.005	
ETP265	328	35	8	8	0.003	
ETP266	852	41	9	19	0.038	
ETP267	685	31	16	10	0.012	
ETP268	567	27	12	11	0.023	
ETP269	482	56	12	11	0.074	
ETP270	676	95	16	28	0.200	
ETP271	499	36	14	36	0.165	0.200
ETP272	456	22	11	15	0.018	
ETP273	774	8	14	18	0.015	0.015
ETP274	418	5	11	8	0.229	0.220
Limit of Detection	2	5	2	1	0.001	0.001

NORTH LTD

Attention: MR E TONUI
YourOrder: PK 02320
SampleType:PULP
Project:

ORANGE

Page-no: 2

Batch-no: 7861
Sub-batch:0
No-samples:104
Received: 07/03/97
Checked: 10/03/97

Element	Cu	Pb	Zn	As	Au	Au PM204
Unit	ppm	ppm	ppm	ppm	ppm	ppm
Method	IC580	IC580	IC580	IC580	PM204	CHECKS
ETP275	785	<5	10	22	0.011	
ETP276	785	<5	12	14	0.021	
ETP277	1200	<5	13	15	0.005	
ETP278	2370	33	32	12	0.058	
ETP279	5080	<5	91	5	<0.001	
ETP280	5580	<5	82	4	0.001	
ETP281	5190	<5	69	5	0.063	0.057
ETP282	1000	<5	48	2	0.011	0.013
[illegible]	[illegible]	[illegible]	[illegible]	[illegible]	[illegible]	
ETP284	S.N.R.	S.N.R.	S.N.R.	S.N.R.	S.N.R.	
ETP285	S.N.R.	S.N.R.	S.N.R.	S.N.R.	S.N.R.	
ETP286	S.N.R.	S.N.R.	S.N.R.	S.N.R.	S.N.R.	
ETP287	S.N.R.	S.N.R.	S.N.R.	S.N.R.	S.N.R.	
ETP288	S.N.R.	S.N.R.	S.N.R.	S.N.R.	S.N.R.	
ETP289	203	23	45	9	0.031	
ETP290	383	30	37	13	0.095	
ETP291	484	35	37	14	0.117	0.111
ETP292	511	40	39	17	0.063	
ETP293	283	57	<2	21	0.031	
ETP294	372	66	4	13	0.027	
ETP295	642	33	8	7	0.023	
ETP296	780	30	8	12	0.016	
ETP297	521	42	10	19	0.061	
ETP298	398	14	16	11	0.346	0.314
ETP299	294	14	23	8	0.035	
ETP300	375	7	35	10	0.032	
ETP301	365	<5	36	8	0.610	1.64
ETP302	760	<5	76	4	0.004	0.006
ETP303	707	5	80	2	0.002	
ETP304	1360	<5	92	5	0.003	
ETP305	1280	5	72	4	0.002	
ETP306	5850	<5	92	2	0.301	0.266
ETP307	5080	<5	74	1	0.004	
ETP308	3460	<5	74	4	0.243	0.219
ETP309	2500	<5	50	5	0.189	
ETP310	518	17	82	8	0.014	
ETP311	696	13	58	5	0.029	
ETP312	710	11	57	7	0.037	
ETP313	1080	<5	41	5	0.011	
ETP314	750	6	45	3	0.013	0.012
ETP315	80	16	47	5	0.025	
ETP316	78	16	48	8	0.020	
ETP317	78	13	48	6	0.024	
ETP318	113	17	42	9	0.038	
ETP319	198	18	34	16	0.034	
Limit of Detection	2	5	2	1	0.001	0.001

Appendix 7

Descriptive statistics

STAT. NONPAR STATS	Descriptive Statistics (all.sta)									
variable	mean	valid N	median	mode	freq-cy of mode	minimum	maximum	25.000th percentl	75.000th percentl	geometrc mean
FE2O3%	14.3168	77	12.0200	no mode	--	1.41000	40.687	5.4300	21.2060	10.9983
MNO%	.3633	77	.0300	.0200000	10	.00300	8.850	.0160	.0600	.0397
TIO2%	1.0665	77	1.0250	.9100000	3	.44300	1.700	.8800	1.2685	1.0314
CAO%	1.2389	77	.1920	multiple	--	.06000	11.890	.1100	1.2550	.3575
K2O%	.4307	77	.3370	multiple	--	.05000	2.106	.1900	.5645	.3350
SO3%	1.0838	77	.1510	.0800000	4	.02000	16.739	.0850	.2725	.2222
P2O5%	.1137	77	.0700	.0900000	5	.02000	.760	.0320	.1280	.0745
SIO2%	44.9687	77	43.0200	no mode	--	27.07000	68.940	35.2100	50.8420	43.6196
AL2O3%	21.2796	77	21.8730	no mode	--	8.56000	31.760	14.2090	27.7900	20.0180
MGO%	.8345	77	.5620	multiple	--	.23000	5.760	.3600	.9825	.6369
NA2O%	.3070	77	.3000	multiple	--	.05000	.642	.2010	.3875	.2756
CU	379.5000	76	297.5000	multiple	--	26.00000	1420.000	124.0000	564.5000	263.8089
PB	29.8158	76	27.0000	16.00000	6	3.00000	66.000	16.5000	43.0000	25.4788
ZN	33.1579	76	23.0000	8.000000	6	-2.00000	262.000	8.0000	42.5000	--
AG	-.9636	55	-1.0000	-1.00000	54	-1.00000	1.000	-1.0000	-1.0000	--
AS	12.3947	76	8.0000	7.000000	8	.50000	63.000	5.0000	14.5000	8.4708
AU	.0411	76	.0200	.0080000	7	.00200	.784	.0080	.0405	.0195

STAT. NONPAR STATS	Descriptive Statistics (all.sta)								
variable	harmonic mean	std.dev.	variance	average deviatn.	range	quartile range	skewness	kurtosis	sum
FE2O3%	8.0818	9.8383	96.79	8.2719	39.277	15.7760	.745913	-.48863	1102.39
MNO%	.0221	1.4311	2.05	.6049	8.847	.0440	5.016818	25.85185	27.97
TIO2%	.9935	.2684	.07	.2207	1.257	.3885	.135734	-.38419	82.12
CAO%	.1766	2.1570	4.65	1.5236	11.830	1.1450	2.659351	8.52240	95.40
K2O%	.2582	.3420	.12	.2418	2.056	.3745	2.401446	8.40132	33.16
SO3%	.1201	2.9954	8.97	1.5764	16.719	.1875	4.201052	18.85303	83.45
P2O5%	.0549	.1389	.02	.0815	.740	.0960	3.055572	9.75019	8.76
SIO2%	42.3402	11.3075	127.86	9.1283	41.870	15.6320	.526588	-.74821	3462.59
AL2O3%	18.6634	6.9413	48.18	5.9628	23.200	13.5810	-.214695	-1.29447	1638.53
MGO%	.5250	.8186	.67	.5054	5.530	.6225	3.628845	17.72092	64.26
NA2O%	.2397	.1336	.02	.1096	.592	.1865	.407328	-.37869	23.64
CU	167.5237	305.5051	93333.35	242.2500	1394.000	440.5000	1.221751	1.39472	28842.00
PB	20.8548	15.9505	254.42	13.3393	63.000	26.5000	.582352	-.74281	2266.00

STAT. NONPAR STATS	Descriptive Statistics (all.sta)								
variable	harmonic mean	std.dev.	variance	average deviatn.	range	quartile range	skewness	kurtosis	sum
ZN	29.2113	62.112	3858.	40.016	473.00	60.000	3.19527	15.5013	9838.0
AG	-1.0669	.543	.	.194	4.00	0.000	5.71596	33.7144	-98.0
AS	2.8339	11.713	137.	6.160	90.00	6.000	4.88935	29.6443	1202.5
AU	.0037	.139	.	.089	.87	.062	2.98198	10.0506	11.9

STAT. NONPAR STATS — Descriptive Statistics (all.sta)

variable	mean	valid N	median	mode	freq-cy of mode	minimum	maximum	25.000th percentl	75.000th percentl	geometrc mean
FE2O3%	8.530	152	7.960	multiple	--	2.13000	39.48	6.1800	9.975	7.787
MNO%	.205	152	.080	.0300000	8	-.01000	6.47	.0300	.130	--
TIO2%	.844	152	.831	multiple	--	.19600	1.39	.7565	.940	.822
CAO%	1.732	152	.291	multiple	--	.10000	17.62	.1900	1.493	.540
K2O%	3.059	152	3.075	multiple	--	.17000	7.87	1.0995	4.553	2.280
SO3%	.126	152	.032	.0100000	16	-.01000	5.50	.0100	.073	--
P2O5%	.188	152	.120	multiple	--	.02000	.80	.0685	.225	.129
SIO2%	47.603	152	48.900	multiple	--	19.94000	65.18	43.6280	52.247	46.884
AL2O3%	22.305	152	23.165	multiple	--	6.99500	32.03	19.1865	26.120	21.543
MGO%	2.125	152	1.513	multiple	--	.27000	12.37	.7885	2.690	1.545
NA2O%	1.075	152	.270	.2000000	5	.03000	5.60	.1800	1.245	.433
CU	2475.151	152	1640.000	5080.000	3	45.00000	18400.00	556.0000	3770.000	1355.659
PB	27.125	152	9.000	-5.00000	22	-5.00000	1880.00	5.0000	16.000	--
ZN	64.724	152	51.000	41.00000	6	6.00000	479.00	23.0000	83.000	44.641
AG	-.899	109	-1.000	-1.00000	105	-1.00000	3.00	-1.0000	-1.000	--
AS	7.911	152	5.000	multiple	--	-1.00000	89.00	2.0000	8.000	--
AU	.078	152	.021	.0005000	15	-.00100	.87	.0060	.068	--

STAT. NONPAR STATS — Descriptive Statistics (all.sta)

variable	harmonic mean	std.dev.	variance	average deviatn.	range	quartile range	skewness	kurtosis	sum
FE2O3%	7.1455	4.362	19.	2.608	37.35	3.795	3.60266	20.9474	1296.6
MNO%	.0402	.662	.	.231	6.48	.100	7.35053	60.6754	31.1
TIO2%	.7921	.177	.	.128	1.19	.184	-.21809	2.1080	128.3
CAO%	.2939	3.254	11.	2.088	17.52	1.303	2.86018	8.5182	263.3
K2O%	1.4451	1.936	4.	1.655	7.70	3.454	.28878	-.9003	464.9
SO3%	.0131	.507	.	.159	5.51	.063	8.76162	86.8679	19.1
P2O5%	.0892	.168	.	.133	.78	.157	1.34348	.9793	28.6
SIO2%	46.0130	7.666	59.	5.644	45.24	8.619	-.87929	1.5869	7235.6
AL2O3%	20.6127	5.360	29.	4.286	25.03	6.933	-.53541	-.1055	3390.3
MGO%	1.1822	2.014	4.	1.364	12.10	1.902	2.53625	7.8925	323.0
NA2O%	.2424	1.545	2.	1.213	5.57	1.065	1.61643	1.1874	163.3
CU	600.5407	2609.847	6811303.	1948.830	18355.00	3214.000	2.22101	8.6173	376223.0
PB	15.7893	153.407	23534.	33.234	1885.00	11.000	11.84051	143.6143	4123.0

STAT. NONPAR STATS	Descriptive Statistics (all.sta)								
variable	harmonic mean	std.dev.	variance	average deviatn.	range	quartile range	skewness	kurtosis	sum
ZN	12.2524	42.5366	1809.36	25.8532	264.000	34.5000	3.234926	13.05132	2520.00
AG	-1.0377	.2697	.07	.0714	2.000	0.0000	7.416198	55.00000	-53.00
AS	5.0361	11.9296	142.32	8.2666	62.500	9.5000	2.247645	5.79230	942.00
AU	.0109	.0926	.01	.0377	.782	.0325	7.119623	56.82451	3.12

STAT. NONPAR STATS	Descriptive Statistics (all.sta)									
variable	mean	valid N	median	mode	freq-cy of mode	minimum	maximum	25.000th percentl	75.000th percentl	geometrc mean
FE2O3%	10.476	229	8.3060	multiple	--	1.41000	40.69	5.8800	11.418	8.7453
MNO%	.258	229	.0510	.0200000	16	-.01000	8.85	.0200	.110	--
TIO2%	.919	229	.8800	.9000000	7	.19600	1.70	.7800	1.030	.8872
CAO%	1.567	229	.2600	multiple	--	.06000	17.62	.1600	1.448	.4700
K2O%	2.175	229	1.1600	multiple	--	.05000	7.87	.4410	3.706	1.1964
SO3%	.448	229	.0600	.0100000	16	-.01000	16.74	.0200	.138	--
P2O5%	.163	229	.1070	.0900000	9	.02000	.80	.0600	.172	.1073
SIO2%	46.717	229	47.7500	multiple	--	19.94000	68.94	41.0400	51.960	45.7602
AL2O3%	21.960	229	22.5980	multiple	--	6.99500	32.03	17.9700	26.575	21.0175
MGO%	1.691	229	1.0400	multiple	--	.23000	12.37	.6000	2.078	1.1471
NA2O%	.816	229	.2800	multiple	--	.03000	5.60	.1820	.472	.3719
CU	1776.601	228	719.5000	multiple	--	26.00000	18400.00	301.5000	2505.000	785.5916
PB	28.022	228	13.0000	-5.00000	22	-5.00000	1880.00	7.0000	27.000	--
ZN	54.202	228	41.0000	8.000000	9	-2.00000	479.00	14.5000	76.000	--
AG	-.921	164	-1.0000	-1.00000	159	-1.00000	3.00	-1.0000	-1.000	--
AS	9.406	228	6.0000	4.000000	24	-1.00000	89.00	3.0000	11.000	--
AU	.066	228	.0205	.0005000	15	-.00100	.87	.0080	.059	--

STAT. NONPAR STATS	Descriptive Statistics (all.sta)								
variable	harmonic mean	std.dev.	variance	average deviatn.	range	quartile range	skewness	kurtosis	sum
FE2O3%	7.4352	7.237	52.	5.039	39.28	5.538	1.96568	3.8398	2399.0
MNO%	.0315	.989	1.	.353	8.86	.090	6.60524	47.3546	59.1
TIO2%	.8501	.236	.	.176	1.50	.250	.52810	1.0320	210.4
CAO%	.2402	2.936	9.	1.894	17.56	1.288	2.99189	9.9195	358.7
K2O%	.5676	2.018	4.	1.758	7.82	3.265	.79212	-.5684	498.1
SO3%	.0187	1.835	3.	.671	16.75	.118	7.02332	55.6857	102.6
P2O5%	.0737	.162	.	.119	.78	.112	1.70651	2.2504	37.4
SIO2%	44.7089	9.115	83.	7.106	49.00	10.920	-.17734	.0071	10698.2
AL2O3%	19.9134	5.943	35.	4.854	25.03	8.605	-.43433	-.6481	5028.8
MGO%	.8320	1.812	3.	1.197	12.14	1.478	2.87472	10.5886	387.3
NA2O%	.2415	1.311	2.	.898	5.57	.291	2.27321	3.9424	187.0
CU	322.5932	2354.134	5541948.	1698.552	18374.00	2203.500	2.67629	11.4618	405065.0
PB	17.1803	125.460	15740.	26.981	1885.00	20.000	14.31462	211.7648	6389.0

STAT. NONPAR STATS	Descriptive Statistics (all.sta)								
variable	harmonic mean	std.dev.	variance	average deviatn.	range	quartile range	skewness	kurtosis	sum
ZN	19.9889	58.193	3386.	38.418	481.00	61.500	3.19251	15.8101	12358.0
AG	-1.0569	.470	.	.154	4.00	0.000	6.37262	42.6806	-151.0
AS	3.3175	11.949	143.	7.149	90.00	8.000	3.78759	18.9352	2144.5
AU	.0048	.127	.	.073	.87	.051	3.65910	15.3116	15.0

Appendix 8

Element-element correlation matrices

ΓAT. ASIC TATS	Correlations (27all.sta) Marked correlations are significant at p < .05000 N=31 (Casewise deletion of missing data)											
ariable	FE2O3%	MNO%	TIO2%	CAO%	K2O%	SO3%	P2O5%	SIO2%	AL2O3%	MGO%	NA2O%	CU
FE2O3%	1.00	.46*	.13	-.37*	-.52*	-.29	.64*	-.68*	-.03	-.33	-.31	.06
MNO%	.46*	1.00	.16	-.09	-.21	-.07	.92*	-.35	-.38*	-.10	-.17	-.23
TIO2%	.13	.16	1.00	-.39*	-.66*	-.43*	.16	-.42*	.59*	-.12	-.28	.13
CAO%	-.37*	-.09	-.39*	1.00	.25	.77*	-.18	-.01	-.45*	.66*	.09	-.01
K2O%	-.52*	-.21	-.66*	.25	1.00	.17	-.20	.65*	-.32	.22	.23	.10
SO3%	-.29	-.07	-.43*	.77*	.17	1.00	-.17	.07	-.47*	.05	.23	-.31
P2O5%	.64*	.92*	.16	-.18	-.20	-.17	1.00	-.52*	-.21	-.16	-.36*	.01
SIO2%	-.68*	-.35	-.42*	-.01	.65*	.07	-.52*	1.00	-.35	.01	.65*	-.35
AL2O3%	-.03	-.38*	.59*	-.45*	-.32	-.47*	-.21	-.35	1.00	-.21	-.50*	.49*
MGO%	-.33	-.10	-.12	.66*	.22	.05	-.16	.01	-.21	1.00	-.05	.30
NA2O%	-.31	-.17	-.28	.09	.23	.23	-.36*	.65*	-.50*	-.05	1.00	-.67*
CU	.06	-.23	.13	-.01	.10	-.31	.01	-.35	.49*	.30	-.67*	1.00
PB	.60*	-.05	-.13	-.39*	-.34	-.24	.11	-.24	.09	-.42*	-.05	.07
ZN	.32	.95*	-.02	.04	-.04	.08	.82*	-.13	-.60*	-.05	.03	-.38*
AG	.39*	.74*	.13	-.06	-.17	-.05	.77*	-.27	-.31	-.07	-.11	-.15
AS	.39*	.20	-.34	-.28	-.01	-.15	.28	.09	-.31	-.29	.08	-.06
AU	-.15	-.11	.05	.01	.03	-.06	-.12	-.02	.23	.09	-.08	.08

;TAT. BASIC ;TATS	Correlations (27all.sta) Marked correlations are significant at p < .05000 N=31 (Casewise deletion of missing data)				
Variable	PB	ZN	AG	AS	AU
FE2O3%	.60*	.32	.39*	.39*	-.15
MNO%	-.05	.95*	.74*	.20	-.11
TIO2%	-.13	-.02	.13	-.34	.05
CAO%	-.39*	.04	-.06	-.28	.01
K2O%	-.34	-.04	-.17	-.01	.03
SO3%	-.24	.08	-.05	-.15	-.06
P2O5%	.11	.82*	.77*	.28	-.12
SIO2%	-.24	-.13	-.27	.09	-.02
AL2O3%	.09	-.60*	-.31	-.31	.23
MGO%	-.42*	-.05	-.07	-.29	.09
NA2O%	-.05	.03	-.11	.08	-.08
CU	.07	-.38*	-.15	-.06	.08
PB	1.00	-.16	-.02	.73*	-.09
ZN	-.16	1.00	.77*	.20	-.12
AG	-.02	.77*	1.00	.24	-.08
AS	.73*	.20	.24	1.00	-.10
AU	-.09	-.12	-.08	-.10	1.00

Appendix 9

Mineral-element correlation matrices

STAT. BASIC STATS	Correlations (all.sta) Marked correlations are significant at p < .05000 N=55 (Casewise deletion of missing data)											
Variable	KAOLIN	QUARTZ	HEMATITE	GOETHITE	MUSCOVIT	ORTHOCLA	MICROCLI	ALBITE	SMECTITE	DOLOMITE	CALCITE	GYPSUM
FE2O3%	.14	-.28*	.24	.25	-.03	--	-.11	-.29*	-.13	.12	-.24	-.33*
MNO%	-.29*	.07	.02	.55*	-.04	--	-.03	-.10	-.10	-.09	-.06	-.10
TIO2%	.25	-.47*	.19	.36*	-.03	--	-.11	-.32*	-.09	.15	-.26	-.46*
CAO%	-.44*	.46*	-.35*	-.18	-.07	--	.04	.42*	.53*	.01	.26	.44*
K2O%	-.12	.16	-.01	-.21	.45*	--	.15	.28*	.02	-.12	.24	.13
SO3%	-.38*	.44*	-.25	-.15	-.04	--	-.04	.27*	.13	-.09	.01	.72*
P2O5%	-.10	-.17	.05	.61*	.03	--	-.08	-.22	-.10	-.04	-.16	-.23
SIO2%	-.36*	.58*	-.31*	-.20	-.05	--	.30*	.40*	-.12	-.17	.44*	.30*
AL2O3%	.74*	-.82*	.43*	-.06	.16	--	-.18	-.39*	-.12	.11	-.39*	-.53*
MGO%	-.20	.16	-.30*	-.14	-.03	--	.10	.27*	.74*	.12	.15	.12
NA2O%	-.50*	.59*	-.33*	.08	-.11	--	.19	.30*	-.15	-.05	.27*	.30*
CU	.50*	-.55*	.13	-.03	.04	--	-.11	-.15	.28*	-.17	-.26	-.32*
PB	.25	-.31*	.15	.30*	-.09	--	-.11	-.35*	-.22	.02	-.19	-.39*
ZN	-.45*	.24	-.18	.57*	-.06	--	.03	.04	-.13	-.02	.02	.01
AG	-.19	.09	.06	.27*	-.02	--	-.02	-.05	-.05	-.04	-.03	-.05
AS	.02	-.06	-.02	.11	-.05	--	-.05	-.19	-.18	.39*	-.15	-.20
AU	.12	-.20	.32*	-.10	-.06	--	-.00	.00	.08	-.09	-.09	-.07

STAT. BASIC STATS	Correlations (all.sta) Marked correlations are significant at p < .05000 N=109 (Casewise deletion of missing data)											
Variable	KAOLIN	QUARTZ	HEMATITE	GOETHITE	MUSCOVIT	ORTHOCLA	MICROCLI	ALBITE	SMECTITE	DOLOMITE	CALCITE	GYPSUM
FE2O3%	.05	-.10	.25*	.35*	-.01	-.02	-.01	-.16	-.03	-.09	-.12	-.07
MNO%	.01	.01	.05	.56*	-.03	-.11	-.07	-.03	-.08	-.08	-.05	-.02
TIO2%	.24*	-.04	.10	-.03	-.05	-.05	-.13	-.17	.06	-.02	-.11	-.06
CAO%	.02	.18	.01	.12	-.24*	-.18	.06	.01	-.03	.09	.15	.35*
K2O%	-.44*	-.40*	-.13	-.39*	.48*	.63*	.10	.24*	.16	-.24*	-.15	-.11
SO3%	.18	.14	.01	.08	-.18	-.18	-.08	-.03	.04	-.01	.12	-.01
P2O5%	-.47*	-.30*	-.00	.07	.18	.30*	.47*	.25*	-.27*	-.17	.05	-.16
SIO2%	-.29*	.16	-.37*	-.28*	.04	.24*	.18	.23*	.06	-.09	.28*	-.11
AL2O3%	.33*	-.23*	.23*	-.14	.19*	-.12	-.29*	-.16	-.06	.11	-.35*	-.25*
MGO%	-.12	-.09	-.05	-.02	-.11	.06	.24*	.07	-.03	.02	-.04	.23*
NA2O%	-.66*	-.34*	-.21*	-.26*	.07	.56*	.71*	.45*	-.15	-.20*	.15	-.09
CU	-.41*	-.33*	-.21*	-.22*	.25*	.57*	.34*	.21*	.05	-.28*	-.10	-.10
PB	.04	-.01	-.08	-.02	.13	.01	-.07	-.05	-.06	-.04	-.04	-.02
ZN	-.28*	-.16	-.27*	-.01	.34*	.30*	.15	.09	.01	-.25*	-.07	-.07
AG	-.05	-.09	.10	-.08	-.06	.18	.07	.06	-.08	-.05	-.05	-.03
AS	.11	.08	.07	.36*	.09	-.21*	-.18	-.17	-.01	.02	-.09	-.05
AU	-.27*	-.09	-.03	-.15	.04	.23*	.29*	.23*	-.15	-.11	.04	-.05

Appendix 10

Partial/selective leaching data

Sample	Name	Nature	Kaolin	Quartz	Hemat.	Goeth.	Musc.	Ortho..	Albite	Smect.	Dolom.	Epidote	Jarosite	PDM
1	E22 P1S3 (5m)	Mottl. clay	73.2	7.9		5.9				5.8	7.3			
2	E27 P1S5 (19m)	Saprolite	56.3	7.7	1.9						34.1			
3	E27 P1S6 (21m)	Saprolite	69.8	1.7	4.4	1.2					22.9			
4	E27P1S10(31m)	Saprolite	28.1	5.3			23.1	12	15.4	13.7				
5	E27 P3S5 (19m)	Mottl. clay	76.5	5.8	15.4	2.3								
6	E27P5S13(32m)	Mottl. clay	77.8	10.7	1.7	7.6				2.2				
7	E27P5S14(34m)	Mottl. clay	79.7	5.5	7.5	7.3				1.7				
8	E27P5S17(40m)	Saprolite	41.2	13.1	1.9	2.1	37.5		0.7				3.4	3.4
9	E27P5S18(42m)	Saprolite	57.8	0.9	3	1.4	12.9	19.1				1.1	1.3	1.3
10	E27 P6S8 (19m)	Mottl. clay	73.2	10.8	9.5	6.5								
11	E27P6S12(29m)	Fe-Mn aggr.	36.9	7.5	8.9	30.6								16
12	E27P6S14(31m)	Fe-Mn aggr.	21	13.7	11.7	35.4								19.2
13	E27P6S15(32m)	Ferr. sapr./Mn	41.7	12.5	6.5	25.2								14
14	E27P6S21(44m)	Sapl./Saprock	50.5	3.8	0.8		26.7	12.3		5.9				
15	E22 P7S2 (8m)	Saprolite	74.9	17	0.5					7.6				
16	E22 P7S3 (11m)	Saprolite	48.2	3.5	6.3	6.1	26.5			1.5	7.9			
17	E27 P9S2 (6m)	Mottl. clay	85.6	2.7	3.6	4.1				4.1				
18	E27 P9S3 (8m)	Mottl. clay	83.6	2.1	7.7	4.3				3.3				
19	E27 P9S5 (12m)	Mottl. clay	68.7	4.3	4.2	2.1				1.2	19.5			
20	E27P8S10(24m)	Mottl. clay	76.3	6.8	4.1	1.9	8			2.8				
21	E27P8S13(29m)	Saprolite	47.6	0.7	1.9	0.8	14.2	30.1		1.4		1.9	1.5	
22	E22P4S9(29m)	Fe-Mn aggrg.	29.3	9.1		47.2								15.4
23	E27P7S2(1m)	Soil	39.7	47.7	0.9	6.8				3.3			Calc.0.5	gyp.2.1
24	E27P6S2 (1m)	Soil	11.3	38.5	3.3	2.7				22.6	0.8		Cal.13.5	gyp.7.3
25	E27 P11S2(1m)	Soil	42.3	16.2	0.4	15.8	12.5	1.3					Cal.7.8	gyp.1.7
26	E27 P8S3 (4m)	Mottl. clay	71.2	11.1	4.7	10.5				1.5				
27	E22P1S10(18m)	Ferr. saprolite	58	8.4	1.1	5.9	26.5							

PDM= Poorly diffracting material (in this case poorly crystalline Mn oxides lithiophorite and hollandite)

Ident	SiO2	Al2O3	Fe2O3	MnO	MgO	CaO	Na2O	K2O	TiO2	P2O5
	%	%	%	%	%	%	%	%	%	%
et-1	44.41	23.94	6.66	0.030	2.75	2.82	0.22	0.53	0.73	0.080
et-2	42.68	22.86	7.56	1.736	2.63	3.34	0.27	0.76	0.87	0.150
et-4	50.74	23.24	6.92	0.020	2.15	0.33	2.17	3.53	0.86	0.152
et-9	58.48	20.05	7.36	0.077	0.80	0.20	0.11	4.36	0.83	0.178
et-10	47.02	22.94	15.29	0.015	0.38	0.11	0.33	0.58	0.82	0.146
et-11	27.05	10.91	33.60	9.324	0.47	0.45	0.24	0.18	1.25	0.741
et-14	53.97	18.61	8.44	0.064	1.85	1.52	5.23	3.33	0.77	0.505
et-16	46.36	33.04	2.20	0.011	0.62	0.25	0.35	0.56	0.96	0.051
et-17	44.58	31.71	5.34	0.017	0.61	0.22	0.22	0.24	1.46	0.061
et-20	43.57	28.11	10.37	0.050	0.70	0.18	0.22	2.87	0.91	0.096
et-22	31.43	19.76	28.10	2.546	0.45	0.19	0.25	0.17	1.17	0.540
et-24	61.92	11.74	4.71	0.085	1.20	2.42	0.56	0.63	0.75	0.022
et-27	47.17	27.47	9.69	0.180	0.54	0.15	0.17	1.75	0.81	0.142

Ident	Ca	Mg	Co	Cu	Fe	Mn	Ni	Pb	Zn	Ba	Ce	Cl	Cr	Ga	La	Nb	Rb	S	Sr	V	Y	Zr	OXIDES
	ppm	ppm	ppm	ppm	ppm	ppm	ppm	ppm	ppm	ppm	ppm	ppm	ppm	ppm	ppm	ppm	ppm	ppm	ppm	ppm	ppm	ppm	%
et-1	20155	11921	1	387	46583	232	6	22	23	327	59	2200	9	25	41	8	16	290	282	176	21	175	82.2
et-2	23871	11401	197	1892	52878	13445	2	12	19	3431	52	3660	8	21	20	3	25	630	242	284	31	114	82.9
et-4	2359	9320	6	5242	48402	155	8	19	77	460	43	280	5	25	21	5	164	10	323	241	21	98	90.1
et-9	1429	3468	19	686	51479	596	-1	15	7	282	31	240	9	22	15	6	99	20	75	320	12	84	92.4
et-10	786	1647	-6	775	106946	116	3	63	14	89	47	1610	26	25	33	4	19	400	134	510	14	104	87.6
et-11	3216	2037	266	231	235015	72211	27	88	260	6817	102	1650	14	13	49	9	16	280	771	458	30	235	84.2
et-14	10864	8020	8	3128	59034	496	6	12	54	700	26	320	11	18	14	5	40	-10	767	256	22	49	94.3
et-16	1787	2688	-1	356	15388	85	8	15	2	297	33	1180	5	33	26	7	20	1150	158	57	10	111	84.4
et-17	1572	2644	-1	538	37351	132	7	26	10	158	41	1200	15	37	32	9	11	90	165	139	19	118	84.5
et-20	1286	3034	9	782	72533	387	3	15	64	650	38	620	3	27	22	8	55	80	169	219	14	173	87.1
et-22	1358	1951	95	954	196545	19718	15	108	128	3237	165	1670	33	23	39	13	14	330	188	516	27	197	84.6
et-24	17296	5202	10	68	32944	658	20	26	43	455	51	550	48	15	22	8	46	10450	150	98	27	333	84.0
et-27	1072	2341	10	1614	67777	1394	7	45	79	536	82	1660	5	30	45	17	42	190	231	181	40	212	88.1

Sample	weight	volume	v/w	Au	Ag	As	Ca	Mg	Co	Cu	Fe	Mn	Ni	Pb	Zn	Sample #	Type
1000				ppb	ppb	ppm	ppm	ppm	ppm	ppm	ppm	ppm	ppm	ppm	ppm	(Eric's)	
Blank A	1	1	1	-0.01	-1	-0.01	1	-0.2	-0	0.06	-0.02	-0.02	-0.02	-0.05	0.02		
Blank B	1	1	1	-0.01	-1	-0.01	0.8	-0.2	-0	-0.02	0.04	-0.02	-0.02	-0.05	-0.02		
Blank C	1	1	1	-0.01	-1	-0.01	0.4	-0.2	-0	-0.02	-0.02	-0.02	-0.02	-0.05	-0.02		
ET1 tot				131		9	126287	75363		117	18324	232		11	16		
ET 1 A	2.5	184	73.6	10.30	-73.6	-0.7	20387	12438	0.7	10.3	3	29	-1.5	-3.7	1.5	E22 P1S3 (5m)	Mottl. clay
ET 1 B	2.5	91	36.4	0.73	-36.4	-0.4	36	15	0.9	-0.73	4	74	-0.7	-1.8	0.7		
ET 1 C	2.5	91	36.4	5.10	-36.4	-0.4	29	116	0.2	13.1	783	12	-0.7	-1.8	0.7		
ET2 tot				131		1.0	97414	58300		307	30704	155		<5	7.0		
ET 2 A	5	184	36.8	10.30	-36.8	-0.4	25392	13616	1.2	132	-1	7	-0.7	-1.8	2.9	E27 P1S5 (19m)	Saprolite
ET 2 B	5	91	18.2	1.09	3676.4	-0.2	1802	957	200	581	706	10884	2.2	0.9	3.6		
ET 2 C	5	91	18.2	0.73	5478.2	-0.2	215	149	44	269	1893	2712	-0.4	0.9	1.5		
ET3 tot				332		2.0	92196	54743		545	71059	232		6.0	10.0		
ET 3 A	5	184	36.8	5.52	-36.8	-0.4	16082	8869	0.9	145	-1	8	-0.7	3.7	2.9	E27 P1S6 (21m)	Saprolite
ET 3 B	5	91	18.2	0.55	200.2	-0.2	113	55	49	92.5	90	901	-0.4	56.4	1.8		
ET 3 C	5	91	18.2	2.91	54.6	-0.2	91	466	16	1529	8063	317	1.5	291.2	16.7		
ET4 tot				428		4.0	1429	12480		4510	54763	387		171.0	157.0		
ET 4 A	5	184	36.8	28.34	-36.8	-0.4	1089	1156	0.6	80.2	33	4	1.5	-1.8	1.5	E27 P1S10 (31m)	Saprolite
ET 4 B	5	91	18.2	-0.18	-18.2	-0.2	22	29	1.4	179	151	8	0.4	-0.9	1.1		
ET 4 C	5	91	18.2	-0.18	-18.2	-0.2	44	462	1.1	2366	3403	7	2.5	-0.9	10.2		
ET5 tot				784		8.0	1001	2894		353	84138	155		25.0	16.0		
ET 5 A	5	184	36.8	0.74	-36.8	-0.4	1008	1281	0.3	3.68	-1	1	-0.7	-1.8	0.7	E27 P3S5 (19m)	Mottl. clay
ET 5 B	5	91	18.2	-0.18	18.2	-0.2	18	22	0.9	4.73	33	9	-0.4	-0.9	1.1		
ET 5 C	5	91	18.2	0.36	36.4	-0.2	15	66	0.3	13.8	644	3	-0.4	1.8	0.7		
ET6 tot				200		28.0	715	2532		676	62037	77		95.0	16.0		
ET 6 A	5	184	36.8	1.10	-36.8	-0.4	824	1170	0.3	16.2	-1	-1	-0.7	3.7	-0.7	E27 P5S13 (32m)	Mottl. clay
ET 6 B	5	91	18.2	-0.18	-18.2	-0.2	15	15	4.4	9.83	27	11	-0.4	8.2	0.7		
ET 6 C	5	91	18.2	-0.18	-18.2	-0.2	15	36	0.5	26.9	1125	3	-0.4	9.1	0.7		
ET7 tot				165		36.0	1001	1628		499	88614	77		36.0	14.0		
ET 7 A	5	184	36.8	0.74	-36.8	-0.4	979	868	0.9	3.68	-1	-1	-0.7	-1.8	-0.7	E27 P5S14 (34m)	Mottl. clay
ET 7 B	5	91	18.2	-0.18	-18.2	-0.2	18	11	0.4	2.55	28	3	-0.4	-0.9	0.7		
ET 7 C	5	91	18.2	-0.18	-18.2	-0.2	25	36	1.4	13.1	675	1	-0.4	2.7	0.7		
ET8 tot				229		8.0	2073	5366		418	37558	0		5.0	11.0		
ET 8 A	5	184	36.8	9.57	-36.8	-0.4	2252	2076	0.4	10.3	1	-1	-0.7	-1.8	0.7	E27 P5S17 (40m)	Saprolite
ET 8 B	5	91	18.2	0.36	-18.2	-0.2	18	18	0.8	5.46	48	20	-0.4	-0.9	0.4		
ET 8 C	5	91	18.2	0.55	-18.2	-0.2	22	91	0.3	20	652	3	-0.4	-0.9	0.7		
ET9 tot				11		22.0	1429	4763		785	52805	542		<5	10.0		
ET 9 A	5	184	36.8	-0.37	-36.8	-0.4	1281	1030	0.9	18.4	18	7	-0.7	-1.8	2.9	E27 P5S18 (42m)	Saprolite
ET 9 B	5	91	18.2	-0.18	54.6	-0.2	22	22	20	25.5	168	451	0.7	0.9	0.7		
ET 9 C	5	91	18.2	-0.18	-18.2	-0.2	36	84	2.2	73.9	1693	44	0.7	-0.9	0.7		
ET10 tot				114		32.0	643	2291		790	106029	155		53.0	14.0		

Sample	weight	volume	v/w	Au	Ag	As	Ca	Mg	Co	Cu	Fe	Mn	Ni	Pb	Zn	Sample #	Type
1000				ppb	ppb	ppm	ppm	ppm	ppm	ppm	ppm	ppm	ppm	ppm	ppm	(Eric's)	
ET21 tot				610		8	1144	3256		365	57491	387		<5	36		
ET 21 A	5	184	36.8	0.74	-36.8	-0.4	1317	4522	0.1	72.9	-1	-1	-0.7	-1.8	2.2	E27 P8S13 (29m)	Saprolite
ET 21 B	5	91	18.2	-0.18	-18.2	-0.2	18	18	17	104	122	608	0.7	2.7	2.2		
ET 21 C	5	91	18.2	-0.18	-18.2	-0.2	22	182	2.4	200	1649	106	-0.4	-0.9	5.1		
ET22 tot				78		29	1429	4522		518	222759	28502		48	137		
ET 22 A	5	184	36.8	12.14	-36.8	-0.4	1200	4035	0.1	3.68	-1	8	-0.7	-1.8	-0.7	E22 P4S9 (29m)	Fe-Mn aggrg.
ET 22 B	5	91	18.2	0.18	145.6	-0.2	91	73	91	98.6	1791	14851	1.8	67.3	13.5		
ET 22 C	5	91	18.2	-0.18	36.4	-0.2	55	160	9.1	45.1	3403	1820	1.1	21.8	4.0		
ET23 tot				38		9	10649	102071		113	36509	852		17	42		
ET 23 A	5	184	36.8	4.78	-36.8	-0.4	11224	7657	0.2	1.47	-1	7	-0.7	-1.8	0.7	E27 P7S2 (1m)	Soil
ET 23 B	5	91	18.2	0.18	-18.2	-0.2	40	109	10	5.82	126	612	6.2	8.2	1.5		
ET 23 C	5	91	18.2	0.55	-18.2	-0.2	15	542	1.8	10.9	1966	85	1.5	4.6	3.6		
ET24 tot				27		6	9363	7657		121	39796	775		13	48		
ET 24 A	5	184	36.8	6.99	-36.8	-0.4	18878	8621	0.1	2.21	-1	7	-0.7	-1.8	-0.7	E27 P6S2 (1m)	Soil
ET 24 B	5	91	18.2	0.55	-18.2	-0.2	51	87	8.4	6.55	98	455	6.2	5.5	0.7		
ET 24 C	5	91	18.2	1.64	-18.2	-0.2	18	386	1.4	9.83	1354	66	1.5	3.6	2.2		
ET25 tot				37		7	6575	8621		710	59939	232		11	57		
ET 25 A	5	184	36.8	4.42	-36.8	-0.4	2296	4642	0.5	38.3	-1	24	-0.7	-1.8	0.7	E27 P11S2 (1m)	Soil
ET 25 B	5	91	18.2	-0.18	18.2	-0.2	18	11	3.1	25.5	67	52	0.4	0.9	0.4		
ET 25 C	5	91	18.2	0.91	36.4	-0.2	18	116	1.5	65.2	2730	33	0.7	3.6	1.8		
ET26 tot				117		14	1286	4642		484	106798	232		35	37		
ET 26 A	5	184	36.8	2.58	-36.8	-0.4	1362	3376	0.3	2.94	-1	5	-0.7	-1.8	0.7	E27 P8S3 (4m)	Mottl. clay
ET 26 B	5	91	18.2	0.55	-18.2	-0.2	36	29	1.3	5.1	70	51	-0.4	3.6	0.4		
ET 26 C	5	91	18.2	1.27	-18.2	-0.2	18	102	0.5	12.4	1387	12	-0.4	6.4	0.7		
ET27 tot				536		9	1001	3376		811	64415	1239		13	66		
ET 27 A	5	184	36.8	1.47	-36.8	0.4	1803	3195	0.9	130	10	2	-0.7	-1.8	2.2	E22 P1S10 (18m)	Ferr. saprolite
ET 27 B	5	91	18.2	0.55	163.8	-0.2	18	11	8.4	72.1	129	1061	-0.4	21.8	1.5		
ET 27 C	5	91	18.2	0.55	327.6	-0.2	33	62	0.8	107	744	108	0.4	2.7	1.5		

Sample	weight	volume	v/w	Au	Ag	As	Ca	Mg	Co	Cu	Fe	Mn	Ni	Pb	Zn	Sample #	Type
1000				ppb	ppb	ppm	ppm	ppm	ppm	ppm	ppm	ppm	ppm	ppm	ppm	(Eric's)	
ET 10 A	5	184	36.8	2.21	-36.8	-0.4	743	1501	0.7	8.83	-1	-1	0.7	-1.8	-0.7	E27 P6S8 (19m)	Mottl. clay
ET 10 B	5	91	18.2	0.18	-18.2	-0.2	15	15	1.5	5.82	29	4	1.1	2.7	1.1		
ET 10 C	5	91	18.2	-0.18	18.2	-0.2	11	33	0.5	16.4	990	2	0.7	3.6	0.4		
ET11 tot				31		12.0	2359	2472		783	184082	61031		16.0	354.0		
ET 11 A1	5	184	36.8	1.84	-36.8	-0.4	3047	1575	0.1	2.21	1	25	-0.7	-1.8	1.5	E27 P6S12 (29m)	Fe-Mn aggr.
ET 11 A2	2.5	184	73.6	1.47	-73.6	-0.7	3209	1634	0.2	4.42	9	78	-1.5	-3.7	4.4		
ET 11 B	2.5	91	36.4	0.36	-36.4	-0.4	415	277	218	2.18	561	50596	8.7	-1.8	27.7		
ET 11 C	2.5	91	36.4	1.82	72.8	-0.4	153	255	98	107	52780	11721	4.4	83.7	107.0		
ET12 tot				77		46.0	3145	2653		553	234019	68698		33.0	331.0		
ET 12 A	5	184	36.8	1.47	-36.8	-0.4	2340	1693	0.2	64.8	-1	18	-0.7	-1.8	2.2	E27 P6S14 (31m)	Fe-Mn aggr.
ET 12 B	5	91	18.2	0.36	91.0	0.2	324	619	166	713	3585	35854	7.6	29.1	37.9		
ET 12 C	5	91	18.2	0.73	36.4	-0.2	98	331	18	451	14524	5296	2.2	41.9	22.2		
ET13 tot				106		22.0	2501	3557		1700	222339	50110		48.0	39.0		
ET 13 A	5	184	36.8	4.05	-36.8	-0.4	1825	2230	0.9	155	-1	26	-0.7	-1.8	2.2	E27 P6S15 (32m)	Ferr. sapr./Mn
ET 13 B	5	91	18.2	0.36	182.0	-0.2	47	47	60	315	582	7116	0.7	21.8	4.4		
ET 13 C	5	91	18.2	0.18	72.8	0.2	25	127	12	240	2748	1090	0.4	7.3	2.5		
ET14 tot				632		1.0	12436	12842		3460	64275	620		6.0	60.0		
ET 14 A	5	184	36.8	0.37	-36.8	-0.4	1597	927	2.3	105	1	4	-0.7	-1.8	1.5	E27 P6S21 (44m)	Sapl./Saprock
ET 14 B	5	91	18.2	-0.18	-18.2	0.9	4350	66	1.8	114	204	46	0.4	-0.9	0.7		
ET 14 C	5	91	18.2	-0.18	36.4	-0.2	389	590	1.8	599	1529	25	1.5	-0.9	5.5		
ET15 tot				123		3.0	1787	3678		312	15806	77		7.0	7.0		
ET 15 A	5	184	36.8	12.88	-36.8	-0.4	2230	2495	0.1	1.47	-1	4	-0.7	-1.8	1.5	E22 P7S2 (8m)	Saprolite
ET 15 B	5	91	18.2	0.91	-18.2	-0.2	29	29	0.1	0.73	17	8	-0.4	-0.9	0.4		
ET 15 C	5	91	18.2	0.36	36.4	-0.2	25	91	0.1	3.64	297	2	0.7	0.9	-0.4		
ET16 tot				132		2.0	39523	26467		267	73087	310		5.0	9.0		
ET 16 A	5	184	36.8	1.84	-36.8	-0.4	2098	1928	0.3	1.47	-1	1	-0.7	-1.8	1.5	E22 P7S3 (11m)	Saprolite
ET 16 B	5	91	18.2	0.36	36.4	-0.2	15	11	0.1	-0.36	1	2	0.4	-0.9	-0.4		
ET 16 C	5	91	18.2	-0.18	109.2	-0.2	15	25	0.1	1.09	27	0.4	-0.4	-0.9	-0.4		
ET17 tot				141		2.0	1572	3678		566	37838	77		16.0	11.0		
ET 17 A	5	184	36.8	11.04	-36.8	-0.4	1722	1744	0.2	2.21	-1	1	-0.7	-1.8	-0.7	E27 P9S2 (6m)	Mottl. clay
ET 17 B	5	91	18.2	0.36	-18.2	-0.2	18	25	0.2	3.28	21	8	0.4	1.8	0.4		
ET 17 C	5	91	18.2	0.73	-18.2	-0.2	15	106	0.1	6.92	450	1	0.4	1.8	-0.4		
ET18 tot				110		2	1429	4281		715	43433	387		12	4		
ET 18 A	5	184	36.8	2.21	-36.8	-0.4	1619	4281	0.1	2.21	-1	19	-0.7	-1.8	1.5	E27 P9S3 (8m)	Mottl. clay
ET 18 B	5	91	18.2	-0.18	-18.2	-0.2	18	33	1.1	3.28	24	220	1.1	-0.9	0.7		
ET 18 C	5	91	18.2	0.91	54.6	-0.2	18	193	0.2	6.92	661	28	-0.4	-0.9	0.7		
ET20 tot				346		11	1358	35028		398	87845	310		14	16		
ET 20 A	5	184	36.8	2.21	-36.8	-0.4	1214	3256	0.1	26.5	-1	-1	-0.7	-1.8	0.7	E27 P8S10 (24m)	Mottl. clay
ET 20 B	5	91	18.2	-0.18	-18.2	-0.2	18	15	5.3	18.6	19	20	-0.4	1.8	1.5		
ET 20 C	5	91	18.2	-0.18	-18.2	-0.2	22	98	0.8	81.2	1605	7	-0.4	2.7	2.2		